mRNA TRANSLATIONAL CONTROL AS A MECHANISM OF POST-TRANSCRIPTIONAL GENE REGULATION

EDITED BY: Daniel L. Kiss, Neva Caliskan, Kiong Ho, Deepika Vasudevan and Kristin S. Koutmou

PUBLISHED IN: Frontiers in Molecular Biosciences

frontiers Research Topics

ISSN 1664-8714
ISBN 978-2-88976-590-4
DOI 10.3389/978-2-88976-590-4

About Frontiers

Frontiers is more than just an open-access publisher of scholarly articles: it is a pioneering approach to the world of academia, radically improving the way scholarly research is managed. The grand vision of Frontiers is a world where all people have an equal opportunity to seek, share and generate knowledge. Frontiers provides immediate and permanent online open access to all its publications, but this alone is not enough to realize our grand goals.

Frontiers Journal Series

The Frontiers Journal Series is a multi-tier and interdisciplinary set of open-access, online journals, promising a paradigm shift from the current review, selection and dissemination processes in academic publishing. All Frontiers journals are driven by researchers for researchers; therefore, they constitute a service to the scholarly community. At the same time, the Frontiers Journal Series operates on a revolutionary invention, the tiered publishing system, initially addressing specific communities of scholars, and gradually climbing up to broader public understanding, thus serving the interests of the lay society, too.

Dedication to Quality

Each Frontiers article is a landmark of the highest quality, thanks to genuinely collaborative interactions between authors and review editors, who include some of the world's best academicians. Research must be certified by peers before entering a stream of knowledge that may eventually reach the public - and shape society; therefore, Frontiers only applies the most rigorous and unbiased reviews.
Frontiers revolutionizes research publishing by freely delivering the most outstanding research, evaluated with no bias from both the academic and social point of view. By applying the most advanced information technologies, Frontiers is catapulting scholarly publishing into a new generation.

What are Frontiers Research Topics?

Frontiers Research Topics are very popular trademarks of the Frontiers Journals Series: they are collections of at least ten articles, all centered on a particular subject. With their unique mix of varied contributions from Original Research to Review Articles, Frontiers Research Topics unify the most influential researchers, the latest key findings and historical advances in a hot research area! Find out more on how to host your own Frontiers Research Topic or contribute to one as an author by contacting the Frontiers Editorial Office: frontiersin.org/about/contact

mRNA TRANSLATIONAL CONTROL AS A MECHANISM OF POST-TRANSCRIPTIONAL GENE REGULATION

Topic Editors:
Daniel L. Kiss, Houston Methodist Research Institute, United States
Neva Caliskan, Helmholtz Institute for RNA-based Infection Research (HIRI), Germany
Kiong Ho, University of Tsukuba, Japan
Deepika Vasudevan, University of Pittsburgh, United States
Kristin S. Koutmou, University of Michigan, United States

Citation: Kiss, D. L., Caliskan, N., Ho, K., Vasudevan, D., Koutmou, K. S., eds. (2022). mRNA Translational Control as a Mechanism of Post-transcriptional Gene Regulation. Lausanne: Frontiers Media SA. doi: 10.3389/978-2-88976-590-4

Table of Contents

frontiers | Frontiers in Molecular Biosciences

EDITORIAL
published: 23 June 2022
doi: 10.3389/fmolb.2022.947516

Editorial: mRNA Translational Control as a Mechanism of Post-transcriptional Gene Regulation

Daniel L. Kiss[1]*, *Deepika Vasudevan*[2], *C. Kiong Ho*[3] and *Neva Caliskan*[4]*

[1]Center for RNA Therapeutics, Weill Cornell Medical College, Houston Methodist Research Institute, Houston, TX, United States, [2]Department of Cell Biology BST, University of Pittsburgh, Pittsburgh, PA, United States, [3]Faculty of Medicine, University of Tsukuba, Tsukuba, Japan, [4]Medical Faculty, Helmholtz Institute for RNA-based Infection Research (HIRI-HZI), University of Würzburg, Würzburg, Germany

Keywords: mRNA translational control, RNA binding proteins, noncanonical translation factors, ribosome frameshifting, translation initiation factors, ribosome profiling, bacterial translation, untranslated regions (UTRs)

Editorial on the Research Topic

mRNA Translational Control as a Mechanism of Post-transcriptional Gene Regulation

INTRODUCTION

Precise control of gene expression is central for every organism. Much research has been done to uncover the network of regulatory pathways controlling the RNA life cycle and how RNA levels change rapidly to modulate the amount of proteins made by the cells. In principle, every point in the life cycle of an mRNA from its transcription, modification, splicing, processing, trafficking, translation, and decay is monitored by one or more RNA surveillance mechanisms. Together, these regulatory mechanisms maintain normal cellular activity and provide timely responses to adapt to changing environments such as during starvation, differentiation, or infections. This special section presents a collection of recent work in prokaryotic and eukaryotic translational control and the role of RNA elements and modifications in regulation of translation.

The contributions to this special section fell into three distinct groups. The first of these groups include three reviews examining the contributions of translational control to stem cells, a second review that helps us better understand the translational impact of RNA binding proteins (RBPs) and microRNAs, and a third review examining ribosome frameshifting. In the first paper, Wang and Amoyel describe recent advances that demonstrate the outsized role of mRNA translational regulation in stem cell proliferation and differentiation. They survey how bulk and mRNA selective translation events dictate stem cell fate and describe translation regulatory mechanisms that affect stem cell specification across many types of stem cells. This is critical as most multicellular life originates from a single totipotent cell that divides and differentiates, giving rise to an entire organism. Next, Jungers and Djuranovic review the literature describing how RBPs and miRNAs act synergistically or antagonistically to regulate mRNAs via 3′UTR sequences. We've known that interactions between trans-acting regulatory factors on individual mRNAs create an elaborate landscape of effects that regulate genes post-transcriptionally. They close by highlighting the implications of these regulatory mechanisms on human disease, particularly cancers. Lastly, many viral, bacterial, and some eukaryotic RNAs contain sequence elements that shift ribosomes to alternative reading frames during translation. Riegger and Caliskan discuss the current knowledge regarding programmed ribosomal frameshifting. They summarize the role(s) of RNA secondary structures and highlight how *trans*-acting RNA modulators can dynamically adjust the timing and

OPEN ACCESS

Edited and reviewed by:
Gian Gaetano Tartaglia,
Italian Institute of Technology (IIT), Italy

***Correspondence:**
Daniel L. Kiss
dlkiss@houstonmethodist.org
Neva Caliskan
neva.caliskan@helmholtz-hiri.de

Specialty section:
This article was submitted to RNA Networks and Biology, a section of the journal Frontiers in Molecular Biosciences

Received: *18 May 2022*
Accepted: *08 June 2022*
Published: *23 June 2022*

Citation:
Kiss DL, Vasudevan D, Ho CK and Caliskan N (2022) Editorial: mRNA Translational Control as a Mechanism of Post-transcriptional Gene Regulation. Front. Mol. Biosci. 9:947516. doi: 10.3389/fmolb.2022.947516

efficiency of frameshifting events. Ribosome frameshifting provides new targets for disrupting viral translation strategies and presents opportunities to impact infections and immune responses.

In the second group of papers, three groups use prokaryotic systems to ask fundamental questions about translational control. High-resolution structures of active ribosomes are critical for understanding translational regulation. Belinite et al. successfully purified stable 30S small ribosome subunits from *S. aureus* and solved their structures complexed with RNA by cryo-electron microscopy in the presence and absence of spermidine. Remarkably, spermidine stabilizes helix 44 to form the active conformation. This study provides important insights into how ribosome structure could be regulated during translation. Next, we've known that certain archaeal transcripts, including tRNA, rRNA, and sRNA, undergo post-transcriptional maturation, often involving a circular RNA intermediate. However, the mechanism underpinning selective circularization occurs was unknown. Liu et al. demonstrated that ATP-dependent RNA ligase (Rnl) generates circular C/D Box sRNAs and validated the structural features required for circularization. Interestingly, their work suggests that, either directly or indirectly via C/D Box sRNA circularization, Rnl also contributes to rRNA processing near the helix 98 region of 23S rRNA. Finally, the anti-Shine-Dalgarno (anti-SD) sequence is a highly conserved rRNA sequence that hybridizes with the Shine-Dalgarno (SD) sequence upstream of the start codon to promote translation initiation. However, species in the phylum Bacteroidota have very few mRNAs with consensus SD sequences. McNutt et al. used comprehensive mutation analysis of anti-SD sequence in *E.coli* and *F. johnsoniae* to gain new insights into the mechanism of SD-independent translation. Together, these three works leverage studies investigating ribosome structure, small RNA processing, and the impact interactions of ribosomal and mRNA sequences to expand our knowledge of prokaryotic translational regulation.

The final group of research articles detail new findings that describe the contributions of RNA modifications and sequences to translational control. Douka et al. describe Ribo-seq approaches tailored for human and Drosophila melanogaster cell lines. They illustrate that even subtle changes in experimental conditions can alter overall quality of ribosome footprinting. Furthermore, the authors show the varying impact of antibiotic pretreatment on different cell types. Overall, this study highlights key attributes that require careful optimization in each new system to obtain high-quality ribosome profiling data. Second, using budding yeast mutants and ribosome profiling Stanciu et al. show that eIF3's (eukaryotic initiation factor 3) contributions were often mediated by sequences in 5′ untranslated regions. eIF3 is a key initiation factor that functions throughout translation initiation including during mRNA recruitment and has been linked to the selective translation of specific classes of mRNAs. Third, IF4B binds and recruits mRNA to preinitiation complexes. Liu et al. disrupted yeast eukaryotic initiation factor 4B (eIF4B) and 40S binding motifs to evaluate how these factors impact adaptation and survival in diverse cellular environments. The authors show that N-terminal domain deletions of eIF4B leads to decreased translation rates, especially on mRNAs with long and structured 5′ UTRs. This work suggests that the NTD of eIF4B affects the translation of a subset of mRNAs, thereby impacting cellular stress responses. Finally, RNA modifications such as N6 methyl-adenosine (m6A) influence post-transcriptional gene regulation. IGF2BP2 (insulin-like growth factor 2 mRNA-binding protein 2) is an RNA binding protein and m6A reader known to regulate the localization, translation, and stability of mRNAs. In their work, Han et al. demonstrate that IGF2BP2 regulates the translation of ATG12 (autophagy-related 12) mRNA indirectly through the MALAT1 lncRNA.

SUMMARY

Overall, these articles highlight the impact of RNA-based regulatory events during translation. These articles also shed light on the interplay of protein factors and mRNA elements that fine tune the dynamics of translation. These aspects will be relevant to understanding the complexity of the gene expression networks and their impact on cellular response in cell proliferation, cell fate and immune regulation.

AUTHOR CONTRIBUTIONS

All authors listed have made a substantial, direct, and intellectual contribution by writing and editing the manuscript and approved it for publication.

FUNDING

DK received funding from National Institutes of Health Grant Nr. R35GM137819. DV received funding from National Institutes of Health Grant Nr. R00EY029013. CKH received funding from National Science Foundation 1050984 and Japan Society for the Promotion of Science Grants-in-Aid for Scientific Research KAKENHI 21K06984. NC received funding from the European Research Council (ERC) Grant Nr. 948636 and Helmholtz Association.

ACKNOWLEDGMENTS

The editors would like to thank all the authors and reviewers that made this special issue a success. We also thank Dr. Kristin Koutmou for her work in helping to edit several manuscripts.

Conflict of Interest: The authors declare that the research was conducted in the absence of any commercial or financial relationships that could be construed as a potential conflict of interest.

Publisher's Note: All claims expressed in this article are solely those of the authors and do not necessarily represent those of their affiliated organizations, or those of the publisher, the editors and the reviewers. Any product that may be evaluated in this article, or claim that may be made by its manufacturer, is not guaranteed or endorsed by the publisher.

frontiers in Molecular Biosciences

ORIGINAL RESEARCH
published: 18 November 2021
doi: 10.3389/fmolb.2021.738752

Stabilization of Ribosomal RNA of the Small Subunit by Spermidine in *Staphylococcus aureus*

Margarita Belinite[1,2,3†‡], Iskander Khusainov[1,4†‡], Heddy Soufari[3], Stefano Marzi[2], Pascale Romby[2], Marat Yusupov[1,4] and Yaser Hashem[2,3]**

[1]Institut de Génétique et de Biologie Moléculaire et Cellulaire (IGBMC), INSERM U964, CNRS UMR7104, Université de Strasbourg, Illkirch, France, [2]Architecture et Réactivité de l'ARN, CNRS 9002, Université de Strasbourg, Strasbourg, France, [3]Institut Européen de Chimie et Biologie (IECB), ARNA U1212, Université de Bordeaux, Pessac, France, [4]Institute of Fundamental Medicine and Biology, Kazan Federal University, Kazan, Russia

Cryo-electron microscopy is now used as a method of choice in structural biology for studying protein synthesis, a process mediated by the ribosome machinery. In order to achieve high-resolution structures using this approach, one needs to obtain homogeneous and stable samples, which requires optimization of ribosome purification in a species-dependent manner. This is especially critical for the bacterial small ribosomal subunit that tends to be unstable in the absence of ligands. Here, we report a protocol for purification of stable 30 S from the Gram-positive bacterium *Staphylococcus aureus* and its cryo-EM structures: in presence of spermidine at a resolution ranging between 3.4 and 3.6 Å and in its absence at 5.3 Å. Using biochemical characterization and cryo-EM, we demonstrate the importance of spermidine for stabilization of the 30 S *via* preserving favorable conformation of the helix 44.

Keywords: ribosome 70 S, ribosomal RNA, *Staphylococcus aureus*, translation, RNA stability

OPEN ACCESS

Edited by:
Kristin S. Koutmou, University of Michigan, United States

Reviewed by:
Emmanuelle Schmitt, UMR7654 Bases moleculaires et regulation de la biosynthese proteique, France
Sunny Sharma, Rutgers, The State University of New Jersey, United States

****Correspondence:***
Marat Yusupov
marat@igbmc.fr
Yaser Hashem
yaser.hashem@inserm.fr

†Present address:
Margarita Belinite, Department of Biochemistry and Biophysics, University of Rochester Medical Center, Rochester, NY, United States
Iskander Khusainov, Department of Molecular Sociology, Max Planck Institute of Biophysics, Frankfurt am Main, Germany

‡These authors have contributed equally to this work and share first authorship

Specialty section:
This article was submitted to Protein and RNA Networks, a section of the journal Frontiers in Molecular Biosciences

Received: *09 July 2021*
Accepted: *07 October 2021*
Published: *18 November 2021*

Citation:
Belinite M, Khusainov I, Soufari H, Marzi S, Romby P, Yusupov M and Hashem Y (2021) Stabilization of Ribosomal RNA of the Small Subunit by Spermidine in Staphylococcus aureus. *Front. Mol. Biosci. 8:738752. doi: 10.3389/fmolb.2021.738752*

INTRODUCTION

Protein synthesis is a tightly regulated biological process performed by the ribosome. High-resolution structures of the ribosome and its functional complexes led to major advances in understanding the functioning and the dynamics of this complex machinery (Javed and Orlova, 2019). The bacterial ribosome (70 S) can be divided into the large (50 S) and the small (30 S) subunits. The latter, which contains the decoding center, consists of 21 proteins (r-proteins) and of the 16 S RNA (rRNA). This flexible subunit faces several conformational changes during translation (Frank et al., 2007; Agirrezabala et al., 2008; Zhang et al., 2009) and its stability is often influenced by ions conditions, making the structural analysis challenging.

The 30 S ribosomal subunit is the main platform, where mRNA and initiator P-tRNA are positioned during translation initiation, as well as accommodation of incoming A-tRNA during the elongation stage. During translation initiation, it interacts with the three Initiation Factors (IFs) and undergoes several rearrangements of the head (swiveling/nodding), which affect the mRNA channel (Hussain et al., 2016). Furthermore, each cycle of tRNA translocation through the ribosome is also accompanied by the reversible rotation of the whole 30 S subunit and swiveling of its head (Ogle et al., 2001; Yusupova et al., 2001; Selmer et al., 2006a; Berk et al., 2006; Pisarev et al., 2008; Demeshkina et al., 2010; Jenner et al., 2010; Guo and Noller, 2012; Pulk and Cate, 2013). The body of the 30 S subunit seems to be less affected by these conformational changes (Hussain et al., 2016). Helix 44 (h44) of the 16S rRNA is among the most crucial regions of the 30 S body because it is

involved in several bridges with the 50 S (Yusupov et al., 2001; Schuwirth et al., 2005; Selmer et al., 2006b), it interacts with both IF1 and IF3, and is part of the decoding center of the ribosome forming the P-site and being involved in the accommodation of tRNA at the A-site (Demeshkina et al., 2012; Rozov et al., 2015; Rozov et al., 2016; Rozov et al., 2019). Its structure needs to be stable enough to be maintained during translation elongation and sufficiently flexible to allow mRNA and factors binding during translation initiation. For these reasons, several proteins (e.g., Era, RbfA, RimM), which are involved in the ribosome biogenesis, perform quality control function of the h44 as one of the last checkpoints of the 16S rRNA maturation (Dammel and Noller, 1995; Bylund et al., 1998; Datta et al., 2007; Guo et al., 2013; Razi et al., 2019; Schedlbauer et al., 2020). Altogether, for efficient participation of the 30 S in protein synthesis, flexibility and structural integrity are required at the same time, and especially proper folding of h44 is essential.

Recent study has shown the importance of magnesium ions on structure stability of the 30 S from *E. coli* (Jahagirdar et al., 2020). Moreover, numerous studies have led to the conclusion that polyamines, which are present in all types of cells, can stabilize the structure of the ribosome (Zillig et al., 1959; Cohen and Lichtenstein, 1960; Stevens, 1969; Weiss and Morris, 1970; Cohen, 1971; Hardy and Turnock, 1971; Turnock and Birch, 1973). It was shown that *E. coli* cells grown in the absence of polyamines contained a large portion of defective 30 S particles (Echandi and Algranati, 1975). Furthermore, polyamines stimulate the assembly of 30 S ribosomal subunits and thereby increase general protein synthesis rate 1.5- to 2.0-fold (Echandi and Algranati, 1975; Igarashi et al., 1980; Igarashi and Kashiwagi, 2018).

In this study, we solved cryo-EM structures of *S. aureus* 30 S subunit bound to *S. aureus*-specific *spa* mRNA that encodes a virulence factor protein A. We show how the addition of spermidine helps to improve the resolution from 5.3 Å to 3.4 Å (for the SSU body) and 3.6 Å (for the SSU head). The main effect of spermidine was on h44 that presents its active conformation only when the polyamine was added. Under these conditions, the 30 S adopts a closed conformation where the decoding channel is properly formed, and the mRNA is naturally adapted inside the channel. Our work highlights the importance of polyamines in determining the structure of the 30 S subunits by cryo-EM and could be even relevant for functional studies. The protocol for 30 S purification can be easily applied for the preparation of various functional complexes of *S. aureus*.

MATERIALS AND METHODS

70 S Ribosome Purification

The protocol described in the article Khusainov et al. (2016b) was used for 70 S purification (Khusainov et al., 2016a). *S. aureus* cells (RN6390 strain) were grown at 37°C (180 rpm) in brain-heart infusion broth (BHI) and harvested in the early logarithmic phase (1 OD^{600} / ml). Then cells were washed in buffer A (20 mM Hepes-KOH pH 7.5, 100 mM NH_4Cl, 21 mM $Mg(OAc)_2$, 1 mM DTT), pelleted at 4,750 g and kept frozen at −80°C. Typically, 5 g of cells were obtained from 2 L of culture. Lysis of the cells (5 g) was performed in buffer A in the presence of 1 mM EDTA, lysostaphin (Sigma-Aldrich), DNase I (Roche), and protease inhibitor cocktail (Roche) at 37°C for 45 min followed by centrifugation at 30,000 g for 90 min.

Ribosomes were precipitated through two stages by adding to the supernatant PEG 20,000 (Hampton Research) with final concentrations of 2.8 and 4.2 % w/v. Solutions were centrifuged at 20,000 g for 5 and 10 min, respectively. The pellet was then resuspended in 35 ml of buffer A and layered to 25 ml cushion of buffer B (10 mM Hepes-KOH pH 7.5, 500 mM KCl, 25 mM $Mg(OAc)_2$, 1.1 M Sucrose, 0.5 mM EDTA, 1 mM DTT), followed by centrifugation at 158,420 g for 15 h using a Beckman Type 45 Ti rotor.

The ribosomal pellet from sucrose cushion was resuspended in buffer E (10 mM Hepes-KOH pH 7.5, 100 mM KCl, 10.5 mM $Mg(OAc)_2$, 0.5 mM EDTA, 1 mM DTT), and loaded on 7–30 % w/v sucrose gradients at a concentration up to 7 mg/ml and centrifuged at 38,694 g for 15.5 h using a Beckman SW28 rotor. Magnesium was adjusted to 25 mM in the pooled fractions. Ribosomes were precipitated by adding PEG 20,000 to a final concentration 4.5 % w/v and centrifuged at 20,000 g for 12 min. The pellet was gently resuspended in buffer G (10 mM Hepes-KOH pH 7.5, 30 mM NH_4Cl, 10 mM $Mg(OAc)_2$, 1 mM DTT), flash-frozen in liquid nitrogen and stored at −80°C in small aliquots.

Effect of Ionic Conditions on the 30 S Ribosomal Subunit Purification

The small ribosomal subunit was isolated from the intact 70 S ribosome under various conditions described below. First, the 70 S ribosome was dialysed in dissociation buffer (1 mM $Mg(OAc)_2$, 200 mM $NaCl_2$ or 200 mM KCl, 10 mM Hepes-KOH pH7.5, 1 mM DTT) for 4 h at 4°C. Then, the subunits were separated with 0–30 % w/v sucrose gradients followed by centrifugation at 35,606 g for 17 h at 4°C using Beckman SW28 rotor. Fractionation of the sucrose gradient is shown on **Supplementary Figure S1A,B**. Fractions from the sucrose gradient in 200 mM KCl were pooled and loaded again on 5–20 % w/v sucrose gradients (35,606 g for 17 h, Beckman SW28 rotor, **Supplementary Figure S1C**). The search for optimal salt conditions for 30 S purification was carried out in 100 and 200 mM KCl or NH_4Cl (1 mM $Mg(OAc)_2$, 10 mM Hepes-KOH pH7.5, 1 mM DTT) and 400 mM NaCl (6 mM or 10 mM $Mg(OAc)_2$, 10 mM Hepes-KOH pH7.5, 1 mM DTT). Dialysis for 4 h at 4°C was followed by subunits separation step with 0–30 % w/v sucrose gradient and centrifuged at 44,556 g for 15 h using Beckman SW41 rotor. Selected fractions were pooled, concentrated with Amicon 0.5 ml MWCO 100K, and analyzed on a 15 % SDS-PAGE (**Supplementary Figures S2A,B**). Re-screening for optimal conditions was performed in 30 and 50 mM NH_4Cl (1 mM $Mg(OAc)_2$, 10 mM Hepes-KOH pH7.5, 1 mM DTT). The 70S ribosome was divided into subunits with 0–30 % w/v sucrose gradient followed by centrifugation at 46,932 g for 14 h 14 min using Beckman SW41 rotor. The obtained sucrose

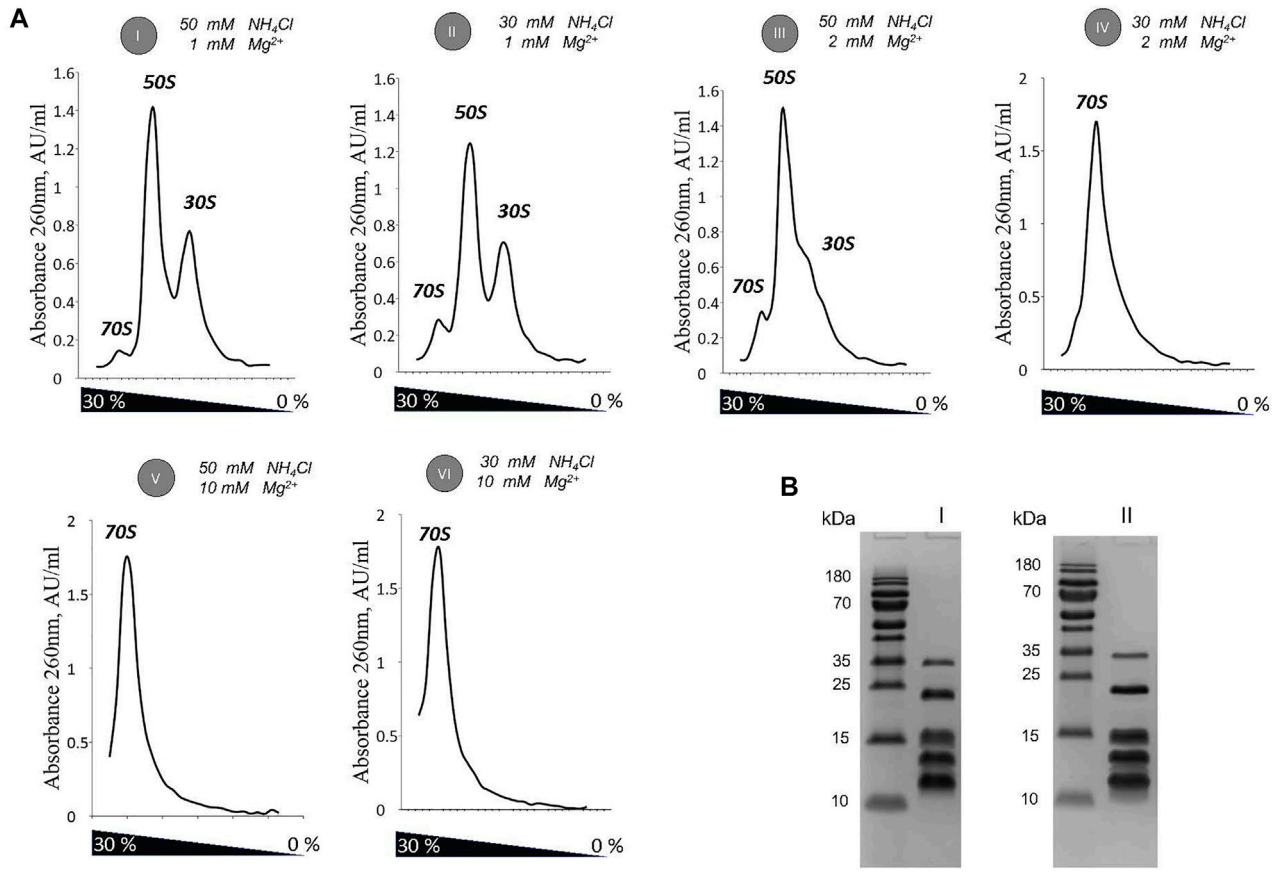

FIGURE 1 | Optimization of 30 S subunit purification by titration of Mg^{2+} / NH_4Cl ratio. **(A)** Sucrose gradients profiles of the 70 S sample exposed to mild dissociation conditions (I–IV), and association conditions (V-VI). **(B)** SDS-PAGE of 30 S purified at conditions determined as optimal (1 mM Mg / 30 mM NH_4Cl) in absence (I) and presence (II) of spermidine.

gradient profiles and respective SDS-PAGE profiles of pooled 30 S peak samples are shown in **Figures 1A,B**.

30 S Ribosomal Subunits Purification

For structural analysis of the 30 S subunit, we first purified 70 S particles as described above, with tiny modification. At the last step, the 70 S ribosomes were dissolved in buffer G' (10 mM Hepes-KOH pH 7.5, 30 mM NH_4Cl, 1 mM $Mg(OAc)_2$, 1 mM DTT) omitting the freezing step ribosomes were directly loaded on 0–30 % w/v sucrose gradients equilibrated in buffer G' and centrifuged at 61,739 g for 14.5 h using a Beckman SW28 rotor. The concentration of $Mg(OAc)_2$ was adjusted to 10 mM in the selected pooled fractions. In addition, the sample was supplemented with 2.5 mM of spermidine and concentrated using 100K Amicon ultra centrifugal filters (Merck Millipore). Aliquots were flash-frozen in liquid nitrogen and stored at −80°C.

mRNA Purification

S. aureus spa mRNA, encoding protein A, has UUG start codon and a strong Shine and Dalgarno (SD) sequence AGGGG. The sequence of the full-length *spa* mRNA used in the study is shown in **Supplementary Figure S2C**. The RNA was transcribed from a plasmid as previously described in (Benito et al., 2000; Huntzinger et al., 2005). In brief, the plasmid was linearized by Bam*HI* during 2 h at 37°C, and the mRNA was *in vitro* transcribed during 3 h at 37°C with T7 RNA polymerase. The mRNA was separated on a 6 % polyacrylamide midi-sized gel and eluted in a solution containing 16 % phenol pH 4.5–5 with 50 mM ammonium acetate and 1 mM EDTA.

In vitro Reconstruction of 30 S With *spa* mRNA

The 30 S ribosomal subunits were incubated with *spa* mRNA during 15 min at 37°C in the buffer containing 10 mM Hepes-KOH pH 7.5, 30 mM NH_4Cl, 10 mM $Mg(OAc)_2$ in the presence or absence of 2.5 mM spermidine.

Cryo-EM Data Acquisition

4 μL of samples (containing the 30 S bound to mRNA) at 90 nM was applied on Quantifoil R2/2300-mesh holey carbon grids covered with carbon in a temperature- and humidity-controlled Vitrobot Mark IV (T = 4°C, humidity 100%, blotting time 2 s,

blotting force 5, waiting time 30 s). The data acquisitions were performed on a Talos Arctica instrument (FEI Company) at 200 kV using the EPU software on the Falcon three direct detector device (FEI Company). Data were collected at a nominal under focus of −0.5 to −2.7 µm at a magnification of 120,000 X yielding a pixel size of 1.24 Å.

Electron Microscopy Image Processing

Drift and gain correction, and dose weighting were performed using MotionCor2 (Zheng et al., 2017). A dose weighted average image of the whole stack was used to determine the contrast transfer function with the software Gctf (Zhang, 2016). The following process has been achieved using RELION 3.0 (Zivanov et al., 2018). Particles were picked using a Laplacian of Gaussian function (min diameter 180 Å, max diameter 290 Å). For the 30S-mRNA complex without polyamine, after 2D classification, 256,000 particles were extracted with a box size of 248 pixels and binned four folds for 3D classification into five classes (final = 5.3 Å resolution). For the 30−S-mRNA complex with spermidine, after 2D classification, 529,602 particles were extracted with a box size of 270 pixels and binned three-fold for 3D classification into six classes. Three classes depicting high-resolution features have been selected for refinement. The obtained structure has been refined up to 3.6 Å resolution. Individual focused refinement of the head and the body of the small ribosomal subunit led to the resolution 3.6 Å and 3.4 Å respectively (**Supplementary Figures S3A,B**). Local resolution estimation was performed in RELION 3.0 using RELION implementation and visualized in Chimera using Surface color option (**Supplementary Figure S3C**).

Structure Building and Model Refinement

As the initial model, we used 30−S extracted from the *S. aureus* vacant 70S ribosome (PBD 5LI0 [https://doi.org/10.2210/pdb5LI0/pdb]). The initial coarse fitting was performed using the NAMDinator web service (Kidmose et al., 2019), which implements the algorithms of molecular dynamics flexible fitting (MDFF) (Trabuco et al., 2009). The default parameters that were used for flexible fitting (start temperature = 298 K; G-force scaling factor = 0.3; minimization steps = 2000; simulation steps = 20,000). Then the real-space refinement was performed in PHENIX (Afonine et al., 2018) (starting temperature = 800 K; cool rate = 100 K). Ribosomal RNA was corrected in ERRASER web service (Chou et al., 2013), which uses enumerative real-space refinement assisted by electron density under Rosetta protocol. Obtained model was corrected manually in Coot (**Supplementary Figure S5**); (Emsley and Cowtan, 2004). The model validation was done in MolProbity web service (Chen et al., 2010). Figures featuring cryo-EM densities as well as atomic models were visualized with UCSF Chimera (Pettersen et al., 2004) and ChimeraX (Goddard et al., 2018). The coordinates of the head and the body parts were rigid body fitted into the 30S-mRNA with spermidine density map to build the full 30 S model followed by manual curation in coot.

RESULTS

Optimization of Salt Conditions for the 30 S Purification

To analyze the effect of ionic conditions on stability of the 30 S subunit, we performed sucrose gradient sedimentation assays of the 70 S ribosome equilibrated in $H_{10}K_{200}M_1$ (10 mM Hepes-KOH pH 7.5 (at 25°C), 200 mM KCl, 1 mM $Mg(OAc)_2$) or $H_{10}Na_{200}M_1$ (10 mM Hepes-KOH pH 7.5 (at 25°C), 200 mM NaCl, 1 mM $Mg(OAc)_2$) buffers. The ribosomes sedimented in $H_{10}K_{200}M_1$ buffer dissociated into 50 S and 30 S subunits (**Supplementary Figure S1A**). Conversely, in presence of 200 mM NaCl, the dissociation of the 70 S ribosomes into the two subunits was not observed (**Supplementary Figure S1A**). However, the shift of the peak towards light fractions of the gradient and the peak asymmetry suggested the loss of structural integrity of these subunits (**Supplementary Figure S1B**). To further monitor the integrity of the dissociated ribosomal subunits, the 50 S and 30 S peaks were loaded onto sucrose gradients equilibrated in a buffer containing 200 mM KCl. A bifurcation of the 30 S peak was detected with the appearance of particles with a lower molecular weight than 30 S (**Supplementary Figure S1C**, right panel) suggesting the inability of the small subunit to withstand 200 mM KCl for a prolonged period of time.

Therefore, we repeated experiments with amended ionic conditions using 100 and 200 mM of NH_4Cl or KCl, respectively at constant 1 mM magnesium acetate. Other conditions included 400 mM NaCl with either six or 10 mM magnesium acetate. For each experiment, the content of the ribosomal proteins within the 30 S peak was analyzed using SDS-PAGE analysis. Despite similarities in the sucrose gradient profiles (**Supplementary Figure S1A**), higher salt concentrations, especially with 200 mM KCl or 400 mM NaCl, led to the loss of several ribosomal proteins (**Supplementary Figure S1B**). Taken together, all further experiments were conducted using NH_4Cl, which has the least dissociating effect on the binding of several ribosomal proteins.

After performing a fine analysis of Mg/NH_4Cl balance effect on ribosome dissociation, we selected 1 mM Mg^{2+} in combination with 30 mM NH_4Cl to isolate 30 S from 70S for further cryo-EM analysis (**Figures 1A,B**). These conditions provided an efficient dissociation of the 70 S ribosome into subunits and concomitantly had their mildest effect on the loss of ribosomal proteins.

Spermidine Effect on the Helix 44 and mRNA Positioning

Using optimized salt concentrations for 30 S purification, we solved the cryo-EM structure of the 30 S in complex with *S. aureus spa* mRNA at a resolution of 3.6 Å. The complex was formed in $H_{10}NH_{30}M_{10}$ (10mM Hepes-KOH pH7.5 (at 25°C), 30mM NH_4Cl, 10 mM $Mg(OAc)_2$ and 1mM DTT). Initially, two different datasets were collected in presence (dataset 2) and in absence (dataset 1) of spermidine.

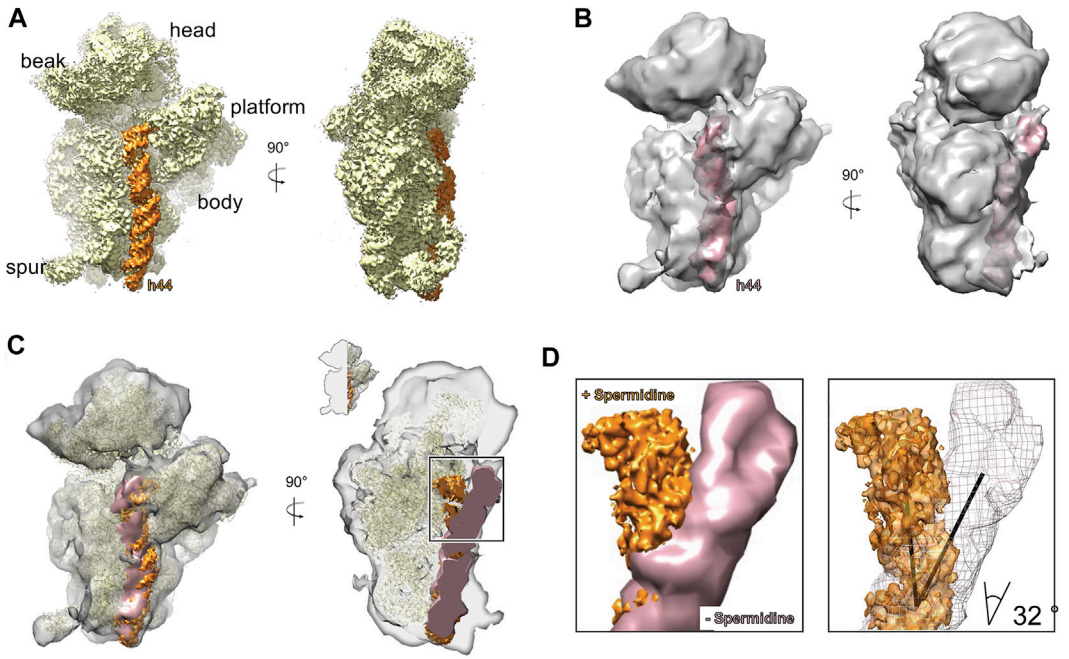

FIGURE 2 | Addition of spermidine stabilizes helix 44 of the 30 S. A. An overview of the structure of 30 S subunit prepared with addition of 2.5 mM spermidine **(A)** and without spermidine **(B)**. The h44 is highlighted in orange and pink respectively. **(C)** An overlay of the structures showing that without spermidine, h44 is destabilized and bent away from the head. For the A-site view (right) structures were clipped as indicated in the inset. **(D)** A close-up view on h44 conformation in 30S with addition of spermidine (orange) and without it (pink/mesh). The calculated angle of the tilt is 32°.

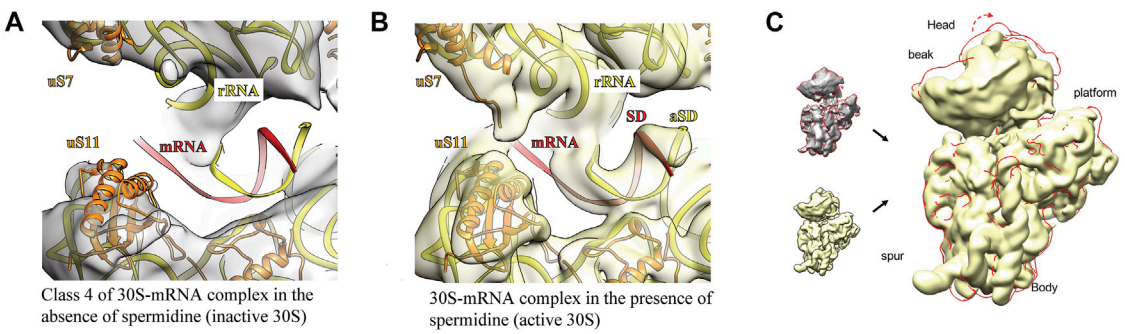

FIGURE 3 | Addition of spermidine helps to close the mRNA channel, allowing mRNA to fully accommodate in it. The ribosomal RNA is highlighted in yellow, ribosomal proteins–in orange and messenger RNA–in red. For the panel **(A)** the same atomic model was used as for panel **(B)** with additional processing in NAMDinator and refitting head and body parts separately. Panel **(C)** represents overlay of the 30 S-mRNA structures in the absence (grey + red contour) and the presence of spermidine (yellow). The 30 S head adopts open conformation (red contour, red arrow) in the absence of spermidine.

In silico sorting the complex lacking spermidine was divided into five classes (**Supplementary Figure S3**). In classes 2, 3, and 4, the upper part of h44 near the decoding center (nucleotides 1,414–1,431 and 1,490–1,508) was tilted by about 32°, whereas the lower part of h44 (1,430–1,489) was only partially visible (**Figures 2B–D**). In addition, in classes 1, 2, and 3, only partial densities of uS2 and bS6 proteins were detected (**Supplementary Figure S4**).

In the presence of spermidine, h44 acquired more stable conformation (**Figure 2A**). It is also worth noting that all small subunit ribosomal proteins except bS21 were present in the structures. Indeed, the density of bS21 protein was not identified due to the positioning of *spa* mRNA in the region where this protein was previously determined (Korostelev et al., 2007; Khusainov et al., 2017). In addition, in both datasets, a high concentration of Mg^{2+} was used for complex formation, which allows us to conclude that polyamines and magnesium ions at these concentrations have different effects on obtained structures.

Open head conformation was observed in all 3D classes obtained from polyamine-deficient 30 S particles; however, mRNA was barely discernible only in class 4 (**Figure 3A**).

When spermidine was added, the mRNA channel was closed by rotation of the 30 S head, allowing *spa* mRNA to fully accommodate in the channel (**Figures 3B,C**) similarly to the 70S•mRNA•fMet-tRNA^{fMet} complex (Golubev et al., 2020). The well-defined density found in the Shine-Dalgarno-anti-Shine-Dalgarno (SD:aSD) region allowed us to fairly accurately build the 30S-mRNA model in this region.

DISCUSSION

In this work, we describe the protocol for obtaining the structure of an intact and homogenous 30 S ribosomal subunit from *Staphylococcus aureus*. We demonstrate a strong dependency of 30 S stability upon ionic conditions during purification. This effect is observed in species-dependent manner. *S. aureus* 30 S showed the inability to withstand 200 mM NaCl concentration and an increased sensitivity to KCl in the same range of concentration (**Supplementary Figures S1A–C**). This is different to *Thermus thermophilus or Escherichia coli* ribosomes that can maintain their structure under similar ionic conditions, even in combination with reverse phase chromatography performed in up to 1.5 M ammonium sulfate concentration (Kirillov et al., 1978; Trakhanov et al., 1987; Clemons et al., 2001). Interestingly, the early studies of the ribosome from *Bacillus subtilis* also suggest an increased stability in lower concentrations of salt (Fahnestock, 1977). This correlates with our findings and suggests that ribosomes from Gram-positive bacteria have evolved different properties (**Figure 1A**).

The biochemical characterization of the 30 S ribosomal subunit revealed favourable ionic conditions to avoid 30 S particle distortions during purification [e.g., changes in sedimentation coefficient (**Supplementary Figure S1**) or loss of ribosomal proteins (**Supplementary Figure S2B**)]. Further, using cryo-EM we showed that even in optimized salts concentration 30S particles show structural disintegration that can be avoided by addition of spermidine. We have shown that the presence of spermidine is crucial for maintaining the correct folding of the helix (h44) of 16S rRNA near the decoding center (**Figure 2**). Spermidine is a polyamine known to stabilize the folding of RNA molecules including rRNA (Cohen and Lichtenstein, 1960; Weiss and Morris, 1970; Cohen, 1971; Hardy and Turnock, 1971; Turnock and Birch, 1973). The upper part of h44 was found as one of the preferred sites for the binding of polyamines (Amarantos et al., 2002) and was particularly observed in the 70S crystal structure from *E. coli* (Noeske et al., 2015). Although polyamines like spermine and putrescine were used in these studies, the binding sites are believed to be identical for spermidine too. Additionally, nucleotides G931, A1400, C1411 of the 16S rRNA were shown to be polyamine-binding sites (Amarantos et al., 2002). Therefore, it is reasonable to suggest that polyamine molecules bound to those positions may control changes in the head conformation.

Interestingly, polyamines were shown to positively affect protein synthesis depending on the uracil content of mRNAs (Igarashi et al., 1975), and spermidine enhanced translation of those mRNAs carrying the less effective UUG initiation codon (Igarashi and Kashiwagi, 2018). These data suggested that at least some mRNAs require the presence of spermidine *in vitro*. Noteworthy, the *spa* mRNA that we used in this study is a *S. aureus* specific mRNA with UUG start-codon. It is unclear whether spermidine can also facilitate the SD:aSD positioning within the mRNA exit tunnel. Even though our structure in the presence of spermidine has a stable SD:aSD interaction, it may be caused by the general effect on ribosome stabilization rather than direct association of polyamine molecules in this region. In *S. aureus spa* mRNA, Shine-Dalgarno sequence is located in the unstructured region that enables its direct binding to the ribosome in the absence of polyamines (Khusainov et al., 2016b). However, many other mRNAs in *S. aureus* have their SD hidden in the step loop. Speculatively spermidine may facilitate the association of such mRNAs with the ribosome through stabilization of SD:aSD interaction.

Spermidine and Mg^{2+} usually bind similarly to the double-stranded regions of rRNA (Igarashi et al., 1982). Here, we have increased the concentration of Mg^{2+} ions from 1 to 10 mM immediately after the dissociation of the subunits and kept it for the complex formation with *spa* mRNA. However, only the addition of spermidine was able to attain the formation of a functional mRNA-30S binary complex. This is well correlated with previous studies showing that polyamines cannot be compensated by Mg^{2+}, and conversely replacement of Mg^{2+} by spermidine leads to a loss of ability to support peptide synthesis (Weiss and Morris, 1970; Teraoka and Tanaka, 1973). Thus, our study provides additional evidence that spermidine and Mg^{2+} are not equivalent in their ability to stabilize the structure of *S. aureus* ribosome.

It was described that helix 44 acquires unfavorable conformation as the result of the absence of several ribosomal proteins located at the interface of the 30 S subunit like uS5, uS12, and bS20 (**Supplementary Figure S6**). However, these ribosomal proteins are present in our structure solved with or without spermidine. It is also plausible that h44 was deformed as an indirect consequence resulting from the flexibility of uS2, bS6, uS7, and uS11 in the absence of spermidine, or also upon exposing of the 30 S interface to the solvent. Similar to our recent observation, destabilization of some regions of 23S rRNA takes place at the interface of the individual 50 S subunit from *S. aureus* in the absence of 30 S counterpart (Khusainov et al., 2020). Conformational changes in important functional motifs on the platform and at the decoding center can also be caused by maturation factors such as RimM, RbfA, and Era (Dammel and Noller, 1995; Bylund et al., 1998; Guo et al., 2013; Razi et al., 2019; Schedlbauer et al., 2020). The obtained structures showed that the binding sites of the maturation factors to the small ribosomal subunit are located in the upper part of h44 (Datta et al., 2007). This may indicate the need for stabilization of h44 at later stages. It remains to be studied whether such conserved maturation factors are also required at a later step of the 30 S ribosomal subunit assembly in *S. aureus*. Interestingly, deletion of *era* in *S. aureus* caused a strong decrease in 70S formation linked to a defect of 30 S processing (Wood et al., 2019).

In conclusion, our data reveals the requirement to maintain particular ionic conditions and the addition of spermidine during *S. aureus* 30 S ribosomal subunit purification. The described protocol can now be used to solve other functional ribosomal complexes in order to better decipher the differences existed between Gram-positive and Gram-negative bacteria at the initiation step of protein synthesis.

DATA AVAILABILITY STATEMENT

The datasets presented in this study can be found in online repositories. The names of the repository/repositories and accession number(s) can be found below: http://www.wwpdb.org/, 7KWG; http://www.wwpdb.org/, 7BGD; http://www.wwpdb.org/, 7BGE; https://www.ebi.ac.uk/pdbe/emdb/, EMD-23052; https://www.ebi.ac.uk/pdbe/emdb/, EMD-12178; https://www.ebi.ac.uk/pdbe/emdb/, EMD-12179; https://www.ebi.ac.uk/pdbe/emdb/, EMD-12091; https://www.ebi.ac.uk/pdbe/emdb/, EMD-12090.

AUTHOR CONTRIBUTIONS

MY, YH, PR, SM conceived the project: MB and IK optimized ribosome purification conditions, MB purified 70S and 30S ribosomes, *spa* mRNA and performed *in vitro* reconstruction of 30S-mRNA complexes. HS performed the cryo-EM experiments. HS and YH performed image processing. MB built the atomic model under supervision of IK MB, IK, and YH interpreted the structures. MB, IK, PR, SM, MY, and YH wrote and edited the manuscript. YH and MY directed the research.

FUNDING

This work was supported by the Institut National de la santé et de la recherche médicale (Inserm), Centre National de la Recherche Scientifique (CNRS), by the Agence Nationale de la Recherche (ANR, grant ANR-16-CE11-0007-01, RIBOSTAPH, to PR and MY), ANR-14-ACHN-0024–CryoEM80S (to YH) and by Russian Foundation for Basic Research (RFBR, project number is 20-54-15001, to MY). It has also been published under the framework of the LABEX: ANR-10-LABX-0036 NETRNA (to PR and YH) and of ANR-17-EURE-0023, funding from the state managed by the French National Research Agency as part of the investments for the future program.

ACKNOWLEDGMENTS

We thank A. Simonetti for useful discussions and critical advices. We thank Dr Armel Bézault for help in Data acquisition on the Talos Arctica microscope.

SUPPLEMENTARY MATERIAL

The Supplementary Material for this article can be found online at: https://www.frontiersin.org/articles/10.3389/fmolb.2021.738752/full#supplementary-material

REFERENCES

Afonine, P. V., Poon, B. K., Read, R. J., Sobolev, O. V., Terwilliger, T. C., Urzhumtsev, A., et al. (2018). Real-space refinement inPHENIXfor cryo-EM and crystallography. *Acta Cryst. Sect D Struct. Biol.* 74, 531–544. doi:10.1107/s2059798318006551

Agirrezabala, X., Lei, J., Brunelle, J. L., Ortiz-Meoz, R. F., Green, R., and Frank, J. (2008). Visualization of the hybrid state of tRNA binding promoted by spontaneous ratcheting of the ribosome. *Mol. Cel.* 32 (2), 190–197. doi:10.1016/j.molcel.2008.10.001

Amarantos, I., Zarkadis, I. K., and Kalpaxis, D. L. (2002). The identification of spermine binding sites in 16S rRNA allows interpretation of the spermine effect on ribosomal 30S subunit functions. *Nucleic Acids Res.* 30, 2832–2843. doi:10.1093/nar/gkf404

Benito, Y., Kolb, F. A., Romby, P., Lina, G., Etienne, J., and Vandenesch, F. (2000). Probing the structure of RNAIII, the Staphylococcus aureus agr regulatory RNA, and identification of the RNA domain involved in repression of protein A expression. *RNA* 6, 668–679. doi:10.1017/s1355838200992550

Berk, V., Zhang, W., Pai, R. D., and Cate, J. H. D. (2006). Structural basis for mRNA and tRNA positioning on the ribosome. *Proc. Natl. Acad. Sci.* 103 (43), 15830–15834. doi:10.1073/pnas.0607541103

Bylund, G. O., Wipemo, L. C., Lundberg, L. A. C., and Wikström, P. M. (1998). RimM and RbfA Are Essential for Efficient Processing of 16S rRNA in Escherichia coli. *J. Bacteriol.* 180, 73–82. doi:10.1128/jb.180.1.73-82.1998

Chen, V. B., Arendall, W. B., 3rd, Headd, J. J., Keedy, D. A., Immormino, R. M., Kapral, G. J., et al. (2010). MolProbity: all-atom structure validation for macromolecular crystallography. *Acta Crystallogr. D Biol. Cryst.* 66, 12–21. doi:10.1107/s0907444909042073

Chou, F.-C., Sripakdeevong, P., Dibrov, S. M., Hermann, T., and Das, R. (2013). Correcting pervasive errors in RNA crystallography through enumerative structure prediction. *Nat. Methods* 10, 74–76. doi:10.1038/nmeth.2262

Clemons, W. M., Brodersen, D. E., McCutcheon, J. P., May, J. L. C., Carter, A. P., Morgan-Warren, R. J., et al. (2001). Crystal structure of the 30 S ribosomal subunit from Thermus thermophilus: purification, crystallization and structure determination. *J. Mol. Biol.* 310, 827–843. doi:10.1006/jmbi.2001.4778

Cohen, S. S. (1971). *Introduction to the Polyamines*. Englewood cliffs, New Jersey: Prentice-Hall.

Cohen, S. S., and Lichtenstein, J. (1960). Polyamines and ribosome structure. *J. Biol. Chem.* 235, 2112–2116. doi:10.1016/s0021-9258(18)69373-1

Dammel, C. S., and Noller, H. F. (1995). Suppression of a cold-sensitive mutation in 16S rRNA by overexpression of a novel ribosome-binding factor, RbfA. *Genes Dev.* 9, 626–637. doi:10.1101/gad.9.5.626

Datta, P. P., Wilson, D. N., Kawazoe, M., Swami, N. K., Kaminishi, T., Sharma, M. R., et al. (2007). Structural aspects of RbfA action during small ribosomal subunit assembly. *Mol. Cel* 28, 434–445. doi:10.1016/j.molcel.2007.08.026

Demeshkina, N., Jenner, L., Westhof, E., Yusupov, M., and Yusupova, G. (2012). A new understanding of the decoding principle on the ribosome. *Nature* 484, 256–259. doi:10.1038/nature10913

Demeshkina, N., Jenner, L., Yusupova, G., and Yusupov, M. (2010). Interactions of the ribosome with mRNA and tRNA. *Curr. Opin. Struct. Biol.* 20 (3), 325–332. doi:10.1016/j.sbi.2010.03.002

Echandi, G., and Algranati, I. D. (1975). Defective 30S ribosomal particles in a polyamine auxotroph of Escherichia coli. *Biochem. Biophysical Res. Commun.* 67, 1185–1191. doi:10.1016/0006-291x(75)90798-6

Emsley, P., and Cowtan, K. (2004). Coot: model-building tools for molecular graphics. *Acta Crystallogr. D Biol. Cryst.* 60, 2126–2132. doi:10.1107/s0907444904019158

Fahnestock, S. R. (1977). Reconstitution of active 50 S ribosomal subunits from Bacillus licheniformis and Bacillus subtilis. *Arch. Biochem. Biophys.* 182, 497–505. doi:10.1016/0003-9861(77)90530-6

Frank, J., Gao, H., Sengupta, J., Gao, N., and Taylor, D. J. (2007). The process of mRNA-tRNA translocation. *Proc. Natl. Acad. Sci.* 104 (50), 19671–19678. doi:10.1073/pnas.0708517104

Goddard, T. D., Huang, C. C., Meng, E. C., Pettersen, E. F., Couch, G. S., Morris, J. H., et al. (2018). UCSF ChimeraX: Meeting modern challenges in visualization and analysis. *Protein Sci.* 27, 14–25. doi:10.1002/pro.3235

Golubev, A., Fatkhullin, B., Khusainov, I., Jenner, L., Gabdulkhakov, A., Validov, S., et al. (2020). Cryo-EM structure of the ribosome functional complex of the human pathogen Staphylococcus aureus at 3.2 Å resolution. *FEBS Lett.* 594, 3551–3567. doi:10.1002/1873-3468.13915

Guo, Q., Goto, S., Chen, Y., Feng, B., Xu, Y., Muto, A., et al. (2013). Dissecting the *in vivo* assembly of the 30S ribosomal subunit reveals the role of RimM and general features of the assembly process. *Nucleic Acids Res.* 41, 2609–2620. doi:10.1093/nar/gks1256

Guo, Z., and Noller, H. F. (2012). Rotation of the head of the 30S ribosomal subunit during mRNA translocation. *Proc. Natl. Acad. Sci.* 109 (50), 20391–20394. doi:10.1073/pnas.1218999109

Hardy, S. J. S., and Turnock, G. (1971). Stabilization of 70S ribosomes by spermidine. *Nat. New Biol.* 229, 17–19. doi:10.1038/newbio229017a0

Huntzinger, E., Boisset, S., Saveanu, C., Benito, Y., Geissmann, T., Namane, A., et al. (2005). Staphylococcus aureus RNAIII and the endoribonuclease III coordinately regulate spa gene expression. *Embo j* 24, 824–835. doi:10.1038/sj.emboj.7600572

Hussain, T., Llácer, J. L., Wimberly, B. T., Kieft, J. S., and Ramakrishnan, V. (2016). Large-Scale Movements of IF3 and tRNA during Bacterial Translation Initiation. *Cell* 167 (1), 133–144. doi:10.1016/j.cell.2016.08.074

Igarashi, K., and Kashiwagi, K. (2018). Effects of polyamines on protein synthesis and growth of Escherichia coli. *J. Biol. Chem.* 293, 18702–18709. doi:10.1074/jbc.tm118.003465

Igarashi, K., Kishida, K., and Hirose, S. (1980). Stimulation by polyamines of enzymatic methylation of two adjacent adenines near the 3′ end of 16S ribosomal RNA of Escherichia coli. *Biochem. Biophysical Res. Commun.* 96, 678–684. doi:10.1016/0006-291x(80)91408-4

Igarashi, K., Sakamoto, I., Goto, N., Kashiwagi, K., HonmaHirose, R. S., and Hirose, S. (1982). Interaction between polyamines and nucleic acids or phospholipids. *Arch. Biochem. Biophys.* 219, 438–443. doi:10.1016/0003-9861(82)90175-8

Igarashi, K., Watanabe, Y., and Hirose, S. (1975). Dependency of spermidine stimulation of polypeptide synthesis on the uracil content of messenger ribonucleic acid. *Biochem. Biophysical Res. Commun.* 67, 407–413. doi:10.1016/0006-291x(75)90330-7

Jahagirdar, D., Jha, V., Basu, K., Gomez-Blanco, J., Vargas, J., and Ortega, J. (2020). Alternative Conformations and Motions Adopted by 30S Ribosomal Subunits Visualized by Cryo-Electron Microscopy. *RNA* 120, 075846.

Javed, A., and Orlova, E. V. (2019). Unravelling ribosome function through structural studies. *Subcell Biochem.* 93, 53–81. doi:10.1007/978-3-030-28151-9_3

Jenner, L., Demeshkina, N., Yusupova, G., and Yusupov, M. (2010). Structural rearrangements of the ribosome at the tRNA proofreading step. *Nat. Struct. Mol. Biol.* 17, 1072–1078. doi:10.1038/nsmb.1880

Khusainov, I., Fatkhullin, B., Pellegrino, S., Bikmullin, A., Liu, W. T., Gabdulkhakov, A., et al. (2020). Mechanism of ribosome shutdown by RsfS in Staphylococcus aureus revealed by integrative structural biology approach. *Nat. Commun.* 11, 1656–1710. doi:10.1038/s41467-020-15517-0

Khusainov, I., Vicens, Q., Bochler, A., Grosse, F., Myasnikov, A., Ménétret, J. F., et al. (2016). Structure of the 70S ribosome from human pathogen Staphylococcus aureus. *Nucleic Acids Res.* 44, 10491–10504. doi:10.1093/nar/gkw933

Khusainov, I., Marenna, A., Cerciat, M., Fechter, P., Hashem, Y., Marzi, S., et al. (2016). A glimpse on Staphylococcus aureus translation machinery and its control. *Mol. Biol.* 50 (4), 477–488. doi:10.1134/s002689331604004x

Khusainov, I., Vicens, Q., Ayupov, R., Usachev, K., Myasnikov, A., Simonetti, A., et al. (2017). Structures and dynamics of hibernating ribosomes from Staphylococcus aureus mediated by intermolecular interactions of HPF. *EMBO J.* 36, 2073–2087. doi:10.15252/embj.201696105

Kidmose, R. T., Juhl, J., Nissen, P., Boesen, T., Karlsen, J. L., and Pedersen, B. P. (2019). Namdinator - automatic molecular dynamics flexible fitting of structural models into cryo-EM and crystallography experimental maps. *Int. Union Crystallogr. J.* 6, 526–531. doi:10.1107/s2052252519007619

Kirillov, S. V., Makhno, V. I., Peshin, N. N., and Semenkov, Y. P. (1978). Separation of ribosomal subunits of Escherichia coli by Sepharose chromatography using reverse salt gradient. *Nucl. Acids Res.* 5, 4305–4316. doi:10.1093/nar/5.11.4305

Korostelev, A., Trakhanov, S., Asahara, H., Laurberg, M., Lancaster, L., and Noller, H. F. (2007). Interactions and dynamics of the Shine Dalgarno helix in the 70S ribosome. *Proc. Natl. Acad. Sci.* 104 (43), 16840–16843. doi:10.1073/pnas.0707850104

Noeske, J., Wasserman, M. R., Terry, D. S., Altman, R. B., Blanchard, S. C., and Cate, J. H. D. (2015). High-resolution structure of the Escherichia coli ribosome. *Nat. Struct. Mol. Biol.* 22, 336–341. doi:10.1038/nsmb.2994

Ogle, J. M., Brodersen, D. E., Clemons, W. M., Tarry, M. J., Carter, A. P., and Ramakrishnan, V. (2001). Recognition of Cognate Transfer RNA by the 30 S Ribosomal Subunit. *Science* 292, 897–902. doi:10.1126/science.1060612

Pettersen, E. F., Goddard, T. D., Huang, C. C., Couch, G. S., Greenblatt, D. M., Meng, E. C., et al. (2004). UCSF Chimera?A visualization system for exploratory research and analysis. *J. Comput. Chem.* 25, 1605–1612. doi:10.1002/jcc.20084

Pisarev, A. V., Kolupaeva, V. G., Yusupov, M. M., Hellen, C. U., and Pestova, T. V. (2008). Ribosomal position and contacts of mRNA in eukaryotic translation initiation complexes. *Embo J.* 27 (11), 1609–1621. doi:10.1038/emboj.2008.90

Pulk, A., and Cate, J. H. (2013). Control of ribosomal subunit rotation by elongation factor G. *Science* 340 (6140), 1235970. doi:10.1126/science.1235970

Razi, A., Davis, J. H., Hao, Y., Jahagirdar, D., Thurlow, B., Basu, K., et al. (2019). Role of Era in assembly and homeostasis of the ribosomal small subunit. *Nucleic Acids Res.* 47, 8301–8317. doi:10.1093/nar/gkz571

Rozov, A., Demeshkina, N., Khusainov, I., Westhof, E., Yusupov, M., and Yusupova, G. (2016). Novel base-pairing interactions at the tRNA wobble position crucial for accurate reading of the genetic code. *Nat. Commun.* 7, 10457–10510. doi:10.1038/ncomms10457

Rozov, A., Demeshkina, N., Westhof, E., Yusupov, M., and Yusupova, G. (2015). Structural insights into the translational infidelity mechanism. *Nat. Commun.* 6, 7251–7259. doi:10.1038/ncomms8251

Rozov, A., Khusainov, I., El Omari, K., Duman, R., Mykhaylyk, V., Yusupov, M., et al. (2019). Importance of potassium ions for ribosome structure and function revealed by long-wavelength X-ray diffraction. *Nat. Commun.* 10, 2519. doi:10.1038/s41467-019-10409-4

Schedlbauer, A., Iturrioz, I., Ochoa-Lizarralde, B., Diercks, T., Lopez-Alonso, J. P., Lavin, J. L., et al. (2021). A Conserved rRNA Switch is Central to Decoding Site Maturation on the Small Ribosomal Subunit. *Sci. Adv.* 7, eabf7547. doi:10.1126/sciadv.abf7547

Schuwirth, B. S., Borovinskaya, M. A., Hau, C. W., Zhang, W., Vila-Sanjurjo, A., Holton, J. M., et al. (2005). Structures of the Bacterial Ribosome at 3.5 A˚ Resolution. *Science* 310 (5749), 827–834. doi:10.1126/science.1117230

Selmer, M., Dunham, C. M., Murphy, F. V., Weixlbaumer, A., Petry, S., Kelley, A. C., et al. (2006). Structure of the 70S ribosome complexed with mRNA and tRNA. *Science* 313 (5795), 1935–1942. doi:10.1126/science.1131127

Selmer, M., Dunham, C. M., Murphy, F. V., Weixlbaumer, A., Petry, S., Kelley, A. C., et al. (2006). Structure of the 70S ribosome complexed with mRNA and tRNA. *Science* 313 (5795), 1935–1942. doi:10.1126/science.1131127

Stevens, L. (1969). The binding of spermine to the ribosomes and ribosomal ribonucleic acid from Bacillus stearothermophilus. *Biochem. J.* 113, 117–121. doi:10.1042/bj1130117

Teraoka, H., and Tanaka, K. (1973). Effect of polyamines on the binding of dihydrostreptomycin and N-acetylphenylalanyl-tRNA to ribosomes from Escherichia coli. *Eur. J. Biochem.* 40, 423–429. doi:10.1111/j.1432-1033.1973.tb03211.x

Trabuco, L. G., Villa, E., Schreiner, E., Harrison, C. B., and Schulten, K. (2009). Molecular dynamics flexible fitting: a practical guide to combine cryo-electron microscopy and X-ray crystallography. *Methods* 49, 174–180. doi:10.1016/j.ymeth.2009.04.005

Trakhanov, S. D., Yusupov, M. M., Agalarov, S. C., Garber, M. B., Ryazantsev, S. N., Tischenko, S. V., et al. (1987). Crystallization of 70 S ribosomes and 30 S ribosomal subunits from Thermus thermophilus. *Febs Lett.* 220, 319–322. doi:10.1016/0014-5793(87)80838-4

Turnock, G., and Birch, B. (1973). Binding of putrescine and spermidine to ribosomes from Escherichia coli. *Eur. J. Biochem.* 33, 467–474. doi:10.1111/j.1432-1033.1973.tb02704.x

Weiss, R. L., and Morris, D. R. (1970). The inability of polyamines to maintain ribosome structure and function. *Biochim. Biophys. Acta (Bba) - Nucleic Acids Protein Synth.* 204, 502–511. doi:10.1016/0005-2787(70)90170-x

Wood, A., Irving, S. E., Bennison, D. J., and Corrigan, R. M. (2019). The (p)ppGpp-binding GTPase Era promotes rRNA processing and cold adaptation in Staphylococcus aureus. *Plos Genet.* 15 (8), e1008346. doi:10.1371/journal.pgen.1008346

Yusupov, M. M., Yusupova, G. Z., Baucom, A., Lieberman, K., Earnest, T. N., Cate, J. H. D., et al. (2001). Crystal Structure of the Ribosome at 5.5 Å Resolution. *science* 292 (5518), 883–896. doi:10.1126/science.1060089

Yusupova, G. Z., Yusupov, M. M., Cate, J. H. D., and Noller, H. F. (2001). The path of messenger RNA through the ribosome. *Cell* 106 (2), 233–241. doi:10.1016/s0092-8674(01)00435-4

Zhang, K. (2016). Gctf: Real-time CTF determination and correction. *J. Struct. Biol.* 193, 1–12. doi:10.1016/j.jsb.2015.11.003

Zhang, W., Dunkle, J. A., and Cate, J. H. D. (2009). Structures of the ribosome in intermediate states of ratcheting. *Science* 325 (5943), 1014–1017. doi:10.1126/science.1175275

Zheng, S. Q., Palovcak, E., Armache, J.-P., Verba, K. A., Cheng, Y., and Agard, D. A. (2017). MotionCor2: anisotropic correction of beam-induced motion for improved cryo-electron microscopy. *Nat. Methods* 14, 331–332. doi:10.1038/nmeth.4193

Zillig, W., Krone, W., and Albers, M. (1959). Untersuchungen zur Biosynthese der Proteine, III. Beitrag zur Kenntnis der Zusammensetzung und Struktur der Ribosomen. *Hoppe-Seyler´s Z. für physiologische Chem.* 317, 131–143. doi:10.1515/bchm2.1959.317.1.131

Zivanov, J., Nakane, T., Forsberg, B. O., Kimanius, D., Hagen, W. J., Lindahl, E., et al. (2018). New tools for automated high-resolution cryo-EM structure determination in RELION-3. *Elife*, 7. doi:10.7554/elife.42166

Conflict of Interest: The authors declare that the research was conducted in the absence of any commercial or financial relationships that could be construed as a potential conflict of interest.

Publisher's Note: All claims expressed in this article are solely those of the authors and do not necessarily represent those of their affiliated organizations, or those of the publisher, the editors and the reviewers. Any product that may be evaluated in this article, or claim that may be made by its manufacturer, is not guaranteed or endorsed by the publisher.

frontiers in Molecular Biosciences

ORIGINAL RESEARCH
published: 13 December 2021
doi: 10.3389/fmolb.2021.787388

Comparative Analysis of anti-Shine-Dalgarno Function in *Flavobacterium johnsoniae* and *Escherichia coli*

*Zakkary A. McNutt[1,2], Mai D. Gandhi[3], Elan A. Shatoff[2,4], Bappaditya Roy[2,3], Aishwarya Devaraj[1,2], Ralf Bundschuh[2,4,5,6] and Kurt Fredrick[1,2,3]**

[1]Ohio State Biochemistry Program, The Ohio State University, Columbus, OH, United States, [2]Center for RNA Biology, The Ohio State University, Columbus, OH, United States, [3]Department of Microbiology, The Ohio State University, Columbus, OH, United States, [4]Department of Physics, The Ohio State University, Columbus, OH, United States, [5]Department of Chemistry and Biochemistry, The Ohio State University, Columbus, OH, United, States, [6]Division of Hematology, Department of Internal Medicine, The Ohio State University, Columbus, OH, United States

The anti-Shine-Dalgarno (ASD) sequence of 16S rRNA is highly conserved across Bacteria, and yet usage of Shine-Dalgarno (SD) sequences in mRNA varies dramatically, depending on the lineage. Here, we compared the effects of ASD mutagenesis in *Escherichia coli*, a Gammaproteobacteria which commonly employs SD sequences, and *Flavobacterium johnsoniae*, a Bacteroidia which rarely does. In *E. coli*, 30S subunits carrying any single substitution at positions 1,535–1,539 confer dominant negative phenotypes, whereas subunits with mutations at positions 1,540–1,542 are sufficient to support cell growth. These data suggest that CCUCC (1,535–1,539) represents the functional core of the element in *E. coli*. In *F. johnsoniae*, deletion of three ribosomal RNA (*rrn*) operons slowed growth substantially, a phenotype largely rescued by a plasmid-borne copy of the *rrn* operon. Using this complementation system, we found that subunits with single mutations at positions 1,535–1,537 are as active as control subunits, in sharp contrast to the *E. coli* results. Moreover, subunits with quadruple substitution or complete replacement of the ASD retain substantial, albeit reduced, activity. Sedimentation analysis revealed that these mutant subunits are overrepresented in the subunit fractions and underrepresented in polysome fractions, suggesting some defect in 30S biogenesis and/or translation initiation. Nonetheless, our collective data indicate that the ASD plays a much smaller role in *F. johnsoniae* than in *E. coli*, consistent with SD usage in the two organisms.

Keywords: ribosome, translation, RF2 (prfB), initiation, bacteroidetes

OPEN ACCESS

Edited by:
Kristin S. Koutmou, University of Michigan, United States

Reviewed by:
Patrick O'Donoghue, Western University, Canada
Allen Buskirk, Johns Hopkins University, United States

****Correspondence:***
Kurt Fredrick
fredrick.5@osu.edu

Specialty section:
This article was submitted to Protein and RNA Networks, a section of the journal Frontiers in Molecular Biosciences

Received: *30 September 2021*
Accepted: *08 November 2021*
Published: *13 December 2021*

Citation:
McNutt ZA, Gandhi MD, Shatoff EA, Roy B, Devaraj A, Bundschuh R and Fredrick K (2021) Comparative Analysis of anti-Shine- Dalgarno Function in Flavobacterium johnsoniae *and* Escherichia coli. *Front. Mol. Biosci. 8:787388. doi: 10.3389/fmolb.2021.787388*

INTRODUCTION

Faithful protein synthesis requires that the translation machinery select the correct start codon over other AUG or similar trinucleotides. In all cells, intrinsic sequence and structural features of the mRNA enable start codon recognition. One well-known feature in prokaryotic cells is the Shine-Dalgarno (SD) sequence, a purine-rich element that lies upstream from the start codon and can pair with the anti-SD (ASD) sequence contained in the 3' tail of 16S rRNA (Shine and Dalgarno, 1974; Steitz and Jakes, 1975). SD-ASD interaction helps position the start codon in the 30S subunit P site during initiation (Vellanoweth and Rabinowitz, 1992; Studer and Joseph, 2006; Hussain et al., 2016).

In *Escherichia coli*, most mRNAs contain a SD (Nakagawa et al., 2017), and numerous genetic studies underscore the functional importance of the SD in such mRNAs (Hui and de Boer, 1987; Jacob et al., 1987; de Smit and van Duin, 1994). At the same time, there are many mRNAs that naturally lack a SD and yet are accurately and efficiently translated, indicating that other features of mRNA can direct start codon selection (Espah Borujeni et al., 2014; Li et al., 2014; Hockenberry et al., 2017).

Genomic studies have revealed that SD usage varies dramatically across Bacteria (Nakagawa et al., 2010; Accetto and Avguštin, 2011; Nakagawa et al., 2017). Certain lineages, such as Bacteroidia (formerly Bacteroidetes), generally lack SD sequences. Baez *et al.* analyzed translation in *Flavobacterium johnsoniae*, a member of Bacteroidia, to understand how start codon selection occurs in these organisms (Baez et al., 2019). They found that reduced secondary structure, a Kozak-like sequence (A-3, A-6), and an upstream A-motif (A-12, A-13) contribute to initiation in *F. johnsoniae*. Additionally, they showed that, across the Bacteroidia, AUG trinucleotides in the vicinity of the start codon are clearly underrepresented. Thus, elimination of alternative AUG trinucleotides in the translation initiation region (TIR) is one means by which these organisms compensate for the absence of SD-ASD pairing (Baez et al., 2019).

Variable usage of SD sequences in Bacteria came as a surprise, because the ASD is highly conserved across the entire domain (Cannone et al., 2002). Reporter gene studies in several representative organisms have shown that Bacteroidia ribosomes fail to recognize SD sequences in the cell (Accetto and Avguštin, 2011; Wegmann et al., 2013; Mimee et al., 2015), as though the ASD is functionally occluded in some way. A recent cryo-EM structure of the *F. johnsoniae* ribosome at 2.8 Å resolution uncovered the basis of ASD inhibition (Jha et al., 2021). The 3′ tail of 16S rRNA binds a pocket formed by bS21, bS18, and bS6 on the 30S platform domain, physically sequestering the ASD nucleotides. Residues of these proteins that interact with the 3' tail are uniquely conserved in the Bacteroidia, suggesting that the mechanism of ASD occlusion is conserved across the class (Jha et al., 2021).

Interestingly, SD sequences are absent from most but not all Bacteroidia genes. In fact, ribosomal protein genes *rpsU* (bS21) and/or *rpsR* (bS18) often contain a "strong" SD, depending on the organism order (Jha et al., 2021). The corresponding proteins, bS21 and bS18, contribute to the mechanism of ASD occlusion, as mentioned above. This implies some type of translational autoregulation, the details of which remain to be elucidated. In Flavobacteriales, SDs are especially rare, and *rpsU* (bS21) is the only ribosomal gene to harbor one. A subset of Flavobacteriales, including Chryseobacteria and related species, has the alternative ASD sequence 5′-UCUCA-3′ rather than the canonical ASD (5′-CCUCC-3′). Remarkably, compensatory substitutions are seen upstream of *rpsU* in these organisms, indicative of natural covariation. Thus, translation of at least one gene, *rpsU*, entails SD-ASD pairing in the Flavobacteriales (Jha et al., 2021).

In this study, we compare the effects of ASD mutations in *E. coli* and *F. johnsoniae*. In *E. coli*, any single substitution of nucleotides 1,535–1,539 confers a dominant negative phenotype, defining the functional core of the ASD. By contrast, *F. johnsoniae* ribosomes carrying analogous single substitutions have no apparent defects in translation. Moreover, ribosomes with four or five substitutions within the 1,535–1,539 region retain substantial, albeit reduced, activity. These data illuminate the divergent functional roles for the ASD in Gammaproteobacteria versus Bacteroidia.

MATERIALS AND METHODS

E. coli Plasmids and Strains

Plasmid p287MS2 carries the *rrnB* operon downstream from the lambda P_L promoter (Youngman et al., 2004). Single mutations were made in the ASD region of p287MS2, generating the plasmids of **Table 1** (pMDxx; where "xx" represents a unique number). To test for dominant lethal/negative phenotypes, each pMDxx plasmid was transformed into DH10 (pcI857), and transformants were evaluated for growth at 30°C and 43°C, as described (Samaha et al., 1995; Cochella et al., 2007). To test the ability of the mutant ribosomes to support cell growth, the Δ7 strain SQZ10 was employed (Qin et al., 2007; Quan et al., 2015). Each pMDxx plasmid was transformed into SQZ10, selecting for ampicillin resistance (100 μg/ml). The resulting transformants were grown in liquid media, and cells were spread onto plates containing ampicillin and sucrose (5%), to select against the resident plasmid pHKrrnC-sacB. Successful plasmid replacement was evident by a high frequency of sucrose resistant (and kanamycin sensitive) colonies, and subsequently confirmed by plasmid purification and DNA sequencing (Qin et al., 2007). Unsuccessful plasmid replacement was indicated by a low frequency of sucrose resistant colonies; i.e., more than four orders of magnitude lower than the control (p278MS2) case. Most of these colonies retained kanamycin resistance, and any rare isolates sensitive to kanamycin were found to contain the wild-type 16S rRNA gene, presumably due to homologous recombination.

F. johnsoniae Plasmids and Strains

All *F. johnsoniae* strains (**Table 2**) were grown on rich CYE medium at 30°C. *F. johnsoniae* plasmids (**Table 2**) were transformed into *E. coli* strain E726 and then moved into *F. johnsoniae* via tri-parental mating as described previously (McBride and Kempf, 1996).

Mutations to the *F. johnsoniae* chromosome were made using precise allelic replacement (Zhu et al., 2017). Alleles were cloned into the Bam HI and Sph I restriction sites of the suicide vector pYT313 (Zhu et al., 2017). This vector has two selectable markers, *bla* (expressed in *E. coli*) and *ermF* (expressed in *F. johnsoniae*), as well as the counter-selectable *sacB* gene (expressed in *F. johnsoniae*). Alleles were generated by separately amplifying ~1 kb regions from the *F. johnsoniae* chromosome both up- and downstream of the target site. These two fragments were then inserted into pYT313 using Gibson Assembly (Gibson et al., 2009). Resulting plasmids were moved into *F. johnsoniae*, and erythromycin (Em, 100 μg/ml) resistant transconjugants were selected. Colonies were then screened for plasmid integration at the appropriate chromosomal locations using PCR. Confirmed recombinants were then grown overnight in the absence of Em, to allow for loss of the plasmid via a second recombination event,

TABLE 1 | Systematic mutagenesis of the 3' end of 16S rRNA in *E. coli*.

Nucleotide	Conservation[a]	Substitution	Plasmid	Dominant negative[b]	Supports growth[c]
A1534	97.9	C	pMD24	–	No
		G	pMD25	–	No
		U	pMD26	–	No
C1535	98.1	A	pMD27	+	No
		G	pMD28	+	No
		U	pMD29	+	No
C1536	98.3	A	pMD14	+	No
		G	pMD15	+++	No
		U	pMD16	+	No
U1537	97.8	A	pMD30	++	No
		C	pMD17	+	No
		G	pMD31	+++	No
C1538	98.4	A	pMD18	++	No
		G	pMD19	+++	No
		U	pMD20	++	No
C1539	98.2	A	pMD21	+++	No
		G	pMD22	++	No
		U	pMD23	+++	No
U1540	98.3	A	pMD42	–	Yes
		C	pMD40	–	No
		G	pMD41	–	Yes
U1541	98.9	A	pMD37	–	Yes
		C	pMD38	–	Yes
		G	pMD39	–	Yes
A1542	16.3	C	pMD43	–	Yes
		G	pMD44	–	Yes
		U	pMD45	–	Yes

[a]*Per cent conservation in Bacteria (Cannone et al., 2002).*

[b]*Dominant negative growth phenotypes were assessed in DH10 (pcl857, pMDxx) by spotting 20 μL of cells (10^{-4}, 10^{-5}, and 10^{-6} dilutions of overnight culture) onto LB, plates and incubating at either 30°C (repressed) or 43°C (derepressed). Results after 24 h of incubation were scored as follows: no effect; +, reduced colony size; ++ evidence for growth only at highest level of inoculation; +++, no growth.*

[c]*A test of whether the mutant allele is sufficient to support growth. Yes: The resident plasmid pHKrrnC-sacB of Δ7 strain SQZ10 was successfully replaced by pMDxx. No: The frequency of sucrose resistant colonies in the counterselection step was >4 orders of magnitude lower than the control (p278MS2) case, and these colonies typically retained kanamycin resistance. Any rare isolates sensitive to kanamycin were found to contain the wild-type 16S rRNA, gene, presumably due to homologous recombination.*

and then cells were plated on 5% sucrose for counterselection. Sucrose resistant/Em sensitive colonies were then screened via colony PCR for replacement of the wild-type allele for the mutant allele. *rrnF* was deleted from *F. johnsoniae* by removal of the chromosomal region 5,118,368 to 5,124,329. *rrnA* was deleted by removal of the chromosomal region 24,082 to 30,164. *rrnB* was deleted by removal of the chromosomal region 49,9700 to 50,6103.

The *F. johnsoniae rrnA* operon (chromosome positions: 29,556–23,688) was cloned into the Bam HI and Sph I restriction sites of expression vector pSCH710 (Baez et al., 2019), downstream of the inducible *ompA* promoter, to generate pZM06. The marker mutation C1451U (phenotypically silent) was introduced into the plasmid-encoded 16S gene, using site-directed mutagenesis, to yield pZM14. Other *rrn* alleles were similarly cloned into pSCH710 using Gibson Assembly. Plasmids were moved into *F. johnsoniae* strains via tri-parental mating and selecting for Em (100 μg/ml) resistance.

Growth Competition Assays

Overnight cultures of *F. johnsoniae* UW101 and ZAM11 were used to seed fresh CYE medium both separately (wild-type and mutant only) or mixed (~1:1, eight replicates). Inoculated cultures were grown up and back-diluted 200-fold to seed another culture, a process repeated daily for 36 days. Aliquots were taken from saturated cultures for use as template for PCR to quantify the fraction of *prfB* mutants. Because the allele of the *prfB* mutant is effectively shortened by the removal of a single base, amplification of the *prfB* gene around the frameshift site resulted in two different size PCR products for the mixed cultures. PCR was done with Phusion DNA polymerase (NEB), since this enzyme leaves clean blunt-ended PCR products. Primers prZM53 (TATTGTGGAGCGCCTTGGTGCGTT) and prZM55 (ATT TCGATTAGCTTGGCATCAACGTC) were used to amplify the *prfB* alleles, producing a 64 bp product for the wild-type allele and 63 bp for the mutant allele. Radiolabeled prZM53 was included in the reaction. Briefly, prZM53 was 5′ end-labeled using γ-[^{32}P]-ATP and T4 polynucleotide kinase (NEB) and purified from free γ-[^{32}P]-ATP by Sephadex G-25 (Amersham Biosciences) chromatography. PCR products were resolved by denaturing 8% PAGE. Gel imaging and quantification were performed with a Typhoon FLA 9000 phosphorimager (GE Healthcare) and associated software (ImageQuant 5.2).

Computational Analysis of *prfB* Frameshifting Usage

A list of 997 organisms from the orders Cytophagales, Bacteroidales, Chitinophagales, Flavobacteriales, and Sphingobacteriales marked as GTDB species representatives and as NCBI type material were

TABLE 2 | List of *F. johnsoniae* strains and plasmids.

Name	Description	References
Strains		
UW101	wild-type	McBride et al. (2009)
ZAM11	*prfB(-FS)*	This work
ZAM18 (Δ1)[a]	*prfB(-FS) ΔrrnF*	This work
ZAM21	UW101 (pZM14)	This work
ZAM23 (Δ2)[a]	*prfB(-FS) ΔrrnF ΔrrnA*	This work
ZAM25 (Δ3)[a]	*prfB(-FS) ΔrrnF ΔrrnA ΔrrnB*	This work
ZAM26	ZAM25 (pZM14)	This work
ZAM28	ZAM25 (pZM17)	This work
ZAM41	ZAM25 (pZM21; GCUCC)	This work
ZAM42	ZAM25 (pZM22; CAUCC)	This work
ZAM43	ZAM25 (pZM23; CCACC)	This work
ZAM46	ZAM25 (pZM26; GAAGC)	This work
ZAM47	ZAM25 (pZM27; AUUGG)	This work
ZAM49	ZAM25 (pZM31; AAAAA)	This work
ZAM50	ZAM25 (pZM32)	This work
Plasmids		
pSCH710	Shuttle vector with IPTG-inducible promoter	Baez et al. (2019)
pYT313	Suicide vector for allelic replacement in Bacteroidia	Zhu et al. (2017)
pZM06	pSCH710 containing *rrnA*	This work
pZM14	pZM06 with 16S mutation C1451U	This work
pZM17	pSCH710 containing $tRNA^{Ile}$-$tRNA^{Ala}$ genes only	This work
pZM21	pZM14 with ASD sequence GCUCC	This work
pZM22	pZM14 with ASD sequence CAUCC	This work
pZM23	pZM14 with ASD sequence CCACC	This work
pZM26	pZM14 with ASD sequence GAAGC	This work
pZM27	pZM14 with ASD sequence AUUGG	This work
pZM31	pZM14 with ASD sequence AAAAA	This work
pZM32	pZM14 with 16S mutation A1492U	This work

[a]*Colloquial name in parentheses.*

downloaded from GTDB (Parks et al., 2021) (Table S2). 740 of these genome assemblies were successfully downloaded and ARFA (Bekaert et al., 2006) was run on these assemblies with default parameters. A *prfB* gene was identified in 726 of these assemblies. Out of the 524 of the 726, in which ARFA detects a frameshift, we manually inspected all five for which the E-value for the detection of the gene fragment upstream of the frameshift (ORF0) was above 0.05, and identified one [*Weeksella virosa*, which had the highest of all E-values (0.32) for ORF0] that was miscalled by ARFA as frameshifted. We visualized the phylogenetic tree of the 726 organisms with a detected *prfB* gene using iTOL (Letunic and Bork, 2021).

Growth Measurements of *F. johnsoniae* Strains

For each strain, cells from overnight cultures were diluted 100-fold into CYE medium. If included, erythromycin was added to a final concentration of 100 μg/ml and IPTG was added to a final concentration of 1 mM. Cultures were shaken at 250 rpm at 30°C, and aliquots were regularly taken throughout growth to measure the optical density (OD) at 600 nm. Doubling times were determined by fitting the data of the logarithmic phase of growth.

Sucrose Gradient Sedimentation Analyses

Ribosomal particles were fractionated using methods described previously (Qin and Fredrick, 2013). Briefly, cells were grown to mid-log phase (OD_{600} 0.4–0.7), poured over crushed ice, and harvested via centrifugation. The cell pellet was resuspended in lysis buffer [10 mM Tris-HCl (pH 8.0), 10 mM $MgCl_2$, 1 mg/ml lysozyme] and flash frozen three times in liquid nitrogen to lyse the cells. Deoxycholate was added (0.3% final), cell debris was pelleted, and clarified lysate (0.4 ml) was loaded onto an 11 ml 10–40% (wt/vol) sucrose gradient and subjected to ultracentrifugation for 3.5 h at 35,000 rpm in an SW41 rotor (Beckman Coulter). Gradients were pumped using a syringe-pump system (Brandel) with in-line UV absorbance detector (UA-6, ISCO; 254 nm), and 1 ml fractions were collected.

Ribosomes were precipitated from sucrose fractions with ethanol, pelleted, and dissolved in 200 μL extraction buffer [0.3 M sodium acetate (pH 6.5), 0.5% SDS, 5 mM EDTA]. RNA was extracted twice with water-saturated phenol and twice with $CHCl_3$/isoamyl alcohol (24:1). Extracted RNA was then precipitated with ethanol, pelleted, and dissolved in water.

To determine the relative amount of mutant 16S rRNA in each fraction, poison primer extension was used as described (Abdi and Fredrick, 2005). Primer prZM66 (GTTACCAGTTTTACC CTAGGCA) was designed to anneal to 16S rRNA at a position 3′ of the marker mutation C1451U such that extension of the primer in the presence of dideoxyadenosine triphosphate (ddATP) results in distinct extension products that reflect the fraction of templates containing the mutation. Briefly, prZM66 was 5′ end-labeled using γ-[^{32}P]-ATP and T4 polynucleotide kinase

(NEB) and purified from free γ-[^{32}P]-ATP by Sephadex G-25 (Amersham Biosciences) chromatography. In a 10-µL reaction containing 50 mM HEPES (pH 7.6) and 100 mM KCl, labeled primer was annealed to ~1.5 pmol 16S rRNA by heating the reaction to 95°C for 1 min and then allowing it to cool slowly. After a brief centrifugation to recover condensation, 10 µL of 2X extension mix [260 mM Tris-HCl (pH 8.5), 20 mM $MgCl_2$, 20 mM DTT, 6 U AMV reverse transcriptase (Life Sciences Advance Technologies Inc.), 340 µM of ddATP, and 340 µM of each other deoxynucleotide triphosphate) was added and the reaction was incubated for 10 min at 42°C. Finally, the primer extension products were passed through a Sephadex G-25 column, dissolved in loading solution (95% formamide, 20 mM EDTA, 0.05% xylene cyanol FF, and 0.05% bromophenol blue), and resolved by denaturing 8% PAGE. Gels were then dried and imaged as described above.

RESULTS

Systematic Mutagenesis of the 3' End of *E. coli* 16S rRNA

The ASD region of the *E. coli* ribosome has been targeted in several previous studies (Hui and de Boer, 1987; Jacob et al., 1987; Lee et al., 1996; Rackham and Chin, 2005; Hui et al., 1988; Yassin et al., 2005). Most of these studies aimed to generate functionally orthogonal ribosomes and hence entailed the simultaneous substitution of multiple nucleotides (e.g., 1,535–1,540). While certain single mutations have been analyzed (Jacob et al., 1987; Yassin et al., 2005), to our knowledge no one has performed a comprehensive analysis of single substitutions across this critical region. We did so here, targeting nine positions (1,534–1,542) of the 16S rRNA gene in plasmid p287MS2 (Youngman et al., 2004). This plasmid contains the ribosomal RNA operon *rrnB* downstream from the P_L promoter, allowing temperature-dependent transcription in cells containing a labile form of lambda repressor (cI857). Each plasmid was moved into *E. coli* strain DH10 (pcI857) (Samaha et al., 1995; Durfee et al., 2008), and cell growth was assessed at 43°C, conditions of P_L de-repression (**Table 1**, **Supplementary Figure S1**). Production of 16S rRNA substituted at position 1,535, 1,536, 1,537, 1,538, or 1,539 conferred dominant negative effects. Certain variants (C1536G, U1537G, C1538G, C1539A, and C1539U) were especially deleterious. Presumably, these strong effects stem from altered specificity of the mutant ribosomes during initiation, consistent with widespread proteomic changes seen in analogous studies (Jacob et al., 1987). Next, each plasmid was tested for its ability to support the growth of SQZ10, an *E. coli* strain lacking all seven chromosomal *rrn* operons (Δ7) (Qin et al., 2007; Quan et al., 2015). Most alleles substituted at positions 1,540–1,542 were able to complement the Δ7 strain, whereas alleles with any mutation further upstream could not (**Table 1**). Collectively, these data indicate the functional importance of nucleotides 1,534–1,539 in *E. coli* and suggest that CCUCC represents the core ASD.

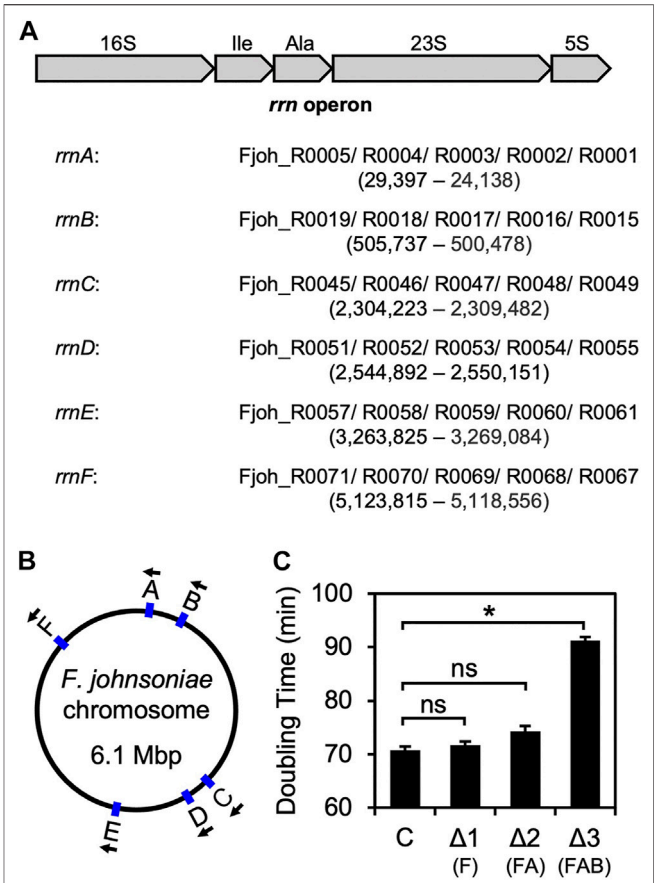

FIGURE 1 | Sequential deletion of *rrn* operons in *F. johnsoniae* **(A)** Common architecture of an *rrn* operon in *F. johnsoniae*. All six operons are virtually identical and encode 16S rRNA (16S), $tRNA^{Ile}$ (Ile), $tRNA^{Ala}$ (Ala), 23S rRNA (23S), and 5S rRNA (5S). Each of the six *rrn* operons in *F. johnsoniae* were assigned a letter, based on chromosomal position. Accession IDs of the component genes for each operon are listed in order, along with the genomic positions (from annotated 5′ end of 16S to 3′ end of 5S) in parenthesis **(B)** A map of the *F. johnsoniae* chromosome with the positions and orientation of each *rrn* operon indicated **(C)** Doubling time (minutes) of the control strain ZAM11 and its deletion derivatives. Data represent the mean ± SEM of three or more independent experiments. Asterisk denotes a significant difference, $p < 0.05$, based on a two-tailed *t* test with the Bonferroni multiple-test correction. ns, not significant. C, control; Δ1, Δ*rrnF*; Δ2, Δ*rrnF*Δ*rrnA*; Δ3, Δ*rrnF*Δ*rrnA*Δ*rrnB*.

Deletion of Three *rrn* Operons Slows the Growth of *F. johnsoniae*

On its single chromosome, *F. johnsoniae* contains six virtually identical *rrn* operons that each encode 16S rRNA, $tRNA^{Ile}$ (anticodon GAU), $tRNA^{Ala}$ (anticodon UGC), 23S rRNA, and 5S rRNA. Starting with ZAM11, a strain which constitutively produces RF2 (see below), we began to progressively delete *rrn* operons (named *rrnA-F*, based on chromosome position; **Figure 1**). Loss of one (Δ*rrnF*) or two (Δ*rrnF*Δ*rrnA*) operons had little if any effect on growth (**Figure 1C**, **Supplementary Table S1**). However, loss of three operons (Δ*rrnF*Δ*rrnA*Δ*rrnB*) slowed growth considerably, increasing the doubling time from 70 to 90 min. These findings are

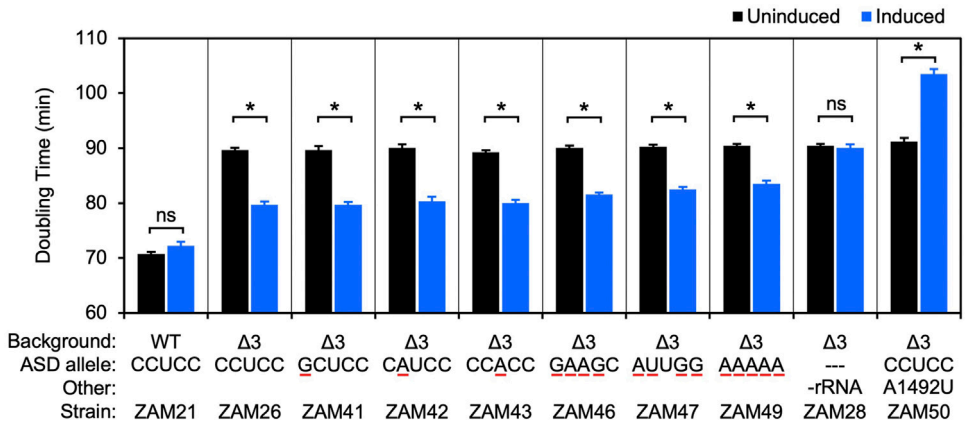

FIGURE 2 | Ribosomes carrying multiple ASD substitutions retain substantial activity *in vivo*. Plasmid pZM14 or one of its derivatives was moved into UW101 (WT) or ZAM25 (Δ3), and cell doubling time in the absence (black bars) or presence (blue bars) of IPTG was measured. The ASD sequence of the plasmid-encoded 16S rRNA is indicated (ASD allele), and substituted nucleotides are underscored in red. In the case of strain ZAM28, only $tRNA^{Ile}$ and $tRNA^{Ala}$ are expressed from the plasmid (-rRNA). Data represent the mean ± SEM of three or more independent experiments. Asterisks denote significant differences, $p < 0.05$, based on a two-tailed *t* test with the Bonferroni multiple-test correction. ns, not significant.

reminiscent of *E. coli* studies which showed that a minimum of four chromosomal operons are needed to sustain rapid growth (Quan et al., 2015).

An *rrn* operon with a marker mutation (C1451U; a base substitution in the tetraloop of h44, predicted to be phenotypically silent) was cloned downstream of an engineered IPTG-inducible promoter in the shuttle vector pSCH710. The resulting plasmid (pZM14) was moved into the Δ3 strain of *F. johnsoniae*, and growth in the absence and presence of IPTG was measured (**Figure 2**, ZAM26; **Supplementary Table S1**). The doubling time decreased from 90 to 80 min in the presence of inducer (1 mM), indicating clear albeit partial complementation by the plasmid-borne *rrn* operon. Expression of $tRNA^{Ile}$ and $tRNA^{Ala}$ only (**Figure 2**, ZAM28) had no effect, indicating the importance of rRNA in the complementation. The marker mutation C1451U allowed us to track the plasmid-encoded 30S subunits in various ribosome fractions, using primer extension with dideoxy-ATP (**Figure 3**, ZAM26). These subunits accounted for ~25% of the total and were distributed evenly across all fractions of the sucrose gradient. This distribution pattern shows that the plasmid-encoded subunits are as active as chromosomally-encoded subunits in these cells.

30S Subunits Carrying Single Mutations in the Core ASD Appear to Be Fully Functional in *F. johnsoniae*

Using this complementation system, we began to evaluate mutations to the ASD core. Derivatives of pZM14 harboring various single mutations were made and introduced into the Δ3 strain. Growth of the resulting strains (ZAM41-43) in the absence and presence of IPTG was measured, and the data were indistinguishable from that of the ZAM26 control (**Figure 2**, **Supplementary Table S1**). In other words, the mutant 30S subunits carrying C1535G, C1536A, or U1537A rescued the growth defect of the Δ3 strain as well as the control subunits and hence have similar activity. Notably, these same mutations confer dominant negative phenotypes in *E. coli* (**Table 1**).

As a separate control, we introduced the A-site mutation A1492U into plasmid pZM14 and moved the resulting plasmid into the Δ3 strain (**Figure 2**, ZAM50; Table S1). Mutation A1492U targets the 30S A site and eliminates translation activity in *E. coli* (Abdi and Fredrick, 2005). Expression of 16S (A1492U) rRNA in the presence of IPTG strongly inhibited growth, increasing the doubling time to 104 min. This dominant negative phenotype is in line with analogous experiments done in *E. coli* (Powers and Noller, 1990; Cochella et al., 2007) and indicates that, in this *F. johnsoniae* system, plasmid-encoded 16S rRNA is expressed at levels high enough to confer such phenotypes.

30S Subunits Carrying Multiple Mutations in the Core ASD Retain Substantial Activity in *F. johnsoniae*

Next, we heavily mutagenized the ASD and tested the ability of the corresponding mutant ribosomes to restore growth of the Δ3 strain (**Figure 2**, **Supplementary Table S1**). Production of subunits with quadruple substitutions within the ASD (CCUCC to GAAGC or AUUGG; mutations underscored) reduced doubling times from 90 to ~82 min, rescues nearly as robust as that provided by control (CCUCC) subunits. Subunits in which the core ASD is replaced with AAAAA also stimulated growth, albeit to smaller degree. Thus, ribosomes lacking the ASD sequence can translate endogenous mRNA in *F. johnsoniae*.

Mutant 16S rRNA Is Enriched in 30S Particles, Indicating Some Defect in Assembly or Initiation

The activity of various mutant ribosomes in the cell was evaluated by quantifying the proportion of plasmid-encoded 16S rRNA in

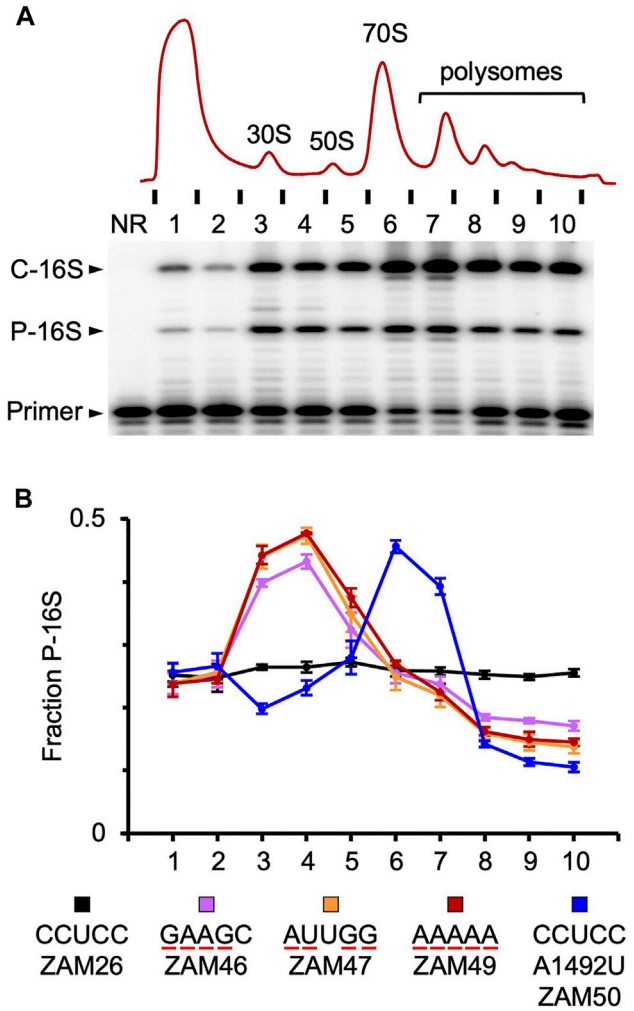

FIGURE 3 | Tracking mutant particles in various ribosomal fractions **(A)** A representative experiment in which ribosomal complexes from induced ZAM26 cells were separated by sucrose gradient sedimentation. RNA isolated from collected fractions (one to ten) was subjected to primer extension analysis to quantify chromosomally-encoded (C-16S) and plasmid-encoded (P-16S) 16S rRNA. NR, no RNA **(B)** The fraction of plasmid-encoded 16S rRNA (P-16S) is plotted as a function of sucrose gradient fraction for various strains (as indicated). For each strain, the experiment was repeated three times, and data points and error bars represent mean ± SEM values. The ASD sequence of the plasmid-encoded 16S rRNA is indicated in the key, and substituted nucleotides are underscored in red. Parallel primer extension analysis of RNA from total (unfractionated) lysates yielded the following values: ZAM26, 0.28 ± 0.01; ZAM46, 0.27 ± 0.01; ZAM47, 0.26 ± 0.01; ZAM49, 0.27 ± 0.01; ZAM50, 0.31 ± 0.01.

ribosomal particles fractionated by sucrose gradient sedimentation (**Figure 3**). Subunits carrying four or five substitutions in the ASD exhibited similar profiles, with overrepresentation in the subunit region (fractions 3–4) and underrepresentation in the polysome region (fractions 8–10). These data indicate that wild-type ribosomes outcompete the mutant ribosomes for mRNA loading. This could stem from a defect in initiation or assembly, as in either case 30S particles would accumulate and fewer ribosomes would enter the actively-translating pool. Notably, A_{260} traces of the lysates were similar across the board (**Supplementary Figure S2**), indicating little or no effects on the overall proportions of subunits, monosomes, and polysomes in these strains.

In the case of A1492U, mutant particles accumulated in the 70S region (fractions 6–7) and were present at reduced levels in both the subunit and polysome regions (**Figure 3**). As this mutation targets an A-site residue critical for decoding, these mutant ribosomes are presumably trapped as 70S initiation complexes, unable to transition to elongation. Their presence in polysomes can be explained by one or more wild-type ribosomes downstream on the mRNA, and their relative underrepresentation in the subunit region might be explained by an inability of "stuck" 70S complexes to dissociate.

Elimination of RF2 Autoregulation in *F. johnsoniae* has No Obvious Effect on Cell Fitness

In many bacteria, the gene encoding RF2, *prfB*, is autoregulated via a +1 programmed frameshifting mechanism (Craigen and Caskey, 1986; Weiss et al., 1987; Baranov et al., 2002). In *E. coli*, the frameshift site corresponds to **AGGGGGU**AUCUU***UGA***C, where the slippery sequence (underscored) overlaps the in-frame stop codon (bold italics), just downstream from a SD-like sequence (bold). When RF2 levels are low in the cell, ribosomes containing peptidyl-$tRNA^{Leu}$:CUU in the P site and codon UGA in the A site pause. Because the SD-like sequence is closely juxtaposed to the P codon, pairing to the ASD causes tension on the mRNA that promotes slippage of peptidyl-$tRNA^{Leu}$ from CUU (zero frame) to UUU (+1 frame) (Devaraj and Fredrick, 2010). Continued translation in the +1 frame allows production of full-length RF2. As RF2 levels rise, the rate of termination at the in-frame UGA increases, down-regulating further production of the factor.

One might expect Bacteroidia to lack this autoregulatory mechanism because it depends on mRNA-rRNA pairing. However, we noticed that the *prfB* gene of *F. johnsoniae* contains a +1 programmed frameshift site, virtually identical to that of *E. coli* but with a "perfect" SD-like sequence: **AGGAGGU**AUCUU***UGA***C (annotated as above). To evaluate the prevalence of *prfB* programmed frameshifting across the class, we used the tool ARFA (Bekaert et al., 2006). Over 700 representative genomes were analyzed, and in 72% of the cases (523/726), *prfB* contains the frameshift. This value is in line with frequencies calculated previously (70–87%), using organisms from multiple phyla (Baranov et al., 2002; Bekaert et al., 2006). Thus, the autoregulatory mechanism seems no less common in the Bacteroidia. Supplementary Figure S3 shows occurrences of programmed frameshifting projected onto the GTDB phylogenetic tree (Parks et al., 2021). The frameshift is present in all Sphingobacteriales analyzed and absent from all Weeksellaceae analyzed. However, the other clades show considerable variability,

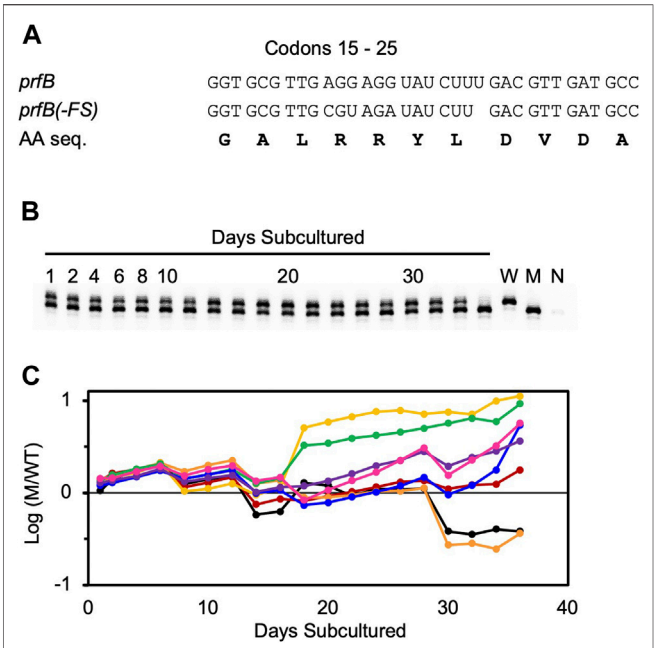

FIGURE 4 | Autoregulation of RF2 synthesis provides no obvious fitness benefit in *F. johnsoniae*. Growth competition between strains UW101 and ZAM11 **(A)** Sequence of codons 15–25 of *prfB* in the wild-type strain UW101 (*prfB*) and the engineered strain ZAM11 (*prfB(-FS)*). Note that the encoded protein sequence (AA seq.) remains unchanged **(B)** An example of the primary data. Mixed cultures were passaged daily, and aliquots were taken and analyzed by PCR to distinguish wild-type and mutant alleles. Control reactions containing pure wild-type cells (W), pure mutant cells (M), or no cells (N) are shown in the rightmost lanes **(C)** The proportion of mutant (M) versus wildtype (W) cells is plotted as a function of time, for eight biological replicates. Each replicate is represented by a different color, and Y values correspond to $\log_{10}$ (M/W).

implying evolutionary loss and/or gain of the autoregulatory mechanism.

Before embarking on genetic analysis of the ASD (described above), we decided to remove the *prfB* frameshift, because we were mainly interested in roles of the ASD beyond this autoregulatory mechanism. We replaced the frameshift site (codons 18–22) with the sequence CGT AGA TAT CTT GAC. The resulting strain, ZAM11, which contains an undisrupted *prfB* open reading frame encoding the wild-type RF2 protein, exhibited no obvious growth defect. To further characterize the strain, we co-cultured ZAM11 and its parent strain UW101 in eight replicate experiments, growing the cells in CYE medium and passaging them every day for 36 days (**Figure 4**). Samples were removed at each passage, and PCR was used to quantify the abundance of ZAM11 versus UW101. The ZAM11/UW101 ratio increased or decreased slowly as a function of time, depending on the particular replicate and time window. In six of the eight experiments, ZAM11 predominated by day 36. Hence, this mutation, which effectively removes *prfB* autoregulation, confers no obvious loss of fitness, at least under these laboratory conditions.

DISCUSSION

In this study, we show that the ASD plays a much smaller role in *F. johnsoniae* than in *E. coli*. In *F. johnsoniae*, ribosomes carrying single mutations at positions 1,535–1,537 are as active as WT ribosomes, based on genetic complementation. In *E. coli*, the same mutations cause a dominant negative or dominant lethal phenotype. Remarkably, *F. johnsoniae* ribosomes retain substantial activity even after quadruple mutation or complete replacement of the ASD (nucleotides 1,535–1,539). This clear difference in ASD dependence can be explained by SD usage in the two organisms. Most *E. coli* genes contain a SD (Nakagawa et al., 2010; Nakagawa et al., 2017), whereas very few *F. johnsoniae* genes do (Jha et al., 2021). In fact, sequences complementary to the 3' end of 16S rRNA are underrepresented upstream of start codons in *F. johnsoniae* (and other Bacteroidia), implying that rRNA-mRNA pairing can be inhibitory for initiation on many mRNAs (Jha et al., 2021).

F. johnsoniae ribosomes carrying multiple ASD mutations are active but functionally compromised. This reduced activity could stem from a defect in 30S assembly. Era, a conserved bacterial GTPase critical for 30S biogenesis, interacts directly with nucleotides 1,530–1,539 of 16S rRNA, which includes the core ASD (nt 1,535–1,539) (Sharma et al., 2005; Tu et al., 2009; Tu et al., 2011; Razi et al., 2019). The mutations we made are predicted to disrupt Era-rRNA contacts, which may slow assembly of the mutant subunits, leading to their enrichment in the 30S region of the gradient and their depletion from the polysome region. Another possibility is that these mutant ribosomes are defective in translation initiation. A recent cryo-EM structure of the *F. johnsoniae* ribosome revealed that the 3′ tail of 16S rRNA binds a pocket formed by bS21, bS18, and bS6 on the 30S platform, explaining why *F. johnsoniae* ribosomes are "blind" to SD sequences *in vivo* and *in vitro* (Jha et al., 2021). Mutations at positions 1,537–1,539 are predicted to disrupt ASD interactions with bS21 and/or bS18 on the platform, effectively liberating the 3' tail. This might be generally detrimental to *F. johnsoniae* initiation, which normally does not entail mRNA-rRNA pairing. Further work will be needed to distinguish whether these ASD mutations influence assembly or initiation (or both), and exactly how they do so.

Translation of *rpsU* in *F. johnsoniae* does involve SD-ASD pairing (Jha et al., 2021), hence bS21 production may be compromised in cells with ASD-substituted ribosomes. While this could impair 30S assembly, both mutant and wild-type subunits would be equivalently affected, which is inconsistent with our gradient sedimentation results. Instead, our data provide strong evidence that the mutant subunits are specifically defective (**Figure 3**), while global translation in the cell is largely unchanged (**Supplementary Figure S2**).

Growth of *F. johnsoniae* slowed substantially after deletion of the third (of six) ribosomal RNA (*rrn*) operons. This is reminiscent of analogous experiments in *E. coli*, where a clear drop in growth occurred upon deletion of the fourth (of seven) operons (Quan et al., 2015). However, the basis of this growth inhibition differs in the two systems. For *E. coli* Δ4, the growth phenotype can be largely rescued by plasmid ptRNA67, which

encodes the various tRNA genes associated with seven *rrn* operons, and the additional presence of a plasmid expressing ribosomal RNA has no further effect. In fact, deletion of two more *rrn* operons (strain Δ6) are needed before growth becomes limited by rRNA levels. For the Δ3 strain of *F. johnsoniae*, complementation depends on plasmid-encoded rRNA, not tRNA (**Figure 2**, ZAM28). In other words, the three intact *rrn* operons on the chromosome are unable to maintain sufficient levels of rRNA in the cell. This hints that feedback regulation of rRNA synthesis in *F. johnsoniae* differs from that in *E. coli* (Paul et al., 2004), a hypothesis worth exploring in the future.

While pZM14 can complement the Δ3 strain of *F. johnsoniae*, the growth rate of ZAM26 does not reach that of wild-type cells. Why only partial complementation is seen remains unclear. One possibility is that production of rRNA from pZM14 is simply not high enough. This plasmid contains the *rrn* operon (*rrnA*) downstream from an engineered *ompA* promoter (Baez et al., 2019), which is probably less active than the native *rrn* promoter. In earlier work (Boleratz, 2016), we cloned the *rrn* operon with its native promoter into an analogous shuttle vector, but we were unable to move the resulting plasmid into *F. johnsoniae*. Further investigation, involving conjugation of numerous deletion derivatives, showed that the *rrn* promoter itself prevents transconjugant formation (Boleratz, 2016). We suspect that high-level transcription directed by P_{rrn} interferes with plasmid replication or stability. Unfortunately, these experiments left us with no useful constructs, and the basis of partial complementation remains unsolved.

All bacteria have two primary release factors—RF1, which recognizes UAA and UAG; and RF2, which recognizes UAA and UGA. In many species, production of RF2 is autoregulated via a +1 programmed frameshifting mechanism, which depends on mRNA-rRNA pairing. In this work, we show that *prfB* autoregulation is also common among Bacteroidia, even though ribosomes of these organisms exhibit an occluded ASD and generally fail to recognize SD sequences (Jha et al., 2021). Presumably, the frameshifting mechanism has adapted in these organisms to account for the altered ASD dynamics. Interestingly, ribo-seq read coverage suggests that ribosomes pause at the slippery site much longer in *F. johnsoniae* than in *E. coli* (Baez et al., 2019). We hypothesize that other *cis*-acting elements and/or trans-acting factors promote this pause, allowing enough time for the ASD to dissociate from the 30S platform and pair with the mRNA. Notably, the *prfB* frameshift appears to be uniformly absent in Weeksellaceae. This clade includes Chryseobacteria and related organisms, whose ribosomes have an alternative ASD (5′-UCUCA-3′) (Jha et al., 2021). This observation is consistent with a critical role for rRNA-mRNA pairing in *prfB* frameshifting and hints that multiple G-C pairs may be needed.

Prior to mutational analysis of the ASD, we removed the frameshift site of *prfB* in *F. johnsoniae*. The resulting strain, ZAM11, constitutively produces the wild-type RF2 protein from one open reading frame. Interestingly, ZAM11 exhibited no obvious phenotype, and growth competition experiments revealed no loss of fitness, at least under the laboratory conditions tested. To our knowledge, analogous work has yet to be performed in *E. coli*, or any other bacterium. The prevalence of the autoregulatory mechanism across Bacteria implies that it must provide some benefit. There is some evidence that overproduction of RF2 can be deleterious, perhaps due to misreading of the tryptophan codon UGG (Abdalaal et al., 2020). Further studies of ZAM11 (and/or analogous strains in other bacteria) will be needed to understand the physiological role of *prfB* autoregulation.

DATA AVAILABILITY STATEMENT

The original contributions presented in the study are included in the article/**Supplementary Material**, further inquiries can be directed to the corresponding author.

AUTHOR CONTRIBUTIONS

ZM and KF designed research; ZM, MD, ES, BR, and AD performed research; ZM, RB and KF analyzed data; ZM, RB and KF wrote the paper; all authors edited the paper.

FUNDING

This work was supported by a grant from the National Science Foundation (MCB-2029502 to KF).

ACKNOWLEDGMENTS

We thank M. McBride for providing pYT313.

SUPPLEMENTARY MATERIAL

The Supplementary Material for this article can be found online at: https://www.frontiersin.org/articles/10.3389/fmolb.2021.787388/full#supplementary-material

REFERENCES

Abdalaal, H., Pundir, S., Ge, X., Sanyal, S., and Näsvall, J. (2020). Collateral Toxicity Limits the Evolution of Bacterial Release Factor 2 toward Total Omnipotence. *Mol. Biol. Evol.* 37 (10), 2918–2930. doi:10.1093/molbev/msaa129

Abdi, N. M., and Fredrick, K. (2005). Contribution of 16S rRNA Nucleotides Forming the 30S Subunit A and P Sites to Translation in *Escherichia coli*. *RNA* 11 (11), 1624–1632. doi:10.1261/rna.2118105

Accetto, T., and Avguštin, G. (2011). Inability of Prevotella Bryantii to Form a Functional Shine-Dalgarno Interaction Reflects Unique Evolution of Ribosome Binding Sites in Bacteroidetes. *PLoS One* 6 (8), e22914. doi:10.1371/journal.pone.0022914

Baez, W. D., Roy, B., McNutt, Z. A., Shatoff, E. A., Chen, S., Bundschuh, R., et al. (2019). Global Analysis of Protein Synthesis in Flavobacterium Johnsoniae Reveals the Use of Kozak-like Sequences in Diverse Bacteria. *Nucleic Acids Res.* 47 (20), 10477–10488. doi:10.1093/nar/gkz855

Baranov, P. V., Gesteland, R. F., and Atkins, J. F. (2002). Release Factor 2 Frameshifting Sites in Different Bacteria. *EMBO Rep.* 3 (4), 373–377. doi:10.1093/embo-reports/kvf065

Bekaert, M., Atkins, J. F., and Baranov, P. V. (2006). ARFA: a Program for Annotating Bacterial Release Factor Genes, Including Prediction of Programmed Ribosomal Frameshifting. *Bioinformatics* 22 (20), 2463–2465. doi:10.1093/bioinformatics/btl430

Boleratz, B. (2016). Studies of Translation Initiation in Flavobacterium Johnsoniae. M.S. Thesis (Columbus, Ohio, United States: The Ohio State University).

Cannone, J. J., Subramanian, S., Schnare, M. N., Collett, J. R., D'Souza, L. M., Du, Y., et al. (2002). The Comparative RNA Web (CRW) Site: an Online Database of Comparative Sequence and Structure Information for Ribosomal, Intron, and Other RNAs. *BMC Bioinformatics* 3, 2. doi:10.1186/1471-2105-3-2

Cochella, L., Brunelle, J. L., and Green, R. (2007). Mutational Analysis Reveals Two Independent Molecular Requirements during Transfer RNA Selection on the Ribosome. *Nat. Struct. Mol. Biol.* 14 (1), 30–36. doi:10.1038/nsmb1183

Craigen, W. J., and Caskey, C. T. (1986). Expression of Peptide Chain Release Factor 2 Requires High-Efficiency Frameshift. *Nature* 322 (6076), 273–275. doi:10.1038/322273a0

de Smit, M. H., and van Duin, J. (1994). Translational Initiation on Structured Messengers. *J. Mol. Biol.* 235 (1), 173–184. doi:10.1016/s0022-2836(05)80024-5

Devaraj, A., and Fredrick, K. (2010). Short Spacing between the Shine-Dalgarno Sequence and P Codon Destabilizes Codon-Anticodon Pairing in the P Site to Promote +1 Programmed Frameshifting. *Mol. Microbiol.* 78 (6), 1500–1509. doi:10.1111/j.1365-2958.2010.07421.x

Durfee, T., Nelson, R., Baldwin, S., Plunkett, G., 3rd, Burland, V., Mau, B., et al. (2008). The Complete Genome Sequence of *Escherichia coli* DH10B: Insights into the Biology of a Laboratory Workhorse. *J. Bacteriol.* 190 (7), 2597–2606. doi:10.1128/JB.01695-07

Espah Borujeni, A., Channarasappa, A. S., and Salis, H. M. (2014). Translation Rate Is Controlled by Coupled Trade-Offs between Site Accessibility, Selective RNA Unfolding and Sliding at Upstream Standby Sites. *Nucleic Acids Res.* 42 (4), 2646–2659. doi:10.1093/nar/gkt1139

Gibson, D. G., Young, L., Chuang, R.-Y., Venter, J. C., Hutchison, C. A., 3rd, and Smith, H. O. (2009). Enzymatic Assembly of DNA Molecules up to Several Hundred Kilobases. *Nat. Methods* 6 (5), 343–345. doi:10.1038/nmeth.1318

Hockenberry, A. J., Pah, A. R., Jewett, M. C., and Amaral, L. A. N. (2017). Leveraging Genome-wide Datasets to Quantify the Functional Role of the Anti-shine-dalgarno Sequence in Regulating Translation Efficiency. *Open Biol.* 7 (1), 160239. doi:10.1098/rsob.160239

Hui, A., and de Boer, H. A. (1987). Specialized Ribosome System: Preferential Translation of a Single mRNA Species by a Subpopulation of Mutated Ribosomes in *Escherichia coli*. *Proc. Natl. Acad. Sci.* 84 (14), 4762–4766. doi:10.1073/pnas.84.14.4762

Hui, A. S., Eaton, D. H., and de Boer, H. A. (1988). Mutagenesis at the mRNA Decoding Site in the 16S Ribosomal RNA Using the Specialized Ribosome System in *Escherichia coli*. *EMBO J.* 7 (13), 4383–4388. doi:10.1002/j.1460-2075.1988.tb03337.x

Hussain, T., Llácer, J. L., Wimberly, B. T., Kieft, J. S., and Ramakrishnan, V. (2016). Large-Scale Movements of IF3 and tRNA during Bacterial Translation Initiation. *Cell* 167 (1), 133–144. doi:10.1016/j.cell.2016.08.074

Jacob, W. F., Santer, M., and Dahlberg, A. E. (1987). A Single Base Change in the Shine-Dalgarno Region of 16S rRNA of *Escherichia coli* Affects Translation of many Proteins. *Proc. Natl. Acad. Sci.* 84 (14), 4757–4761. doi:10.1073/pnas.84.14.4757

Jha, V., Roy, B., Jahagirdar, D., McNutt, Z. A., Shatoff, E. A., Boleratz, B. L., et al. (2021). Structural Basis of Sequestration of the Anti-shine-dalgarno Sequence in the Bacteroidetes Ribosome. *Nucleic Acids Res.* 49 (1), 547–567. doi:10.1093/nar/gkaa1195

Lee, K., Holland-Staley, C. A., and Cunningham, P. R. (1996). Genetic Analysis of the Shine-Dalgarno Interaction: Selection of Alternative Functional mRNA-rRNA Combinations. *RNA* 2 (12), 1270–1285.

Letunic, I., and Bork, P. (2021). Interactive Tree of Life (iTOL) V5: an Online Tool for Phylogenetic Tree Display and Annotation. *Nucleic Acids Res.* 49 (W1), W293–W296. doi:10.1093/nar/gkab301

Li, G.-W., Burkhardt, D., Gross, C., and Weissman, J. S. (2014). Quantifying Absolute Protein Synthesis Rates Reveals Principles Underlying Allocation of Cellular Resources. *Cell* 157 (3), 624–635. doi:10.1016/j.cell.2014.02.033

McBride, M. J., and Kempf, M. J. (1996). Development of Techniques for the Genetic Manipulation of the Gliding Bacterium Cytophaga Johnsonae. *J. Bacteriol.* 178 (3), 583–590. doi:10.1128/jb.178.3.583-590.1996

McBride, M. J., Xie, G., Martens, E. C., Lapidus, A., Henrissat, B., Rhodes, R. G., et al. (2009). Novel Features of the Polysaccharide-Digesting Gliding Bacterium Flavobacterium Johnsoniae as Revealed by Genome Sequence Analysis. *Appl. Environ. Microbiol.* 75 (21), 6864–6875. doi:10.1128/AEM.01495-09

Mimee, M., Tucker, A. C., Voigt, C. A., and Lu, T. K. (2015). Programming a Human Commensal Bacterium, Bacteroides Thetaiotaomicron, to Sense and Respond to Stimuli in the Murine Gut Microbiota. *Cell Syst.* 1 (1), 62–71. doi:10.1016/j.cels.2015.06.001

Nakagawa, S., Niimura, Y., and Gojobori, T. (2017). Comparative Genomic Analysis of Translation Initiation Mechanisms for Genes Lacking the Shine-Dalgarno Sequence in Prokaryotes. *Nucleic Acids Res.* 45 (7), 3922–3931. doi:10.1093/nar/gkx124

Nakagawa, S., Niimura, Y., Miura, K.-i., and Gojobori, T. (2010). Dynamic Evolution of Translation Initiation Mechanisms in Prokaryotes. *Proc. Natl. Acad. Sci.* 107 (14), 6382–6387. doi:10.1073/pnas.1002036107

Parks, D. H., Chuvochina, M., Rinke, C., Mussig, A. J., Chaumeil, P.-A., and Hugenholtz, P. (2021). GTDB: an Ongoing Census of Bacterial and Archaeal Diversity through a Phylogenetically Consistent, Rank Normalized and Complete Genome-Based Taxonomy. *Nucleic Acids Res.* doi:10.1093/nar/gkab776

Paul, B. J., Ross, W., Gaal, T., and Gourse, R. L. (2004). rRNA Transcription in *Escherichia coli*. *Annu. Rev. Genet.* 38, 749–770. doi:10.1146/annurev.genet.38.072902.091347

Powers, T., and Noller, H. F. (1990). Dominant Lethal Mutations in a Conserved Loop in 16S rRNA. *Proc. Natl. Acad. Sci.* 87 (3), 1042–1046. doi:10.1073/pnas.87.3.1042

Qin, D., Abdi, N. M., and Fredrick, K. (2007). Characterization of 16S rRNA Mutations that Decrease the Fidelity of Translation Initiation. *RNA* 13 (12), 2348–2355. doi:10.1261/rna.715307

Qin, D., and Fredrick, K. (2013). Analysis of Polysomes from Bacteria. *Methods Enzymol.* 530, 159–172. doi:10.1016/B978-0-12-420037-1.00008-7

Quan, S., Skovgaard, O., McLaughlin, R. E., Buurman, E. T., and Squires, C. L. (2015). Markerless *Escherichia coli* Rrn Deletion Strains for Genetic Determination of Ribosomal Binding Sites. *G3 (Bethesda)* 5 (12), 2555–2557. doi:10.1534/g3.115.022301

Rackham, O., and Chin, J. W. (2005). A Network of Orthogonal Ribosome·mRNA Pairs. *Nat. Chem. Biol.* 1 (3), 159–166. doi:10.1038/nchembio719

Razi, A., Davis, J. H., Hao, Y., Jahagirdar, D., Thurlow, B., Basu, K., et al. (2019). Role of Era in Assembly and Homeostasis of the Ribosomal Small Subunit. *Nucleic Acids Res.* 47 (15), 8301–8317. doi:10.1093/nar/gkz571

Samaha, R. R., Green, R., and Noller, H. F. (1995). A Base Pair between tRNA and 23S rRNA in the Peptidyl Transferase centre of the Ribosome. *Nature* 377 (6547), 309–314. doi:10.1038/377309a0

Sharma, M. R., Barat, C., Wilson, D. N., Booth, T. M., Kawazoe, M., Hori-Takemoto, C., et al. (2005). Interaction of Era with the 30S Ribosomal Subunit. *Mol. Cell* 18 (3), 319–329. doi:10.1016/j.molcel.2005.03.028

Shine, J., and Dalgarno, L. (1974). The 3'-terminal Sequence of *Escherichia coli* 16S Ribosomal RNA: Complementarity to Nonsense Triplets and Ribosome Binding Sites. *Proc. Natl. Acad. Sci.* 71 (4), 1342–1346. doi:10.1073/pnas.71.4.1342

Steitz, J. A., and Jakes, K. (1975). How Ribosomes Select Initiator Regions in mRNA: Base Pair Formation between the 3' Terminus of 16S rRNA and the mRNA during Initiation of Protein Synthesis in *Escherichia coli*. *Proc. Natl. Acad. Sci.* 72 (12), 4734–4738. doi:10.1073/pnas.72.12.4734

Studer, S. M., and Joseph, S. (2006). Unfolding of mRNA Secondary Structure by the Bacterial Translation Initiation Complex. *Mol. Cell* 22 (1), 105–115. doi:10.1016/j.molcel.2006.02.014

Tu, C., Zhou, X., Tarasov, S. G., Tropea, J. E., Austin, B. P., Waugh, D. S., et al. (2011). The Era GTPase Recognizes the GAUCACCUCC Sequence and Binds

helix 45 Near the 3' End of 16S rRNA. *Proc. Natl. Acad. Sci.* 108 (25), 10156–10161. doi:10.1073/pnas.1017679108

Tu, C., Zhou, X., Tropea, J. E., Austin, B. P., Waugh, D. S., Court, D. L., et al. (2009). Structure of ERA in Complex with the 3' End of 16S rRNA: Implications for Ribosome Biogenesis. *Proc. Natl. Acad. Sci.* 106 (35), 14843–14848. doi:10.1073/pnas.0904032106

Vellanoweth, R. L., and Rabinowitz, J. C. (1992). The Influence of Ribosome-Binding-Site Elements on Translational Efficiency in Bacillus Subtilis and *Escherichia coli In Vivo*. *Mol. Microbiol.* 6 (9), 1105–1114. doi:10.1111/j.1365-2958.1992.tb01548.x

Wegmann, U., Horn, N., and Carding, S. R. (2013). Defining the bacteroides Ribosomal Binding Site. *Appl. Environ. Microbiol.* 79 (6), 1980–1989. doi:10.1128/AEM.03086-12

Weiss, R. B., Dunn, D. M., Atkins, J. F., and Gesteland, R. F. (1987). Slippery Runs, Shifty Stops, Backward Steps, and Forward Hops: -2, -1, +1, +2, +5, and +6 Ribosomal Frameshifting. *Cold Spring Harbor Symposia Quantitative Biol.* 52, 687–693. doi:10.1101/sqb.1987.052.01.078

Yassin, A., Fredrick, K., and Mankin, A. S. (2005). Deleterious Mutations in Small Subunit Ribosomal RNA Identify Functional Sites and Potential Targets for Antibiotics. *Proc. Natl. Acad. Sci.* 102 (46), 16620–16625. doi:10.1073/pnas.0508444102

Youngman, E. M., Brunelle, J. L., Kochaniak, A. B., and Green, R. (2004). The Active Site of the Ribosome Is Composed of Two Layers of Conserved Nucleotides with Distinct Roles in Peptide Bond Formation and Peptide Release. *Cell* 117 (5), 589–599. doi:10.1016/s0092-8674(04)00411-8

Zhu, Y., Thomas, F., Larocque, R., Li, N., Duffieux, D., Cladière, L., et al. (2017). Genetic Analyses Unravel the Crucial Role of a Horizontally Acquired Alginate Lyase for Brown Algal Biomass Degradation by Z Obellia Galactanivorans. *Environ. Microbiol.* 19 (6), 2164–2181. doi:10.1111/1462-2920.13699

Conflict of Interest: The authors declare that the research was conducted in the absence of any commercial or financial relationships that could be construed as a potential conflict of interest.

Publisher's Note: All claims expressed in this article are solely those of the authors and do not necessarily represent those of their affiliated organizations, or those of the publisher, the editors and the reviewers. Any product that may be evaluated in this article, or claim that may be made by its manufacturer, is not guaranteed or endorsed by the publisher.

frontiers in Molecular Biosciences

ORIGINAL RESEARCH
published: 03 January 2022
doi: 10.3389/fmolb.2021.787781

Deletion of the N-Terminal Domain of Yeast Eukaryotic Initiation Factor 4B Reprograms Translation and Reduces Growth in Urea

*Xiaozhuo Liu, Houtan Moshiri, Qian He, Ansuman Sahoo and Sarah E. Walker**

Department of Biological Sciences, SUNY at Buffalo, Buffalo, NY, United States

OPEN ACCESS

Edited by:
Neva Caliskan, Helmholtz Institute for RNA-based Infection Research (HIRI), Germany

Reviewed by:
Clément Charenton, INSERM U964 Institut de Génétique et de Biologie Moléculaire et Cellulaire (IGBMC), France
Sohani Das Sharma, Weill Cornell Medical Center, United States

***Correspondence:**
Sarah E. Walker
walker47@buffalo.edu

Specialty section:
This article was submitted to RNA Networks and Biology, a section of the journal Frontiers in Molecular Biosciences

Received: *01 October 2021*
Accepted: *03 December 2021*
Published: *03 January 2022*

Citation:
Liu X, Moshiri H, He Q, Sahoo A and Walker SE (2022) Deletion of the N-Terminal Domain of Yeast Eukaryotic Initiation Factor 4B Reprograms Translation and Reduces Growth in Urea. Front. Mol. Biosci. 8:787781. doi: 10.3389/fmolb.2021.787781

The yeast eukaryotic initiation factor 4B binds the 40S subunit in translation preinitiation complexes (PICs), promoting mRNA recruitment. Recent evidence indicates yeast mRNAs have variable dependence on eIF4B under optimal growth conditions. Given the ability of eIF4B to promote translation as a function of nutrient conditions in mammalian cells, we wondered if eIF4B activities in translation could alter phenotypes in yeast through differential mRNA selection for translation. Here we compared the effects of disrupting yeast eIF4B RNA- and 40S-binding motifs under ~1400 growth conditions. The RNA-Recognition Motif (RRM) was dispensable for stress responses, but the 40S-binding N-terminal Domain (NTD) promoted growth in response to stressors requiring robust cellular integrity. In particular, the NTD conferred a strong growth advantage in the presence of urea, which may be important for pathogenesis of related fungal species. Ribosome profiling indicated that similar to complete eIF4B deletion, deletion of the NTD dramatically reduced translation, particularly of those mRNAs with long and highly structured 5-prime untranslated regions. This behavior was observed both with and without urea exposure, but the specific mRNA pool associated with ribosomes in response to urea differed. Deletion of the NTD led to relative increases in ribosome association of shorter transcripts with higher dependence on eIF4G, as was noted previously for eIF4B deletion. Gene ontology analysis indicated that proteins encoded by eIF4B NTD-dependent transcripts were associated with the cellular membrane system and the cell wall, while NTD-independent transcripts encoded proteins associated with cytoplasmic proteins and protein synthesis. This analysis highlighted the difference in structure content of mRNAs encoding membrane versus cytoplasmic housekeeping proteins and the variable reliance of specific gene ontology classes on various initiation factors promoting otherwise similar functions. Together our analyses suggest that deletion of the eIF4B NTD prevents cellular stress responses by affecting the capacity to translate a diverse mRNA pool.

Keywords: eukaryotic translation, translation initiation, eIF4B, ribosome, mRNA control

INTRODUCTION

Translation initiation begins with the formation of a translation preinitiation complex (PIC) comprised of an initiator Met-tRNA•eIF2•GTP ternary complex bound to the 40S ribosomal subunit along with eIFs 1, 1A, 5 and the multisubunit eIF3. Simultaneously, mRNAs are complexed with the eIF4F complex and Ded1/Ddx3, which are proposed to unwind secondary structure and promote PIC binding to mRNA. The eIF4F complex is comprised of three factors. eIF4E binds the 5′cap structure and eIF4G. eIF4G acts as a scaffold linking the cap to the helicase, and as such binds to mRNAs, eIF4E, eIF4A, and other proteins. eIF4A is a DEAD-box RNA helicase with activity modulated by changes in conformation upon binding to RNA, eIF4G, eIF4B, and in mammalian cells, eIF4H (Mitchell et al., 2011). This complex is thought to serve multiple purposes: *1*) interactions of the 5′cap bound to eIF4E with other components of the PIC bound to eIF4G direct PIC loading to the 5′end of mRNAs, and *2*) helicase activity of eIF4A melts mRNA secondary structure near the cap and throughout the 5-prime untranslated region (5′UTR) to allow effective loading at the cap and scanning through 5′UTRs. The associated protein eIF4B promotes the activity of the eIF4F complex (Rozovsky et al., 2008; Özeş et al., 2011).

A number of observations indicate the importance of eIF4B in translating structured mRNAs and promoting the activity of eIF4A/eIF4F both *in vitro* and *in vivo* (Dmitriev et al., 2003; Mitchell et al., 2010; Sen et al., 2016). In fact, eIF4B in yeast was first discovered by two groups as both a multicopy suppressor of a temperature-sensitive eIF4A mutation, as well as a protein that interacted with antibodies against the 5′-cap complex (Altmann et al., 1993; Coppolecchia et al., 1993). This indicates important functional interaction between eIF4F and eIF4B. One model for eIF4B function suggests that eIF4B enhances eIF4A mRNA helicase activity at the step of mRNA activation or scanning to allow structured mRNA translation (Rogers et al., 2001; Özeş et al., 2011; Andreou and Klostermeier, 2014). However, recent work indicates that some classes of mRNAs have a hyperdependence on eIF4B while showing less relative dependence on eIF4A. This could suggest eIF4B performs both eIF4A-dependent and eIF4A/eIF4F-independent activities during translation, or that functions of eIF4A are universally important for translation (Park et al., 2011; Sen et al., 2015; Sen et al., 2016). These eIF4A-independent functions could stem from the ability of eIF4B to bind to the 40S subunit and promote conformational changes in the mRNA binding channel (Walker et al., 2013; Sen et al., 2016).

Yeast eIF4B can be divided into four functional domains: an N-terminal domain (NTD), an RNA-recognition motif (RRM), a 7-repeats domain, and a C-terminal domain (**Figure 1A**; (Altmann et al., 1993; Coppolecchia et al., 1993). While the RRM has a defined globular structure with conserved RNA-binding motifs (Fleming et al., 2003), the other three domains are predicted to be disordered (by analysis of the S288C eIF4B sequence in PONDR (Xue et al., 2010)). Our previous work demonstrated that eIF4B binds directly to the 40S subunit using both the NTD and 7-repeats domains of the protein, independently of the RRM (Walker et al., 2013). The 7-repeats domain consists of imperfect repetitions of a ~26 amino acid motif that can also bind directly to single-stranded RNA (Altmann et al., 1993; Coppolecchia et al., 1993; Niederberger et al., 1998; Walker et al., 2013). Binding the 40S by either the NTD or 7-repeats domain promotes the movement of a ribosomal protein, Rps20/uS10 (Walker et al., 2013). This induces changes in the conformation of multiple rRNA residues on both the solvent and subunit interfaces of the 40S near domains of Rps20/uS10 that reach into the mRNA binding channel. Both the NTD and the 7-repeats domain of eIF4B enhance its affinity to the 40S and are required for robust mRNA recruitment to the PIC, suggesting these ribosome binding activities are critical for translation. Deletion of either domain resulted in decreased rates of mRNA recruitment and translation. However, the defect conferred by deleting the seven repeats was partially rescued by increasing the concentration of the Δ7-repeats variant *in vitro* or overexpressing the Δ7-repeats protein in cells. The heightened concentration of the Δ7-repeats mutant required for maximal rate suggests the repeats must interact with the 40S or another binding partner for maximal affinity and activity. In contrast, increasing concentrations of the Δntd protein did not rescue the decreased rate, suggesting the NTD affects the mechanism by which eIF4B accelerates mRNA recruitment (Walker et al., 2013). Deletion of the NTD, but not other eIF4B domains also confers a dominant-negative overexpression phenotype in cells harboring temperature-sensitive mutant eIF4F alleles, repressing growth even under permissive temperature (Zhou et al., 2014). This suggests the NTD is needed to activate eIF4F. Deletion of either the NTD or 7-repeats domain also increases the amount of eIF4A needed to achieve maximal rate of mRNA recruitment to the PIC, suggesting both domains are needed for optimal functional interaction of eIF4A with the preinitiation complex (Walker et al., 2013). Evidence was recently provided for RNA-dependent interaction of the 7-repeats domain with eIF4A *in vitro* (Andreou et al., 2017), and for an RNA-independent interaction of eIF4B with eIF4F *in vitro* and *in vivo* (Park et al., 2013). These observations together suggest a model in which the seven repeats domain of eIF4B binds the preinitiation complex, where the NTD can effectively promote eIF4A activity or a conformation of the PIC that allows effective loading and scanning of mRNAs.

In contrast to the 40S binding activities of the NTD and the seven repeats domains, disrupting the RNA-binding activity of the RRM of yeast eIF4B did not affect growth or translation activity *in vitro* or *in vivo*, unless combined with other mutations that affect function on their own, such as deletion of the NTD or 7-repeats (Walker et al., 2013). This suggests that the RNA-binding RRM can stimulate the required function of the NTD and seven repeats, although to a limited extent which does not accelerate growth rate under standard laboratory conditions. The RRM is the only large functional domain with considerable sequence conservation between yeast and human eIF4B (Altmann et al., 1995) outside of small motifs of homology in the NTD and a segment of homology to the core sequence of a single yeast repeat just downstream of the RRM in human eIF4B.

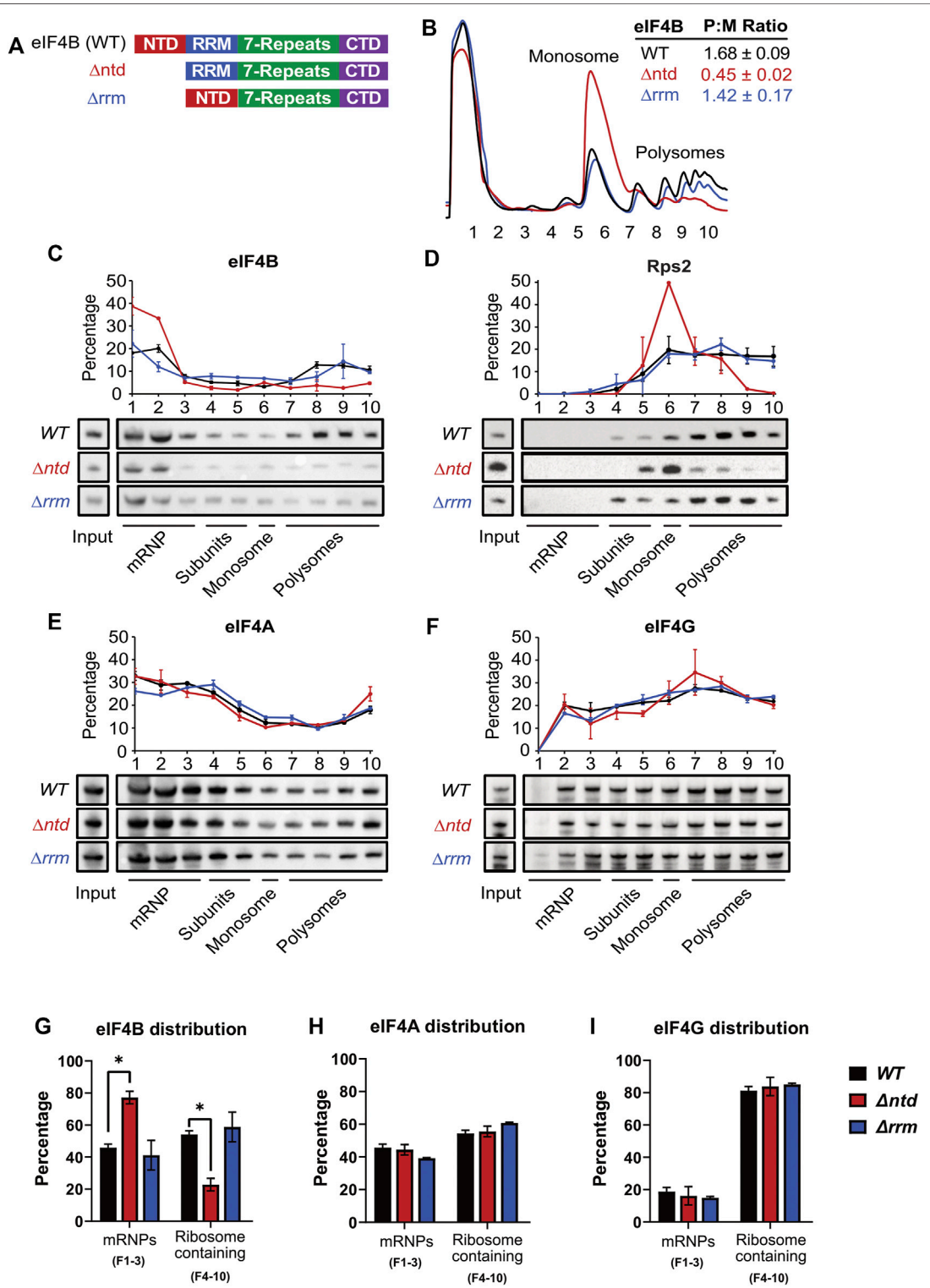

FIGURE 1 | The N-terminal domain of eIF4B binds the ribosome and promotes translation in a prototrophic yeast strain. **(A)** Schematic of eIF4B functional domains in WT, Δntd, and Δrrm constructs. **(B)** Lysates from strains harboring WT (black), Δntd (red), or Δrrm (blue) eIF4B were fractionated on 5–45% sucrose gradients and monitored by absorbance at 254 nm. Polysome to monosome (P:M) ratios were calculated by quantifying the area under the curve for the indicated monosome and polysome peaks. The Mean P:M ratios from three or more biological replicates (representative traces shown) are reported ± standard error of the mean. **(C–F)** Lysates were crosslinked with 1% formaldehyde prior to running on 5–45% sucrose gradients. The distributions of eIF4B **(C)**, Rps2 (**D**, an indicator of 40S subunits/monosomes/polysomes), eIF4A **(E)**, and eIF4G **(F)** in mRNP, subunit, monosome, and polysome fractions were determined by western blotting indicated gradient fractions. The line graphs show the mean percentages of total indicated protein (quantified across the gradient) that was present in each fraction. **(G–I)** The distributions of eIF4B **(G)**, eIF4A **(H)** and eIF4G **(I)** in mRNP vs. ribosome containing fractions were analyzed by an unpaired students *t* test. The only significant differences observed were for Δntd versus WT eIF4B distributions. Asterisk indicates *p* value ≤0.05.

These motifs in the human factor are sufficient to rescue function of yeast eIF4B variants lacking the analogous motifs, suggesting they may provide a conserved function (Zhou et al., 2014).

Here we investigated the ability of the RNA-binding RRM and the 40S-binding NTD of eIF4B to stimulate translation and growth under various stress conditions. We found that the NTD enhanced growth in conditions that require robust cellular integrity, including in the presence of 3% w/v urea. Deletion of the NTD resulted in reduced eIF4B association with ribosome fractions and large decreases in translation as expected based on our previous work. Analysis of the structural content of mRNAs that strongly depended on the NTD for translation supports the model that eIF4B is necessary to enhance translation of mRNAs with long, structured 5′UTRs that showed less enrichment with eIF4G and other closed-loop factors, and further implicates the NTD in promoting this function (Sen et al., 2016). As expected, eIF4B interaction with translating polysomes was disrupted by truncation of the NTD, in agreement with our previous claim that this domain stabilizes binding to free 40S subunits (Walker et al., 2013). The mRNAs that responded to eIF4B NTD-deletion encode cell wall, membrane and ER/Golgi-associated proteins. Further analysis of the full complement of mRNAs in gene ontology classes associated with high NTD-dependence showed that mRNAs encoding membrane and trafficking proteins, irrespective of strong NTD-dependent changes in this study, had more structured 5′UTRs than other yeast mRNAs. The mRNAs that showed relative increases when the NTD was deleted were in contrast associated with cytoplasmic proteins, and especially with cytoplasmic translation. The mRNAs in these NTD-independent gene ontology classes showed significantly less structure. The divergence in mRNA structure propensity and likewise, eIF4B-dependence, of cytoplasmic proteins versus membrane-associated factors may allow the cellular responses to various stressors garnered by the eIF4B NTD. Together these data suggest eIF4B-NTD activity is needed to reprogram translation and allow cells to adapt to diverse cellular environments.

MATERIALS AND METHODS

Construction of Yeast Strain and Plasmids

Yeast strains (**Supplementary Table S1**) YSW3 and YSW4 were generated by tetrad dissection of strain FJZ001 (*MATa/MATα, his3Δ1/his3Δ1 leu2Δ0/leu2Δ0 met15Δ0/MET15 LYS2/lys2Δ0 ura3Δ0/ura3Δ0 TIF3/ tif3Δ::hisG-URA3-hisG*) (Walker et al., 2013), followed by isolation of LYS+, HIS−, LEU−, and MET− haploid clones, and finally counterselection on 5-FOA for removal of the *URA3-HisG* cassette of the URA+ *tif3*Δ strain. *TIF3* alleles with the native promoter and terminator encoding C-terminal hexahistidine tagged-eIF4B or variants were Gibson-assembled (NEB, United States) into the BamHI site of single-copy vector pHLUM (Mülleder et al., 2012). DNA sequences of the entire PCR-amplified regions were verified in the assembled plasmids (**Supplementary Table S2**). Plasmids were transformed into YSW4 to generate prototrophic strains. Transformed strains were verified by Western blot for correct eIF4B variant expression (**Figure 2D** and **Supplementary Table S1**).

Plasmids (**Supplementary Table S2**) for monitoring translation reporter expression were constructed using the Mo-Clo yeast toolkit Golden Gate cloning system as described (Lee et al., 2015). The promoter, 5′UTR, and first 30 nucleotides of FIG2 and VBA2 genes were amplified from yeast (BY4741) genomic DNA and cloned into parts vector pYTK001 *via* BsaI assembly. An intermediate vector (pAS45) containing an *E. coli* GFP cassette (pYTK047) for screening green/white colonies by replacement of GFP was combined with the FIG2 and VBA2 parts vectors, the C-terminal Venus fusion tag (pYTK045), and a terminator part vector (pYTK053) for BsmBI assembly of the complete reporter vectors. Plasmids were verified by sequencing.

Phenotype Microarrays

Previous work showed that inclusion on the same plasmid of the four requisite metabolic genes lacking in the parental genome of the barcoded yeast knockout collection (*HIS3*, *LEU2*, *URA3*, and *MET17*) provided a selective growth advantage, regardless of whether the metabolites these genes produce were included in the media. Hence, the plasmid with four metabolic markers is effectively retained even in rich growth media without selection, and synthetic growth effects between metabolic gene deletion and the mutation of interest can be avoided (Mülleder et al., 2012). Prototrophic strains YSW5, 6, and 7 were sent to Biolog for Phenotype Microarray screening at 30°C in duplicate, using plates 1–10 and 20–25 (Biolog Inc, United States) (Bochner et al., 2001). Plates were read every 30 min for 48 h.

Yeast Growth

Yeast were cultivated in liquid or on solid (2% agar) Synthetic Drop-out (SD) media (20 g/L glucose, 1.71 g/L yeast nitrogen base without amino acids containing 5 g/L ammonium sulfate; Sunrise Scientific Products, United States) at 30°C. For assays with additives, yeast cells from an overnight culture in SD media were diluted to an OD_{600} of 0.05 in SD media or SD media supplemented with additive (e.g. 2% or 3% urea), and allowed to grow to mid-log phase with shaking at 30°C, unless otherwise noted. Automated growth curves were performed in 96-well plates (200 µl SD and additives per well) by taking OD_{600} measurements every 2 h for 48 h while incubating at 30°C with double-orbital shaking in a Spark plate reader (Tecan, Switzerland). The same trends in growth rate were observed on solid media (data not shown).

Analysis of Polysome:Monosome Ratios

Polysome analysis was performed as described previously (Lee et al., 2007; Walker et al., 2013). For **Figure 1B**, yeast cells were cultured in SD medium with or without additives as noted at 30°C to an OD_{600} of 1.5. Cycloheximide (Gold biotechnology, United States) was added to a final concentration of 50 µg/ml and incubated for 5 min at 30°C with shaking before collecting cells by pelleting in centrifuge bottles packed with ice. Pellets were resuspended in 1/3 of the pellet weight of breaking buffer (20 mM Tris-HCl at pH 7.5, 50 mM KCl, 10 mM MgCl2, 1 mM DTT, 200 µg/ml heparin, 50 µg/ml cycloheximide, and one Complete

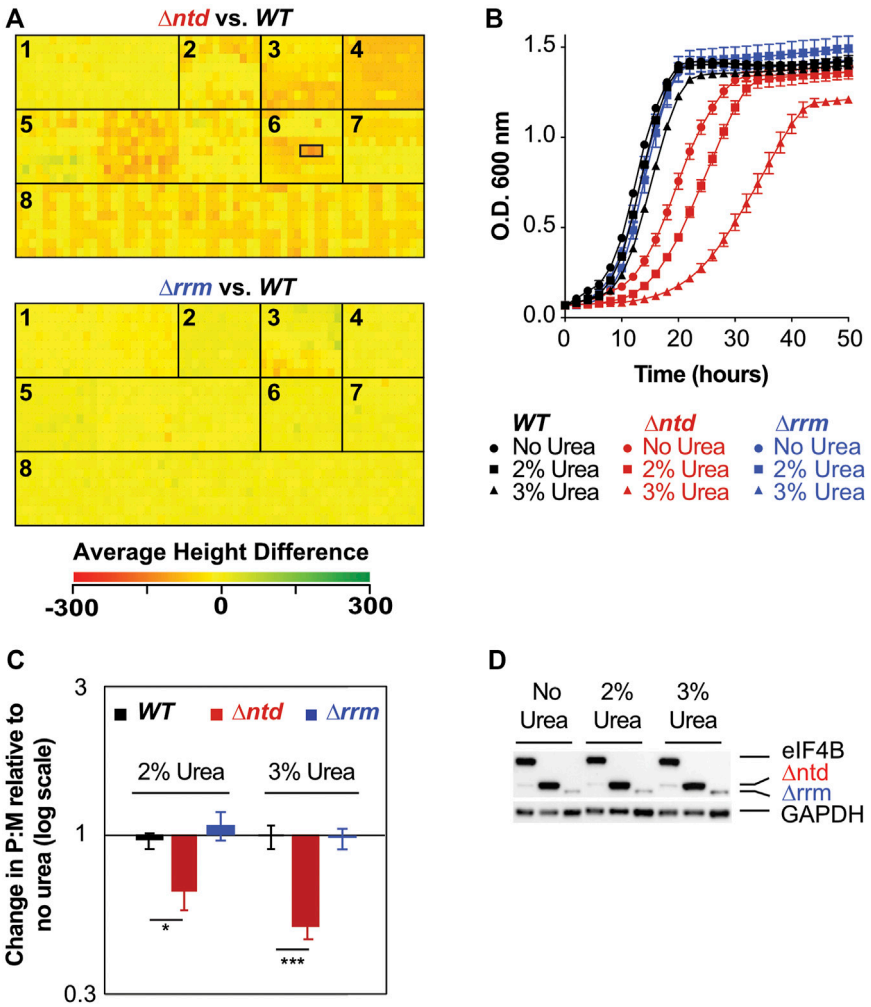

FIGURE 2 | eIF4B binding to the 40S promotes resistance to stressors that challenge cellular integrity through changes in translation. **(A)** Heatmap of average height differences for cellular fitness between the NTD **(top)** or RRM **(bottom)** deletion mutant (green) and WT (red) under 1440 metabolic and chemical conditions as assayed by Phenotype microarray, which includes seven panels in 15 96-well plates: 1. Carbon Sources; 2. Nitrogen Sources; 3. Phosphorus and Sulfur Sources; 4. Nutrient Supplements; 5. Peptide Nitrogen Sources; 6. Osmolytes; 7. pH; and 8. Chemical Sensitivity. Wells containing 2, 3, and 4% urea are outlined by a black box, left to right, for Δntd. 3% Urea gave the largest difference in WT and Δ*ntd* fitness. There were no conditions that gave a significant change for Δrrm **(B)**. Growth curves of WT (black), Δntd (red), and Δrrm (blue) grown with 0% (circles), 2% (squares), or 3% urea (triangles). Results from biological triplicates ± SEM are shown. **(C)** Relative change in polysome to monosome (P:M) ratio upon exposure to urea was determined as in 1B with representative traces shown in **Supplementary Figure S2** in the presence and absence of 3% urea. Biological triplicates ± SEM are shown with *p* values from Student's t test indicated (*$p < 0.05$). **(D)** eIF4B levels in WT, Δntd, and Δrrm strains after growth with 0, 2%, or 3% urea in Synthetic Dextrose media.

EDTA-free Protease Inhibitor Tablet [Roche]/50 ml buffer), dropped into liquid nitrogen, and lysed in a Nitrogen Mill for 10 Cycles following a precool of 15 min with the following parameters: 1 min run, 2 min cool, rate = 15 (Spex Sample Prep, United States). 25 A_{260} units of lysates were resuspended in 1.5 volumes of the pellet weight of ice-cold breaking buffer and clarified by spinning at 14,000 rpm for 15 min at 4°C prior to separation by velocity sedimentation on 5–45% sucrose gradients (20 mM Tris-HCl [pH 7.5], 50 mM KCl, 10 mM $MgCl_2$, 1 mM DTT, 5–45% sucrose mixed using the 5–45% SW-41 gradient program on the BioComp gradient station) by centrifugation at 39,000 rpm for 2.5 h at 4°C in a Beckman SW41 rotor. Gradient fractions were separated on a gradient station (BioComp, Canada) while scanning at 254 nm. The areas under the monosome and polysome peaks, determined in GraphPad Prism software, were used to calculate the P/M ratio.

Analysis of Initiation Factor Association With Subunits and Polysomes by Crosslinking and Gradient Ultracentrifugation

To monitor association of eIF4B and other proteins with 40S subunits, formaldehyde crosslinking analysis was performed as described (Herrmannová et al., 2020) with the following differences: Yeast cells were grown to an OD_{600} of ~0.8 in SD

media at 30°C. Cultures were poured into bottles packed with ice containing formaldehyde for a final concentration of 2% and incubated for 60 min prior to collection and lysis. Cells were lysed in a nitrogen mill as described above and resuspended to 20 A_{260} units per 300 µl. 300 µl of crosslinked lysates were then loaded and separated by spinning at 41,000 rpms for 5 h on 7.5–30% sucrose gradients in an SW-41 rotor, and 0.63 ml fractions were collected upon fractionation on a Biocomp gradient station. Fractions 1–2 were combined prior to loading. Fractions up to the 40S peak were analyzed by western analysis. Three biological replicates were performed.

For observing polysome association, Cycloheximide was added to the culture to a final concentration of 50 µg/ml and incubated for 5 min at 30°C with shaking before harvesting cells on ice. Cells were lysed and resuspended in BBK buffer as above, then formaldehyde was added to the resuspended lysates at a final concentration of 1%. Crosslinking was carried out for 30 min on ice before quenching with glycine at 0.1 M. Crosslinked cell lysates were layered on 5–45% gradients and 10 1 ml fractions were collected for analysis by western blotting (Herrmannová et al., 2020). Two biological replicates were performed.

Western Analysis

Antibodies and samples were used at concentrations that showed linear increases when samples were titrated. TGS and TGX-Stain-free gels were transferred to PVDF membranes using the Trans-blot Turbo system (Biorad, United States). Visualization of blots was performed using BioRad ECL or ECL Max sensitivity HRP substrate as needed for the secondary antibody. When blotting the same protein on multiple blots for comparison, the acquisition time was kept approximately the same. The stain-free visualization of total protein was carried out using a Biorad touch imager according to the manufacturer's protocol.

To verify that eIF4B variants were expressed under stress conditions, yeast cells were grown in SD media with or without 2 or 3% urea, and harvested at an OD_{600} of 1.0. Whole cell extracts (WCEs) were prepared by extraction with trichloroacetic acid (TCA) and subjected to Western blot analysis as described previously (Walker et al., 2013) using antibody against the His6 epitope (EMD Millipore/Novagen 70796, 1:2000 dilution) Experiments were repeated three or more times from biological replicates.

For analysis of eIF4B position within gradients, 0.5 ml of each gradient fraction was precipitated by addition of 1 ml 100% Ethanol and spinning for 30 min at 13,000 × g, resuspended in SDS loading buffer, and resolved by SDS-PAGE, followed by Western blotting using anti-His antibody. 40S subunit (and 80S/polysome) containing fractions were verified from the same samples by blotting yeast ribosomal small subunit protein Rps2 (Aviva ARP63572_P050, 1:2000 dilution.) Rabbit antibodies to purified recombinant yeast eIF4A (1:20,000 dilution) and eIF4G1 (1:1000 dilution), generated by Invitrogen/Pierce custom antibody services and verified against the recombinant proteins, were used to determine the position of those proteins within gradients (Liu et al., 2019). Each experiment was repeated three or more times from biological replicates.

To determine changes in *FIG2* and *VBA2* translation reporter fusions, TCA-precipitated lysates were prepared as above from cells grown in media with or without 3% urea to an OD_{600} of 0.5–0.8. Lysates were separated on a stain-free SDS-PAGE gel (Bio-rad), then blotted with mouse anti-GFP antibody (Roche 11814460001, 1:1000 dilution) and anti-mouse-HRP secondary (Cell Signaling 7076, 1:3500). GFP was normalized to total protein bands per lane (visualized by a stain-free scan on a Bio-rad gel doc), which was also normalized prior to loading lysates. Each experiment was repeated at least two times from biological replicates.

RiboSeq and RNASeq Library Preparation

Ribosome footprint profiling was conducted as described (Ingolia et al., 2009; Guydosh and Green, 2014; McGlincy and Ingolia, 2017) with minor modifications. Yeast cells at an OD_{600} of approximately 0.8 were rapidly harvested by vacuum filtration through a 0.45 µm Whatman cellulose nitrate membrane filter (GE Healthcare Life Sciences, United States) at room temperature by scraping the slurry into liquid nitrogen. Cells were lysed as above in a Nitrogen mill, and thawed and suspended in lysis buffer (20 mM Tris [pH 8], 140 mM KCl, 1.5 mM $MgCl_2$, 1% Triton X-100, 100 µg/ml cycloheximide). 25 A_{260} units of extract were treated with 87.5 Units of RNase If (M0243, NEB, United States) for 1 h at 22°C on a rotator, then separated on 10–50% sucrose gradients (20 mM Tris [pH 8], 140 mM KCl, 1.5 mM $MgCl_2$, 1 mM DTT, 100 µg/ml cycloheximide, 10–50% sucrose) by centrifugation at 40,000 rpm for 3 h at 4°C in a Beckman SW41 rotor and fractionated as above. Ribosome-protected RNA footprints were purified from the nuclease-treated monosome fraction by addition of SDS to 0.8% at 65°C, followed by extraction with acid phenol [pH 4.5] (Ambion, United States) and then chloroform/isoamyl alcohol extraction. 300 mM NaOAc [pH 5.2] was added to the aqueous phase and RNA was precipitated with one volume of isopropanol before resuspending in 10 mM Tris-HCl [pH 8]. RNA footprints from 25 to 35 nt were size-selected on a 15% denaturing PAGE gel, eluted by crushing and soaking gel fragments in RNA elution buffer (300 mM NaOAc [pH 5.5], 1 mM EDTA, 0.1 U/µl SUPERaseIn (Life Technologies, United States)), and dephosphorylated using T4 Polynucleotide Kinase (M0201, NEB, United States) prior to isopropanol precipitation and resuspension in 10 mM Tris [pH8]). A pre-adenylated universal linker (5′-rAppCTGTAGGCACCATCAAT-NH_2-3′) was prepared in house or purchased from NEB (S1315S) and ligated to the 3′ ends of the dephosphorylated footprints using T4 RNA Ligase 2, truncated (MO242L, NEB). rRNA was depleted using the Yeast Ribo-Zero Gold rRNA removal kit (Illumina, United States). First strand synthesis was performed with Superscript III (Life Technologies, United States) and reverse transcription primer NINI9 (5'-/5Phos/ AGA TCG GAA GAG CGT CGT GTA G GGA AAG AGT GTA GAT CTC GGT GGT CGC/SpacerC18/ CAC TCA/SpacerC18/ TTC AGA CGT GTG CTC TTC CGA TCT ATT GAT GGT GCC TAC AG), followed by circularization with Circligase (Epicenter, United States). Circularized cDNA was then PCR amplified using primer NINI2 (AAT GAT ACG GCG ACC ACC GAG ATC TAC

AC) and a primer with a barcode (CAA GCA GAA GAC GGC ATA CGA GAT XXX XXX GTG ACT GGA GTT CAG ACG TGT GCT CTT CCG), where XXXXXX denotes a six-nucleotide-barcode used to distinguish samples run in the same lane (**Supplementary Table S4**). For RNA-seq, total RNA was isolated from the same cell extracts using SDS/hot acid phenol/chloroform extraction. The Ribo-Zero Gold Yeast kit was used to remove rRNA, and total RNA was randomly fragmented by incubating for 20 min at 95°C in freshly made fragmentation buffer (100 mM sodium carbonate-bicarbonate [pH 9.2], 2 mM EDTA). RNA was then precipitated and fragments of 40–60 nt were purified from a denaturing PAGE gel, and library generation carried out as above. Ribo-Seq and RNA-Seq were performed for two independent cultures for each condition (WT and Δntd cells grown in SD both with and without 3% Urea), and the 16 libraries sequenced in two lanes with 150 bp reads on an Illumina HiSeq 4000 instrument by Genewiz.

Analysis of Ribosome Profiling Libraries

The Ribogalaxy platform (https://ribogalaxy.ucc.ie, (Michel et al., 2016)) was used for trimming linker sequences (Cutadapt version 1.1.a; (Martin, 2011)), subtractive alignment of *S. cerevisiae* non-coding RNAs (Bowtie version 1.1.a; (Langmead et al., 2009); using the R64.2.1 S288C genome from Saccharomyces Genome Database (SGD, RefSeq ID: 285498), alignment of rRNA subtracted libraries to the transcriptome (Bowtie version 0.1.3 using the SGD transcriptome dataset and counting of uniquely mapped reads (Ingolia et al., 2009) using Ribocount version 0.3.1. Statistical analyses of differences in total RNA counts, ribosome footprints, or TE values between WT, mutant, urea-treated, and untreated samples were conducted using DESeq2 and are presented in **Supplementary Table S6** along with the calculated false discovery rates (Love et al., 2014). Gene ontology categorization of library-specific differences was performed at SGD, using all genes within the four classes, NTD dependent increase/decrease in urea, NTD dependent increase/decrease in SD (Thompson et al., 2016). Cumulative PARS scores (Kertesz et al., 2010) and strong-closed loop association (Costello et al., 2015) for yeast mRNAs were obtained from published works and were analyzed for those mRNAs showing reduced or enhanced dependence on the NTD with and without urea, as described previously for cells lacking eIF4B (Sen et al., 2016).

Gene set enrichment analysis (GSEA) was carried out by using the curated gene sets of Gene Ontology for *S. cerevisiae* (http://ge-lab.org/gskb/), (**Supplementary Figure S5**) The list of the entire detectable genes with $\log_2$ ratios derived from each comparison was used for the pre-rank GSEA, and we followed the standard procedure described by GSEA user guide (http://www.broadinstitute.org/gsea/doc/GSEAUserGuideFrame.html). The nominal *p*-value is the statistical significance of the enrichment score.

qRT-PCR

Cell lysates were prepared and 12 fractions were collected from polysomes fractionated using the protocol for Riboseq gradient preparation above (without nuclease treatment.) 0.3 ml of each gradient fraction was spiked with equal amounts of control RNA (Fluc mRNA, Trilink Biotechnologies, United States), then total RNA was extracted using the hot acid phenol-chloroform method (Thompson et al., 2016). First strand synthesis was performed with iScript Advanced Reverse Transcriptase (Biorad, United States) using oligo-dT primers and random hexamer primers. Quantitative PCR was performed with iQ SYBR Supermix reagents (Biorad, United States) using CFX384 Touch Real-Time PCR detection system (Biorad, United States) two times per sample. Gene-specific primer sequences are listed in **Supplementary Table S3**.

RESULTS

Previous work demonstrated that the N-terminal domain (NTD) of eIF4B promotes both affinity for the 40S subunit *in vitro* and recruitment of mRNAs to the preinitiation complex *in vitro* and *in vivo*, while the RRM of eIF4B is dispensable in auxotrophic yeast strains (Walker et al., 2013; Zhou et al., 2014). Given the diverse dependencies of cellular mRNAs on eIF4B function (Sen et al., 2016), we thought it likely that differential mRNA selection promoted by eIF4B could confer phenotypic advantages. We wondered if the ability of the NTD to promote translation would afford cells the ability to resist different stressors, and whether the RRM could provide additional function under stress, so we constructed prototrophic strains for phenotype microarray analysis. We previously reported that deletion of the NTD conferred slow growth and cold-sensitivity in a strain auxotrophic for histidine, uracil, and methionine on solid media (Coppolecchia et al., 1993; Walker et al., 2013). For this work, an eIF4B null mutant was transformed with a plasmid that complemented all four existing auxotrophic markers and provided a WT, Δntd, or Δrrm eIF4B gene copy (*TIF3, tif3 Δntd,* or *tif3 Δrrm*) under the native promoter and terminator (**Figure 1A**). As previously reported, deletion of the NTD, but not the RRM reduced growth rate (**Figure 2B**, (Walker et al., 2013)).

Polysome profiles from these prototrophic strains expressing WT, Δntd, and Δrrm eIF4B confirmed that NTD deletion led to a gross reduction of polysomes and an increase in monosomes in the mutant (**Figure 1B** and **Supplementary Figure S2**), indicating the NTD promotes global translation initiation *in vivo* in a prototrophic background. RRM deletion had only a minor effect on polysome to monosome ratio when expressed from this single copy plasmid (**Figure 1B**, blue), in agreement with our previous findings (Walker et al., 2013).

The NTD of Yeast eIF4B Enhances Association With Ribosome Complexes *In Vivo*

We previously reported that deletion of the NTD decreased binding affinity of eIF4B for purified 40S subunits. In addition, deletion of the NTD decreased the rate constants and endpoints of mRNA binding to the PIC *in vitro*, while affecting the conformation of two areas of the rRNA near protein RPS20/uS10 (Walker et al., 2013). To determine

whether deletion of the NTD affected association of eIF4B with ribosomes in yeast, we performed velocity gradient fractionation of formaldehyde-crosslinked lysates followed by Western blotting of eIF4B, eIF4A, eIF4G, and Rps2. We performed two types of gradients to observe changes in association of eIF4B with both translating ribosome complexes and 40S subunits and PICs as a function of NTD and RRM deletion (**Figures 1C–I** and **Supplementary Figure S1**). Running crosslinked lysates on a 5–45% gradient effectively separates polysome-, monosome-, and mRNP-fractions. We then blotted for eIF4B in each fraction of the gradient and determined distribution of eIF4B within each fraction of the gradient. Importantly, we found that ~55% of WT eIF4B comigrated with Rps2/40S subunit-containing fractions (**Figures 1C,D** fractions 4–10, **Figure 1H**), both as part of the 40S/PIC and moreso with the later fractions containing translating polysome complexes, which make up more of the ribosome pool. Upon deletion of the NTD we saw that Rps2 shifted from later to earlier fractions, confirming the polysome to monosome shift observed by UV spectroscopy in this paper (Compare **Figures 1B,D**) and in prior work (Walker et al., 2013). This indicates deletion of the NTD led to less ribosomes associated with mRNAs, suggesting reduced translation initiation rate in these cells, as we previously reported. In addition, we found that upon deletion of the NTD, eIF4B position in the gradient was shifted such that ~80% of the protein moved to the first two fractions that lack 40S subunits and ribosomes (**Figure 1C**, compare black and red.) This is in contrast to deletion of the RRM, which conferred only a minor decrease in translating ribosome capacity, judged by similar polysome:monosome ratio as WT (**Figure 1B**, compare black and blue), and also did not grossly affect eIF4B association with translating ribosomes (**Figures 1C,D**).

Ultracentrifugation of crosslinked lysates on 7.5–30% sucrose gradients optimally separates 40S/PIC fractions (**Supplementary Figure S1**) We found that WT eIF4B was present in fractions 10–13 that contain RPS2 and indicate 40S, 43S, and 48S complexes. As we saw in **Figure 1**, eIF4B was also present in early fractions containing mRNPs (**Supplementary Figures S1A,C**). Deletion of the NTD reduced the amount of eIF4B in these Rps2-containing fractions by 93%, with increased eIF4B in early fractions containing proteins and mRNPs.

We also found that while the RRM did not change the amount of eIF4B comigrating with the overall ribosome pool (**Figure 1**), deletion of this domain did decrease occupancy of eIF4B on 40S/PICs, although not to the extent observed for NTD deletion, which nearly eliminated eIF4B occupancy in PIC fractions (**Supplementary Figure S1**). It is notable that deletion of the RRM decreased the concentration of eIF4B in cells (**Figure 2D**), and was previously shown to have a minor effect on 40S binding affinity and apparent affinity for the PIC in an mRNA recruitment assay (Walker et al., 2013), so this decrease in RRM occupancy of PICs outside of polysomes could be a reflection of that decreased ribosome affinity.

As a control we blotted the same gradient fractions for additional 48S components, eIF4A and/or eIF4G (**Figures 1E,F** and **Supplementary Figure S1B**). In contrast to eIF4B, we found that eIF4A and eIF4G remained distributed across gradient fractions when the NTD or RRM of eIF4B were deleted. This suggests the affinity of eIF4A and eIF4G for the PIC are not mediated by eIF4B. Moreover, this suggests that shift of Δntd eIF4B from polysome and 40S fractions to ribosome-free fractions is the result of decreased ribosome binding affinity of the mutant, and less likely to be due to eIF4F not associating with mRNPs as a result of eIF4B inactivation, since these other components of 48S PICs did not show a PIC and polysome to mRNP shift.

Deletion of the NTD of eIF4B Results in Decreased Resistance to Stressors and Associated Decreases in Translation

To determine conditions under which the NTD of eIF4B, which promoted association with ribosomes, plays a specific role in regulating growth and translation, we performed phenotype microarrays of cells expressing WT or Δntd eIF4B from a single copy plasmid that also restored nutrient prototrophy. As an additional control, we performed phenotype microarray analysis on cells expressing Δrrm eIF4B. Phenotype microarray analysis was not performed on cells expressing eIF4B lacking the seven repeats or a strain lacking eIF4B entirely, because the growth rates of these strains are too slow under optimal growth conditions to clearly assess additional effects of stressors in these assays. Phenotype microarray analysis showed a large number of conditions in which the prototrophic Δntd eIF4B-expressing strain grew at a reduced rate compared to the wild-type eIF4B expressing cells (**Figure 2A**). The strongest responses (**Supplementary Table S5**) include osmolytes, detergents, a number of peptides as nitrogen sources, and antibiotics. Urea, which gave the strongest negative phenotype when present at 3% w/v in the media, acts as a denaturing agent, can cause membrane blebbing at high concentrations (Lambert and Draper, 2012; Necas and Svoboda, 1973), and can readily cross the yeast cell wall and membrane to act as a nitrogen source (Cooper and Sumrada, 1975). Tamoxifen, which targets the estrogen receptor in higher eukaryotes, targets the calmodulin protein in yeast, which regulates stress responses through Hog1 interaction (Dolan et al., 2009; Kim et al., 2016). Poly-L-Lysine can act as a cationic detergent or a charged adherent for various molecules, and likely interacts with the cell wall or membrane. The strain lacking the NTD of eIF4B also showed heightened sensitivity to antibiotics that target the small ribosomal subunit, apramycin sulfate and to a lesser extent tobramycin. WT yeast are not sensitive to these antibiotics, which when combined with the sensitivity to various salts (Potassium chloride, Chromium chloride, and to a lesser extent, sodium chloride) and other phenotypes described above, suggests a defect in membrane and/or cell wall permeability in the mutant. Growth defects were verified for Δntd-expressing cells in the presence of urea, which conferred the largest reduction in the mutant (**Figure 2B**, red). These experiments confirmed that WT growth rate is nearly unaffected by urea (**Figure 2B**, black) while the mutant shows slow growth. In contrast, deletion of the RNA-binding RRM domain, which diminishes *in vitro* RNA-binding affinity (Walker

et al., 2013), conferred no large reproducible advantage or hindrance in the phenotype microarray, and supported levels of growth similar to WT eIF4B, suggesting the RNA-binding activity of eIF4B, at least that provided by the RRM, is dispensable for growth in all conditions tested (**Figure 2B**, blue). Together these results suggest the eIF4B 40S-binding NTD is required for resistance to a number of growth conditions that challenge cellular integrity, and that the mutant may have a defect in membrane and/or cell wall permeability.

To further investigate the mechanisms by which the NTD promoted growth in the presence of stressors, we compared polysome traces for WT and Δntd eIF4B-expressing cells grown in the presence and absence of 2% or 3% urea (**Figure 2C**, traces shown in **Supplementary Figure S2**). Whereas WT eIF4B-containing cells showed minor decreases in polysome to monosome (P:M) ratio upon addition of either concentration of urea (7% reduction in 2 and 10% reduction in 3% urea; **Figure 2C**, black), Δntd cells showed further 36 and 50% decreases in P:M ratio due to urea exposure (**Figure 2C**, red). In contrast, deletion of the RRM resulted in less than 5% change in P:M ratio (**Figure 2C**, blue).

The reduction in translation conferred by NTD deletion was not due to altered levels of eIF4B, as immunoblotting for a His tag on the eIF4BC-terminus showed similar protein levels when grown in media with varied urea concentrations (**Figure 2D**). As noted before (Walker et al., 2013), deletion of the RRM resulted in reduced detection of that protein. As previously stated (Walker et al., 2013), the reduction in Δrrm protein levels without a large decrease in polysome:monosome levels or growth rate suggests eIF4B may normally be present in excess of what is required to stimulate translation and growth. While perplexing that the factor level can be reduced to such a large extent without corresponding functional defects, this is in agreement with the observation that targeted reduction of WT eIF4B levels by ~55–75% resulted in only a minor reduction in translation rate in yeast (cells retained ~80–95% of WT translation rate, (Firczuk et al., 2013).) However, the level of detectable Δrrm protein, while lower than that of WT and Δntd eIF4B, was unaffected by urea addition, suggesting urea did not affect the expression or stability of the protein. Together, these data suggest interactions and activities promoted by the NTD within WT eIF4B allow robust translation in the presence of urea.

Activities Supported by the NTD Promote Translation of mRNAs Encoding Membrane-Associated Proteins

We next performed ribosome profiling on the yeast cells expressing WT or Δntd eIF4B, both with and without urea to determine how eIF4B•40S association affects translation of individual mRNAs. Ribosome profiling maps the positions of translating ribosomes on mRNAs to determine which sequences are translated more and less effectively in response to changes. We prepared illumina-indexed cDNA libraries for RNAseq and Riboseq from WT and Δntd eIF4B-expressing cells in the presence or absence of 3% urea. Comparison of replicates indicates sufficient reproducibility for each sample, with slightly higher variability in the Riboseq libraries from Δntd eIF4B-expressing cells with 3% urea (**Supplementary Figure S3**). This sample showed the strongest global repression of translation by polysome:monosome assessment (**Supplementary Figure S2**) and therefore had the least ribosome footprints, so the increased noise is expected. After mapping and quantifying footprints on RNAs in the yeast transcriptome, we compared the $\log_2$fold-changes in RNAseq, Riboseq, and TE (translation efficiency, the ratio of Riboseq/RNAseq) in response to urea exposure in WT versus the urea-dependent change ($\log_2$fold change in TE for the same strain with and without urea) in Δntd eIF4B-expressing cells (**Figure 3** and **Supplementary Figure S3** and **Supplementary Table S6**). Changes in individual RNA levels in response to urea were more similar between the two strains (**Figure 3A**, r = 0.622), while changes in ribosome footprints and TE for individual RNAs in response to urea showed less correlation between the two strains (**Figure 3B**, Riboseq, r = 0.361; 3C, TE, r = 0.156). This is further evidenced by evaluation of the RNAs with ≥1.5-fold increase in RNAseq, Riboseq, and TE in response to urea. There were fewer RNAs overall showing ≥1.5-fold urea-dependent increases in RNA levels (**Figure 3D**; WT = 39, Δntd = 108). In contrast, there were large numbers of RNAs with ≥1.5-fold changes in Riboseq (**Figure 3E**, WT = 141 RNAs, Δntd = 543 RNAs) and TE in response to urea (**Figure 3F**, WT = 210 RNAs, Δntd = 163 RNAs), both in the WT and Δntd eIF4B-expressing cells. The pools of RNAs showing increased TE upon exposure to urea were almost completely distinct in control cells versus those RNAs whose TE increased in the Δntd mutant (3.8% of the WT TE change was also observed in Δntd, which represented 4.9% of the Δntd change; p value for overlap = 0.13). This is in contrast to the urea-dependent changes observed for RNA and Riboseq, in which the normal WT response to urea was represented significantly in the pools of RNAs also showing changes in the mutant (RNASeq, 44% of WT RNA change occurred in Δntd, $p = 3.54 \times 10^{-21}$; Riboseq, 38% of the WT Riboseq change occurred in Δntd, $p = 5.55 \times 10^{-24}$.) These overlapping RNAs constituted considerably less of the RNA and riboseq changes in Δntd (RNASeq, 16% of Δntd change; Riboseq, 9.9% of Δntd change overlaps with WT change). It is important to note that while there are more RNAs showing a urea-dependent increase in ribosome footprint density in Δntd than WT, the Δntd cells show an overall decrease in global translation initiation capacity as evidenced by decreased P:M ratio (**Figures 1B**, **2C**). Together these data suggest that the mutation primarily prevents increased ribosome loading of specific mRNAs in urea, but that there are also dysregulated changes in RNA levels in the mutant.

Changes in ribosome occupancy of nine selected RNAs were verified by performing qRT-PCR on RNA from polysome gradient fractions (**Figure 1B** and **Supplementary Figure S4**) of cells expressing WT and Δntd eIF4B in the presence and absence of 3% urea in the growth media. The trends observed by ribosome profiling were confirmed by this independent method for mRNAs and 18S rRNA (**Supplementary Figure S4** and **Supplementary Table S10**). Moreover, to determine whether changes in ribosome footprint density correlated with changes in

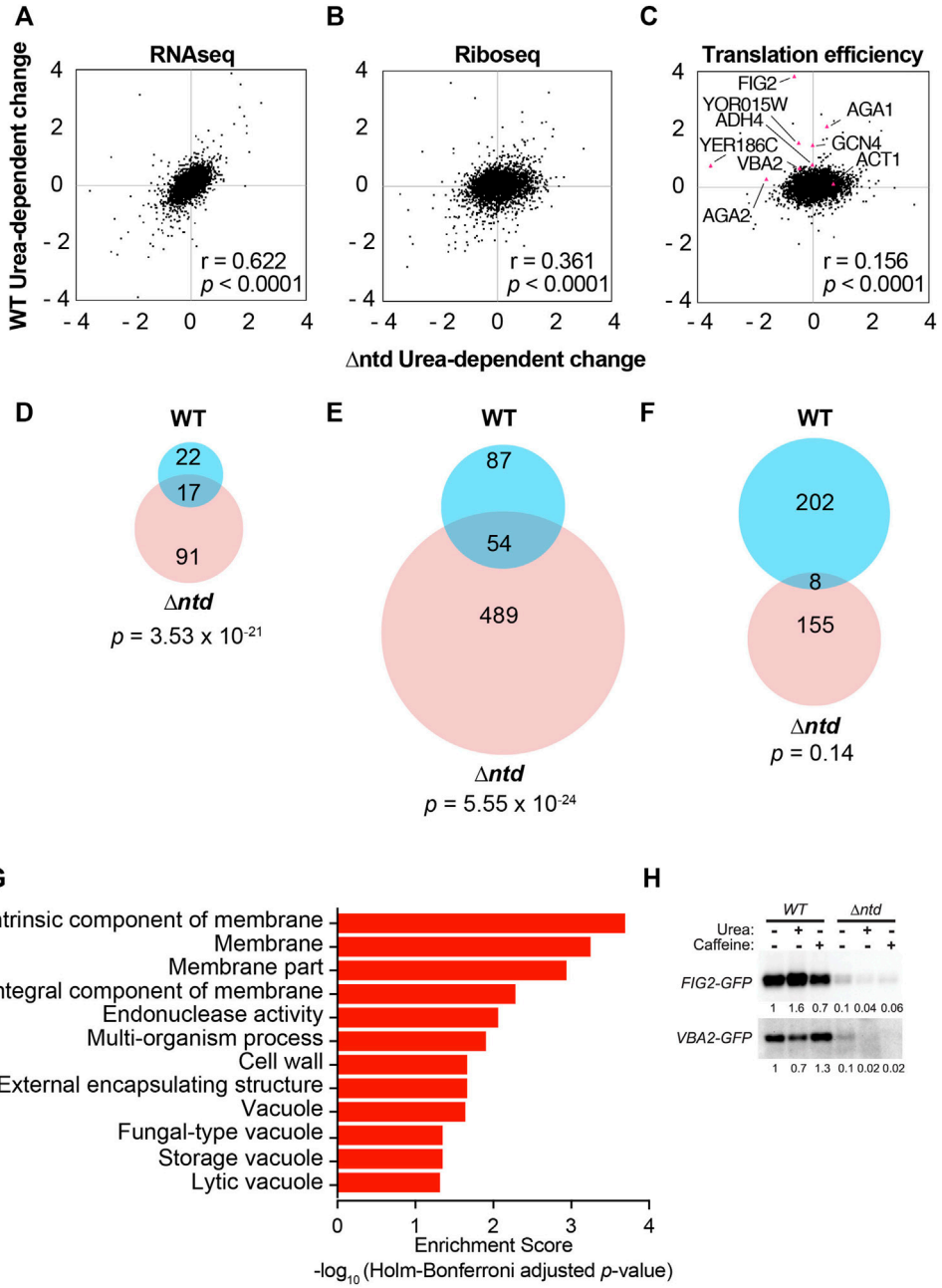

FIGURE 3 | The NTD of eIF4B promotes translation of mRNAs encoding proteins associated with the membrane and cell wall. **(A–C)** Comparison of Log_2 values for changes in RNAseq **(A)**, Riboseq **(B)**, or TE **(C**, Translation efficiency) in response to 3% urea for WT are plotted vs. the Log_2 values for changes observed in the NTD deletion mutant for each of the 4070 genes with measurable expression in each group. Nine mRNAs are indicated in **(C)**, which were analyzed by qRT-PCR of polysome gradient fractions in **Supplementary Figure S3** Pearson correlation coefficients are shown. **(D–F)** Overlap of urea-dependent genes exhibiting 1.5-fold or greater increase in RNAseq **(D)**, Riboseq **(E)**, or TE **(F)** for WT and Δ*ntd*. The Fisher's exact *p*-values were shown to indicate the statistical significance of overlap between two datasets. **(G)** Gene ontology analysis for urea-dependent RNAs (e.g. increased TE in WT in response to urea.) **(H)**. Western analysis of GFP translation reporters. The 5′UTR and first 30 nucleotides of the FIG2 and VBA2 genes were fused to GFP in a plasmid under the native promoters for each. Indicated transformants of WT and Δntd eIF4B-expressing yeast were subjected to anti-GFP western analysis following growth in the absence or presence of 3% urea or 1.5 mg/ml caffeine. The fractions of reporter band intensity per total protein bands for each lane on the gel were normalized to WT eIF4B without additive for each reporter.

protein production, we designed two translation reporters in which the 5′ UTR and first 30 nucleotides of two RNAs that showed NTD-dependent reductions (*FIG2* and *VBA2*) were cloned in frame in front of a GFP gene (**Supplementary Table S2**). Western blotting for GFP in extracts of cells harboring both a *FIG2-GFP* reporter and WT or Δntd eIF4B showed that addition of urea to WT cultures increased the level of FIG2-GFP protein by 1.6-fold (relative to total protein quantified per lane on gel after

loading a normalized amount of lysate in each lane; **Figure 3H**). In contrast, addition of urea to WT cells did not increase steady state levels of VBA2-GFP, and instead resulted in a minor decrease (**Figure 3H**). This result is consistent with the increased polysome association observed for *FIG2* upon urea addition, but little to no change in polysome association observed for *VBA2* in WT cells upon urea addition (**Supplementary Figure S4**). In addition to monitoring the effects of urea, we determined the effect of caffeine on production of these reporters. Caffeine severely impaired growth of the Δntd mutant in the phenotype microarray assay (**Figure 2A** and **Supplementary Table S5**), so we reasoned that it may also affect reporter protein production if both conditions require function of eIF4B's NTD. We found that caffeine incurred a modest decrease in *FIG2-GFP* production and a minor increase in *VBA2-GFP* production in the *WT* strain. In contrast, large decreases in translation were observed upon addition of caffeine in the Δ*ntd* mutant, leading to little production of either reporter, even though *WT* and Δ*ntd* cells were grown to the same degree prior to the western. Importantly, deletion of the NTD reduced the steady state levels of both reporter proteins by 90% or more, supporting a claim that reduced translation initiation upon deletion of the NTD may lead to reduced levels of some proteins that are highly reliant on eIF4B in order to be synthesized. GFP production in both strains was also verified by following fluorescence, and accumulated at a reduced rate in Δntd cells in the presence of urea (data not shown). Together these data suggest that the eIF4B•40S binding NTD may confer changes in growth by differentially affecting translation of specific mRNAs in response to stressors, although further analyses of proteome changes are needed to support that claim.

To understand how eIF4B NTD-dependent TE changes relate to enhanced growth in urea, we first performed gene ontology (GO) analysis of the mRNAs showing ≥1.5-fold increased TE in response to urea in WT or mutant cells (**Figure 3G** and **Supplementary Figure S5**). Of the 202 mRNAs with ≥1.5-fold increased translation in WT cells upon exposure to urea, 102 mRNAs were associated with the parental membrane (GO) term. Significant numbers of mRNAs were also associated with the cell wall, cellular periphery, and other related terms, suggesting the eIF4B NTD enhanced translation of mRNAs encoding proteins that remodel or otherwise localize to the cellular membrane. In contrast, of 155 mRNAs showing ≥1.5-fold increased translation in Δntd-expressing cells in response to urea, 151 of those mRNAs were associated with the cytoplasm GO term (**Supplementary Table S7**). Likewise, analysis of the mRNAs showing increased TE in Δntd cells showed strong association with GO terms for ribosomes and cytosolic components, even without urea (**Supplementary Table S8**). Furthermore, mRNAs that showed decreased TE in Δ*ntd* cells in the absence of urea were associated with membrane-bound organelles (**Supplementary Table S9**). This suggests the NTD promotes translation of mRNAs encoding membrane-associated proteins, and the loss of this ability results in the mutant translating mRNAs that encode cytoplasmic proteins, leading to urea and other stress sensitivities.

TABLE 1 | Gene Ontology analysis for genes with decreased translational efficiency in Δ*ntd* compared to WT in the presence of urea.

GO term	*p*-Value
Transferase activity, transferring hexosyl groups [GO:0016758]	1.62E–06
Endomembrane system [GO:0012505]	1.44E–05
Transferase activity, transferring glycosyl groups [GO:0016757]	2.22E–04
Protein glycosylation [GO:0006486]	3.76E–04
Macromolecule glycosylation [GO:0043413]	3.76E–04
Mannosylation [GO:0097502]	5.19E–04
Glycoprotein biosynthetic process [GO:0009101]	8.19E–04
Cellular bud [GO:0005933]	1.55E–03
Protein N-linked glycosylation [GO:0006487]	1.91E–03
Glycosylation [GO:0070085]	2.40E–03
Glycoprotein metabolic process [GO:0009100]	2.85E–03
Cell periphery [GO:0071944]	4.09E–03
Golgi cisterna [GO:0031985]	4.70E–03
Cell part [GO:0044464]	8.14E–03
Cell [GO:0005623]	8.81E–03
Protein O-linked glycosylation [GO:0006493]	1.98E–02
Golgi stack [GO:0005795]	2.26E–02
Mannosyltransferase activity [GO:0000030]	3.04E–02
Organelle subcompartment [GO:0031984]	3.65E–02
Membrane part [GO:0044425]	4.69E–02

Finally, we analysed the 281 mRNAs showing more than 1.5-fold decreased translation efficiency in response to urea in the mutant cells relative to WT. In this case we saw decreased translation for 84 mRNAs associated with the endomembrane system (p-value = 0.000026), including association with the ER, Golgi, transferase activities, glycosylation, and mannosylation (**Table 1**). This suggests effective translation of mRNAs for proteins trafficked through the ER/Golgi network to the membrane and cell wall may be dependent on eIF4B NTD activities. Together these results suggest that the eIF4B 40S-binding NTD may affect critical changes in translation of RNAs that remodel the cellular periphery in response to urea exposure. This function is necessary for translation of the optimal pool of mRNAs to promote rapid growth in standard media as well.

Deletion of the NTD of eIF4B Reduces Translation Efficiency of mRNAs With Long and Structured 5′UTRs

Previous studies have shown that mammalian eIF4B is necessary for PIC assembly at the start codon of mRNAs with 5′UTR secondary structure *in vitro* (Dmitriev et al., 2003). Likewise, yeast eIF4B is associated with robust loading and scanning of PICs and translation of mRNAs and synthetic reporters containing higher than average secondary structure *in vitro* and *in vivo* (Mitchell et al., 2010; Sen et al., 2016). We speculated that the effect of the NTD on translation of mRNAs needed to combat extracellular urea is related to the ability of eIF4B to promote translation of structured mRNAs. To test this hypothesis, we analysed existing parallel analysis of RNA structure (PARS) scores (Kertesz et al., 2010) for the RNAs exhibiting changes in TE as a result of eIF4B NTD deletion, in the presence or absence of

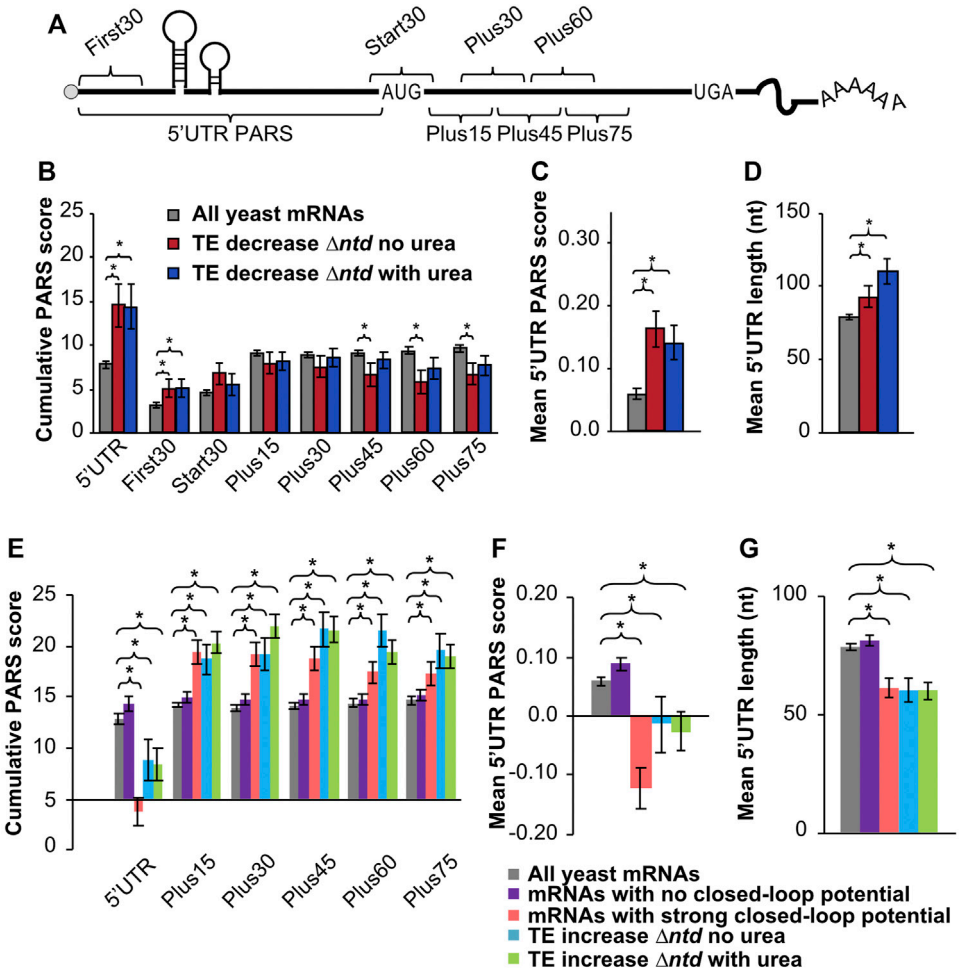

FIGURE 4 | Comparison of PARS (Parallel analysis of RNA structure) scores indicates a higher propensity for secondary structure in the 5′UTRs of mRNAs that are dependent on the NTD for translation, and less associated with closed-loop factors. **(A)** Schematic showing 5′-UTR and CDS intervals for cumulative PARS scores. The sum of scores for all 5′-UTR nucleotides (5′UTR PARS); for the first 30 nucleotides (First 30 PARS); for 30 nucleotides surrounding the start codon (Start 30 PARS); and for nucleotides within the ORF, from +1 to +30 (Plus15), +16 to +45 (Plus30), +31 to +60 (Plus45), +46 to +75 (Plus60), and +61 to +90 (Plus75). **(B**,**C)** The mean PARS scores (calculated from data reported in reference (Kertesz et al., 2010)) for indicated cumulative regions **(B)**, or for individual nucleotides in the 5′UTR **(C)** are indicated for all yeast mRNAs with available PARS scores (gray, $n = 2679$); mRNAs with decreased TE (≥1.5-fold) in Δ*ntd* relative to WT in media lacking urea (red, $n = 138$); and for mRNAs with decreased TE in Δ*ntd* relative to WT in 3% urea (navy, $n = 156$). **(D)** Average length of 5′-UTR for the indicated sets of mRNAs. **(E–G)** PARS and 5′UTR length analysis calculated for the indicated gene sets, with p values from Student's t test indicated (*$p < 0.05$): grey bar, all yeast mRNAs with available PARS scores ($n = 2679$); purple bar, mRNAs with no closed-loop potential, characterized for de-enrichment in immunoprecipitation of eIF4F and Pab1, and enrichment in immunoprecipitation of eIF4E-binding proteins as shown in (Costello et al., 2015); red bar, mRNAs with strong closed-loop potential, characterized for de-enrichment in immunoprecipitation of eIF4E-binding proteins and enrichment in immunoprecipitation of eIF4F and Pab1, as shown in (Costello et al., 2015); blue bar, mRNAs with increased TE in NTD deletion mutant as compared to WT without urea; green bar, mRNAs with increased TE in NTD deletion mutant as compared to WT in 3% urea. **(E)** Average PARS scores calculated for the indicated sets of mRNAs for each 5′-UTR or CDS interval described in **Figure 4A**. **(F)** Average PARS score calculated for entire 5′-UTR for the indicated sets of mRNAs. **(G)** Average length of 5′-UTR for the indicated sets of mRNAs.

urea. PARS scores provide the relative propensity of each nucleotide to a single- or double-strand specific nuclease, with a higher PARS score indicating a higher propensity for secondary structure. Cumulative PARS scores can be compared for specific regions of mRNAs to determine the likelihood that the e.g. first 30 nucleotides, total 5′ UTR, or regions in the ORF have more structure (**Figure 4A**), which would present an impediment for PIC loading, PIC scanning, or translation elongation, respectively (Sen et al., 2016). A previous analysis reported that deletion of eIF4B in yeast led to reduced translation of mRNAs with long, structured 5′UTRs (Sen et al., 2016). We found that, likewise, deletion of the NTD led to lower translation efficiency (≥1.5-fold decrease) of mRNAs with significantly higher PARS scores for the first 30 nucleotides of the 5′UTR (**Figure 4B**, First30), (comparison of Δ*tif3* and Δ*ntd* in **Supplementary Figure S10**). An even larger difference was observed for the total 5′UTR, suggesting interactions of the eIF4B NTD promote effective mRNA loading and possibly scanning through structured mRNA 5′UTRs (**Figure 4B**, 5′UTR). The average individual

nucleotide PARS score averaged for the full 5′UTRs was likewise significantly higher for these groups of mRNAs that showed reduced TE in the Δ*ntd* strain, e.g. presumably higher dependence on the NTD for translation (**Figure 4C**). In contrast, there was not a significant change in the PARS scores for the 30 nucleotides surrounding the start codon (**Figure 4B**, Start30), or the first 30 nucleotides of the ORF, suggesting structure around the start site and in the ORF does not strongly require eIF4B activity. In fact, the PARS scores for the Plus45, Plus60 and Plus75 regions were significantly lower for the group of mRNAs that showed higher dependence on the NTD of eIF4B (in the absence of urea). This suggests that the eIF4B NTD is not required for translation of mRNAs with structured ORFs or structured RNAs in general, but instead is important for PIC loading and movement through structured 5′UTRs (**Figures 4A,B**). The mean length of 5′UTR was also significantly higher for the group of mRNAs that were less efficiently translated (≥1.5-fold) when the NTD of eIF4B was deleted, similar to what was reported for complete eIF4B deletion (Sen et al., 2016). This further suggests the NTD plays a role in effective scanning of PICs through long structured 5′UTRs (**Figure 4D**). This effect was more pronounced when cells were grown in the presence of 3% urea prior to ribosome profiling, suggesting the effect of the NTD on urea resistance may stem from the ability of eIF4B to promote effective scanning.

We also found that 155 mRNAs showed a relative increase in TE in Δntd cells (**Figure 3F**), indicating ribosomes were able to be loaded on these mRNAs without eIF4B NTD activities. We assessed the degree of secondary structure in the 5′UTRs and coding sequences of these mRNAs (**Figures 4E–G**, cyan and green) as well as the closed-loop potential. Previous analysis of the tif3Δ mutant demonstrated that mRNAs showing less reliance on eIF4B had shown increased enrichment with components of the closed-loop complex (Sen et al., 2016): eIF4E, eIF4G and PABP (Costello et al., 2015). We likewise compared mRNAs classified as strong-closed loop potential (higher crosslinking immunoprecipitation association with closed-loop components) and no closed-loop potential (enriched in inhibitors of the closed-loop complex(36)) to mRNAs that were translated ≥1.5-fold more efficiently in the Δ*ntd* mutant. We found that mRNAs that showed increased TE in Δ*ntd* (with or without urea, cyan and green) showed similar trends with respect to PARS scores as those mRNAs defined as having strong closed-loop potential, and the opposite behavior as those mRNAs defined as having no closed-loop potential. Both the Total 5′UTR region and the average per nucleotide PARS scores for the 5′UTRs of these mRNAs showing eIF4B NTD-independence were significantly lower than the average yeast mRNA. In contrast, the mRNAs that showed increased translation efficiency in the Δntd mutant and strong-closed-loop associated mRNAs were more structured than the average yeast mRNA in the ORF. This suggests that mRNAs that rely on closed-loop components for mRNA loading do not require the eIF4B NTD or its interaction with the ribosome (Walker et al., 2013), and reinforces the conclusions of the previous manuscript that mRNAs requiring eIF4B activity are less associated with closed-loop components (Sen et al., 2016).

RNAs Encoding Proteins Trafficked Through the ER and Golgi Have Long and Structured 5′UTRs, Imposing a Heightened Requirement for eIF4B

Phenotype microarray analysis suggested the NTD of eIF4B stimulated growth in a number of diverse conditions that challenge cellular integrity (**Figure 2A** and **Supplementary Table S5**). The findings that mRNAs translated more effectively by full-length eIF4B had longer and more structured 5′-untranslated regions than those translated when the NTD was deleted led us to question whether proteins for different functions in cells may rely on distinct translational mechanisms. For instance, mRNAs for proteins that promote rapid growth may have less structure and rely less on eIF4B, whereas proteins that allow adaption to stressors, such as the membrane and cell wall proteins, may have more structure and require eIF4B function for translation. If true, the degree of structure would be expected to impose regulatory capacity as cells encounter stresses that require membrane changes, and may explain how the NTD of eIF4B affords resistance to diverse stressors that may require different membrane composition. To investigate this further, we compared the PARS scores for all yeast mRNAs versus the PARS scores for all yeast mRNAs associated with GO terms for mRNAs that required eIF4B for translation in response to urea (**Figures 5A–C**.) This group includes: intrinsic component of the membrane (the GO term with the lowest *p* value for RNAs showing increased translation in response to urea in WT cells); as well as transferase activity, endomembrane system, glycosylation, and mannosylation (parent GO terms for mRNAs with decreased translation in response to urea in Δ*ntd* cells.) Interestingly, we found that the 5′UTRs of mRNAs associated with each of these GO terms had higher average Total PARS scores than the average yeast mRNA (**Figure 5A**, 5′UTR). However, only those mRNAs encoding intrinsic components of the membrane had significantly longer 5′UTRs (**Figure 5B**). The mean 5′UTR PARS scores for individual nucleotides was also significantly higher than the average yeast mRNA for all classes (**Figure 5C**), indicating these classes of mRNAs associated with dependence on the ribosome binding NTD of eIF4B have inherently more structure in the 5′UTRs. This suggests functional importance of structural elements in regulating translation of membrane-associated and trafficked proteins. We then compared the structural composition of mRNAs from two gene ontology categories that were enriched under eIF4B NTD independent translation (**Figures 5D–F**). We found that as expected, given the observed NTD-independent translation associated with these classes of mRNAs, cytoplasmic translation and structural constituent of the ribosome mRNA categories as whole showed a dearth of structure in their 5′UTRs, with overall negative cumulative PARS scores and mean 5′UTR scores per nucleotide, indicating the 5′UTR regions of these mRNAs are likely to be single stranded. Interestingly, the

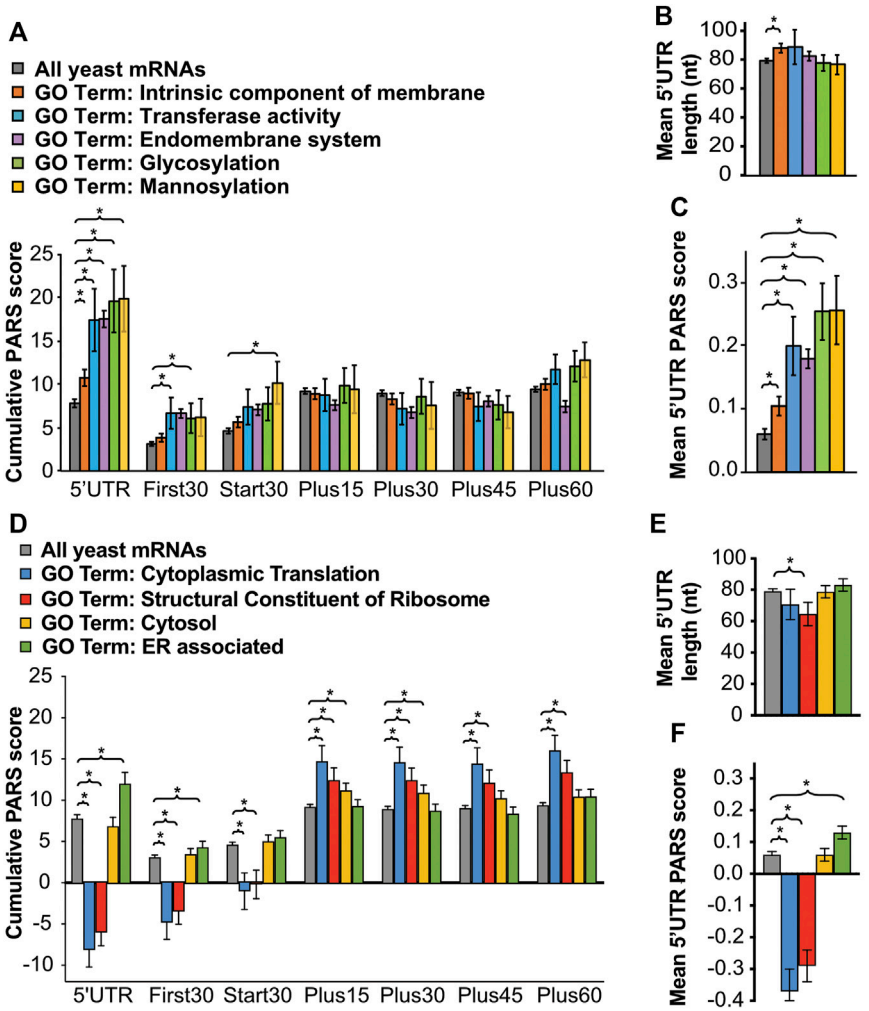

FIGURE 5 | RNAs encoding proteins trafficked through the ER and Golgi have long and structured 5′UTRs, imposing a heightened requirement for eIF4B. Averaged cumulative **(A**,**D)** and single nucleotide **(C**,**F)** PARS scores and 5′UTR lengths **(B**,**E)** for all genes associated with indicated gene ontology categories: intrinsic component of membrane (orange, n = 1360), transferase **(A–C**, blue, n = 86**)**, endomembrane system (purple, n = 1098), glycosylation **(A–C**, green, n = 87**)**, mannosylation **(A–C**, yellow, n = 46**)**, cytoplasmic translation **(D–F**, blue, n = 161**)**, structural constituent of ribosome (red, n = 190), cytosol **(D–F**, yellow n = 426**)**, or ER associated **(D–F**, green, n = 405**)** for each 5′-UTR or CDS interval described as in **Figure 4A**, with p values from Student's t test indicated (*p < 0.05).

cytoplasmic translation mRNAs had no significant difference in lengths of their 5′UTRs from the pool of all yeast mRNAs. In contrast to the 5′UTR however, the regions just downstream of the start codon showed higher than average PARS scores for these translation-associated gene ontology classes (**Figure 5D**, blue and red).

We finally compared the structural content of the two broad gene ontology classes: cytosol and ER. Whereas the cytosol class showed no significant difference in 5′UTR PARs scores from average yeast mRNA, the ER-associated gene ontology class showed significantly higher Total 5′UTR and mean 5′UTR PARS scores than all yeast mRNAs. Moreover, the open reading frames of the ER- associated mRNA pool showed the opposite trend. The cytosol class showed slightly elevated PARS scores for the region immediately downstream of the start site than observed for all yeast mRNAs. Together this suggests higher structure in the 5′UTRs of ER-associated mRNAs than cytosolic mRNAs.

We also took an unbiased approach to exploring the relationship between gene ontology classes, 5′UTR features, and eIF4B NTD-dependence. We ranked all yeast mRNAs based on their cumulative 5′UTR PARS scores (**Supplementary Figures S6A–C**) or 5′UTR lengths (**Supplementary Figures S6D–F**) and performed gene ontology analysis to determine enrichment of specific biological processes for the top (B, E) and bottom (C, F) 30% of mRNAs from each group. We compared the degree of overlap between the resulting GO term lists, and found that eIF4B NTD-independence, low 5′UTR structure propensity, and short 5′UTR gene ontology terms showed striking overlap, particularly for the highest enriched GO terms. These mRNAs encode proteins associated with cytoplasmic translation, ribosome biogenesis,

and other processes related to ramping up protein synthesis. In contrast, those GO terms enriched for transcripts exhibiting higher NTD-dependence showed some overlap with those enriched in mRNAs with high 5′UTR structure, but considerably less overlap with those enriched for mRNAs with long 5′UTRs. We investigated this relationship further by plotting the $\log_2$ fold-change in TE as a result of urea and/or NTD-deletion (**Supplementary Figure S7**). We found that while there was a significant effect correlation of change in TE in urea (for WT or Δntd) with 5′UTR lencth, and correlations of 5′UTR PARS with change in TE upon NTD deletion, there may be a threshold level of structure or length at which the NTD becomes necessary to effect change in TE. Overall, these data suggest a complex relationship between the ability of eIF4B to promote translation of mRNAs with structured 5′UTRs and regulation of translation that promotes growth versus regulatory changes.

Finally, we further analyzed the overlap in TE effects for Δ*tif3* (Lambert and Draper, 2012) and Δ*ntd* strains (**Supplementary Figure S8**). We found that while there was a correlation between the changes imparted by both mutations, there were also changes in TE that were unrelated between the two mutants. These anticorrelated changes in TE (**Supplementary Figure S8D**) could be an effect of the seven repeats, or simply an effect of the differences in experimental setup of the previously-published work on the Δ*tif3* strain grown at 37°C versus the 30° growth in this work. Interestingly the RNAs showing correlated TEs for the full deletion and Δntd have different GO terms than those that are anticorrelated for TE change in the two strains.

DISCUSSION

In this study, we characterized the contribution of eIF4B RNA- and 40S subunit-binding domains to translational control as well as the ability to promote adaptation of yeast to diverse stressors. We found that the NTD of eIF4B promoted association of eIF4B with PICs and polysomes in yeast while allowing higher TE for RNAs with longer than average and highly structured 5′UTRs, and repression of shorter highly translated mRNAs. These effects were similar to what was observed for deletion of eIF4B. The NTD also afforded higher TE for RNAs encoding proteins trafficked through and modified in the ER and Golgi to reside in cellular membranes. These proteins are expected to remodel the cellular periphery and allow yeast to cope with external stressors.

The RRM of eIF4B was thought to promote mRNA recruitment to ribosomes by providing an RNA anchoring point on a ribosome or eIF3-bound molecule (namely for mammalian eIF4B, (Méthot et al., 1996; Methot et al., 1996; Naranda et al., 1994; Méthot et al., 1994)) or by promoting RNA strand-exchange activities of eIF4B (Niederberger et al., 1998). Our previous work suggested that instead, the RNA-binding activities of the RRM are dispensable for eIF4B function in yeast (Walker et al., 2013). However, because the experiments in our previous work analysed the function of Δrrm-expressing eIF4B under optimal growth conditions, it remained plausible that the RRM provides additional functions to cells under stress, when additional interactions may be needed to direct ribosomes to specific mRNAs. Our phenotype microarray analysis of the Δ*rrm* mutant provides strong evidence that the RRM domain is in fact dispensable for function of this protein in yeast, at least in liquid media. The only plate in which we saw mild phenotypes for the Δ*rrm* mutant was in the presence of certain alternative sulfur sources (**Figure 2A**), but the changes observed were well below the cutoff for significance and were not reproducible. It remains possible that survival in non-vegetative differentiated states could depend on the RRM, and this may explain why the RRM is more important in multicellular organisms (Méthot et al., 1994; Naranda et al., 1994). Alternatively, the contribution of the RRM to cellular processes may not be sufficient to detect a change in growth rate or cellular fitness, but could allow RRM-containing yeast to outcompete mutants defective in RNA-binding. This could have led to retention of the RRM over the course of evolution (Altmann et al., 1993).

In contrast to yeast lacking the eIF4B RRM, we found that yeast lacking the NTD were highly sensitive to a number of conditions that WT cells are able to tolerate, and that at least two of these conditions (urea and caffeine) conferred additional changes in translation in the NTD-less mutant (**Figure 2** and **Supplementary Figure S2**, data not shown for caffeine). The mRNAs that showed decreased TE when the NTD was lacking had a number of features similar to those observed for an eIF4B null strain. The 5′UTRs of NTD-dependent mRNAs were longer and more structured than the average yeast mRNA (**Figure 4**), reinforcing many observations that eIF4B promotes translation of structured mRNAs (Özeş et al., 2011; Dmitriev et al., 2003; Sen et al., 2016; Rogers et al., 2001). The mechanism by which eIF4B is proposed to promote translation of these mRNAs resides in its ability to interact with eIF4A and stimulate helicase activity. However, a report for direct interaction of these factors suggests that the 7-repeats domain of eIF4B binds eIF4A (Andreou et al., 2017). In our study, we observed decreased translation of structured mRNAs when interaction of eIF4B with ribosome complexes was reduced by 80% upon NTD deletion (**Figures 1**, **4** and **Supplementary Figure S1**). Related components of the PIC, eIF4A and eIF4G, remained associated with ribosome fractions (**Figure 1** and **Supplementary Figure S1**). This suggests that the mechanism for eIF4B stimulation of structured mRNA translation resides at least to some extent in its ability to bind the ribosome (**Figure 6**). We have also previously reported defects in functional interaction of eIF4A with eIF4B when either the seven repeats or the NTD is deleted, and observed that overexpression of Δ*ntd* has a dominant negative effect on an eIF4A mutant (Walker et al., 2013; Zhou et al., 2014). Together these observations could indicate that deletion of the eIF4B NTD sequesters eIF4A in an inactive state off of the ribosome. However, we did not observe changes in the amount of eIF4A associated with small subunits and translating polysomes when eIF4B occupancy was decreased, arguing against this possibility and suggesting any interactions of the NTD with eIF4A do not drive affinity for ribosome complexes. An alternative possibility is that deletion of the NTD prevents a PIC

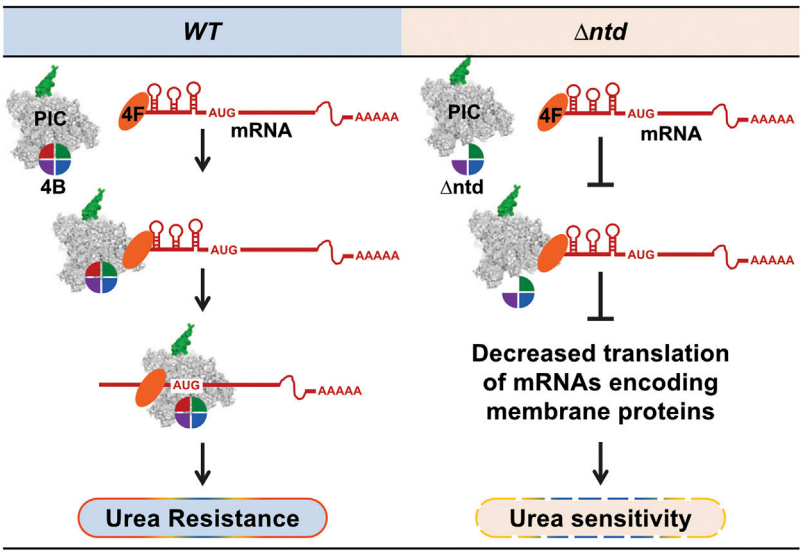

FIGURE 6 | The NTD of eIF4B enhances translation efficiency of mRNAs with structured 5′-UTRs and allows a robust cellular response to urea. WT eIF4B promotes PIC loading and scanning of all mRNAs. Deletion of the NTD of eIF4B reduces translation efficiency of mRNAs with long structured 5′UTRs to a greater extent, indicating eIF4B promotes ribosome loading and scanning while bound to the PIC. Translation of these highly structured mRNAs may be required to reconfigure the membrane proteome and balance translation of cytoplasmic proteins, providing urea resistance.

conformation required for optimal eIF4F activity. In either case, our data suggest the NTD of eIF4B contributes to effective scanning through structured 5′UTRs while bound to the ribosome.

The effect of the eIF4B NTD on recruitment of highly structured mRNAs to the ribosome is in keeping with long-standing models for translational control suggesting that factors which increase the rate of initiation would preferentially benefit mRNAs that are poorly translated (Lodish, 1974). Ribosome profiling data have shown that translation initiation helicases Ded1, Dbp1, and the related human protein DDX3, similarly stimulate translation of specific highly structured mRNAs to a higher degree than unstructured mRNAs that are typically highly translated. Interestingly, despite sharing an ability to promote translation of mRNAs with structured 5′UTRs, analysis of the specific mRNAs that were hyperdependent on the helicases Ded1 (Sen et al., 2015), Dbp1 (Sen et al., 2019), and eIF4A (Sen et al., 2015) showed little overlap with one another or eIF4B, and there was no overlap in the gene ontology enrichment observed for mRNAs hyperdependent on each of these factors. In contrast there was partial overlap between the gene ontology enrichment for mRNAs showing hyperdependence in an eIF4B null strain (Sen et al., 2016) versus the NTD domain deletion that retains some eIF4B activity. This suggests that each of these helicase factors and eIF4B contribute distinct functions to selection of varying classes of mRNAs, perhaps due to varied types and locations of secondary structures.

The strongest NTD-specific growth defect was observed in the presence of urea, which had very little effect on WT or Δrrm growth rate or translation (P:M ratio) at concentrations that strongly repressed growth and translation of the mutant (**Figures 2A–C**). Urea affects several processes in *S. cerevisiae*, where it can serve as a nitrogen source, lead to membrane blebbing, and can denature structured nucleic acids. At the concentrations used in this work, it was reported that urea can readily cross the cellular membrane (Cooper and Sumrada, 1975), presumably *via* the Dur3 transporter (Navarathna et al., 2011), and be used as a nitrogen source. Membrane blebbing and denaturation of nucleic acids are unlikely to occur at the ~0.5 M urea used here (Necas and Svoboda, 1973; Lambert and Draper, 2012). We conclude that translation reprogramming observed in WT cells grown in urea are responsible for growth of those cells at this level of urea. Upon deletion of the eIF4B NTD, the normal translation program is disrupted leading to urea sensitivity.

It is possible that NTD-dependent TE enhancements are needed to produce more of some proteins, or to prevent unregulated derepression of eIF4B-independent mRNAs. Gene ontology enrichment analysis of ≥1.5-fold translation efficiency changes indicated mRNAs encoding proteins associated with the membrane, and to a lesser extent cell wall, showed higher TE in WT cells in response to urea (**Figure 3**). Likewise, mRNAs encoding proteins associated with endomembrane system and modifications that arise within the ER and Golgi showed decreased TE in response to urea in the mutant cells (**Figure 3**; **Table 1**). The resulting membrane proteins are involved in a number of cellular processes. For instance, several paralogous proteins associated with adhesion during a-cell mating (Fig2, Aga1, and Aga2; **Supplementary Table S6** and **Supplementary Figure S4**) showed TE decreases in cells lacking the eIF4B NTD (TE decrease in WT vs Δntd in urea of 30-, 5- and 4-fold, respectively, FDR<0.0003). We confirmed an NTD-dependent change in protein level for a *FIG2* 5′UTR driven

translation reporter. Recent analyses of uORF usage of yeast cells exposed to temperature shifts indicated that *AGA1* and *AGA2* showed changes in uORF usage in response to temperature shifts (Kulkarni et al., 2019). In the presence of urea, or in response to NTD deletion we did not observe changes in uORF usage of the *AGA2* mRNA. We did not observe ribosome occupancy consistent with translation of the *AGA1* uORF in any of our experiments, and did not observe substantial changes in uORF occupancy overall genome-wide (analysis using uORF seqR not shown, (Spealman et al., 2018)). This suggests the uORF occupancy changes observed in the former study were specific to changes in start codon fidelity in the high temperature response that do not apply in the conditions tested here.

While we found that eIF4B promoted TE of RNAs associated with specific gene ontology classes in response to urea, deletion of the NTD also led to relative increases in TE of RNAs encoding proteins associated with cytoplasmic translation and ribosome biogenesis, which lack structure in their 5′UTRs. In fact, we found substantial overlap in our analysis of gene ontology enrichment for the most unstructured yeast mRNAs (**Supplementary Figure S5**) and eIF4B NTD-independent gene ontology (**Supplementary Tables S7, S8**). In some conditions it is likely that derepression of strong closed-loop mRNAs that promote growth could be equally or more detrimental to cells as not producing membrane associated proteins needed for a particular stress response. An analogous scenario has been described for eIF4G-phosphorylation-mediated control of mRNAs in response to glucose starvation in yeast (Chang and Huh, 2018). Reprogramming upon NTD deletion that increases translation of unstructured mRNAs could occur as a result of competition between structured and unstructured mRNA pools for degradation and/or translation machinery. In one scenario, eIF4B may be unable to engage 40S subunits using the NTD to enhance recruitment to structured mRNAs. Ribosomes not being loaded onto eIF4B NTD-dependent mRNAs may be more available to translate mRNAs that do not require eIF4B for ribosome transit through the 5′ UTR. In an alternative scenario, which is not mutually exclusive, increased structured mRNA lacking ribosomes may quench the degradation machinery in RNA granules to prevent proper turnover of housekeeping mRNAs. These additional questions will be of great interest in future work.

DATA AVAILABILITY STATEMENT

The datasets presented in this study can be found in online repositories. The names of the repository/repositories and accession number(s) can be found below: https://www.ncbi.nlm.nih.gov/geo/, GSE139097.

AUTHOR CONTRIBUTIONS

All authors designed and performed experiments. XL and SW conceived and performed bioinformatic analyses and wrote the manuscript. SW conceived and oversaw the project and secured funding. All authors contributed to the final draft of the manuscript.

FUNDING

This work was supported by the National Institutes of Health (R00GM119173 to SW); and start-up funds from the University at Buffalo College of Arts and Sciences.

ACKNOWLEDGMENTS

The authors would like to thank Fujun Zhou for assistance generating yeast strain YSW4 used in this study; Alan Hinnebusch and Jon Lorsch for providing reagents and strains; Mary Thompson, Shardul Kulkarni, Audrey Michel, Onta Lin, Marie Saitou, Zhe Ji, and Michael Love for protocols and technical advice; and Paul Cullen, Joseph Barbi, Alan Hinnebusch and members of the Walker lab for helpful feedback on the manuscript.

SUPPLEMENTARY MATERIAL

The Supplementary Material for this article can be found online at: https://www.frontiersin.org/articles/10.3389/fmolb.2021.787781/full#supplementary-material

REFERENCES

Altmann, M., Müller, P. P., Wittmer, B., Ruchti, F., Lanker, S., and Trachsel, H. (1993). A Saccharomyces cerevisiae Homologue of Mammalian Translation Initiation Factor 4B Contributes to RNA Helicase Activity. *EMBO J.* 12, 3997–4003. doi:10.1002/j.1460-2075.1993.tb06077.x

Altmann, M., Wittmer, B., Méthot, N., Sonenberg, N., and Trachsel, H. (1995). The Saccharomyces cerevisiae Translation Initiation Factor Tif3 and its Mammalian Homologue, eIF-4B, Have RNA Annealing Activity. *EMBO J.* 14, 3820–3827. doi:10.1002/j.1460-2075.1995.tb00051.x

Andreou, A. Z., Harms, U., and Klostermeier, D. (2017). eIF4B Stimulates eIF4A ATPase and Unwinding Activities by Direct Interaction Through its 7-repeats Region. *RNA Biol.* 14, 113–123. doi:10.1080/15476286.2016.1259782

Andreou, A. Z., and Klostermeier, D. (2014). eIF4B and eIF4G Jointly Stimulate eIF4A ATPase and Unwinding Activities by Modulation of the eIF4A Conformational Cycle. *J. Mol. Biol.* 426, 51–61. doi:10.1016/j.jmb.2013.09.027

Bochner, B. R., Gadzinski, P., and Panomitros, E. (2001). Phenotype Microarrays for High-Throughput Phenotypic Testing and Assay of Gene Function. *Genome Res.* 11, 1246–1255. doi:10.1101/gr.186501

Chang, Y., and Huh, W.-K. (2018). Ksp1-dependent Phosphorylation of eIF4G Modulates Post-transcriptional Regulation of Specific mRNAs Under Glucose Deprivation Conditions. *Nucleic Acids Res.* 46, 3047–3060. doi:10.1093/nar/gky097

Cooper, T. G., and Sumrada, R. (1975). Urea Transport in Saccharomyces cerevisiae. *J. Bacteriol.* 121, 571–576. doi:10.1128/jb.121.2.571-576.1975

Coppolecchia, R., Buser, P., Stotz, A., and Linder, P. (1993). A New Yeast Translation Initiation Factor Suppresses a Mutation in the eIF-4A RNA Helicase. *EMBO J.* 12, 4005–4011. doi:10.1002/j.1460-2075.1993.tb06078.x

Costello, J., Castelli, L. M., Rowe, W., Kershaw, C. J., Talavera, D., Mohammad-Qureshi, S. S., et al. (2015). Global mRNA Selection Mechanisms for Translation Initiation. *Genome Biol.* 16, 10. doi:10.1186/s13059-014-0559-z

Dmitriev, S. E., Terenin, I. M., Dunaevsky, Y. E., Merrick, W. C., and Shatsky, I. N. (2003). Assembly of 48S Translation Initiation Complexesfrom Purified Components with mRNAs that Have Some Base Pairingwithin Their 5′ Untranslated Regions. *Mol. Cel Biol* 23, 8925–8933. doi:10.1128/mcb.23.24.8925-8933.2003

Dolan, K., Montgomery, S., Buchheit, B., Didone, L., Wellington, M., and Krysan, D. J. (2009). Antifungal Activity of Tamoxifen: In Vitro and In Vivo Activities and Mechanistic Characterization. *Antimicrob. Agents Chemother.* 53, 3337–3346. doi:10.1128/aac.01564-08

Firczuk, H., Kannambath, S., Pahle, J., Claydon, A., Beynon, R., Duncan, J., et al. (2013). An In Vivo Control Map for the Eukaryotic mRNA Translation Machinery. *Mol. Syst. Biol.* 9, 635. doi:10.1038/msb.2012.73

Fleming, K., Ghuman, J., Yuan, X., Simpson, P., Szendröi, A., Matthews, S., et al. (2003). Solution Structure and RNA Interactions of the RNA Recognition Motif from Eukaryotic Translation Initiation Factor 4B. *Biochemistry* 42, 8966–8975. doi:10.1021/bi034506g

Guydosh, N. R., and Green, R. (2014). Dom34 Rescues Ribosomes in 3′ Untranslated Regions. *Cell* 156, 950–962. doi:10.1016/j.cell.2014.02.006

Herrmannová, A., Prilepskaja, T., Wagner, S., Šikrová, D., Zeman, J., Poncová, K., et al. (2020). Adapted Formaldehyde Gradient Cross-Linking Protocol Implicates Human eIF3d and eIF3c, K and L Subunits in the 43S and 48S Pre-initiation Complex Assembly, Respectively. *Nucleic Acids Res.* 48, 1969–1984. doi:10.1093/nar/gkz1185

Ingolia, N. T., Ghaemmaghami, S., Newman, J. R. S., and Weissman, J. S. (2009). Genome-wide Analysis In Vivo of Translation with Nucleotide Resolution Using Ribosome Profiling. *Science* 324, 218–223. doi:10.1126/science.1168978

Kertesz, M., Wan, Y., Mazor, E., Rinn, J. L., Nutter, R. C., Chang, H. Y., et al. (2010). Genome-wide Measurement of RNA Secondary Structure in Yeast. *Nature* 467, 103–107. doi:10.1038/nature09322

Kim, J., Oh, J., and Sung, G.-H. (2016). Regulation of MAP Kinase Hog1 by Calmodulin During Hyperosmotic Stress. *Biochim. Biophys. Acta (Bba) - Mol. Cel Res.* 1863, 2551–2559. doi:10.1016/j.bbamcr.2016.07.003

Kulkarni, S. D., Zhou, F., Sen, N. D., Zhang, H., Hinnebusch, A. G., and Lorsch, J. R. (2019). Temperature-dependent Regulation of Upstream Open reading Frame Translation in S. cerevisiae. *BMC Biol.* 17, 101. doi:10.1186/s12915-019-0718-5

Lambert, D., and Draper, D. E. (2012). Denaturation of RNA Secondary and Tertiary Structure by Urea: Simple Unfolded State Models and Free Energy Parameters Account for Measured M-Values. *Biochemistry* 51, 9014–9026. doi:10.1021/bi301103j

Langmead, B., Trapnell, C., Pop, M., and Salzberg, S. L. (2009). Ultrafast and Memory-Efficient Alignment of Short DNA Sequences to the Human Genome. *Genome Biol.* 10, R25. doi:10.1186/gb-2009-10-3-r25

Lee, B., Udagawa, T., Singh, C. R., and Asano, K. (2007). Yeast Phenotypic Assays on Translational Control. *Methods Enzymol.* 429, 105–137. doi:10.1016/s0076-6879(07)29006-8

Lee, M. E., DeLoache, W. C., Cervantes, B., and Dueber, J. E. (2015). A Highly Characterized Yeast Toolkit for Modular, Multipart Assembly. *ACS Synth. Biol.* 4, 975–986. doi:10.1021/sb500366v

Liu, X., Schuessler, P. J., Sahoo, A., and Walker, S. E. (2019). Reconstitution and Analyses of RNA Interactions with Eukaryotic Translation Initiation Factors and Ribosomal Preinitiation Complexes. *Methods* 162-163, 42–53. doi:10.1016/j.ymeth.2019.03.024

Lodish, H. F. (1974). Model for the Regulation of mRNA Translation Applied to Haemoglobin Synthesis. *Nature* 251, 385–388. doi:10.1038/251385a0

Love, M. I., Huber, W., and Anders, S. (2014). Moderated Estimation of Fold Change and Dispersion for RNA-Seq Data with DESeq2. *Genome Biol.* 15, 550. doi:10.1186/s13059-014-0550-8

Martin, M. (2011). Cutadapt Removes Adapter Sequences from High-Throughput Sequencing Reads. *EMBnet j.* 17, 10–12. doi:10.14806/ej.17.1.200

McGlincy, N. J., and Ingolia, N. T. (2017). Transcriptome-wide Measurement of Translation by Ribosome Profiling. *Methods* 126, 112–129. doi:10.1016/j.ymeth.2017.05.028

Methot, N., Pickett, G., Keene, J. D., and Sonenberg, N. (1996). In Vitro RNA Selection Identifies RNA Ligands that Specifically Bind to Eukaryotic Translation Initiation Factor 4B: The Role of the RNA Remotif. *RNA* 2, 38–50.

Méthot, N., Pause, A., Hershey, J. W., and Sonenberg, N. (1994). The Translation Initiation Factor eIF-4B Contains an RNA-Binding Region that Is Distinct and Independent from its Ribonucleoprotein Consensus Sequence. *Mol. Cel Biol* 14, 2307–2316. doi:10.1128/mcb.14.4.2307-2316.1994

Méthot, N., Song, M. S., and Sonenberg, N. (1996). A Region Rich in Aspartic Acid, Arginine, Tyrosine, and glycine (DRYG) Mediates Eukaryotic Initiation Factor 4B (eIF4B) Self-Association and Interaction with eIF3. *Mol. Cel Biol* 16, 5328–5334. doi:10.1128/mcb.16.10.5328

Michel, A. M., Mullan, J. P. A., Velayudhan, V., O'Connor, P. B. F., Donohue, C. A., and Baranov, P. V. (2016). RiboGalaxy: A Browser Based Platform for the Alignment, Analysis and Visualization of Ribosome Profiling Data. *RNA Biol.* 13, 316–319. doi:10.1080/15476286.2016.1141862

Mitchell, S. F., Walker, S. E., Algire, M. A., Park, E.-H., Hinnebusch, A. G., and Lorsch, J. R. (2010). The 5′-7-Methylguanosine Cap on Eukaryotic mRNAs Serves Both to Stimulate Canonical Translation Initiation and to Block an Alternative Pathway. *Mol. Cel*, 39, 950–962. doi:10.1016/j.molcel.2010.08.021

Mitchell, S. F., Walker, S. E., Rajagopal, V., Aitken, C. E., and Lorsch, J. R. (2011). "The Roles of Translation Initiation Factors in mRNA Recruitment to the Eukaryotic Ribosome," in *Ribosomes* Editors M. V. Rodnina, W. Wintermeyer, and R. Green (Vienna, Austria: Springer) Vol. 39, 155–169. doi:10.1007/978-3-7091-0215-2_13

Mülleder, M., Capuano, F., Pir, P., Christen, S., Sauer, U., Oliver, S. G., et al. (2012). A Prototrophic Deletion Mutant Collection for Yeast Metabolomics and Systems Biology. *Nat. Biotechnol.* 30, 1176–1178. doi:10.1038/nbt.2442

Naranda, T., Strong, W. B., Menaya, J., Fabbri, B. J., and Hershey, J. W. (1994). Two Structural Domains of Initiation Factor eIF-4B Are Involved in Binding to RNA. *J. Biol. Chem.* 269, 14465–14472. doi:10.1016/s0021-9258(17)36646-2

Navarathna, D. H. M. L. P., Das, A., Morschhäuser, J., Nickerson, K. W., and Roberts, D. D. (2011). Dur3 Is the Major Urea Transporter in Candida Albicans and Is Co-regulated with the Urea Amidolyase Dur1,2. *Microbiology* 157, 270–279. doi:10.1099/mic.0.045005-0

Necas, O., and Svoboda, A. (1973). Effect of Urea on the Plasma Membrane Particles in Yeast Cells and Protoplasts. *Protoplasma* 77, 453–466. doi:10.1007/BF01275721

Niederberger, N., Trachsel, H., and Altmann, M. (1998). The RNA Recognition Motif of Yeast Translation Initiation Factor Tif3/eIF4B Is Required but Not Sufficient for RNA Strand-Exchange and Translational Activity. *RNA* 4, 1259–1267. doi:10.1017/s1355838298980487

Özeş, A. R., Feoktistova, K., Avanzino, B. C., and Fraser, C. S. (2011). Duplex Unwinding and ATPase Activities of the DEAD-Box Helicase eIF4A Are Coupled by eIF4G and eIF4B. *J. Mol. Biol.* 412, 674–687. doi:10.1016/j.jmb.2011.08.004

Park, E.-H., Walker, S. E., Zhou, F., Lee, J. M., Rajagopal, V., Lorsch, J. R., et al. (2013). Yeast Eukaryotic Initiation Factor 4B (eIF4B) Enhances Complex Assembly between eIF4A and eIF4G In Vivo. *J. Biol. Chem.* 288, 2340–2354. doi:10.1074/jbc.m112.398537

Park, E.-H., Zhang, F., Warringer, J., Sunnerhagen, P., and Hinnebusch, A. G. (2011). Depletion of eIF4G from Yeast Cells Narrows the Range of Translational Efficiencies Genome-wide. *BMC Genomics* 12, 68. doi:10.1186/1471-2164-12-68

Rogers, G. W., Jr., Richter, N. J., Lima, W. F., and Merrick, W. C. (2001). Modulation of the Helicase Activity of eIF4A by eIF4B, eIF4H, and eIF4F. *J. Biol. Chem.* 276, 30914–30922. doi:10.1074/jbc.m100157200

Rozovsky, N., Butterworth, A. C., and Moore, M. J. (2008). Interactions Between eIF4AI and its Accessory Factors eIF4B and eIF4H. *RNA* 14, 2136–2148. doi:10.1261/rna.1049608

Sen, N. D., Gupta, N., Stuart, K. A., Preiss, T., Lorsch, J. R., and Hinnebusch, A. G. (2019). Functional Interplay Between DEAD-Box RNA Helicases Ded1 and Dbp1 in Preinitiation Complex Attachment and Scanning on Structured mRNAs In Vivo. *Nucleic Acids Res.* 47 (16), 8785–8806. doi:10.1093/nar/gkz595

Sen, N. D., Zhou, F., Harris, M. S., Ingolia, N. T., and Hinnebusch, A. G. (2016). eIF4B Stimulates Translation of Long mRNAs with Structured 5′ UTRs and Low Closed-Loop Potential but Weak Dependence on eIF4G. *Proc. Natl. Acad. Sci. USA* 113, 10464–10472. doi:10.1073/pnas.1612398113

Sen, N. D., Zhou, F., Ingolia, N. T., and Hinnebusch, A. G. (2015). Genome-wide Analysis of Translational Efficiency Reveals Distinct but Overlapping Functions of Yeast DEAD-Box RNA Helicases Ded1 and eIF4A. *Genome Res.* 25, 1196–1205. doi:10.1101/gr.191601.115

Spealman, P., Naik, A. W., May, G. E., Kuersten, S., Freeberg, L., Murphy, R. F., et al. (2018). Conserved Non-AUG uORFs Revealed by a Novel Regression Analysis of Ribosome Profiling Data. *Genome Res.* 28, 214–222. doi:10.1101/gr.221507.117

Thompson, M. K., Rojas-Duran, M. F., Gangaramani, P., and Gilbert, W. V. (2016). The Ribosomal Protein Asc1/RACK1 Is Required for Efficient Translation of Short mRNAs. *Elife* 5, e11154. doi:10.7554/eLife.11154

Walker, S. E., Zhou, F., Mitchell, S. F., Larson, V. S., Valasek, L., Hinnebusch, A. G., et al. (2013). Yeast eIF4B Binds to the Head of the 40S Ribosomal Subunit and Promotes mRNA Recruitment Through its N-Terminal and Internal Repeat Domains. *RNA* 19, 191–207. doi:10.1261/rna.035881.112

Xue, B., Dunbrack, R. L., Williams, R. W., Dunker, A. K., and Uversky, V. N. (2010). PONDR-FIT: A Meta-Predictor of Intrinsically Disordered Amino Acids. *Biochim. Biophys. Acta (Bba) - Proteins Proteomics* 1804, 996–1010. doi:10.1016/j.bbapap.2010.01.011

Zhou, F., Walker, S. E., Mitchell, S. F., Lorsch, J. R., and Hinnebusch, A. G. (2014). Identification and Characterization of Functionally Critical, Conserved Motifs in the Internal Repeats and N-Terminal Domain of Yeast Translation Initiation Factor 4B (yeIF4B). *J. Biol. Chem.* 289, 11860. doi:10.1074/jbc.a113.529370

Conflict of Interest: The authors declare that the research was conducted in the absence of any commercial or financial relationships that could be construed as a potential conflict of interest.

Publisher's Note: All claims expressed in this article are solely those of the authors and do not necessarily represent those of their affiliated organizations, or those of the publisher, the editors and the reviewers. Any product that may be evaluated in this article, or claim that may be made by its manufacturer, is not guaranteed or endorsed by the publisher.

frontiers in Molecular Biosciences

ORIGINAL RESEARCH
published: 17 January 2022
doi: 10.3389/fmolb.2021.780089

IGF2BP2 Regulates MALAT1 by Serving as an N6-Methyladenosine Reader to Promote NSCLC Proliferation

Le Han[1,2†], Guangyan Lei[1†], Zhenghong Chen[3], Yili Zhang[4], Chen Huang[2†] and Wenjuan Chen[5*]*

[1]Department of Thoracic Surgery, Tumor Hospital of Shaanxi Province, Affiliated to the Medical College of Xi'an Jiaotong University, Xi'an, China, [2]Department of Cell Biology and Genetics/Key Laboratory of Environment and Genes Related to Diseases, School of Basic Medical Sciences, Xi'an Jiaotong University Health Science Center, Xi'an, China, [3]Department of Integrated Chinese and Western Medicine, Tumor Hospital of Shaanxi Province, Affiliated to the Medical College of Xi'an Jiaotong University, Xi'an, China, [4]Tumor Hospital of Shaanxi Province, Affiliated to the Medical College of Xi'an Jiaotong University, Xi'an, China, [5]Department of Third Oncology, Tumor Hospital of Shaanxi Province, Affiliated to the Medical College of Xi'an Jiaotong University, Xi'an, China

OPEN ACCESS

Edited by:
Daniel L. Kiss,
Houston Methodist Research Institute, United States

Reviewed by:
Poonam Ramsevak Pandey,
University of Texas MD Anderson Cancer Center, United States
Yun Wang,
Sun Yat-sen University, China

***Correspondence:**
Chen Huang
hchen@mail.xjtu.edu.cn
Wenjuan Chen
chenwenjuan1984@aliyun.com

[†]These authors have contributed equally to this work

Specialty section:
This article was submitted to RNA Networks and Biology, a section of the journal Frontiers in Molecular Biosciences

Received: 20 September 2021
Accepted: 13 December 2021
Published: 17 January 2022

Citation:
Han L, Lei G, Chen Z, Zhang Y, Huang C and Chen W (2022) IGF2BP2 Regulates MALAT1 by Serving as an N6-Methyladenosine Reader to Promote NSCLC Proliferation. Front. Mol. Biosci. 8:780089. doi: 10.3389/fmolb.2021.780089

Insulin-like growth factor 2 (IGF2) mRNA-binding protein 2 (IGF2BP2) is an important posttranscriptional regulatory for stability and m6A modification. Here, we investigated the role of IGF2BP2 in non–small-cell lung cancer (NSCLC) proliferation. TCGA database was used to predict the expression and clinical significance of IGF2BP2 in normal and NSCLC samples. The expression of IGF2BP2 was further validated in NSCLC samples from surgery. Then we performed the functional study in NSCLC cell lines through overexpressing and knocking down IGF2BP2 in NSCLC cell lines *in vitro* and *in vivo*. The mechanism of interaction between IGF2BP2 and lncRNA metastasis associated lung adenocarcinoma transcript 1 (MALAT1) in NSCLC proliferation was determined by RIP assay. We demonstrated that IGF2BP2 is highly expressed in NSCLC and positively associated with poor overall survival (OS) and disease-free survival (DFS). We identified that lncRNA MALAT1 is a target of IGF2BP2 in NSCLC. IGF2BP2 promotes MALAT1 stability in an m6A-dependent mechanism, thus promoting its downstream target autophagy-related (ATG)12 expression and NSCLC proliferation.

Keywords: NSCLC, IGF2BP2, M6A, MALAT1, ATG12

INTRODUCTION

Lung cancer is one of the most diagnosed cancers with high morbidity and mortality in most countries (Bray et al., 2018). Non–small-cell lung cancer (NSCLC), including lung adenocarcinoma (LUAD), lung squamous cell carcinoma (LUSC), and large cell carcinoma histologic subtypes, constitutes about 85% of lung cancer. Despite improvement of basic research and treatment methods of NSCLC, the overall survival rate remains relatively poor

Abbreviations: NSCLC, non–small-cell lung cancer; LUAD, lung adenocarcinoma; LUSC, lung squamous cell carcinoma; IGF2BP2, insulin-like growth factor 2 (IGF2) mRNA-binding protein 2; RBP, RNA-binding protein; OS, overall survival; DFS, disease-free survival; MALAT1, metastasis associated lung adenocarcinoma transcript 1; ATG, autophagy-related; m6A, N6-methyladenosine.

(Hirsch et al., 2017; Jones and Baldwin, 2018). Therefore, exploring and figuring out detailed molecular mechanisms of NSCLC is necessary for NSCLC management. Insulin-like growth factor 2 (IGF2) mRNA-binding protein 2 (IGF2BP2) is an RNA-binding protein (RBP) with an important posttranscriptional regulatory role for mRNA localization, stability, and translational control (Li et al., 2019; Liu et al., 2019; Hu et al., 2020). Importantly, IGF2BP2 is a distinct m6A reader that targets lots of mRNA transcripts, promoting the stability and storage of target mRNAs in carcinogenesis. For example, IGF2BP2 promotes liver cancer proliferation in an N6-methyladenosine (m6A)-FEN1-dependent manner (Pu et al., 2020). METTL3 facilitates colorectal carcinoma progression in an m6A-IGF2BP2-dependent way (Li et al., 2019). Recent advances unveiled that IGF2BP2 is a major player in NSCLC progression. For instance, circNDUFB2 inhibits NSCLC progression *via* destabilizing IGF2BPs and activating antitumor immunity (Li B. et al., 2021). MiR-485-5p suppresses growth and metastasis in NSCLC by targeting IGF2BP2 (Huang R. Set al., 2018). However, it remains largely unclear how IGF2BP2 can regulate NSCLC progression.

In this study, we demonstrated that IGF2BP2 is highly expressed in NSCLC and positively associated with poor prognosis. We identified that lncRNA metastasis associated lung adenocarcinoma transcript 1 (MALAT1) is a target of IGF2BP2 in NSCLC. IGF2BP2 promotes MALAT1 stability in an m6A-dependent mechanism, thus promoting its downstream target autophagy-related (ATG)12 expression and NSCLC proliferation.

MATERIALS AND METHODS

NSCLC Tissues

A total of 24 paired samples of tumorous and non-tumorous tissues were collected from surgery at Tumor Hospital of Shaanxi Province with the consent of patients. The histological analysis of each sample was confirmed by pathologists in a double-blind manner. All the procedures were approved by the Ethics Committee of the Tumor Hospital of Shaanxi Province Hospital.

Cell Lines

Human NSCLC cell lines NCI157, A549, H1299, H460, H1703, H1975, and BEAS control cells were purchased from the Cell Bank of the Chinese Academy of Sciences (Shanghai, China). The cells were grown in RPMI-1640 medium with 10% fetal bovine serum (Gibco, United States). All the NSCLC cell lines were authenticated by short tandem repeat (STR) analysis and were tested for Mycoplasma contamination.

Quantitative Real-Time PCR

Total RNA of NSCLC cells was extracted with TRIzol reagent (Invitrogen, United States). The relative fold expression was calculated using the comparative threshold cycle ($2^{-\Delta\Delta Ct}$). The primer is presented as follows: β-actin: Forward (5′-3′): CCCACT CCTCCACCTTTGAC, Reverse (5′-3′): CATACCAGGAAA TGAGCTTGACAA; IGF2BP2: Forward (5′-3′): GTTGGTGCC ATCATCGGAAAGG, Reverse (5′-3′): TGGATGGTGACAGGC TTCTCTG; MALTA1: Forward (5′-3′): GAATTGCGTCATTTA AAGCCTAGTT, Reverse (5′-3′): GTTTCATCCTACCACTCC CAATTAAT.

Western Blot

Total protein of NSCLC cells was extracted with RIPA reagent (Beyotime Biotechnology, China). An equal amount of total protein lysate (30 μg) was separated by 7.5–12% SDS-PAGE and transferred onto a PVDF membrane, followed by incubation with primary antibody overnight at 4°C. Then the bands were incubated with secondary antibody for 1 h at room temperature (RT). The bands were detected using a Bio-Rad ChemiDoc XRS system. The primary antibodies were presented as follows: anti-IGF2BP2 (1: 1,000, abcam, ab124930), anti-ATG12 (1:1,000, abcam, ab109491), and anti–β-actin (1:2,000, abcam, ab8226).

Cell Proliferation Assay

Cell proliferation was analyzed using CCK8 assay and colony formation assay. CCK8 assay was performed using a Cell Counting Kit-8 (CCK-8, Biotool, China). Cells were seeded in 96-well plates at a density of 3.5×10^3 cells/well. The CCK8 reagent was added to each well at different time points. After incubation for 4 h at 37°C, the absorbance at 450 nm was measured. For colony formation assay, cells were seeded in 6-well plates and cultured for 14 days. Then the cells were fixed and stained with crystal violet. The number of colonies was countered for five representative fields.

Subcutaneous Tumor Bearing Nude Mice Model

All animal experiments were approved by the Institutional Animal Care and Use Committee of Xi'an Jiaotong University. Mice (male and 6 weeks old) were subcutaneously injected with NSCLC cells ($1.0*10^6$ cells/200 μl). The mice were terminated after 4 weeks of induction, and the tumor volume and tumor weight were measured.

RNA Immunoprecipitation

IGF2BP2 antibody was used to pull down MALTA1. The IGF2BP2 antibody was then recovered with protein A/G beads, and RNA level of MALTA1 in the precipitates was measured by qRT-PCR. For m6A RIP, m6A antibody (MABE1006) (Millipore Sigma, Burlington, MA) was used to pull down m6A modified MALTA1, and RNA level of MALTA1 in the precipitates was measured by qRT-PCR.

Statistical Analysis

Statistical analyses were performed using the GraphPad Prism program. The *t*-test was used to compare the mean of a continuous variable between two groups. OS and disease-free survival (DFS) curves were calculated using the Kaplan–Meier method and were analyzed with the log-rank test. p values < 0.05 were considered as significant.

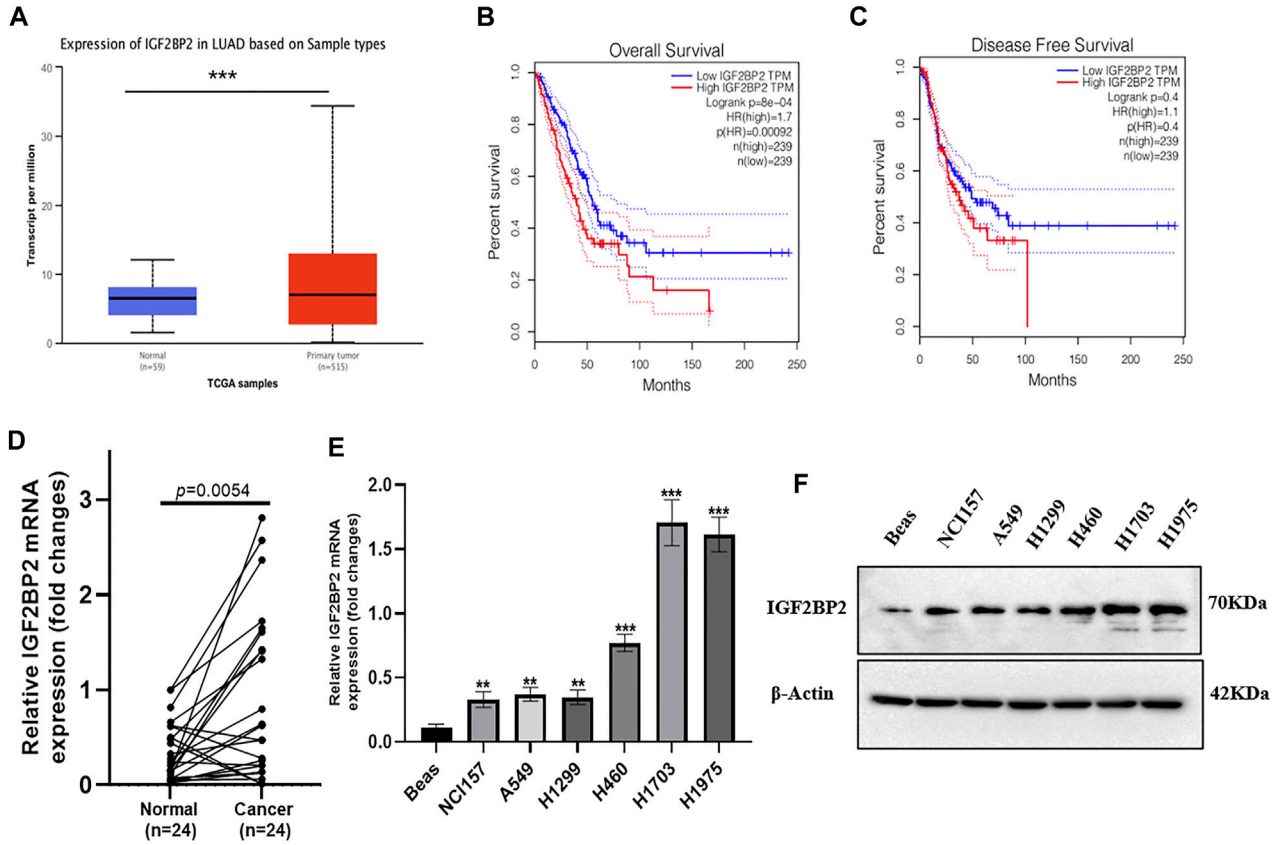

FIGURE 1 | IGF2BP2 is an unfavorable prognostic marker in NSCLC. **(A)** The expression difference of IGF2BP2 in the TCGA database. **(B,C)** The expression of IGF2BP2 is related to the survival and prognosis of patients with non-small cell lung cancer. **(D)** The expression difference of IGF2BP2 in non-small cell lung cancer tissues and adjacent tissues ($n = 24$). **(E,F)**. The expression of IGF2BP2 in non-small cell lung cancer cell lines. Data are presented as mean ± SD. p values are calculated by unpaired two-sided t-test.

RESULTS

IGF2BP2 Is an Unfavorable Prognostic Marker in NSCLC

We first checked the TCGA database to investigate the role of IGF2BP2 in NSCLC patients. As compared with normal tissues, the IGF2BP2 mRNA level was upregulated in primary NSCLC tissues (**Figure 1A**). Moreover, a higher IGF2BP2 mRNA level was positively correlated with poor overall survival (OS) and disease-free survival (DFS) (**Figures 1B,C**). The upregulation of IGF2BP2 mRNA was further validated in fresh NSCLC samples and the paired adjacent non-tumor sites (**Figure 1D**, $n = 24$, $p < 0.01$). Consistently, the upregulation of IGF2BP2 was presented in NSCLC cell lines compared with the BEAS cells (**Figures 1E,F**). These results highlight the clinical significance of IGF2BP2 in NSCLC.

IGF2BP2 Promotes NSCLC Cell Proliferation *In Vitro* and *In Vivo*

To gain an insight into IGF2BP2 in NSCLC progression, we ectopically expressed IGF2BP2 in A549 cells (**Figures 2A,B**) and generated IGF2BP2 knockdown in H1975 cells (**Figures 2C,D**). We found that IGF2BP2 promoted cell proliferation, as determined using CCK8 and colony formation assays (**Figures 2E,F**). However, knockdown of IGF2BP2 showed an opposite effect on NSCLC cell proliferation (**Figures 2G,H**). Then we established the subcutaneous tumor bearing nude mice model to better understand the oncogenic role of IGF2BP2 in NSCLC. The results confirmed that IGF2BP2 promoted NCCLC proliferation, as indicated by larger tumor volume and heavier tumor weight (**Figures 2I–K**). Conversely, IGF2BP2 knockdown repressed tumor growth in nude mice (**Figures 2L–N**). All the results indicate the oncogenic role of IGF2BP2 in NSCLC.

IGF2BP2 Regulates MALTA1 Expression in NSCLC

It is widely recognized that lncRNA MALAT1 is a key regulator in NSCLC initiation, progression, and metastasis (Tang et al., 2018; Song J. et al., 2020; Li M. et al., 2021). Because IGF2BP2 usually functions as a key regulator of IncRNAs, we speculate whether lncRNA MALAT1 can be regulated by IGF2BP2. As expected, IGF2BP2 overexpression upregulated the MALAT1 level, whereas MALAT1 was significantly downregulated by IGF2BP2 knockdown

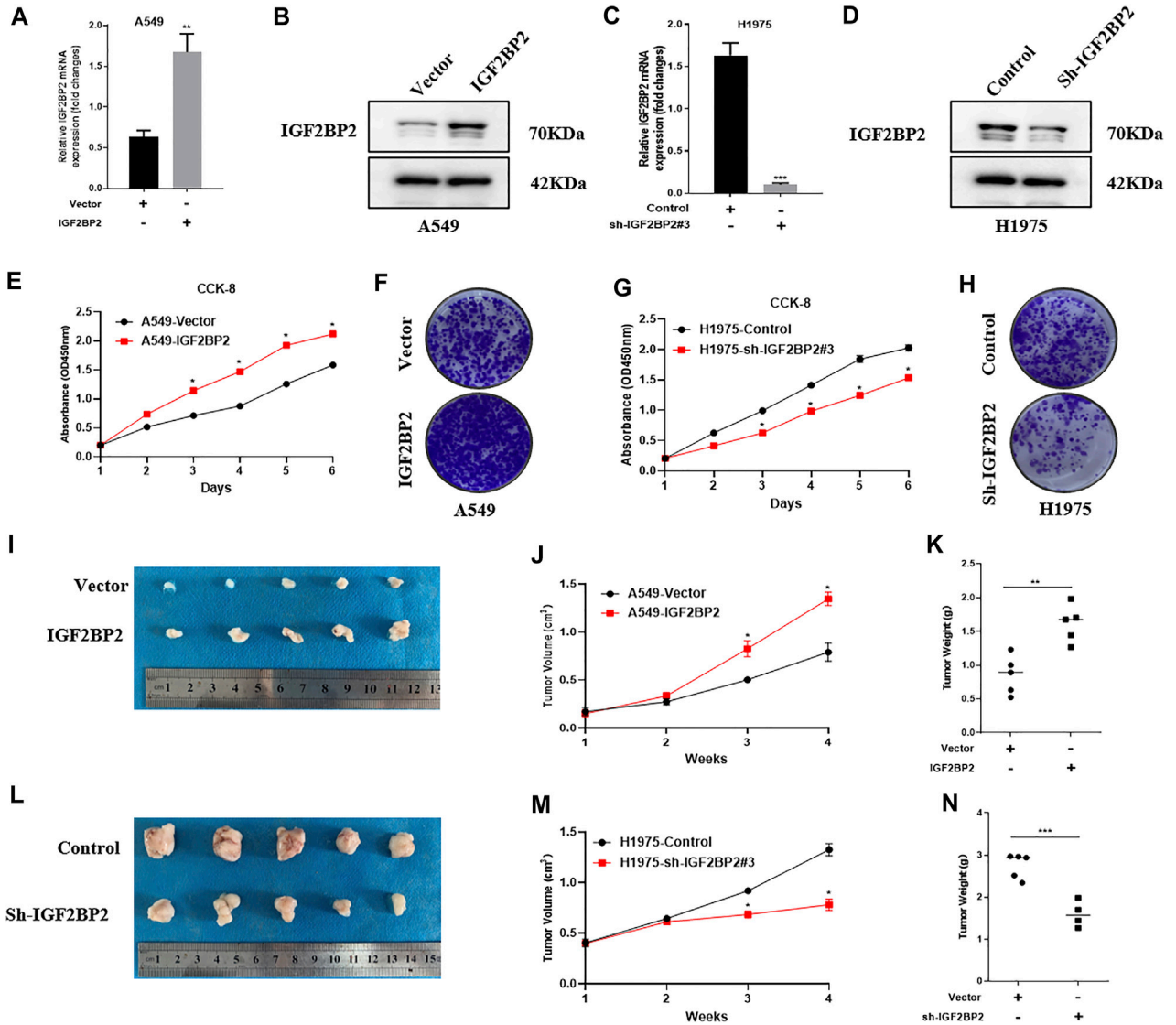

FIGURE 2 | IGF2BP2 promotes NSCLC cell proliferation *in vitro* and *in vivo*. **(A,B)** Real-time quantitative PCR and western blot analysis overexpress IGF2BP2 in A549 cells. **(C,D)**. Real-time quantitative PCR and western blot analysis knocked out IGF2BP2 in H1975 cells. **(E–H)**. CCK-8 and clone formation experiments analyze the effect of IGF2BP2 on the proliferation of non-small cell lung cancer cell lines. **(I–N)**. *In vivo* tumor formation experiments in nude mice analyzed the effect of IGF2BP2 on the proliferation of non-small cell lung cancer cell lines. Data are presented as mean ± SD. *p* values are calculated by unpaired two-sided *t*-test.

(**Figures 3A,B**). We further investigate the mechanisms by which IGF2PB2 regulates MALAT1 expression. Since a central role of IGF2BP2 in carcinogenesis is to regulate RNA stability, we examined the stability of MALAT1 by using actinomycin D (2 μg/ml). The results showed that the MALAT1 decay was slowed down *via* upregulating of IGF2BP2 (**Figure 3C**). Conversely, knockdown of IGF2BP2 accelerates MALAT1 decay compared with control cells (**Figure 3D**). In addition, RIP-PCR assay further validated the interaction between IGF2BP2 and MALAT1 (**Figure 3E**). As for N6-methyladenosine (m6A), it is the most abundant internal modification on RNAs (Jin et al., 2019; Xue et al., 2021). We detected whether IGF2BP2 promotes MALAT1 stability *via* m6A modification. RIP assays with m6A antibody identified enrichment of MALAT1 *via* upregulating of IGF2BP2 (**Figure 3F**). All these data suggested that IGF2BP2 regulates MALTA1 stability in NSCLC.

IGF2BP2 Promotes NSCLC Proliferation *via* Upregulating ATG12 Expression

It is known that ATG12 is a key downstream regulator of MALAT1, and ATG12 is required for NSCLC progression (He et al., 2020). Therefore, we tested whether IGF2BP2 can regulate ATG12 expression *via* MALAT1 in NSCLC. Western blot assay revealed that IGF2BP2 overexpression upregulated the ATG12 level, whereas

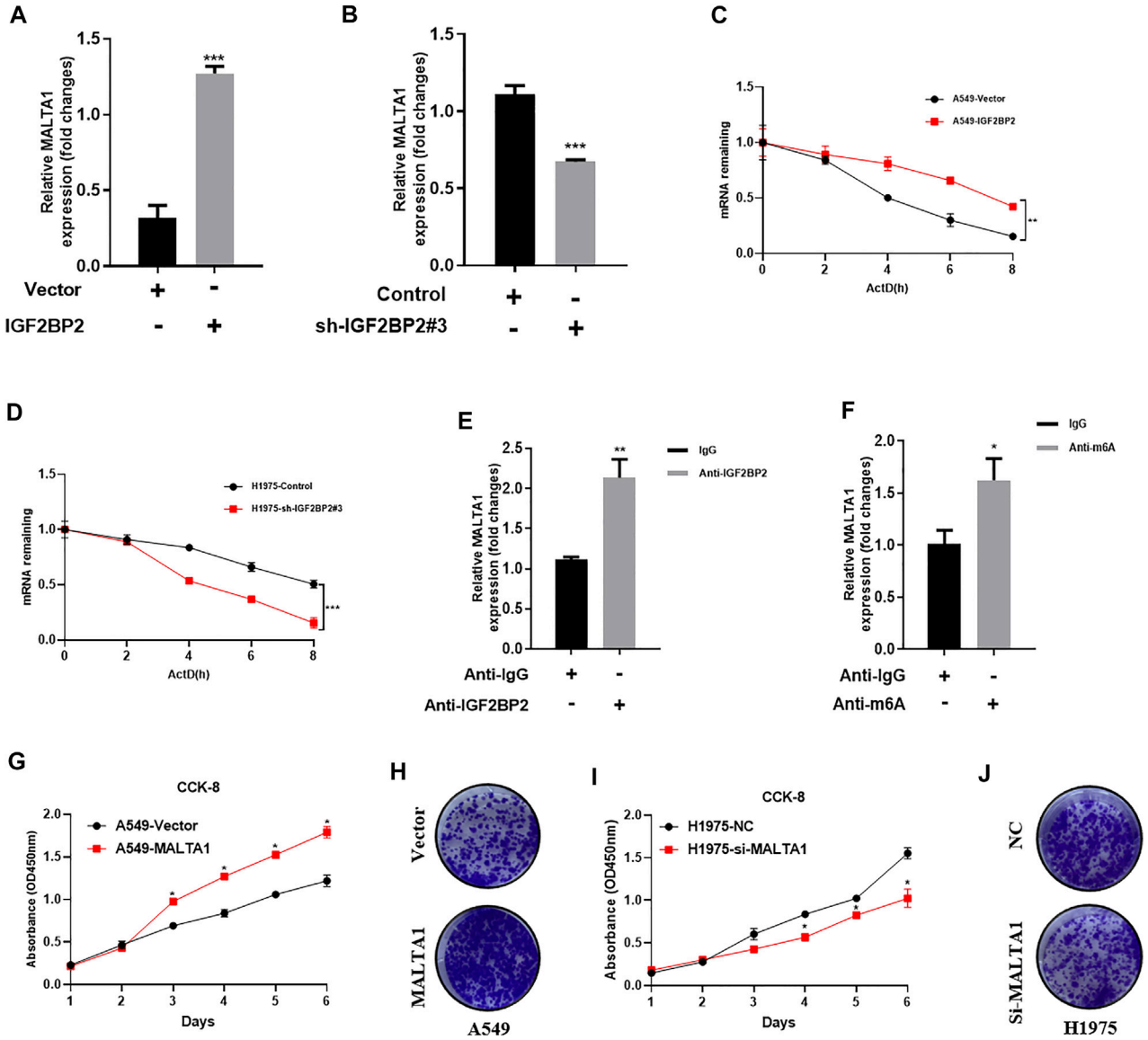

FIGURE 3 | IGF2BP2 regulates MALTA1 expression in NSCLC. **(A,B)** Real-time quantitative PCR analysis IGF2BP2 regulates the expression of MALAT1. **(C,D)** MALAT1 half-life determination. **(E)** RIP-PCR analysis of the interaction between IGF2BP2 and MALAT1. **(F)** mRIP-PCR analysis of m6A modification of MALAT1. **(G–J)** CCK-8 and clone formation experiments analyze the effect of MALAT1 on the proliferation of non-small cell lung cancer cell lines. Data are presented as mean ± SD. *p* values are calculated by unpaired two-sided *t*-test.

ATG12 was significantly downregulated by IGF2BP2 knockdown (**Figures 4A,B**). We also confirmed that MALAT1 overexpression upregulated the ATG2 level, whereas ATG12 was significantly downregulated by MALAT1 knockdown (**Figures 4C,D**). To further validate whether IGF2BP2 can regulate NSCLC proliferation *via* ATG12, we knocked down ATG12 expression in IGF2BP2 overexpressing cells and ectopically expressed ATG2 in IGF2BP2 knockdown cells (**Figures 4E,F**). CCK8 assay indicated that knockdown ATG12 expression can repress cell proliferation in IGF2BP2 overexpressing cells, while ectopically expressed ATG12 promotes cell proliferation in IGF2BP2 knockdown cells (**Figures 4G,I**). Colony formation assay showed the same trend as the CCK8 experiment (**Figures 4H,J**). All the data suggested that IGF2BP2 promotes NSCLC proliferation *via* the lncRNA MALAT1/ATG12 axis.

DISCUSSION

In the present study, we showed that high expression of IGF2BP2 in NSCLC is correlated with unsatisfied OS and DFS. lncRNA MALAT1 is a direct target of IGF2BP2 in NSCLC. Mechanistically, IGF2BP2 promotes MALAT1 stability *via* m6A modification and promoting its downstream target ATG12 expression.

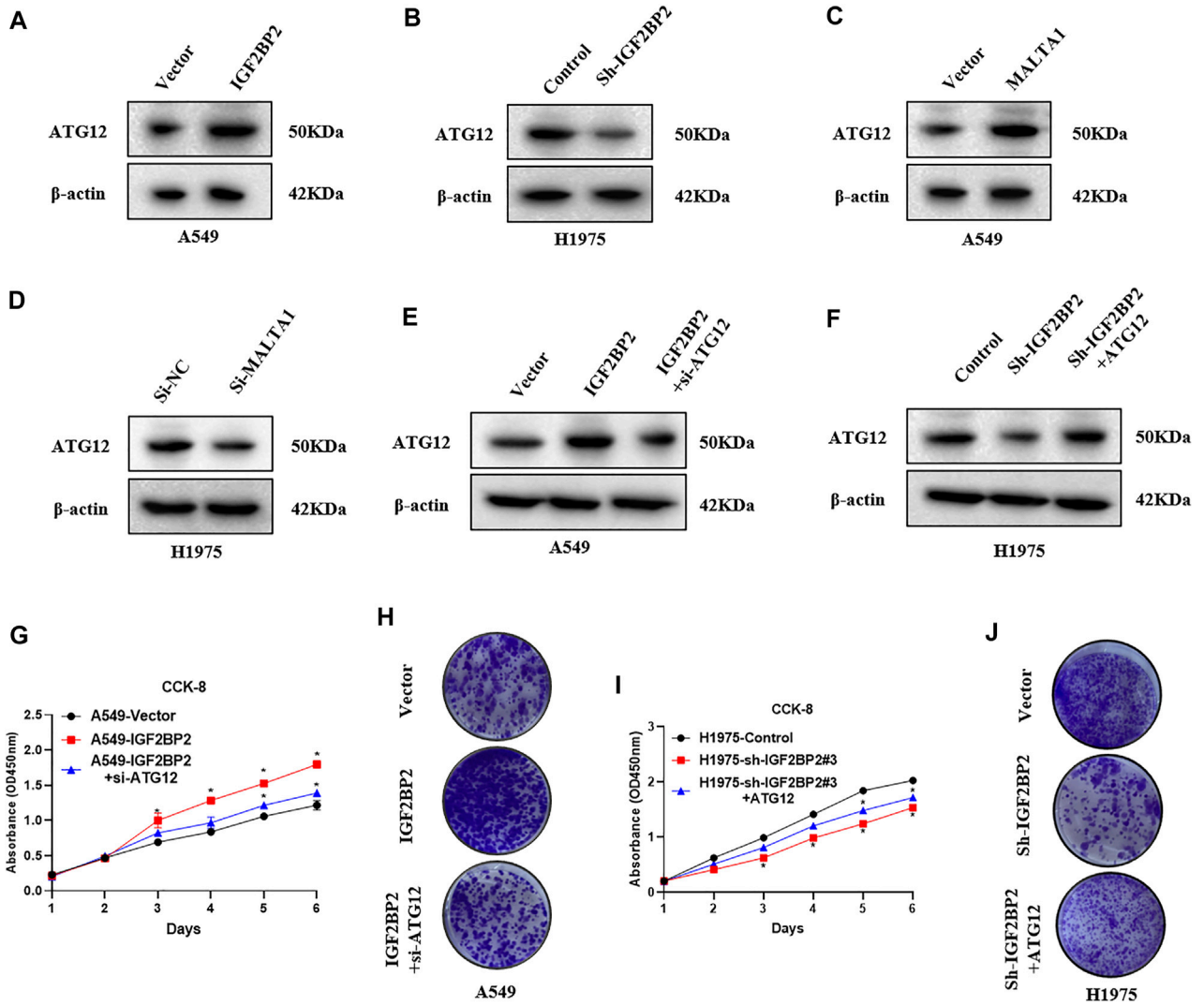

FIGURE 4 | IGF2BP2 promote NSCLC proliferation via upregulating ATG12 expression. **(A,B)** Western blot analysis of the effect of IGF2BP2 on the expression of ATG12 protein. **(C,D)** Western blot analysis of the effect of MALAT1 on the expression of ATG12 protein. **(E,F)** Western blot analysis of the effect of MALAT1 and IGF2BP2 on the expression of ATG12 protein. **(G–J)** CCK-8 and clone formation experiments analyze the effect of MALAT1 and IGF2BP2 on the proliferation of non-small cell lung cancer cell lines. Data are presented as mean ± SD. *p* values are calculated by unpaired two-sided *t*-test.

Using TCGA database, we identified the clinical significance of upregulating IGF2BP2 in NSCLC. To support the findings of TCGA database, we further highlight elevated IGF2BP2 expression in NSCLC samples and cell lines. To further unveil the function of IGF2BP2 in NSCLC progression, we performed the functional study in NSCLC cell lines through overexpressing and knocking down IGF2BP2 in NSCLC cell lines. We showed that IGF2BP2 promotes cell proliferation and viability *in vitro* and *in vivo*, indicating the oncogenic role of IGF2BP2 in NSCLC. Since IGF2BP2 functions as a key regulator of IncRNAs, we speculate whether lncRNA MALAT1 can be regulated by IGF2BP2. MALAT1 is a most widely studied lncRNA in tumorigenesis. MALAT1 act as a metastasis-suppressing lncRNA in breast cancer (Kim et al., 2018). However, MALAT1 serves as an oncogenic lncRNA in NSCLC proliferation and Gefitinib resistance by acting as a miR-200a sponge (Feng et al., 2019). Consistently, lncRNA MALAT1 also plays a pro-oncogenic role in ovarian cancer (Jin et al., 2017), osteosarcoma (Zhang et al., 2020), acute lymphoblastic leukemia (Song Y. et al., 2020), and colorectal cancer (Guo et al., 2020). Our results showed that IGF2BP2 overexpression increased the MALAT1 level, whereas MALAT1 was significantly downregulated by IGF2BP2 knockdown, suggesting that lncRNA MALAT1 can be regulated by IGF2BP2. Regulating the RNA stability is the major way of IGF2BP2 to interact with target RNAs (Huang H. et al., 2018; Chen et al., 2019). To figure out the mechanisms by which IGF2PB2 regulates MALAT1 expression, we tested the stability of lncRNA MALAT1 by overexpressing and knocking down IGF2BP2 and found that the MALAT1 decay was slowed down *via* upregulating of IGF2BP2. Conversely, knockdown of IGF2BP2 accelerates MALAT1 decay. Moreover, RIP-PCR assay further validated the interaction between

IGF2BP2 and MALAT1. As for N6-methyladenosine (m6A), it is the most abundant internal modification on RNAs (Jin et al., 2019; Xue et al., 2021). We detected whether IGF2BP2 promotes MALAT1 stability *via* m6A modification. RIP assays with m6A antibody identified enrichment of MALAT1 *via* upregulating of IGF2BP2. All these data suggested that IGF2BP2 regulates MALTA1 stability in NSCLC. It is known that ATG12 is a key downstream regulator of MALAT1, and ATG12 is required for NSCLC progression (He et al., 2020). Therefore, we tested whether IGF2BP2 can regulate ATG12 expression *via* MALAT1 in NSCLC. The results revealed that IGF2BP2 overexpression upregulated the ATG12 level, whereas ATG12 was significantly downregulated by IGF2BP2 knockdown. In addition, to further validate whether IGF2BP2 can regulate NSCLC proliferation *via* ATG12, we knock down ATG12 expression in IGF2BP2 overexpressing cells and ectopically expressed ATG2 in IGF2BP2 knockdown cells. We showed that knockdown ATG12 expression can repress cell proliferation in IGF2BP2 overexpressing cells, while ectopically expressed ATG12 promotes cell proliferation in IGF2BP2 knockdown cells, suggesting that IGF2BP2 promotes NSCLC proliferation *via* the lncRNA MALAT1/ATG12 axis.

In summary, we found that upregulation of IGF2BP2 in NSCLC is correlated with unsatisfied OS and DFS. IGF2BP2 promotes NSCLC proliferation *via* regulation of lncRNA MALAT1 stability in an m6A-dependent manner. Targeting the IGF2BP2/lncRNA MALAT1/ATG12 axis may be beneficial for NSCLC treatment.

DATA AVAILABILITY STATEMENT

The original contributions presented in the study are included in the article/Supplementary Material, further inquiries can be directed to the corresponding authors.

ETHICS STATEMENT

The studies involving human participants were reviewed and approved by the Ethics Committee of the Tumor Hospital of Shaanxi Province Hospital. The patients/participants provided their written informed consent to participate in this study. The animal study was reviewed and approved by the Institutional Animal Care and Use Committee of Xi'an Jiaotong University.

AUTHOR CONTRIBUTIONS

LH and GL drafted the manuscript, participated in research design, conducted experiments, and validated the data; ZC and YZ participated in research design and conducted experiments; CH and WC contributed to the writing of the manuscript, discussed data, and supervised the study. All authors performed data analysis and interpretation and read and approved the final manuscript.

FUNDING

This project is supported by the National Natural Science Foundation of China (Grant No. 81902321) and the China Postdoctoral Science Foundation (Grant No. 2020M683511).

ACKNOWLEDGMENTS

We thank all patients who have participated in this study. We thank the members of our group who participated in this work.

REFERENCES

Bray, F., Ferlay, J., Soerjomataram, I., Siegel, R. L., Torre, L. A., and Jemal, A. (2018). Global Cancer Statistics 2018: GLOBOCAN Estimates of Incidence and Mortality Worldwide for 36 Cancers in 185 Countries. *CA: A Cancer J. Clinicians* 68, 394–424. doi:10.3322/caac.21492

Chen, R.-X., Chen, X., Xia, L.-P., Zhang, J.-X., Pan, Z.-Z., Ma, X.-D., et al. (2019). N6-methyladenosine Modification of circNSUN2 Facilitates Cytoplasmic export and Stabilizes HMGA2 to Promote Colorectal Liver Metastasis. *Nat. Commun.* 10, 4695. doi:10.1038/s41467-019-12651-2

Feng, C., Zhao, Y., Li, Y., Zhang, T., Ma, Y., and Liu, Y. (2019). LncRNA MALAT1 Promotes Lung Cancer Proliferation and Gefitinib Resistance by Acting as a miR-200a Sponge. *Archivos de Bronconeumología* 55, 627–633. doi:10.1016/j.arbres.2019.03.026

Guo, J., Ding, Y., Yang, H., Guo, H., Zhou, X., and Chen, X. (2020). RETRACTED: Aberrant Expression of lncRNA MALAT1 Modulates Radioresistance in Colorectal Cancer *In Vitro* via miR-101-3p Sponging. *Exp. Mol. Pathol.* 115, 104448. doi:10.1016/j.yexmp.2020.104448

He, H., Song, X., Yang, Z., Mao, Y., Zhang, K., Wang, Y., et al. (2020). Upregulation of KCNQ1OT1 Promotes Resistance to Stereotactic Body Radiotherapy in Lung Adenocarcinoma by Inducing ATG5/ATG12-Mediated Autophagy via miR-372-3p. *Cell Death Dis.* 11, 883. doi:10.1038/s41419-020-03083-8

Hirsch, F. R., Scagliotti, G. V., Mulshine, J. L., Kwon, R., Curran, W. J., Wu, Y.-L., et al. (2017). Lung Cancer: Current Therapies and New Targeted Treatments. *The Lancet* 389, 299–311. doi:10.1016/s0140-6736(16)30958-8

Hu, X., Peng, W.-X., Zhou, H., Jiang, J., Zhou, X., Huang, D., et al. (2020). IGF2BP2 Regulates DANCR by Serving as an N6-Methyladenosine Reader. *Cell Death Differ* 27, 1782–1794. doi:10.1038/s41418-019-0461-z

Huang, R.-S., Zheng, Y.-l., Li, C., Ding, C., Xu, C., and Zhao, J. (2018). MicroRNA-485-5p Suppresses Growth and Metastasis in Non-small Cell Lung Cancer Cells by Targeting IGF2BP2. *Life Sci.* 199, 104–111. doi:10.1016/j.lfs.2018.03.005

Huang, H., Weng, H., Sun, W., Qin, X., Shi, H., Wu, H., et al. (2018). Recognition of RNA N6-Methyladenosine by IGF2BP Proteins Enhances mRNA Stability and Translation. *Nat. Cel Biol* 20, 285–295. doi:10.1038/s41556-018-0045-z

Jin, D., Guo, J., Wu, Y., Du, J., Yang, L., Wang, X., et al. (2019). m6A mRNA Methylation Initiated by METTL3 Directly Promotes YAP Translation and Increases YAP Activity by Regulating the MALAT1-miR-1914-3p-YAP axis to Induce NSCLC Drug Resistance and metastasisA mRNA Methylation Initiated by METTL3 Directly Promotes YAP Translation and Increases YAP Activity by Regulating the MALAT1-miR-1914-3p-YAP axis to Induce NSCLC Drug Resistance and Metastasis. *J. Hematol. Oncol.* 12, 135. doi:10.1186/s13045-019-0830-6

Jin, Y., Feng, S. J., Qiu, S., Shao, N., and Zheng, J. H. (2017). LncRNA MALAT1 Promotes Proliferation and Metastasis in Epithelial Ovarian Cancer via the PI3K-AKT Pathway. *Eur. Rev. Med. Pharmacol. Sci.* 21, 3176–3184.

Jones, G. S., and Baldwin, D. R. (2018). Recent Advances in the Management of Lung Cancer. *Clin. Med.* 18, s41–s46. doi:10.7861/clinmedicine.18-2-s41

Kim, J., Piao, H.-L., Kim, B.-J., Yao, F., Han, Z., Wang, Y., et al. (2018). Long Noncoding RNA MALAT1 Suppresses Breast Cancer Metastasis. *Nat. Genet.* 50, 1705–1715. doi:10.1038/s41588-018-0252-3

Li, B., Zhu, L., Lu, C., Wang, C., Wang, H., Jin, H., et al. (2021). circNDUFB2 Inhibits Non-small Cell Lung Cancer Progression via Destabilizing IGF2BPs and Activating Anti-tumor Immunity. *Nat. Commun.* 12, 295. doi:10.1038/s41467-020-20527-z

Li, M., Shi, M., Hu, C., Chen, B., and Li, S. (2021). MALAT1 Modulated FOXP3 Ubiquitination Then Affected GINS1 Transcription and Drived NSCLC Proliferation. *Oncogene* 40, 3870–3884. doi:10.1038/s41388-021-01816-3

Li, T., Hu, P.-S., Zuo, Z., Lin, J.-F., Li, X., Wu, Q.-N., et al. (2019). METTL3 Facilitates Tumor Progression via an m6A-igf2bp2-dependent Mechanism in Colorectal Carcinoma. *Mol. Cancer* 18, 112. doi:10.1186/s12943-019-1038-7

Liu, H. B., Muhammad, T., Guo, Y., Li, M. J., Sha, Q. Q., Zhang, C. X., et al. (2019). RNA-Binding Protein IGF2BP2/IMP2 Is a Critical Maternal Activator in Early Zygotic Genome Activation. *Adv. Sci.* 6, 1900295. doi:10.1002/advs.201900295

Pu, J., Wang, J., Qin, Z., Wang, A., Zhang, Y., Wu, X., et al. (2020). IGF2BP2 Promotes Liver Cancer Growth through an m6A-FEN1-dependent Mechanism. *Front. Oncol.* 10, 578816. doi:10.3389/fonc.2020.578816

Song, J., Su, Z. Z., and Shen, Q. M. (2020). Long Non-coding RNA MALAT1 Regulates Proliferation, Apoptosis, Migration and Invasion via miR-374b-5p/SRSF7 axis in Non-small Cell Lung Cancer. *Eur. Rev. Med. Pharmacol. Sci.* 24, 1853–1862. doi:10.26355/eurrev_202002_20363

Song, Y., Guo, N. H., and Zheng, J. F. (2020). LncRNA-MALAT1 Regulates Proliferation and Apoptosis of Acute Lymphoblastic Leukemia Cells via miR-205-PTK7 Pathway. *Pathol. Int.* 70, 724–732. doi:10.1111/pin.12993

Tang, Y., Xiao, G., Chen, Y., and Deng, Y. (2018). LncRNA MALAT1 Promotes Migration and Invasion of Non-small-cell Lung Cancer by Targeting miR-206 and Activating Akt/mTOR Signaling. *Anticancer Drugs* 29, 725–735. doi:10.1097/cad.0000000000000650

Xue, L., Li, J., Lin, Y., Liu, D., Yang, Q., Jian, J., et al. (2021). m 6 A Transferase METTL3-induced lncRNA ABHD11-AS1 Promotes the Warburg Effect of Non-small-cell Lung cancerA Transferase METTL3-Induced lncRNA ABHD11-AS1 Promotes the Warburg Effect of Non-small-cell Lung Cancer. *J. Cel Physiol* 236, 2649–2658. doi:10.1002/jcp.30023

Zhang, J., Piao, C.-D., Ding, J., and Li, Z.-W. (2020). LncRNA MALAT1 Facilitates Lung Metastasis of Osteosarcomas through miR-202 Sponging. *Sci. Rep.* 10, 12757. doi:10.1038/s41598-020-69574-y

Conflict of Interest: The authors declare that the research was conducted in the absence of any commercial or financial relationships that could be construed as a potential conflict of interest.

Publisher's Note: All claims expressed in this article are solely those of the authors and do not necessarily represent those of their affiliated organizations, or those of the publisher, the editors, and the reviewers. Any product that may be evaluated in this article, or claim that may be made by its manufacturer, is not guaranteed or endorsed by the publisher.

frontiers in Molecular Biosciences

ORIGINAL RESEARCH
published: 25 January 2022
doi: 10.3389/fmolb.2021.791455

Optimization of Ribosome Footprinting Conditions for Ribo-Seq in Human and *Drosophila melanogaster* Tissue Culture Cells

Katerina Douka[1,2], *Michaela Agapiou*[1,2], *Isabel Birds*[1,2] *and Julie L. Aspden*[1,2]*

[1]School of Molecular and Cellular Biology, Faculty of Biological Sciences, University of Leeds, Leeds, United Kingdom, [2]LeedsOmics, University of Leeds, Leeds, United Kingdom

Our understanding of mRNA translation and its regulation has been transformed by the development of ribosome profiling. This approach relies upon RNase footprinting of translating ribosomes in a precise manner to generate an accurate snapshot of ribosome positions with nucleotide resolution. Here we tested a variety of conditions, which contribute to the preciseness of ribosome footprinting and therefore the success of ribosome profiling. We found that NaCl concentration, RNaseI source, RNaseI amount, and temperature of footprinting all contributed to the quality of ribosome footprinting in human neuroblastoma SH-SY5Y cells. These ideal conditions for footprinting also improved footprint quality when used with *Drosophila melanogaster* S2 cells. Footprinting under the same conditions generated different footprints sizes and framing patterns in human and *D. melanogaster* cells. We also found that treatment of S2 cells with cycloheximide prior to footprinting impacted the distribution of footprints across ORFs, without affecting overall read length distribution and framing pattern, as previously found in other organisms. Together our results indicate that a variety of factors affect ribosome footprint quality and the nature of precise footprinting varies across species.

Keywords: Ribo-seq, ribosome profiling, footprinting, mRNA translation, ORF

OPEN ACCESS

Edited by:
Neva Caliskan, Helmholtz Institute for RNA-Based Infection Research (HIRI), Germany

Reviewed by:
Can Cenik, University of Texas at Austin, United States
Neelanjan Mukherjee, University of Colorado Anschutz Medical Campus, United States

***Correspondence:**
Julie L. Aspden
j.aspden@leeds.ac.uk

Specialty section:
This article was submitted to RNA Networks and Biology, a section of the journal Frontiers in Molecular Biosciences

Received: *08 October 2021*
Accepted: *03 December 2021*
Published: *25 January 2022*

Citation:
Douka K, Agapiou M, Birds I and Aspden JL (2022) Optimization of Ribosome Footprinting Conditions for Ribo-Seq in Human and Drosophila melanogaster *Tissue Culture Cells. Front. Mol. Biosci. 8:791455. doi: 10.3389/fmolb.2021.791455*

INTRODUCTION

Next-generation sequencing approaches have transformed our understanding of gene expression and its regulation. RNA-seq based methods revolutionised the measurement of RNA species, levels, and splicing. However, mRNA translation lagged behind in its study at the genome-wide level until the development of ribosome profiling (Ribo-Seq) (Ingolia et al., 2009). The use of Ribo-Seq has transformed our understanding of the translatome, revealing translation of novel ORFs (Douka et al., 2021), stop-codon read through (Dunn et al., 2013), use of alternative initiation codons, (Van Damme et al., 2014) and providing mechanistic insights into translation elongation (Wu et al., 2019) and ribosome stalling (Rubio et al., 2021). This approach has been employed across a wide range of species and systems (Ingolia et al., 2009; Guo et al., 2010; Baltz et al., 2012; Ingolia et al., 2013; Aspden et al., 2014; Duncan and Mata, 2014; Chung et al., 2015; Heyer and Moore, 2016; Hsu et al., 2016). By isolating and sequencing the portion of RNA covered by the translational machinery, the ribosome, we can now perform transcriptome-wide assessments of protein translation and translational regulation.

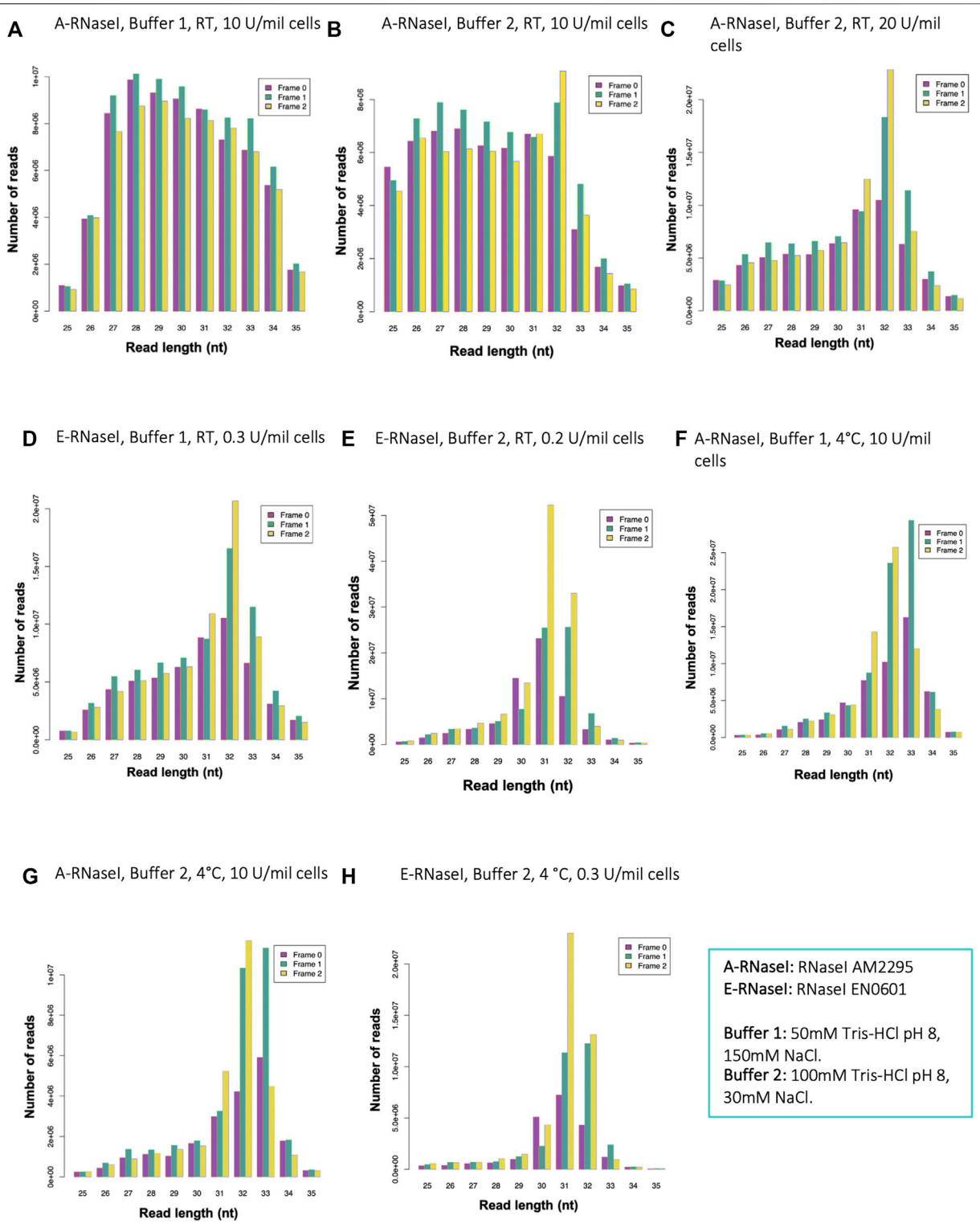

FIGURE 1 | Changes to RNaseI footprinting affects size and framing of ribosome footprints in human SH-SY5Y cells. Read length distribution and frame plots, generated by RiboSeqR, from ribosome footprinting in cells SH-SY5Y under different conditions: **(A)** Buffer 1 (50 mM Tris-HCl pH8, 150 mM NaCl), RT 1 h, with A-RNaseI 10 U/million cells, **(B)** Buffer 2 (100 mM Tris-HCl pH8, 30 mM NaCl), RT 1 h, with A-RNaseI 10 U/million cells, **(C)** Buffer 2, RT 1 h, with A-RNaseI 20 U/million cells, **(D)** Buffer 1, RT 1 h, with E-RNaseI 0.3 U/million cells, **(E)** Buffer 2, RT 1 h, with E-RNaseI 0.2 U/million cells, **(F)** Buffer 1, O/N at 4°C, with A-RNaseI 10 U/million cells, **(G)** Buffer 2, O/N at 4°C, with A-RNaseI 10 U/million cells, **(H)** Buffer 2, O/N at 4°C, with E-RNaseI 0.3 U/million cells. See **Table 1** for full details of each condition tested.

Central to the success of ribosome profiling experiments is the ability to isolate ribosome footprints. The key experimental step in the generation of footprints is the RNase treatment of cytoplasmic lysate. Ribosome footprints are typically around 28–32 nucleotides (nt), although this varies by organism, cell or tissue type, and experimental protocol (Ingolia et al., 2013; Aspden et al., 2014). For Ribo-Seq data to be useful in the study of translation, the fragments of RNA sequenced need to originate from ribosome protected fragments rather than other RNA-protein complexes. Therefore, it is important to isolate RNA fragments corresponding to 28–32 nt ribosome footprints rather other smaller non-translation dependent fragments.

One of the important and distinctive features of Ribo-Seq data compared to RNA-seq data is its triplet periodicity. This is a bias in the mapping of reads toward one of the three possible reading frames, reflecting the codon-by-codon decoding activity of the ribosome. This pattern is not observed in RNA-seq, and a strong framing preference is indicative of high quality Ribo-Seq data. Triplet periodicity is assessed using metagene plots; aggregate plots which illustrate the distance between one end of the Ribo-Seq read (generally 5′) and the annotated start and stop codons of consensus coding sequence (CCDS). A clear preference for a single reading frame is expected. Metaplots can also be used to infer the position of the P-site of the ribosome with respect of the ribosome footprint read. This feature is important in determining precisely which codon is being decoded by each read. Together with framing, this information enables quality assessment of the ribosome profiling to be performed, and can also provide insight into the movement of the ribosome (Lareau et al., 2014; Wu et al., 2019).

The majority of standard Ribo-Seq reads are expected to map to canonical coding sequences, with a low percentage mapping to 5′-untranslated regions (UTRs) and very few to 3′-UTRs. Ribosome footprints mapping to 5′-UTRs generally represent scanning ribosomes, or the translation of upstream ORFs (uORFs) (Heyer & Moore, 2016; Rodriguez et al., 2019; Chen et al., 2020), while reads in the 3′-UTR may represent rarer downstream ORF (dORF) translation events. RNA-binding proteins (RBPs) can also create footprints, but these will not exhibit a framing bias, and may be of different lengths to true ribosome footprints (Ruiz-Orera and Albà, 2019). Although many technical improvements have been made to the original ribosome profiling protocol, there are several experimental variables that can be altered to optimise footprinting conditions. These include buffer conditions, temperature, amount and type of RNAseI. When working with a new organism or tissue type, or starting up ribosome profiling in a new lab, it is not always clear where to start, or how much variation from published data should be expected. Here we describe work to optimise footprinting conditions in human neuroblastoma SH-SY5Y cells and *Drosophila melanogaster* S2 cells. Together these experiments indicate key attributes which can affect the quality of ribosome profiling data in two different organisms although comparisons are only qualitative because additional replicates were not performed. Our results illustrate the impact experimental conditions can have on the final outputs of such experiments.

MATERIALS AND METHODS

Cell Culture

Human neuroblastoma SH-SY5Y cells were cultured in Dulbecco's Modified Eagle Medium (DMEM; 4.5 g/L Glucose with L-Glutamine) supplemented with 1% (v/v) Penicillin/Streptomycin (GE Healthcare) and 10% Fetal Bovine Serum (FBS, Sigma) at 37°C, 5% CO_2. Semi-adherent *D. melanogaster* S2 cells were maintained in Schneider's medium containing L-glutamine (Sigma) supplemented with 1% (v/v) Penicillin/Streptomycin/amphotericin B (GE Healthcare), 10% FBS, and maintained at 26°C in non-vented, adherent flasks (Sarstedt).

Poly-Ribo-Seq

Cells were treated with cycloheximide (Sigma) at 100 μg/ml for 3 min at 37°C, washed (1X PBS, 100 μg/ml cycloheximide) and trypsinised for 5 min at 37°C. Subsequently, cells were pelleted, washed (1X PBS, 100 μg/ml cycloheximide), and resuspended in ice cold lysis buffer (**Supplementary Table S1**); 50 mM Tris-HCl pH8, 150 mM NaCl, 10mM $MgCl_2$, 1 mM DTT, 1% IGEPAL, 100 μg/ml cycloheximide, Turbo DNase 24 U/mL (Invitrogen), RNasin Plus RNase Inhibitor 90 U (Promega), cOmplete Protease Inhibitor (Roche), for 45 min. Cells were then subjected to centrifugation at 17,000 × g for 5 min, to pellet nuclei. Cytoplasmic lysate was loaded onto 18–60% sucrose gradients (~70×10^6 cells per gradient) at 4°C and subjected to ultracentrifugation (121,355 × g_{avg} 3.5h, 4°C) in SW-40 rotor. Polysome fractions were pooled and diluted in either Buffer 1 (50 mM Tris-HCl pH8, 150 mM NaCl, 10 mM $MgCl_2$) or Buffer 2 (100 mM Tris-HCl pH8, 30 mM NaCl, 10 mM $MgCl_2$). RNaseI (either AM2295 at 10–20U/million cells, or EN601, 10 U/μl 0.7–1 U/million cells) was subsequently added incubated either for 1 h at RT or overnight at 4°C. RNaseI was deactivated using SUPERase inhibitor (200U/gradient) for 5 min at 4°C. Samples were concentrated using 30 kDa molecular weight cut-off columns (Merck) and loaded on sucrose cushion (1 M sucrose, 50 mM Tris-HCl pH8, 150 mM NaCl, 10mM $MgCl_2$, 40U RNase Inhibitor) and subjected to ultracentrifugation at 204,428 × g_{avg} at 4°C for 4 h (TLA110). Pellets were resuspended in TRIzol (Ambion, Life Technologies) and processed for RNA purification followed by TURBO DNase treatment (Thermofisher) (according to manufacturer's instructions), acidic phenol/chloroform RNA purification and ethanol precipitation at −80°C overnight. RNA concentration was determined by Nano-drop 2000 software. 28–34 nt ribosome footprints were gel purified in 10% (w/v) polyacrylamide-TBE-urea gel at 300 V for 3.5 h in 1X TBE. Ribosome footprints were subjected to rRNA depletion (Illumina, RiboZero rRNA removal kit).

Ribo-Seq

Cycloheximide treated cells were treated for 3 min with 100 μg/ml cycloheximide before being pelleted. All cells were pelleted (8 min at 800 ×g), washed (1 × PBS, 100 μg/ml cycloheximide) and resuspended in ice cold lysis buffer and left to lyse for 45 min. Nuclei were removed via centrifugation (17,000 × g for 5 min) and cytoplasmic lysates were footprinted overnight at 4°C. Two different footprinting conditions were tested on both cycloheximide treated and untreated lysates: 1) A-RNAseI (AM2295) in Buffer 1 (50 mM Tris-HCl pH8, 150 mM NaCl, 10 mM $MgCl_2$), 2)

E-RNAseI (EN0601) in Buffer 2 (100 mM Tris-HCl pH8, 30 mM NaCl, 10 mM $MgCl_2$). RNaseI was deactivated using SUPERase inhibitor (500°U/gradient) for 5 min at 4°C. Footprinted lysates were loaded onto sucrose gradients and subjected to ultracentrifugation at 4°C and subjected to ultracentrifugation (121,355 × g_{avg} 3.5h, 4°C) in SW-40 rotor. 80S ribosomes were purified away from ribosomal subunits and polysomes. RNA was isopropanol precipitated, TURBO DNase treated, acidic phenol/chloroform purified and ethanol precipitated at -80°C overnight. 28–34 nt ribosome footprints were gel purified via a 10% (w/v) polyacrylamide-TBE-urea gel (300°V, 3.5°h, 1X TBE), T4 PNK treated and isopropanol precipitated. rRNA depletion for S2 cells carried out with custom made beads. rRNA depleted footprints were ethanol precipitated again.

Library Preparation and Sequencing

5′ stranded libraries were constructed using NEB Next Multiplex Small RNA Library Prep. Resulting cDNA was PCR amplified and gel purified prior to sequencing. Libraries were subjected to 75bp single end RNA Seq using NextSeq500 Illumina sequencer, High Output Kit v2.5 (75 Cycles) (Next Generation Sequencing Facility, Faculty of Medicine, University of Leeds).

Ribosome Footprinting Analysis

Poly-Ribo-Seq and Ribo-Seq fastq files were uploaded on Ribogalaxy (Michel et al., 2016) and subjected to quality control using FastQC (v.0.11.5) (Andrews, 2010). 3′ end adapter sequence AGATCGGAAGAGCACACGTCT was trimmed from the reads using Cutadapt (v.1.1) (Martin, 2011), discarding untrimmed footprint reads. Trimmed reads were further filtered, so that 90% of each read passed the quality threshold Phred score of 20, using the Filter by quality tool (Gordon, 2010) on Galaxy (Afgan et al., 2018). Subsequently, rRNA and tRNA reads were removed, using Bowtie (v.0.12.7) (Langmead and Salzberg, 2012) and 1 base trimmed from the 3′ end of reads. For assessment of the framing quality of ribosome footprinting, reads were mapped to the human (version hg38, Gencode v29) or the *D. melanogaster* (version dm3, BDGP Release 5) transcriptome and were subsequently processed with the RiboSeqR pipeline (Hardcastle, 2014). The analysis was performed on read lengths 25–35 nt, in order to assess the number of reads of each specific length that are in each frame. A metagene analysis was performed on the reads that display the best triplet periodicity (31 and 33 nt for human, 28 and 29 nt for fly) with parameters for filtering those reads (filterHits parameters) set as: lengths = 31, 33 (or 28, 29); frames = 1, 2, 3; hitMean = 50; unqhitMean = 10. Plots were generated and the plotCDS (parameters set as: lengths = 31, 33 (or 28, 29); min5p = -100; max5p = 100; min3p = −100; max3p = 100). In this analysis, reads were globally mapped to 5′ and 3′ UTRs and coding regions (CDS) and the mean number of reads that is mapped to each region is plotted.

Translated ORF Detection

Quality reports of *D. melanogaster* Ribo-Seq and RNA-seq data were made using Fastqc (v.0.11.9) (Andrews, 2010). Adapter sequences (AGATCGGAAGAGCACACGTCT) were trimmed using Cutadapt (v.2.10) (Martin, 2011) with minimum read length of 25bp, and untrimmed outputs retained for RNA-seq reads. Low-quality reads (score < 20 for 10% or more of read) were then discarded using FASTQ Quality Filter, FASTX-Toolkit (v.0.0.14) (Gordon, 2010). *D. melanogaster* rRNA sequences were retrieved from RiboGalaxy (Michel et al., 2016) and tRNA sequences from FlyBase release FB 2020_04 (Larkin et al., 2021). One base was removed from 3′ end of reads to improve alignment quality, and reads originating from rRNA and tRNA were aligned and removed using Bowtie2 (v.2.4.1) (Langmead and Salzberg, 2012).

The splice aware aligner STAR (v2.7.5c) (Dobin et al., 2012) was used to map remaining reads to the *D. melanogaster* reference genome (r6.35) from FlyBase (Larkin et al., 2021). The STAR (v2.7.5c) (Dobin et al., 2012) genome index was built with a sjdbOverhang of 99. Samtools (v.1.10) (Li et al., 2009) was used to create sorted, indexed bam files of the resulting alignments. These bam files were then subsampled to ~2,000,000 reads per sample to create a fairer comparison. Alignments were visualised using Golden Helix GenomeBrowse (v3.0.0).

Metaplots of aligned Ribo-Seq data were generated using create_metaplots.bash script from Ribotaper (v1.3) pipeline (Calviello et al., 2016). These show the distance between the 5′ ends of Ribo-Seq and annotated start and stop codons from CCDS ORFs, allowing the locations of P-sites to be inferred. Read lengths exhibiting the best triplet periodicity were selected for each replicate, along with appropriate offsets (**Supplementary Table S2**).

Translated smORFs were then identified using Ribotaper (v1.3) (Calviello et al., 2016). Initially, this requires an exon to contain more than 5 P-sites in order to pass to quality control steps. Identified ORFs were then required to have a 3-nt periodic pattern of Ribo-Seq reads, with 50% or more of the P-sites in-frame. In the case of multiple start codons, the most upstream in-frame start codon with a minimum of 5 P-sites in between it and the next ATG was selected. ORFs for which >30% of the Ribo-Seq coverage was only supported by multimapping reads were also subsequently filtered (Chothani et al., 2019).

General Statistics and Plots

Statistical analyses were performed in R (R Core Team, 2020) using packages including stringr (Wickham, 2019), dplyr (Wickham et al., 2017), ggplot2 (Wickham, 2016), knitr (Xie, 2020), eulerr (Larsson, 2020), viridis (Garnier et al., 2021) and tidyverse (Wickham et al., 2019).

RESULTS

Changes to RNaseI Footprinting Affects Size and Framing of Ribosome Footprints in Human SH-SY5Y Cells

The precise conditions in which ribosome footprinting is performed can have substantial impact on the quality of the ribosome profiling experiment, as judged by the preciseness of the footprint and the level of triplet periodicity (framing). Although

additional attributes can be used to assess the reproducibility of transcript-specific ribosome occupancy, we have focused on footprint size and triplet periodicity to specifically assess the quality of ribosome footprinting rather than other aspects of ribosome profiling. Triplet periodicity is particularly important when attempting to identify novel ORFs to ensure footprints represent elongating ribosomes rather than non-specific protein or ribosome binding. We previously developed an adaptation to Ribo-Seq, Poly-Ribo-Seq in *D. melanogaster* S2 cells (Aspden et al., 2014) (**Supplementary Figure S1**). By ribosome footprinting polysomal complexes rather than all ribosomal complexes, i.e., monosomes and polysomes, Poly-Ribo-Seq aids detection of genuine translation events in small or noncanonical ORFs.

To employ Poly-Ribo-Seq for the first time in human neuroblastoma SH-SY5Y cells, and identify novel translation events, we initially tried the same footprinting conditions previously performed in *D. melanogaster* S2 cells. This included 50 mM Tris-HCl pH8, 150 mM NaCl, 10 mM $MgCl_2$ and RNase I (AM2295) at 10 U/million cells, but with footprinting performed at room temperature (RT) for 1 h, as is standard for human cells (McGlincy, 2017; Wu et al., 2019). On the urea-acrylamide gel used to purify footprints, a smeary band corresponding to ribosome footprints was visible between the RNA markers of 28 and 34 nt (**Supplementary Figure S2A**). However, ribosome footprinting under these conditions resulted in ribosome footprint reads with a wide length distribution and virtually no triplet periodicity (**Figure 1A**). Most footprints did map to CCDSs indicating that they represented ribosomes (**Supplementary Figure S3A**), but with some noise within 5′-UTRs and imprecisely footprinted. Therefore, we sought to test a range of factors to improve the preciseness of the ribosome footprinting. Given these experiments were simply testing conditions only single replicates were performed.

Previously others have found in *Arabidopsis thaliana* that the buffer conditions of the footprinting buffer can affect RNAseI activity and therefore footprinting (Hsu et al., 2016). To emulate these conditions, we modified the buffer to reduce NaCl from 150 to 30 mM, and increased Tris-HCl pH8 from 50 to 100 mM, to test if this improved footprinting. We refer to the 50 mM Tris-HCl pH8, 150 mM NaCl buffer as Buffer 1, and the 100 mM Tris-HCl pH8, 30 mM NaCl buffer as Buffer 2. These changes to the buffer conditions did have a small effect on improving triplet periodicity of reads (**Figure 1B**). However, reads still showed a wide length distribution and low triplet periodicity. Therefore, we modified aspects of the RNase treatment to try and improve quality of footprinting. Increasing the amount of RNaseI present in the footprinting reaction dramatically improved both length distribution and framing (**Figure 1C**). The ratio of the amount of RNaseI enzyme to the RNA present in the reaction is important to ensure precise footprinting. Therefore the amount of RNaseI used in each experiment was adjusted based on the number of cells being subjected to footprinting, to maintain a consistent ratio between RNaseI and RNA.

Several Ribo-Seq publications have used alternative sources of RNaseI (McGlincy, 2017). Therefore, we tested EN0601 RNase (Thermofisher), E-RNaseI, alongside the AM2295 (Ambion), A-RNaseI, we previously used (**Table 1**). This E-RNaseI, when used in Buffer 1, also led to an improvement in triplet periodicity and footprint length distribution (**Figure 1D**). A combination of E-RNaseI and Buffer 2, together resulted in a substantial improvement to preciseness of footprinting (**Figure 1E**). Under these conditions 72% of footprints were 31–32 nt in length. The most abundant read length (31 nt) exhibits high levels of framing with 52% of 31 nt read in frame 2 (**Supplementary Figure S3B**).

Previously in *D. melanogaster* we had performed footprinting at 4°C overnight to maintain stable ribosomes. However, the majority of Ribo-Seq experiments in human cells are performed at RT for 1 h (McGlincy, 2017; Wu et al., 2019). Performing footprinting at 4°C overnight with the A-RNaseI in Buffer 1, resulted in footprints with precise footprint of 31–33 nt, with good framing (**Figure 1F**, compared to **Figure 1A**). The temperature of footprinting clearly contributes a substantial improvement. An almost identical pattern was found when performed with Buffer 2 (**Figure 1G**), suggesting that the buffer has less of an effect on footprinting when performed at 4°C overnight compared to at RT for 1 h. In attempt to maximise the number of ribosomes remaining intact as 80S ribosomes bound to mRNAs, samples were also loaded onto gradients at 4°C, as well as footprinted at 4°C. This combination had little effect in the context of E-RNaseI (**Figure 1H** compared to **Figure 1E**).

Together the ribosome profiling conditions tested (**Table 1**) indicate that a number of factors contribute to the effectiveness of ribosome footprinting (**Table 2**). Buffer conditions can be modified to improve quality of footprints but in general it was more straightforward to achieve high quality footprints with E-RNaseI. Reducing the temperature, changing the buffer, and increasing amount of RNaseI all helped improved quality. For our cells of interest, human SH-SY5Y cells, we identified the best conditions (of those we tested) to be E-RNAaseI, 100 mM Tris-HCl pH8, 30 mM NaCl, ON at 4°C (**Figure 1H**), which produced the highest level of periodicity (**Supplementary Figures S3C,D**). Comparing metagene plots from these 'best' conditions, with those we started with (A-RNAaseI, 50 mM Tris-HCl pH8, 150 mM NaCl, RT for 1 h), at their ideal read lengths, background signal has been reduced substantially. Specifically, there are fewer reads mapping to UTRs in these improved conditions (**Supplementary Figures S3D,E**) compared to starting conditions (**Supplementary Figure S3A**).

Changes to RNaseI Footprinting Affects Size and Framing of Ribosome Footprints in *Drosophila* S2 Cells

To determine whether the improvements tested in human SH-SY5Y cells would also affect footprinting in *D. melanogaster* we performed Ribo-Seq on S2 cells in the best conditions we identified in SH-SY5Y cells (Buffer 2: 100 mM Tris-HCl pH8, 30 mM NaCl and ~0.4 U/million cells E-RNaseI). Bands corresponding to ribosome footprints were visible on urea-acrylamide gels between 28 and 34 nt RNA markers (**Supplementary Figure S2B**). When compared with the 'old' conditions (Buffer 1: 50 mM Tris-HCl pH 8 and 150 mM NaCl

TABLE 1 | Summary of ribosome footprinting conditions tested with human SH-SY5Y cells.

Panel in Figure 2	RNaseI	Tris-HCl and NaCl concentrations	Footprinting temperature	Footprinting time
A	AM2295 10 U/million cells	50 mM Tris-HCl pH8, 150 mM NaCl (Buffer 1)	RT	1 h
B	AM2295 10 U/million cells	100 mM Tris-HCl pH8, 30 mM NaCl (Buffer 2)	RT	1 h
C	AM2295 20 U/million cells	100 mM Tris-HCl pH8, 30 mM NaCl (Buffer 2)	RT	1 h
D	EN0601 0.3 U/million cells	50 mM Tris-HCl pH8, 150 mM NaCl (Buffer 1)	RT	1 h
E	EN0601 0.2 U/million cells	100 mM Tris-HCl pH8, 30 mM NaCl (Buffer 2)	RT	1 h
F	AM2295 10 U/million cells	50 mM Tris-HCl pH8, 150 mM NaCl (Buffer 1)	4°C	overnight
G	AM2295 10 U/million cells	100 mM Tris-HCl pH8, 30 mM NaCl (Buffer 2)	4°C	overnight
H	EN0601 0.3 U/million cells	100 mM Tris-HCl pH8, 30 mM NaCl (Buffer 2)	4°C	overnight

*Ribosome footprinting conditions tested in human SH-SY5Y cells with reference to data in **Figure 1**, RNaseI type and units, Tris-HCl pH8 and NaCl concentrations, incubation temperature and incubation time.*

TABLE 2 | Summary conclusions from conditions tested.

Test	Background	Panels	Conclusion	Triplet periodicty (%)	Read length
Buffer conditions	A-RNaseI RT for 1 h	A and B	100 mM Tris-HCl, 30 mM NaCl > 50 mM Tris-HCl, 150 mM NaCl	2	Little difference
Buffer conditions	E-RNaseI RT for 1 h	D and E	100 mM Tris-HCl, 30 mM NaCl > 50 mM Tris-HCl, 150 mM NaCl	9	Increase in % of 31-32 nt reads
Buffer conditions	A-RNaseI, 4°C ON	F and G	100 mM Tris-HCl, 30 mM NaCl = 50 mM Tris-HCl, 150 mM NaCl	1	No difference. Both high % of 31-33 nt reads
RNaseI quantity	100 mM Tris-HCl pH8, 30 mM NaCl, A-RNaseI RT for 1 h	B and C	20U/million cells >> 10U/million cells	4	Large increase in % of 31-33 nt reads
RNaseI source	50 mM Tris-HCl pH8, 150 mM NaCl, RT for 1 h	A and D	E-RNaseI >>> A-RNaseI	6	Large increase in % of 31-33 nt reads
RNaseI source	100 mM Tris-HCl pH8, 30 mM NaCl, 4°C ON	G and H	E-RNaseI = A-RNaseI	3	Shift from 32 to 33 nt to 31–32 nt reads
RNaseI source	100 mM Tris-HCl pH8, 30 mM NaCl, RT for 1 h	C and E	E-RNaseI >> A-RNaseI	8	Moderate increase in % of 31-32 nt reads. Shift from 31 to 33 nt to 30–32 nt
Temperature	A-RNaseI, 50 mM Tris-HCl pH8, 150 mM NaCl,	A and F	4°C ON >>> RT for 1 h	13	Large increase in % of 31-33 nt reads
Temperature	E-RNaseI, 100 mM Tris-HCl pH8, 30 mM NaCl,	E and H	4°C ON = RT for 1 h	3	No difference in % of 31-32 nt reads
Temperature	E-RNaseI, 100 mM Tris-HCl pH8, 30 mM NaCl,	B and G	4°C ON >>> RT for 1 h	12	Large increase in % of 31-33 nt reads

*Details of different tests performed and in what background conditions, which panels in **Figure 1** show the results and conclusion of which condition achieved better footprint length and framing. Measures of changes in triplet periodicity (% difference in dominant frame for read length with best framing) and read length distribution (difference in % read length distribution and read length with best periodicity).*

and ~20 U/million cells A-RNaseI, these new conditions made a substantial improvement to effectiveness of footprinting in *D. melanogaster* S2 cells (compare **Figures 2A,B**). The majority of footprints are 28–29 nt under these Buffer 2 and E-RNaseI conditions, compared to 28–31 nt in Buffer 1 with A-RNaseI conditions (**Figures 2A,B**). The proportion of reads exhibiting triplet periodicity is improved substantially from 51% of 29 nt reads in frame 0 (**Figure 2A**) to 61% of 28 nt reads in frame 0 (**Figure 2B**). The improvements to footprint length distribution and triplet periodicity were seen both in the presence (**Figures 2A,B**), absence of cycloheximide (**Supplementary Figures S4A,B**). Both footprinting conditions tested in S2 cells resulted in the majority of footprints mapping to coding sequences (CDSs), as evident in metagene analysis (**Figures 2C,D**).

Downstream analysis of the Ribo-Seq data revealed that the improved footprinting conditions identified more actively translated ORFs, both in the presence and absence of cycloheximide (**Table 3**). The number of CCDS ORFs - ORFs which overlap known coding regions in CCDS genes - increased by ~1/5 in the new conditions (from 7,511 to 9,654), while the number of upstream ORFs (uORFs) detected nearly doubled (from 39 to 71). This indicates that the improved ribosome footprinting conditions not only increase triplet periodicity and preciseness of footprints, but also lead to the better detection of translation.

Cycloheximide Treatment Affects Ribosome Footprint Distribution and Length

Previous Poly-Ribo-Seq in *D. melanogaster* S2 cells had only achieved modest framing and was performed in the presence of cycloheximide (Aspden et al., 2014). Therefore, we sought to determine the effect the addition of cycloheximide has in *D. melanogaster*. This is of particular interest for dissected tissues from numerous individual organisms (e.g. *D. melanogaster* testes) because batch flash freezing is not straightforward, and therefore cycloheximide is likely useful to trap elongating ribosomes.

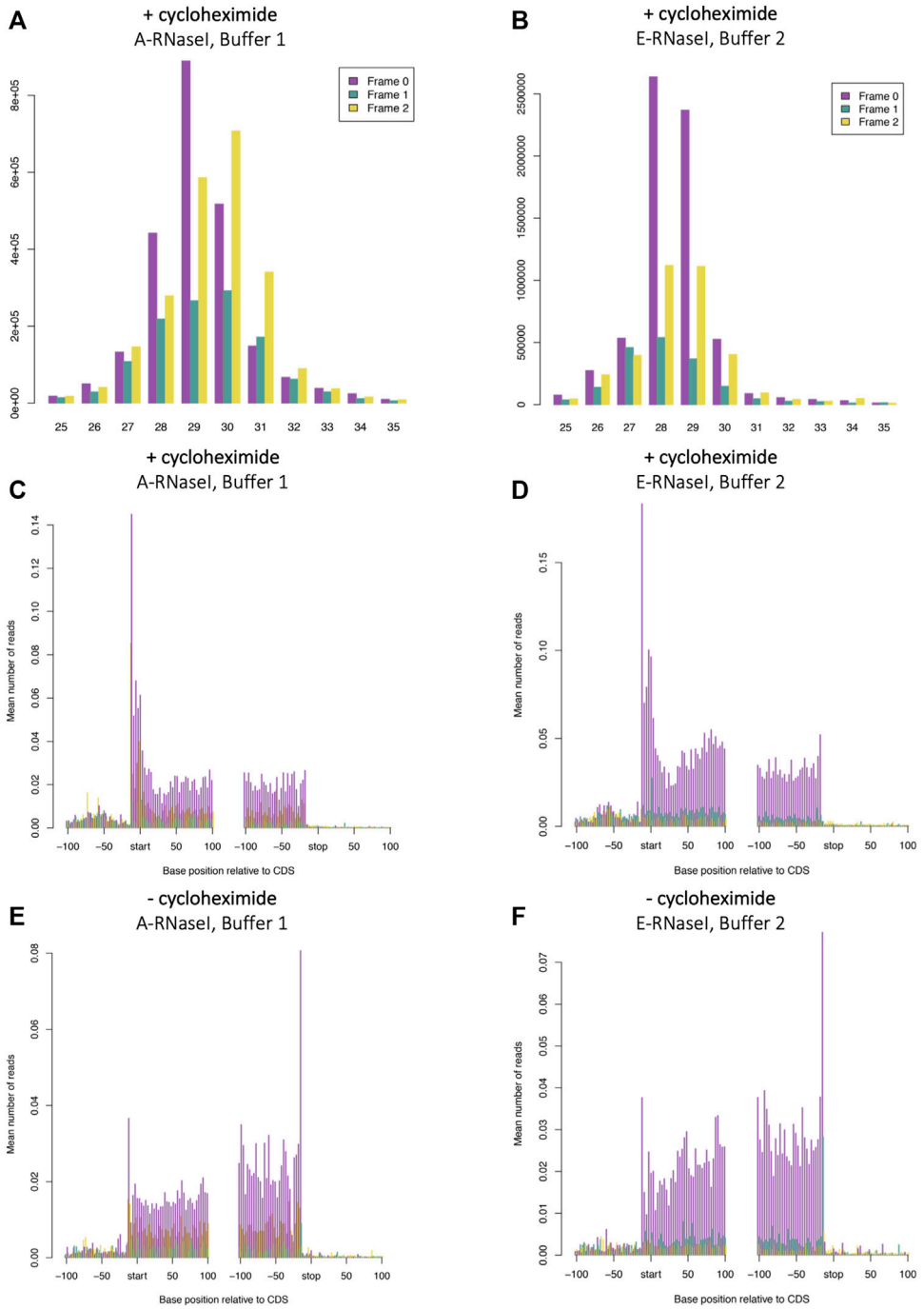

FIGURE 2 | Changes to RNaseI footprinting affects size and framing of ribosome footprints in *Drosophila* S2 cells. Read length distribution and frame plots from Ribosome footprinting in *D. melanogaster* S2 cells in **(A)** A-RNaseI and Buffer 1 (50 mM Tris-HCl pH8, 150 mM NaCl) and **(B)** E-RNaseI and Buffer 2 (100 mM Tris-HCl pH8, 30 mM NaCl) footprinting conditions, both in presence of cycloheximide (100 µg/ml). Metagene plots from 29 nt ribosome footprints **(C and E)** A-RNaseI and Buffer 1 and metagene plots from 28 nt ribosome footprints **(D and F)** E-RNaseI and Buffer 2 footprinting conditions, either in **(C and D)** the presence or **(E and F)** absence of cycloheximide. Plots were generated with RiboSeqR.

To assess the effect of cycloheximide treatment Ribo-Seq was performed with S2 cells in the presence or absence of cycloheximide (final 100 µM), in the footprinting conditions used previously in *D. melanogaster* S2 cells (Aspden et al., 2014). These were 50 mM Tris-HCl pH8, 150 mM NaCl, 10 mM $MgCl_2$ (i.e. Buffer 1) and A-RNaseI (~20U/million cells). Metagene analysis revealed that cycloheximide treatment had a limited effect on footprint length or

TABLE 3 | Summary of translated ORFs identifed in *Drosophila* S2 cells.

ORF type	A-RNaseI, Buffer 1 (+cycloheximide)	E-RNaseI, Buffer 2 (+cycloheximide)	*A-RNaseI, Buffer 1 (- cycloheximide)*	*E-RNaseI, Buffer 2 (-cycloheximide)*
dORFs	**1**	**3**	*1*	*2*
ncORFS	**5**	**4**	*2*	*1*
CCDS ORFs	**7511**	**9654**	*5957*	*8407*
uORFs	**39**	**71**	*7*	*23*

Translated ORFs identified from ribosome profiling in D. melanogaster *S2 cells in A-RNaseI, Buffer 1 and E-RNaseI, Buffer 2, footprinting conditions, in the presence (bold) or absence of cycloheximide (italic). The E-RNaseI, Buffer 2, conditions, which produce better quality framing find more ORFs both with and without cycloheximide. ORF types include downstream ORFs (dORFs) found downstream of the main ORF, non-coding ORFs (ncORFs) found on transcripts currently annotated as non-coding, CCDS ORFs overlap known coding regions in CCDS genes, and upstream ORFs (uORFs) are found upstream of the main ORF.*

periodicity with Buffer 1, A-RNaseI (comparing **Supplementary Figure S4A** and **Figure 3A**) and Buffer 2 E-RNAseI (comparing **Supplementary Figure S4B** and **Figure 2B**). The distribution of reads across CDSs is affected by cycloheximide treatment, as previously described in other organisms (Duncan and Mata, 2017; Gerashchenko and Gladyshev, 2014; Hussmann et al., 2015; Sharma et al., 2019). Specifically, cycloheximide treatment results in a build-up of Ribo-Seq reads at the start codon and in the first ~15 nt of CDSs (**Figure 2C**). Whilst in the absence of cycloheximide there is a build up around the stop codon (**Figure 2E**). These footprints around the stop codon are of a different frame compared within the main part of the CDS (frame 1 rather than 0), reflecting a ribosomal rearrangement at the stop codon (Lareau et al., 2014; Wu et al., 2019). This same pattern of effect by cycloheximide can also be seen in the improved conditions that used E-RNaseI and Buffer 2 by metagene analysis (comparing **Figure 2D** and **Figure 2F**), footprint length and framing (comparing **Supplementary Figure S4B** and **Figure 2B**).

The changes of Ribo-Seq read build up caused by cycloheximide can also be seen at the transcript level (**Figure 3A**). Ribosomal protein L40 (RpL40) was found to be translated (from transcript FBtr0334787) in all conditions. In samples treated with cycloheximide there is a build-up of reads at the start of the ORF, whereas in untreated samples we can see a pile up at the 3′ end of the ORF. The effects of cycloheximide on global changes to footprinting caused by cycloheximide can also be observed, with more ORFs detected in presence of cycloheximide (**Table 3**). At the ORF level, only ~50% of the translated ORFs detected (in Buffer 2, E-RNase) in the absence of cycloheximide were also identified in the presence of cycloheximide (**Figure 3B**). At the transcript level, 94% of the transcripts were detected as translated in the absence of cycloheximide were also translated in presence of cycloheximide (**Figure 3C**), and 96% at the gene level (**Figure 3D**). Although this analysis is based on single samples, biological replicates would likely increase this overlap. This indicates that although the same translation events are likely to be taking place in both presence and absence of cycloheximide, the exact ORF a translation event is attributed to can be affected by the accumulation of reads at the start codon upon cycloheximide treatment.

Length of Footprints and Nature of Framing is Different Between Humans and *Drosophila*

One of the most time-consuming aspects of performing Ribo-Seq is the requirement to find ideal conditions for footprinting. An added complication is that comparing your data to published data sets can indicate that there may be a problem with your own footprinting, but this may represent an actual difference in footprint length and pattern of framing between different systems. Here we have performed Poly-Ribo-Seq on human SH-SY5Y cells and Ribo-Seq on *D. melanogaster* S2 cells under the same conditions: 100 mM Tris-HCl pH8, 30 mM NaCl, 10 mM $MgCl_2$ (Buffer 2) and E-RNaseI (~0.4 U/million cells). This allows us to make direct comparisons of differences between the two. Under these conditions the majority (57.1%) of *D. melanogaster* S2 cells footprints are 28–29 nt in length (**Figure 4A**), whilst in human SH-SY5Y cells they are longer: 31–32 nt (**Figure 4B**). The pattern of triplet periodicity is also different with Frame 0 the dominant frame in S2 cells and Frame 2 in SH-SY5Y cells (**Figures 4A,B**). There are also differences in the metagene profiles, with S2 cells exhibiting a higher peak of reads around the start codon and stop codon (in presence of cycloheximide) (**Figure 4C**) when compared with human SH-SY5Y cells (**Figure 4D**) (also in the presence of cycloheximide). Signal in 5′-UTRs and 3′-UTRs is higher in Poly-Ribo-Seq of human SH-SY5Y cells (**Figure 4D**) compared with Ribo-Seq of S2 cells (**Figure 4C**). This may have more to do with the different sucrose gradients used in Poly-Ribo-Seq compared to Ribo-Seq, but we cannot be sure. Comparing similar footprinting conditions between different organisms and systems can generate subtle differences in footprinting nature, but as long as footprints display substantial framing and precise length distribution, translation can be detected and measured.

DISCUSSION

In this work we have tested a variety of experimental conditions which affect the quality of ribosome footprinting in human neuroblastoma SH-SY5Y cells and *D. melanogaster* S2 cells. Since no replicates were performed, the comparisons we report are only qualitative but our results could be beneficial to those

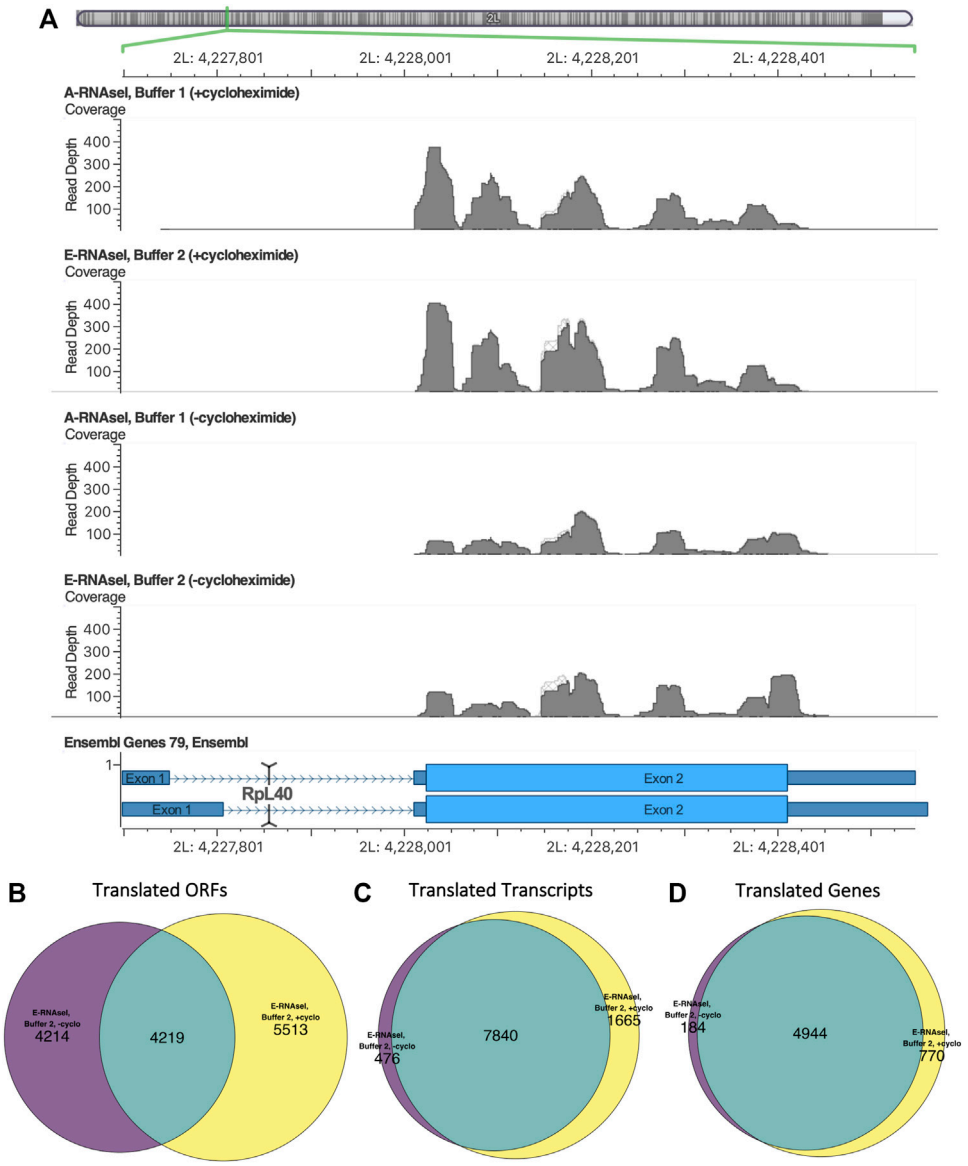

FIGURE 3 | Differences in footprinting in the presence and absence of cycloheximide in *Drosophila* S2 cells. **(A)** Ribo-seq reads mapping to RpL40 in *D. melanogaster* S2 cells viewed using Golden Helix GenomeBrowse (v3.0.0). The presence/absence of cycloheximide causes changes in footprint build up. Replicates with cycloheximide exhibit build up at the start of the ORF, and replicates without cycloheximide have a build up at the end of the ORF, reflecting a ribosomal rearrangement at the stop codon. The overlap in translation events identified in the presence and absence of cycloheximide at the **(B)** ORF, **(C)** transcript and **(D)** gene level in *D. melanogaster* S2 cells, footprinted with E-RNaseI in Buffer 2.

performing ribosome profiling and adapting to new systems. NaCl and Tris-HCl concentrations, RNaseI source, RNaseI amount, and temperature of footprinting all contributed to the quality of ribosome footprinting. This highlights some key contributing factors to the success of ribosome footprinting that may not be obvious to the beginner. Although many standard ribosome profiling protocols perform ribosome footprinting at RT, others have also found that reducing the temperature to 4°C can reduce ribosome sensitivity to RNaseI in human cell lines (Cenik et al., 2015). The amount of nuclease has also been shown to affect footprinting efficiency in other systems (Dunn et al., 2013) and small quantities of ribosomes are particularly sensitive to the amount of RNaseI during footprinting (Liu et al., 2019). We, like others, have found it important to optimize ribosome footprinting conditions for the type of material and RNase that is being used. Not all RNases respond in the same way to changes in the other conditions, as we found for the two RNaseI we tested. An additional consideration is the wide variation in activity between *E. coli* RNAseI enzymes, that use different unit definitions to measure the enzyme activity (McGlincy, 2017; Liu et al., 2019) and the need to adjust for this, as well as potential variation between RNase batches. Our results

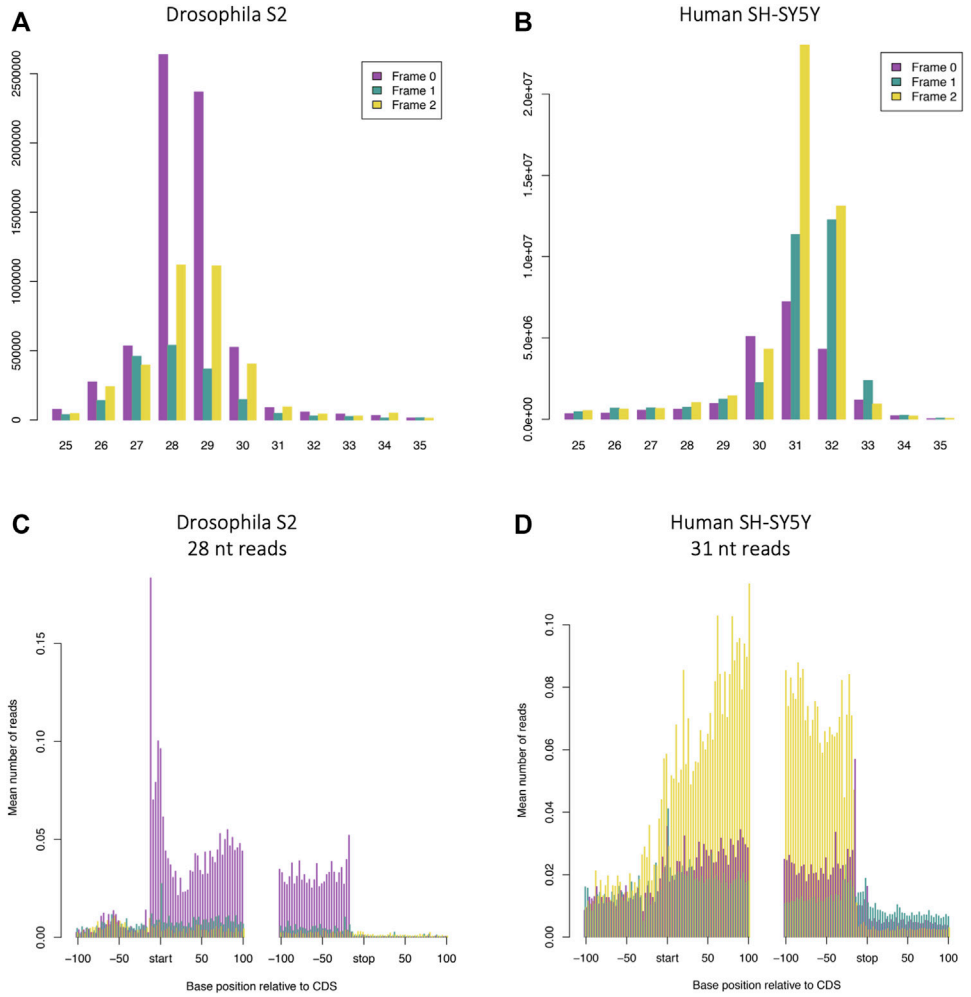

FIGURE 4 | Length of footprints and nature of framing is different between Poly-Ribo-Seq in humans and Ribo-Seq in *Drosophila*. Read length distribution and framing of ribosome footprinting **(A)** *Drosophila* S2 cells **(**same as **Figure 2B)** and **(B)** human neuroblastoma SH-SY5Y cells **(**same as **Figure 1G)**, with E-RNaseI, in Buffer 2 at ON at 4°C, in presence of cycloheximide. Metagene analysis of ribosome profiling in **(C)** *Drosophila* S2 cells: 28 nt reads **(**same as **Figure 2D)** and **(D)** human neuroblastoma SH-SY5Y cells 31 nt reads **(**same as **Supplementary Figure S3D)**. Plots generated with RiboSeqR.

were generated from single batches of both RNaseI sources. The type of RNase has also been previously shown to impact ribosome footprinting. For example, *Drosophila* ribosomes have been shown to be sensitive to digestion of their rRNA by RNaseI at higher temperatures (e.g. RT) so alternative RNases have been employed such as micrococcal nuclease (Dunn et al., 2013). The disadvantage of several alternatives to RNaseI, such as micrococcal nuclease, RNaseA and RNaseT1, is weaker triplet periodicity (Gerashchenko and Gladyshev, 2017). Several labs are now also using combinations of RNases for footprinting to reduce bias, minimise degradation of ribosomes and maximise triplet periodicity (Liu et al., 2019).

By comparing the optimisation of the ribosome footprinting in these disparate organisms, we demonstrate that footprinting under the same conditions can generate different footprint sizes and framing patterns. We therefore recommend you use existing literature and consult experts to plan experimental conditions and establish a reasonable range of expected footprint lengths when working with a new species. Even within the same species, variation should be expected when working with a different cell or tissue type. A key consideration for undertaking optimisation such as we describe is the balance between time and money spent, and the resulting improvement in footprinting quality. If one is establishing a protocol to support multiple studies in the same model and multiple replicates, this step is worth sustained investment.

An important consideration for ribosome profiling is the 'trapping' of ribosomes in the act of translation to provide an accurate snapshot of translation. Many researchers have relied upon cycloheximide treatment to aid this stabilisation of 80S ribosomes on the mRNA. However, as others have previously shown in yeast (Duncan and Mata, 2017), we found that cycloheximide can affect read distribution and ORF detection in *Drosophila* cells. However, it seems likely that cycloheximide

treatment has less of an effect in humans and some other organisms, compared to yeast and fly, not impacting transcript-specific ribosome occupancy (Sharma et al., 2021). Both the results presented here in *Drosophila* and other studies have shown that cycloheximide treatment does not affect either footprint size distribution or framing (Sharma et al., 2019). Snap freezing material is an alternative to 'trapping' ribosomes during elongation using cycloheximde, which does not seem to affect framing, read length or distribution. Flash freezing can also be of benefit when collecting difficult or biologically challenging tissues. But there are circumstances where collecting tissues from individual animals over long time frames when cycloheximide treatment is logistically more appropriate. Overall, this study shows the importance of testing ribosome footprinting conditions in a new system and in combination different conditions can vary in their contribution to generating high quality ribosome profiling data.

DATA AVAILABILITY STATEMENT

D. melanogaster S2 cell Ribo-seq data is deposited in GEO, record GSE166408. Human SH-SY5Y Ribo-seq data is deposited in SRA, BioProject PRJNA753469. Previously published *D. melanogaster* RNA-seq is available from GEO record GSE60384, run SRR1548661 (Aspden et al. 2014).

AUTHOR CONTRIBUTIONS

KD designed and performed experiments acquired, analysed and interpreted data, MA conceived, designed and performed experiments for the study. IB analysed and interpreted data. JA conceived the work and interpreted data. All authors contributed to manuscript writing, revision and have approved the submitted version.

FUNDING

This work was funded by MRC (MR/N000471/1). KD was funded by Leeds Anniversary Research Scholarship (LARS). MA was funded from BBSRC DTP, BB/M011151/1. IB has had financial support from Faculty of Biological Sciences, University of Leeds and the Sir Richard Stapley Educational Trust. JA was funded by the University of Leeds (University Academic Fellow scheme).

ACKNOWLEDGMENTS

We thank the Next Generation Sequencing facility, at St James University Hospital, Leeds, United Kingdom for performing Next Generation Sequencing. Parts of this work were undertaken on ARC4, part of the High Performance Computing facilities at the University of Leeds, United Kingdom.

SUPPLEMENTARY MATERIAL

The Supplementary Material for this article can be found online at: https://www.frontiersin.org/articles/10.3389/fmolb.2021.791455/full#supplementary-material

REFERENCES

Andrews, S. (2010). *FastQC: a Quality Control Tool for High Throughput Sequence Data*.

Aspden, J. L., Eyre-Walker, Y. C., Phillips, R. J., Amin, U., Mumtaz, M. A., Brocard, M., et al. (2014). Extensive Translation of Small Open Reading Frames Revealed by Poly-Ribo-Seq. *Elife* 3, e03528. doi:10.7554/eLife.03528

Baltz, A. G., Munschauer, M., Schwanhäusser, B., Vasile, A., Murakawa, Y., Schueler, M., et al. (2012). The mRNA-Bound Proteome and its Global Occupancy Profile on Protein-Coding Transcripts. *Mol. Cel* 46 (5), 674–690. doi:10.1016/j.molcel.2012.05.021

Calviello, L., Mukherjee, N., Wyler, E., Zauber, H., Hirsekorn, A., Selbach, M., and Ohler, U. (2016). Detecting Actively Translated Open reading Frames in Ribosome Profiling Data. *Nat. Methods*, 13(2), 165. doi:10.1038/nmeth.3688

Cenik, C., Cenik, E. S., Byeon, G. W., Grubert, F., Candille, S. I., Spacek, D., et al. (2015). Integrative Analysis of RNA, Translation, and Protein Levels Reveals Distinct Regulatory Variation across Humans. *Genome Res.* 25 (11), 1610–1621. doi:10.1101/gr.193342.115

Chen, J., Brunner, A.-D., Cogan, J. Z., Nuez, J. K., Fields, A. P., Adamson, B., et al. (2020). Pervasive Functional Translation of Noncanonical Human Open reading Frames. *Science* 367 (6482), 1140–1146. doi:10.1126/science.aay0262

Chothani, S., Adami, E., Ouyang, J. F., Viswanathan, S., Hubner, N., Cook, S. A., et al. (2019). deltaTE: Detection of Translationally Regulated Genes by Integrative Analysis of Ribo-Seq and RNA-Seq Data. *Curr. Protoc. Mol. Biol.* 129 (1), e108.

Chung, B. Y. H., Thomas, J., Jones, J. D., Irigoyen, N. F., Andrew, E., Baulcombe, D. C., et al. (2015). The Use of Duplex-specific Nuclease in Ribosome Profiling and a User-Friendly Software Package for Ribo-Seq Data Analysis. *RNA journal* 1731–1745.

Dobin, A., Davis, C. A., Schlesinger, F., Drenkow, J., Zaleski, C., Jha, S., et al. (2012). STAR: Ultrafast Universal RNA-Seq Aligner. *Bioinformatics* 29 (1), 15–21. doi:10.1093/bioinformatics/bts635

Douka, K., Wang, D., Kosteletos, A., Clayton, S., Byford, A., and Aspden, J. L. (2021). Birds, ICytoplasmic Long Non-coding RNAs Are Differentially Regulated and Translated during Human Neuronal Differentiation. *RNA*. doi:10.1261/rna.078782.121

Duncan, C. D. S., and Mata, J. (2017). Effects of Cycloheximide on the Interpretation of Ribosome Profiling Experiments in *Schizosaccharomyces pombe*. *Sci. Rep.* 7 (1), 10331. doi:10.1038/s41598-017-10650-1

Duncan, C. D. S., and Mata, J. (2014). The Translational Landscape of Fission-Yeast Meiosis and Sporulation. *Nat. Struct. \\& Mol. Biol.* 21 (7), 641–647. doi:10.1038/nsmb.2843

Dunn, J. G., Foo, C. K., Belletier, N. G., Gavis, E. R., and Weissman, J. S. (2013). Ribosome Profiling Reveals Pervasive and Regulated Stop Codon Readthrough in *Drosophila melanogaster*. *Elife* 2, e01179. doi:10.7554/eLife.01179

Garnier, S., Ross, N., Rudis, R., Camargo, A. P., Sciaini, M., and Scherer, C. é. (2021). Rvision - Colorblind-Friendly Color Maps for R. (Version R package version 0.6.1) https://sjmgarnier.github.io/viridis/.

Gerashchenko, M. V., and Gladyshev, V. N. (2017). Ribonuclease Selection for Ribosome Profiling. *Nucleic Acids Res.* 45 (2), e6. doi:10.1093/nar/gkw822

Gerashchenko, M. V., and Gladyshev, V. N. (2014). Translation Inhibitors Cause Abnormalities in Ribosome Profiling Experiments. *Nucleic Acids Res.* 42 (17), e134. doi:10.1093/nar/gku671

Gordon, A. (2010). *FASTQ/A Short-Reads Pre-processing Tools*.

Guo, H., Ingolia, N. T., Weissman, J. S., and Bartel, D. P. (2010). Mammalian microRNAs Predominantly Act to Decrease Target mRNA Levels. *Nature* 466 (7308), 835–840. doi:10.1038/nature09267

Heyer, E. E., and Moore, M. J. (2016). Redefining the Translational Status of 80S Monosomes. *Cell* 164 (4), 757–769. doi:10.1016/j.cell.2016.01.003

Hsu, P. Y., Lorenzo, C., Larry, W. H.-Y., Fay-Wei, L., Uwe, O., et al. (2016). Super-resolution Ribosome Profiling Reveals Unannotated Translation Events in Arabidopsis. *Proc. Natl. Acad. Sci.* 113 (45), E7126–E7135. doi:10.1073/pnas.1614788113

Hussmann, J. A., Patchett, S., Johnson, A., Sawyer, S., and Press, W. H. (2015). Understanding Biases in Ribosome Profiling Experiments Reveals Signatures of Translation Dynamics in Yeast. *Plos Genet.* 11 (12), e1005732. doi:10.1371/journal.pgen.1005732

Ingolia, N. T., Brar, G. A., Rouskin, S., McGeachy, A. M., and Weissman, J. S. (2013). Genome-Wide Annotation and Quantitation of Translation by Ribosome Profiling. *Curr. Protoc. Mol. Biol.* 418, 11–14. doi:10.1002/0471142727.mb0418s103

Ingolia, N. T., Ghaemmaghami, S., Newman, J. R., and Weissman, J. S. (2009). Genome-wide Analysis *In Vivo* of Translation with Nucleotide Resolution Using Ribosome Profiling. *Science* 324 (5924), 218–223. doi:10.1126/science.1168978

Langmead, B., and Salzberg, S. L. (2012). Fast Gapped-Read Alignment with Bowtie 2. *Nat. Methods* 9 (4), 357–U354. doi:10.1038/nmeth.1923

Lareau, L. F., Hite, D. H., Hogan, G. J., and Brown, P. O. (2014). Distinct Stages of the Translation Elongation Cycle Revealed by Sequencing Ribosome-Protected mRNA Fragments. *Elife* 3, e01257. doi:10.7554/eLife.01257

Larkin, A., Marygold, S. J., Antonazzo, G., Attrill, H., Dos Santos, G., Garapati, P. V., et al. (2021). FlyBase: Updates to the *Drosophila melanogaster* Knowledge Base. *Nucleic Acids Res.* 49 (D1), D899–D907. doi:10.1093/nar/gkaa1026

Larsson, J. (2020). Eulerr: Area-Proportional Euler and Venn Diagrams with Ellipses. https://cran.r-project.org/package=eulerr.

Li, H., Handsaker, B., Wysoker, A., Fennell, T., Ruan, J., Homer, N., et al. (2009). The Sequence Alignment/Map Format and SAMtools. *Bioinformatics (Oxford, England)* 25 (16), 2078–2079. doi:10.1093/bioinformatics/btp352

Liu, B., Molinaro, G., Shu, H., Stackpole, E. E., Huber, K. M., and Richter, J. D. (2019). Optimization of Ribosome Profiling Using Low-Input Brain Tissue from Fragile X Syndrome Model Mice. *Nucleic Acids Res.* 47 (5), e25. doi:10.1093/nar/gky1292

Martin, M. (2011). Cutadapt Removes Adapter Sequences from High-Throughput Sequencing Reads. *EMBnet.journal*, 17(1), 3. doi:10.14806/ej.17.1.200

McGlincy, N. J. a. I. N. T. (2017). Transcriptome-wide Measurement of Translation by Ribosome Profiling. *Methods* 126, 112–129. doi:10.1016/j.ymeth.2017.05.028

Michel, A. M., Mullan, J. P. A., Velayudhan, V., O'Connor, P. B. F., Donohue, C. A., and Baranov, P. V. (2016). RiboGalaxy: A Browser Based Platform for the Alignment, Analysis and Visualization of Ribosome Profiling Data [Article]. *Rna Biol.* 13 (3), 316–319. doi:10.1080/15476286.2016.1141862

R Core Team (2020). "R: A Language and Environment for Statistical Computing," in *R Foundation for Statistical Computing* (Vienna, Austria.

Rodriguez, C. M., Chun, S. Y., Mills, R. E., and Todd, P. K. (2019). Translation of Upstream Open reading Frames in a Model of Neuronal Differentiation. *BMC Genomics* 20 (1), 391. doi:10.1186/s12864-019-5775-1

Rubio, A., Ghosh, S., Mülleder, M., Ralser, M., and Mata, J. (2021). Ribosome Profiling Reveals Ribosome Stalling on Tryptophan Codons and Ribosome Queuing upon Oxidative Stress in Fission Yeast. *Nucleic Acids Res.* 49 (1), 383–399. doi:10.1093/nar/gkaa1180

Ruiz-Orera, J., and Albà, M. M. (2019). Conserved Regions in Long Non-coding RNAs Contain Abundant Translation and Protein-RNA Interaction Signatures. *NAR Genom Bioinform* 1 (1), e2. doi:10.1093/nargab/lqz002

Sharma, P., Nilges, B. S., Wu, J., and Leidel, S. A. (2019). The Translation Inhibitor Cycloheximide Affects Ribosome Profiling Data in a Species-specific Manner. *bioRxiv*, 746255. doi:10.1101/746255

Sharma, P., Wu, J., Nilges, B. S., and Leidel, S. A. (2021). Humans and Other Commonly Used Model Organisms Are Resistant to Cycloheximide-Mediated Biases in Ribosome Profiling Experiments. *Nat. Commun.* 12 (1), 5094. doi:10.1038/s41467-021-25411-y

Van Damme, P., Gawron, D., Van Criekinge, W., and Menschaert, G. (2014). N-terminal Proteomics and Ribosome Profiling Provide a Comprehensive View of the Alternative Translation Initiation Landscape in Mice and Men. *Mol. Cel Proteomics* 13 (5), 1245–1261. doi:10.1074/mcp.M113.036442

Wickham, H., Averick, M., Bryan, J., Chang, W., D'Agostino McGowan, L., François, R., and Yutani, H. (2019). Welcome to the Tidyverse. *J. Open Source Softw.* 4 (43), 1686. doi:10.21105/joss.01686

Wickham, H., François, R., Henry, L., and Müller, K. (2015). *Dplyr: A Grammar of Data Manipulation*. R Package Version 0.4 3, 156.

Wickham, H. (2016). *ggplot2: Elegant Graphics for Data Analysis*. New York, NY: Springer-Verlag.

Wickham, H. (2019). Stringr: Simple, Consistent Wrappers for Common String Operations. https://CRAN.R-project.org/package=stringr.

Wu, C. C., Zinshteyn, B., Wehner, K. A., and Green, R. (2019). High-Resolution Ribosome Profiling Defines Discrete Ribosome Elongation States and Translational Regulation during Cellular Stress. *Mol. Cel* 73 (5), 959–970. doi:10.1016/j.molcel.2018.12.009

Xie, Y. (2020). *Knitr: A General-Purpose Package for Dynamic Report Generation in R*. R package version 1.36. Available at https://yihui.org/knitr/.

Conflict of Interest: The authors declare that the research was conducted in the absence of any commercial or financial relationships that could be construed as a potential conflict of interest.

Publisher's Note: All claims expressed in this article are solely those of the authors and do not necessarily represent those of their affiliated organizations, or those of the publisher, the editors, and the reviewers. Any product that may be evaluated in this article, or claim that may be made by its manufacturer, is not guaranteed or endorsed by the publisher.

frontiers in Molecular Biosciences

REVIEW
published: 14 February 2022
doi: 10.3389/fmolb.2022.832916

Modulation of miRISC-Mediated Gene Silencing in Eukaryotes

*Courtney F. Jungers and Sergej Djuranovic**

Department of Cell Biology and Physiology, Washington University School of Medicine, St. Louis, MO, United States

Gene expression is regulated at multiple levels in eukaryotic cells. Regulation at the post-transcriptional level is modulated by various *trans*-acting factors that bind to specific sequences in the messenger RNA (mRNA). The binding of different *trans* factors influences various aspects of the mRNA such as degradation rate, translation efficiency, splicing, localization, etc. MicroRNAs (miRNAs) are short endogenous ncRNAs that combine with the Argonaute to form the microRNA-induced silencing complex (miRISC), which uses base-pair complementation to silence the target transcript. RNA-binding proteins (RBPs) contribute to post-transcriptional control by influencing the mRNA stability and translation upon binding to *cis*-elements within the mRNA transcript. RBPs have been shown to impact gene expression through influencing the miRISC biogenesis, composition, or miRISC-mRNA target interaction. While there is clear evidence that those interactions between RBPs, miRNAs, miRISC and target mRNAs influence the efficiency of miRISC-mediated gene silencing, the exact mechanism for most of them remains unclear. This review summarizes our current knowledge on gene expression regulation through interactions of miRNAs and RBPs.

Keywords: miRNA, miRISC, RNA binding protein, mRNA, miRISC activity, RBP binding models

OPEN ACCESS

Edited by:
Deepika Vasudevan, University of Pittsburgh, United States

Reviewed by:
Jeffrey Vedanayagam, Memorial Sloan Kettering Cancer Center, United States
Ubaldo Gioia, IFOM - The FIRC Institute of Molecular Oncology, Italy

****Correspondence:***
Sergej Djuranovic
sergej.djuranovic@wustl.edu

Specialty section:
This article was submitted to RNA Networks and Biology, a section of the journal Frontiers in Molecular Biosciences

Received: *10 December 2021*
Accepted: *18 January 2022*
Published: *14 February 2022*

Citation:
Jungers CF and Djuranovic S (2022) Modulation of miRISC-Mediated Gene Silencing in Eukaryotes. Front. Mol. Biosci. 9:832916. doi: 10.3389/fmolb.2022.832916

INTRODUCTION

The central dogma of biology follows the flow of genetic information; DNA is transcribed into RNA and RNA is translated into protein. Correct gene expression in a timely and quantitative way is essential for maintaining cellular homeostasis as dysregulated protein production can lead to various diseased states. RNA is not just a simple intermediate for conveying the genetic code, but it also regulates when, where, and how much protein will be produced. RNA has a complex, multistage lifecycle starting in the nucleus, where it is transcribed from DNA. After maturation, which includes co- and post-transcriptional processing, including 5′ capping, polyadenylation, and splicing, the mRNA is exported into the cytoplasm from the nucleus. In the cytoplasm ribosomes translate coding mRNAs into protein. From its initial transcription until its degradation, mRNAs are highly regulated at both a global and individual level. Individual mRNAs are regulated by various *trans*-acting factors that bind to specific *cis*-regulatory elements within the mRNA and influence the stability, localization, modifications, and translation of the information encoded in the mRNA (Gebauer and Hentze, 2004; Fukao et al., 2021).

Several classes of small noncoding RNAs (ncRNAs) have been shown to bind to specific sequences within mRNAs, mainly in the 3′ untranslated region (UTR), and influence the extent of expression of encoded genes. The three main classes of small ncRNAs, within 19–31 nucelotide length, are microRNAs (miRNA), small interfering RNAs (siRNAs), and piwi-interacting RNAs (piRNA). Each class of these small ncRNAs associates with distinct sets of effector proteins to carry out their function, both miRNAs and siRNAs associated with the Ago-clade, while piwi-RNAs associate with

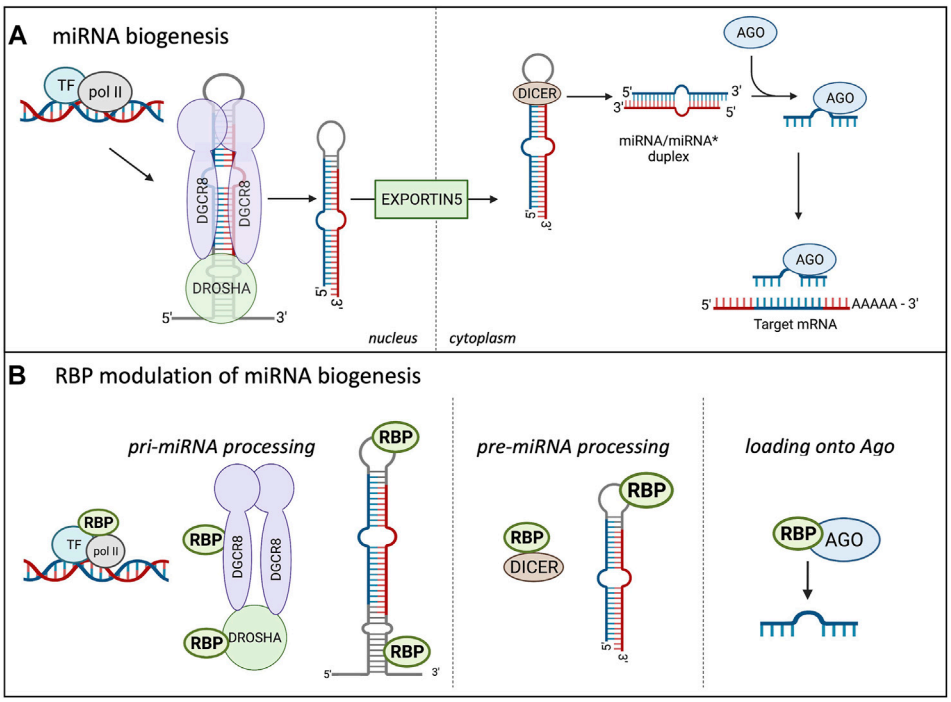

FIGURE 1 | Canonical miRNA biogenesis in Eukaryotes and the influence of RBPs. **(A)** shows the miRNA biogenesis in eukaryotes. miRNAs are transcribed in the nucleus by RNA polymerase II (pol II), creating the pri-miRNA, two sequential cleavage reactions follow. The microprocessor consists of Drosha and DGCR8 and performs the first cleavage reaction in the nucleus, creating the pre-miRNA. The pre-miRNA is transported into the cytoplasm through Exportin5 where the second cleavage reaction occurs. Dicer cleaves the terminal loop of the pre-miRNA, creating the miRNA/miRNA* duplex. The miRNAs are incorporated into the Ago protein, forming the minimal effector RNA induced silencing complex (miRISC) and target mRNA sequences. **(B)** Highlights the modulation of miRNA biogenesis by RBPs. RBPs can bind to the promoter region of certain miRNAs and influence their transcription. RBPs modulate miRNA expression at the pri-miRNA processing level through binding to Drosha and enhance or repress the cleavage. RBPs can also bind to the terminal loop or other sequences in the pri- and pre-miRNAs to influence the cleavage reactions. Additionally, RBPs can bind to DICER and influence this cleavage reaction through modulating DICER expression and availability. Lastly, RBPs can bind to AGO and increase the miRNA loading onto the AGO, increasing the miRISC silencing.

the PIWI-clade (Parker and Barford, 2006; Peters and Meister, 2007; Farazi et al., 2008; Thomson and Lin, 2009; Juliano et al., 2011). miRNAs and siRNAs are the most well understood and similar of the three; they are mostly derived from endogenous encoded double-stranded hairpin-shaped RNA. The main difference between miRNAs and siRNAs is their complementarity; siRNAs are derived from stem-loop with perfect complementarity while miRNAs contain imperfect complementarity. This review focuses on miRNAs, but siRNAs and piRNAs have been well-documented in recent reviews (Farazi et al., 2008; Carthew and Sontheimer, 2009; Thomson and Lin, 2009; Dana et al., 2017; Czech et al., 2018).

miRNAs are conserved, endogenous, short (19–22 nt) ncRNAs that combine with Argonaute (Ago) proteins to form the microRNA-induced silencing complex (miRISC). The miRISC uses imperfect base pair complementarity to bind to specific sequences found mostly in the 3′UTR of target mRNAs and repress the gene expression of that transcript (Siegel et al., 2011; Lin and Gregory, 2015; Duchaine and Fabian, 2019). While there were hints of miRNAs in the 1980's in developmental and cell lineage screens (Horvitz and Sulston, 1980), the first miRNA, lin-4, was discovered in 1993 by the Ambros lab (Lee et al., 1993). Lin-4 was found to bind to the lin-14 mRNA and post-transcriptionally repress the expression of the Lin-14 protein. Lin-14 is necessary for proper timing of larval development in *Caenorhabditis elegans* (*C. elegans*) as loss-of-function lin-4 mutants revert to an early developmental stage later in their development. Seven years later the, second miRNA, let-7, was discovered (Reinhart et al., 2000). As let-7 was also found to be a heterochromatic switching factor, it was first thought that these short, hence the name micro, ncRNAs must target mRNAs that code for developmental genes. However, as more miRNAs continued to be discovered, their roles became more diverse, suggesting a much broader role in biological processes (Bartel, 2018). Over 60% of human protein-coding genes have been shown to be targeted by miRNAs (Friedman et al., 2008). As miRNAs modulate the expression of genes involved in cellular differentiation, division, growth, and apoptosis it comes to no surprise that the miRNAs themselves must be highly regulated to avoid diseased states (Siomi and Siomi, 2010). In addition to small ncRNAs, RNA-binding proteins (RBPs) are another class of *trans*-factors that bind to *cis* elements within mRNA transcripts. RBPs regulate many aspects of processes associated with RNAs; splicing, transcription, modification, localization, translation, and decay (Díaz-Muñoz and Turner, 2018; Hentze et al., 2018). RBPs have been found to greatly influence both miRNA biogenesis and

miRNA-mediated gene silencing. This review focuses on miRNA-mediated gene silencing and investigates the influence of RBPs on the modulation of miRISC function (Gebauer et al., 2021).

miRNA BIOGENESIS IN EUKARYOTES

As miRNAs play a major role in controlling protein abundance, the expression and number of miRNAs is highly important. As depicted in **Figure 1A**, prior to silencing their target transcripts, miRNAs are transcribed in the nucleus mostly by RNA polymerase II, forming the primary (pri) miRNA. The pri-miRNA is composed of a local stem loop containing 3 helical stems that are flanked by basal and apical junctions at both ends (Ha and Kim, 2014; Nguyen et al., 2015; Bartel, 2018; Duchaine and Fabian, 2019). **Figure 1A** shows how the pri-miRNA is processed in the nucleus to form the shorter pre-miRNA. The pre-miRNA is created through two sequential processing reactions; first, the pri-miRNA hairpin is recognized and cleaved from the transcript by the microprocessor, which comprises Drosha and the double-strand RNA (dsRNA) binding protein DGCR8 (DiGeorge Critical Regulator 8). DGCR8 helps provide the affinity for the microprocessor as it acts as a molecular anchor to position Drosha's catalytic site at the desired distance from the stem flanking region (Bartel, 2004, 2018). DGCR8 interacts with the stem and apical portion of the stem-loop structure in the pri-miRNA and positions Drosha for cleavage (Nguyen et al., 2015; **Figure 1A**). Drosha, a member of the Rnase III family, localizes at the pri-miRNA basal junction and cleaves the stem-loop from the rest of the transcript, creating a pre-miRNA product ~60–75 nucleotides long (Ha and Kim, 2014). There are multiple transcripts with the ability to fold backward and form hairpins, but not all are selected to become pri-miRNAs and enter the miRNA biogenesis pathway. The microprocessor is the gate-keeper of this process and seems to have a preference for pri-miRNAs containing hairpins with a stem that is ~35 base pairs long, an unstructured apical loop that is over 10 nucleotides long, single-stranded sequences flanking the hairpin, and there are 4 sequence motifs at sites correlating to the position of the microprocessor. These sequence motifs include a basal UG motif, an apical UGU motif, a CNNC flanking motif, and a mismatched GHG motif with 6 nucleotides of the basal stem (Fang and Bartel, 2020; Shang et al., 2020). However, not all pri-miRNAs are optimal substrates of the microprocessor so they rely on neighboring canonical pri-miRNAs (Fang and Bartel, 2020; Shang et al., 2020).

The pre-miRNA is transported to the cytoplasm via exportin V where it undergoes the second cleavage reaction to form the mature miRNA/miRNA* duplex, which consists of the guide and passenger (*) strand (reviewed in Duchaine and Fabian, 2019; Loffreda et al., 2015). Dicer functions in miRNA maturation and helps to facilitate loading of the mature miRNA onto Argonaute (Foulkes et al., 2014). Dicer cleaves the terminal loop from the pre-miRNA stem creating the mature duplex that is 18–21 base pairs long and contains 3′ overhangs (Murphy et al., 2008). Dicer contains 2 catalytic RNAse III domains, C-terminal dsRBD, ATPase/RNA helicase, Piwi-Argonaute-Zwille (PAZ) domain, and the DUF283 domain (Foulkes et al., 2014; Gebauer et al., 2021). The PAZ domain recognizes the 5′ terminal phosphate of authentic pre-miRNAs and acts as a ruler to measure the cleavage site at the 3′ overhang where the RNAse III domains will cut a strand to create the mature miRNA duplex (Connerty et al., 2015). The mature miRNA duplex associates with the Ago protein to form the minimal effector miRNA-induced silencing complex (miRISC). The guide strand from the duplex becomes associated with the Ago protein and is unwound while the passenger strand is lost. This process is referred to as differential strand retention, which is based on the thermodynamic stability of the ends of the duplex (Bartel, 2018). The miRNA biogenesis involving the microprocessor is the canonical pathway and is depicted in **Figure 1A**. Research has shown that there are microprocessor-independent, or non-canonical, pathways for miRNA biogenesis (Miyoshi et al., 2010; Connerty et al., 2015; Bartel, 2018). Probably the most well-defined alternative miRNA biogenesis pathway is the one which combines intron splicing with dicing of the miRNA. These miRNAs are known as "mirtrons" and they are processed from RNAs that are both pre-miRNAs and introns (Westholm and Lai, 2011). Upon splicing of introns from transcribed RNAs, the processing of pri-miRNAs and pre-miRNAs is preceded by linearization of intron lariat by debranching enzymes. While it was originally thought that mirtrons are *Drosophila* and *C. elegans* specific pathways further studies found mirtrons throughout the animal kingdom (Siomi and Siomi, 2010; Salim et al., 2021). There are also miRNAs that are dicer-independent, but rely on the nuclear canonical machinery for miRNA biogenesis usually through cluster assistance, which will be discussed in detail in the next section (Fang and Bartel, 2020; Shang et al., 2020).

While this review focuses on miRNAs in the context of mammalian cells, it is important to note that miRNA biogenesis in plants is very similar to mammals, however, there are some key differences that should be highlighted. Similar to animal miRNA biogenesis, pri-miRNAs are transcribed in the nucleus by RNA polymerase II, followed by stabilization in a region known as the D-body (Voinnet, 2009; Wang et al., 2019). While in the D-body region the pri-miRNA interacts with a complex composed of zinc finger protein serrate (SE), a double-stranded binding protein hyponastic leaves 1 (Hyl1), dicer like 1 (Dcl1), and other accessory proteins depending on the specific type of miRNA (Wang et al., 2019). Dc11 functions much like Dicer in animal miRNA biogenesis, dc11 performs two cleavage reactions on the pri-miRNA; the first creating the shorter pre-miRNA, which then proceeds to another round of processing by dc11 to form the mature miRNA/miRNA* duplex. The mature duplex is exported out of the nucleus through HASTY (homolog to the animal exportin-V) (Bartel., 2004; Voinnet, 2009). Once in the cytoplasm, the guide strand interacts with Ago to guide the RISC to its target mRNA through near-perfect complementarity to silence the gene through direct cleavage and/or translational inhibition.

RBPs IN CONTROL OF miRNA BIOGENESIS

As the proper expression of miRNAs is essential for maintaining cellular homeostasis, their biogenesis is highly regulated at all steps, as highlighted in **Figure 1B** (Treiber et al., 2017; Nussbacher and Yeo, 2018). Analyses of crosslinking immunoprecipitation (CLIP) data with proteins involved in the miRNA biogenesis has helped identify specific RBPs involved in miRNA processing (Ramanathan et al., 2019). Post-transcriptional modifications of the RNA, as well as post-translational control of the biogenesis machinery and effector proteins involved in these processes, can impact the production of miRNAs and formation of the miRISC. Multiple modifications take place on miRNAs and the majority of them are important for their biogenesis, function, and stability; in addition, ubiquitination and phosphorylation of Ago proteins can play a role in miRISC formation (Peters and Meister, 2007; Meister, 2013; Müller et al., 2020; Wu et al., 2020). Some modifications have been extensively studied, including uridylation, editing of adenosine to inosine, or methylation of miRNAs, but many of them still need to be functionally characterized (Wyman et al., 2011; Michlewski and Cáceres, 2019). As an example, uridylation of pre-let7a miRNA by TUT4 or TUT7 blocks its processing and marks the miRNA for degradation (Heo et al., 2012; Michlewski and Cáceres, 2019). Deamination of specific adenosine to inosine by ADAR in pri-miR-142 (Yang et al., 2006) and pri-miR-151 (Kawahara et al., 2007) targets these miRNAs for degradation or blocks their processing, respectively. It was also shown that N6-methyladenosine (m6A) methylation by both mammalian or plant METTL3 homolog affects proper levels of mature microRNA (miRNA) biogenesis in human tissue cultures (Alarcón et al., 2015) and *Arabidopsis* (Bhat et al., 2020). The proposed mechanism involves specific methylation of a set of pri-miRNAs affecting proper folding of the RNA and recruitment of the microprocessor for proper and efficient pri-miRNA processing. In this case it's the loss of the modification (m6A) in pri-miRNA that leads to the reduction of pri-miRNA-microprocessor interactions and reduction in the levels of mature miRNAs in both mammalian and plant studies. Additionally, experiments with an introduction of m6A marks by *in vitro* transcription in pri-miRNAs indicated more efficient processing of the modified pri-miRNA by the microprocessor, thus confirming the role of m6a modifications in miRNA biogenesis (Alarcón et al., 2015). Certain RBPs have been shown to increase or decrease efficiency of miRNA biogenesis through direct binding to the miRNA precursor and/or altering the machinery involved in the biogenesis. RBPs can influence pre-miRNAs through directly binding to the miRNA sequence or indirectly through binding to DICER and impacting its expression and/or function (Bicker et al., 2013; Connerty et al., 2015; Loffreda et al., 2015). PACT and TRBP are two RBPs that have been shown to bind to and stabilize the expression of DICER, thus indirectly increasing the fidelity of miRNA biogenesis (Peters and Meister, 2007; Ha and Kim, 2014). At the pri-miRNA level, RBPs have been shown to bind to the miRNA's terminal loop. hnRNPA1 can bind to the stem loop of the pri-miR-18a (Díaz-Muñoz and Turner, 2018; Kooshapur et al., 2018). This binding alters the secondary structure, creating a more relaxed loop conformation which provides more accessibility for the microprocessor. On the other hand, RBPs can bind to the pri-miRNA and inhibit the biogenesis reaction through blocking the binding site for the microprocessor or other RBPs that are necessary for miRNA biogenesis (Loffreda et al., 2015; Michlewski and Cáceles, 2019). As depicted in **Figure 1B** the production of miRNAs is highly regulated by RBPs at multiple levels. As shown in **Figure 1B**, the two cleavage reactions that take place during miRNA biogenesis require the assistance of multiple RNA-binding proteins (RBPs). Fused in Sarcoma (FUS) protein is a ubiquitously expressed RBP that has been shown to directly interact with the microprocessor and recruit it to the transcription site of the miRNA (Morlando et al., 2012). Besides the FUS protein, a TAR DNA-binding protein-43 (TDP-43) has been shown to interact with both the microprocessor and Dicer complexes promoting the biogenesis of specific subsets of miRNAs and playing a role in neuronal differentiation (Kawahara and Mieda-Sato, 2012; Di Carlo et al., 2013). The RBP Ewing Sarcoma Protein (EWS) can inhibit the expression of DROSHA, likely through direct binding to the promoter (Ouyang et al., 2017), and thus regulate the overall efficiency of miRNA biogenesis. Another RBP that has been shown to interact with Drosha to influence miRNA biogenesis is SRSF3, a serine arginine splicing factor. SRSF3 regulates a large portion of canonical miRNAs (Kim et al., 2018). The CNNC motif lies about 17 nucleotides from the microprocessor and has been shown to interact with SRSF3 to aid in stimulating the processing of pri-miRNAs. It is thought that SRSF3 binding to the CNNC motif helps Drosha bind to the basal junction, thus aiding in pri-miRNA processing (Kim et al., 2018). Treiber and others performed a systematic analysis of pre-, pri- and mature miRNAs and identified a set of 72 human pre-miRNAs and found that 180 RBPs had preferential binding to a single or multiple miRNA precursor (Treiber et al., 2017). While it's clear RBPs play a critical role in the biogenesis of miRNAs, most of these studies have been performed *in vitro* which could result in unphysiological binding. It will be important to investigate these interactions of RBPs with miRNA biogenesis pathways *in vivo* to identify their physiological significance as well as connect this type of regulation to cell type specific biogenesis of miRNAs.

There are multiple miRNAs that are made from pri-miRNAs that contain multiple clustered stem loop structures that were originally thought to be treated as independent units and thus individually cleaved by the microprocessor. However, it is becoming clear that certain pri-miRNAs that are poor substrates of the microprocessor are dependent on a close pri-miRNA neighbor for proper miRNA biogenesis, this process is known as cluster assistance. miR-451 is a miRNA that is dicer-independent but requires the canonical nuclear miRNA processing for its biogenesis as indicated with decreased miR-451 expression upon knockout of Drosha (Shang et al., 2020). miR-451 is a poor substrate for the microprocessor due to its short step loop, however, despite this, miR-451 is somehow a substrate of the microprocessor. Interestingly, miR-451 has been found to be tightly clustered by miR-144 throughout evolution

(Fang and Bartel., 2020; Shang et al., 2020). miR-144 is an optimal substrate of the microprocessor and several groups have demonstrated that miR-451 biogenesis is dependent on its close proximity to miR-144. Shang and colleauges replaced miR-144 with miR-7a and miR-454, which are optimal substrates of the microprocessor, and miR-451 biogenesis was still promoted. This suggests a general mechanism whereby miRNAs that are suboptimal substrates of the microprocessor require canonical miRNAs in close proximity for their biogenesis (Shang et al., 2020). Additionally, several groups are identifying RBPs that are shown to assist in this clustering process (Fang and Bartel, 2020; Hutter et al., 2020; Kwon et al., 2020). Enhancer of rudimentary homolog (ERH) is a recently discovered component of the microprocessor that has been shown to aid in the cluster assistance process of miR-451 and miR-144 (Fang and Bartel., 2020; Hutter et al., 2020; Kwon et al., 2020). During cluster assistance the microprocessor is loaded onto the poor substrate with the aid of its neighboring high affinity miRNA substrate and ERH increases the processing of the suboptimal miRNA substrate through binding to the N-terminus of DGCR8 (Kwon et al., 2020).

Using a CRISPR/Cas9 LOF screen Hutter and colleuges found ERH and SAFB2 to be critical factors for cluster-mediated assistance (Hutter et al., 2020). Scaffold attachment factor B2 (SAFB2) is an RBP that has been found to be an accessory protein of the microprocessor in mammals (Hutter et al., 2020). The study by Hutter et al. looked at the miR-15a-16-1 cluster. Due to a large unpaired region in its basal stem, miR-15a is a suboptimal substrate of the microprocessor and therefore cannot be efficiently processed without the assistance from an optimal miRNA neighbor. Through use of a CRISPR/Cas9 screen they were able to identify SAFB2 as an essential cofactor for the efficient cleavage of pri-miR-15a through miR-16-1 assistance. Cluster assistance has also been observed in plants. In *Arabidopsis*, MAC5 is a component of the MOS4-associated complex which is needed for immunity and development (Palma et al., 2007; Li et al., 2020). MAC5 is an RBP that binds to stem loops and appears to help with cluster assistance. MAC5 is essential for plant development, as loss of function mutants of MAC5a and MAC5b have been shown to be embryonic lethal. Recently, MAC5 was shown to interact with the SE to promote pri-miRNA processing in plants via protecting the pri-miRNA from SE-dependent exoribonuclease activity (Li et al., 2020). Interestingly there is a human counterpart to MAC5, but it remains to be tested whether or not it interacts with the microprocessor in humans.

miRISC FUNCTION AND NATURE OF THE miRISC

As mentioned above, once the miRNA combines with the Ago protein, the functional miRISC is formed. The Ago protein is the minimal effector needed for the miRNA to carry out its silencing mechanism (Connerty et al., 2015). Ago is made up of 4 domains; the N-terminal domain, Piwi-Argonaute-Zwille (PAZ) domain, the middle domain (MID), and the p-element induced wimpy testis (PIWI) domain (Song et al., 2004; Carthew and Sontheimer, 2009; Djuranovic et al., 2011; Sheu-Gruttadauria and MacRae, 2017). The N-terminal domain facilitates small RNA loading and unwinding of the duplex. The PAZ domain recognizes and anchors to the 3′ ends of miRNA. The MID domain binds the 5′ terminal monophosphate moiety and the 5′ terminal nucleotide of the miRNA-guide strand. Finally, the PIWI domain shows extensive homology to RNase H. Of note, it is important to mention that mammalian genomes encode 4 Ago proteins, Ago one to four, with Ago2 being most highly expressed and the only one to have endonucleolytic activity allowing it to cleave target mRNAs with full complementarity to miRNAs (Bhattacharyya et al., 2006; Gebert and MacRae, 2019; Kakumani et al., 2021). Plants and *C. elegans* have multiple Ago proteins that are further specialized in their cellular function and association with particular miRNA/small RNAs based on their length or 5′ nucleotide (Lim et al., 2003; Wang et al., 2019). The structure and function of Ago proteins have been well characterized (Hutvagner and Simard, 2008; Meister, 2013; Müller et al., 2020; Wu et al., 2020). The miRISC functions to identify the target transcripts first and then silence the gene expression of the target mRNA. The miRISC uses imperfect base complementarity to identify the target sequence in the mRNA. The target sites for the miRNA are usually located in the 3′UTR of the mRNA. Target site prediction is strengthened based on complementarity to the seed region. The seed region of the miRNA is from nucleotide 2 to 7 from the 5′ end, and its complementarity is one of the main criteria for target-site prediction (Bartel, 2009).

Unlike siRNA, miRNAs have imperfect base pair complementarity making target mRNA cleavage a rare event for mammalian miRNAs (Gebauer et al., 2021). miRNAs employ their silencing function mostly through translational repression and mRNA decay (Braun et al., 2012; Djuranovic et al., 2011; Fabian and Sonenberg, 2012; Bartel, 2018). While the exact mechanism of silencing remains a topic of debate, the "default" mechanism agreed upon includes inhibition of translation, followed by deadenylation, decapping, and decay of the mRNA transcript, as shown in **Figure 2A** (Djuranovic et al., 2011; Braun et al., 2013; Gardiner et al., 2015; Nawalpuri et al., 2020). Even though research has shown translational repression occurs first and might be one mode of controlling gene expression, it is the mRNA decay that ultimately consolidates and silences the target mRNAs (Bazzini et al., 2012; Bêthune et al., 2012; Djuranovic et al., 2011; Hu and Coller, 2012). However, it is important to note that this model of miRISC function will vary depending on additional factors as depicted in **Figure 2B**. There are several proposed models for miRISC-mediated translational repression, and they are not mutually exclusive (Gu and Kay, 2010; Fabian and Sonenberg, 2012). While the mature miRNA and Ago protein are part of the minimal miRISC, this association alone is insufficient to carry out miRISC-mediated translational repression. The more complete miRISC, including GW182, or its mammalian homologs TNRC6, is needed for translational repression (Eulalio et al., 2009; Huntzinger et al., 2013). GW182 is also a bridging factor between Ago proteins and the poly(A) binding protein

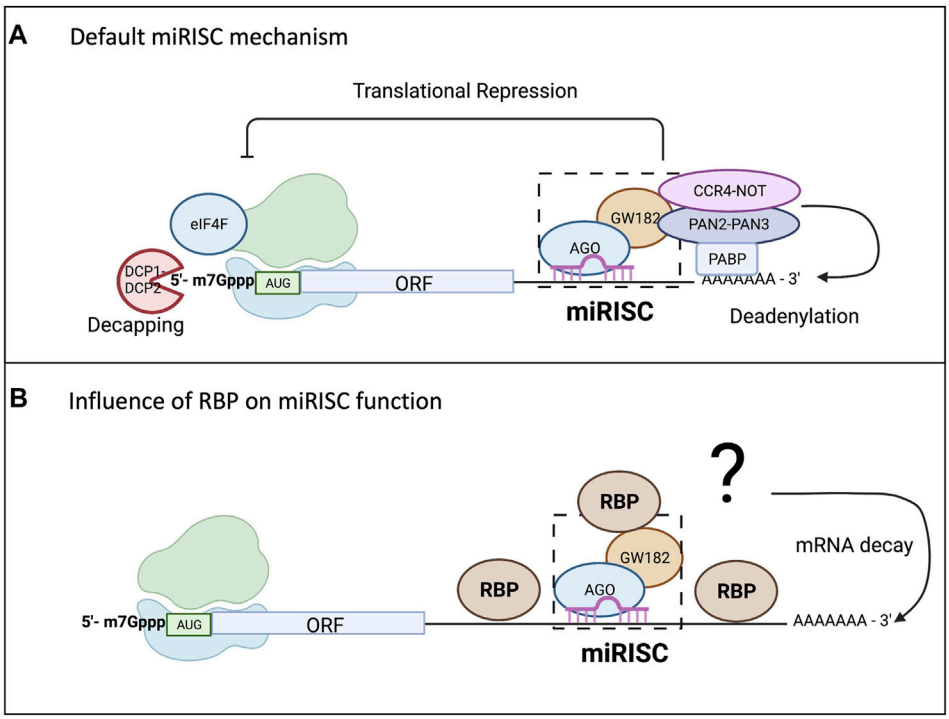

FIGURE 2 | miRISC-mediated gene repression and the influence from RBPs. While there are conflicting models of miRISC-mediated gene silencing that are not mutually exclusive, scientists have agreed upon a "default" mechanism as all the proposed mechanisms for miRNA-mediated repression involve repression of translation and mRNA decay. As shown in **(A)**, Ago interacts with the PABP complex to promote mRNA deadenylation through recruitment of poly(A) nuclease deadenylation complex subunit 2 (PAN2)-PAN3 and carbon catabolite repressor protein 4 (CCR4)-NOT. Deadenylation promotes decapping by the mRNA-decapping enzyme subunit DCP1-DCP2, making the mRNA vulnerable to degradation by exoribonuclease 1 (XRN1). **(B)** Highlights the influence RBP binding in the 3′UTR can have on miRISC-mediated gene repression. The RBP can bind up or downstream of the miRISC and either enhance the repression, usually through increasing mRNA degradation, or it could reduce the silencing efficiency of the miRISC.

(PABP) (Duchaine and Fabian, 2019), binding both of these proteins through the N-terminal domain. However, it is the carboxy terminal domain of GW182, which is referred to as the silencing domain, that recruits effector proteins such as deadenylases (PAN2-PAN3 and CCR4-NOT) and mRNA decapping factors (DCP1/2) (Eulalio et al., 2009; Braun et al., 2012; Wilczynska and Bushell, 2015). In a sequential series of actions, the miRISC is thought to induce translational repression of targeted mRNAs, which are later deadenylated by action of deadenylases, decapped by DCP1/2, and then degraded by the exosome and XRN1 (Rehwinkel et al., 2005; Braun et al., 2012). The presence of PABP aids in regulating both mRNA translation and mRNA turnover since it enhances miRNA-mediated deadenylation (Roy and Jacobson, 2013; Wigington et al., 2014). However, the presence of PABP on targeted mRNAs or its interaction with the miRISC is not necessary for translational repression (Djuranovic et al., 2011). Recently, 4EHP and GIGYF2 have been shown to bind to a conserved proline rich region of GW182 and impact miRISC-induced translational repression potentially at the step of 5′ mRNA cap binding (Chapat et al., 2017; Schopp et al., 2017). Regardless of whether there are multiple modes or one unifying model of translational repression by miRISC, it is becoming clearer that miRISC composition may influence outcome of the miRISC-target mRNA interaction. Both Ago and GW182 proteins may serve as molecular hubs for multiple ribonucleoprotein complexes (RNPs) or other enzymes involved in RNA metabolism further define their role in gene expression control.

RBPs AND A FUNCTIONAL miRISC

Multiple RBPs fulfill their gene regulation function independently of the miRISC but may impact the actions of the miRISC on target mRNAs. These RBPs can directly influence the functional outcome of the miRISC by modulating the actual composition of the miRISC or indirectly through interactions with the translational machinery involved in miRISC regulation. As previously mentioned, the FUS protein is an RBP that has been shown to directly associate with the core miRISC and influence the downstream function (Zhang et al., 2021). It is proposed that FUS facilitates the association between miRISC components such as the Ago protein, a set of mature miRNAs, and interacting with their mRNA targets, thus increasing efficiency of miRNA-mediated silencing. Since the interaction of FUS with the Ago protein is miRNA-independent, it may impact global miRNA regulation. FUS-enabled and selective

miRISC targeting through direct interactions with "preferred" miRNAs and mRNA targets could create an even bigger challenge for "non-preferred" miRISC complexes and their ability to locate targets among the other RNAs in the cell.

In a very similar fashion, Smaug, an important RBP in the early development of *Drosophila,* has been shown to recruit the minimal miRISC complex or Ago proteins, regardless of the miRNA targeting (Pinder and Smibert, 2013). Smaug interaction with the miRISC or Ago proteins is driven by a direct protein-protein interaction (Smaug-Ago1/2) and recruitment of such a complex to the 3′UTR of targeted mRNAs is purely driven by Smaug-recognition elements (SREs). As such, the *Drosophila* Smaug-Ago1 complex does not require miRNAs for translational repression of Nanos mRNA. This direct recruitment of miRISC without the involvement of miRNA-mRNA target recognition has not been found in other cases, but several members of the Hu family of RBPs have been found to reduce miRISC function by preventing the formation of the repressive miRISC on target mRNAs or directly competing for components of translation machinery targeted by the miRISC (Fukao et al., 2015). The HuD member of the Hu family is known to stimulate eIF4A activity on bound mRNAs and thus prevent potential miRISC translational repression through the translation initiation scanning mechanism (Fukao et al., 2015). The ability of other members of Hu family, as well as other AU-rich element-binding proteins (ARE-BPs) to oligomerize on target mRNAs can also abrogate miRISC-mRNA interaction (as discussed in the next section).

There are multiple reports that the miRISC is indeed not a homogenous complex. The factors that make miRISC variations are associated with cell types as well as cellular processes such as cellular stress, growth, and differentiation. The heterogeneity of the miRISC complex allows for diversity in its function (Sheu-Gruttadauria and MacRae, 2017; Dallaire et al., 2018; Nawalpuri et al., 2020). The different cell-specific cofactors will contribute to the miRISC function, potentially changing the function of the same miRNA-Ago complex depending on the cell type. A recent study looked at miRNAs in somatic and germline cells and found that they formed distinct miRISC depending on the cell type (Dallaire et al., 2018). They used an *in vivo* fluorescent reporter with binding sites for miR-228 and germline- and somatic-specific promoters. They observed that in intestinal cells the miR-228 reporter was repressed at both the protein and mRNA level. However, they discovered stabilization of the miR-228 reporter in germline cells, suggesting a different mechanism where translational repression is uncoupled from mRNA destabilization. Using RNA affinity assays to purify specific miRISCs they identified a GW182-independent silencing mechanism used in germline cells of *C. elegans* compared to somatic cells. As such a single mRNA can have flexible regulation that changes based on cellular and developmental context, RBP presence, and miRISC composition, adding another layer of complexity to miRISC-mediated mechanisms and differential target regulation.

CROSSTALK BETWEEN miRNAs AND RBPs ON TARGET mRNAs

Historically miRNA research has focused on one individual miRNA, however, in an endogenous system there can be multiple miRNA binding sites in the 3′UTR of a single target mRNA. Currently miRbase has identified 1917 precursor and 2654 mature miRNAs. Additionally, over 1,000 RBPs have been identified in the human genome, so it is no surprise that their binding sites can be right next to each other, or even overlapping as depicted in **Figures 3A,B** (van Kouwenhove et al., 2011; Jiang et al., 2013; Cottrell et al., 2018). It has become apparent that in order to understand miRNA-mediated gene silencing fully, the miRNA must be studied in combination with other miRNAs and RBPs. Computational analysis has been helpful to predict crosstalk between RBPs and miRNAs (Jiang et al., 2013; Loffreda et al., 2015). PAR-CLIP and RIP-Seq experiments have been critical for identifying enrichment of RBP binding sites next to or overlapping with miRNA recognition target sites (Jiang and Coller, 2012; Iadevaia and Gerber, 2015; Ramanathan et al., 2019).

RBPs can have an antagonistic effect on miRISC gene silencing when competing for the same or nearby binding site within the 3′UTR of the target mRNA as demonstrated in **Figure 3B**. The best-known examples for this are Hu and ARE-BP family members (Jiang and Coller, 2012). Multiple groups have found that the CAT1 mRNA can be targeted by miR-122 and HuR (Filipowicz et al., 2008; Fabian and Sonenberg, 2012; Kundu et al., 2012). Under normal conditions, miR-122 targets CAT1 and represses its expression. However, it has been shown that when stimulated with stress, HuR can rescue CAT1 from miRNA-mediated repression by miR-122 (Filipowicz et al., 2008; Kundu et al., 2012). The mechanism by which HuR rescues CAT1 expression remains unclear; it could be through dissociation of miRNPs from the mRNA or prevention of the miRISC from binding to its target site in the 3′UTR. Another example of competition between miRNAs and RBPs is with HuR and miR-16. They both have binding sites in the 3′UTR of prostaglandin synthase cyclooxtgenesis-2 (COX-2). miR-16 normally binds to the 3′UTR of COX-2 and promotes rapid repression and degradation of the transcript. However, when HuR levels are increased, HuR can outcompete miR-16 for the binding site and stabilize COX2, thus increasing its expression (Young et al., 2012). Similarly, AU-rich element-binding protein 1 (AUF1) binds to AU-rich elements (AREs) in the 3′UTR of target mRNAs and potentially oligomerizes, preventing or enabling miRISC binding (Wilson et al., 1999; Zucconi et al., 2010). However, scientists have shown that AUF1 also has a high affinity for the let-7b miRNA. When AUF1 binds to the miRNA, let-7b, it facilitates its transfer onto Ago2, thus enhancing the miRNA-mediated repression (Yoon et al., 2014) in a way similar to FUS.

On the other hand, RBPs can cooperate with miRNAs to enhance the silencing of the target mRNA as shown in **Figure 3A**. This can be done through recruitment of the miRISC to the binding site on the target mRNA (example of Smaug and FUS above) or the binding of the RBP can change the secondary

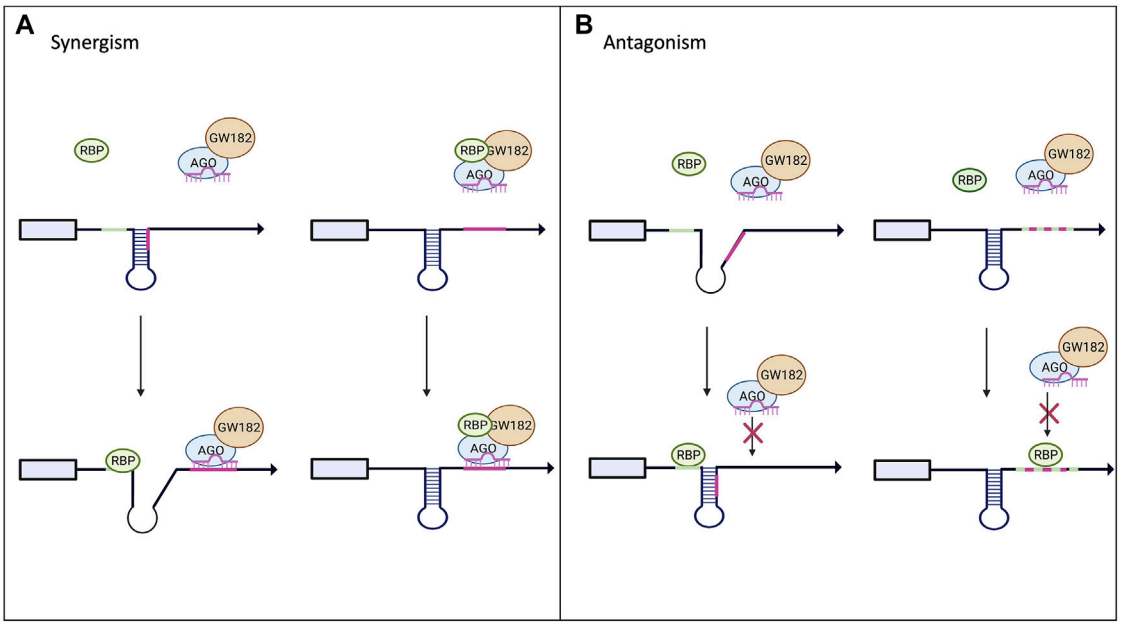

FIGURE 3 | Interplay between RBPs and miRNAs on miRISC-mediated gene expression. Panel **(A)** shows potential models of synergism between RBPs and miRNAs. Upon binding to the mRNA target the RBP can alter the secondary structure and increase the exposure of the miRNA binding site allowing for increased miRISC binding. The RBP could also bind to the miRISC and increase its binding affinity to its target mRNA. **(B)** Highlights the possible antagonistic mechanism between RBPs and miRNAs. RBP binding to its target could alter the secondary structure, decreasing the miRISC's access to its binding site. RBPs and miRNA can also compete for the same binding site and the RBP can outcompete and block the miRISC from binding to its site (Loffreda et al., 2015).

TABLE 1 | Known interactions of RNA-binding proteins and microRNAs.

Target	RNA-binding protein	microRNA	Action	References
Antagonistic interactions				
Transcription sites of miRNA	FUS	miR-9, miR-125b, miR-132	Drosha recruitment lost	Morlando et al. (2012)
CAT1 3′UTR	HuR	miR-122	HuR prevents miRISC from binding to target	Fabian and Sonenberg (2012); Kundu et al. (2012)
COX-2 3′UTR	HuR	miR-16	Compete for binding site in 3′UTR	Young et al. (2012)
VEGFA 3′UTR	hnRNPL	miR-297, miR-299	Competes with miRNAs for binding to VEGFA in 3′UTR	Shih and Claffey, (1999)
βTrCP1 (coding region)	CRD-BP	miR-183	Compete for binding in 3′UTR	Elcheva et al. (2009)
Stretches of uridine in 3′UTR	Dnd1	miR-430	Dnd1 makes target site inaccessible	Kedde et al. (2010)
Synergistic interactions				
RhoB	HuR	miR-19	Binding of HuR to recruits loaded miRISC	Sun et al. (2010)
p27, E2F3	Pumilio	miR-221/222 miR-503	Pumilio binding alters secondary structure, increasing binding accessibility for miRISC	Kedde et al. (2010) Miles et al. (2012)
c-myc	HuR	let-7	HuR recruits loaded let-7 RISC	Kim et al. (2009)
TNF-α	TTP	miR-16	TTP interacts with Ago to increase miR-16 loading	Jing et al. (2005)
Ago	AUF1	let-7a	Increase let-7 loading onto Ago	Yoon et al. (2014)
pre-miR18a	hnRNP1	miR-18a	Increase binding accessibility for miRISC	Michlewski et al. (2008)
pre-let7	DDX5	let-7	Facilitate miRISC loading to let-7 precurser	van Kouwenhove et al. (2011)

structure of the mRNA to increase the binding accessibility for the miRISC. Pumilio, a member of the Puf family, is an RBP that has been shown to enhance miRISC activity through unwinding the mRNA 3′UTR, thus promoting miRISC binding (Kedde et al., 2010; Miles et al., 2012; Nawalpuri et al., 2020). Pumilio is known to promote cell-cycle re-entry of quiescent cells upon binding to the 3′UTR of the mRNA that encodes for the tumor suppressor p27. Binding of Pumilo to the Pumilio-recognition elements (PREs) in the 3′UTR of p27 mRNA induces a change in the secondary structure of p27 mRNA that increases the accessibility

of the target sites for miR-221 and miR-222, thus enabling the repression of this mRNA (Kedde et al., 2010). The similar mode of miRISC binding regulation and activity by Pumilio was found in a 3′UTR of transcription factors important for regulating cell proliferation, such as E2F3 (Miles et al., 2012).

While scientists have found examples showing antagonism and synergism between RBPs and miRNAs on miRISC gene silencing, it is important to note that all of these actions are co-occurring inside of the cell. **Table 1** highlights certain known RBPs and miRISC interactions on common target mRNAs and you can see that a single RBP can either enhance or repress miRNA-mediated repression depending on the miRISC and RBPs binding sites. This suggests that there cannot be a universal model for the crosstalk between RBPs and miRNAs. A single mRNA can have binding sites for multiple RBPs and miRNAs, therefore the additive or countering effects of the different interactions will determine the final outcome of miRISC silencing efficiency.

POSITIONAL-DEPENDENT INTERACTIONS OF RBPs AND miRNAs ON miRISC SILENCING

Many studies have indicated the influence of RBPs on miRISC-mediated gene silencing, but as different cells have varying RBP expression profiles, the same miRNA may have a different silencing mechanism or the transcript may be under control of both miRNAs and RBPs, depending on the specific cell type (Jiang et al., 2013; Cottrell et al., 2018). Many groups have investigated combined effects of miRNAs and RBPs, but studies are usually limited to a single mRNA or reporter 3′UTRs. As such, it is hard to conclude whether the exact mechanism that causes the antagonistic or synergistic effect of RBPs and miRISC on gene repression in a single 3′UTR is applicable in global analyses of other regulated genes. The answer to this question may lie in the positions of the miRNA and RBP binding sites in relation to one another in the 3′UTR of the target mRNA as well as in cell types. In an endogenous system the RBP binding site can be close to or far away from the miRNA binding site.

Recently two groups have identified that proximity of the binding sites influences the cross talk between RBPs and miRNAs (Cottrell et al., 2018). These studies identified that the closer the RBP and miRNA binding sites were to one another on target mRNA, the larger the influence of RBPs on miRISC gene targeting. One study indicated that nearby RBP binding was associated with enhanced miRISC targeting, which could potentially mean an increase in gene silencing. The other study used a massively parallel reporter (MPRA) assay with an eGFP plasmid library containing synthetic or endogenously encoded 3′UTRs, covering all possible combinations of several repressive translation elements (let-7 miRNA binding sites, AREs, PREs and SREs). Authors discovered positional effects between miRNA binding sites and AREs. AREs positioned upstream of the miRNA binding site of let-7 caused an increase in miRISC-silencing efficiency, while a decrease in let-7 silencing was observed when the AREs were downstream of the let-7 binding site (Cottrell et al., 2018). This effect was not only specific for miRNA binding sites but it was also seen in the combination of Pumilio binding sites (PREs) and AREs.

Interestingly, a study that looked at the ARE-BP, HuR, found that this RBP was able to mediate de-repression of Cat1 mRNA from miRISC silencing by binding to AREs located next to miRNA binding sites (Kundu et al., 2012). Given that HuR and other ARE-BPs are known to oligomerize upon binding to their target sites the group sought to investigate if the multimerization of HuR contributed to its ability to rescue Cat1 from miRNA repression. They created several mutants of HuR and found that the mutants with compromised multimerization of HuR did not interfere with the miRISC activity arguing for a steric occlusion model as a potential mechanism (Kundu et al., 2012). Such a model suggests the positional effect and distance-dependence through directional oligomerization of the RBPs may play a role in ARE-dependent modulation of miRISC activity. However, not all RBPs are known to oligomerize so this would not explain the mechanism for all RBP-miRNA crosstalk. Another possibility is that the RNA structure within the 3′UTR alters which would change the availability of the binding sites for both the miRISC and RBP, as described in models for Pumilio and miRISC on p27 and E2F3 mRNAs (Kedde et al., 2010; Miles et al., 2012).

A study in the zebrafish model demonstrated the impact of the RNA structure and RBP-binding sequence motifs during the maternal-to-zygotic transition (MZT) (Beaudoin et al., 2018; Vejnar et al., 2019). They found that certain AREs, U-rich and C-rich motifs, and miR-430 activity are responsible for variation in gene expression seen during the development. They identified multiple sequence and RNA structural elements can have antagonistic effects on the same mRNAs. Combination of these elements on the same mRNAs such as stabilizing U-rich motifs and destabilizing miR-430 target sites leads to differential temporal or spatial regulation and creates specific patterns of gene expression. The transcripts would be stabilized by maternally provided poly(U)-binding proteins and then deadenylated and degraded later in development. These actions are carried by combinatorial effects of the miR-430 miRISC and ARE-BPs by a dose-dependent mechanism established through either maternally deposited or newly synthesized RBPs and RNPs. It is clear the outcome of the interaction between RBPs and miRNAs can vary depending on their position from one another, primarily the distance between the binding sites and the local mRNA structure, thus further enforcing the idea that there is no single mechanism of miRISC function due to the these variations in mRNA targets. Scientists will need to identify methods to predict how certain miRNAs and RBPs interact with one another and identify their impact on gene expression regulation and then validate these results experimentally in endogenous targets. Additionally, other factors will be also at play, such as mRNA modifications or alternative splicing, that influence the structure within the 3′UTR, which in turn would alter miRISC and/or RBPs activity.

DISEASE-ASSOCIATED STATES RESULTING FROM INTERACTIONS BETWEEN RBPs AND miRNAs

Upon their initial discovery, miRNAs were believed to play a role in just development, but as more miRNAs were uncovered, scientists recognized their roles were much more diverse (Bartel, 2018). miRNAs likely play a role in every single biological process, and their dysregulation is seen in many diseased states, such as cancer and neurodegenerative disorders. Timed and correct expression of miRNAs in specific cell types is critical as mRNAs that are not silenced through miRNA-mediated repression will be translated into proteins and may impact cell growth, proliferation, or differentiation. The above-mentioned interplay between RBPs and miRNAs on certain targeted mRNA transcripts can easily contribute to pathogenesis if the levels of RBPs and miRNAs are altered. Most cancer cells see a decrease in global miRNA levels, but individual miRNAs have been shown to increase and accumulate in cancers (Peng and Croce, 2016; Vos et al., 2019; Zhang et al., 2021). Such variation in miRNA levels can indeed lead to tumorigenesis. For example, if there were an increase in miRNA regulators that target tumor suppressors, then there would be a decrease in the tumor suppressor genes (Cheng et al., 2017). In the opposite scenario, an increase in oncogenes can occur if there is a decrease in levels of their regulatory miRNAs. While the importance of miRNAs in cancer is evident, their role in cancer progression should be studied in parallel with RBPs. RBPs may be one of the key factors in determining miRNA function and mutations or changes in the expression of RBPs can impair miRNA biogenesis and miRISC activity. For instance, DEAD-Box 5 (DDX5) and DDX17 RNA helicases are RBPs that help regulate the Drosha-mediated cleavage to produce pri-miRNA. Studies have shown that there is an increase in DDX5 and DDX17 expression levels in breast, cervix, colon, and prostate cancer (Connerty et al., 2015; Shen and Hung, 2015; Khan et al., 2019). Knockdown of both DDX5 and DDX17, in human cervical carcinoma cells suppressed cellular proliferation indicating their association with abnormal cell growth. On the other hand, overexpression of DDX5 caused a proliferation of keratinocytes (van Kouwenhove et al., 2011) thus confirming its role in tumor phenotypes of these cells. It is worth mentioning that DDX5 exerts helicase activity when in the cytoplasm, and it facilitates miRISC loading by unwinding the let-7 precursor duplex.

Another example is an increased expression of COX-2 gene as a hallmark of colorectal cancer (Asting et al., 2011; Young et al., 2012). Under normal physiological conditions, miR-16 degrades COX-2, but miR-16 is decreased by about two-fold in colorectal cancer cells, thus its likelihood of binding and regulating COX-2 mRNA is drastically decreased. HuR expression is increased in colorectal cancer cells and since HuR also binds in the 3′UTR of COX-2 mRNA, additional stabilization of this mRNA and overexpression of COX-2 protein is warranted through the multimerization of HuR, a mechanism described in Kundu et al. (2012).

As Dicer is a major modulator of miRNA biogenesis it comes to no surprise that its level is important. Low levels of Dicer have been identified in several cancers associated with a poor outcome, such as breast, endometrial, lung, and ovarian cancer (Foulkes et al., 2014). However, there is also an observed increase in Dicer1 levels in the metastatic lesions in prostate cancer (Foulkes et al., 2014). This inconsistency in Dicer1 levels led scientist to focus on the specific mutations in the DICER gene rather than the levels. Both germline and somatic mutations in the DICER gene have been found in various cancers (Foulkes et al., 2014). Dicer1 syndrome is a rare genetic condition where specific mutations in the dicer gene predispose the patient for hereditary cancers (Caroleo et al., 2020). Only a third of Dicer1 pathogenic variant carriers present neoplasms during their life, suggesting there may be multiple additive events needed to create the neoplasm (Foulkes et al.,. 2014; Stewart et al., 2019; Caroleo et al., 2020). As the type of mutation in DICER gene can vary, future work will be needed to uncover how the specific type of mutation will alter the role of Dicer in recognition, binding, and processing of pre-miRNAs in addition to identifying the other events that may increase the chances of neoplasms occurring.

Neuronal development is another process that requires the function of genes whose expression is highly dependent on miRNAs. The proper expression of miRNAs is necessary for normal neuronal development, as altered levels of miRNA are observed for numerous neurodegenerative diseases (Juźwik et al., 2019). As we mentioned above, the components of the miRISC determine the function and mechanism of the miRISC and disruptions to these components, which are often due to RBPs, are observed in multiple neurodegenerative disorders. For example, brain atrophy, neurodegeneration, and gliosis are observed when Dicer is depleted in certain regions of the brain (Júzwik et al., 2019). FUS is involved in several biological processes and mutations in this RBP are observed in various neurodegenerative diseases, such as Amyotrophic Lateral Sclerosis (ALS) and Fronto-Temporal Lobar Degeneration (FTLD) (Loffreda et al., 2015; Nakaya et al., 2013). FUS has been shown to enhance the processing of certain miRNA by binding to the terminal loop of the pre-miRNA, these include miR-9, miR-125, and miR-132 (Morlando et al., 2012) which are all known to play important roles in neuronal functions (Loffreda et al., 2015). Cyclin-dependent kinases regulate the cell cycle and can initiate cell death. Their misregulation is often observed in neurodegenerative diseases, such as ALS, Parkinson's and Alzheimer's (Nguyen et al., 2002). CDK4 and CDK6 are known targets of the miRNA, miR-663a. miR-663a promotes cellular senescence by decreasing CDK4 and CDK6 expression (Kinoshita et al., 2021). Recent reports have found increased levels of CDK4 and CDK6 in the blood of ALS patients and connected this observation with combinatorial miRNA and RBP regulation (Katerina et al., 2018; Li et al., 2020; Kinoshita et al., 2021). Authors indicate that hnRNPH is an RBP that has been shown to indirectly decrease the expression of miR-663a. hnRNPH binds to RP11-670E13.6, which is a long noncoding RNA that, upon activation from hnRNPH binds to miR-663a and prevents miR-663a from binding to and repressing CDK4 and CDK6 mRNAs (Li et al., 2020:; Kinoshita et al., 2021). Exactly

how increased levels of CDK4 and CDK6 contribute to ALS remains unclear, but it is evident that the interplay of RBPs and miRNAs contributes to this observation.

While there is clear evidence that disruption of miRISC machinery is seen in many neurodegenerative diseases, there is still a lack in understanding whether these disruptions of machinery cause the diseased state, or perhaps the disruption is a side-effect from another mishap that caused the disease (Kinoshita et al., 2021). Similarly, as an increase in pre-miRNAs is observed in tumor cells compared to normal cells, and might be a cause for tumorigenesis or metastasis, it would seem useful to study how changes in RBP expression influences miRNA biogenesis in certain cell types and cancers. Such data would clearly be beneficial in disentangling the complicated interactions between miRISC and RBPs.

CONCLUSION

miRNAs play an essential role in gene regulation as they control the expression of genes involved in nearly all biological processes. Dysregulation of miRISC-mediated gene silencing is prevalent in human diseases, especially in neurological disorders and cancers. The importance of miRNAs is evident, and it's becoming clear that in order to understand the biogenesis and function of miRNAs fully, RBPs, developmental stage, and cell types must be considered. Translational repression, modulated by RBPs and miRISCs, has been shown to be reversible (Bhattacharyya et al., 2006) so it is important to consider such regulation in spatial-temporal relations. The reversibility of translational repression modulated by RBPs and miRISCs allows for flexible control of the expression of targeted genes in a wide pool of mRNAs in a timely manner. This is, as mentioned earlier, important in cases such as cellular stress, cellular growth, or proliferation as well as during cellular specification (Nawalpuri et al., 2020). In some cases, "interruptions" in translation induced by miRISC and RBPs translational control will be enough to buffer cellular stress or developmental transition states. In other cases, additional gene expression control of transcribed but "unwanted" mRNAs would be further enforced by the miRISCs associated with mRNA decay factors or by interaction with RBPs. Establishing these connections between RBPs and miRISC components will be important as they will determine mechanisms by which miRISC complexes and RBPs regulate gene expression in biological systems. These studies require the novel design of experimental setups and new biochemical, genetic, and bioinformatics methodologies. Previous methods used to study the mechanism of miRISC mediated gene silencing focused on a single miRNA or a single RBP, looking at either single reporters or multiple endogenous genes but without a good overview of miRISC and RBP interactions. Current and future methods focus on uncovering RBPs and miRNAs' combinatorial mechanism during miRISC- or RPB-mediated gene regulation. RNA element selection assays (RESA) have been useful for selecting RNA elements based on their activity *in vivo,* followed by high throughput sequencing to measure their regulatory function (Yartseva et al., 2017). The use of massively parallel reporter assay libraries (MPRAs) will be critical to study the individual and combined effects of miRNAs and RBPs both *in vitro* and *in vivo*. As there are infinite combinations of miRNAs and RBPs, the use of computational analysis for predicting the interactions of RBPs and miRNAs, followed by experimental validation, will help uncover the mechanism of certain RBPs and novel RNPs. Deciphering this crosstalk between RBPs and the miRISC in development stages and disease will be critical to identify new therapeutics.

AUTHOR CONTRIBUTIONS

All authors listed have made a substantial, direct, and intellectual contribution to the work and approved it for publication.

FUNDING

Authors are funded by NIH T32GM007067-46 (CJ), NIH R01 GM112824 (CJ and SD), NIH R01 GM136823 (SD), NIMH R01 MH116999 (SD), The Simons Foundation (571009 to SD) and Siteman Investment Program funds (823924 to SD).

ACKNOWLEDGMENTS

We are thankful to the members of the Djuranovic lab for their help in revising this review.

REFERENCES

Alarcón, C. R., Lee, H., Goodarzi, H., Halberg, N., and Tavazoie, S. F. (2015). N6-methyladenosine marks Primary microRNAs for Processing. *Nature* 519 (7544), 482–485. doi:10.1038/nature14281

Asting, A. G., Carén, H., Andersson, M., Lönnroth, C., Lagerstedt, K., and Lundholm, K. (2011). COX-2 Gene Expression in colon Cancer Tissue Related to Regulating Factors and Promoter Methylation Status. *BMC Cancer* 11 (1), 238. doi:10.1186/1471-2407-11-238

Bartel, D. P. (2018). Metazoan MicroRNAs. *Cell* 173 (1), 20–51. doi:10.1016/j.cell.2018.03.006

Bartel, D. P. (2004). MicroRNAs: Genomics, Biogenesis, Mechanism, and Function. *Cell* 116 (2), 281–297. doi:10.1016/s0092-8674(04)00045-5

Bartel, D. P. (2009). MicroRNAs: Target Recognition and Regulatory Functions. *Cell* 136 (2), 215–233. doi:10.1016/j.cell.2009.01.002

Bazzini, A. A., Lee, M. T., and Giraldez, A. J. (2012). Ribosome Profiling Shows that miR-430 Reduces Translation before Causing mRNA Decay in Zebrafish. *Science* 336 (6078), 233–237. doi:10.1126/science.1215704

Beaudoin, J.-D., Novoa, E. M., Vejnar, C. E., Yartseva, V., Takacs, C. M., Kellis, M., et al. (2018). Analyses of mRNA Structure Dynamics Identify Embryonic Gene Regulatory Programs. *Nat. Struct. Mol. Biol.* 25 (8), 677–686. doi:10.1038/s41594-018-0091-z

Béthune, J., Artus-Revel, C. G., and Filipowicz, W. (2012). Kinetic Analysis Reveals Successive Steps Leading to miRNA-mediated Silencing in Mammalian Cells. *EMBO Rep.* 13 (8), 716–723. doi:10.1038/embor.2012.82

Bhat, S. S., Bielewicz, D., Gulanicz, T., Bodi, Z., Yu, X., Anderson, S. J., et al. (2020). mRNA Adenosine Methylase (MTA) Deposits m6A on pri-miRNAs to

Modulate miRNA Biogenesis inArabidopsis Thaliana. *Proc. Natl. Acad. Sci. USA* 117 (35), 21785–21795. doi:10.1073/pnas.2003733117

Bhattacharyya, S. N., Habermacher, R., Martine, U., Closs, E. I., and Filipowicz, W. (2006). Relief of microRNA-Mediated Translational Repression in Human Cells Subjected to Stress. *Cell* 125 (6), 1111–1124. doi:10.1016/j.cell.2006.04.031

Bicker, S., Khudayberdiev, S., Weiss, K., Zocher, K., Baumeister, S., and Schratt, G. (2013). The DEAH-Box Helicase DHX36 Mediates Dendritic Localization of the Neuronal Precursor-microRNA-134. *Genes Dev.* 27 (9), 991–996. doi:10.1101/gad.211243.112

Braun, J. E., Huntzinger, E., and Izaurralde, E. (2012). A Molecular Link between miRISCs and Deadenylases Provides New Insight into the Mechanism of Gene Silencing by MicroRNAs. *Cold Spring Harbor Perspect. Biol.* 4 (12), a012328. doi:10.1101/cshperspect.a012328

Braun, J. E., Huntzinger, E., and Izaurralde, E. (2013). The Role of GW182 Proteins in miRNA-Mediated Gene Silencing. *Adv. Exp. Med. Biol.* 768, 147–163. doi:10.1007/978-1-4614-5107-5_9

Caroleo, A. M., De Ioris, M. A., Boccuto, L., Alessi, I., Del Baldo, G., Cacchione, A., et al. (2020). DICER1 Syndrome and Cancer Predisposition: From a Rare Pediatric Tumor to Lifetime Risk. *Front. Oncol.* 10, 614541. doi:10.3389/fonc.2020.614541

Carthew, R. W., and Sontheimer, E. J. (2009). Origins and Mechanisms of miRNAs and siRNAs. *Cell* 136 (4), 642–655. doi:10.1016/j.cell.2009.01.035

Chapat, C., Jafarnejad, S. M., Matta-Camacho, E., Hesketh, G. G., Gelbart, I. A., Attig, J., et al. (2017). Cap-binding Protein 4EHP Effects Translation Silencing by microRNAs. *Proc. Natl. Acad. Sci. USA* 114 (21), 5425–5430. doi:10.1073/pnas.1701488114

Cheng, J., Maier, K. C., Avsec, Ž., Rus, P., and Gagneur, J. (2017). Cis-regulatory Elements Explain Most of the mRNA Stability Variation across Genes in Yeast. *Rna* 23 (11), 1648–1659. doi:10.1261/rna.062224.117

Connerty, P., Ahadi, A., and Hutvagner, G. (2015). RNA Binding Proteins in the miRNA Pathway. *Ijms* 17 (1), 31. doi:10.3390/ijms17010031

Cottrell, K. A., Chaudhari, H. G., Cohen, B. A., and Djuranovic, S. (2018). PTRE-seq Reveals Mechanism and Interactions of RNA Binding Proteins and miRNAs. *Nat. Commun.* 9 (1), 301. doi:10.1038/s41467-017-02745-0

Czech, B., Munafò, M., Ciabrelli, F., Eastwood, E. L., Fabry, M. H., Kneuss, E., et al. (2018). piRNA-Guided Genome Defense: From Biogenesis to Silencing. *Annu. Rev. Genet.* 52 (1), 131–157. doi:10.1146/annurev-genet-120417-031441

Dallaire, A., Frédérick, P.-M., and Simard, M. J. (2018). Somatic and Germline MicroRNAs Form Distinct Silencing Complexes to Regulate Their Target mRNAs Differently. *Develop. Cel* 47 (2), 239–247. e4. doi:10.1016/j.devcel.2018.08.022

Dana, H., Chalbatani, G. M., Mahmoodzadeh, H., Karimloo, R., Rezaiean, O., Moradzadeh, A., et al. (2017). Molecular Mechanisms and Biological Functions of siRNA. *Int. J. Biomed. Sci.* 13 (2), 48–57.

Di Carlo, V., Grossi, E., Laneve, P., Morlando, M., Dini Modigliani, S., Ballarino, M., et al. (2013). TDP-43 Regulates the Microprocessor Complex Activity during *In Vitro* Neuronal Differentiation. *Mol. Neurobiol.* 48 (3), 952–963. doi:10.1007/s12035-013-8564-x

Díaz-Muñoz, M. D., and Turner, M. (2018). Uncovering the Role of RNA-Binding Proteins in Gene Expression in the Immune System. *Front. Immunol.* 9, 1094. doi:10.3389/fimmu.2018.01094

Djuranovic, S., Nahvi, A., and Green, R. (2011). A Parsimonious Model for Gene Regulation by miRNAs. *Science* 331 (6017), 550–553. doi:10.1126/science.1191138

Duchaine, T. F., and Fabian, M. R. (2019). Mechanistic Insights into MicroRNA-Mediated Gene Silencing. *Cold Spring Harb Perspect. Biol.* 11 (3), a032771. doi:10.1101/cshperspect.a032771

Elcheva, I., Goswami, S., Noubissi, F. K., and Spiegelman, V. S. (2009). CRD-BP Protects the Coding Region of βTrCP1 mRNA from miR-183-Mediated Degradation. *Mol. Cel* 35 (2), 240–246. doi:10.1016/j.molcel.2009.06.007

Eulalio, A., Huntzinger, E., Nishihara, T., Rehwinkel, J., Fauser, M., and Izaurralde, E. (2009). Deadenylation is a Widespread Effect of miRNA Regulation. *RNA*. 15 (1), 21–32. doi:10.1261/rna.1399509

Fabian, M. R., and Sonenberg, N. (2012). The Mechanics of miRNA-Mediated Gene Silencing: A Look under the Hood of miRISC. *Nat. Struct. Mol. Biol.* 19 (6), 586–593. doi:10.1038/nsmb.2296

Fang, W., and Bartel, D. P. (2020). MicroRNA Clustering Assists Processing of Suboptimal MicroRNA Hairpins through the Action of the ERH Protein. *Mol. Cel* 78 (2), 289–302. e6. doi:10.1016/j.molcel.2020.01.026

Farazi, T. A., Juranek, S. A., and Tuschl, T. (2008). The Growing Catalog of Small RNAs and Their Association with Distinct Argonaute/Piwi Family Members. *Development (Cambridge, England)* 135 (7), 1201–1214. doi:10.1242/dev.005629

Filipowicz, W., Bhattacharyya, S. N., and Sonenberg, N. (2008). Mechanisms of post-transcriptional Regulation by microRNAs: Are the Answers in Sight?. *Nat. Rev. Genet.* 9 (2), 102–114. doi:10.1038/nrg2290

Foulkes, W. D., Priest, J. R., and Duchaine, T. F. (2014). DICER1: Mutations, microRNAs and Mechanisms. *Nat. Rev. Cancer* 14 (10), 662–672. doi:10.1038/nrc3802

Friedman, R. C., Farh, K. K.-H., Burge, C. B., and Bartel, D. P. (2008). Most Mammalian mRNAs Are Conserved Targets of microRNAs. *Genome Res.* 19 (1), 92–105. doi:10.1101/gr.082701.108

Fukao, A., Aoyama, T., and Fujiwara, T. (2015). The Molecular Mechanism of Translational Control via the Communication Between the MicroRNA Pathway and RNA-binding Proteins. *RNA Biology.* 12 (9), 922–926. doi:10.1080/15476286.2015.1073436

Fukao, A., Tomohiro, T., and Fujiwara, T. (2021). Translation Initiation Regulated by RNA-Binding Protein in Mammals: The Modulation of Translation Initiation Complex by Trans-acting Factors. *Cells* 10 (7), 1711. doi:10.3390/cells10071711

Gardiner, A., Twiss, J., and Perrone-Bizzozero, N. (2015). Competing Interactions of RNA-Binding Proteins, MicroRNAs, and Their Targets Control Neuronal Development and Function. *Biomolecules* 5 (4), 2903–2918. doi:10.3390/biom5042903

Gebauer, F., and Hentze, M. W. (2004). Molecular Mechanisms of Translational Control. *Nat. Rev. Mol. Cel Biol* 5 (10), 827–835. doi:10.1038/nrm1488

Gebauer, F., Schwarzl, T., Valcárcel, J., and Hentze, M. W. (2021). RNA-binding Proteins in Human Genetic Disease. *Nat. Rev. Genet.* 22 (3), 185–198. doi:10.1038/s41576-020-00302-y

Gebert, L. F. R., and MacRae, I. J. (2019). Regulation of microRNA Function in Animals. *Nat. Rev. Mol. Cel Biol* 20 (1), 21–37. doi:10.1038/s41580-018-0045-7

Gu, S., and Kay, M. A. (2010). How Do miRNAs Mediate Translational Repression?. *Silence* 1 (1), 11. doi:10.1186/1758-907X-1-11

Ha, M., and Kim, V. N. (2014). Regulation of microRNA Biogenesis. *Nat. Rev. Mol. Cel Biol* 15 (8), 509–524. doi:10.1038/nrm3838

Hentze, M. W., Castello, A., Schwarzl, T., and Preiss, T. (2018). A Brave New World of RNA-Binding Proteins. *Nat. Rev. Mol. Cel Biol* 19 (5), 327–341. doi:10.1038/nrm.2017.130

Heo, I., Ha, M., Lim, J., Yoon, M-J., Park, J-E., Kwon, S. C., et al. (2012). Mono-Uridylation of Pre-MicroRNA as a Key Step in the Biogenesis of Group II let-7 MicroRNAs. *Cell* 151 (3), 521–532. doi:10.1016/j.cell.2012.09.022

Horvitz, H. R., and Sulston, J. E. (1980). Isolation and Genetic Characterization of Cell-Lineage Mutants of the Nematode Caenorhabditis Elegans. *Genetics* 96 (2), 435–454. doi:10.1093/genetics/96.2.435

Hu, W., and Coller, J. (2012). What Comes First: Translational Repression or mRNA Degradation? the Deepening Mystery of microRNA Function. *Cell Res* 22 (9), 1322–1324. doi:10.1038/cr.2012.80

Huntzinger, E., Kuzuoğlu-Öztürk, D., Braun, J. E., Eulalio, A., Wohlbold, L., and Izaurralde, E. (2013). The Interactions of GW182 Proteins with PABP and Deadenylases Are Required for Both Translational Repression and Degradation of miRNA Targets. *Nucleic Acids Res.* 41 (2), 978–994. doi:10.1093/nar/gks1078

Hutter, K., Lohmüller, M., Jukic, A., Eichin, F., Avci, S., Labi, V., et al. (2020). SAFB2 Enables the Processing of Suboptimal Stem-Loop Structures in Clustered Primary miRNA Transcripts. *Mol. Cel* 78 (5), 876–889. e6. doi:10.1016/j.molcel.2020.05.011

Hutvagner, G., and Simard, M. J. (2008). Argonaute Proteins: Key Players in RNA Silencing. *Nat. Rev. Mol. Cel Biol* 9 (1), 22–32. doi:10.1038/nrm2321

Iadevaia, V., and Gerber, A. (2015). Combinatorial Control of mRNA Fates by RNA-Binding Proteins and Non-coding RNAs. *Biomolecules* 5 (4), 2207–2222. doi:10.3390/biom5042207

Jiang, P., and Coller, H. (2012). Functional Interactions between microRNAs and RNA Binding Proteins. *Mirna* 1 (1), 70–79. doi:10.2174/2211536611201010070

Jiang, P., Singh, M., and Coller, H. A. (2013). Computational Assessment of the Cooperativity between RNA Binding Proteins and MicroRNAs in Transcript Decay. *Plos Comput. Biol.* 9 (5), e1003075. doi:10.1371/journal.pcbi.1003075

Jing, Q., Huang, S., Guth, S., Zarubin, T., Motoyama, A., Chen, J., et al. (2005). Involvement of microRNA in AU-Rich Element-Mediated mRNA Instability. *Cell* 120 (5), 623–634. doi:10.1016/j.cell.2004.12.038

Juliano, C., Wang, J., and Lin, H. (2011). Uniting Germline and Stem Cells: The Function of Piwi Proteins and the piRNA Pathway in Diverse Organisms. *Annu. Rev. Genet.* 45 (1), 447–469. doi:10.1146/annurev-genet-110410-132541

Juźwik, C. A., Drake, S. S., Zhang, Y., Paradis-Isler, N., Sylvester, A., Amar-Zifkin, A., et al. (2019). microRNA Dysregulation in Neurodegenerative Diseases: A Systematic Review. *Prog. Neurobiol.* 182, 101664. doi:10.1016/j.pneurobio.2019.101664

Kakumani, P. K., Guitart, T., Houle, F., Harvey, L.-M., Goyer, B., Germain, L., et al. (2021). CSDE1 Attenuates microRNA-Mediated Silencing of PMEPA1 in Melanoma. *Oncogene* 40 (18), 3231–3244. doi:10.1038/s41388-021-01767-9

Kanellopoulou, C., Muljo, S. A., Kung, A. L., Ganesan, S., Drapkin, R., Jenuwein, T., et al. (2005). Dicer-deficient Mouse Embryonic Stem Cells Are Defective in Differentiation and Centromeric Silencing. *Genes Dev.* 19 (4), 489–501. doi:10.1101/gad.1248505

Kawahara, Y., and Mieda-Sato, A. (2012). TDP-43 Promotes microRNA Biogenesis as a Component of the Drosha and Dicer Complexes. *Proc. Natl. Acad. Sci.* 109 (9), 3347–3352. doi:10.1073/pnas.1112427109

Kawahara, Y., Zinshteyn, B., Chendrimada, T. P., Shiekhattar, R., and Nishikura, K. (2007). RNA Editing of the microRNA-151 Precursor Blocks Cleavage by the Dicer-TRBP Complex. *EMBO Rep.* 8 (8), 763–769. doi:10.1038/sj.embor.7401011

Kedde, M., van Kouwenhove, M., Zwart, W., Oude Vrielink, J. A. F., Elkon, R., and Agami, R. (2010). A Pumilio-Induced RNA Structure Switch in P27-3′ UTR Controls miR-221 and miR-222 Accessibility. *Nat. Cel Biol* 12 (10), 1014–1020. doi:10.1038/ncb2105

Khan, S., Ayub, H., Khan, T., and Wahid, F. (2019). MicroRNA Biogenesis, Gene Silencing Mechanisms and Role in Breast, Ovarian and Prostate Cancer. *Biochimie* 167, 12–24. doi:10.1016/j.biochi.2019.09.001

Kim, H. H., Kuwano, Y., Srikantan, S., Lee, E. K., Martindale, J. L., and Gorospe, M. (2009). HuR Recruits Let-7/RISC to Repress C-Myc Expression. *Genes Dev.* 23 (15), 1743–1748. doi:10.1101/gad.1812509

Kim, K., Nguyen, T. D., Li, S., and Nguyen, T. A. (2018). SRSF3 Recruits DROSHA to the Basal junction of Primary microRNAs. *Rna* 24 (7), 892–898. doi:10.1261/rna.065862.118

Kinoshita, C., Kubota, N., and Aoyama, K. (2021). Interplay of RNA-Binding Proteins and microRNAs in Neurodegenerative Diseases. *Ijms* 22 (10), 5292. doi:10.3390/ijms22105292

Kooshapur, H., Choudhury, N. R., Simon, B., Mühlbauer, M., Jussupow, A., Fernandez, N., et al. (2018). Structural Basis for Terminal Loop Recognition and Stimulation of Pri-miRNA-18a Processing by hnRNP A1. *Nat. Commun.* 9 (1), 2479. doi:10.1038/s41467-018-04871-9

Kundu, P., Fabian, M. R., Sonenberg, N., Bhattacharyya, S. N., and Filipowicz, W. (2012). HuR Protein Attenuates miRNA-Mediated Repression by Promoting miRISC Dissociation from the Target RNA. *Nucleic Acids Res.* 40 (11), 5088–5100. doi:10.1093/nar/gks148

Kwon, S. C., Jang, H., Shen, S., Baek, S. C., Kim, K., Yang, J., et al. (2020). ERH Facilitates microRNA Maturation through the Interaction with the N-Terminus of DGCR8. *Nucleic Acids Res.* 48 (19), 11097–11112. doi:10.1093/nar/gkaa827

Lee, R. C., Feinbaum, R. L., and Ambros, V. (1993). The C. elegans Heterochronic Gene Lin-4 Encodes Small RNAs with Antisense Complementarity to Lin-14. *Cell* 75 (5), 843–854. doi:10.1016/0092-8674(93)90529-y

Li, S., Li, M., Liu, K., Zhang, H., Zhang, S., Zhang, C., et al. (2020). MAC5, an RNA-Binding Protein, Protects Pri-miRNAs from SERRATE-dependent Exoribonuclease Activities. *Proc. Natl. Acad. Sci. USA* 117 (38), 23982–23990. doi:10.1073/pnas.2008283117

Lim, L. P., Lau, N. C., Weinstein, E. G., Abdelhakim, A., Yekta, S., Rhoades, M. W., et al. (2003). The microRNAs ofCaenorhabditis Elegans. *Genes Dev.* 17 (8), 991–1008. doi:10.1101/gad.1074403

Lin, S., and Gregory, R. I. (2015). MicroRNA Biogenesis Pathways in Cancer. *Nat. Rev. Cancer* 15 (6), 321–333. doi:10.1038/nrc3932

Loffreda, A., Rigamonti, A., Barabino, S., and Lenzken, S. (2015). RNA-binding Proteins in the Regulation of miRNA Activity: A Focus on Neuronal Functions. *Biomolecules* 5 (4), 2363–2387. doi:10.3390/biom5042363

Martin, J. C., Tippie, M. A., McGee, D. P. C., and Verheyden, J. P. H. (1987). Synthesis and Antiviral Activity of Various Esters of 9-[(1,3-Dihydroxy-2-Propoxy)methyl]guanine. *J. Pharm. Sci.* 76 (2), 180–184. doi:10.1002/jps.2600760221

Meister, G. (2013). Argonaute Proteins: Functional Insights and Emerging Roles. *Nat. Rev. Genet.* 14 (7), 447–459. doi:10.1038/nrg3462

Michlewski, G., and Cáceres, J. F. (2019). Post-transcriptional Control of miRNA Biogenesis. *RNA* 25 (1), 1–16. doi:10.1261/rna.068692.118

Michlewski, G., Guil, S., Semple, C. A., and Cáceres, J. F. (2008). Posttranscriptional Regulation of miRNAs Harboring Conserved Terminal Loops. *Mol. Cel* 32 (3), 383–393. doi:10.1016/j.molcel.2008.10.013

Miles, W. O., Tschöp, K., Herr, A., Ji, J.-Y., and Dyson, N. J. (2012). Pumilio Facilitates miRNA Regulation of the E2F3 Oncogene. *Genes Dev.* 26 (4), 356–368. doi:10.1101/gad.182568.111

Miyoshi, K., Miyoshi, T., and Siomi, H. (2010). Many Ways to Generate microRNA-like Small RNAs: Non-canonical Pathways for microRNA Production. *Mol. Genet. Genomics* 284 (2), 95–103. doi:10.1007/s00438-010-0556-1

Morlando, M., Dini Modigliani, S., Torrelli, G., Rosa, A., Di Carlo, V., Caffarelli, E., et al. (2012). FUS Stimulates microRNA Biogenesis by Facilitating Co-transcriptional Drosha Recruitment. *EMBO J.* 31 (24), 4502–4510. doi:10.1038/emboj.2012.319

Müller, M., Fazi, F., and Ciaudo, C. (2020). Argonaute Proteins: From Structure to Function in Development and Pathological Cell Fate Determination. *Front. Cel Dev. Biol.* 7, 360. doi:10.3389/fcell.2019.00360

Murphy, D., Dancis, B., and Brown, J. R. (2008). The Evolution of Core Proteins Involved in microRNA Biogenesis. *BMC Evol. Biol.* 8 (1), 92. doi:10.1186/1471-2148-8-92

Nakaya, T., Alexiou, P., Maragkakis, M., Chang, A., and Mourelatos, Z. (2013). FUS Regulates Genes Coding for RNA-Binding Proteins in Neurons by Binding to Their Highly Conserved Introns. *RNA* 19 (4), 498–509. doi:10.1261/rna.037804.112

Nawalpuri, B., Ravindran, S., and Muddashetty, R. S. (2020). The Role of Dynamic miRISC during Neuronal Development. *Front. Mol. Biosci.* 7, 8. doi:10.3389/fmolb.2020.00008

Nguyen, M. D., Mushynski, W. E., and Julien, J.-P. (2002). Cycling at the Interface between Neurodevelopment and Neurodegeneration. *Cell Death Differ* 9 (12), 1294–1306. doi:10.1038/sj.cdd.4401108

Nguyen, T. A., Jo, M. H., Choi, Y-G., Park, J., Kwon, S. C., Hohng, S., et al. (2015). Functional Anatomy of the Human Microprocessor. *Cell* 161 (6), 1374–1387. doi:10.1016/j.cell.2015.05.010

Nolde, M. J., Saka, N., Reinert, K. L., and Slack, F. J. (2007). The Caenorhabditis elegans Pumilio Homolog, Puf-9, Is Required for the 3′UTR-Mediated Repression of the Let-7 microRNA Target Gene, Hbl-1. *Develop. Biol.* 305 (2), 551–563. doi:10.1016/j.ydbio.2007.02.040*hbl-1*. 25

Nussbacher, J. K., and Yeo, G. W. (2018). Systematic Discovery of RNA Binding Proteins that Regulate MicroRNA Levels. *Mol. Cel* 69 (6), 1005–1016. e7. doi:10.1016/j.molcel.2018.02.012

Ouyang, H., Zhang, K., Fox-Walsh, K., Yang, Y., Zhang, C., Huang, J., et al. (2017). The RNA Binding Protein EWS Is Broadly Involved in the Regulation of Pri-miRNA Processing in Mammalian Cells. *Nucleic Acids Res.* 45 (21), 12481–12495. doi:10.1093/nar/gkx912

Palma, K., Zhao, Q., Cheng, Y. T., Bi, D., Monaghan, J., Cheng, W., et al. (2007). Regulation of Plant Innate Immunity by Three Proteins in a Complex Conserved across the Plant and Animal Kingdoms. *Genes Dev.* 21 (12), 1484–1493. doi:10.1101/gad.1559607

Parker, J. S., and Barford, D. (2006). Argonaute: A Scaffold for the Function of Short Regulatory RNAs. *Trends Biochem. Sci.* 31 (11), 622–630. doi:10.1016/j.tibs.2006.09.010

Peng, Y., and Croce, C. M. (2016). The Role of MicroRNAs in Human Cancer. *Sig Transduct Target. Ther.* 1 (1), 15004. doi:10.1038/sigtrans.2015.4

Peters, L., and Meister, G. (2007). Argonaute Proteins: Mediators of RNA Silencing. *Mol. Cel* 26 (5), 611–623. doi:10.1016/j.molcel.2007.05.001

Pinder, B. D., and Smibert, C. A. (2013). microRNA-Independent Recruitment of Argonaute 1 to Nanos mRNA through the Smaug RNA-binding Protein. *EMBO Rep.* 14 (1), 80–86. doi:10.1038/embor.2012.192

Ramanathan, M., Porter, D. F., and Khavari, P. A. (2019). Methods to Study RNA-Protein Interactions. *Nat. Methods* 16 (3), 225–234. doi:10.1038/s41592-019-0330-1

Rehwinkel, J., Behm-Ansmant, I., Gatfield, D., and Izaurralde, E. (2005). A Crucial Role for GW182 and the DCP1:DCP2 Decapping Complex in miRNA-Mediated Gene Silencing. *RNA* 11 (11), 1640–1647. doi:10.1261/rna.2191905

Reinhart, B. J., Slack, F. J., Basson, M., Pasquinelli, A. E., Bettinger, J. C., Rougvie, A. E., et al. (2000). The 21-nucleotide Let-7 RNA Regulates Developmental Timing in *Caenorhabditis elegans*. *Nature* 403 (6772), 901–906. doi:10.1038/35002607

Roy, B., and Jacobson, A. (2013). The Intimate Relationships of mRNA Decay and Translation. *Trends Genet.* 29 (12), 691–699. doi:10.1016/j.tig.2013.09.002

Salim, U., Kumar, A., Kulshreshtha, R., and Vivekanandan, P. (2021). Biogenesis, Characterization, and Functions of Mirtrons. *WIREs RNA* 13 (1), e1680. doi:10.1002/wrna.1680

Schopp, I. M., Amaya Ramirez, C. C., Debeljak, J., Kreibich, E., Skribbe, M., Wild, K., et al. (2017). Split-BioID a Conditional Proteomics Approach to Monitor the Composition of Spatiotemporally Defined Protein Complexes. *Nat. Commun.* 8 (1), 15690. doi:10.1038/ncomms15690

Shang, R., Baek, S. C., Kim, K., Kim, B., Kim, V. N., and Lai, E. C. (2020). Genomic Clustering Facilitates Nuclear Processing of Suboptimal Pri-miRNA Loci. *Mol. Cel* 78 (2), 303–316. e4. doi:10.1016/j.molcel.2020.02.009

Shenoy, A., and Blelloch, R. H. (2014). Regulation of microRNA Function in Somatic Stem Cell Proliferation and Differentiation. *Nat. Rev. Mol. Cel Biol* 15 (9), 565–576. doi:10.1038/nrm3854

Sheu-Gruttadauria, J., and MacRae, I. J. (2017). Structural Foundations of RNA Silencing by Argonaute. *J. Mol. Biol.* 429 (17), 2619–2639. doi:10.1016/j.jmb.2017.07.018

Shih, S.-C., and Claffey, K. P. (1999). Regulation of Human Vascular Endothelial Growth Factor mRNA Stability in Hypoxia by Heterogeneous Nuclear Ribonucleoprotein L. *J. Biol. Chem.* 274 (3), 1359–1365. doi:10.1074/jbc.274.3.1359

Siegel, G., Saba, R., and Schratt, G. (2011). microRNAs in Neurons: Manifold Regulatory Roles at the Synapse. *Curr. Opin. Genet. Develop.* 21 (4), 491–497. doi:10.1016/j.gde.2011.04.008

Siomi, H., and Siomi, M. C. (2010). Posttranscriptional Regulation of MicroRNA Biogenesis in Animals. *Mol. Cel* 38 (3), 323–332. doi:10.1016/j.molcel.2010.03.013

Song, J.-J., Smith, S. K., Hannon, G. J., and Joshua-Tor, L. (2004). Crystal Structure of Argonaute and its Implications for RISC Slicer Activity. *Science* 305 (5689), 1434–1437. doi:10.1126/science.1102514

Stewart, D. R., Best, A. F., Williams, G. M., Harney, L. A., Carr, A. G., Harris, A. K., et al. (2019). Neoplasm Risk Among Individuals with a Pathogenic Germline Variant in DICER1. *Jco* 37 (8), 668–676. doi:10.1200/JCO.2018.78.4678

Sun, G., Li, H., and Rossi, J. J. (2010). Sequence Context outside the Target Region Influences the Effectiveness of miR-223 Target Sites in the RhoB 3′UTR. *Nucleic Acids Res.* 38 (1), 239–252. doi:10.1093/nar/gkp870

Thomson, T., and Lin, H. (2009). The Biogenesis and Function of PIWI Proteins and piRNAs: Progress and prospect. *Annu. Rev. Cel Dev. Biol.* 25, 355–376. doi:10.1146/annurev.cellbio.24.110707.175327

Treiber, T., Treiber, N., Plessmann, U., Harlander, S., Daiß, J.-L., Eichner, N., et al. (2017). A Compendium of RNA-Binding Proteins that Regulate MicroRNA Biogenesis. *Mol. Cel* 66 (2), 270–284. e13. doi:10.1016/j.molcel.2017.03.014

van Kouwenhove, M., Kedde, M., and Agami, R. (2011). MicroRNA Regulation by RNA-Binding Proteins and its Implications for Cancer. *Nat. Rev. Cancer* 11 (9), 644–656. doi:10.1038/nrc3107

Vejnar, C. E., Abdel Messih, M., Takacs, C. M., Yartseva, V., Oikonomou, P., Christiano, R., et al. (2019). Genome Wide Analysis of 3′ UTR Sequence Elements and Proteins Regulating mRNA Stability during Maternal-To-Zygotic Transition in Zebrafish. *Genome Res.* 29 (7), 1100–1114. doi:10.1101/gr.245159.118

Voinnet, O. (2009). Origin, Biogenesis, and Activity of Plant MicroRNAs. *Cell* 136 (4), 669–687. doi:10.1016/j.cell.2009.01.046

Vos, P. D., Leedman, P. J., Filipovska, A., and Rackham, O. (2019). Modulation of miRNA Function by Natural and Synthetic RNA-Binding Proteins in Cancer. *Cell. Mol. Life Sci.* 76 (19), 3745–3752. doi:10.1007/s00018-019-03163-9

Vrabec, K., Boštjančič, E., Koritnik, B., Leonardis, L., Dolenc Grošelj, L., Zidar, J., et al. (2018). Differential Expression of Several miRNAs and the Host Genes AATK and DNM2 in Leukocytes of Sporadic ALS Patients. *Front. Mol. Neurosci.* 11, 106. doi:10.3389/fnmol.2018.00106

Wang, J., Mei, J., and Ren, G. (2019). Plant microRNAs: Biogenesis, Homeostasis, and Degradation. *Front. Plant Sci.* 10, 360. doi:10.3389/fpls.2019.00360

Westholm, J. O., and Lai, E. C. (2011). Mirtrons: MicroRNA Biogenesis via Splicing. *Biochimie* 93 (11), 1897–1904. doi:10.1016/j.biochi.2011.06.017

Wigington, C. P., Williams, K. R., Meers, M. P., Bassell, G. J., and Corbett, A. H. (2014). Poly(A) RNA-Binding Proteins and Polyadenosine RNA: New Members and Novel Functions. *WIREs RNA* 5 (5), 601–622. doi:10.1002/wrna.1233

Wilczynska, A., and Bushell, M. (2015). The Complexity of miRNA-Mediated Repression. *Cel Death Differ* 22 (1), 22–33. doi:10.1038/cdd.2014.112

Wilson, G. M., Sun, Y., Lu, H., and Brewer, G. (1999). Assembly of AUF1 Oligomers on U-Rich RNA Targets by Sequential Dimer Association. *J. Biol. Chem.* 274 (47), 33374–33381. doi:10.1074/jbc.274.47.33374

Wu, J. e., Yang, J., Cho, W. C., and Zheng, Y. (2020). Argonaute Proteins: Structural Features, Functions and Emerging Roles. *J. Adv. Res.* 24, 317–324. doi:10.1016/j.jare.2020.04.017

Wyman, S. K., Knouf, E. C., Parkin, R. K., Fritz, B. R., Lin, D. W., Dennis, L. M., et al. (2011). Post-transcriptional Generation of miRNA Variants by Multiple Nucleotidyl Transferases Contributes to miRNA Transcriptome Complexity. *Genome Res.* 21 (9), 1450–1461. doi:10.1101/gr.118059.110

Yang, W., Chendrimada, T. P., Wang, Q., Higuchi, M., Seeburg, P. H., Shiekhattar, R., et al. (2006). Modulation of microRNA Processing and Expression through RNA Editing by ADAR Deaminases. *Nat. Struct. Mol. Biol.* 13 (1), 13–21. doi:10.1038/nsmb1041

Yartseva, V., Takacs, C. M., Vejnar, C. E., Lee, M. T., and Giraldez, A. J. (2017). RESA Identifies mRNA-Regulatory Sequences at High Resolution. *Nat. Methods* 14 (2), 201–207. doi:10.1038/nmeth.4121

Yoon, J.-H., De, S., Srikantan, S., Abdelmohsen, K., Grammatikakis, I., Kim, J., et al. (2014). PAR-CLIP Analysis Uncovers AUF1 Impact on Target RNA Fate and Genome Integrity. *Nat. Commun.* 5, 5248. doi:10.1038/ncomms6248

Young, L. E., Moore, A. E., Sokol, L., Meisner-Kober, N., and Dixon, D. A. (2012). The mRNA Stability Factor HuR Inhibits MicroRNA-16 Targeting of COX-2. *Mol. Cancer Res.* 10 (1), 167–180. doi:10.1158/1541-7786.MCR-11-0337

Zhang, Y., Wei, Z., Dong, H., Zhou, J., Yuan, J., Ni, B., et al. (2021). Regulation of mRNA Stability by RBPs and Noncoding RNAs Contributing to the Pathogenicity of Th17 Cells. *RNA Biol.* 18 (5), 647–656. doi:10.1080/15476286.2020.1862567

Zucconi, B. E., Ballin, J. D., Brewer, B. Y., Ross, C. R., Huang, J., Toth, E. A., et al. (2010). Alternatively Expressed Domains of AU-Rich Element RNA-Binding Protein 1 (AUF1) Regulate RNA-Binding Affinity, RNA-Induced Protein Oligomerization, and the Local Conformation of Bound RNA Ligands. *J. Biol. Chem.* 285 (50), 39127–39139. doi:10.1074/jbc.M110.180182

Conflict of Interest: The authors declare that the research was conducted in the absence of any commercial or financial relationships that could be construed as a potential conflict of interest.

Publisher's Note: All claims expressed in this article are solely those of the authors and do not necessarily represent those of their affiliated organizations, or those of the publisher, the editors and the reviewers. Any product that may be evaluated in this article, or claim that may be made by its manufacturer, is not guaranteed or endorsed by the publisher.

frontiers in Molecular Biosciences

REVIEW
published: 14 February 2022
doi: 10.3389/fmolb.2022.842261

Thinking Outside the Frame: Impacting Genomes Capacity by Programmed Ribosomal Frameshifting

Ricarda J. Riegger[1,2] *and Neva Caliskan*[1,3]*

[1]Helmholtz Centre for Infection Research (HZI), Helmholtz Institute for RNA-Based Infection Research (HIRI), Würzburg, Germany, [2]Graduate School of Life Sciences (GSLS), University of Würzburg, Würzburg, Germany, [3]Medical Faculty, University of Würzburg, Würzburg, Germany

Translation facilitates the transfer of the genetic information stored in the genome via messenger RNAs to a functional protein and is therefore one of the most fundamental cellular processes. Programmed ribosomal frameshifting is a ubiquitous alternative translation event that is extensively used by viruses to regulate gene expression from overlapping open reading frames in a controlled manner. Recent technical advances in the translation field enabled the identification of precise mechanisms as to how and when ribosomes change the reading frame on mRNAs containing *cis*-acting signals. Several studies began also to illustrate that *trans*-acting RNA modulators can adjust the timing and efficiency of frameshifting illuminating that frameshifting can be a dynamically regulated process in cells. Here, we intend to summarize these new findings and emphasize how it fits in our current understanding of PRF mechanisms as previously described.

Keywords: RNA, viruses, frameshifting, ribosome, translational regulation, translation

OPEN ACCESS

Edited by:
Norbert Polacek,
University of Bern, Switzerland

Reviewed by:
Jonathan Dinman,
University of Maryland, College Park, United States
John Atkins,
University College Cork, Ireland

***Correspondence:**
Neva Caliskan
Neva.Caliskan@helmholtz-hiri.de

Specialty section:
This article was submitted to RNA Networks and Biology, a section of the journal Frontiers in Molecular Biosciences

Received: *23 December 2021*
Accepted: *26 January 2022*
Published: *14 February 2022*

Citation:
Riegger RJ and Caliskan N (2022) Thinking Outside the Frame: Impacting Genomes Capacity by Programmed Ribosomal Frameshifting. Front. Mol. Biosci. 9:842261. doi: 10.3389/fmolb.2022.842261

INTRODUCTION

Protein synthesis is essential for any living cell. Based on the genetic information encoded in the messenger RNA (mRNA) sequence, the ribosome catalyzes the peptide bond formation of each amino acid to the nascent polypeptide chain. The incorporation of the correct amino acid is facilitated by the match between the mRNA codon and its cognate anticodon of the tRNA that delivers the appropriate amino acid. The genetic code is universal and read in triplets directed from the mRNA 5′ to 3′ end. The movement of tRNAs and the mRNA through the ribosome is maintained by coordinated, inter- and intra-subunit conformational changes and rotations of the ribosome (Rodnina and Wintermeyer, 2011; Achenbach and Nierhaus, 2015; Noller et al., 2017; Rodnina, 2018). During canonical translation, the elongation process is synchronized with translocation of the ribosome by exactly one codon after resolving intra-molecular base-pairs by the ribosomal mRNA helicase located at the mRNA tunnel entrance (Takyar et al., 2005). Errors in the maintenance of the correct reading frame, referred to as spontaneous frameshifting, occur less than 10^{-5} times per codon during translation (Kurland, 1992). An interesting feature of many genomes is that they contain overlapping open reading frames (ORF) (Veeramachaneni et al., 2004; Firth, 2014; Pavesi et al., 2018; Schlub and Holmes, 2020) some of which can be accessed during translation via recoding (Jacks and Varmus, 1985; Brierley et al., 1987; Jacks et al., 1988a). Translational recoding events are employed to fine-tune gene expression and expand the genomic coding capacity. Unlike erroneous translation, these translational recoding sites contain specific features embedded in the mRNA to signal the

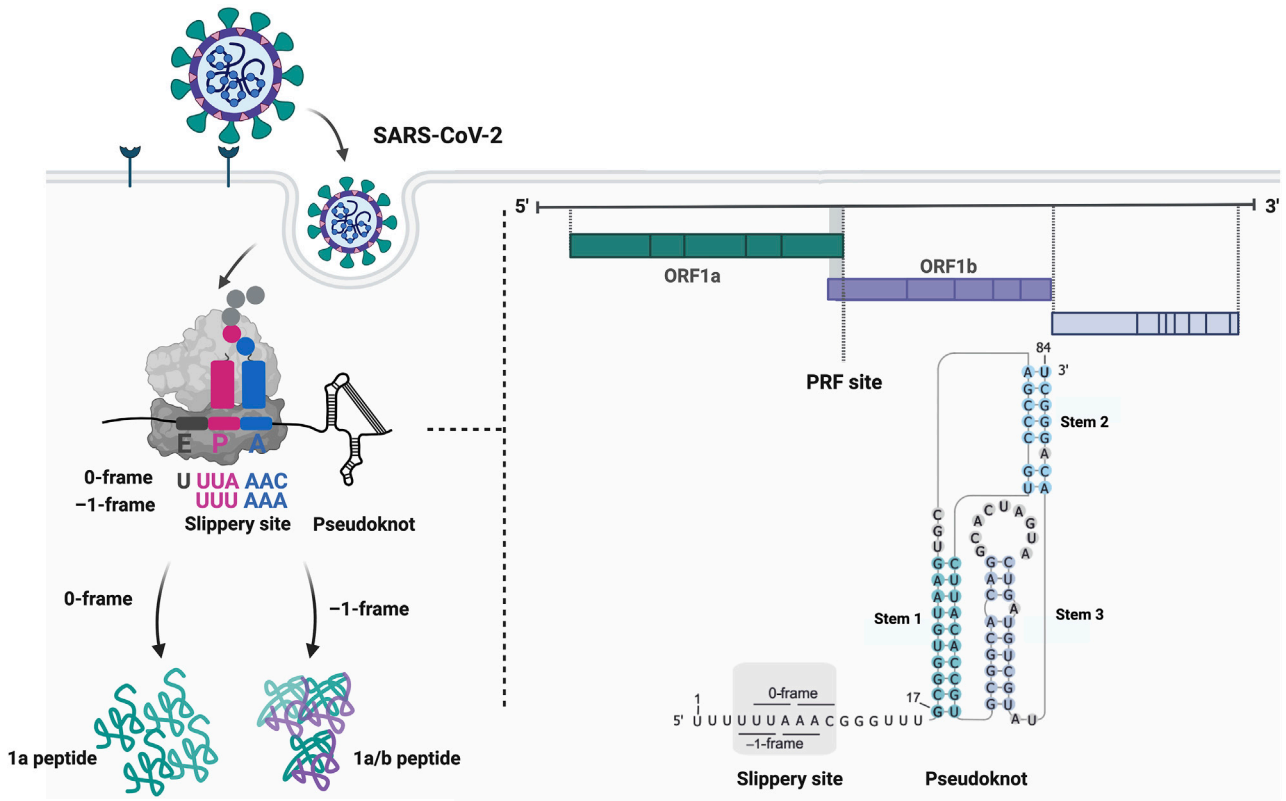

FIGURE 1 | Programmed ribosomal frameshifting on the SARS-CoV-2 mRNA. Frameshifting on the Severe Acute Respiratory Syndrome Coronavirus 2 (SARS-CoV-2) mRNA occurs on the slippery sequence located at the overlap of the open reading frames 1a (ORF1a) and 1b (ORF1b). Here, the slippery sequence has the motif U_UUA_AAC followed by a short spacer and the frameshift stimulatory pseudoknot. This secondary structure element comprises a kinetic roadblock that precisely stalls the ribosome on the slippery sequence potentially leading to the movement of the ribosome by one nucleotide into the 5′ direction. The translocation continues in the −1-frame with the peptidyl P- and aminoacyl A-site codons UUU_AAA resulting in the synthesis of the 1a/b peptide. Created with BioRender.com.

ribosome to move to the alternative ORF in a programmed manner. Several forms of recoding exist: 1) programmed ribosomal frameshifting (PRF); 2) translational bypassing or leaky scanning of the first start codon by the 48S pre-initiation complex; and 3) stop-codon readthrough (Atkins and Gesteland, 2010; Brierley et al., 2010; Caliskan et al., 2015; Miras et al., 2017; Dinman, 2019a; Rodnina et al., 2020). While there are numerous reviews which extensively detail general mechanisms and occurrences of recoding events, namely (Gesteland and Atkins, 1996; Ketteler, 2012; Caliskan et al., 2015; Atkins et al., 2016; Dever et al., 2018; Dinman, 2019b; Rodnina et al., 2020), in this review we focus mainly on PRF, where a different reading frame is accessed through controlled slippage of the ribosome on an mRNA (**Figure 1**).

Cases of PRF have been reported in many viruses and domains of life such as on the bacterial *Escherichia coli dnaX* gene (Tsuchihashi and Kornberg, 1990), in archaea like in *Sulfolobus solfataricus* on the *α-l-fucosidase fucA1* mRNA (Cobucci-Ponzano et al., 2006), as well as in eukaryotes on the human embryonic *Paternally Expressed Gene 10* (*PEG-10*) (Manktelow et al., 2005; Clark et al., 2007). Movement of ribosomes during PRF can occur in both the + or − direction relative to the 5′ end of the mRNA by one to even six nucleotides (Weiss et al., 1987; Lainé et al., 2008; Fang et al., 2012; Yan et al., 2015). −1PRF, where the ribosome slips by one nucleotide in the 5′ direction is the best-known variety of PRF, but +1PRF (slippage by one nucleotide in the 3′ direction), e.g., first discovered on a transposon element in yeast (Ty) (Clare and Farabaugh, 1985; Clare et al., 1988; Belcourt and Farabaugh, 1990) and −2PRF in case of the Porcine Reproductive and Respiratory Syndrome Virus (PRRSV) (Fang et al., 2012) have been reported as well.

−1PRF is extensively studied in RNA viruses, including the coronaviruses [e.g., Infectious Bronchitis Virus (IBV), Severe Acute Respiratory Syndrome Coronavirus (SARS-CoV)] (**Figure 1**) and retroviruses [e.g., Human Immunodeficiency Virus (HIV)]. While the 5′ end of viral frameshift genomes usually encodes for structural proteins, the 3′ alternative ORF mostly encodes for proteins involved in replication and processing (Atkins et al., 2016). Therefore, PRF events represent an elegant way to regulate packaging and replication of viral genomes. The ratio of the upstream and the downstream, alternative translation products is referred to as frameshifting efficiency. Perturbations in frameshifting levels can alter viral spread and pathogenesis (Brierley et al., 1991; Dinman and Wickner, 1992; Hung et al., 1998; Shehu-Xhilaga et al., 2001;

Plant et al., 2005; Dulude et al., 2006). The frameshifting efficiency varies widely from only 1% of all translation events on the Barley Yellow Dwarf Virus (BYDV) genome (Barry and Miller, 2002), to up to 80% in Theiler's Murine Encephalomyelitis Virus (TMEV) (Finch et al., 2015). In yeast, predicted -1PRFs mostly would result in the termination of protein synthesis at premature termination codons in the alternative frame (Jacobs et al., 2007), which was shown to also trigger nonsense-mediated mRNA decay (NMD) and no-go decay (NGD) in order to clear the cells from non-functional mRNAs (Belew et al., 2011). Furthermore, when ribosomes stall or collide on frameshift sites, NGD is also commanded to dissolve stalled or collided elongation complexes by degrading the mRNA (Simms et al., 2019; Smith et al., 2019). Therefore, in addition to its role in expanding the genomes repertoire, frameshifting events allow adaptation of the encoded proteome to changes in cellular and environmental conditions or infections (Rom and Kahana, 1994; Matsufuji et al., 1995; Baranov et al., 2002; Caliskan et al., 2017; Meydan et al., 2017; Korniy et al., 2019).

CIS-ACTING ELEMENTS ARE CRUCIAL FOR –1PRF

In most cases, the propensity of a ribosome to undergo –1PRF depends on two crucial *cis*-acting elements in the mRNA that are separated by a spacer sequence: a heptanucleotide slippery sequence on which the ribosome can slip into the alternative frame (Jacks et al., 1988a) and a downstream secondary structure element that causes the ribosome to slow down on the slippery sequence (Brierley et al., 1989).

The canonical slippery sequence is mostly a heptanucleotide motif that allows codon and anticodon base-pairing in both, the 0 and the alternative –1 reading frames (Jacks et al., 1988a; Jacks et al., 1988b; Icho and Wickner, 1989; Horsfield et al., 1995) (**Figure 1**). The most common slippery motif is X_XXY_YYZ (0-frame), where X can be any nucleotide, Y either adenine or uridine and Z any nucleotide except for guanine (Jacks et al., 1988a; Jacks et al., 1988b; Brierley et al., 1989; Dinman et al., 1991; Brierley et al., 1992), however also divergent patterns have been reported (Firth and Atkins, 2009; Loughran et al., 2011). Prior to slippage, the ribosome P- and the A-sites occupy the XXY and YYZ codons (0-frame) and during frameshifting, the ribosome moves to the XXX and YYY codons (–1-frame), which may lead to a mismatch of the anticodon and the codon in the wobble position. The spacer (five to nine nucleotides in eukaryotes, five to six nucleotides in prokaryotes) separating the slippery sequence and the secondary structure element ensures correct positioning of the ribosome on the slippery sites (Kontos et al., 2001; Howard et al., 2004; Lin et al., 2012; Napthine et al., 2017). The secondary structure element constitutes a kinetic barrier that slows down or stalls the translating ribosome (Brierley et al., 2010; Caliskan et al., 2014; Kim et al., 2014). This *cis*-acting element varies from a simple stem-loop [e.g., in the HIV-1 mRNA (Jacks et al., 1988a)], to a more complex H-type pseudoknot [e.g., in coronaviral mRNAs (Brierley et al., 1989)]. In exceptional cases, guanine-rich sequences that form four-stranded G-tracts referred to as G-quadruplexes, can form a physical barrier that is capable of stalling the ribosome similar to the stem-loops or pseudoknots reflecting the structural diversity of stimulatory RNA structures (Endoh et al., 2013; Yu et al., 2014). Of note, frameshift RNAs likely exist in several conformations with different stimulatory potentials (Houck-Loomis et al., 2011; Halma et al., 2019; Schlick et al., 2021). Also, the high structural variation of different stimulatory elements suggests that there could be mechanistic differences in how they act on the ribosome during translation elongation (Dinman, 1995; Kontos et al., 2001; Plant and Dinman, 2005). For instance, forming a translational roadblock is not the only way structured RNAs can alter recoding (Plant and Dinman, 2005). Frameshift RNA elements can also sterically obstruct the tRNA binding: Cryo-EM studies of the HIV-1 frameshift site have recently proposed this –1PRF activating function by revealing that the stimulatory HIV-1 stem-loop sterically hinders the binding of an aminoacylated tRNA to the A-site of the bacterial ribosome (Bao et al., 2020; Bao et al., 2021).

In addition to the slippery sequence and the downstream RNA structures, the presence of additional upstream RNA elements, such as Shine-Dalgarno-like sequences interacting with the 16S ribosomal RNA in *E. coli* (Larsen et al., 1994; Choi et al., 2020) or the frameshift attenuator sequence found upstream of the SARS-CoV frameshift site (Su et al., 2005; Kelly et al., 2020) were shown to modulate the levels of PRF. Another interesting feature of the SARS-CoV mRNA is that it does not only regulate frameshifting via its secondary structure in *cis*, but also in *trans* by forming dimers through kissing loop-loop interactions involving the stem 3 of the genomic RNA (Ishimaru et al., 2013; Bao et al., 2020; Bao et al., 2021). Such kissing loop interactions likely compete with the folding of the pseudoknot structure and thereby reduce the level of frameshifting. Overall, these illuminate that the regulatory *cis*-elements can vary in their structural folds and functions and how they work together with the canonical *cis*-acting stimulators of frameshifting remains to be studied.

TRANS-ACTING REGULATORS OF –1PRF EFFICIENCY

Although classically, PRF was thought to depend on *cis*-acting RNA elements, similar to other RNA-based regulatory events, frameshifting levels can be modulated by *trans*-acting factors in cells. These *trans*-factors are pathogen- or host-encoded proteins or other molecules that either directly bind to specific mRNA motifs or the ribosome, or indirectly affect translation by interacting with other proteins (Penn et al., 2020). Such interactions would likely alter the thermodynamic stability of the stimulatory structure or impair kinetics of ribosomal translocation resulting in changed recoding rates.

Earliest examples of frameshifting regulation were reported to occur on the +1 frameshift mRNAs, human ornithine decarboxylase antizyme (Rom and Kahana, 1994; Matsufuji et al., 1995) and the *E. coli* release factor 2 (RF2) (Baranov et al., 2002), where the levels of polyamines and RF2 in cell have autoregulatory functions.

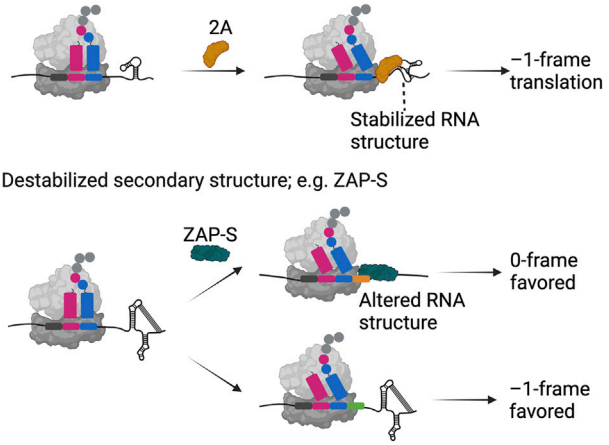

FIGURE 2 | Examples of *trans*-factor-mediated frameshifting. Two examples, namely **(A)** the cardioviral 2A protein and **(B)** the zinc-finger antiviral protein ZAP-S are shown as representatives of how host- and pathogen-encoded proteins can alter the secondary structure of a frameshift mRNA resulting in enhanced or decreased frameshifting efficiencies. Both proteins specifically bind to the appropriate mRNA and interact with the ribosome. While the 2A protein binds and stabilizes the secondary structure of the EMCV mRNA leading to −1 frameshifting, ZAP-S binding contrastingly destabilizes the secondary structure element on the SARS-CoV-2 mRNA resulting in significantly decreased frameshifting efficiencies. Created with BioRender.com.

Protein-mediated −1 frameshifting has been more recently discovered on the cellular poly-(C) binding proteins (PCBP) that promote −1 as well as −2 frameshifting in arteriviruses such as the PRRSV by directly interacting with the viral nonstructural protein nsp1β (Napthine et al., 2016; Li et al., 2019). In addition to stimulation of −2 frameshifting, here also the lack of a typical downstream RNA structure is remarkable. Instead, frameshifting is mediated through the binding of the PCBP and the viral nsp1β to a cytosine-rich sequence (CCCANCUCC) on the mRNA downstream to the slippery sequence, which mimics a stimulatory secondary structure (Napthine et al., 2016; Li et al., 2019).

Another elegant example of a pathogen-encoded *trans*-factor-mediated translational regulation has been discovered in the cardioviruses Encephalomyocarditis Virus (EMCV) and Theiler's Murine Encephalomyelitis Virus (TMEV) (Loughran et al., 2011; Hill et al., 2021b). The coding region of cardioviruses contain a conserved frameshift site at the 2A-2B ORF junction. Frameshifting occurs on the slippery motif G_GUU_UX eleven to twelve codons from the start of the 2B gene, producing a shorter 2B* protein, with undefined functions (Loughran et al., 2011; Napthine et al., 2017). However, it is assumed that the main function of this frameshift is the downregulation of the downstream encoded proteins, which in a way acts like a regulator of viral replication and assembly. Similar to PRRSV (Li et al., 2014), the downstream RNA motif, in this case a 35-nucleotide long stem loop, downstream of the slippery sequence is not sufficient alone to stimulate frameshifting. Frameshifting depends on an RNA-protein complex formed between the stem loop and the 2A protein. Cardioviral 2A is regarded as a multifunctional protein with key functions in virulence (Caliskan and Hill, 2022). In addition to regulating apoptosis, 2A was previously shown to bind to ribosomes and regulate translation (Groppo and Palmenberg, 2007; Hill et al., 2021b). Furthermore, it was discovered that 2A expression increases over the course of EMCV infection correlating with an increasing frameshifting efficiency of up to 70% (Napthine et al., 2017). The increase in 2A levels thus shuts down translation of downstream lying genes in the 0-frame, thereby ensuring appropriate levels of viral replicative proteins at early versus late stages of infection.

Recent work combining structural, biochemical and single-molecule analysis illuminated how the unique RNA binding fold found in the 2A structure allows it to interact with translating ribosomes and the downstream RNA element (Hill et al., 2021a; Hill et al., 2021b) (**Figure 2A**). The 2A protein interacts with the RNA at high affinity in a 1:1 stoichiometry (Hill et al., 2021a; Hill et al., 2021b). Furthermore, it also interacts with empty and translating ribosomes in a 3:1 stoichiometry possibly interfering with the binding of elongation factors on the ribosome. Detailed single-molecule analysis of the RNA-protein interactions of the wild type and mutant RNAs explained that 2A binding indeed stabilizes the EMCV RNA structure to a level that it alters the speed of translation elongation (Hill et al., 2021b) (**Figure 2A**). Combination of the higher force needed to unfold the structure and interference in binding of elongation factors caused by cardioviral 2A protein binding may thus explain the increase in the frameshifting efficiency (Groppo and Palmenberg, 2007; Loughran et al., 2011; Napthine et al., 2017; Hill et al., 2021b).

Such viral-encoded factors seem to selectively recognize particular RNA motifs and stabilize the RNA to impede translational elongation. Pausing at these sites likely opens a favorable time-window for codon-anticodon interactions to be re-established in the alternative reading frame, however, exactly which step of translation elongation is affected is still an open question.

The aforementioned findings also bring up the question whether modulation of frameshifting is a common feature of other cellular RNA-binding proteins as well. In this context, an earlier study by Kwak et al. showed that human annexin A2 (ANXA2) protein is associated with the IBV frameshift RNA element *in vitro* (Kwak et al., 2011). Interestingly, the knockdown of this factor increases frameshifting levels, suggesting a different mode-of-action than viral regulators of frameshifting. However, since ANXA2 is one of the most abundant proteins in the human cytoskeleton, it remains unclear how selective and conserved the interaction of ANXA2 and the IBV mRNA is or how the factor actually modulates frameshifting.

Other host factors also seem to recognize frameshifting ribosomes including the eukaryotic release factor 1 (eRF1) (Kobayashi et al., 2010) and the interferon-induced shiftless (SHFL) (Wang et al., 2019; Napthine et al., 2021; Zimmer et al., 2021). The cellular eRF1 was shown to interact with at least 30 other proteins in the cell together with HIV-1 proteins, therefore, what causes the decrease in HIV-1 frameshifting upon overexpression of the eRF1 remains open (Kobayashi et al., 2010).

Another cellular protein SHFL, previously named RyDEN or C19orf66 is an interferon-induced protein which was reported to inhibit replication of some viruses like Dengue Virus (DENV) (Suzuki et al., 2016). Contrary to Dengue Virus which does not frameshift, HIV-1 mRNA frameshifting decreases through SHFL interaction suggesting multiple antiviral functions for SHFL (Wang et al., 2019). This results in altered stoichiometry of the structural Gag protein to the Gag-Pol polypeptide ultimately leading to inhibition of HIV-1 replication. It was suggested that SHFL recruits cellular release factors to stalled ribosomes (Wang et al., 2019), but how the factors recognize frameshifting versus other stalled ribosomes awaits investigation. Beyond HIV-1, SHFL was shown to act broadly on other viral and cellular recoding sites including SARS-CoV-2 (Napthine et al., 2021; Schmidt et al., 2021; Zimmer et al., 2021) and the cellular *PEG-10* mRNA (Wang et al., 2019). In summary, these studies suggested that cellular proteins work in a concerted way to interfere with viral RNA frameshifting regimes. However, whether this also occurs in an mRNA-specific manner like in the case of viral 2A protein has been unclear.

The short isoform of the cellular zinc-finger antiviral protein ZAP, ZAP-S was recently identified as a *trans*-acting factor directly influencing −1PRF during SARS-CoV-2 infections (Zimmer et al., 2021). This interferon-induced protein (Yang and Li, 2020) impairs −1PRF, which is pertinent for the synthesis of the viral RNA polymerase through its specific interactions with the frameshift RNA pseudoknot (Zimmer et al., 2021) (**Figure 2B**). Among other frameshift sites tested, the effect was only observed for SARS-CoV-1 and-2, which differ by only one nucleotide in the primary sequence of the putative structure, suggesting specific interactions of ZAP-S with the SARS-CoV frameshift RNA element and an alternative mode-of-action compared to the host factor SHFL. By *in vitro* ensemble and single-molecule analysis, Zimmer and Kibe et al. showed that ZAP-S preferentially binds to the stem-loops 2 and 3 of the pseudoknot. Accordingly, unlike the cardioviral 2A protein, human ZAP-S does not stabilize the viral frameshift RNA, instead it interferes with the folding of the pseudoknot (**Figure 2B**). The interaction of ZAP-S with the frameshift site thus alters the stability of the secondary structure, which then no longer constitutes a blockade for the translating ribosome. Reduced frameshifting rates would lead to a drop in the viral polymerase level and consequently impede viral replication (Zimmer et al., 2021). Overall, despite following different modulatory mechanisms, host factors seem to have a common inhibitory effect on ribosomal frameshifting on viral mRNAs, suggesting that cells developed this type of global or gene-specific strategies as part of the antiviral response.

Interestingly, not only proteins have been categorized as *trans*-factors influencing the frameshifting efficiency but also other molecules: Small molecules including small RNAs [e.g., locked nucleic acids (LNAs), micro RNAs (miRNAs)] have already been successfully used for *in vitro* studies on frameshifting and consequently be suggested to act as potential effectors of the frameshifting process (Plant and Dinman, 2005; Henderson et al., 2006; Yu et al., 2010; Matsumoto et al., 2018; Puah et al., 2018; Chen et al., 2020; Sun et al., 2021). Whether such molecules are stable and specific enough to allow a precise tuning of gene expression warrants further studies.

In conclusion, ultimately it can be assumed that many more *trans*-factors await discovery. Whether in the form of proteins or other molecules affecting the frameshifting process, regulation of PRF seems to be a layer of host-pathogen interaction which is only recently been recognized. Furthermore, despite the fact that numerous studies already contributed pieces to better understand this recoding event, the molecular mechanisms by which these modulators act on the ribosomal frameshifting routes need to be further elucidated.

OTHER FACTORS THAT ALTER FRAMESHIFTING

The efficiency of frameshifting can be modulated by a variety of other effectors that tune the overall fidelity and rate of translation. Among those, limitations of aminoacylated tRNA supply can lead to an alternative frameshifting pathway, also referred to as hungry-codon frameshifting (Clare and Farabaugh, 1985; Clare et al., 1988; Belcourt and Farabaugh, 1990; Barak et al., 1996; Caliskan et al., 2017) (**Figure 3C**). Here, the frameshifting occurs when the A-site of the ribosome is vacant since the aminoacylated tRNA substrate is limited. After the slippage of the tRNA bound in the P-site, decoding continues in the alternative reading frame. Furthermore, it was shown that this conditional frameshifting can occur even by two nucleotides in consecutive steps and does not depend on the stimulatory secondary structure element (Caliskan et al., 2017). In addition, not only the aminoacylated tRNA supply, but also the presence and degree of certain tRNA modifications influences frameshifting: Particularly ones in the anticodon loop or on position 37 of the tRNA can lead to weakened and inefficient base-stacking interactions between the codon and the anticodon and alter the frameshifting process (Bjork et al., 1989; Urbonavicius et al., 2001; Licznar et al., 2003; Tükenmez et al., 2015). Similar to −1 frameshifting, also +1 frameshifting levels can be affected when tRNAs contain mutations like insertions in the anticodon stem-loop or when modifications are missing (O'Mahony et al., 1989; Atkins and Bjork, 2009; Hoffer et al., 2020; Gamper et al., 2021b).

Interactions of the nascent polypeptide chain with the ribosomal exit tunnel can lead to translational stalling (Wilson and Beckmann, 2011). +1PRF efficiency was previously shown to be regulated by the interactions of the nascent peptide (Yordanova et al., 2015). Recently, stalling caused by co-translational folding of the polypeptide was reported to influence −1PRF (Harrington et al., 2020; Carmody et al., 2021). It was shown that co-translational folding during the integration of an isomer of the structural polypeptide of the alphavirus Sindbis Virus (SINV) into the endoplasmic reticulum (ER) membrane correlates with frameshifting efficiency (Harrington et al., 2020). Especially, mutations altering the composition of the nascent polypeptide, especially charged amino acids located immediate upstream of the slippery sequence could be crucial for this effect (Harrington et al., 2020; Carmody et al., 2021). Based on molecular dynamic simulations, the group suggested that the folding of the protein generates a mechanical tension on the nascent polypeptide chain which alters −1PRF rates (Carmody et al.,

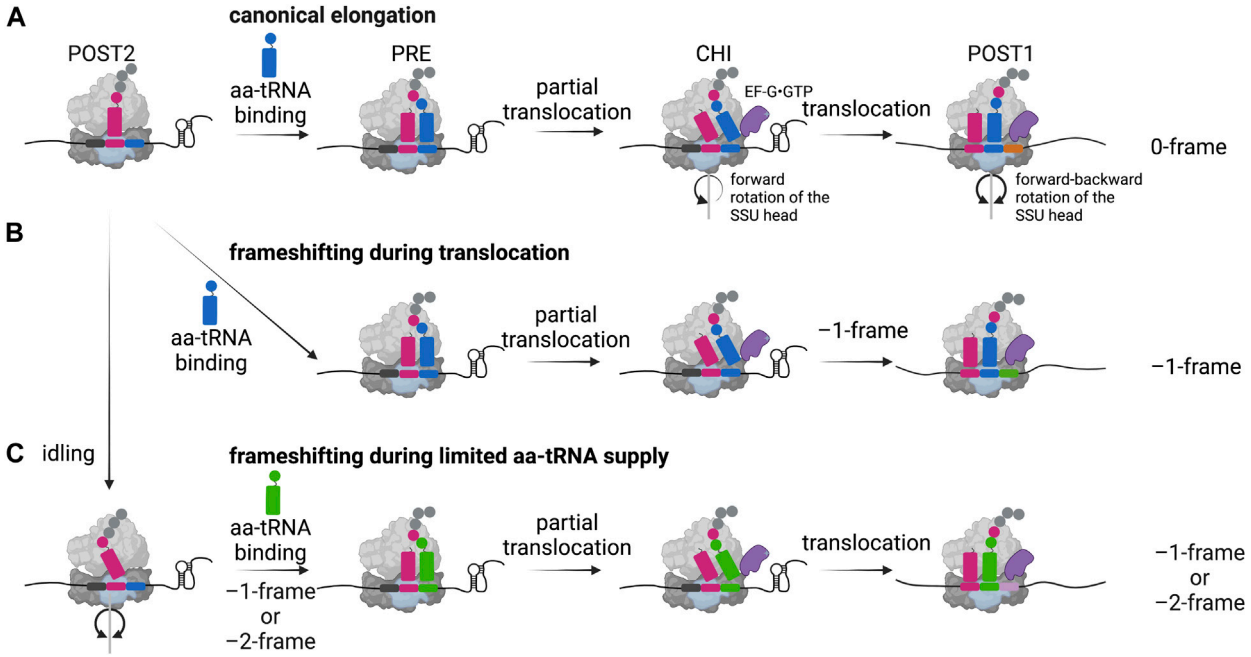

FIGURE 3 | –1 Programmed ribosomal frameshifting models. **(A)** In the canonical elongation pathway, movement of the ribosome along the mRNA and the peptide bond formation is facilitated by specific forward and backward movements of the small subunit (SSU) head and the hydrolysis of GTP by the elongation factor EF-G (eEF-2 in eukaryotes). POST: post-translocation state, PRE: pre-translocation state, CHI: chimeric state. **(B)** In case of canonical –1 frameshifting, ribosomal stalling is caused by a secondary structure of the mRNA leading to frameshifting during translocation. **(C)** An alternative frameshifting pathway is mediated by the limitation of the aminoacyl-site codon respective aminoacylated tRNA (aa-tRNA), here an idling step gives the time to overcome the limitation by shifting into the –1- or –2-frame. Created with BioRender.com.

2021). More recently, the co-translational folding of the nascent polypeptide chain of the viral non-structural protein 10 (Nsp10) was determined to distinctly interact with the ribosomal tunnel resulting in an upregulated frameshifting level on SARS-CoV-2 mRNA (Bhatt et al., 2021). Furthermore, mutations within the ribosome affecting their translation accuracy (Brunelle et al., 1999), mutations in the 16S ribosomal RNA platform region of the small ribosomal subunit (Leger et al., 2007) as well as mutations in proximity to the ribosomal exit E-site (Robert and Brakier-Gingras, 2003) were shown to alter the reading frame. Dependent on the ribosome loading on a given mRNA, frameshifting events may be altered and regulated by trailing ribosomes (Smith et al., 2019). Evidence has also been presented for the possibility that loading of the ribosome and rate of initiation on an mRNA inversely correlates with the formation of the stimulatory structure and thus alters frameshifting (Gendron et al., 2008).

In addition, components of the translational machinery can affect the overall fidelity of translation and therefore are important for the maintenance of the reading frame. Especially the elongation factors eEF1A and eEF2 in eukaryotes and their counterparts EF-Tu and EF-G in prokaryotes are crucial: Through their GTPase activities, elongation factors deliver the essential energy for binding of the aminoacylated tRNA to the A-site and the ribosomal translocation along the mRNA. Mutants of EF-Tu or eEF1A were shown to promote frameshifting (Dinman and Kinzy, 1997). Also, the eukaryotic translocation elongation factor 2 (eEF2) driving tRNA translocation was highlighted to be important for maintaining the reading frame since mutations in only one amino acid can affect translation fidelity leading to frameshifts (Ortiz et al., 2006). In particular, mutants of the domain IV of eEF2 in yeast (Ortiz et al., 2006; Peng et al., 2019) and mice (Liu et al., 2012) increased -1 frameshifting occurrence despite unaffected ribosome binding and GTP hydrolysis.

All in all, these suggest that the level of frameshifting is defined by multiple factors in the cell and support that the reading frame can be modulated in a time- and/or tissue-specific manner. Furthermore, the aforementioned examples show that, when ribosomal frameshifting is investigated, light should be also shed on the ribosomal exit tunnel to consider the influence that the interaction of the nascent polypeptide chain and the tunnel has on regulating frameshifting. The complex regulatory network also raises the question, what the molecular determinants are that cause the ribosome to slip into the alternative reading frame on a given coding sequence?

MOLECULAR DETERMINANTS OF RIBOSOME PAUSING AT SECONDARY STRUCTURES

A fundamental understanding of how various *cis*-acting elements and *trans*-acting factors act in a concerted way during the transition from the regular to the alternative translation route

requires a detailed kinetic framework of the molecular events defining PRF. Current knowledge points to the existence of several determinants of how RNA elements can mediate pausing and lead to frameshifting. These include the thermodynamic stability of the stimulatory elements as well as the conformational heterogeneity and structural plasticity of the stimulatory secondary structure. Regardless of how the kinetic barrier is formed, it is commonly accepted that such elements should sufficiently slow down or stall the ribosome, thereby increase the time-window that the tRNA dwells on the slippery codons (Caliskan et al., 2014; Chen et al., 2014; Kim et al., 2014; Choi et al., 2020).

Thermodynamic stability and the unfolding kinetics of the frameshift stimulatory structures are crucial determinants of the translational pause (Plant and Dinman, 2005; Chen et al., 2009; Giedroc and Cornish, 2009; Mouzakis et al., 2013; Caliskan et al., 2014; Choi et al., 2020). Evidence comes from earlier findings reporting that the local thermodynamic stability of the bottom part of the stem in the *dnaX* frameshift mRNA is more stable than the upper part (Larsen et al., 1997) and the stability of the first three to four base-pairs of the HIV-1 frameshift-mediating stem-loop positively correlates with frameshifting efficiency (Mouzakis et al., 2013). Here, the replacement with base-pairs of slightly higher stability results in an enhanced frameshifting efficiency. Studies comparing various stimulatory elements demonstrated that the local stability of the mRNA secondary structure is important for pausing and energetic restraints during ribosome movement due to the high energy needed for unwinding of the supercoiled stem is crucial for the frameshifting process (Plant and Dinman, 2005; Mouzakis et al., 2013; Caliskan et al., 2014). In addition, Choi et al. proposed a correlation between the duration of ribosome pausing and the number of base-pairs that has to be resolved before the ribosome fully translocates (Choi et al., 2020). Moreover, the precise length of the spacer region between the slippery codon and the frameshift stimulatory element on the mRNA ensures the correct positioning of the ribosome at the P-site codon during frameshifting (Kontos et al., 2001; Howard et al., 2004), which seem to place the base of the pseudoknot at the active site of the ribosomal helicase (Takyar et al., 2005; Caliskan et al., 2014). Consistently, kinetic studies of ribosomes stalled on the IBV frameshift mRNA showed a four-fold faster translocation in case the ribosome slipped into the −1-frame compared to continued translation in the 0-frame (Caliskan et al., 2014). This confirms that the helicase activity associated with the ribosomal mRNA entry channel highly depends on its precise positioning relative to the secondary structure and changing the position by a single nucleotide into the −1-frame assists the ribosome to better unwind the highly structured stimulatory RNAs (Qu et al., 2011; Caliskan et al., 2014; Choi et al., 2020).

Two recent studies provided the mechanistic insights into the interactions of the frameshift RNA structures and the ribosomal helicase. Bao et al. observed an inhibitory interaction of the secondary structures on the *E. coli dnaX* as well as the HIV-1 mRNA with ribosomes, that could also interfere with A-site binding (Bao et al., 2020). Using ribosomes primed at the SARS-CoV-2 frameshift site, Bhatt and Scaiola et al. illustrated that the pausing prior to the frameshift and that specific interactions of ribosomal helicase proteins and the helix h16 of the 18S ribosomal RNA (rRNA) and the bases within the pseudoknot were important for frameshifting. A particular position on the stem loop 1, the guanine at position 13,486, was shown to flip out from its stacked position within the loop and interact with the ribosomal helicase protein uS3 (Bhatt et al., 2021). The authors also underlined an important role of this guanine residue of the pseudoknot by showing an up to 45% reduction in frameshifting rates when this base was mutated (Bhatt et al., 2021). Overall, these studies reveal mechanistic and regulatory features that influence the pause duration at the frameshift sites.

FRAMESHIFT MRNAS CAN EXIST IN SEVERAL CONFORMATIONS

Others also proposed that structural plasticity and conformational heterogeneity of the secondary structure strongly correlates with translational pause and frameshifting efficiencies (Ritchie et al., 2012; Wu et al., 2018; Dinman, 2019a; Halma et al., 2019; Neupane et al., 2021). Wu et al. proposed that the ribosomal helicase unwinds only single base-pairs at once but not the entire structure, leaving time for the secondary structure to fold into other intermediates (Wu et al., 2018). These intermediates may enhance the frameshifting efficiency since translation might be faster when continuing in the −1-frame than overcoming the higher energy barrier to unfold the new, more stable structure (Wu et al., 2018). Furthermore, different mRNA secondary structures divergent from the initial structure might be formed due to different orders in refolding during or after the ribosome moves over the sequence, resulting in an altered frameshifting rate after the initial round of translation (Lyon et al., 2019; Halma et al., 2021; Hsu et al., 2021; Neupane et al., 2021). Moreover, considering the aforementioned importance of the spacer length, frameshifting might also be affected by secondary structures including parts of the spacer sequence since the effective length between the two frameshift stimulatory sequences would be altered in this case (Napthine et al., 2017; Hill et al., 2021b; Omar et al., 2021). Ultimately, the conformational heterogeneity of the frameshift-stimulating structure has been revealed to correlate with the frameshifting efficiency (Halma et al., 2021; Neupane et al., 2021; Schlick et al., 2021). Nevertheless, these conclusions are based on diverse mRNA structures and differences between *in vivo* and *in vitro* studies should be taken into account.

THERMODYNAMIC MODEL OF FRAMESHIFTING

The thermodynamic stability and the structural heterogeneity of the downstream RNA elements are important determinants defining the strength of the RNA roadblock and duration of the pause. However, propensity to frameshift on a given mRNA and the rate of frameshifting is primarily determined by

thermodynamics of base-pairing between the individual bases of the codon and the anticodon of the slippery heptanucleotides. Early on, the interaction of the tRNA anticodon and the mRNA codon was highlighted to influence frameshifting (Tsuchihashi and Brown, 1992). Furthermore, the nature of the mRNA bases, wobble propensity of the tRNAs and the presence of certain modified and unmodified bases dictates how much frameshifting will take place (Licznar et al., 2003; Nguyen et al., 2019). Bock et al. confirmed that the frameshifting efficiency on a given mRNA is not defined by kinetic determinants of unfolding the secondary structure, but is mainly controlled by the free energy of base-pairing between the codon and the anticodon of the slippery sequence (Bock et al., 2019). Long pause of the ribosome at an mRNA secondary structure may serve to achieve sufficient time for the ribosome to explore the energetically more favorable state in the 0- or –1-frame to continue translation. Based on thermodynamic modelling of the energy landscapes of individual codon-anticodon interactions on the *dnaX* frameshift site, the authors illustrated that the frameshifting efficiencies on a given frameshift sequence can be predicted quantitatively (Bock et al., 2019).

In conclusion, these findings suggest that the thermodynamic constraints of the frameshift stimulatory elements, as well as the conformations might synergistically work to mediate stalling of translating ribosomes thus providing the essential time-window in which the ribosome can explore an alternative reading frame. However, ribosomes are thought to be already primed for frameshifting due to the thermodynamically favorable nature of base-pairing in the alternative reading frame.

TIMING OF –1PRF DURING TRANSLOCATION

Based on these molecular constraints, when exactly does ribosomal frameshifting happen during translation?

During protein synthesis, following the accommodation of the correct aminoacylated tRNA in the A-site and peptide bond formation, the resulting pre-translocation state (PRE) ribosome undergoes large conformational changes facilitating the translocation of the tRNAs from the P- and A-sites into the E- and P-sites, along the mRNA in one codon steps (Rodnina and Wintermeyer, 2011) (**Figure 3A**). Since ribosomes are highly dynamic during this process, the exact determination of when ribosomal frameshifting happens during translation requires observation of the elemental steps of the elongation cycle over frameshift motifs in real time. Several studies employed single-molecule and ensemble kinetic analysis techniques to directly follow the translation process shortly upstream, at and downstream of the frameshift site to explain the precise position of the ribosome during slippage as well as the timing of frameshifting (Caliskan et al., 2014; Chen et al., 2014; Kim et al., 2014; Yan et al., 2015; Caliskan et al., 2017; Kim and Tinoco, 2017). There is evidence from genetic mutational studies of elongation factors that reading frame can be altered in both directions during accommodation or translocation (Dinman and Kinzy, 1997; Ortiz et al., 2006; Liu et al., 2012; Peng et al., 2019). A computational model predicted that the kinetic parameters of aminoacylated tRNA binding, peptide bond formation and translocation define the simultaneous accessibility of –1PRF through different pathways (Liao et al., 2011). *In vitro* structural and biochemical studies suggested that translocation of the tRNAs is the step of elongation cycle when codon-anticodon interactions most likely are broken and reestablished in the new reading frame (Giedroc and Cornish, 2009). The codon resolved, stepwise kinetic analysis of –1PRF on the IBV frameshift site demonstrated that canonical slippage occurs at a late step of tRNA translocation, when the tRNAs both bound on the slippery codons move from the P- and A-sites into the E- and P-sites (Caliskan et al., 2014) (**Figure 3B**). Supporting these findings, frameshifting on the bacterial *dnaX* gene, which is stimulated by a stem loop, was shown to occur when the translocation of the two tRNAs bound to the slippery sequence codons is slowed down (Chen et al., 2014; Kim et al., 2014; Caliskan et al., 2017; Kim and Tinoco, 2017). Accordingly, the recruitment of EF-G to the PRE complex was shown to facilitate the tRNA movement into the chimeric (CHI) state, however, the presence of the secondary structure prevents the backward rotation of the small subunit head, which is essential for completion of translocation (Caliskan et al., 2014; Chen et al., 2014; Yan et al., 2015). This slow translocation results in delayed dissociation of the E-site tRNA and EF-G (Caliskan et al., 2014), in part also explaining an earlier reported eukaryotic frameshifting complex during pausing at the IBV pseudoknot with eEF2 bound to the ribosome (Namy et al., 2006). Biochemical studies also suggest that the ribosome would be trapped in an unusual chimeric state, which would undergo several futile attempts of incomplete translocation allowing the ribosome to explore alternative routes to resume translation (Caliskan et al., 2014; Kim et al., 2014; Yan et al., 2015; Kim and Tinoco, 2017; Desai et al., 2019). It was reported that the unfolding of the secondary structure only happens after EF-G binding and directly depends on the force generated when the small subunit head undergoes the forward rotation (Desai et al., 2019). In addition, the delay in the reverse rotation of the small ribosomal subunit head into the non-rotated state and thus the increased lifetime of the rotated state of the ribosome correlates with the frameshifting efficiency (Choi et al., 2020). Nevertheless, although simultaneous translocation seems to be the predominant pathway in these *in vitro* systems, other –1PRF routes can also operate, e.g., when aminoacylated tRNAs supply is limited (Clare and Farabaugh, 1985; Clare et al., 1988; Belcourt and Farabaugh, 1990; Barak et al., 1996; Caliskan et al., 2017) (**Figure 3C**). Furthermore, as mentioned earlier, mutations of the ribosome, translation factors and tRNA modifications can alter the kinetic parameters of frameshifting and favor alternative translocation pathways (Atkins et al., 2016). For instance, Chen et al. Reported that *dnaX* frameshifting can occur before accommodation of the second codon of the slippery sequence, but still when the ribosome is in the long paused hyper-rotated state (Chen et al., 2014).

Recent studies employing a +1 frameshift-prone mRNA and native *E. coli* tRNA ($tRNA^{Pro}$) also suggested that timing of +1 frameshifting could be similar to canonical –1 frameshifting

occurring during late steps of translocation (Demo et al., 2021). Structural studies of +1 frameshift complexes reported extensive conformational rearrangements of the 30S head and body domains mimicking what is observed in a translocation intermediate state interacting with EF-G (Hong et al., 2018). In this scenario, while the tRNA-mRNA base-pairing is dynamic during swiveling movement of the small subunit head, in frameshift-prone ribosomes EF-G fails to some extent to maintain the codon-anticodon interactions and allows slippage into the +1 reading frame (Demo et al., 2021). This points that both, +1 and −1 frameshifting can be driven by swiveling movement of the small subunit head domain (Gamper et al., 2021a; Demo et al., 2021). Nonetheless, in the absence of EF-G, +1 frameshifting can also be mediated by quadruplet interactions between the codon and the extended or modified anticodon loop of a single tRNA (Maehigashi et al., 2014). Whether the present models of frameshifting apply also to other organisms and details of frameshifting pathways in eukaryotes remain to be further investigated.

CONCLUDING REMARKS

Despite fundamental knowledge gained about frameshifting events over the past years, there are still many outstanding questions concerning the detailed molecular mechanisms and occurrences of PRF. For instance, both upstream and downstream regions of frameshift RNAs seem to influence folding and the function of *cis*-acting canonical frameshift elements. Also, discovery of novel cellular and viral *trans*-acting factors, nascent polypeptide chain interactions and modifications on the RNAs affecting frameshifting, continuously reveal new levels of complexity. In the long run, the accumulated knowledge about this recoding mechanism and its regulation in cells will help to pave the way for therapeutic studies inhibiting frameshifting on pathogen mRNAs. Potential antiviral therapeutics could be designed to bind the frameshift RNA in a way that the stimulatory secondary structure either cannot be formed or cannot be unwound, hence prohibiting viral protein synthesis. In this respect, small synthetic, complementary oligonucleotides have already been suggested as possible therapeutic agents (Vickers and Ecker, 1992; Howard et al., 2004; Olsthoorn et al., 2004). Artificial, peptide nucleic acids (PNAs) can be designed to target secondary structures like hairpins and forming stable triplexes, thus enabling impacting −1PRF. Nevertheless, designing PNAs is challenging since the specificity and efficacy need to be high to prevent off-target effects. However, in potential cases where frameshifting might be supposed to be enhanced, the triplex needs to be resolved allowing the ribosome to continue translation in the −1-frame (Puah et al., 2018). Additionally, the discovery and optimization of novel small molecules that modulate frameshifting efficiencies such as the benzene derivative reagent RG501 (Hung et al., 1998), doxorubicin (Marcheschi et al., 2009), naphthyridine carbamate tetramer (Matsumoto et al., 2018) or merafloxacin (Sun et al., 2021) are desirable to find effective antiviral therapeutics. Collectively it is evident, that more research is imperative to fully understand the mechanism and all players involved in reinterpretation of the genetic code by frameshifting.

AUTHOR CONTRIBUTIONS

RR and NC contributed to conceptualisation of the manuscript, wrote the draft and edited it.

FUNDING

The work in our laboratory is supported by the Helmholtz Association, Helmholtz Centre for Infection Research. NC received funding from the European Research Council (ERC) Grant Nr. 948636.

ACKNOWLEDGMENTS

We thank Dr. Anke Sparmann and Anuja Kibe and members of Caliskan lab for critical reading of the manuscript. We thank Anuja Kibe for help with figure preparation in Biorender.

REFERENCES

Achenbach, J., and Nierhaus, K. H. (2015). The Mechanics of Ribosomal Translocation. *Biochimie* 114, 80–89. doi:10.1016/j.biochi.2014.12.003

Atkins, J. F., and Gesteland, R. F. (2010). *Recoding: Expansion of Decoding Rules Enriches Gene Expression*. New York, NY: Springer.

Atkins, J. F., Loughran, G., Bhatt, P. R., Firth, A. E., and Baranov, P. V. (2016). Ribosomal Frameshifting and Transcriptional Slippage: From Genetic Steganography and Cryptography to Adventitious Use. *Nucleic Acids Res.* 44, 7007–7078. doi:10.1093/nar/gkw530

Atkins, J. F., and Björk, G. R. (2009). A Gripping Tale of Ribosomal Frameshifting: Extragenic Suppressors of Frameshift Mutations Spotlight P-Site Realignment. *Microbiol. Mol. Biol. Rev.* 73, 178–210. doi:10.1128/mmbr.00010-08

Bao, C., Loerch, S., Ling, C., Korostelev, A. A., Grigorieff, N., and Ermolenko, D. N. (2020). mRNA Stem-Loops Can Pause the Ribosome by Hindering A-Site tRNA Binding. *eLife* 9, e55799. doi:10.7554/eLife.55799

Bao, C., Zhu, M., Nykonchuk, I., Wakabayashi, H., Mathews, D. H., and Ermolenko, D. N. (2021). Specific Length and Structure rather Than High Thermodynamic Stability Enable Regulatory mRNA Stem-Loops to Pause Translation. *bioRxiv, Cold Spring Harbor Lab.*. doi:10.1101/2021.08.16.456581

Barak, Z., Lindsley, D., and Gallant, J. (1996). On the Mechanism of Leftward Frameshifting at Several Hungry Codons. *J. Mol. Biol.* 256, 676–684. doi:10.1006/jmbi.1996.0117

Baranov, P. V., Gesteland, R. F., and Atkins, J. F. (2002). Release Factor 2 Frameshifting Sites in Different Bacteria. *EMBO Rep.* 3, 373–377. doi:10.1093/embo-reports/kvf065

Barry, J. K., and Miller, W. A. (2002). A -1 Ribosomal Frameshift Element that Requires Base Pairing across Four Kilobases Suggests a Mechanism of Regulating Ribosome and Replicase Traffic on a Viral RNA. *Proc. Natl. Acad. Sci.* 99, 11133–11138. doi:10.1073/pnas.162223099

Belcourt, M. F., and Farabaugh, P. J. (1990). Ribosomal Frameshifting in the Yeast Retrotransposon Ty: tRNAs Induce Slippage on a 7 Nucleotide Minimal Site. *Cell* 62, 339–352. doi:10.1016/0092-8674(90)90371-k

Belew, A. T., Advani, V. M., and Dinman, J. D. (2011). Endogenous Ribosomal Frameshift Signals Operate as mRNA Destabilizing Elements through at Least Two Molecular Pathways in Yeast. *Nucleic Acids Res.* 39, 2799–2808. doi:10.1093/nar/gkq1220

Bhatt, P. R., Scaiola, A., Loughran, G., Leibundgut, M., Kratzel, A., Meurs, R., et al. (2021). Structural Basis of Ribosomal Frameshifting during Translation of the SARS-CoV-2 RNA Genome. *Science* 372, 1306–1313. doi:10.1126/science.abf3546

Björk, G. R., Wikström, P. M., and Byström, A. S. (1989). Prevention of Translational Frameshifting by the Modified Nucleoside 1-methylguanosine. *Science* 244, 986–989. doi:10.1126/science.2471265

Bock, L. V., Caliskan, N., Korniy, N., Peske, F., Rodnina, M. V., and Grubmüller, H. (2019). Thermodynamic Control of -1 Programmed Ribosomal Frameshifting. *Nat. Commun.* 10, 4598. doi:10.1038/s41467-019-12648-x

Brierley, I., Boursnell, M. E., Binns, M. M., Bilimoria, B., Blok, V. C., Brown, T. D., et al. (1987). An Efficient Ribosomal Frame-Shifting Signal in the Polymerase-Encoding Region of the Coronavirus IBV. *EMBO J.* 6, 3779–3785. doi:10.1002/j.1460-2075.1987.tb02713.x

Brierley, I., Digard, P., and Inglis, S. C. (1989). Characterization of an Efficient Coronavirus Ribosomal Frameshifting Signal: Requirement for an RNA Pseudoknot. *Cell* 57, 537–547. doi:10.1016/0092-8674(89)90124-4

Brierley, I., Gilbert, R. J. C., and Pennell, S. (2010). "Pseudoknot-Dependent Programmed -1 Ribosomal Frameshifting: Structures, Mechanisms and Models," in *Recoding: Expansion of Decoding Rules Enriches Gene Expression* (New York, NY: Springer), 149–174. doi:10.1007/978-0-387-89382-2_7

Brierley, I., Jenner, A. J., and Inglis, S. C. (1992). Mutational Analysis of the "Slippery-Sequence" Component of a Coronavirus Ribosomal Frameshifting Signal. *J. Mol. Biol.* 227, 463–479. doi:10.1016/0022-2836(92)90901-u

Brierley, I., Rolley, N. J., Jenner, A. J., and Inglis, S. C. (1991). Mutational Analysis of the RNA Pseudoknot Component of a Coronavirus Ribosomal Frameshifting Signal. *J. Mol. Biol.* 220, 889–902. doi:10.1016/0022-2836(91)90361-9

Brunelle, M., Payant, C., Lemay, G., and Brakier-Gingras, L. (1999). Expression of the Human Immunodeficiency Virus Frameshift Signal in a Bacterial Cell-free System: Influence of an Interaction between the Ribosome and a Stem-Loop Structure Downstream from the Slippery Site. *Nucleic Acids Res.* 27, 4783–4791. doi:10.1093/nar/27.24.4783

Caliskan, N., and Hill, C. H. (2022). Insights from Structural Studies of the Cardiovirus 2A Protein. *Biosci. Rep.* 42, BSR20210406. doi:10.1042/bsr20210406

Caliskan, N., Katunin, V. I., Belardinelli, R., Peske, F., and Rodnina, M. V. (2014). Programmed -1 Frameshifting by Kinetic Partitioning during Impeded Translocation. *Cell* 157, 1619–1631. doi:10.1016/j.cell.2014.04.041

Caliskan, N., Peske, F., and Rodnina, M. V. (2015). Changed in Translation: mRNA Recoding by −1 Programmed Ribosomal Frameshifting. *Trends Biochem. Sci.* 40, 265–274. doi:10.1016/j.tibs.2015.03.006

Caliskan, N., Wohlgemuth, I., Korniy, N., Pearson, M., Peske, F., and Rodnina, M. V. (2017). Conditional Switch between Frameshifting Regimes upon Translation of dnaX mRNA. *Mol. Cel* 66, 558–567. e4. doi:10.1016/j.molcel.2017.04.023

Carmody, P. J., Zimmer, M. H., Kuntz, C. P., Harrington, H. R., Duckworth, K. E., Penn, W. D., et al. (2021). Coordination of -1 Programmed Ribosomal Frameshifting by Transcript and Nascent Chain Features Revealed by Deep Mutational Scanning. *Nucleic Acids Res.* 49, 12943–12954. doi:10.1093/nar/gkab1172

Chen, G., Chang, K.-Y., Chou, M.-Y., Bustamante, C., and Tinoco, I. (2009). Triplex Structures in an RNA Pseudoknot Enhance Mechanical Stability and Increase Efficiency of -1 Ribosomal Frameshifting. *Proc. Natl. Acad. Sci.* 106, 12706–12711. doi:10.1073/pnas.0905046106

Chen, J., Petrov, A., Johansson, M., Tsai, A., O'Leary, S. E., and Puglisi, J. D. (2014). Dynamic Pathways of −1 Translational Frameshifting. *Nature* 512, 328–332. doi:10.1038/nature13428

Chen, Y., Tao, H., Shen, S., Miao, Z., Li, L., Jia, Y., et al. (2020). A Drug Screening Toolkit Based on the -1 Ribosomal Frameshifting of SARS-CoV-2. *Heliyon* 6, e04793. doi:10.1016/j.heliyon.2020.e04793

Choi, J., O'Loughlin, S., Atkins, J. F., and Puglisi, J. D. (2020). The Energy Landscape of -1 Ribosomal Frameshifting. *Sci. Adv.* 6, eaax6969. doi:10.1126/sciadv.aax6969

Clare, J., and Farabaugh, P. (1985). Nucleotide Sequence of a Yeast Ty Element: Evidence for an Unusual Mechanism of Gene Expression. *Proc. Natl. Acad. Sci.* 82, 2829–2833. doi:10.1073/pnas.82.9.2829

Clare, J. J., Belcourt, M., and Farabaugh, P. J. (1988). Efficient Translational Frameshifting Occurs within a Conserved Sequence of the Overlap between the Two Genes of a Yeast Ty1 Transposon. *Proc. Natl. Acad. Sci.* 85, 6816–6820. doi:10.1073/pnas.85.18.6816

Clark, M. B., Jänicke, M., Gottesbühren, U., Kleffmann, T., Legge, M., Poole, E. S., et al. (2007). Mammalian Gene PEG10 Expresses Two Reading Frames by High Efficiency -1 Frameshifting in Embryonic-Associated Tissues. *J. Biol. Chem.* 282, 37359–37369. doi:10.1074/jbc.m705676200

Cobucci-Ponzano, B., Conte, F., Benelli, D., Londei, P., Flagiello, A., Monti, M., et al. (2006). The Gene of an Archaeal α-l-fucosidase Is Expressed by Translational Frameshifting. *Nucleic Acids Res.* 34, 4258–4268. doi:10.1093/nar/gkl574

Demo, G., Gamper, H. B., Loveland, A. B., Masuda, I., Carbone, C. E., Svidritskiy, E., et al. (2021). Structural Basis for +1 Ribosomal Frameshifting during EF-G-Catalyzed Translocation. *Nat. Commun.* 12, 4644. doi:10.1038/s41467-021-24911-1

Desai, V. P., Frank, F., Lee, A., Righini, M., Lancaster, L., Noller, H. F., et al. (2019). Co-temporal Force and Fluorescence Measurements Reveal a Ribosomal Gear Shift Mechanism of Translation Regulation by Structured mRNAs. *Mol. Cel* 75, 1007–1019. e5. doi:10.1016/j.molcel.2019.07.024

Dever, T. E., Dinman, J. D., and Green, R. (2018). Translation Elongation and Recoding in Eukaryotes. *Cold Spring Harb Perspect. Biol.* 10, a032649. doi:10.1101/cshperspect.a032649

Dinman, J. D., and Kinzy, T. G. (1997). Translational Misreading: Mutations in Translation Elongation Factor 1alpha Differentially Affect Programmed Ribosomal Frameshifting and Drug Sensitivity. *RNA* 3, 870–881.

Dinman, J. D., Icho, T., and Wickner, R. B. (1991). A -1 Ribosomal Frameshift in a Double-Stranded RNA Virus of Yeast Forms a Gag-Pol Fusion Protein. *Proc. Natl. Acad. Sci.* 88, 174–178. doi:10.1073/pnas.88.1.174

Dinman, J. D. (1995). Ribosomal Frameshifting in Yeast Viruses. *Yeast* 11, 1115–1127. doi:10.1002/yea.320111202

Dinman, J. D. (2019a). Slippery Ribosomes Prefer Shapeshifting mRNAs. *Proc. Natl. Acad. Sci. USA* 116, 19225–19227. doi:10.1073/pnas.1913074116

Dinman, J. D. (2019b). Translational Recoding Signals: Expanding the Synthetic Biology Toolbox. *J. Biol. Chem.* 294, 7537–7545. doi:10.1074/jbc.rev119.006348

Dinman, J. D., and Wickner, R. B. (1992). Ribosomal Frameshifting Efficiency and Gag/gag-Pol Ratio Are Critical for Yeast M1 Double-Stranded RNA Virus Propagation. *J. Virol.* 66, 3669–3676. doi:10.1128/jvi.66.6.3669-3676.1992

Dulude, D., Berchiche, Y. A., Gendron, K., Brakier-Gingras, L., and Heveker, N. (2006). Decreasing the Frameshift Efficiency Translates into an Equivalent Reduction of the Replication of the Human Immunodeficiency Virus Type 1. *Virology* 345, 127–136. doi:10.1016/j.virol.2005.08.048

Endoh, T., Kawasaki, Y., and Sugimoto, N. (2013). Suppression of Gene Expression by G-Quadruplexes in Open Reading Frames Depends on G-Quadruplex Stability. *Angew. Chem. Int. Ed.* 52, 5522–5526. doi:10.1002/anie.201300058

Fang, Y., Treffers, E. E., Li, Y., Tas, A., Sun, Z., Van Der Meer, Y., et al. (2012). Efficient -2 Frameshifting by Mammalian Ribosomes to Synthesize an Additional Arterivirus Protein. *Proc. Natl. Acad. Sci.* 109, E2920–E2928. doi:10.1073/pnas.1211145109

Finch, L. K., Ling, R., Napthine, S., Olspert, A., Michiels, T., Lardinois, C., et al. (2015). Characterization of Ribosomal Frameshifting in Theiler's Murine Encephalomyelitis Virus. *J. Virol.* 89, 8580–8589. doi:10.1128/jvi.01043-15

Firth, A. E., and Atkins, J. F. (2009). A Conserved Predicted Pseudoknot in the NS2A-Encoding Sequence of West Nile and Japanese Encephalitis Flaviviruses Suggests NS1' May Derive from Ribosomal Frameshifting. *Virol. J.* 6, 14. doi:10.1186/1743-422X-6-14

Firth, A. E. (2014). Mapping Overlapping Functional Elements Embedded within the Protein-Coding Regions of RNA Viruses. *Nucleic Acids Res.* 42, 12425–12439. doi:10.1093/nar/gku981

Gamper, H., Li, H., Masuda, I., Miklos Robkis, D., Christian, T., Conn, A. B., et al. (2021a). Insights into Genome Recoding from the Mechanism of a Classic +1-frameshifting tRNA. *Nat. Commun.* 12, 328. doi:10.1038/s41467-020-20373-z

Gamper, H., Mao, Y., Masuda, I., McGuigan, H., Blaha, G., Wang, Y., et al. (2021b). Twice Exploration of tRNA +1 Frameshifting in an Elongation Cycle of Protein Synthesis. *Nucleic Acids Res.* 49, 10046–10060. doi:10.1093/nar/gkab734

Gendron, K., Charbonneau, J., Dulude, D., Heveker, N., Ferbeyre, G., and Brakier-gingras, L. (2008). The Presence of the TAR RNA Structure Alters the Programmed -1 Ribosomal Frameshift Efficiency of the Human Immunodeficiency Virus Type 1 (HIV-1) by Modifying the Rate of Translation Initiation. *Nucleic Acids Res.* 36, 30–40. doi:10.1093/nar/gkm906

Gesteland, R. F., and Atkins, J. F. (1996). Recoding: Dynamic Reprogramming of Translation. *Annu. Rev. Biochem.* 65, 741–768. doi:10.1146/annurev.bi.65.070196.003521

Giedroc, D. P., and Cornish, P. V. (2009). Frameshifting RNA Pseudoknots: Structure and Mechanism. *Virus. Res.* 139, 193–208. doi:10.1016/j.virusres.2008.06.008

Groppo, R., and Palmenberg, A. C. (2007). Cardiovirus 2A Protein Associates with 40S but Not 80S Ribosome Subunits during Infection. *J. Virol.* 81, 13067–13074. doi:10.1128/jvi.00185-07

Halma, M. T. J., Ritchie, D. B., and Woodside, M. T. (2021). Conformational Shannon Entropy of mRNA Structures from Force Spectroscopy Measurements Predicts the Efficiency of -1 Programmed Ribosomal Frameshift Stimulation. *Phys. Rev. Lett.* 126, 038102. doi:10.1103/PhysRevLett.126.038102

Halma, M. T. J., Ritchie, D. B., Cappellano, T. R., Neupane, K., and Woodside, M. T. (2019). Complex Dynamics under Tension in a High-Efficiency Frameshift Stimulatory Structure. *Proc. Natl. Acad. Sci. USA* 116, 19500–19505. doi:10.1073/pnas.1905258116

Harrington, H. R., Zimmer, M. H., Chamness, L. M., Nash, V., Penn, W. D., Miller, T. F., et al. (2020). Cotranslational Folding Stimulates Programmed Ribosomal Frameshifting in the Alphavirus Structural Polyprotein. *J. Biol. Chem.* 295, 6798–6808. doi:10.1074/jbc.ra120.012706

Henderson, C. M., Anderson, C. B., and Howard, M. T. (2006). Antisense-induced Ribosomal Frameshifting. *Nucleic Acids Res.* 34, 4302–4310. doi:10.1093/nar/gkl531

Hill, C. H., Pekarek, L., Napthine, S., Kibe, A., Firth, A. E., Graham, S. C., et al. (2021b). Structural and Molecular Basis for Cardiovirus 2A Protein as a Viral Gene Expression Switch. *Nat. Commun.* 12, 7166. doi:10.1038/s41467-021-27400-7

Hill, C. H., Cook, G. M., Napthine, S., Kibe, A., Brown, K., Caliskan, N., et al. (2021a). Investigating Molecular Mechanisms of 2A-Stimulated Ribosomal Pausing and Frameshifting in Theilovirus. *Nucleic Acids Res.* 49, 11938–11958. doi:10.1093/nar/gkab969

Hoffer, E. D., Hong, S., Sunita, S., Maehigashi, T., Gonzalez, R. L., Whitford, P. C., et al. (2020). Structural Insights into mRNA reading Frame Regulation by tRNA Modification and Slippery Codon-Anticodon Pairing. *Elife* 9, e51898. doi:10.7554/eLife.51898

Hong, S., Sunita, S., Maehigashi, T., Hoffer, E. D., Dunkle, J. A., and Dunham, C. M. (2018). Mechanism of tRNA-Mediated +1 Ribosomal Frameshifting. *Proc. Natl. Acad. Sci. USA* 115, 11226–11231. doi:10.1073/pnas.1809319115

Horsfield, J. A., Wilson, D. N., Mannering, S. A., Adamski, F. M., and Tate, W. P. (1995). Prokaryotic Ribosomes Recode the HIV-1gag-Pol-1 Frameshift Sequence by an E/P Site post-translocation Simultaneous Slippage Mechanism. *Nucl. Acids Res.* 23, 1487–1494. doi:10.1093/nar/23.9.1487

Houck-Loomis, B., Durney, M. A., Salguero, C., Shankar, N., Nagle, J. M., Goff, S. P., et al. (2011). An Equilibrium-dependent Retroviral mRNA Switch Regulates Translational Recoding. *Nature* 480, 561–564. doi:10.1038/nature10657

Howard, M. T., Gesteland, R. F., and Atkins, J. F. (2004). Efficient Stimulation of Site-specific Ribosome Frameshifting by Antisense Oligonucleotides. *RNA* 10, 1653–1661. doi:10.1261/rna.7810204

Hsu, C.-F., Chang, K.-C., Chen, Y.-L., Hsieh, P.-S., Lee, A.-I., Tu, J.-Y., et al. (2021). Formation of Frameshift-Stimulating RNA Pseudoknots Is Facilitated by Remodeling of Their Folding Intermediates. *Nucleic Acids Res.* 49, 6941–6957. doi:10.1093/nar/gkab512

Hung, M., Patel, P., Davis, S., and Green, S. R. (1998). Importance of Ribosomal Frameshifting for Human Immunodeficiency Virus Type 1 Particle Assembly and Replication. *J. Virol.* 72, 4819–4824. doi:10.1128/jvi.72.6.4819-4824.1998

Icho, T., and Wickner, R. B. (1989). The Double-Stranded RNA Genome of Yeast Virus L-A Encodes its Own Putative RNA Polymerase by Fusing Two Open reading Frames. *J. Biol. Chem.* 264, 6716–6723. doi:10.1016/s0021-9258(18)83488-3

Ishimaru, D., Plant, E. P., Sims, A. C., Yount, B. L., Roth, B. M., Eldho, N. V., et al. (2013). RNA Dimerization Plays a Role in Ribosomal Frameshifting of the SARS Coronavirus. *Nucleic Acids Res.* 41, 2594–2608. doi:10.1093/nar/gks1361

Jacks, T., Madhani, H. D., Masiarz, F. R., and Varmus, H. E. (1988a). Signals for Ribosomal Frameshifting in the Rous Sarcoma Virus Gag-Pol Region. *Cell* 55, 447–458. doi:10.1016/0092-8674(88)90031-1

Jacks, T., Power, M. D., Masiarz, F. R., Luciw, P. A., Barr, P. J., and Varmus, H. E. (1988b). Characterization of Ribosomal Frameshifting in HIV-1 Gag-Pol Expression. *Nature* 331, 280–283. doi:10.1038/331280a0

Jacks, T., and Varmus, H. E. (1985). Expression of the Rous Sarcoma Virus Pol Gene by Ribosomal Frameshifting. *Science* 230, 1237–1242. doi:10.1126/science.2416054

Jacobs, J. L., Belew, A. T., Rakauskaite, R., and Dinman, J. D. (2007). Identification of Functional, Endogenous Programmed −1 Ribosomal Frameshift Signals in the Genome of Saccharomyces cerevisiae. *Nucleic Acids Res.* 35, 165–174. doi:10.1093/nar/gkl1033

Kelly, J. A., Olson, A. N., Neupane, K., Munshi, S., San Emeterio, J., Pollack, L., et al. (2020). Structural and Functional Conservation of the Programmed −1 Ribosomal Frameshift Signal of SARS Coronavirus 2 (SARS-CoV-2). *J. Biol. Chem.* 295, 10741–10748. doi:10.1074/jbc.ac120.013449

Ketteler, R. (2012). On Programmed Ribosomal Frameshifting: The Alternative Proteomes. *Front. Genet.* 3, 242. doi:10.3389/fgene.2012.00242

Kim, H.-K., Liu, F., Fei, J., Bustamante, C., Gonzalez, R. L., and Tinoco, I. (2014). A Frameshifting Stimulatory Stem Loop Destabilizes the Hybrid State and Impedes Ribosomal Translocation. *Proc. Natl. Acad. Sci.* 111, 5538–5543. doi:10.1073/pnas.1403457111

Kim, H. K., and Tinoco, I. (2017). EF-G Catalyzed Translocation Dynamics in the Presence of Ribosomal Frameshifting Stimulatory Signals. *Nucleic Acids Res.* 45, 2865–2874. doi:10.1093/nar/gkw1020

Kobayashi, Y., Zhuang, J., Peltz, S., and Dougherty, J. (2010). Identification of a Cellular Factor that Modulates HIV-1 Programmed Ribosomal Frameshifting. *J. Biol. Chem.* 285, 19776–19784. doi:10.1074/jbc.m109.085621

Kontos, H., Napthine, S., and Brierley, I. (2001). Ribosomal Pausing at a Frameshifter RNA Pseudoknot Is Sensitive to Reading Phase but Shows Little Correlation with Frameshift Efficiency. *Mol. Cel Biol* 21, 8657–8670. doi:10.1128/mcb.21.24.8657-8670.2001

Korniy, N., Goyal, A., Hoffmann, M., Samatova, E., Peske, F., Pöhlmann, S., et al. (2019). Modulation of HIV-1 Gag/Gag-Pol Frameshifting by tRNA Abundance. *Nucleic Acids Res.* 47, 5210–5222. doi:10.1093/nar/gkz202

Kurland, C. G. (1992). Translational Accuracy and the Fitness of Bacteria. *Annu. Rev. Genet.* 26, 29–50. doi:10.1146/annurev.ge.26.120192.000333

Kwak, H., Park, M. W., and Jeong, S. (2011). Annexin A2 Binds RNA and Reduces the Frameshifting Efficiency of Infectious Bronchitis Virus. *PLoS ONE* 6, e24067. doi:10.1371/journal.pone.0024067

Lainé, S., Thouard, A., Komar, A. A., and Rossignol, J. M. (2008). Ribosome Can Resume the Translation in Both +1 or -1 Frames after Encountering an AGA Cluster in Escherichia coli. *Gene* 412, 95–101. doi:10.1016/j.gene.2008.01.018

Larsen, B., Gesteland, R. F., and Atkins, J. F. (1997). Structural Probing and Mutagenic Analysis of the Stem-Loop Required for Escherichia coli dnaX Ribosomal Frameshifting: Programmed Efficiency of 50%. *J. Mol. Biol.* 271, 47–60. doi:10.1006/jmbi.1997.1162

Larsen, B., Wills, N. M., Gesteland, R. F., and Atkins, J. F. (1994). rRNA-mRNA Base Pairing Stimulates a Programmed -1 Ribosomal Frameshift. *J. Bacteriol.* 176, 6842–6851. doi:10.1128/jb.176.22.6842-6851.1994

Leger, M., Dulude, D., Steinberg, S. V., and Brakier-Gingras, L. (2007). The Three Transfer RNAs Occupying the A, P and E Sites on the Ribosome Are Involved in Viral Programmed -1 Ribosomal Frameshift. *Nucleic Acids Res.* 35, 5581–5592. doi:10.1093/nar/gkm578

Li, Y., Firth, A. E., Brierley, I., Cai, Y., Napthine, S., Wang, T., et al. (2019). Programmed -2/-1 Ribosomal Frameshifting in Simarteriviruses: an Evolutionarily Conserved Mechanism. *J. Virol.* 93, e00370–19. doi:10.1128/JVI.00370-19

Li, Y., Treffers, E. E., Napthine, S., Tas, A., Zhu, L., Sun, Z., et al. (2014). Transactivation of Programmed Ribosomal Frameshifting by a Viral Protein. *Proc. Natl. Acad. Sci.* 111, E2172–E2181. doi:10.1073/pnas.1321930111

Liao, P.-Y., Choi, Y. S., Dinman, J. D., and Lee, K. H. (2011). The many Paths to Frameshifting: Kinetic Modelling and Analysis of the Effects of Different Elongation Steps on Programmed -1 Ribosomal Frameshifting. *Nucleic Acids Res.* 39, 300–312. doi:10.1093/nar/gkq761

Licznar, P., Mejlhede, N., Prère, M. F., Wills, N., Gesteland, R. F., Atkins, J. F., et al. (2003). Programmed Translational -1 Frameshifting on Hexanucleotide Motifs

and the Wobble Properties of tRNAs. *EMBO J.* 22, 4770–4778. doi:10.1093/emboj/cdg465

Lin, Z., Gilbert, R. J. C., and Brierley, I. (2012). Spacer-length Dependence of Programmed −1 or −2 Ribosomal Frameshifting on a U 6 A Heptamer Supports a Role for Messenger RNA (mRNA) Tension in Frameshifting. *Nucleic Acids Res.* 40, 8674–8689. doi:10.1093/nar/gks629

Liu, S., Bachran, C., Gupta, P., Miller-Randolph, S., Wang, H., Crown, D., et al. (2012). Diphthamide Modification on Eukaryotic Elongation Factor 2 Is Needed to Assure Fidelity of mRNA Translation and Mouse Development. *Proc. Natl. Acad. Sci.* 109, 13817–13822. doi:10.1073/pnas.1206933109

Loughran, G., Firth, A. E., and Atkins, J. F. (2011). Ribosomal Frameshifting into an Overlapping Gene in the 2B-Encoding Region of the Cardiovirus Genome. *Proc. Natl. Acad. Sci.* 108, E1111–E1119. doi:10.1073/pnas.1102932108

Lyon, K., Aguilera, L. U., Morisaki, T., Munsky, B., and Stasevich, T. J. (2019). Live-Cell Single RNA Imaging Reveals Bursts of Translational Frameshifting. *Mol. Cel* 75, 172–183. doi:10.1016/j.molcel.2019.05.002

Maehigashi, T., Dunkle, J. A., Miles, S. J., and Dunham, C. M. (2014). Structural Insights into +1 Frameshifting Promoted by Expanded or Modification-Deficient Anticodon Stem Loops. *Proc. Natl. Acad. Sci.* 111, 12740–12745. doi:10.1073/pnas.1409436111

Manktelow, E., Shigemoto, K., and Brierley, I. (2005). Characterization of the Frameshift Signal of Edr, a Mammalian Example of Programmed -1 Ribosomal Frameshifting. *Nucleic Acids Res.* 33, 1553–1563. doi:10.1093/nar/gki299

Marcheschi, R. J., Mouzakis, K. D., and Butcher, S. E. (2009). Selection and Characterization of Small Molecules that Bind the HIV-1 Frameshift Site RNA. *ACS Chem. Biol.* 4, 844–854. doi:10.1021/cb900167m

Matsufuji, S., Matsufuji, T., Miyazaki, Y., Murakami, Y., Atkins, J. F., Gesteland, R. F., et al. (1995). Autoregulatory Frameshifting in Decoding Mammalian Ornithine Decarboxylase Antizyme. *Cell* 80, 51–60. doi:10.1016/0092-8674(95)90450-6

Matsumoto, S., Caliskan, N., Rodnina, M. V., Murata, A., and Nakatani, K. (2018). Small Synthetic Molecule-Stabilized RNA Pseudoknot as an Activator for -1 Ribosomal Frameshifting. *Nucleic Acids Res.* 46, 8079–8089. doi:10.1093/nar/gky689

Meydan, S., Klepacki, D., Karthikeyan, S., Margus, T., Thomas, P., Jones, J. E., et al. (2017). Programmed Ribosomal Frameshifting Generates a Copper Transporter and a Copper Chaperone from the Same Gene. *Mol. Cel* 65, 207–219. doi:10.1016/j.molcel.2016.12.008

Miras, M., Miller, W. A., Truniger, V., and Aranda, M. A. (2017). Non-canonical Translation in Plant RNA Viruses. *Front. Plant Sci.* 8, 494. doi:10.3389/fpls.2017.00494

Mouzakis, K. D., Lang, A. L., Vander Meulen, K. A., Easterday, P. D., and Butcher, S. E. (2013). HIV-1 Frameshift Efficiency Is Primarily Determined by the Stability of Base Pairs Positioned at the mRNA Entrance Channel of the Ribosome. *Nucleic Acids Res.* 41, 1901–1913. doi:10.1093/nar/gks1254

Namy, O., Moran, S. J., Stuart, D. I., Gilbert, R. J. C., and Brierley, I. (2006). A Mechanical Explanation of RNA Pseudoknot Function in Programmed Ribosomal Frameshifting. *Nature* 441, 244–247. doi:10.1038/nature04735

Napthine, S., Hill, C. H., Nugent, H. C. M., and Brierley, I. (2021). Modulation of Viral Programmed Ribosomal Frameshifting and Stop Codon Readthrough by the Host Restriction Factor Shiftless. *Viruses* 13, 1230. doi:10.3390/v13071230

Napthine, S., Ling, R., Finch, L. K., Jones, J. D., Bell, S., Brierley, I., et al. (2017). Protein-directed Ribosomal Frameshifting Temporally Regulates Gene Expression. *Nat. Commun.* 8, 15582. doi:10.1038/ncomms15582

Napthine, S., Treffers, E. E., Bell, S., Goodfellow, I., Fang, Y., Firth, A. E., et al. (2016). A Novel Role for Poly(C) Binding Proteins in Programmed Ribosomal Frameshifting. *Nucleic Acids Res.* 44, 5491–5503. doi:10.1093/nar/gkw480

Neupane, K., Zhao, M., Lyons, A., Munshi, S., Ileperuma, S. M., Ritchie, D. B., et al. (2021). Structural Dynamics of Single SARS-CoV-2 Pseudoknot Molecules Reveal Topologically Distinct Conformers. *Nat. Commun.* 12, 4749. doi:10.1038/s41467-021-25085-6

Nguyen, H. A., Hoffer, E. D., and Dunham, C. M. (2019). Importance of a tRNA Anticodon Loop Modification and a Conserved, Noncanonical Anticodon Stem Pairing in tRNACGGPro for Decoding. *J. Biol. Chem.* 294, 5281–5291. doi:10.1074/jbc.ra119.007410

Noller, H. F., Lancaster, L., Zhou, J., and Mohan, S. (2017). The Ribosome Moves: RNA Mechanics and Translocation. *Nat. Struct. Mol. Biol.* 24, 1021–1027. doi:10.1038/nsmb.3505

O'Mahony, D. J., Mims, B. H., Thompson, S., Murgola, E. J., and Atkins, J. F. (1989). Glycine tRNA Mutants with normal Anticodon Loop Size Cause -1 Frameshifting. *Proc. Natl. Acad. Sci.* 86, 7979–7983. doi:10.1073/pnas.86.20.7979

Olsthoorn, R. C. L., Laurs, M., Sohet, F., Hilbers, C. W., Heus, H. A., and Pleij, C. W. A. (2004). Novel Application of sRNA: Stimulation of Ribosomal Frameshifting: FIGURE 1. *RNA* 10, 1702–1703. doi:10.1261/rna.7139704

Omar, S. I., Zhao, M., Sekar, R. V., Moghadam, S. A., Tuszynski, J. A., and Woodside, M. T. (2021). Modeling the Structure of the Frameshift-Stimulatory Pseudoknot in SARS-CoV-2 Reveals Multiple Possible Conformers. *Plos Comput. Biol.* 17, e1008603. doi:10.1371/journal.pcbi.1008603

Ortiz, P. A., Ulloque, R., Kihara, G. K., Zheng, H., and Kinzy, T. G. (2006). Translation Elongation Factor 2 Anticodon Mimicry Domain Mutants Affect Fidelity and Diphtheria Toxin Resistance. *J. Biol. Chem.* 281, 32639–32648. doi:10.1074/jbc.m607076200

Pavesi, A., Vianelli, A., Chirico, N., Bao, Y., Blinkova, O., Belshaw, R., et al. (2018). Overlapping Genes and the Proteins They Encode Differ Significantly in Their Sequence Composition from Non-overlapping Genes. *PLoS One* 13, e0202513. doi:10.1371/journal.pone.0202513

Peng, B. Z., Bock, L. V., Belardinelli, R., Peske, F., Grubmüller, H., and Rodnina, M. V. (2019). Active Role of Elongation Factor G in Maintaining the mRNA reading Frame during Translation. *Sci. Adv.* 5, eaax8030. doi:10.1126/sciadv.aax8030

Penn, W. D., Harrington, H. R., Schlebach, J. P., and Mukhopadhyay, S. (2020). Regulators of Viral Frameshifting: More Than RNA Influences Translation Events. *Annu. Rev. Virol.* 7, 219–238. doi:10.1146/annurev-virology-012120-101548

Plant, E. P., and Dinman, J. D. (2005). Torsional Restraint: a New Twist on Frameshifting Pseudoknots. *Nucleic Acids Res.* 33, 1825–1833. doi:10.1093/nar/gki329

Plant, E. P., Pérez-Alvarado, G. C., Jacobs, J. L., Mukhopadhyay, B., Hennig, M., and Dinman, J. D. (2005). A Three-Stemmed mRNA Pseudoknot in the SARS Coronavirus Frameshift Signal. *Plos Biol.* 3, e172. doi:10.1371/journal.pbio.0030172

Puah, R. Y., Jia, H., Maraswami, M., Kaixin Toh, D.-F., Ero, R., Yang, L., et al. (2018). Selective Binding to mRNA Duplex Regions by Chemically Modified Peptide Nucleic Acids Stimulates Ribosomal Frameshifting. *Biochemistry* 57, 149–159. doi:10.1021/acs.biochem.7b00744

Qu, X., Wen, J.-D., Lancaster, L., Noller, H. F., Bustamante, C., and Tinoco, I., Jr (2011). The Ribosome Uses Two Active Mechanisms to Unwind Messenger RNA during Translation. *Nature* 475, 118–121. doi:10.1038/nature10126

Ritchie, D. B., Foster, D. A. N., and Woodside, M. T. (2012). Programmed -1 Frameshifting Efficiency Correlates with RNA Pseudoknot Conformational Plasticity, Not Resistance to Mechanical Unfolding. *Proc. Natl. Acad. Sci.* 109, 16167–16172. doi:10.1073/pnas.1204114109

Robert, F., and Brakier-Gingras, L. (2003). A Functional Interaction between Ribosomal Proteins S7 and S11 within the Bacterial Ribosome. *J. Biol. Chem.* 278, 44913–44920. doi:10.1074/jbc.m306534200

Rodnina, M. V. (2018). Translation in Prokaryotes. *Cold Spring Harb Perspect. Biol.* 10, a032664. doi:10.1101/cshperspect.a032664

Rodnina, M. V., Korniy, N., Klimova, M., Karki, P., Peng, B.-Z., Senyushkina, T., et al. (2020). Translational Recoding: Canonical Translation Mechanisms Reinterpreted. *Nucleic Acids Res.* 48, 1056–1067. doi:10.1093/nar/gkz783

Rodnina, M. V., and Wintermeyer, W. (2011). The Ribosome as a Molecular Machine: the Mechanism of tRNA-mRNA Movement in Translocation. *Biochem. Soc. Trans.* 39, 658–662. doi:10.1042/bst0390658

Rom, E., and Kahana, C. (1994). Polyamines Regulate the Expression of Ornithine Decarboxylase Antizyme *In Vitro* by Inducing Ribosomal Frame-Shifting. *Proc. Natl. Acad. Sci.* 91, 3959–3963. doi:10.1073/pnas.91.9.3959

Schlick, T., Zhu, Q., Dey, A., Jain, S., Yan, S., and Laederach, A. (2021). To Knot or Not to Knot: Multiple Conformations of the SARS-CoV-2 Frameshifting RNA Element. *J. Am. Chem. Soc.* 143, 11404–11422. doi:10.1021/jacs.1c03003

Schlub, T. E., and Holmes, E. C. (2020). Properties and Abundance of Overlapping Genes in Viruses. *Virus. Evol.* 6, veaa009. doi:10.1093/ve/veaa009

Schmidt, N., Lareau, C. A., Keshishian, H., Ganskih, S., Schneider, C., Hennig, T., et al. (2021). The SARS-CoV-2 RNA-Protein Interactome in Infected Human Cells. *Nat. Microbiol.* 6, 339–353. doi:10.1038/s41564-020-00846-z

Shehu-Xhilaga, M., Crowe, S. M., and Mak, J. (2001). Maintenance of the Gag/Gag-Pol Ratio Is Important for Human Immunodeficiency Virus Type 1 RNA Dimerization and Viral Infectivity. *J. Virol.* 75, 1834–1841. doi:10.1128/jvi.75.4.1834-1841.2001

Simms, C. L., Yan, L. L., Qiu, J. K., and Zaher, H. S. (2019). Ribosome Collisions Result in +1 Frameshifting in the Absence of No-Go Decay. *Cel Rep.* 28, 1679–1689. e4. doi:10.1016/j.celrep.2019.07.046

Smith, A. M., Costello, M. S., Kettring, A. H., Wingo, R. J., and Moore, S. D. (2019). Ribosome Collisions Alter Frameshifting at Translational Reprogramming Motifs in Bacterial mRNAs. *Proc. Natl. Acad. Sci. USA* 116, 21769–21779. doi:10.1073/pnas.1910613116

Su, M.-C., Chang, C-T., Chu, C-H., Tsai, C-H., and Chang, K-Y. (2005). An Atypical RNA Pseudoknot Stimulator and an Upstream Attenuation Signal for -1 Ribosomal Frameshifting of SARS Coronavirus. *Nucleic Acids Res.* 33, 4265–4275. doi:10.1093/nar/gki731

Sun, Y., Abriola, L., Niederer, R. O., Pedersen, S. F., Alfajaro, M. M., Monteiro, V. S., et al. (2021). Restriction of SARS-CoV-2 Replication by Targeting Programmed -1 Ribosomal Frameshifting. *Proc. Natl. Acad. Sci. United States America* 118, e2023051118. doi:10.1073/pnas.2023051118

Suzuki, Y., Chin, W. X., Han, Q., Ichiyama, K., Lee, C. H., Eyo, Z. W., et al. (2016). Characterization of RyDEN (C19orf66) as an Interferon-Stimulated Cellular Inhibitor against Dengue Virus Replication. *Plos Pathog.* 12, e1005357. doi:10.1371/journal.ppat.1005357

Takyar, S., Hickerson, R. P., and Noller, H. F. (2005). mRNA Helicase Activity of the Ribosome. *Cell* 120, 49–58. doi:10.1016/j.cell.2004.11.042

Tsuchihashi, Z., and Brown, P. O. (1992). Sequence Requirements for Efficient Translational Frameshifting in the Escherichia coli dnaX Gene and the Role of an Unstable Interaction between tRNA(Lys) and an AAG Lysine Codon. *Genes Dev.* 6, 511–519. doi:10.1101/gad.6.3.511

Tsuchihashi, Z., and Kornberg, A. (1990). Translational Frameshifting Generates the Gamma Subunit of DNA Polymerase III Holoenzyme. *Proc. Natl. Acad. Sci.* 87, 2516–2520. doi:10.1073/pnas.87.7.2516

Tükenmez, H., Xu, H., Esberg, A., and Byström, A. S. (2015). The Role of Wobble Uridine Modifications in +1 Translational Frameshifting in Eukaryotes. *Nucleic Acids Res.* 43, 9489–9499. doi:10.1093/nar/gkv83

Urbonavicius, J., Qian, Q., Durand, J. M., Hagervall, T. G., and Bjork, G. R. (2001). Improvement of reading Frame Maintenance Is a Common Function for Several tRNA Modifications. *EMBO J.* 20, 4863–4873. doi:10.1093/emboj/20.17.4863

Veeramachaneni, V., Makalowski, W., Galdzicki, M., Sood, R., and Makalowska, I. (2004). Mammalian Overlapping Genes: the Comparative Perspective. *Genome Res.* 14, 280–286. doi:10.1101/gr.1590904

Vickers, T. A., and Ecker, D. J. (1992). Enhancement of Ribosomal Frameshifting by Oligonucleotides Targeted to the HIVgag-Polregion. *Nucl. Acids Res.* 20, 3945–3953. doi:10.1093/nar/20.15.3945

Wang, X., Xuan, Y., Han, Y., Ding, X., Ye, K., Yang, F., et al. (2019). Regulation of HIV-1 Gag-Pol Expression by Shiftless, an Inhibitor of Programmed -1 Ribosomal Frameshifting. *Cell* 176, 625–635. e14. doi:10.1016/j.cell.2018.12.030

Weiss, R. B., Dunn, D. M., Atkins, J. F., and Gesteland, R. F. (1987). Slippery Runs, Shifty Stops, Backward Steps, and Forward Hops: -2, -1, +1, +2, +5, and +6 Ribosomal Frameshifting. *Cold Spring Harbor Symposia Quantitative Biol.* 52, 687–693. doi:10.1101/sqb.1987.052.01.078

Wilson, D. N., and Beckmann, R. (2011). The Ribosomal Tunnel as a Functional Environment for Nascent Polypeptide Folding and Translational Stalling. *Curr. Opin. Struct. Biol.* 21, 274–282. doi:10.1016/j.sbi.2011.01.007

Wu, B., Zhang, H., Sun, R., Peng, S., Cooperman, B. S., Goldman, Y. E., et al. (2018). Translocation Kinetics and Structural Dynamics of Ribosomes Are Modulated by the Conformational Plasticity of Downstream Pseudoknots. *Nucleic Acids Res.* 46, 9736–9748. doi:10.1093/nar/gky636

Yan, S., Wen, J.-D., Bustamante, C., and Tinoco, I. (2015). Ribosome Excursions during mRNA Translocation Mediate Broad Branching of Frameshift Pathways. *Cell* 160, 870–881. doi:10.1016/j.cell.2015.02.003

Yang, E., and Li, M. M. H. (2020). All about the RNA: Interferon-Stimulated Genes that Interfere with Viral RNA Processes. *Front. Immunol.* 11, 605024. doi:10.3389/fimmu.2020.605024

Yordanova, M. M., Wu, C., Andreev, D. E., Sachs, M. S., and Atkins, J. F. (2015). A Nascent Peptide Signal Responsive to Endogenous Levels of Polyamines Acts to Stimulate Regulatory Frameshifting on Antizyme mRNA. *J. Biol. Chem.* 290, 17863–17878. doi:10.1074/jbc.m115.647065

Yu, C.-H., Noteborn, M. H. M., and Olsthoorn, R. C. L. (2010). Stimulation of Ribosomal Frameshifting by Antisense LNA. *Nucleic Acids Res.* 38, 8277–8283. doi:10.1093/nar/gkq650

Yu, C.-H., Teulade-Fichou, M.-P., and Olsthoorn, R. C. L. (2014). Stimulation of Ribosomal Frameshifting by RNA G-Quadruplex Structures. *Nucleic Acids Res.* 42, 1887–1892. doi:10.1093/nar/gkt1022

Zimmer, M. M., Kibe, A., Rand, U., Pekarek, L., Ye, L., Buck, S., et al. (2021). The Short Isoform of the Host Antiviral Protein ZAP Acts as an Inhibitor of SARS-CoV-2 Programmed Ribosomal Frameshifting. *Nat. Commun.* 12, 7193. doi:10.1038/s41467-021-27431-0

Conflict of Interest: The authors declare that the research was conducted in the absence of any commercial or financial relationships that could be construed as a potential conflict of interest.

Publisher's Note: All claims expressed in this article are solely those of the authors and do not necessarily represent those of their affiliated organizations, or those of the publisher, the editors and the reviewers. Any product that may be evaluated in this article, or claim that may be made by its manufacturer, is not guaranteed or endorsed by the publisher.

frontiers in Molecular Biosciences

ORIGINAL RESEARCH
published: 25 March 2022
doi: 10.3389/fmolb.2022.811548

Genetic and Functional Analyses of Archaeal ATP-Dependent RNA Ligase in C/D Box sRNA Circularization and Ribosomal RNA Processing

Yancheng Liu[1†], *Yuko Takagi*[2†], *Milyadi Sugijanto*[3], *Kieu Duong My Nguyen*[1], *Akira Hirata*[4], *Hiroyuki Hori*[5] *and C. Kiong Ho*[1,3*]

[1]Human Biology Program, University of Tsukuba, Tsukuba, Japan, [2]Biomedical Research Institute, National Institute of Advanced Industrial Science and Technology, Tsukuba, Japan, [3]Doctoral Program in Medical Sciences, Faculty of Medicine, University of Tsukuba, Tsukuba, Japan, [4]Department of Natural Science, Graduate School of Technology, Industrial and Social Science, Tokushima University, Tokushima, Japan, [5]Department of Materials Science and Biotechnology, Graduate School of Science and Engineering, Ehime University, Matsuyama, Japan

OPEN ACCESS

Edited by:
Teng Ma,
Capital Medical University, China

Reviewed by:
Jinwei Zhang,
National Institutes of Health (NIH), United States
Jörg Soppa,
Goethe University Frankfurt, Germany

***Correspondence:**
C. Kiong Ho
kiongho@md.tsukuba.ac.jp

[†]These authors have contributed equally to this work and share first authorship

Specialty section:
This article was submitted to RNA Networks and Biology, a section of the journal Frontiers in Molecular Biosciences

Received: 09 November 2021
Accepted: 08 February 2022
Published: 25 March 2022

Citation:
Liu Y, Takagi Y, Sugijanto M, Nguyen KDM, Hirata A, Hori H and Ho CK (2022) Genetic and Functional Analyses of Archaeal ATP-Dependent RNA Ligase in C/D Box sRNA Circularization and Ribosomal RNA Processing. Front. Mol. Biosci. 9:811548. doi: 10.3389/fmolb.2022.811548

RNA ligases play important roles in repairing and circularizing RNAs post-transcriptionally. In this study, we generated an allelic knockout of ATP-dependent RNA ligase (Rnl) in the hyperthermophilic archaeon *Thermococcus kodakarensis* to identify its biological targets. A comparative analysis of circular RNA reveals that the Rnl-knockout strain represses circularization of C/D box sRNAs without affecting the circularization of tRNA and rRNA processing intermediates. Recombinant archaeal Rnl could circularize C/D box sRNAs with a mutation in the conserved C/D box sequence element but not when the terminal stem structures were disrupted, suggesting that proximity of the two ends could be critical for intramolecular ligation. Furthermore, *T. kodakarensis* accumulates aberrant RNA fragments derived from ribosomal RNA in the absence of Rnl. These results suggest that Rnl is responsible for C/D box sRNA circularization and may also play a role in ribosomal RNA processing.

Keywords: circular RNA, RNA ligase, thermococcus kodakarensis KOD1, rRNA processing, C/D box sRNAs

INTRODUCTION

Numerous RNA molecules are involved in controlling gene expression to maintain cellular RNA metabolism. In addition to tRNA, mRNA and rRNA, cells also contain a striking diversity of additional RNA types, such as edited RNAs, circularized RNAs, trans-spliced RNAs, and other non-coding RNAs (Brennicke et al., 1999; Burroughs and Aravind, 2016; Kristensen et al., 2019). We hypothesize that RNA ligase, an enzyme that joins free RNA ends together, is a key player in producing a diverse set of RNAs by altering their structures. The recent finding that RNA ligase is responsible for generating a circular RNA molecule (circRNA) and could selectively modify the ends of the RNA raises the possibility that RNA ligase may also function to regulate cellular RNA metabolism.

ATP-dependent RNA ligase (Rnl) catalyzes the formation of phosphodiester bonds between the 5′-phosphate and 3′-hydroxyl termini of RNA (Uhlenbeck and Gumport, 1982). Rnl can join two single-stranded RNA molecules with or without a complementary bridging polynucleotide. It can also catalyze intramolecular ligation, leading to the formation of a covalently-closed circRNA. The biological functions of Rnl are firmly established in bacterial tRNA restriction/repair (Amitsur, 1987;

Omari et al., 2006; Wang et al., 2007; Nandakumar et al., 2008), yeast and plant tRNA splicing (Sidrauski et al., 1996; Abelson et al., 1998; Englert and Beier, 2005), and kinetoplastid mitochondrial RNA editing pathways (McManus et al., 2001; Rusché et al., 2001; Schnaufer et al., 2001).

Many archaea species encode Rnl, and its structure is unique among polynucleotide ligases in that it forms a homodimeric quaternary structure. The crystal structure of *Pyrococccus abyssi* (PabRnl) and *Methanobacterium thermoautotrophicum* Rnl (MthRnl) have been solved and were shown to catalyze an intramolecular ligation of single-stranded RNA to form a covalently closed circRNA (Brooks et al., 2008; Gu et al., 2016). MthRnl can also transfer AMP to RNA containing 3′- phosphate termini to form 2′,3′-cyclic phosphate, and can selectively cleave adenosine from the 3′-hydroxyl end of the RNA, to form the 2′,3′-cyclic phosphate (Zhelkovsky and McReynolds, 2014; Yoshinari et al., 2017). Although the biological function of archaea Rnl is not known, RNA immunoprecipitation studies in *P. abyssi* suggest that it can interact with circular non-coding RNAs, including C/D box guide RNA (Becker et al., 2017).

Here we generated an allelic knockout of the Rnl gene in *Thermococcus kodakarensis* (TkoRnl; *TK1545*) and analyzed the change in RNA metabolism using high-throughput RNA-Seq technology. We showed that deletion of TkoRnl selectively dissipates circular C/D box sRNAs and other small RNA species. The conserved C/D box sequence elements were not strictly required for ligation activity of the archaeal Rnl. We also found that deletion of TkoRnl produces aberrant rRNA fragments, suggesting that TkoRnl may also participate in rRNA maturation process.

MATERIALS AND METHODS

Strains, Media, and Culture Conditions

The *T. kodakarensis* KUW1 (Sato et al., 2005) and gene disruptant strain were cultivated under anaerobic conditions at 85°C (optimum growth temperature) in a nutrient-rich medium (ASW-YT) or a synthetic medium (ASW-AA). ASW-YT medium (1 L) contains 5 g yeast extract (Y) and 5 g tryptone (T) dissolved in artificial seawater (ASW) (Sato et al., 2003a). ASW-AA medium is a synthetic medium that contains a mixture of vitamins, modified Wolfe's trace minerals, and the 20 canonical amino acids dissolved in 0.8 × ASW (Sato et al., 2003a; Atomi et al., 2004). Elemental sulfur (2 g) was added into 1 L ASW-YT and ASW-AA media before culturing. For all liquid media, resazurin (0.5 mg/L) was supplemented as an oxygen indicator, and 5.0% Na_2S was added until the medium became colorless. For colony isolation, solid ASW-AA medium containing 1 g of Gelrite and 0.4 g of polysulfide per 0.1 L was used. The *E. coli* Mach1-T1 was used to construct the targeting plasmids and was grown at 37°C in LB medium containing ampicillin (100 mg/L). For RNA isolation and growth analysis, cells were cultured in MA-YT-P medium (0.8 × Marine Art SF1 reagent [Osaka Yakken Co. Ltd., Osaka, Japan], 5 g/L of yeast extract, 5 g/L of trypton, and 5 g/L of sodium pyruvate) which lacks elementary sulfur.

Deletion of *TK1545* Gene

A DNA fragment containing the *TK1545* gene along with its 5′- and 3′-flanking regions (~1.0 kbp) was amplified with forward (5′ACTCTCTCCTTTTCTCCAATTTCGG-3′) and reverse (5′-TCAGGATTTTGCAAA GTACTGACTGG-3′) primers using *T. kodakarensis* KUW1 genomic DNA as a template for PCR and was cloned into the Hinc II site of pUC118 to obtain pUC-*TK1545*. The *RNL* coding sequence in pUC-*TK1545* was replaced with a DNA fragment containing *pyrF* gene (*TK2276*: orotidine 5′-phosphate decarboxylase) and its promoter element as described (Sato et al., 2003b). This was accomplished by amplifying pUC-*TK1545* using two outward primers (5′-AGC TGTAAGGGGCCTGTGGACATTTC-3′ and 5′- GATATCACC GAGAAGAGTGGGAGC-3′) complementary to the upstream and downstream sequence of the *TkoRNL* coding sequence. The amplified plasmid fragment was ligated with a PvuII-PvuII restriction fragment (763 bp) containing the *pyrF* marker gene derived from pUD2 plasmid (Sato et al., 2003b). All the sequences of the inserted region were verified with DNA sequencing. The resulting targeting plasmid, with *pyrF* marker gene inserted between the 5′- and 3′-flanking regions of *RNL* gene, was used to transform *T. kodakarensis* KUW1 strain. Cells grown in ASW-YT-S0 medium at 85°C for 10 h were harvested and suspended in 200 μL of 0.8 × ASW and kept on ice for 30 min. Then, 3 μg of the plasmid was gently added into the suspended cells and kept on ice for 1 h. Transformants were cultivated in an uracil-free ASW-AA-S0 at 85°C for 40 h. Next, 200 μL of the culture was transferred to a fresh medium and cultivated under the same conditions to enrich transformants displaying uracil prototrophy. The cultures (100 μL) were spread onto ASW-AA-S0 solid medium and incubated at 85°C for 3 days. Only cells that obtained a phenotype exhibiting uracil prototrophy by homologous recombination can grow in the absence of uracil. Single colonies were selected and then cultured in ASW-YT-S0 medium at 85°C for 10 h. Throughout this article, the term wild-type (WT) refers to KUW1 and *tk1545* KO refers to TkoRnl deletion in the KUW1 strain. The cells of the *tk1545* KO strain were harvested and suspended in distilled water. Genomic DNA was extracted from the cells using phenol-chloroform treatment. The replacement of *TK1545* gene with *pyrF* gene was verified with PCR (**Figure 1A**).

RNA Isolation and RNA-Seq Analysis

T. kodakarensis WT and *tk1545* KO (1.6 L) were cultured in MA-YT-P medium at 85°C and harvested when the absorbance at 660 nm reached ~0.7 (late-log phase). Total RNA was isolated using TRIzol reagent (Invitrogen) following the manufacture's instruction. The total RNA and small RNA libraries were prepared using standard Illumina protocol by UB Genomics and Bioinformatics Core at The State University of New York (SUNY) at Buffalo, United States. The high-throughput RNA-sequencing was performed using Illumina HighSeq2500 technology (51-base; pair-ended read). Raw reads were trimmed, and FastQC was used to determine the clean reads.

For both WT and *tk1545* KO datasets, 80 percent of the reads had Phred quality scores >35. The reads were mapped to *T. kodakarensis* reference genome (NC_006624.1) using bowtie2-2.2.9 with the option preset set to sensitive and alignment type set to local mode. The reads per kilo-base per million mapped reads (RPKM) were calculated using featureCount (Liao et al., 2014). From the WT dataset, 101 million reads were obtained, of which 94.86% mapped to the reference genome, with a median RPKM of 9.8. From the *tk1545* KO dataset, 58 million pairs of reads were obtained, of which 94.54% were mapped to the reference genome with a median RPKM of 10.9 (**Supplementary Data S1**).

For the small RNA-Seq, the 5′-adaptor sequence (5′-GTT CAGAGTTCTACAGTCCGACGATC) and 3′-adaptor sequence (5′-TGGAATTCTCGGGTGCCAAGG) were trimmed using Cutadapt, with 80 percent of the reads having Phred quality scores of >35. The reads aligned to reference genome as described above. We obtained 22 million pairs of reads from the WT sample, of which 79.94% mapped to the reference genome. From the *tk1545* KO sample, 16 million reads were obtained, and 81.43% mapped to the genome (**Supplementary Data S1**).

Analysis of circRNA from RNA-Seq Data

A custom Perl script was used to identify RNA-Seq reads containing circular junction sequences. The screening was done to identify RNA-Seq reads containing two segments of at least 20-nts matching the reference genome; the two matched segments should be encoded in the same direction but inverse order in the reference genome. From total RNA Seq data, 410,073 and 281,828 reads containing circular junctions from the WT and *tk1545* KO were identified, respectively (**Supplementary Data S2**). To reduce redundancy, reads containing similar junction sequences within five nucleotide variations were classified into the same group, which decreased the number of candidate circRNA reads to 12,632 for WT and 9,744 for *tk1545* KO. Subsequently, circRNA junction reads with less than 100 independent read counts were eliminated. This criterion identified 113 and 63 reads containing circRNA junction sequences from WT and *tk1545* KO, respectively. A similar strategy was used to identify circRNAs from the small RNA-Seq datasets, except that circRNA reads predicted to be longer than 10 kb and read counts of less than 20 were eliminated (**Supplementary Data S3**).

Detection of circRNA Using RT-PCR

We performed RT-PCR to detect predicted circular RNAs. Primers containing gene-specific sequences were used for reverse transcription reaction. The reaction mixture (40 μL) containing total RNA (200 ng) from either WT or *tk1545* KO was incubated with 25 μM gene-specific primer, 0.5 mM dNTP, and 50 U ReverTra Ace-α (Toyobo, Japan) in a supplied reaction buffer at 55°C for 10 min (for primer sequences, see **Supplementary Table S1**). The reaction was terminated at 95°C for 10 min, and an aliquot (1 μL) was used as a template for PCR. PCR (50 μL) contained 0.2 μM circular junction primer and gene-specific primer, 2.5 U Paq5000 DNA polymerase (Toyobo, Japan) programmed for 25 cycles (95°C for 30 s; 60°C for 30 s; 72°C for 10 s). PCR products were separated on 3% low-range ultra-agarose gel, stained with ethidium bromide, and visualized using UV.

RNA Ligase and RNA Substrates

His-tagged MthRnl and His-tagged T4 RNA Ligase 2 (T4 Rnl2) were produced in *E. coli* and purified from soluble bacterial extracts using Ni-agarose chromatography as described previously (Ho and Shuman, 2002; Torchia et al., 2008). *In vitro* transcription was used to synthesize RNAs from PCR amplified linear DNA templates containing a T7 RNA polymerase promoter. RNAs containing 5′ triphosphate were purified by electrophoresis through a non-denaturing 8% polyacrylamide gel. The RNAs were then treated with calf intestinal alkaline phosphatase, extracted by phenol-chloroform, and ethanol precipitated. The *in vitro* transcribed RNAs and the chemically synthesized 24-mer RNA were labeled at the 5′-end with [γ-^{32}P] ATP using T4 polynucleotide kinase and purified on the non-denaturing polyacrylamide gel.

Cloning of Small RNA Fragments

Total RNA (15 μg) from WT and *tk1545* KO were separated using 10% denaturing polyacrylamide gel, and RNA ranging from 70 to 120 nt was isolated by elution from the gel with Tris-EDTA (TE) buffer. RNA was ethanol-precipitated and resuspended to 50 μL with TE buffer. The isolated small RNA was used for the adapter-mediated RNA cloning with SOLiD Small RNA Expression Kit (Ambion). Ligation and reverse-transcription were performed according to the manufacturers' instructions. cDNA was amplified using Taq DNA polymerase, inserted into TOPO cloning vector (Invitrogen), and transformed into *E. coli* DH5α. The region of cDNA insertion within the TOPO vector was PCR amplified directly from the bacterial colonies, and product size was analyzed on 1.8% agarose gel. The majority (90%) of the plasmid recovered contained primer-dimer insert. Therefore, PCR product corresponding to >40 bp cDNA insert was regarded as a "positive" clone and was sequenced to reveal the identity of cloned RNA species. PCR product length corresponding to <40 bp insert was omitted, as it likely represented a fragment derived from a primer dimer.

RESULTS

Deletion of *T. kodakarensis* Rnl Gene

TK1545 encoding for *T. kodakarensis* ATP-dependent RNA ligase (TkoRnl) was removed via homologous recombination using a non-replicating targeting vector carrying orotidine-5′-monophosphate decarboxylase gene (*pyrF*) flanked by ~700 bp of upstream and downstream *TK1545* DNA sequence. The plasmid was transformed into *T. kodakarensis* strain KUW1 (Δ*pryF*) and the *Ura*$^{+}$ transformants were recovered. Deletion of *TK1545* locus was confirmed using PCR analysis (**Figure 1A**). Expression of *TK1545* was verified using RNA-Seq analysis, as described below. No significant difference in growth phenotype was observed between the WT and *tk1545* KO strains in nutrient-rich medium, at optimal (85°C) and elevated temperatures (93°C) (**Supplementary Figure S1**), which implies that TkoRnl is not

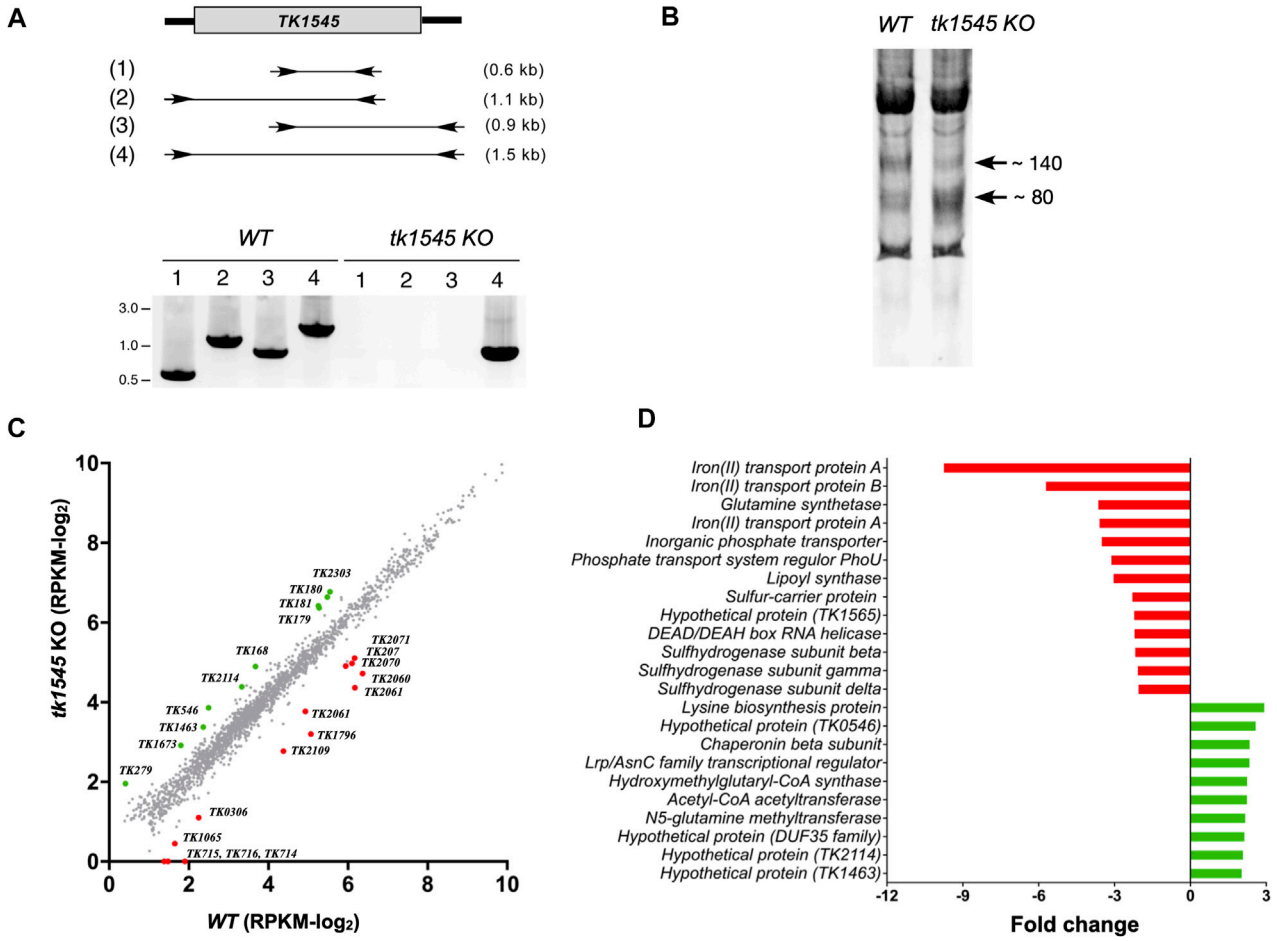

FIGURE 1 | Differentially expressed genes by deletion of TkoRnl gene. **(A)** Generation of RNA ligase knockout in *T. kodakarensis*. The *TK1545* gene was replaced with the *pyrF* selectable marker (763 bp). The positions of four pairs of PCR primers and their expected product sizes are depicted in (1–4). The lower panel shows an agarose gel electrophoresis of PCR products derived from WT and *tk1545* KO genomic DNAs. **(B)** Total RNA extracted from WT and *tk1545* KO strains were separated using 10% denaturing polyacrylamide gel electrophoresis. Ethidium bromide staining of the gel is shown. **(C)** Transcriptosome analysis of WT and *tk1545* KO. Total RNA isolated from WT and *tk1545* KO cells were subjected to RNA-Seq analysis. Each dot represents an individual gene and are depicted according to read per million mapped reads (RPKM) values. The RPKM value with less than one RPKM were set to 0. Genes with RPKM of <2.0 in both WT and *tk1545* KO were omitted. Differentially expressed genes are depicted as colored dots. Green dots represent the 10 genes that are up-regulated, and red dots represent 13 genes that are down-regulated by more than 2-fold in *tk1545* KO (excluding the *tk1545* gene). The RPKM for *tk1545* from the WT and *tk1545* KO were 9.05 and 0.04, respectively. Genes that show greater than two-fold change are listed in **(D)** and in **Supplementary Table S2**.

essential for viability. Polyacrylamide gel electrophoresis analysis of the small RNA population suggested that the relative distribution of short RNA species, ranging from 80 to 140 nt, differed significantly between the two strains (**Figure 1B**). Compared to the parental strain, the level of ~140-nt species was reduced while that of the ~80-nt species was increased in the *tk1545* KO strains. Therefore, both total and small RNA-Seq analyses were performed to evaluate the physiological consequences of TkoRnl deletion.

Transcriptome Analysis

Total and small RNAs isolated from the wild-type and *tk1545* KO strains were sequenced on an Illumina HighSeq platform sized at 51-bp and mapped uniquely to the annotated genome. The gene expression abundance was normalized using RPKM (**Supplementary Data S2**), and scatterplots were used to assess the expression variation of the genes between the WT and *tk1545* KO from the total RNA-Seq dataset (**Figure 1C**). Finally, 23 genes were identified that showed altered expression changes of >2-fold, of which 13 were up-regulated, and 10 were down-regulated in *tk1545* KO compared to the WT (**Figure 1D**; **Supplementary Table S2**). Many of these genes that exhibit differential gene expression are encoded on the same polycistronic transcription unit; iron transport proteins (*TK0714*, *TK0715*, and *TK0716*), phosphate transporter proteins (*TK2060* and *TK2061*), sulfur reductase subunits (*TK2071* and *TK2072*), and Acetyl-CoA acetyltransferase pathway (*TK0179*, *TK0180*, and *TK0181*). The genes encoded within each operon were either enhanced or reduced to a similar

TABLE 1 | List of circRNAs in *T. kodakarensis*. The top part of the table shows list of circRNAs that were detected in WT but were either absent or significantly reduced in *tk1545* KO small RNA-Seq dataset. The bottom part of the table shows a list of circRNAs that were detected in both WT and *tk1545* KO. The value in parenthesis shows the number of reads detected in total RNA-Seq dataset.

Locus/ CircRNA name	Circular junction (+/− 5 nucleotides)	Predicted length[a]	*T. kodakarensis* (WT)		*T. kodakarensis* (*tk1545* KO)		Alias and predicted transcription start site[b]	
			Number of aligned read	Number of circular reads	Number of aligned read	Number of circular reads		
sR01	47786 to 47847	62	2,167 (368)	395 (18)	1,776 (193)	7 (0)	TKOc and Sno. 19	47910
sR05	116401 to 116466	66	445,142 (531)	354 (54)	333,035 (286)	0 (0)	Tko-sR07	116468
sR13	279797 to 279863	67	59,144 (142)	47 (2)	58,048 (62)	0 (0)	Tko-sR14	279865
sR15	316130 to 316191	62	1,629,229 (611)	698 (113)	1,523,609 (352)	8 (0)	Tko-sR16	316202
sR20	558818 to 558879	62	1,622 (84)	21 (46)	1,400 (37)	0 (0)	Tko-sR20	558914
sR28	832364 to 832425	62	65,322 (340)	72 (123)	54,801 (156)	1 (0)	Tko-sR26	832424
sR29	940146 to 940209	64	475,600 (551)	36 (11)	283,215 (335)	0 (0)	Tko-sR29	940134
sR31	963853 to 963919	67	562,648 (252)	4,655 (343)	721,884 (11)	34 (1)	Tko-sR31	963842
sR34	1103565 to 1103626	62	20,161 (797)	119 (14)	19,347 (478)	0 (0)	Tko-sR35	1103625
sR37	1159583 to 1159644	62	356,961 (139)	44 (21)	195,173 (94)	1 (0)	Tko-sR37	1159732
sR38	1167276 to 1167338	63	11,287 (111)	106 (3)	4,940 (94)	0 (0)		
sR41	1226838 to 1226899	62	1,967 (359)	31 (202)	610 (19)	0 (0)	Tko-sR41	1226903
sR42	1226948 to 1227017	70	12,085 (226)	7,194 (145)	17,658 (83)	10 (0)	Tko-sR42	1226948
sR46	1371729 to 1371790	62	176,232 (540)	188 (258)	79,569 (118)	3 (3)	Tko-sR50	1371720
sR49	1446209 to 1446268	60	62,328 (224)	358 (376)	36,039 (104)	1 (0)	Tko-sR52	1446266
sR52	1476851 to 1476917	67	28,701 (349)	467 (4)	42,613 (208)	6 (0)	Tko-sR54	1476850
sR58	1947796 to 1947856	61	926 (66)	95 (5)	845 (52)	0 (0)		
sR61	2070055 to 2070116	62	100,212 (235)	92 (22)	31,284 (188)	0 (0)	Tko-sR67	2070114
ncRNA01	1053772 to 1053834	63	1,267,983 (198)	68 (48)	587,087 (113)	3 (0)	Tko-sR33	1053770
ncRNA02	1257020 to 1257081	62	8,320 (42)	139 (135)	6,342 (3)	0 (0)	TKOcandSno66	1257078
ncRNA03	1593064 to 1593134	71	7,565 (149)	403 (4)	9,633 (83)	1 (0)		
TK0058	51411 to 51477	67	1,816 (535)	589 (493)	780 (194)	1 (1)	Tko-sR01	51477
TK2034	1826865 to 1826930	66	771 (159)	66 (22)	477 (84)	2 (0)	Tko-sR22[c]	1826865
TK2109	1894519 to 1894579	61	14,240 (1,092)	28 (857)	11,134 (164)	0 (4)		
tRNA-Trp	1945728 to 1945789	62	28,907 (3,195)	2,023 (1,415)	23,156 (1,680)	1,292 (987)		
TK0135	108461 to 116468	8,008	457,060 (1,94,213)	90 (0)	576,950 (114,857)	110 (0)		
TK0894	779653 to 779796	144	317 (1,487)	28 (0)	215 (1,207)	28 (0)		
TK1980	1784662 to 1785579	918	1,322 (104,981)	42 (0)	739 (72,305)	53 (0)		
16S RNA-c1	2022801 to 2024382	1,582	404,505 (55,116,954)	96,319 (6,836)	268,720 (30,650,056)	53,186 (4,733)		

(Continued on following page)

TABLE 1 | (*Continued*) List of circRNAs in *T. kodakarensis*. The top part of the table shows list of circRNAs that were detected in WT but were either absent or significantly reduced in *tk1545* KO small RNA-Seq dataset. The bottom part of the table shows a list of circRNAs that were detected in both WT and *tk1545* KO. The value in parenthesis shows the number of reads detected in total RNA-Seq dataset.

Locus/ CircRNA name	Circular junction (+/− 5 nucleotides)	Predicted length[a]	*T. kodakarensis* (WT)		*T. kodakarensis* (*tk1545* KO)		Alias and predicted transcription start site[b]
			Number of aligned read	Number of circular reads	Number of aligned read	Number of circular reads	
23S RNA-c1	2024584 to 2027631	3,048	867,077 (109,488,453)	27,733 (282,955)	610,944 (62,941,809)	11,628 (205,719)	
23S RNA-c2	2024595 to 2027605	3,011	867,051 (109,486,015)	83 (42,016)	610,939 (62,940,686)	35 (23,246)	

[a]*Position of circular junction and predicted length of each circRNAs, were determined by mapping to the T. kodakarensis reference genome (See* ***Supplementary Data S3****).*
[b]*The alias and predicted start site of transcription are from (Jäger et al., 2014).*
[c]*Annotated as sR22 in (Jäger et al., 2014).*

extent in *tk1545* KO. Transcriptome analysis from the small RNA-Seq data is shown in **Supplementary Figure S2**.

Computational Predictions of Circular RNAs

It has been widely reported that non-coding RNAs, including tRNAs, C/D box sRNA, and rRNA processing intermediates are circularized in archaea (Tang et al., 2002; Starostina et al., 2004; Danan et al., 2012; Randau, 2012; Su et al., 2013; Becker et al., 2017). We hypothesize that if Rnl is responsible for generating circRNAs, we would identify its RNA target by comparing the circRNA reads obtained from WT and *tk1545* KO. Our criteria for detecting circular reads from the RNA-Seq data were as follows: 1) the 51-nts RNA-Seq reads containing two segments, and each segment has a minimum 20-nts match to the reference genome sequence; 2) the two matched segments within the read are encoded in the same transcriptional direction, but are positioned in inverse order in the reference genome (Danan et al., 2012); and 3) the two matched segments are fused to form a unique circular junction sequence. Variation in the circular junction within five nucleotides in the locus was classified into the same group to reduce redundancy (**Supplementary Data S2**). The predicted length of individual circRNA was deduced from the distance between the two homologous segments in the genome reference. For the total RNA-Seq data, we selected reads that support more than 100 counts (**Supplementary Data S2**). For the small RNA-Seq data, we selected read supported more than 20 counts and did not include reads that were predicted to be longer than 10 kb (**Supplementary Data S3**).

In the WT *T. kodakarensis,* 31 circRNA reads were detected from the small RNA Seq data set, many of which were derived from C/D box sRNAs (**Supplementary Table S2**). The C/D box sRNA molecule has four sequence elements: the C box and C' box motifs with the consensus sequence RUGAUGA, and the D box and D' box motifs with the consensus sequence CUGA. Of the 61 putative *T. kodakarensis* C/D box sRNAs we identified, 26 C/D Box sRNAs had circRNA reads (**Supplementary Table S3**). Analysis of *P. abyssi* RNA-Seq dataset detected 24 circRNA reads (Toffano-Nioche et al., 2013), many of which were shown to be circularized (Becker et al., 2017). Other circRNA reads detected from *T. kodakarensis* include protein coding genes (*TK0058* [HAD superfamily hydrolase], *TK2034* [Universal stress protein], *TK2109* [lipoyl synthase], *TK0894* [hypothetical protein], *TK1980* [ferredoxin oxidoreductase, alpha subunit], *TK0135* [ferredoxin oxidoreductase, beta subunit]) and non-coding RNAs designated here as ncRNA01, ncRNA02, and ncRNA03 (**Table 1**; **Supplementary Data S2**). Some of these RNAs were previously reported as C/D box sRNA (Jäger et al., 2014). CircRNAs were also detected in abundance from rRNA operon and $tRNA^{Trp}$ as previously reported (Danan et al., 2012).

TK1545 is Required for C/D Box sRNA Circularization

Analysis of *tk1545* KO RNA-Seq data revealed that 24 out of 31 circRNAs that were detected in WT were either absent or significantly reduced in *tk1545* KO (**Table 1**). These included 18 C/D box sRNAs, three non-coding RNAs, and three protein-coding genes (*TK0058*, *TK2109*, and *TK 2034*). Similar results were obtained when RNA-Seq analysis of WT and *tk1545* KO were analyzed on a SOLiD sequencing platform (**Supplementary Table S4**) (Liu, 2022). **Figure 2A** shows a sequence alignment of circRNAs that were affected in *tk1545* KO. All these circRNAs have a similar length (61–71 nts) and homology to the C/D box sRNA. The terminal ends are generally GC-rich, and sequences at the termini can hybridize to form a stem, a structural characteristic found in C/D box sRNA. Secondary structure analysis suggests that hybridization between the two terminal ends could be critical for RNA circularization (**Supplementary Figure S3**). The majority of the RNAs that were circularized (21 out of 24 shown in **Figure 2A**) could potentially form three or more base pairings to form a terminal stem (**Supplementary Figure S3A**). In contrast, 16 out of 17 non-circular C/D box sRNAs are less likely to form a terminal stem with two or less base pairings (**Supplementary Figure S3B**). We note that relative abundance of six C/D box sRNAs (sR14, sR35, sR38, sR41, sR54, and sR61) out of sixty-one C/D box sRNAs that we identified, were reduced by 2-fold or more in *tk1545* KO compared to the WT (**Figure 2B**).

There were no significant changes in the level of circRNA reads derived from $tRNA^{Trp}$ intron and 16S and 23S rRNAs. We note that circularization of *TK0135*, *TK0894* and *TK1980*, all of which have predicted circRNA size of >100 nts, were not significantly affected by TkoRnl deletion. Circular *TK0894,*

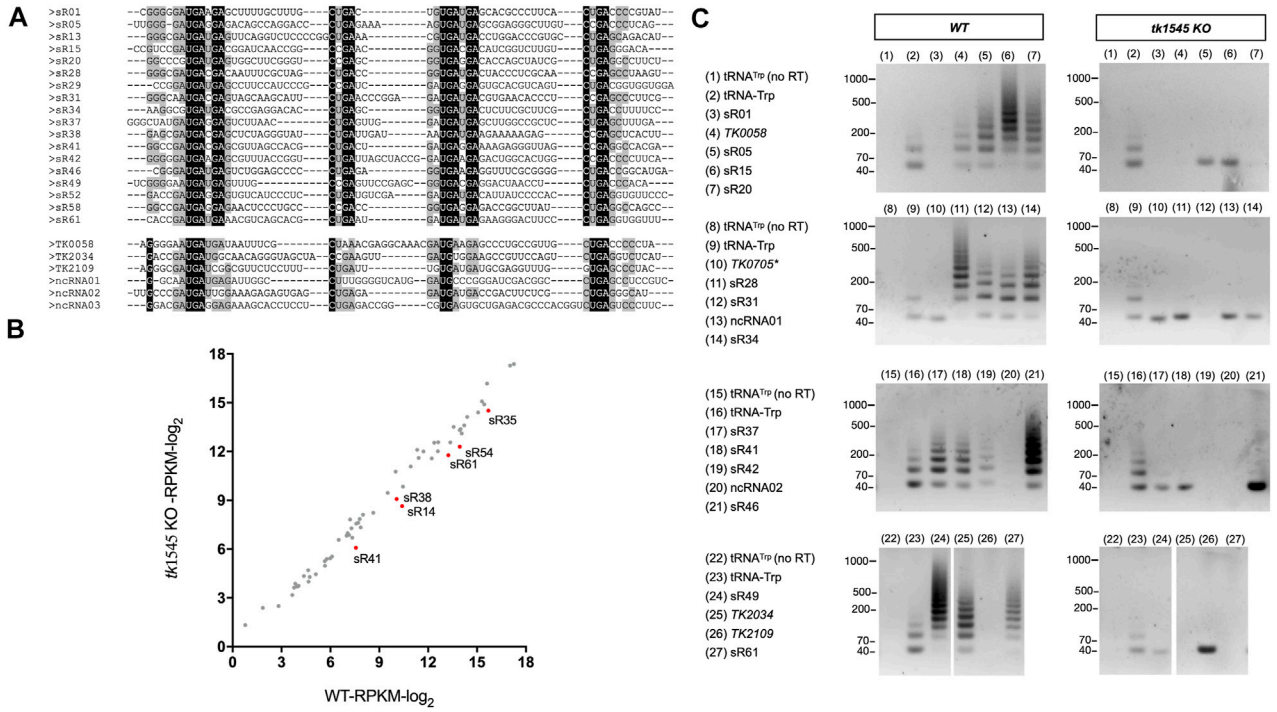

FIGURE 2 | Effect on RNA circularization by *TK1545* knockout. **(A)** Sequence alignment of circRNAs which were reduced or absent in *tk1545* KO (see **Table 1**). Putative circular C/D box RNAs are listed on top and other circRNAs are listed on the bottom. The positions of conserved motifs (C box, C′ box, D box, and D′ box) are indicated. Identical nucleotides are highlighted in black with white text and conserved nucleotides are highlighted in gray. **(B)** Expression of C/D box RNA. Expression analysis of sixty-one *T. kodakarensis* C/D box RNA listed on **Supplementary Table S3**. Red dots represent the six C/D box RNAs reduced by more than 2-fold in *tk1545* KO. **(C)** RT-PCR analysis was used to detect circRNAs from total RNA isolated from WT and *tk1545* KO. The primer set used to detect circular RNA species is indicated on the right of the gel. A circular $tRNA^{Trp}$ intron primer was used as a positive control (tRNA-Trp). As a negative control, assay was performed without reverse transcriptase treatment using $tRNA^{Trp}$ intron primers [$tRNA^{Trp}$ (no RT)], or with the *TK0705* primers (Gene ID 3234407: NADP-dependent glyceraldehyde-3-phosphate dehydrogenase, which is not circularized in both WT and *tk1545* KO). The size of the molecular weight markers is indicated on the left. PCR product that migrates ~40 nts most likely represented a product derived from a primer dimer.

TK1980 and *TK0135* were not detected in the whole RNA-seq data (**Table 1**), suggesting that these RNAs may likely circularize after the degradation or processing of the transcript into small RNA.

RT-PCR analysis was performed to verify whether the circular RNA species are present in *T. kodakarensis* (**Figure 2C**). In this procedure, reverse transcription primer was designed to hybridize the gene specific sequence. If this primer hybridizes to circular RNA, reverse transcription will generate a long "rolling-circle" single-stranded cDNA. Subsequent PCR with circular junction and gene specific primers generate a ladder of DNA fragments, which can be visualized on the gel electrophoresis (Starostina et al., 2004). A $tRNA^{Trp}$ primer was used as a positive control because $tRNA^{Trp}$ introns accumulate circRNA reads in both WT and *tk1545* KO, generating a ladder of DNA fragments from WT and *tk1545* KO RNAs (**Figure 2C**, tRNA-Trp) but not when reverse transcriptase was omitted in the reaction (no RT). Out of the 18 candidate circRNAs, 16 were detected circularized in the WT, but not in *tk1545* KO. A circular form of C/D box sR01 and *TK2109* could not be detected in WT or *tk1545* KO (**Figure 2C**; lanes 3 and 26, respectively), possibly due to a heterogeneous mixture of circular junction sequences in these RNAs. While most of the circular junction sequences represent ligation between the predicted 5′-end and 3′-end, some of the circRNA reads had a few nucleotides missing at the circular junction, which may have affected the PCR amplification step.

RNA Ligation Activity on C/D Box sRNA

To determine whether Rnl preferentially recognizes C/D box sRNA sequence elements, we assayed for the ligation activity *in vitro* using a 5′-monophosphate terminated C/D box sR42 and sR31 sRNAs as substrates. These two C/D box sRNAs were selected because both are highly enriched and circularized in the WT sample (**Table 1**; **Figure 2C**). We previously showed that TkoRnl is capable of circularizing 24-mer single-stranded RNA, but the circularization activity was weak compared to the *M. thermoautotrophicus* enzyme (MthRnl) (Yoshinari et al., 2017; Zhang and Tripathi, 2017); thus, MthRnl was used for the ligation assay. MthRnl is a homolog of TkoRnl (NCBI BLAST E-value of 6×10^{-60}). The biochemical activity of MthRnl has been extensively characterized and all amino acid residues found to be essential for the MthRnl ligation activity are conserved in TkoRnl (Zhelkovsky and McReynolds, 2014; Torchia et al., 2008; Gu et al., 2016; Yoshinari et al., 2017).

Incubation of MthRnl with either 5′-monophosphate terminated sR42 or sR31 RNAs generates a circRNA molecule that migrates slower than the linear pRNA on a denaturing PAGE (**Figure 3A**). The circularity of the slower migrating RNA product was verified by its resistance to alkaline phosphatase and RNase R treatment (data not shown). Under identical conditions, MthRnl could not ligate a non-structured 67-mer RNA, suggesting that a structure on the C/D box sRNAs is necessary for RNA circularization. Ligation in the absence of added ATP reflects the presence of pre-adenylated ligase intermediate in the enzyme preparation (Torchia et al., 2008; Gu et al., 2016). We also note that inclusion of ATP in the reaction did not affect circularization of sR42 and sR31 RNAs. This contrasts with ligation of a 24-mer pRNA substrate, which accumulates AppRNA intermediate and suppress the circularization in the presence of ATP, as shown previously for MthRnl (Torchia et al., 2008; Gu et al., 2016), and T4 Rnl2 (Ho and Shuman, 2002; Yin et al., 2003; Nandakumar et al., 2004).

The circularization activity was not significantly affected when the conserved C/D box sequence was substituted with different bases (**Figure 3A**; sR42-a and sR31-a). However, a mutant form of sR31 RNA that can alleviate hybridization between the terminus was a poor substrate for ligation (**Figures 3A,B**; sR31-b). Furthermore, MthRnl was inert for circularizing the RNA when both the C/D box and the 3′-terminal sequences were altered (**Figures 3A,B**; sR31-c). As a control reaction, we showed that bacteriophage T4 Rnl2 could efficiently circularize both the linear 67-mer and sR31-c RNAs (**Supplementary Figure S4**). We conclude that conserved C/D box sequence elements are not

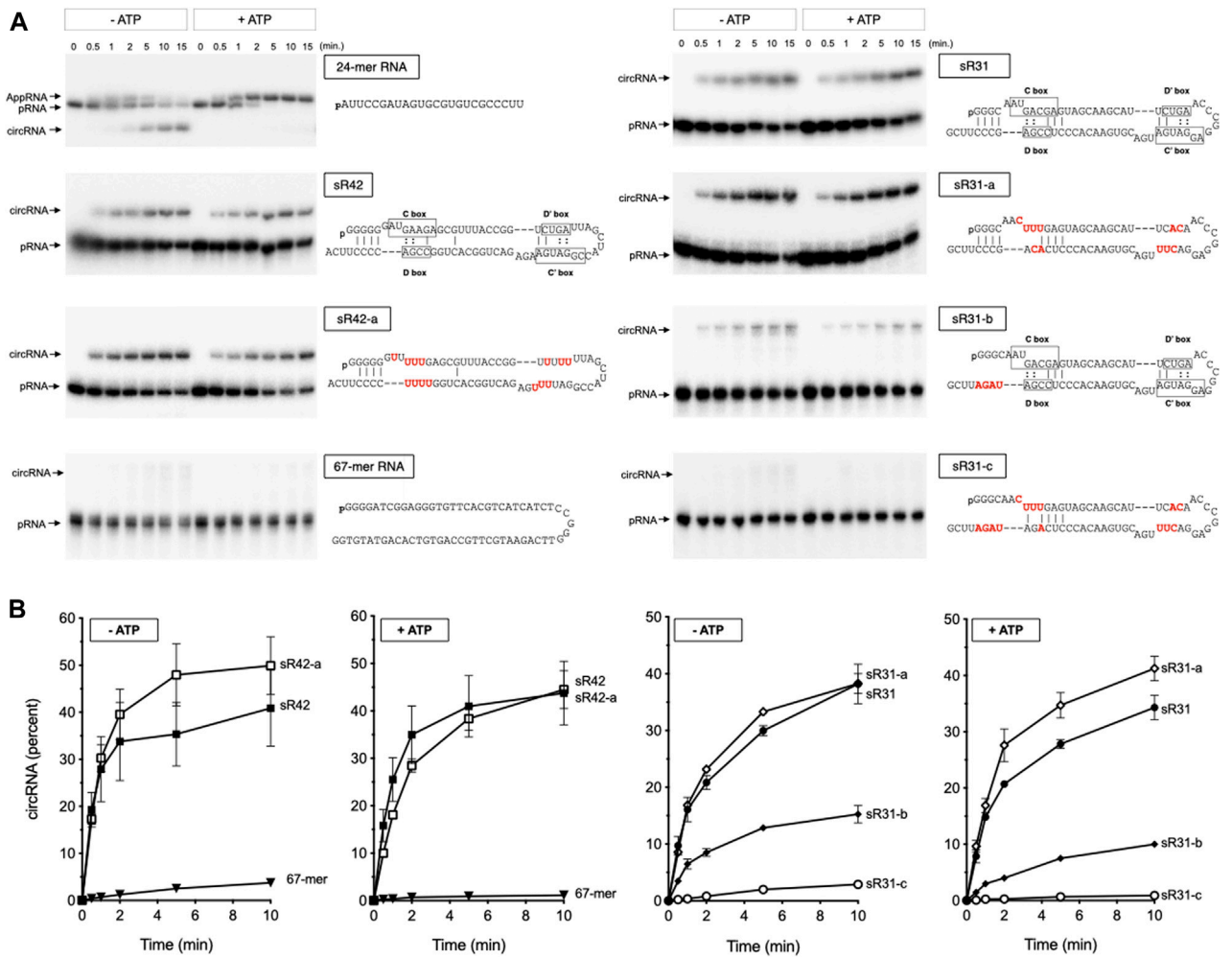

FIGURE 3 | Characterization of RNA circularization activity of MthRnl on C/D box sRNA. **(A)** MthRnl (360 ng) was incubated with 2 pmol of indicated pRNA at 70°C in a reaction mixture (40 μL) that contained 50 mM Tris-HCl (pH 6.5), 1 mM $MgCl_2$, in the presence or absence of 1 mM ATP. Aliquots (3 μL) were withdrawn at the times indicated and the products were separated by denaturing polyacrylamide gel. Positions of pRNA, AppRNA, and circRNA are indicated on the left. The sequences of pRNA substrates are illustrated on the right. The conserved C/D box sequence elements in sR42 and sR31 are highlighted, and the variant nucleotides in a mutant form of sR42 and sR31 RNAs are colored in red. **(B)** The yield of circular RNA products by MthRnl in the presence (+ATP) and absence (–ATP) of ATP is plotted as a function of time. The data shown represent the average of three separate experiments with SE bars.

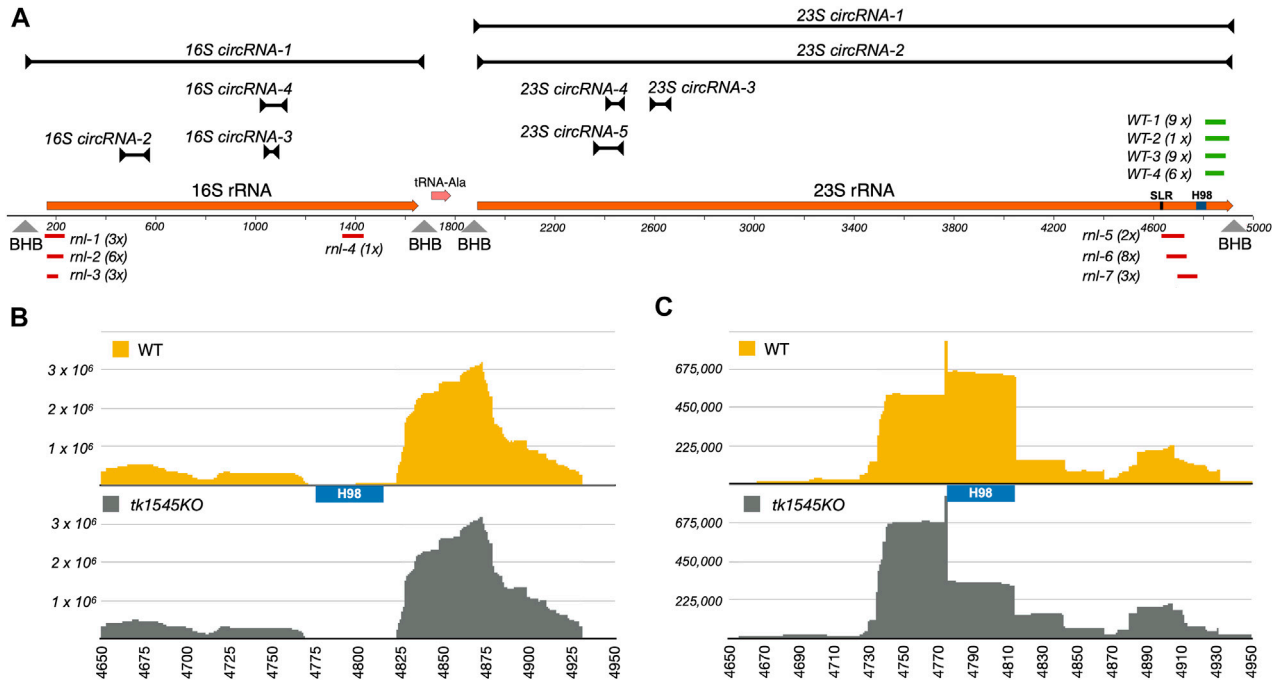

FIGURE 4 | Effect of *TK1545* knockout on rRNA circularization and processing. **(A)** Circular RNAs derived from *T. kodakarensis* 16S-tRNA^{Ala}-23S rRNA operon. A diagram on the bottom represents a 5 kb segment of *T. kodakarensis* 16S-tRNA^{Ala}-23S rRNA operon, corresponding to 2022701–2027700 of NC_006624.1 reference sequence. The 16S rRNA, tRNA^{Ala}, and 23S rRNA genes are colored in orange. Positions of SRL and H98 are annotated. Arrowheads indicate predicted positions of bulge-helix-bulge motifs (BHB) on the primary transcript. The black lines above the diagram represent the expected size and position of highly represented circRNAs (**Supplementary Data S2**). Predicted length and position were determined from total RNA-Seq reads containing the junction sequence. Small RNAs fragments derived from WT and *T. kodakarensis* were cloned into TOPO vector via adaptor-mediate RNA ligation. The cloned fragments derived from WT (*WT*: green) or *tk1545* KO (*rnl*: red) were aligned to the reference genome. The number on the right represents number of identical RNA fragments recovered in the RNA cloning experiment (i.e., *2 x indicates twice*). See **Supplementary Figure S5** for circular junction and alignment of small RNA fragments with the 16S-tRNA^{Ala}-23S rRNA operon. **(B)** Read-coverage in 23S rRNA at the 3′-end from total RNA-Seq dataset from WT (top) and *tk1545* KO (bottom). **(C)** Read-coverage in 23S rRNA at the 3′-end from small RNA-Seq dataset from WT (top) and *tk1545* KO (bottom). The read counts (*y*-axis) for the *tk1545* KO were normalized to the WT read counts. The position of H98 is marked below the WT read-coverage.

strictly required for circularization by MthRnl. The sequence surrounding the termini could be important for guiding the two termini in close proximity to be recognized by archaea Rnl to allow for intramolecular ligation.

Other circRNAs in *T. kodakarensis*

It has been widely reported that tRNA introns and rRNA processing intermediates are circularized in various archaea species (Danan et al., 2012; Su et al., 2013; Becker et al., 2017; Jüttner et al., 2019; Qi et al., 2020; Breuer et al., 2021). In both WT and *tk1545* KO, high-levels of circRNA reads were detected from the 16S-23S rRNA operon and tRNA^{Trp} intron (**Supplementary Data S2**). Inspection of circular junction sequences in total RNA-Seq data reveal that tRNA^{Trp} intron (1,415 reads), 16S circRNA-1 (6,835 reads) and 23S circRNA-1 (282,955 reads) are likely cleaved at the Bulge-Helix-Bulge (BHB) motifs by tRNA splicing endonuclease and joined by tRNA ligase RtcB to form a circular rRNA processing intermediate, as reported (Trotta et al., 1997; Englert et al., 2011; Popow et al., 2011). The circularized tRNA^{Trp} intron was also detected in our RT-PCR analysis in abundance, both in WT and *tk1545* KO (**Figure 2C**), implying that deletion of TkoRnl does not have an impact on the RtcB ligation pathway.

Effect on rRNA Processing by Rnl Knock-Out

In addition to the circular rRNA processing intermediate, we also detected a high level of circular junction reads (42,016 reads) near the predicted 5′-and 3′-ends of 23S rRNA (**Figure 4A**; 23S circRNA-2). Recent studies in *Pyrococcus furiosus* suggest that 3′-end of 23S rRNA could be fused to the 5′-end by an RNA rearrangement as a consequence of excision of 40-nts helix 98 (H98) located ~100 nucleotides upstream of the mature 3′-end (Birkedal et al., 2020). Similar to *P. furiosus* rRNA, the H98 could be excised in *T. kodakarensis*, evinced by low coverage of RNA-Seq reads within the equivalent segment (**Figure 4B**).

We noted earlier that the relative distribution of small RNA species was altered in *tk1545* KO (**Figure 1B**). While this change is partially attributable to the reduced level of circular C/D box sRNAs in *tk1545* KO, it cannot solely account for the observed differences because a fraction of C/D box sRNAs are likely

circularized. We therefore cloned and sequenced the small RNA fragments accumulated in WT and *tk1545* KO. RNA populations in the range of 70–120 nts were isolated from WT and *tk1545* KO cells by gel electrophoresis, annealed to an adapter oligonucleotide containing six degenerate nucleotides at the 3′ end, ligated, and then converted into cDNAs by reverse transcription. The cDNA fragment was cloned into a plasmid using TA cloning and transformed into bacteria. Plasmids isolated from the individual colonies were sequenced using the Sanger method. Note that the adaptor sequence used for RNA cloning has a degenerate sequence at the ends, which allowed us to verify that each obtained clone was derived from an independent RNA and that no single clone was over-represented during PCR amplification.

Alignment of sequences retrieved from small RNA cloning shows that all the fragments obtained were derived from 16S and 23S rRNAs. There were no overlaps between the fragments recovered from WT and *tk1545* KO, indicating that this difference is a consequence of Rnl deletion. Fragments isolated from WT were all derived from 23S rRNA, between the excision site of H98 to the 3′-end of the predicted 23S rRNA (*WT-1* through *WT-4* colored as green in **Figure 4A**; **Supplementary Figure S5**). In the *tk1545* KO, nearly half of the cDNA fragments matched the 23S rRNA. Notably, all the fragments mapped upstream of the H98 near the sarcin-ricin loop (SRL) (*rnl-5* through *rnl-7*; colored in red and **Supplementary Figure S5**). The remaining half of the fragments were derived from 16S rRNA that mapped at the 5′-end of 16S rRNA (*rnl-1* through *rnl-3*; colored in red). Consistent with this finding, analysis of small RNA-Seq data reveals that the reads-coverage upstream of H98 are more abundant in the TkoRnl deletion strain than the WT. (**Figure 4C**). Taken together, our results suggest that Rnl may participate in rRNA processing, either directly by joining the breaks near the SRL or indirectly through the formation of circular C/D box sRNA.

DISCUSSION

Here we generated an allelic knock-out of ATP-dependent RNA ligase in *T. kodakarensis* to determine the biological targets of archaeal Rnl. Whereas TkoRnl was not essential for the growth of *T. kodakarensis* under standard laboratory conditions, we showed that its absence abolishes circularization of C/D box sRNAs. The conserved C/D box sequence element, however, was not sufficient for circularization because not all C/D box sRNAs were circularized in *T. kodakarensis*. Furthermore, we demonstrated that recombinant Rnl was capable of forming circular C/D box sRNA with a mutation in the conserved sequence element. The archaeal Rnl could not circularize unstructured RNA of a similar length or C/D box sRNAs that have disrupted terminal stem structures. We conclude that archaeal Rnl may preferentially recognize the terminal stem, and the proximity of the two ends could be critical for intramolecular ligation.

We also detected numerous circular RNA-Seq reads derived from 16S and 23S rRNAs in *T. kodakarensis*. As expected, circularization of tRNA intron or rRNA processing intermediates was not affected in the absence of Rnl, which implies that Rnl does not affect the RtcB ligation pathway. Our finding that C/D box sRNAs are prime substrates for archaeal Rnl is consistent with the previous findings that circular C/D box sRNA-Rnl complexes were detected in *P. abyssi* (Becker et al., 2017).

The functional significance of circular C/D Box sRNA is unclear. C/D box sRNAs have been reported to function as a guide RNA for methylating tRNAs and rRNAs. Circular C/D Box sRNA may alter the specificity to guide RNA to regulate rRNA methylation. However, we did not detect significant differences in the expression, or the overall read coverage, of rRNA genes from the whole transcriptome RNA-seq analysis, between the WT and TkoRnl deletion strains. Comparative transcriptomics analysis revealed that TkoRnl may alter that abundance of subset of C/D Box sRNAs (**Figure 2B**). TkoRnl could also be involved by regulating the expression of genes involved in sulfur or iron metabolism (**Figure 1**; **Supplementary Table S2**). We note that only one biological replicate was analyzed in this study. While it is clear that TkoRnl is responsible for C/D box sRNA circularization, further analysis is necessary to evaluate the biological function of Rnl in archaea.

Similar to *P. furiosus*, *T. kodakarensis* appears to excise H98 from 23S rRNA (**Figure 4B**), consistent with the finding that the H98 is not present in the cryo-EM structure of *T. kodakarensis* 70S rRNA (Birkedal et al., 2020; Sas-Chen et al., 2020). We found that *T. kodakarensis* accumulates ~90 nts fragments consisting of a sequence that matches the H98 3′-cleavage site to the predicted 3′-end of 23S rRNA. We speculate that the excision of H98 releases the 3′-end fragment and may have accumulated in *T. kodakarensis*. Intriguingly, we did not retrieve the same fragments from the TkoRnl deletion strain. Instead, we recovered fragments that mapped upstream of H98 near the SRL. SRL interacts with the translational elongation factors that hydrolyze GTP during translocation (Wool et al., 1992; Szewczak et al., 1993; Schmeing et al., 2009), and the cleavage or modification by ribotoxins could block ribosome translocation (Wool et al., 1992; Szewczak et al., 1993; Schmeing et al., 2009).

While it is tempting to speculate that Rnl directly participates in joining the breakage upon excision of H98, we fail to detect any RNA-Seq reads suggesting such "*cis*-splicing" events near the 3′-end of *T. kodakarensis* 23S rRNA. Furthermore, TkoRnl is not likely involved in rearranging the 3′- and 5′-ends of the 23S rRNA as observed in *P. furious* (Birkedal et al., 2020) because permuted reads containing junction sequence between the 5′- and 3′- ends of 23S rRNA were detected in both WT and TkoRnl deletion strain (**Table 1**; **Supplementary Data S2, S3**). Therefore, Rnl ligation activity may not act on rRNA directly. It is plausible that Rnl may act indirectly through the formation of circular C/D box sRNA, which in turn could regulate rRNA processing.

Nonetheless, the phylogenetic analysis suggests a possible link between the archaea Rnl, C/D box sRNA circularization, and H98 processing. A high abundance of circular C/D box sRNA molecules was detected in *T. kodakarensis*, *P. furiosus*, *P. abyssi*, *and Methanopyrus kandleri* (Starostina et al., 2004; Danan et al., 2012; Su et al., 2013; Toffano-Nioche et al., 2013). They all encode a homodimeric type-3 Rnl (Gu et al., 2016) and possess H98 or an equivalent structural element in

their large subunit of rRNA. In *T. kodakarensis* and *P. furiosus*, H98 is excised evinced by discontinuous RNA-Seq map coverage ((Birkedal et al., 2020) and this study). While many species from *Methanomicrobiales* and *Archaeoglobales* encode Rnl, the helix equivalent of H98 is replaced with a short linker sequence (Birkedal et al., 2020). In contrast, *Haloferax volcanii*, *Nanoarchaeum equitans*, *Sulfolobus solfataricus*, *Sulfolobus acidocaldarius*, and *Pyrobaculum aerophilum*, do not encode homolog of type-3 Rnl. Circular tRNA intron and rRNA intermediates are present in abundance, but only a modest number of circular C/D box RNAs were reported in *H. volcanii*, *S. solfataricu*, *S. acidocaldarius*, and *N. equitans* (Danan et al., 2012; Randau, 2012; Becker et al., 2019). The large subunits of *S. acidocaldarius* and *P. aerophilum* rRNAs were shown to retain H98 evinced by a continuous read coverage at the 3′-end (Birkedal et al., 2020). Because many RNA-Seq data are depleted for rRNA, it is difficult to evaluate its read coverage. Availability of complete RNA-Seq data from other archaea species could provide further insight into the role of Rnl and its relationship to small RNA circularization and rRNA processing.

DATA AVAILABILITY STATEMENT

The datasets presented in this study can be found in online repositories. The names of the repository/repositories and accession number(s) can be found below: https://www.ncbi.nlm.nih.gov/, GSE186817.

AUTHOR CONTRIBUTIONS

CKH designed research. YL, YT, AH, and CKH performed research. YL, YT, and CKH analyzed data. KM and MS data curation. HH and CKH provide resources. CKH wrote the paper.

FUNDING

This material is based upon work supported by National Science Foundation 1050984 (to CKH) and Japan Society for the Promotion of Science Grants-in-Aid for Scientific Research KAKENHI 21K06984 (to CKH). Open Access publication charge was provided by National Institute of Advanced Industrial Science and Technology.

ACKNOWLEDGMENTS

We thank Katsuhiko Murakami (Penn State University) for valuable discussion and Thomas Mayers (University of Tsukuba) for editing the manuscript.

SUPPLEMENTARY MATERIAL

The Supplementary Material for this article can be found online at: https://www.frontiersin.org/articles/10.3389/fmolb.2022.811548/full#supplementary-material

REFERENCES

Abelson, J., Trotta, C. R., and Li, H. (1998). tRNA Splicing. *J. Biol. Chem.* 273, 12685–12688. doi:10.1074/jbc.273.21.12685

Amitsur, M., Levitz, R., and Kaufmann, G. (1987). Bacteriophage T4 Anticodon Nuclease, Polynucleotide Kinase and RNA Ligase Reprocess the Host Lysine tRNA. *EMBO J.* 6, 2499–2503. doi:10.1002/j.1460-2075.1987.tb02532.x

Atomi, H., Fukui, T., Kanai, T., Morikawa, M., and Imanaka, T. (2004). Description ofThermococcus Kodakaraensissp. nov., a Well Studied Hyperthermophilic Archaeon Previously Reported asPyrococcussp. KOD1. *Archaea* 1, 263–267. doi:10.1155/2004/204953

Becker, H. F., Héliou, A., Djaout, K., Lestini, R., Regnier, M., and Myllykallio, H. (2017). High-throughput Sequencing Reveals Circular Substrates for an Archaeal RNA Ligase. *RNA Biol.* 14, 1075–1085. doi:10.1080/15476286.2017.1302640

Becker, H. F., L'Hermitte-Stead, C., and Myllykallio, H. (2019). Diversity of Circular RNAs and RNA Ligases in Archaeal Cells. *Biochimie* 164, 37–44. doi:10.1016/j.biochi.2019.06.011

Birkedal, U., Beckert, B., Wilson, D. N., and Nielsen, H. (2020). The 23S Ribosomal RNA from Pyrococcus Furiosus Is Circularly Permuted. *Front. Microbiol.* 11, 582022. doi:10.3389/fmicb.2020.582022

Brennicke, A., Marchfelder, A., and Binder, S. (1999). RNA Editing. *Fems Microbiol. Rev.* 23, 297–316. doi:10.1111/j.1574-6976.1999.tb00401.x

Breuer, R., Gomes-Filho, J.-V., and Randau, L. (2021). Conservation of Archaeal C/D Box sRNA-Guided RNA Modifications. *Front. Microbiol.* 12, 654029. doi:10.3389/fmicb.2021.654029

Brooks, M. A., Meslet-Cladiére, L., Graille, M., Kuhn, J., Blondeau, K., Myllykallio, H., et al. (2008). The Structure of an Archaeal Homodimeric Ligase Which Has RNA Circularization Activity. *Protein Sci.* 17, 1336–1345. doi:10.1110/ps.035493.108

Burroughs, A. M., and Aravind, L. (2016). RNA Damage in Biological Conflicts and the Diversity of Responding RNA Repair Systems. *Nucleic Acids Res.* 44, 8525–8555. doi:10.1093/nar/gkw722

Danan, M., Schwartz, S., Edelheit, S., and Sorek, R. (2012). Transcriptome-wide Discovery of Circular RNAs in Archaea. *Nucleic Acids Res.* 40, 3131–3142. doi:10.1093/nar/gkr1009

Englert, M., and Beier, H. (2005). Plant tRNA Ligases Are Multifunctional Enzymes that Have Diverged in Sequence and Substrate Specificity from RNA Ligases of Other Phylogenetic Origins. *Nucleic Acids Res.* 33, 388–399. doi:10.1093/nar/gki174

Englert, M., Sheppard, K., Aslanian, A., Yates, J. R., and Söll, D. (2011). Archaeal 3'-phosphate RNA Splicing Ligase Characterization Identifies the Missing Component in tRNA Maturation. *Proc. Natl. Acad. Sci.* 108, 1290–1295. doi:10.1073/pnas.1018307108

Gu, H., Yoshinari, S., Ghosh, R., Ignatochkina, A. V., Gollnick, P. D., Murakami, K. S., et al. (2016). Structural and Mutational Analysis of Archaeal ATP-dependent RNA Ligase Identifies Amino Acids Required for RNA Binding and Catalysis. *Nucleic Acids Res.* 44, 2337–2347. doi:10.1093/nar/gkw094

Ho, C. K., and Shuman, S. (2002). Bacteriophage T4 RNA Ligase 2 (gp24.1) Exemplifies a Family of RNA Ligases Found in All Phylogenetic Domains. *Proc. Natl. Acad. Sci.* 99, 12709–12714. doi:10.1073/pnas.192184699

Jäger, D., Förstner, K. U., Sharma, C. M., Santangelo, T. J., and Reeve, J. N. (2014). Primary Transcriptome Map of the Hyperthermophilic Archaeon Thermococcus Kodakarensis. *BMC Genomics* 15, 684–699. doi:10.1186/1471-2164-15-684

Jüttner, M., Weiß, M., Ostheimer, N., Reglin, C., Kern, M., Knüppel, R., et al. (2019). A Versatile Cis-Acting Element Reporter System to Study the Function, Maturation and Stability of Ribosomal RNA Mutants in Archaea. *Nucleic Acids Res.* 48, 2073–2090. doi:10.1093/nar/gkz1156

Kristensen, L. S., Andersen, M. S., Stagsted, L. V. W., Ebbesen, K. K., Hansen, T. B., and Kjems, J. (2019). The Biogenesis, Biology and Characterization of Circular RNAs. *Nat. Rev. Genet.* 20, 675–691. doi:10.1038/s41576-019-0158-7

Liao, Y., Smyth, G. K., and Shi, W. (2014). Featurecounts: An Efficient General Purpose Program For Assigning Sequence Reads To Genomic Features. *Bioinformat.* 30, 923–930. doi:10.1093/bioinformatics/btt656

Liu, Y. (2022). Genetic And Functional Analyses Of Archaeal ATP-Dependent RNA Ligase. Ph.D. thesis Tsukuba (Japan): University of Tsukuba.

McManus, M. T., Shimamura, M., Grams, J., and Hajduk, S. L. (2001). Identification of Candidate Mitochondrial RNA Editing Ligases from Trypanosoma Brucei. *Rna-A Publ. Rna Soc.* 7, 167–175. doi:10.1017/s1355838201002072

Nandakumar, J., Ho, C. K., Lima, C. D., and Shuman, S. (2004). RNA Substrate Specificity and Structure-Guided Mutational Analysis of Bacteriophage T4 RNA Ligase 2. *J. Biol. Chem.* 279, 31337–31347. doi:10.1074/jbc.m402394200

Nandakumar, J., Schwer, B., Schaffrath, R., and Shuman, S. (2008). RNA Repair: an Antidote to Cytotoxic Eukaryal RNA Damage. *Mol. Cel.* 31, 278–286. doi:10.1016/j.molcel.2008.05.019

Omari, K. E., Ren, J., Bird, L. E., Bona, M. K., Klarmann, G., LeGrice, S. F. J., et al. (2006). Molecular Architecture and Ligand Recognition Determinants for T4 RNA Ligase. *J. Biol. Chem.* 281, 1573–1579. doi:10.1074/jbc.m509658200

Popow, J., Englert, M., Weitzer, S., Schleiffer, A., Mierzwa, B., Mechtler, K., et al. (2011). HSPC117 Is the Essential Subunit of a Human tRNA Splicing Ligase Complex. *Science* 331, 760–764. doi:10.1126/science.1197847

Qi, L., Li, J., Jia, J., Yue, L., and Dong, X. (2020). Comprehensive Analysis of the Pre-ribosomal RNA Maturation Pathway in a Methanoarchaeon Exposes the Conserved Circularization and Linearization Mode in Archaea. *RNA Biol.* 17, 1427–1441. doi:10.1080/15476286.2020.1771946

Randau, L. (2012). RNA Processing in the Minimal Organism Nanoarchaeum Equitans. *Genome Biol.* 13, R63. doi:10.1186/gb-2012-13-7-r63

Rusche´, L. N., Huang, C. E., Piller, K. J., Hemann, M., Wirtz, E., and Sollner-Webb, B. (2001). The Two RNA Ligases of the Trypanosoma Brucei RNA Editing Complex: Cloning the Essential Band IV Gene and Identifying the Band V Gene. *Mol. Cel. Biol.* 21, 979–989. doi:10.1128/mcb.21.4.979-989.2001

Sas-Chen, A., Thomas, J. M., Matzov, D., Taoka, M., Nance, K. D., Nir, R., et al. (2020). Dynamic RNA Acetylation Revealed by Quantitative Cross-Evolutionary Mapping. *Nature* 583, 638–643. doi:10.1038/s41586-020-2418-2

Sato, T., Fukui, T., Atomi, H., and Imanaka, T. (2005). Improved and Versatile Transformation System Allowing Multiple Genetic Manipulations of the Hyperthermophilic Archaeon Thermococcus Kodakaraensis. *Appl. Environ. Microbiol.* 71, 3889–3899. doi:10.1128/aem.71.7.3889-3899.2005

Sato, T., Fukui, T., Atomi, H., and Imanaka, T. (2003a). Targeted Gene Disruption by Homologous Recombination in the Hyperthermophilic Archaeon Thermococcus Kodakaraensis KOD1. *J. Bacteriol.* 185, 210–220. doi:10.1128/jb.185.1.210-220.2003

Sato, T., Fukui, T., Atomi, H., and Imanaka, T. (2003b). Targeted Gene Disruption by Homologous Recombination in the Hyperthermophilic Archaeon Thermococcus Kodakaraensis KOD1. *J. Bacteriol.* 185, 210–220. doi:10.1128/jb.185.1.210-220.2003

Schmeing, T. M., Voorhees, R. M., Kelley, A. C., Gao, Y.-G., Murphy, F. V., Weir, J. R., et al. (2009). The Crystal Structure of the Ribosome Bound to EF-Tu and Aminoacyl-tRNA. *Science* 326, 688–694. doi:10.1126/science.1179700

Schnaufer, A., Panigrahi, A. K., Panicucci, B., Igo, R. P., Salavati, R., Stuart, K., et al. (2001). An RNA Ligase Essential for RNA Editing and Survival of the Bloodstream Form of Trypanosoma Brucei. *Science* 291, 2159–2162. doi:10.1126/science.1058955

Sidrauski, C., Cox, J. S., and Walter, P. (1996). tRNA Ligase Is Required for Regulated mRNA Splicing in the Unfolded Protein Response. *Cell* 87, 405–413. doi:10.1016/s0092-8674(00)81361-6

Starostina, N. G., Marshburn, S., Johnson, L. S., Eddy, S. R., Terns, R. M., and Terns, M. P. (2004). Circular Box C/D RNAs in Pyrococcus Furiosus. *Proc. Natl. Acad. Sci.* 101, 14097–14101. doi:10.1073/pnas.0403520101

Su, A. A. H., Tripp, V., and Randau, L. (2013). RNA-seq Analyses Reveal the Order of tRNA Processing Events and the Maturation of C/D Box and CRISPR RNAs in the Hyperthermophile Methanopyrus Kandleri. *Nucleic Acids Res.* 41, 6250–6258. doi:10.1093/nar/gkt317

Szewczak, A. A., Moore, P. B., Chang, Y. L., and Wool, I. G. (1993). The Conformation of the Sarcin/ricin Loop from 28S Ribosomal RNA. *Proc. Natl. Acad. Sci.* 90, 9581–9585. doi:10.1073/pnas.90.20.9581

Tang, T. H., Rozhdestvensky, T. S., d'Orval, B. C., Bortolin, M.-L., Huber, H., Charpentier, B., et al. (2002). RNomics in Archaea Reveals a Further Link between Splicing of Archaeal Introns and rRNA Processing. *Nucleic Acids Res.* 30, 921–930. doi:10.1093/nar/30.4.921

Toffano-Nioche, C., Ott, A., Crozat, E., Nguyen, A. N., Zytnicki, M., Leclerc, F., et al. (2013). RNA at 92°C. *RNA Biol.* 10, 1211–1220. doi:10.4161/rna.25567

Torchia, C., Takagi, Y., and Ho, C. K. (2008). Archaeal RNA Ligase Is a Homodimeric Protein that Catalyzes Intramolecular Ligation of Single-Stranded RNA and DNA. *Nucleic Acids Res.* 36, 6218–6227. doi:10.1093/nar/gkn602

Trotta, C. R., Miao, F., Arn, E. A., Stevens, S. W., Ho, C. K., Rauhut, R., et al. (1997). The Yeast tRNA Splicing Endonuclease: A Tetrameric Enzyme with Two Active Site Subunits Homologous to the Archaeal tRNA Endonucleases. *Cell* 89, 849–858. doi:10.1016/s0092-8674(00)80270-6

Uhlenbeck, O. C., and Gumport, R. I. (1982). 2 T4 RNA Ligase. *The Enzymes* 15, 31–58. doi:10.1016/s1874-6047(08)60274-7

Wang, L. K., Nandakumar, J., Schwer, B., and Shuman, S. (2007). The C-Terminal Domain of T4 RNA Ligase 1 Confers Specificity for tRNA Repair. *Rna* 13, 1235–1244. doi:10.1261/rna.591807

Wool, I. G., Glück, A., and Endo, Y. (1992). Ribotoxin Recognition of Ribosomal RNA and a Proposal for the Mechanism of Translocation. *Trends Biochem. Sci.* 17, 266–269. doi:10.1016/0968-0004(92)90407-z

Yin, S., Ho, C. K., and Shuman, S. (2003). Structure-function Analysis of T4 RNA Ligase 2. *J. Biol. Chem.* 278, 17601–17608. doi:10.1074/jbc.m300817200

Yoshinari, S., Liu, Y., Gollnick, P., and Ho, C. K. (2017). Cleavage of 3′-terminal Adenosine by Archaeal ATP-dependent RNA Ligase. *Sci. Rep.* 7, 11662. doi:10.1038/s41598-017-11693-0

Zhang, L., and Tripathi, A. (2017). Archaeal RNA Ligase from Thermoccocus Kodakarensis for Template Dependent Ligation. *RNA Biol.* 14, 36–44. doi:10.1080/15476286.2016.1239688

Zhelkovsky, A. M., and McReynolds, L. A. (2014). Polynucleotide 3′-terminal Phosphate Modifications by RNA and DNA Ligasess. *J. Biol. Chem.* 289, 33608–33616. doi:10.1074/jbc.m114.612929

Conflict of Interest: The authors declare that the research was conducted in the absence of any commercial or financial relationships that could be construed as a potential conflict of interest.

Publisher's Note: All claims expressed in this article are solely those of the authors and do not necessarily represent those of their affiliated organizations, or those of the publisher, the editors and the reviewers. Any product that may be evaluated in this article, or claim that may be made by its manufacturer, is not guaranteed or endorsed by the publisher.

frontiers in Molecular Biosciences

REVIEW
published: 31 March 2022
doi: 10.3389/fmolb.2022.863885

mRNA Translation Is Dynamically Regulated to Instruct Stem Cell Fate

*Ruoxu Wang and Marc Amoyel**

Department of Cell and Developmental Biology, University College London, London, United Kingdom

Stem cells preserve tissue homeostasis by replacing the cells lost through damage or natural turnover. Thus, stem cells and their daughters can adopt two identities, characterized by different programs of gene expression and metabolic activity. The composition and regulation of these programs have been extensively studied, particularly by identifying transcription factor networks that define cellular identity and the epigenetic changes that underlie the progressive restriction in gene expression potential. However, there is increasing evidence that post-transcriptional mechanisms influence gene expression in stem cells and their progeny, in particular through the control of mRNA translation. Here, we review the described roles of translational regulation in controlling all aspects of stem cell biology, from the decision to enter or exit quiescence to maintaining self-renewal and promoting differentiation. We focus on mechanisms controlling global translation rates in cells, mTOR signaling, eIF2α phosphorylation, and ribosome biogenesis and how they allow stem cells to rapidly change their gene expression in response to tissue needs or environmental changes. These studies emphasize that translation acts as an additional layer of control in regulating gene expression in stem cells and that understanding this regulation is critical to gaining a full understanding of the mechanisms that underlie fate decisions in stem cells.

Keywords: stem cell, self-renewal, differentiation, translation, protein synthesis, mTOR, eIF2 kinase, ribosome biogenesis

OPEN ACCESS

Edited by:
Deepika Vasudevan,
University of Pittsburgh, United States

Reviewed by:
Marianthi Kiparaki,
Alexander Fleming Biomedical Sciences Research Center, Greece
Greco Hernández,
National Institute of Cancerology (INCAN), Mexico

****Correspondence:***
Marc Amoyel
marc.amoyel@ucl.ac.uk

Specialty section:
This article was submitted to RNA Networks and Biology, a section of the journal Frontiers in Molecular Biosciences

Received: *27 January 2022*
Accepted: *25 February 2022*
Published: *31 March 2022*

Citation:
Wang R and Amoyel M (2022) mRNA Translation Is Dynamically Regulated to Instruct Stem Cell Fate. Front. Mol. Biosci. 9:863885. doi: 10.3389/fmolb.2022.863885

INTRODUCTION

Stem cells share the unique property of being able to both self-renew and differentiate, generating progeny with specialized functions. Nonetheless, stem cells encompass a wide variety of cells with a broad range of behaviors, from multipotent embryonic stem cells, which give rise to all cell types in an embryo, to lineage-restricted adult stem cells. For instance, in some mammalian tissues such as the blood, muscle, or brain, stem cells are mostly quiescent and proliferate only when activated by environmental signals, while in other tissues such as the intestine or epidermis, stem cells are highly proliferative to maintain tissue integrity despite continued turnover of differentiated cells. Even in those tissues, differentiation or proliferation can be modulated in response to stimuli from dying cells, or systemic signals including nutrition. Thus, adult stem cells are capable of rapidly altering their behavior and fate in response to the needs of the tissue or the organism, emphasizing the flexibility in their gene expression programs.

How gene expression programs controlling quiescence, proliferation, self-renewal, and differentiation can be both stable and plastic is the subject of much study, often focusing on understanding the transcriptional networks that maintain cell identity and the inputs that destabilize these networks and allow cells to change fate. Our understanding of these networks has grown and is

continually being refined, showing that various stable network states exist and explaining transitions between these states (Kim et al., 2008; Moignard et al., 2013; Theunissen and Jaenisch, 2017; Kim et al., 2020; Sagner et al., 2021). Furthermore, we have gained considerable understanding of the epigenetic changes that reinforce these transcriptional changes and ensure that stem cells maintain plasticity in gene expression while differentiating cells gradually become restricted in potential (Lunyak and Rosenfeld, 2008; Ohbo and Tomizawa, 2015; Theunissen and Jaenisch, 2017; Ding et al., 2021).

However, technological advances enabling the comparison of the proteins in cells with their transcriptome led to the discovery that the two are often poorly correlated and that changes in the proteome can occur without accompanying transcriptional changes (Unwin et al., 2006; de Sousa Abreu et al., 2009; Lu et al., 2009; Maier et al., 2009; Schwanhausser et al., 2011), indicating that there are additional layers of regulation of gene expression beyond transcription. This mismatch has been described in many cell types, including stem cells (Lu et al., 2009; Ingolia et al., 2011; Baser et al., 2019; Habowski et al., 2020; Spevak et al., 2020), suggesting that post-transcriptional control of gene expression is common. The protein content of a cell depends on both synthesis and degradation: work describing extensive links between protein degradation and stem cell fate has been reviewed elsewhere (Strikoudis et al., 2014; Suresh et al., 2016; Yan et al., 2020); here, we will focus on the mechanisms affecting stem cell fate through the regulation of protein synthesis.

Bulk Translation Rates Change During Stem Cell Activation and Differentiation

Until recently, precise measurement of translation rates was mostly restricted to cell culture models where newly synthesized proteins could be labeled by providing a pulse of radioactive amino acids. For instance, in *ex vivo* cultures, differentiating murine embryonic stem cells (mESCs) into structures known as embryoid bodies resulted in a ~2-fold increase in their translation rate, as indicated by [^{35}S] methionine incorporation (Sampath et al., 2008). Consistently, embryoid bodies display an increased content of the Golgi apparatus and rough endoplasmic reticulum (ER) and an increased proportion of polysomes (multiple ribosomes bound to the same mRNA), indicating higher rates of protein synthesis. Similarly, cultured human embryonic stem cells (hESCs) show immature Golgi and rough ER and much lower translation rates than differentiated derivatives (Easley et al., 2010).

However, new techniques, known as bio-orthogonal non-canonical amino acid tagging (BONCAT) (Dieterich et al., 2007; Dieterich et al., 2006) and fluorescent non-canonical amino acid tagging (FUNCAT) (Dieterich et al., 2010), have enabled direct visualization of translation in tissue samples and comparison between cell types *in situ*, leading to a different conclusion. In this case, a transient decrease in the overall translation rate was observed as mESCs differentiated into epiblasts, increasing again during neuroectodermal differentiation (**Figure 1A**) (Corsini et al., 2018). One likely explanation for the discrepancy in translation rates between cultured and *in vivo* mESCs is that protein synthesis is artificially repressed by the factors added to maintain pluripotency in *ex vivo* cultures, leukemia inhibitory factor (LIF) and bone morphogenetic protein 4 (BMP4) (Friend et al., 2015).

In adult stem cells, however, a clearer picture emerges of how the translation rate changes during differentiation. In most stem cell models, translation is low in stem cells, increasing their differentiating progeny, but this increase is reversed when cells terminally differentiate and become postmitotic (**Figure 1B**).

This was first shown in one of the best characterized adult stem cell populations, hematopoietic stem cells (HSCs), which show low translation rates. As the progeny of HSCs progress along the differentiation pathway through highly proliferative transit-amplifying stages, translation rates increase, remaining high as these progenitors become more lineage-restricted, but eventually dropping in further differentiated cell types (Signer et al., 2014). This latter observation was consistent with previous work showing that the polysome fraction decreased during myeloid differentiation from a promyelocytic cell line in culture, indicating an overall decrease in protein synthesis during terminal differentiation (Krichevsky et al., 1999). Similarly, adult neural stem cells (NSCs) in the sub-ventricular zone have lower translation rates than the neuronal progenitors they give rise to, while differentiation of the latter into postmitotic neuroblasts correlates with decreased levels of protein synthesis (Llorens-Bobadilla et al., 2015; Baser et al., 2019). Hair follicle stem cells (HFSCs) also show a similar pattern of increasing translation rates during differentiation into progenitors, followed by a decrease in terminally differentiated cells (Blanco et al., 2016).

Intriguingly, HSCs, NSCs, and HFSCs can all exist in a quiescent state, in which they do not proliferate; in all cases, quiescent stem cells have significantly lower translation rates than activated stem cells (Signer et al., 2014; Llorens-Bobadilla et al., 2015; Blanco et al., 2016). Although this observation, together with the fact that postmitotic cells tend to have lower translation rates than proliferative progenitors, suggests a link between the translation rate and cell proliferation, proliferation only accounts for part of the difference in protein synthesis rates observed, at least in both blood and hair follicle lineages (Signer et al., 2016; Blanco et al., 2016).

One interesting exception to the general trend that stem cells have lower translation rates than their differentiating offspring is seen in intestinal stem cells (ISCs) in *Drosophila*, which give rise to daughters that are postmitotic, without a transit-amplifying stage (Micchelli and Perrimon, 2006; Ohlstein and Spradling, 2006). Obata et al. (2018) showed that ISCs have the highest bulk translation rate of all cell types in the *Drosophila* intestine, suggesting that differentiating stem cell daughters that immediately become postmitotic does not increase their translation rate, consistent with observations of lower protein synthesis in non-dividing cells in other tissues.

Altogether, these studies indicate that global translation is dynamically regulated during stem cell activation and differentiation and suggest a general pattern (**Figure 1B**): each

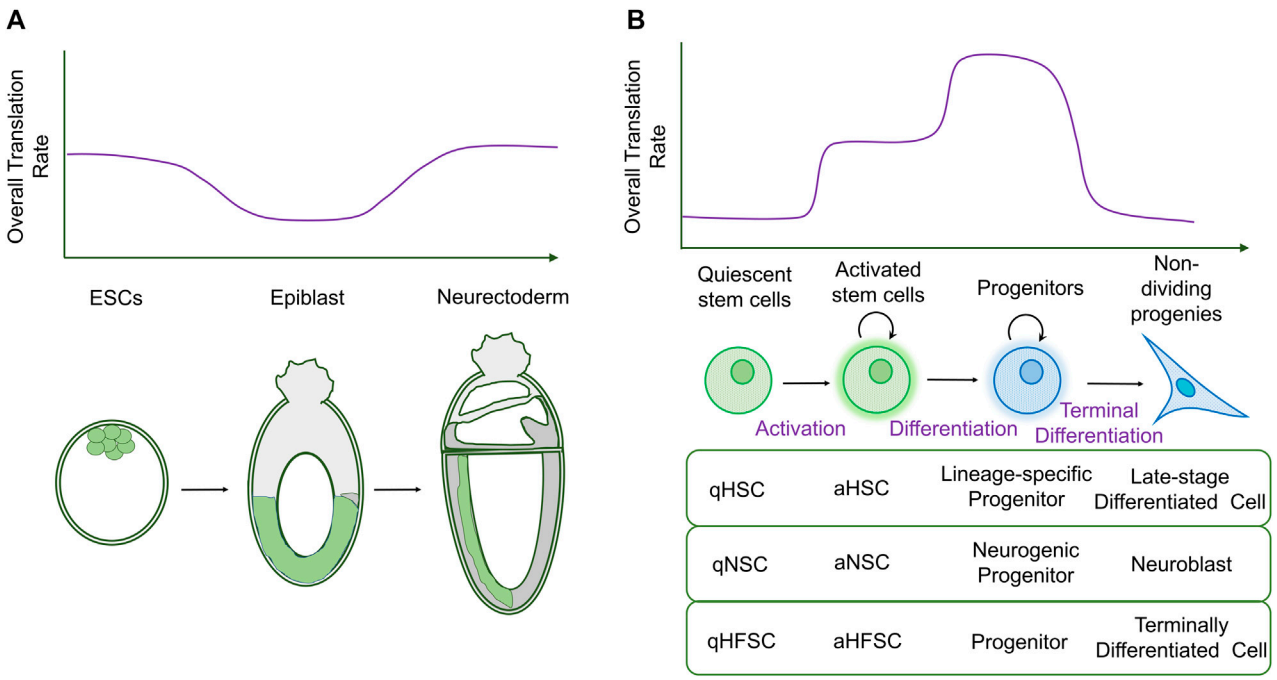

FIGURE 1 | Changes in global translation during stem cell differentiation. **(A)** Diagram schematizing bulk translation rates during early mammalian embryogenesis (top), with stages shown later. Bulk translation rates are initially high in ESCs and decrease during differentiation into the epiblast. Global translation levels rise again during neurectodermal development. **(B)** In adult stem cells, quiescent stem cells have low rates of bulk translation. Translation increases in activated stem cells and is highest in proliferating progenitors that initiate differentiation. Terminally differentiated cells display low rates of translation. The table shows examples of stem cells in which translation rates follow this pattern: hematopoietic stem cells (HSCs), neural stem cells (NSCs), and hair follicle stem cells (HFSCs). q: quiescent; a: activated.

step from the activation of quiescent stem cells to differentiation into proliferative progenitors results in an increase in the translation rate. This high rate of protein synthesis is sustained in proliferating progenitors as they continue to mature, until differentiation into postmitotic cells is associated with a decrease in translation. Given this tight control of overall translation rates during development, we focus on the regulation of global protein synthesis in stem cells and their differentiated offspring and how this contributes to gene expression and the maintenance of cell identity.

Several mechanisms have been described to regulate the translation of individual mRNAs, and these include regulating mRNA splicing, stability, and methylation, as well as microRNAs (Jackson et al., 2010; Zhang M. et al., 2020). The *Drosophila* germline provides an excellent example to understand how RNA-binding proteins can affect the translation of key factors regulating self-renewal and differentiation (Slaidina and Lehmann, 2014; Blatt et al., 2020); however, in this review, we will focus on mechanisms that affect global translation rates, in particular translation initiation and ribosome biogenesis, and how they influence stem cell identity.

Translation Initiation and Its Regulation

Initiation is thought to be the rate-limiting step of protein synthesis, determining which transcripts are translated and how much protein is produced (Duncan et al., 1987; Shah et al., 2013), and it is subjected to regulation by multiple upstream inputs, including nutrient-responsive signals, growth factor signaling, and the amount of ribosomes available in the cell (Sonenberg and Hinnebusch, 2009; Jackson et al., 2010; Roux and Topisirovic, 2018). These regulatory interactions determine both the total rate of translation and the specificity of translated mRNAs. Many signals governing translation rates converge either on controlling the rate of assembly of initiation factors at the m^7G 5' cap of the mRNA or the availability of the initiator tRNA carrying methionine (Met-$tRNA_i^{Met}$).

Canonical translation begins with the eukaryotic initiation factor (eIF) 4E binding to the 5′cap of mRNAs, and assembling a complex known as eIF4F, composed of eIF4E, the helicase eIF4A which unwinds secondary structure and eIF4G. eIF4G acts as a scaffold to bring other initiation complexes, together with the 40S small ribosome subunit to the 5′ end of the mRNA, from where the ribosome will begin scanning for a start codon (**Figure 2**). Initiation of translation requires Met-$tRNA_i^{Met}$, which is brought to the ribosome as part of the so-called ternary complex formed of eIF2 bound to GTP and Met-$tRNA_i^{Met}$.

A major regulator of global cellular translation rates is the mechanistic target of rapamycin (mTOR) pathway (Albert and Hall, 2015; Liu and Sabatini, 2020; Ma and Blenis, 2009), which regulates cell growth and metabolism in response to extracellular growth factors and amino acid levels (Showkat et al., 2014). Two of the best characterized effectors of mTOR are ribosomal protein

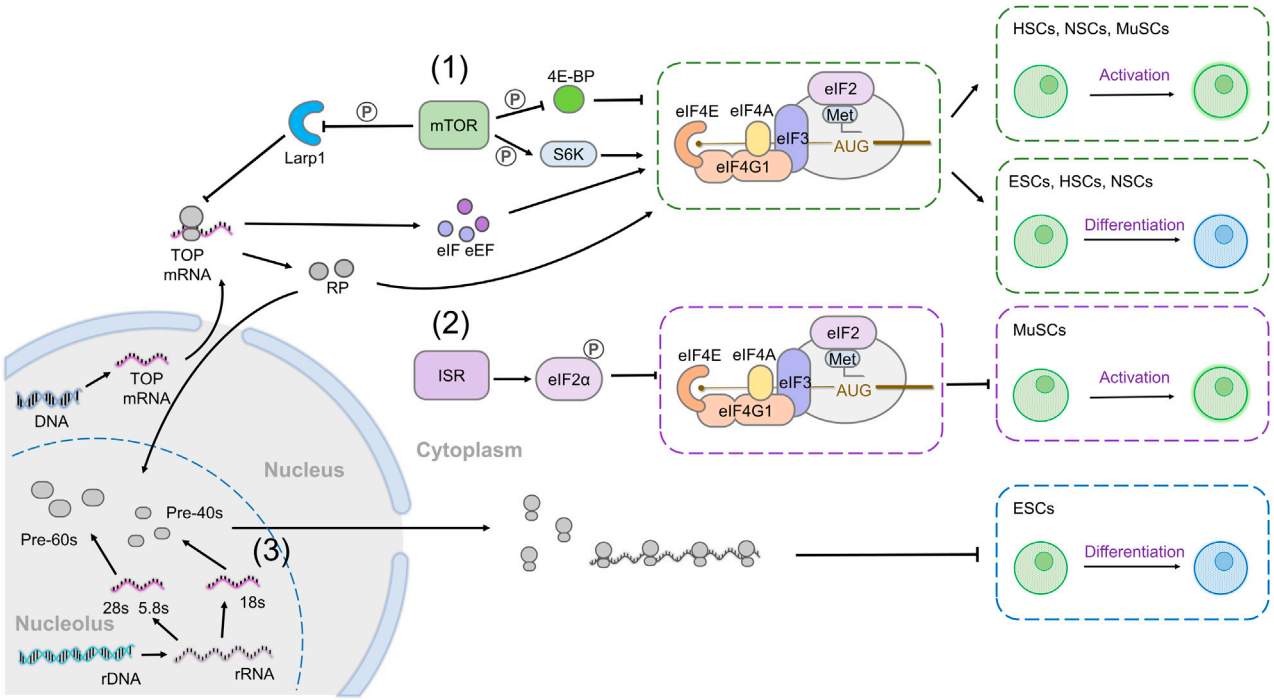

FIGURE 2 | Global mechanisms of translation regulation and their roles in stem cell maintenance. (1) mTOR activity increases global translation through its effectors 4E-BP and S6K and promotes cap-dependent translation. In addition, mTOR increases the translation of TOP mRNAs, which include most components of the translation machinery including translation initiation factors (eIFs), translation elongation factors (eEFs), and ribosomal proteins (RPs). Increased mTOR signaling leads to the activation of HSCs, NSCs, and MuSCs from quiescence and induces differentiation of ESCs, HSCs, and NSCs (green boxes). (2) The integrated stress response (ISR) pathway promotes eIF2α phosphorylation, which reduces eIF2α association with Met-tRNA$_i^{Met}$ and impairs global translation. P-eIF2α prevents MuSC activation from quiescence (purple box). (3) Ribosomes are assembled in the nucleolus. Decreasing the rate of ribosome biogenesis results in ESC differentiation (blue box).

S6 kinase 1 (S6K1) and eIF4E-binding protein (4E-BP), both of which are phosphorylated upon mTOR activation. 4E-BP binds and sequesters eIF4E, preventing it from interacting with the 5′ mRNA cap, but phosphorylation of 4E-BP by mTOR inactivates it, releasing eIF4E and promoting cap-dependent translation (**Figure 2** (1)) (Brunn et al., 1997; Hara et al., 1997; Gingras et al., 1999). Phosphorylated S6K1 increases the activity of several proteins involved in mRNA translation, including eIF4B and ribosomal protein S6 (RpS6), and inactivates translational repressors such as eukaryotic elongation factor-2 kinase (eEF2K), programmed cell death 4 (PDCD4), and La ribonucleoprotein 1 (Larp1) (Ferrari et al., 1991; Wang et al., 2001; Yang et al., 2003; Raught et al., 2004; Fonseca et al., 2015; Hong et al., 2017). Through various targets, activation of mTOR specifically increases the translation of mRNAs containing 5′ terminal oligopyrimidine (TOP) or TOP-like motifs, which consist of a 5’ cytidine at the cap immediately followed by a stretch of 4–15 pyrimidines (Hsieh et al., 2012; Thoreen et al., 2012; Meyuhas and Kahan, 2015; Hong et al., 2017; Iezaki et al., 2018; Philippe et al., 2018; Jia et al., 2021). Interestingly, many mRNAs encoding components of the translation machinery, including but not limited to translation elongation factors (eEFs), some translation initiation factors (eIFs) and most ribosomal proteins, have a TOP motif (Iadevaia et al., 2008; Meyuhas and Kahan, 2015; Hong et al., 2017). Thus, activation of mTOR and its effectors dramatically increases the synthesis of the translation machinery itself, as well as increasing the efficiency of existing translation factors.

Another critical regulator of cellular translation rates is a signaling pathway known as the integrated stress response (ISR). The ISR dramatically decreases mRNA translation following cellular stresses by phosphorylating eIF2α, which prevents its assembly into the ternary complex with GTP and Met-tRNA$_i^{Met}$ (**Figure 2** (2)) (Wek et al., 2006; Pakos-Zebrucka et al., 2016; Costa-Mattioli and Walter, 2020). There are four known kinases that phosphorylate eIF2α in response to various physiological or environmental stresses: PKR-like ER kinase (PERK) is activated downstream of ER stress; general control non-derepressible 2 (GCN2) is responsive to amino acid deprivation; protein kinase RNA-activated (PKR) senses infection-derived dsRNA; and heme-regulated inhibitor (HRI) binds hemin and is disinhibited upon cellular heme deficiency. ISR activation is thought to restore homeostasis and save energy under adverse conditions, particularly by restraining translation; however, a subset of transcripts is specifically translated when eIF2α is phosphorylated, providing a mechanism for the upregulation of stress response genes when most translation is inhibited.

Finally, in addition to these pathways which are dedicated to growth control, other signaling pathways that control patterning during development and influence self-renewal decisions in stem cells can also affect translation. In particular, the Ras/mitogen-activated protein kinase (MAPK) pathway also promotes cellular growth and translation through promoting the activity of eIF4F, *via* its effector MAPK-interacting kinase 1 (Mnk1) (Waskiewicz et al., 1999). In sum, translation initiation is under the control of multiple signaling pathways, enabling the coordination of protein synthesis rates with other inputs into cell identity.

Ribosomal Biogenesis

Another critical parameter affecting the amount of protein produced in a cell is the number of ribosomes available for translation. Ribosome biogenesis is a complex process bringing together the ribosomal RNAs (rRNAs) and ribosomal proteins into the small and large ribosomal subunits, with the cooperation of non-ribosomal factors, such as small nucleolar ribonucleoproteins (SnoRNPs) (**Figure 2** (3)). The amount of rRNA and protein available and the rate of assembly depend on several factors, including cellular stress, nutrient availability, and signaling (de la Cruz et al., 2018; Pelletier et al., 2018; Klinge and Woolford, 2019). The rRNAs are transcribed from nuclear DNA by two specific RNA polymerases (RNA Pol), RNA Pol I, which transcribes most rRNAs and RNA Pol III, which transcribes the 5s rRNA and tRNAs. However, rRNA synthesis and ribosome biogenesis also requires the action of RNA Pol II (Abraham et al., 2020). mTOR has emerged as a critical regulator of ribosome assembly, as its activity coordinately increases the transcription of rRNA and ribosomal proteins. Indeed, mTOR directly regulates the activity of RNA Pol I and RNA Pol III (Powers and Walter, 1999). Similarly, Ras/MAPK signaling increases rRNA synthesis to mediate its effects on growth (Stefanovsky et al., 2001).

Finally, although ribosomes were assumed to be equal and identical, recent work has identified that the composition of ribosomal proteins can change from cell-to-cell, and that, in turn, this composition can affect the mRNAs which are translated (Genuth and Barna, 2018). Thus, both abundance and specificity of ribosomes can be regulated to control overall translation rates and specificity in cells.

CHANGES IN BULK TRANSLATION INFLUENCE STEM CELL MAINTENANCE AND DIFFERENTIATION

mTOR Promotes Stem Cell Activation and Differentiation Through Increased Translation

mTOR activity changes during stem cell differentiation or activation, and in many cases increased mTOR signaling is sufficient to induce differentiation. The differentiation of *ex vivo*-cultured ESCs, derived from both human and mouse, is coupled with the activation of mTOR activation indicated by phosphorylation of 4E-BP1, RPS6, and eIF4B (Sampath et al., 2008; Easley et al., 2010; Zhou et al., 2020). Similarly, mTOR activity is reduced during the early stages of reprogramming somatic cells into induced pluripotent stem cells (iPSCs) (Wang et al., 2013; Wu et al., 2015). Importantly, while mTOR activity is not required to maintain ESC self-renewal, activating mTOR or its effector S6K primes ESCs to differentiate and mTOR hyperactivity prevents the reprogramming of somatic cells into iPSCs (Murakami et al., 2004; Easley et al., 2010; He et al., 2012; Wang et al., 2013; Wu et al., 2015). Reprogramming also requires the presence of 4E-BPs (Tahmasebi et al., 2014), further implicating translation as one of the key cellular processes by which mTOR activity leads to the loss of pluripotency (**Figure 2** (1)).

Similarly, increasing mTOR activity is sufficient to promote differentiation and loss of self-renewal ability in a variety of adult stem cell types across organisms, from HSCs and NSCs in mouse to *Drosophila* intestinal stem cells and both somatic and germline stem cells in the gonads (Zhang et al., 2006; Chen et al., 2009; Sun et al., 2010; Magri et al., 2011; Kapuria et al., 2012; Quan et al., 2013; Yuen et al., 2021). In HSCs, the deletion of *Pten*, a repressor of mTOR, or constitutive activation of mTOR, lead to ectopic proliferation of transit-amplifying progenitors, resulting in leukemia. However, despite this over-proliferation, increases in mTOR activity result in a depletion of HSCs, as determined by a deficiency in reconstituting the blood lineage upon transplantation into an immunodeficient host (Yilmaz et al., 2006; Zhang et al., 2006; Guo et al., 2008; Chen et al., 2009; Magee et al., 2012). In elegant genetic experiments, Signer et al. (2014) showed that *Pten* mutant HSCs had higher translation rates than control, and, importantly, that introducing a mutant copy of the *belly spot and tail* (Ferretti et al., 2017), encoding the ribosomal protein Rpl24, could decrease overall translation and restore the self-renewal and reconstitutive capacity of *Pten* mutant HSCs. Further work identified 4E-BP1 and 4E-BP2 as mediators of translational repression in HSCs, and their loss results in a similar decrease in long-term self-renewal ability to that of *Pten* mutant HSCs (Signer et al., 2016). Thus, an increased translation downstream of mTOR activation results in the loss of quiescence, increased proliferation, and eventual loss of the stem cell pool (**Figure 2** (1)).

mTOR plays similar roles in regulating NSC quiescence and differentiation, in two different NSC populations, in the sub-ventricular zone (SVZ) of the lateral ventricle and the dentate gyrus. In both postnatal and adult SVZ NSCs, activating mTOR through loss of function of the negative regulators *Pten* or *TSC1*, or gain of function of the activator Rheb, led to increased production of neurons, at the expense of stem cell maintenance (Groszer et al., 2006; Gregorian et al., 2009; Magri et al., 2011; Hartman et al., 2013; Mahoney et al., 2016). Loss of NSCs was attributed to an increased frequency of symmetric divisions generating two proliferative progenitors, rather than self-renewing asymmetric divisions. Similarly, in the dentate gyrus, *Pten* loss mobilizes quiescent NSCs and induces them to proliferate through symmetric self-renewing divisions, but eventually results in increased terminal differentiation and stem cell loss (Bonaguidi et al., 2011). As in HSCs, 4E-BP2 is a critical downstream effector of mTORC1, controlling cap-

dependent translation during neuronal differentiation in the SVZ (Hartman et al., 2013; Mahoney et al., 2016) (**Figure 2** (1)).

The function of mTOR in controlling exit from quiescence is remarkably conserved across tissues and even species. Indeed, TOR activation in quiescent *Drosophila* NSCs arrested in either G_0 or G_2 leads to cell cycle entry and differentiation (Chell and Brand, 2010; Sousa-Nunes et al., 2011; Otsuki and Brand, 2018). In muscle stem cells (MuSCs, also known as satellite cells), mTOR activity promotes an "alert" state of quiescence in which cells are primed for reactivation, leading them to re-enter the cell cycle upon injury or stress (Rodgers et al., 2014). Moreover, in the intestine of both flies and mice, mTOR controls the ability of the population of quiescent stem cells to contribute to the regenerative response following fasting and refeeding (Richmond et al., 2015); however, repeated regenerative episodes and bouts of mTOR activity lead to eventual loss of stem cell maintenance (Haller et al., 2017). In sum, the mTOR pathway is widely associated with stem cell activation and differentiation, and persistent activation leads to the loss of self-renewing potential. In several instances, the effects of mTOR are mediated through its effects on translation through its effectors, 4E-BP, and S6K (**Figure 2** (1)).

Of note, although the global translation rate correlates with mTOR activity throughout differentiation in the neural lineage, this is not true in all tissues (Paliouras et al., 2012; Cloetta et al., 2013; Baser et al., 2019). In myeloid progenitors derived from HSCs, mTOR is degraded by the proteasome, yet translation is still regulated by the mTOR target 4E-BP1 (Spevak et al., 2020). In this case, the cell cycle-dependent kinase CDK1 phosphorylates 4E-BP1 to promote eIF4E-dependent translation and maintain high translation rates. Thus, mTOR activity does not always linearly correlate with the overall translation rate and many other regulators may independently regulate translation initiation factors to achieve a precise rate of global translation.

eIF2α Phosphorylation in Stem Cell Maintenance

eIF2α phosphorylation has also emerged as an important regulator of stem cell maintenance through effects on global translation. High levels of p-eIF2α are observed in both *ex vivo*-cultured mESCs and murine MuSCs (Friend et al., 2015; Zismanov et al., 2016). Although in mESCs, there are conflicting data as to whether p-eIF2α levels decrease with differentiation, the signaling factors BMP4 and LIF, which maintain pluripotency in ESCs, both increase eIF2α phosphorylation (Friend et al., 2015). Indeed, preventing dephosphorylation of eIF2α is sufficient to prevent differentiation even in the absence of LIF. Similarly, in intestinal stem cells in *Drosophila*, eIF2α is phosphorylated by PERK in response to ER stress, and promotes stem cell proliferation. Continued eIF2α phosphorylation results in tissue dysplasia with an accumulation of undifferentiated cells, consistent with a role for p-eIF2 in maintaining stem cell identity (Wang et al., 2015).

In MuSCs, eIF2α is highly phosphorylated in quiescent cells. Indeed, replacing endogenous eIF2α with a non-phosphorylatable mutant, results in the short-term activation of quiescent stem cells, increased translation and proliferation, and myogenic differentiation. In the long term, however, MuSCs unable to phosphorylate eIF2α are lost from the stem cell population (Zismanov et al., 2016) (**Figure 2** (2)). Thus, in MuSCs at least, eIF2 is a critical regulator of both overall translation rates and quiescence, precise regulation of which is essential to maintain long-term self-renewal potential.

Ribosome Biogenesis Is Highly Regulated and Required for Stem Cell Maintenance

Given the importance of translation in regulating stem cell biology, ribosome biogenesis has also emerged as a critical factor controlling self-renewal and differentiation. In hematopoietic and muscle lineages, rRNA transcription follows a similar pattern to the bulk translation rate, increasing during the differentiation of stem cells into proliferative progenitor cells and decreasing in terminally differentiated cells (Larson et al., 1993; Hayashi et al., 2014; Stedman et al., 2015; Gayraud-Morel et al., 2018). In addition to rRNA, the expression of regulators controlling rRNA transcription or maturation also correlates with the bulk translation rate during stem cell differentiation. In zebrafish, the expression of *ddx27*, encoding a regulator of rRNA maturation, is detected in activated MuSCs and proliferating myoblasts, and decreases when cells terminally differentiate (Bennett et al., 2018). In mESCs and hESCs, the expression of rRNA and the regulators of ribosome biogenesis correlate with the overall translation rate both *in vivo* and *in vitro* (Watanabe-Susaki et al., 2014; Zaidi et al., 2016; Corsini et al., 2018).

Despite this broad correlation, it is notable that ribosome biogenesis is proportionally higher in stem cells than that in differentiating cells, relative to the rate of translation (Stedman et al., 2015; Zaidi et al., 2016; Gayraud-Morel et al., 2018). Strikingly, in the *Drosophila* germline, rRNA transcription is the highest in germline stem cells (GSCs), while translation is lower in GSCs than in differentiated offspring (Zhang et al., 2014; Sanchez et al., 2016). These observations suggest a specific requirement for increased ribosome biogenesis in stem cells.

Indeed, disrupting ribosomal biogenesis in many stem cell models leads to defects in both survival and self-renewal (Stedman et al., 2015; Sanchez et al., 2016; Bennett et al., 2018; Baral et al., 2020; Farooq et al., 2020; Saez et al., 2020), while fully differentiated somatic cells demonstrate less dependency on ribosome biogenesis (Bennett et al., 2018; Gayraud-Morel et al., 2018; Saez et al., 2020). Impairing rRNA transcription induces differentiation in *Drosophila* GSCs and mouse hematopoietic progenitor cells (Hayashi et al., 2014; Zhang et al., 2014). Importantly, this effect on hematopoiesis is not mediated by a global repression of translation or a cell cycle arrest as inhibiting overall protein synthesis by cycloheximide and puromycin, or inhibiting cell cycle by roscovitine, a CDK inhibitor, does not have the same effect (Pilz et al., 1987; Hayashi et al., 2014). Similarly, disrupting ribosomal biogenesis in mESCs or hESCs by either repressing rRNA maturation or transcription triggers the expression of differentiation-related genes, and this is coupled with a reduced expression of pluripotent mRNAs such as

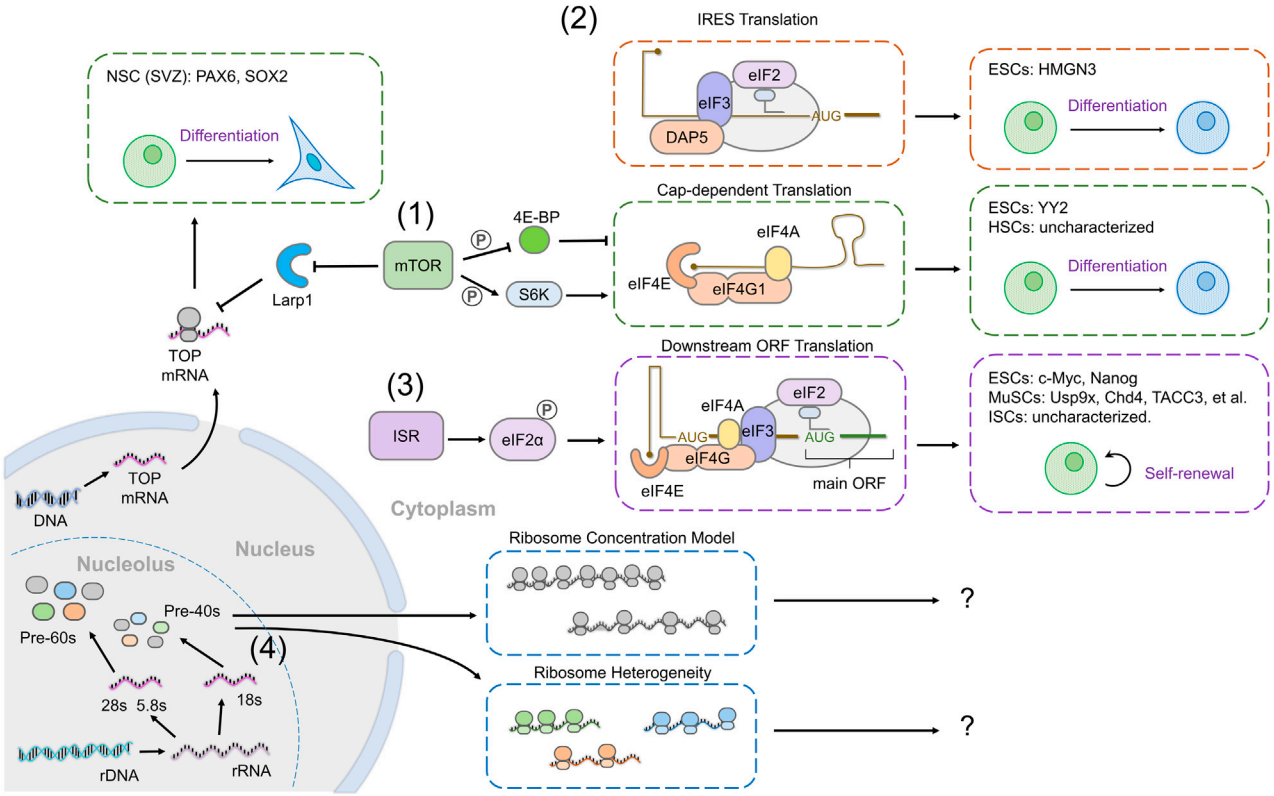

FIGURE 3 | Global translation mechanisms result in selective translation of specific transcripts to regulate stem cell fate. (1) Increased cap-dependent translation downstream of mTOR activity can result in selective translation of transcripts that have low translation efficiency. In ESCs, the mRNA encoding YY2 is one such target, in other tissues (HSCs), whether mTOR activity results in specific target expression is unknown (green box). mTOR also promotes the translation of mRNAs with TOP-like motifs, such as PAX6 and SOX2, which are translationally repressed during neuronal differentiation, in response to reduced mTOR activity. (2) Internal ribosome entry site (IRES)-mediated translation occurs when cap-binding is inhibited and can direct transcript-specific translation. In ESCs, DAP5 replaces eIF4G to promote IRES-dependent translation and ESC differentiation, through translation of HMGN3 (orange boxes). (3) p-eIF2α selectively promotes the translation of mRNAs with an upstream open reading frame (uORF). In ESCs, p-eIF2α promotes the translation of the mRNAs encoding c-Myc and Nanog. In MuSCs, p-eIF2α promotes the translation of mRNAs coding for Usp9x, Chd4, TACC3, etc. (purple box). (4) Ribosomes can selectively regulate mRNA translation. Two models have been proposed, the ribosome concentration model in which the amount of ribosomes available affects the translation of transcripts with high or low translation efficiency differently, or ribosome heterogeneity in which different ribosomal subunit composition directs specific translation of particular transcripts (blue boxes). Although ribosomes impact stem cell fate, no evidence directly supports either model to date.

OCT4 or SOX2 (You et al., 2015; Woolnough et al., 2016; Zhang H. et al., 2020). Importantly, the overexpression of fibrillarin, an important regulator of ribosomal RNA processing, can sustain pluripotency in the absence of LIF(Watanabe-Susaki et al., 2014) (**Figure 2** (3)).

Altogether, ribosomal biogenesis has begun to be recognized as a major factor maintaining pluripotency and self-renewal potential. Little work to date has sought to identify the upstream regulators ensuring the coordinated production of high levels of rRNA, ribosomal proteins, and assembly factors in stem cells. Nonetheless, it is clear that elevated ribosome levels are required to maintain stem cell potential. Together with strong evidence showing lower translation in stem cells, this suggests that ribosome levels and translation rates are not correlated in stem cells; one suggestion is that a large pool of ribosomes is required to prepare cells to rapidly increase their translation rates and change their proteome during differentiation (Saba et al., 2021). However, this is hard to reconcile with the fact that decreasing ribosome biogenesis promotes differentiation, indicating that either ribosome biogenesis itself or the availability of large numbers of ribosomes relative to the amount of transcripts is in itself important for stem cell biology.

FROM GLOBAL TRANSLATIONAL CONTROL TO SPECIFIC PROTEIN EXPRESSION: MECHANISMS ENSURING SELECTIVITY IN TRANSLATION IN STEM CELLS

How do changes in global translation rates or ribosome biogenesis affect stem cell maintenance? At least in part, the answer to this question lies in the selective translation of specific transcripts in response to changes that globally alter translation rates. Indeed, accumulating evidence show that specific mRNAs

are translated in stem or differentiated cells, without always being accompanied by changes in mRNA abundance (Unwin et al., 2006; Lu et al., 2009; Habowski et al., 2020). In other words, mRNA translation is a regulatory mechanism allowing gene expression changes independently of transcription.

Specific Targets of mTOR Activity

Although mTOR activity increases bulk translation by increasing the activity of initiation complexes, it disproportionally targets mRNAs containing TOP motifs for increased translation (Hsieh et al., 2012; Thoreen et al., 2012; Meyuhas and Kahan, 2015; Hong et al., 2017; Iezaki et al., 2018; Philippe et al., 2018; Jia et al., 2021). For instance, during the differentiation of SVZ neurogenic progenitors into neurons, both mTOR activity and bulk translation levels decrease (Baser et al., 2019). Notably, transcripts containing a pyrimidine-rich motif, similar to the TOP motif, are specifically repressed during differentiation; these encode both ribosomal proteins and transcription factors regulating stem cell identity such as Pax6 and Sox2, providing a mechanism by which mTOR activity correlates both with translation rates and with fate acquisition (Baser et al., 2019) (**Figure 3** (1)).

eIF4F-Mediated Cap-Dependent Translation and Non-Canonical Translation

Regulation of the activity and ability of the eIF4F complex to bind the mRNA cap also provides a means to achieve specificity in translation (Hernández et al., 2020). 4E-BP is a major regulator of eIF4F activity, and its regulation by mTOR and other signals makes it an ideal modulator to act as a switch for gene expression. Surprisingly, in mESCs, loss of function of *4E-BP1/2* does not influence the global translation rate, but results in the loss of pluripotency marker expression (Tahmasebi et al., 2016). This effect is mediated by the selective translation of Yin Yang 2 (YY2) upon ablation of 4E-BP. The *YY2* mRNA retains an intron in its 5' UTR, making its translation acutely sensitive to eIF4E activity due to a complex secondary structure (**Figure 3** (1)).

Other regulators of the assembly of the eIF4F complex also contribute to specific gene expression. In SVZ neural precursors, 4E-T competes with eIF4G for binding to eIF4E1, forming a complex which represses the translation of neurogenic mRNAs (Yang et al., 2014). Knock down of eIF4E1 or 4E-T promotes precursor differentiation while knocking down eIF4G1, on the contrary, impairs differentiation, indicating that in the SVZ, the main function of eIF4E1 in neural precursors is to repress the translation of neurogenic mRNAs.

Another regulator of eIF4F function is eIF4G2 (also named death-associated protein 5 (DAP5) or the novel APOBEC1 target 1 (NAT1)). eIF4G2 contains a similar C-terminal region to eIF4G1, enabling it to interact with eIF3 and eIF4A, but lacks an N-terminal eIF4E-binding domain, meaning that eIF4G2 promotes translation independently of eIF4F, and instead stimulates the translation of mRNAs containing an element known as an internal ribosome entry site (IRES) (Henis-Korenblit et al., 2002). DAP5 is required for neural and mesodermal differentiation of hESCs (Yoffe et al., 2016). The block in differentiation observed upon DAP5 depletion is not the consequence of a global translational repression, but instead it is due to selective IRES-driven translation by DAP5, in particular of the chromatin modifier HMGN3. Similarly, NAT1, the mouse homolog of DAP5, is required for the differentiation of mESCs (Sugiyama et al., 2017; Yamanaka et al., 2000). This was ascribed to NAT1 promoting the translation of two components of the ERK signaling pathway, which is required for ESC differentiation (**Figure 3** (2)). However, the role of DAP5 in ESCs is still not fully understood, and may differ between mouse and humans, as loss of DAP5 in primed mESCs results in reduced self-renewal and defects in neural differentiation, in contrast to loss of DAP5 in naïve mESCs, which prevents differentiation into all cell types (Takahashi et al., 2020).

Thus, the eIF4F complex is a central node through which multiple regulators can control bulk protein synthesis and the translation of specific subsets of mRNAs. Indeed, due to the presence of the eIF4A helicase in the eIF4F complex, mRNAs with long and/or complex secondary structures are particularly sensitive to eIF4F activity. Thus, changes in eIF4F activity (in the absence of some of the more specific regulations described earlier) can result in a binary regulation of individual mRNA translation (Leppek et al., 2018), enabling the fine control of gene expression. It is highly likely that in other situations where bulk translation is increased during stem cell differentiation, such as in HSCs, the effects of translation increase on cell identity are mediated by such mechanisms.

eIF2α-p Selectively Regulates mRNAs With uORFs

Although eIF2α phosphorylation dramatically reduces bulk translation, a subset of mRNAs is translated under these conditions (Baird et al., 2014). The best characterized example is the translation of the mRNA encoding ATF4 (Vattem and Wek, 2004; Asano, 2021), which contains two upstream open reading frames (uORFs), preventing the translation of the main open reading frame. Phosphorylation of eIF2 delays re-initiation of translation at the second uORF, resulting in initiation and translation at the main ATF-coding open reading frame.

Ribosome profiling in mESCs has revealed higher translation of uORFs in ESCs than EBs (Ingolia et al., 2011). Intriguingly, transcripts encoding the pluripotency factors, c-*Myc* and *Nanog*, have multiple uORFs (**Figure 3** (3)). Whether this change in uORF translation during ESC differentiation is related to eIF2 activity, and whether it plays a role in fate determination is yet to be established.

A more direct example of p-eIF2α-dependent expression of specific transcripts is seen in MuSCs, in which quiescence and self-renewal depend on eIF2α phosphorylation (Zismanov et al., 2016). A study of proteins upregulated by eIF2 phosphorylation without accompanying changes in mRNA levels identified several genes encoding mitotic spindle assembly factors, in particular *TACC3*. The *TACC3* transcript contains multiple uORFs and the protein is present in stem cells but downregulated in differentiating myoblasts. Importantly, TACC3 is required for MuSC expansion and self-renewal, demonstrating the functional

importance of selective translation of uORF-containing transcripts in stem cell maintenance (Vattem and Wek, 2004; Fujita et al., 2021) (**Figure 3** (3)).

Translational Specificity From Ribosomes: Effects of Ribosome Concentration and Subunit Composition

Stem cells require high levels of ribosome biogenesis for maintenance, despite lower translation rates, raising the possibility that ribosome numbers may play a role in specifically regulating stem cell gene expression. One model put forward to explain this is that different transcripts are differentially sensitive to ribosome concentration; mRNAs that are less efficiently translated would require a higher concentration of ribosomes to be expressed (Gabut et al., 2020; Lodish, 1974; Mills and Green, 2017) (**Figure 3** (4)). Evidence in support of this model has been found in the case of a mutation in a ribosomal protein chaperone that causes Diamond-Blackfan anemia, which leads to reduced ribosome numbers but specifically alters the translation of a susbset of transcripts (Khajuria et al., 2018). This study linked a lineage commitment decision in progenitors with ribosome levels for the first time, but as yet, the same findings have not been reproduced in a stem cell model. Future work will determine whether this model does indeed apply to stem cells, and importantly, what determines the sensitivity of particular mRNAs to ribosome concentration.

Another means by which specificity in transcript translation can be achieved by ribosomes is through the specific subunit composition of each ribosome (**Figure 3** (4)). Although ribosomes were initially assumed to be equivalent and to translate all mRNAs equally, work in the past decade has established that different ribosomes incorporate different ribosomal proteins. Different ribosomal proteins can confer mRNA sequence recognition (Genuth and Barna, 2018) and direct specific translation through IRES-dependent mechanisms. Intriguingly, mESCs display different ribosome subunit stoichiometries in monosomes and polysomes, and these associate with different mRNAs (Shi et al., 2017). Recent work in the *Drosophila* germline has shown that a paralogue of RpS5 is required for normal progression of differentiation and preferentially promotes translation of a subset of transcripts (Kong et al., 2019; Jang et al., 2021). These tantalizing observations raise the possibility that different incorporation of ribosomal subunits into ribosomes may regulate stem cell behavior; however, this has not yet been demonstrated.

CONCLUSIONS AND PERSPECTIVES

From an initial view of mRNA translation as a "housekeeping" function that is performed equally in all cells and for all transcripts, our understanding has evolved to grasp the complexity and precision of translational regulation and its ability to tune cell fate. This is especially evident in stem cells where the decision to self-renew and differentiate is exquisitely sensitive to changes in protein synthesis. This raises the important question as to why translational regulation is such a pervasive mechanism to control identity across stem cells. One possible explanation is that stem cell differentiation requires a large remodeling of the cell's proteome. Indeed, another important cellular function in stem cell biology is protein degradation, emphasizing the importance of accurate regulation of the cellular protein content in stem cell fate decisions (Llamas et al., 2020). Additionally, transcription is an inherently noisy process (Elowitz et al., 2002; Raj et al., 2010; Raser and O'Shea, 2005); this noise may play important roles in enabling cell decisions (Eldar and Elowitz, 2010). However, overlaying selective translation onto noisy gene expression could be a way to ensure that cells with the potential to adopt two different fates can only commit to one of these.

As our ability to probe translation increases, it is becoming more apparent that regulatory mechanisms-controlling global translation do not affect all transcripts equally; translation efficiency varies for individual mRNAs in different conditions. Thus, whether bulk translation changes are relevant to stem cell differentiation, or whether all the effects of changes in translation are mediated by the altered translation of a few key transcripts is still an open question.

In addition to contributing to our understanding of the mechanisms underlying self-renewal and differentiation and to our ability to manipulate those processes, and studying translation in stem cells will yield important advances in the study of aging. Reducing mTOR activity has long been known to extend the lifespan and promote continued health of organisms (Liu and Sabatini, 2020). Although other targets of mTOR have been implicated, S6K or eIF4E reduction, or 4E-BP overexpression, can contribute to lifespan extension, suggesting that decreased translation rates are at least partly responsible (Hansen et al., 2007; Syntichaki et al., 2007; Selman et al., 2009; Zid et al., 2009). Moreover, recent work has shown that both RNA Pol I and RNA Pol III, which synthesize rRNAs, mediate lifespan control downstream of mTOR, and that, in *Drosophila*, they exert their effects on lifespan specifically in intestinal stem cells (Filer et al., 2017; Martinez Corrales et al., 2020). As we deepen our understanding of how translational regulation influences stem cell behavior, new avenues for interventions that mitigate the effects of aging will be opened up.

AUTHOR CONTRIBUTIONS

RW and MA contributed to conceptualization of the manuscript, wrote the draft, and edited it.

FUNDING

This work was funded by an MRC Career Development Award MR/P009646/2.

ACKNOWLEDGMENTS

The authors thank members of the Amoyel lab for discussions.

REFERENCES

Abraham, K. J., Khosraviani, N., Chan, J. N. Y., Gorthi, A., Samman, A., Zhao, D. Y., et al. (2020). Nucleolar RNA Polymerase II Drives Ribosome Biogenesis. *Nature* 585, 298–302. doi:10.1038/s41586-020-2497-0

Albert, V., and Hall, M. N. (2015). mTOR Signaling in Cellular and Organismal Energetics. *Curr. Opin. Cel Biol.* 33, 55–66. doi:10.1016/j.ceb.2014.12.001

Asano, K. (2021). Origin of Translational Control by eIF2α Phosphorylation: Insights from Genome-wide Translational Profiling Studies in Fission Yeast. *Curr. Genet.* 67, 359–368. doi:10.1007/s00294-020-01149-w

Baird, T. D., Palam, L. R., Fusakio, M. E., Willy, J. A., Davis, C. M., McClintick, J. N., et al. (2014). Selective mRNA Translation during eIF2 Phosphorylation Induces Expression of IBTKα. *MBoC* 25, 1686–1697. doi:10.1091/mbc.e14-02-0704

Baral, S. S., Lieux, M. E., and DiMario, P. J. (2020). Nucleolar Stress in Drosophila Neuroblasts, a Model for Human Ribosomopathies. *Biol. Open* 9. doi:10.1242/bio.046565

Baser, A., Skabkin, M., Kleber, S., Dang, Y., Gülcüler Balta, G. S., Kalamakis, G., et al. (2019). Onset of Differentiation Is post-transcriptionally Controlled in Adult Neural Stem Cells. *Nature* 566, 100–104. doi:10.1038/s41586-019-0888-x

Bennett, A. H., O'Donohue, M.-F., Gundry, S. R., Chan, A. T., Widrick, J., Draper, I., et al. (2018). RNA Helicase, DDX27 Regulates Skeletal Muscle Growth and Regeneration by Modulation of Translational Processes. *Plos Genet.* 14, e1007226. doi:10.1371/journal.pgen.1007226

Blanco, S., Bandiera, R., Popis, M., Hussain, S., Lombard, P., Aleksic, J., et al. (2016). Stem Cell Function and Stress Response Are Controlled by Protein Synthesis. *Nature* 534, 335–340. doi:10.1038/nature18282

Blatt, P., Martin, E. T., Breznak, S. M., and Rangan, P. (2020). Post-transcriptional Gene Regulation Regulates Germline Stem Cell to Oocyte Transition during Drosophila Oogenesis. *Curr. Top. Dev. Biol.* 140, 3–34. doi:10.1016/bs.ctdb.2019.10.003

Bonaguidi, M. A., Wheeler, M. A., Shapiro, J. S., Stadel, R. P., Sun, G. J., Ming, G.-l., et al. (2011). *In Vivo* clonal Analysis Reveals Self-Renewing and Multipotent Adult Neural Stem Cell Characteristics. *Cell* 145, 1142–1155. doi:10.1016/j.cell.2011.05.024

Brunn, G. J., Hudson, C. C., Sekulic´, A., Williams, J. M., Hosoi, H., Houghton, P. J., et al. (1997). Phosphorylation of the Translational Repressor PHAS-I by the Mammalian Target of Rapamycin. *Science* 277, 99–101. doi:10.1126/science.277.5322.99

Chell, J. M., and Brand, A. H. (2010). Nutrition-responsive Glia Control Exit of Neural Stem Cells from Quiescence. *Cell* 143, 1161–1173. doi:10.1016/j.cell.2010.12.007

Chen, C., Liu, Y., Liu, Y., and Zheng, P. (2009). mTOR Regulation and Therapeutic Rejuvenation of Aging Hematopoietic Stem Cells. *Sci. Signal.* 2, ra75. doi:10.1126/scisignal.2000559

Cloetta, D., Thomanetz, V., Baranek, C., Lustenberger, R. M., Lin, S., Oliveri, F., et al. (2013). Inactivation of mTORC1 in the Developing Brain Causes Microcephaly and Affects Gliogenesis. *J. Neurosci.* 33, 7799–7810. doi:10.1523/jneurosci.3294-12.2013

Corsini, N. S., Peer, A. M., Moeseneder, P., Roiuk, M., Burkard, T. R., Theussl, H.-C., et al. (2018). Coordinated Control of mRNA and rRNA Processing Controls Embryonic Stem Cell Pluripotency and Differentiation. *Cell Stem Cell* 22, 543–558 e512. doi:10.1016/j.stem.2018.03.002

Costa-Mattioli, M., and Walter, P. (2020). The Integrated Stress Response: From Mechanism to Disease. *Science* 368. doi:10.1126/science.aat5314

de la Cruz, J., Gómez-Herreros, F., Rodríguez-Galán, O., Begley, V., de la Cruz Muñoz-Centeno, M., and Chávez, S. (2018). Feedback Regulation of Ribosome Assembly. *Curr. Genet.* 64, 393–404. doi:10.1007/s00294-017-0764-x

de Sousa Abreu, R., Penalva, L. O., Marcotte, E. M., and Vogel, C. (2009). Global Signatures of Protein and mRNA Expression Levels. *Mol. Biosyst.* 5, 1512–1526. doi:10.1039/b908315d

Dieterich, D. C., Hodas, J. J. L., Gouzer, G., Shadrin, I. Y., Ngo, J. T., Triller, A., et al. (2010). *In Situ* visualization and Dynamics of Newly Synthesized Proteins in Rat Hippocampal Neurons. *Nat. Neurosci.* 13, 897–905. doi:10.1038/nn.2580

Dieterich, D. C., Lee, J. J., Link, A. J., Graumann, J., Tirrell, D. A., and Schuman, E. M. (2007). Labeling, Detection and Identification of Newly Synthesized Proteomes with Bioorthogonal Non-canonical Amino-Acid Tagging. *Nat. Protoc.* 2, 532–540. doi:10.1038/nprot.2007.52

Dieterich, D. C., Link, A. J., Graumann, J., Tirrell, D. A., and Schuman, E. M. (2006). Selective Identification of Newly Synthesized Proteins in Mammalian Cells Using Bioorthogonal Noncanonical Amino Acid Tagging (BONCAT). *Proc. Natl. Acad. Sci.* 103, 9482–9487. doi:10.1073/pnas.0601637103

Ding, Y., Liu, Z., and Liu, F. (2021). Transcriptional and Epigenetic Control of Hematopoietic Stem Cell Fate Decisions in Vertebrates. *Dev. Biol.* 475, 156–164. doi:10.1016/j.ydbio.2021.03.003

Duncan, R., Milburn, S. C., and Hershey, J. W. (1987). Regulated Phosphorylation and Low Abundance of HeLa Cell Initiation Factor eIF-4F Suggest a Role in Translational Control. Heat Shock Effects on eIF-4F. *J. Biol. Chem.* 262, 380–388. doi:10.1016/s0021-9258(19)75938-9

Easley, C. A., Ben-Yehudah, A., Redinger, C. J., Oliver, S. L., Varum, S. T., Eisinger, V. M., et al. (2010). mTOR-Mediated Activation of P70 S6K Induces Differentiation of Pluripotent Human Embryonic Stem Cells. *Cell Reprogramming* 12, 263–273. doi:10.1089/cell.2010.0011

Eldar, A., and Elowitz, M. B. (2010). Functional Roles for Noise in Genetic Circuits. *Nature* 467, 167–173. doi:10.1038/nature09326

Elowitz, M. B., Levine, A. J., Siggia, E. D., and Swain, P. S. (2002). Stochastic Gene Expression in a Single Cell. *Science* 297, 1183–1186. doi:10.1126/science.1070919

Farooq, M., Lindbæk, L., Krogh, N., Doganli, C., Keller, C., Mönnich, M., et al. (2020). RRP7A Links Primary Microcephaly to Dysfunction of Ribosome Biogenesis, Resorption of Primary Cilia, and Neurogenesis. *Nat. Commun.* 11, 5816. doi:10.1038/s41467-020-19658-0

Ferrari, S., Bandi, H. R., Hofsteenge, J., Bussian, B. M., and Thomas, G. (1991). Mitogen-activated 70K S6 Kinase. Identification of *In Vitro* 40 S Ribosomal S6 Phosphorylation Sites. *J. Biol. Chem.* 266, 22770–22775. doi:10.1016/s0021-9258(18)54634-2

Ferretti, M. B., Ghalei, H., Ward, E. A., Potts, E. L., and Karbstein, K. (2017). Rps26 Directs mRNA-specific Translation by Recognition of Kozak Sequence Elements. *Nat. Struct. Mol. Biol.* 24, 700–707. doi:10.1038/nsmb.3442

Filer, D., Thompson, M. A., Takhaveev, V., Dobson, A. J., Kotronaki, I., Green, J. W. M., et al. (2017). RNA Polymerase III Limits Longevity Downstream of TORC1. *Nature* 552, 263–267. doi:10.1038/nature25007

Fonseca, B. D., Zakaria, C., Jia, J.-J., Graber, T. E., Svitkin, Y., Tahmasebi, S., et al. (2015). La-related Protein 1 (LARP1) Represses Terminal Oligopyrimidine (TOP) mRNA Translation Downstream of mTOR Complex 1 (mTORC1). *J. Biol. Chem.* 290, 15996–16020. doi:10.1074/jbc.m114.621730

Friend, K., Brooks, H. A., Propson, N. E., Thomson, J. A., and Kimble, J. (2015). Embryonic Stem Cell Growth Factors Regulate eIF2α Phosphorylation. *PLoS One* 10, e0139076. doi:10.1371/journal.pone.0139076

Fujita, R., Jamet, S., Lean, G., Cheng, H. C. M., Hebert, S., Kleinman, C. L., et al. (2021). Satellite Cell Expansion Is Mediated by P-eIF2alpha-dependent Tacc3 Translation. *Development*, 148. doi:10.1242/dev.194480

Gabut, M., Bourdelais, F., and Durand, S. (2020). Ribosome and Translational Control in Stem Cells. *Cells* 9. doi:10.3390/cells9020497

Gayraud-Morel, B., Le Bouteiller, M., Commere, P. H., Cohen-Tannoudji, M., and Tajbakhsh, S. (2018). Notchless Defines a Stage-specific Requirement for Ribosome Biogenesis during Lineage Progression in Adult Skeletal Myogenesis. *Development*, 145. doi:10.1242/dev.162636

Genuth, N. R., and Barna, M. (2018). The Discovery of Ribosome Heterogeneity and its Implications for Gene Regulation and Organismal Life. *Mol. Cel* 71, 364–374. doi:10.1016/j.molcel.2018.07.018

Gingras, A.-C., Gygi, S. P., Raught, B., Polakiewicz, R. D., Abraham, R. T., Hoekstra, M. F., et al. (1999). Regulation of 4E-BP1 Phosphorylation: a Novel Two-step Mechanism. *Genes Dev.* 13, 1422–1437. doi:10.1101/gad.13.11.1422

Gregorian, C., Nakashima, J., Le Belle, J., Ohab, J., Kim, R., Liu, A., et al. (2009). Pten Deletion in Adult Neural Stem/progenitor Cells Enhances Constitutive Neurogenesis. *J. Neurosci.* 29, 1874–1886. doi:10.1523/jneurosci.3095-08.2009

Groszer, M., Erickson, R., Scripture-Adams, D. D., Dougherty, J. D., Le Belle, J., Zack, J. A., et al. (2006). PTEN Negatively Regulates Neural Stem Cell Self-Renewal by Modulating G0-G1 Cell Cycle Entry. *Proc. Natl. Acad. Sci.* 103, 111–116. doi:10.1073/pnas.0509939103

Guo, W., Lasky, J. L., Chang, C.-J., Mosessian, S., Lewis, X., Xiao, Y., et al. (2008). Multi-genetic Events Collaboratively Contribute to Pten-Null Leukaemia Stem-Cell Formation. *Nature* 453, 529–533. doi:10.1038/nature06933

Habowski, A. N., Flesher, J. L., Bates, J. M., Tsai, C.-F., Martin, K., Zhao, R., et al. (2020). Transcriptomic and Proteomic Signatures of Stemness and Differentiation in the colon Crypt. *Commun. Biol.* 3, 453. doi:10.1038/s42003-020-01181-z

Haller, S., Kapuria, S., Riley, R. R., O'Leary, M. N., Schreiber, K. H., Andersen, J. K., et al. (2017). mTORC1 Activation during Repeated Regeneration Impairs Somatic Stem Cell Maintenance. *Cell Stem Cell* 21, 806–818 e805. doi:10.1016/j.stem.2017.11.008

Hansen, M., Taubert, S., Crawford, D., Libina, N., Lee, S.-J., and Kenyon, C. (2007). Lifespan Extension by Conditions that Inhibit Translation in *Caenorhabditis elegans*. *Aging Cell* 6, 95–110. doi:10.1111/j.1474-9726.2006.00267.x

Hara, K., Yonezawa, K., Kozlowski, M. T., Sugimoto, T., Andrabi, K., Weng, Q.-P., et al. (1997). Regulation of eIF-4E BP1 Phosphorylation by mTOR. *J. Biol. Chem.* 272, 26457–26463. doi:10.1074/jbc.272.42.26457

Hartman, N. W., Lin, T. V., Zhang, L., Paquelet, G. E., Feliciano, D. M., and Bordey, A. (2013). mTORC1 Targets the Translational Repressor 4E-BP2, but Not S6 Kinase 1/2, to Regulate Neural Stem Cell Self-Renewal *In Vivo*. *Cel Rep.* 5, 433–444. doi:10.1016/j.celrep.2013.09.017

Hayashi, Y., Kuroda, T., Kishimoto, H., Wang, C., Iwama, A., and Kimura, K. (2014). Downregulation of rRNA Transcription Triggers Cell Differentiation. *PLoS One* 9, e98586. doi:10.1371/journal.pone.0098586

He, J., Kang, L., Wu, T., Zhang, J., Wang, H., Gao, H., et al. (2012). An Elaborate Regulation of Mammalian Target of Rapamycin Activity Is Required for Somatic Cell Reprogramming Induced by Defined Transcription Factors. *Stem Cell Dev.* 21, 2630–2641. doi:10.1089/scd.2012.0015

Henis-Korenblit, S., Shani, G., Sines, T., Marash, L., Shohat, G., and Kimchi, A. (2002). The Caspase-Cleaved DAP5 Protein Supports Internal Ribosome Entry Site-Mediated Translation of Death Proteins. *Proc. Natl. Acad. Sci.* 99, 5400–5405. doi:10.1073/pnas.082102499

Hernández, G., García, A., Sonenberg, N., and Lasko, P. (2020). Unorthodox Mechanisms to Initiate Translation Open Novel Paths for Gene Expression. *J. Mol. Biol.* 432, 166702. doi:10.1016/j.jmb.2020.10.035

Hong, S., Freeberg, M. A., Han, T., Kamath, A., Yao, Y., Fukuda, T., et al. (2017). LARP1 Functions as a Molecular Switch for mTORC1-Mediated Translation of an Essential Class of mRNAs. *Elife* 6. doi:10.7554/eLife.25237

Hsieh, A. C., Liu, Y., Edlind, M. P., Ingolia, N. T., Janes, M. R., Sher, A., et al. (2012). The Translational Landscape of mTOR Signalling Steers Cancer Initiation and Metastasis. *Nature* 485, 55–61. doi:10.1038/nature10912

Iadevaia, V., Caldarola, S., Tino, E., Amaldi, F., and Loreni, F. (2008). All translation elongation factors and the e, f, and h subunits of translation initiation factor 3 are encoded by 5′-terminal oligopyrimidine (TOP) mRNAs. *RNA* 14, 1730–1736. doi:10.1261/rna.1037108

Iezaki, T., Horie, T., Fukasawa, K., Kitabatake, M., Nakamura, Y., Park, G., et al. (2018). Translational Control of Sox9 RNA by mTORC1 Contributes to Skeletogenesis. *Stem Cel Rep.* 11, 228–241. doi:10.1016/j.stemcr.2018.05.020

Ingolia, N. T., Lareau, L. F., and Weissman, J. S. (2011). Ribosome Profiling of Mouse Embryonic Stem Cells Reveals the Complexity and Dynamics of Mammalian Proteomes. *Cell* 147, 789–802. doi:10.1016/j.cell.2011.10.002

Jackson, R. J., Hellen, C. U. T., and Pestova, T. V. (2010). The Mechanism of Eukaryotic Translation Initiation and Principles of its Regulation. *Nat. Rev. Mol. Cel Biol* 11, 113–127. doi:10.1038/nrm2838

Jang, S., Lee, J., Mathews, J., Ruess, H., Williford, A. O., Rangan, P., et al. (2021). The Drosophila Ribosome Protein S5 Paralog RpS5b Promotes Germ Cell and Follicle Cell Differentiation during Oogenesis. *Development*, 148. doi:10.1242/dev.199511

Jia, J.-J., Lahr, R. M., Solgaard, M. T., Moraes, B. J., Pointet, R., Yang, A.-D., et al. (2021). mTORC1 Promotes TOP mRNA Translation through Site-specific Phosphorylation of LARP1. *Nucleic Acids Res.* 49, 3461–3489. doi:10.1093/nar/gkaa1239

Kapuria, S., Karpac, J., Biteau, B., Hwangbo, D., and Jasper, H. (2012). Notch-mediated Suppression of TSC2 Expression Regulates Cell Differentiation in the Drosophila Intestinal Stem Cell Lineage. *Plos Genet.* 8, e1003045. doi:10.1371/journal.pgen.1003045

Khajuria, R. K., Munschauer, M., Ulirsch, J. C., Fiorini, C., Ludwig, L. S., McFarland, S. K., et al. (2018). Ribosome Levels Selectively Regulate Translation and Lineage Commitment in Human Hematopoiesis. *Cell* 173, 90–103. doi:10.1016/j.cell.2018.02.036

Kim, H. J., Osteil, P., Humphrey, S. J., Cinghu, S., Oldfield, A. J., Patrick, E., et al. (2020). Transcriptional Network Dynamics during the Progression of Pluripotency Revealed by Integrative Statistical Learning. *Nucleic Acids Res.* 48, 1828–1842. doi:10.1093/nar/gkz1179

Kim, J., Chu, J., Shen, X., Wang, J., and Orkin, S. H. (2008). An Extended Transcriptional Network for Pluripotency of Embryonic Stem Cells. *Cell* 132, 1049–1061. doi:10.1016/j.cell.2008.02.039

Klinge, S., and Woolford, J. L., Jr. (2019). Ribosome Assembly Coming into Focus. *Nat. Rev. Mol. Cel Biol* 20, 116–131. doi:10.1038/s41580-018-0078-y

Kong, J., Han, H., Bergalet, J., Bouvrette, L. P. B., Hernández, G., Moon, N.-S., et al. (2019). A Ribosomal Protein S5 Isoform Is Essential for Oogenesis and Interacts with Distinct RNAs in *Drosophila melanogaster*. *Sci. Rep.* 9, 13779. doi:10.1038/s41598-019-50357-z

Krichevsky, A. M., Metzer, E., and Rosen, H. (1999). Translational Control of Specific Genes during Differentiation of HL-60 Cells. *J. Biol. Chem.* 274, 14295–14305. doi:10.1074/jbc.274.20.14295

Larson, D. E., Xie, W., Glibetic, M., O'Mahony, D., Sells, B. H., and Rothblum, L. I. (1993). Coordinated Decreases in rRNA Gene Transcription Factors and rRNA Synthesis during Muscle Cell Differentiation. *Proc. Natl. Acad. Sci.* 90, 7933–7936. doi:10.1073/pnas.90.17.7933

Leppek, K., Das, R., and Barna, M. (2018). Functional 5′ UTR mRNA Structures in Eukaryotic Translation Regulation and How to Find Them. *Nat. Rev. Mol. Cel Biol* 19, 158–174. doi:10.1038/nrm.2017.103

Liu, G. Y., and Sabatini, D. M. (2020). mTOR at the Nexus of Nutrition, Growth, Ageing and Disease. *Nat. Rev. Mol. Cel Biol* 21, 183–203. doi:10.1038/s41580-019-0199-y

Llamas, E., Alirzayeva, H., Loureiro, R., and Vilchez, D. (2020). The Intrinsic Proteostasis Network of Stem Cells. *Curr. Opin. Cel Biol.* 67, 46–55. doi:10.1016/j.ceb.2020.08.005

Llorens-Bobadilla, E., Zhao, S., Baser, A., Saiz-Castro, G., Zwadlo, K., and Martin-Villalba, A. (2015). Single-Cell Transcriptomics Reveals a Population of Dormant Neural Stem Cells that Become Activated upon Brain Injury. *Cell Stem Cell* 17, 329–340. doi:10.1016/j.stem.2015.07.002

Lodish, H. F. (1974). Model for the Regulation of mRNA Translation Applied to Haemoglobin Synthesis. *Nature* 251, 385–388. doi:10.1038/251385a0

Lu, R., Markowetz, F., Unwin, R. D., Leek, J. T., Airoldi, E. M., MacArthur, B. D., et al. (2009). Systems-level Dynamic Analyses of Fate Change in Murine Embryonic Stem Cells. *Nature* 462, 358–362. doi:10.1038/nature08575

Lunyak, V. V., and Rosenfeld, M. G. (2008). Epigenetic Regulation of Stem Cell Fate. *Hum. Mol. Genet.* 17, R28–R36. doi:10.1093/hmg/ddn149

Ma, X. M., and Blenis, J. (2009). Molecular Mechanisms of mTOR-Mediated Translational Control. *Nat. Rev. Mol. Cel Biol* 10, 307–318. doi:10.1038/nrm2672

Magee, J. A., Ikenoue, T., Nakada, D., Lee, J. Y., Guan, K.-L., and Morrison, S. J. (2012). Temporal Changes in PTEN and mTORC2 Regulation of Hematopoietic Stem Cell Self-Renewal and Leukemia Suppression. *Cell Stem Cell* 11, 415–428. doi:10.1016/j.stem.2012.05.026

Magri, L., Cambiaghi, M., Cominelli, M., Alfaro-Cervello, C., Cursi, M., Pala, M., et al. (2011). Sustained Activation of mTOR Pathway in Embryonic Neural Stem Cells Leads to Development of Tuberous Sclerosis Complex-Associated Lesions. *Cell Stem Cell* 9, 447–462. doi:10.1016/j.stem.2011.09.008

Mahoney, C., Feliciano, D. M., Bordey, A., and Hartman, N. W. (2016). Switching on mTORC1 Induces Neurogenesis but Not Proliferation in Neural Stem Cells of Young Mice. *Neurosci. Lett.* 614, 112–118. doi:10.1016/j.neulet.2015.12.042

Maier, T., Güell, M., and Serrano, L. (2009). Correlation of mRNA and Protein in Complex Biological Samples. *FEBS Lett.* 583, 3966–3973. doi:10.1016/j.febslet.2009.10.036

Martínez Corrales, G., Filer, D., Wenz, K. C., Rogan, A., Phillips, G., Li, M., et al. (2020). Partial Inhibition of RNA Polymerase I Promotes Animal Health and Longevity. *Cel Rep.* 30, 1661–1669 e1664. doi:10.1016/j.celrep.2020.01.017

Meyuhas, O., and Kahan, T. (2015). The Race to Decipher the Top Secrets of TOP mRNAs. *Biochim. Biophys. Acta (Bba) - Gene Regul. Mech.* 1849, 801–811. doi:10.1016/j.bbagrm.2014.08.015

Micchelli, C. A., and Perrimon, N. (2006). Evidence that Stem Cells Reside in the Adult Drosophila Midgut Epithelium. *Nature* 439, 475–479. doi:10.1038/nature04371

Mills, E. W., and Green, R. (2017). Ribosomopathies: There's Strength in Numbers. *Science* 358. doi:10.1126/science.aan2755

Moignard, V., Macaulay, I. C., Swiers, G., Buettner, F., Schütte, J., Calero-Nieto, F. J., et al. (2013). Characterization of Transcriptional Networks in Blood Stem and Progenitor Cells Using High-Throughput Single-Cell Gene Expression Analysis. *Nat. Cel Biol* 15, 363–372. doi:10.1038/ncb2709

Murakami, M., Ichisaka, T., Maeda, M., Oshiro, N., Hara, K., Edenhofer, F., et al. (2004). mTOR Is Essential for Growth and Proliferation in Early Mouse Embryos and Embryonic Stem Cells. *Mol. Cel Biol* 24, 6710–6718. doi:10.1128/mcb.24.15.6710-6718.2004

Obata, F., Tsuda-Sakurai, K., Yamazaki, T., Nishio, R., Nishimura, K., Kimura, M., et al. (2018). Nutritional Control of Stem Cell Division through S-Adenosylmethionine in Drosophila Intestine. *Dev. Cel* 44, 741–751. doi:10.1016/j.devcel.2018.02.017

Ohbo, K., and Tomizawa, S.-i. (2015). Epigenetic Regulation in Stem Cell Development, Cell Fate Conversion, and Reprogramming. *Biomol. Concepts* 6, 1–9. doi:10.1515/bmc-2014-0036

Ohlstein, B., and Spradling, A. (2006). The Adult Drosophila Posterior Midgut Is Maintained by Pluripotent Stem Cells. *Nature* 439, 470–474. doi:10.1038/nature04333

Otsuki, L., and Brand, A. H. (2018). Cell Cycle Heterogeneity Directs the Timing of Neural Stem Cell Activation from Quiescence. *Science* 360, 99–102. doi:10.1126/science.aan8795

Pakos-Zebrucka, K., Koryga, I., Mnich, K., Ljujic, M., Samali, A., and Gorman, A. M. (2016). The Integrated Stress Response. *EMBO Rep.* 17, 1374–1395. doi:10.15252/embr.201642195

Paliouras, G. N., Hamilton, L. K., Aumont, A., Joppe, S. E., Barnabe-Heider, F., and Fernandes, K. J. L. (2012). Mammalian Target of Rapamycin Signaling Is a Key Regulator of the Transit-Amplifying Progenitor Pool in the Adult and Aging Forebrain. *J. Neurosci.* 32, 15012–15026. doi:10.1523/jneurosci.2248-12.2012

Pelletier, J., Thomas, G., and Volarević, S. (2018). Ribosome Biogenesis in Cancer: New Players and Therapeutic Avenues. *Nat. Rev. Cancer* 18, 51–63. doi:10.1038/nrc.2017.104

Philippe, L., Vasseur, J.-J., Debart, F., and Thoreen, C. C. (2018). La-related Protein 1 (LARP1) Repression of TOP mRNA Translation Is Mediated through its Cap-Binding Domain and Controlled by an Adjacent Regulatory Region. *Nucleic Acids Res.* 46, 1457–1469. doi:10.1093/nar/gkx1237

Pilz, R. B., Van den Berghe, G., and Boss, G. R. (1987). Induction of HL-60 Differentiation by Starvation for a Single Essential Amino Acid but Not by Protein Synthesis Inhibitors. *J. Clin. Invest.* 79, 1006–1009. doi:10.1172/jci112867

Powers, T., and Walter, P. (1999). Regulation of Ribosome Biogenesis by the Rapamycin-Sensitive TOR-Signaling Pathway inSaccharomyces Cerevisiae. *MBoC* 10, 987–1000. doi:10.1091/mbc.10.4.987

Quan, Z., Sun, P., Lin, G., and Xi, R. (2013). TSC1/2 Regulates Intestinal Stem Cell Maintenance and Lineage Differentiation through Rheb-TORC1-S6k but Independently of Nutritional Status or Notch Regulation. *J. Cel Sci* 126, 3884–3892. doi:10.1242/jcs.125294

Raj, A., Rifkin, S. A., Andersen, E., and van Oudenaarden, A. (2010). Variability in Gene Expression Underlies Incomplete Penetrance. *Nature* 463, 913–918. doi:10.1038/nature08781

Raser, J. M., and O'Shea, E. K. (2005). Noise in Gene Expression: Origins, Consequences, and Control. *Science* 309, 2010–2013. doi:10.1126/science.1105891

Raught, B., Peiretti, F., Gingras, A.-C., Livingstone, M., Shahbazian, D., Mayeur, G. L., et al. (2004). Phosphorylation of Eucaryotic Translation Initiation Factor 4B Ser422 Is Modulated by S6 Kinases. *EMBO J.* 23, 1761–1769. doi:10.1038/sj.emboj.7600193

Richmond, C. A., Shah, M. S., Deary, L. T., Trotier, D. C., Thomas, H., Ambruzs, D. M., et al. (2015). Dormant Intestinal Stem Cells Are Regulated by PTEN and Nutritional Status. *Cel Rep.* 13, 2403–2411. doi:10.1016/j.celrep.2015.11.035

Rodgers, J. T., King, K. Y., Brett, J. O., Cromie, M. J., Charville, G. W., Maguire, K. K., et al. (2014). mTORC1 Controls the Adaptive Transition of Quiescent Stem Cells from G0 to GAlert. *Nature* 510, 393–396. doi:10.1038/nature13255

Roux, P. P., and Topisirovic, I. (2018). Signaling Pathways Involved in the Regulation of mRNA Translation. *Mol. Cel Biol* 38. doi:10.1128/MCB.00070-18

Saba, J. A., Liakath-Ali, K., Green, R., and Watt, F. M. (2021). Translational Control of Stem Cell Function. *Nat. Rev. Mol. Cel Biol* 22, 671–690. doi:10.1038/s41580-021-00386-2

Saez, I., Gerbracht, J. V., Koyuncu, S., Lee, H. J., Horn, M., Kroef, V., et al. (2020). The E3 Ubiquitin Ligase UBR 5 Interacts with the H/ACA Ribonucleoprotein Complex and Regulates Ribosomal RNA Biogenesis in Embryonic Stem Cells. *FEBS Lett.* 594, 175–188. doi:10.1002/1873-3468.13559

Sagner, A., Zhang, I., Watson, T., Lazaro, J., Melchionda, M., and Briscoe, J. (2021). A Shared Transcriptional Code Orchestrates Temporal Patterning of the central Nervous System. *Plos Biol.* 19, e3001450. doi:10.1371/journal.pbio.3001450

Sampath, P., Pritchard, D. K., Pabon, L., Reinecke, H., Schwartz, S. M., Morris, D. R., et al. (2008). A Hierarchical Network Controls Protein Translation during Murine Embryonic Stem Cell Self-Renewal and Differentiation. *Cell Stem Cell* 2, 448–460. doi:10.1016/j.stem.2008.03.013

Sanchez, C. G., Teixeira, F. K., Czech, B., Preall, J. B., Zamparini, A. L., Seifert, J. R. K., et al. (2016). Regulation of Ribosome Biogenesis and Protein Synthesis Controls Germline Stem Cell Differentiation. *Cell Stem Cell* 18, 276–290. doi:10.1016/j.stem.2015.11.004

Schwanhäusser, B., Busse, D., Li, N., Dittmar, G., Schuchhardt, J., Wolf, J., et al. (2011). Global Quantification of Mammalian Gene Expression Control. *Nature* 473, 337–342. doi:10.1038/nature10098

Selman, C., Tullet, J. M. A., Wieser, D., Irvine, E., Lingard, S. J., Choudhury, A. I., et al. (2009). Ribosomal Protein S6 Kinase 1 Signaling Regulates Mammalian Life Span. *Science* 326, 140–144. doi:10.1126/science.1177221

Shah, P., Ding, Y., Niemczyk, M., Kudla, G., and Plotkin, J. B. (2013). Rate-limiting Steps in Yeast Protein Translation. *Cell* 153, 1589–1601. doi:10.1016/j.cell.2013.05.049

Shi, Z., Fujii, K., Kovary, K. M., Genuth, N. R., Röst, H. L., Teruel, M. N., et al. (2017). Heterogeneous Ribosomes Preferentially Translate Distinct Subpools of mRNAs Genome-wide. *Mol. Cel* 67, 71–83. doi:10.1016/j.molcel.2017.05.021

Showkat, M., Beigh, M. A., and Andrabi, K. I. (2014). mTOR Signaling in Protein Translation Regulation: Implications in Cancer Genesis and Therapeutic Interventions. *Mol. Biol. Int.* 2014, 686984. doi:10.1155/2014/686984

Signer, R. A. J., Magee, J. A., Salic, A., and Morrison, S. J. (2014). Haematopoietic Stem Cells Require a Highly Regulated Protein Synthesis Rate. *Nature* 509, 49–54. doi:10.1038/nature13035

Signer, R. A. J., Qi, L., Zhao, Z., Thompson, D., Sigova, A. A., Fan, Z. P., et al. (2016). The Rate of Protein Synthesis in Hematopoietic Stem Cells Is Limited Partly by 4E-BPs. *Genes Dev.* 30, 1698–1703. doi:10.1101/gad.282756.116

Slaidina, M., and Lehmann, R. (2014). Translational Control in Germline Stem Cell Development. *J. Cel Biol* 207, 13–21. doi:10.1083/jcb.201407102

Sonenberg, N., and Hinnebusch, A. G. (2009). Regulation of Translation Initiation in Eukaryotes: Mechanisms and Biological Targets. *Cell* 136, 731–745. doi:10.1016/j.cell.2009.01.042

Sousa-Nunes, R., Yee, L. L., and Gould, A. P. (2011). Fat Cells Reactivate Quiescent Neuroblasts via TOR and Glial Insulin Relays in Drosophila. *Nature* 471, 508–512. doi:10.1038/nature09867

Spevak, C. C., Elias, H. K., Kannan, L., Ali, M. A. E., Martin, G. H., Selvaraj, S., et al. (2020). Hematopoietic Stem and Progenitor Cells Exhibit Stage-specific Translational Programs via mTOR- and CDK1-dependent Mechanisms. *Cell Stem Cell* 26, 755–765. doi:10.1016/j.stem.2019.12.006

Stedman, A., Beck-Cormier, S., Le Bouteiller, M., Raveux, A., Vandormael-Pournin, S., Coqueran, S., et al. (2015). Ribosome Biogenesis Dysfunction Leads to P53-Mediated Apoptosis and Goblet Cell Differentiation of Mouse Intestinal Stem/progenitor Cells. *Cell Death Differ* 22, 1865–1876. doi:10.1038/cdd.2015.57

Stefanovsky, V. Y., Pelletier, G., Hannan, R., Gagnon-Kugler, T., Rothblum, L. I., and Moss, T. (2001). An Immediate Response of Ribosomal Transcription to Growth Factor Stimulation in Mammals Is Mediated by ERK Phosphorylation of UBF. *Mol. Cel* 8, 1063–1073. doi:10.1016/s1097-2765(01)00384-7

Strikoudis, A., Guillamot, M., and Aifantis, I. (2014). Regulation of Stem Cell Function by Protein Ubiquitylation. *EMBO Rep.* 15, 365–382. doi:10.1002/embr.201338373

Sugiyama, H., Takahashi, K., Yamamoto, T., Iwasaki, M., Narita, M., Nakamura, M., et al. (2017). Nat1 Promotes Translation of Specific Proteins that Induce Differentiation of Mouse Embryonic Stem Cells. *Proc. Natl. Acad. Sci. USA* 114, 340–345. doi:10.1073/pnas.1617234114

Sun, P., Quan, Z., Zhang, B., Wu, T., and Xi, R. (2010). TSC1/2 Tumour Suppressor Complex maintainsDrosophilagermline Stem Cells by Preventing Differentiation. *Development* 137, 2461–2469. doi:10.1242/dev.051466

Suresh, B., Lee, J., Kim, H., and Ramakrishna, S. (2016). Regulation of Pluripotency and Differentiation by Deubiquitinating Enzymes. *Cel Death Differ* 23, 1257–1264. doi:10.1038/cdd.2016.53

Syntichaki, P., Troulinaki, K., and Tavernarakis, N. (2007). eIF4E Function in Somatic Cells Modulates Ageing in *Caenorhabditis elegans*. *Nature* 445, 922–926. doi:10.1038/nature05603

Tahmasebi, S., Alain, T., Rajasekhar, V. K., Zhang, J.-P., Prager-Khoutorsky, M., Khoutorsky, A., et al. (2014). Multifaceted Regulation of Somatic Cell Reprogramming by mRNA Translational Control. *Cell Stem Cell* 14, 606–616. doi:10.1016/j.stem.2014.02.005

Tahmasebi, S., Jafarnejad, S. M., Tam, I. S., Gonatopoulos-Pournatzis, T., Matta-Camacho, E., Tsukumo, Y., et al. (2016). Control of Embryonic Stem Cell Self-Renewal and Differentiation via Coordinated Alternative Splicing and Translation of YY2. *Proc. Natl. Acad. Sci. USA* 113, 12360–12367. doi:10.1073/pnas.1615540113

Takahashi, K., Jeong, D., Wang, S., Narita, M., Jin, X., Iwasaki, M., et al. (2020). Critical Roles of Translation Initiation and RNA Uridylation in Endogenous Retroviral Expression and Neural Differentiation in Pluripotent Stem Cells. *Cel Rep.* 31, 107715. doi:10.1016/j.celrep.2020.107715

Theunissen, T. W., and Jaenisch, R. (2017). Mechanisms of Gene Regulation in Human Embryos and Pluripotent Stem Cells. *Development* 144, 4496–4509. doi:10.1242/dev.157404

Thoreen, C. C., Chantranupong, L., Keys, H. R., Wang, T., Gray, N. S., and Sabatini, D. M. (2012). A Unifying Model for mTORC1-Mediated Regulation of mRNA Translation. *Nature* 485, 109–113. doi:10.1038/nature11083

Unwin, R. D., Smith, D. L., Blinco, D., Wilson, C. L., Miller, C. J., Evans, C. A., et al. (2006). Quantitative Proteomics Reveals Posttranslational Control as a Regulatory Factor in Primary Hematopoietic Stem Cells. *Blood* 107, 4687–4694. doi:10.1182/blood-2005-12-4995

Vattem, K. M., and Wek, R. C. (2004). Reinitiation Involving Upstream ORFs Regulates ATF4 mRNA Translation in Mammalian Cells. *Proc. Natl. Acad. Sci.* 101, 11269–11274. doi:10.1073/pnas.0400541101

Wang, L., Ryoo, H. D., Qi, Y., and Jasper, H. (2015). PERK Limits Drosophila Lifespan by Promoting Intestinal Stem Cell Proliferation in Response to ER Stress. *Plos Genet.* 11, e1005220. doi:10.1371/journal.pgen.1005220

Wang, S., Xia, P., Ye, B., Huang, G., Liu, J., and Fan, Z. (2013). Transient Activation of Autophagy via Sox2-Mediated Suppression of mTOR Is an Important Early Step in Reprogramming to Pluripotency. *Cell Stem Cell* 13, 617–625. doi:10.1016/j.stem.2013.10.005

Wang, X., Li, W., Williams, M., Terada, N., Alessi, D. R., and Proud, C. G. (2001). Regulation of Elongation Factor 2 Kinase by p90RSK1 and P70 S6 Kinase. *EMBO J.* 20, 4370–4379. doi:10.1093/emboj/20.16.4370

Waskiewicz, A. J., Johnson, J. C., Penn, B., Mahalingam, M., Kimball, S. R., and Cooper, J. A. (1999). Phosphorylation of the Cap-Binding Protein Eukaryotic Translation Initiation Factor 4E by Protein Kinase Mnk1 *In Vivo*. *Mol. Cel Biol* 19, 1871–1880. doi:10.1128/mcb.19.3.1871

Watanabe-Susaki, K., Takada, H., Enomoto, K., Miwata, K., Ishimine, H., Intoh, A., et al. (2014). Biosynthesis of Ribosomal RNA in Nucleoli Regulates Pluripotency and Differentiation Ability of Pluripotent Stem Cells. *Stem Cells* 32, 3099–3111. doi:10.1002/stem.1825

Wek, R. C., Jiang, H.-Y., and Anthony, T. G. (2006). Coping with Stress: eIF2 Kinases and Translational Control. *Biochem. Soc. Trans.* 34, 7–11. doi:10.1042/bst0340007

Woolnough, J. L., Atwood, B. L., Liu, Z., Zhao, R., and Giles, K. E. (2016). The Regulation of rRNA Gene Transcription during Directed Differentiation of Human Embryonic Stem Cells. *PLoS One* 11, e0157276. doi:10.1371/journal.pone.0157276

Wu, Y., Li, Y., Zhang, H., Huang, Y., Zhao, P., Tang, Y., et al. (2015). Autophagy and mTORC1 Regulate the Stochastic Phase of Somatic Cell Reprogramming. *Nat. Cel Biol* 17, 715–725. doi:10.1038/ncb3172

Yamanaka, S., Zhang, X. Y., Maeda, M., Miura, K., Wang, S., Farese, R. V., Jr., et al. (2000). Essential Role of NAT1/p97/DAP5 in Embryonic Differentiation and the Retinoic Acid Pathway. *EMBO J.* 19, 5533–5541. doi:10.1093/emboj/19.20.5533

Yan, P., Ren, J., Zhang, W., Qu, J., and Liu, G.-H. (2020). Protein Quality Control of Cell Stemness. *Cell Regen* 9, 22. doi:10.1186/s13619-020-00064-2

Yang, G., Smibert, C. A., Kaplan, D. R., and Miller, F. D. (2014). An eIF4E1/4E-T Complex Determines the Genesis of Neurons from Precursors by Translationally Repressing a Proneurogenic Transcription Program. *Neuron* 84, 723–739. doi:10.1016/j.neuron.2014.10.022

Yang, H.-S., Jansen, A. P., Komar, A. A., Zheng, X., Merrick, W. C., Costes, S., et al. (2003). The Transformation Suppressor Pdcd4 Is a Novel Eukaryotic Translation Initiation Factor 4A Binding Protein that Inhibits Translation. *Mol. Cel Biol* 23, 26–37. doi:10.1128/mcb.23.1.26-37.2003

Yilmaz, Ö. H., Valdez, R., Theisen, B. K., Guo, W., Ferguson, D. O., Wu, H., et al. (2006). Pten Dependence Distinguishes Haematopoietic Stem Cells from Leukaemia-Initiating Cells. *Nature* 441, 475–482. doi:10.1038/nature04703

Yoffe, Y., David, M., Kalaora, R., Povodovski, L., Friedlander, G., Feldmesser, E., et al. (2016). Cap-independent Translation by DAP5 Controls Cell Fate Decisions in Human Embryonic Stem Cells. *Genes Dev.* 30, 1991–2004. doi:10.1101/gad.285239.116

You, K. T., Park, J., and Kim, V. N. (2015). Role of the Small Subunit Processome in the Maintenance of Pluripotent Stem Cells. *Genes Dev.* 29, 2004–2009. doi:10.1101/gad.267112.115

Yuen, A. C., Hillion, K.-H., Wang, R., and Amoyel, M. (2021). Germ Cells Commit Somatic Stem Cells to Differentiation Following Priming by PI3K/Tor Activity in the Drosophila Testis. *Plos Genet.* 17, e1009609. doi:10.1371/journal.pgen.1009609

Zaidi, S. K., Boyd, J. R., Grandy, R. A., Medina, R., Lian, J. B., Stein, G. S., et al. (2016). Expression of Ribosomal RNA and Protein Genes in Human Embryonic Stem Cells Is Associated with the Activating H3K4me3 Histone Mark. *J. Cel. Physiol.* 231, 2007–2013. doi:10.1002/jcp.25309

Zhang, H., Wu, Z., Lu, J. Y., Huang, B., Zhou, H., Xie, W., et al. (2020a). DEAD-box Helicase 18 Counteracts PRC2 to Safeguard Ribosomal DNA in Pluripotency Regulation. *Cel Rep.* 30, 81–97. doi:10.1016/j.celrep.2019.12.021

Zhang, J., Grindley, J. C., Yin, T., Jayasinghe, S., He, X. C., Ross, J. T., et al. (2006). PTEN Maintains Haematopoietic Stem Cells and Acts in Lineage Choice and Leukaemia Prevention. *Nature* 441, 518–522. doi:10.1038/nature04747

Zhang, M., Zhai, Y., Zhang, S., Dai, X., and Li, Z. (2020b). Roles of N6-Methyladenosine (m6A) in Stem Cell Fate Decisions and Early Embryonic Development in Mammals. *Front. Cel Dev. Biol.* 8, 782. doi:10.3389/fcell.2020.00782

Zhang, Q., Shalaby, N. A., and Buszczak, M. (2014). Changes in rRNA Transcription Influence Proliferation and Cell Fate within a Stem Cell Lineage. *Science* 343, 298–301. doi:10.1126/science.1246384

Zhou, X., Lv, X., Zhang, L., Yan, J., Hu, R., Sun, Y., et al. (2020). Ketamine Promotes the Neural Differentiation of Mouse Embryonic Stem Cells by Activating mTOR. *Mol. Med. Rep.* 21, 2443–2451. doi:10.3892/mmr.2020.11043

Zid, B. M., Rogers, A. N., Katewa, S. D., Vargas, M. A., Kolipinski, M. C., Lu, T. A., et al. (2009). 4E-BP Extends Lifespan upon Dietary Restriction by Enhancing Mitochondrial Activity in Drosophila. *Cell* 139, 149–160. doi:10.1016/j.cell.2009.07.034

Zismanov, V., Chichkov, V., Colangelo, V., Jamet, S., Wang, S., Syme, A., et al. (2016). Phosphorylation of eIF2α Is a Translational Control Mechanism Regulating Muscle Stem Cell Quiescence and Self-Renewal. *Cell Stem Cell* 18, 79–90. doi:10.1016/j.stem.2015.09.020

Conflict of Interest: The authors declare that the research was conducted in the absence of any commercial or financial relationships that could be construed as a potential conflict of interest.

frontiers in Molecular Biosciences

ORIGINAL RESEARCH
published: 11 January 2022
doi: 10.3389/fmolb.2021.787664

eIF3 and Its mRNA-Entry-Channel Arm Contribute to the Recruitment of mRNAs With Long 5′-Untranslated Regions

*Andrei Stanciu[1], Juncheng Luo[2], Lucy Funes[3], Shanya Galbokke Hewage[3], Shardul D. Kulkarni[4] and Colin Echeverría Aitken[2,3]**

[1]Computer Science Department, Vassar College, Poughkeepsie, NY, United States, [2]Biochemistry Program, Vassar College, Poughkeepsie, NY, United States, [3]Biology Department, Vassar College, Poughkeepsie, NY, United States, [4]Department of Biochemistry and Molecular Biology, Penn State Eberly College of Medicine, University Park, PA, United States

OPEN ACCESS

Edited by:
Daniel L. Kiss,
Houston Methodist Research Institute,
United States

Reviewed by:
Amy Lee,
Dana–Farber Cancer Institute,
United States
Leos Valasek,
Academy of Sciences of the Czech
Republic (ASCR), Czechia
Angie Hilliker,
University of Richmond, United States

***Correspondence:**
Colin Echeverría Aitken
caitken@vassar.edu

Specialty section:
This article was submitted to
RNA Networks and Biology,
a section of the journal
Frontiers in Molecular Biosciences

Received: 01 October 2021
Accepted: 13 December 2021
Published: 11 January 2022

Citation:
Stanciu A, Luo J, Funes L,
Galbokke Hewage S, Kulkarni SD and
Aitken CE (2022) eIF3 and Its mRNA-
Entry-Channel Arm Contribute to the
Recruitment of mRNAs With Long 5′-
Untranslated Regions.
Front. Mol. Biosci. 8:787664.
doi: 10.3389/fmolb.2021.787664

Translation initiation in eukaryotes is a multi-step pathway and the most regulated phase of translation. Eukaryotic initiation factor 3 (eIF3) is the largest and most complex of the translation initiation factors, and it contributes to events throughout the initiation pathway. In particular, eIF3 appears to play critical roles in mRNA recruitment. More recently, eIF3 has been implicated in driving the selective translation of specific classes of mRNAs. However, unraveling the mechanism of these diverse contributions—and disentangling the roles of the individual subunits of the eIF3 complex—remains challenging. We employed ribosome profiling of budding yeast cells expressing two distinct mutations targeting the eIF3 complex. These mutations either disrupt the entire complex or subunits positioned near the mRNA-entry channel of the ribosome and which appear to relocate during or in response to mRNA binding and start-codon recognition. Disruption of either the entire eIF3 complex or specific targeting of these subunits affects mRNAs with long 5′-untranslated regions and whose translation is more dependent on eIF4A, eIF4B, and Ded1 but less dependent on eIF4G, eIF4E, and PABP. Disruption of the entire eIF3 complex further affects mRNAs involved in mitochondrial processes and with structured 5′-untranslated regions. Comparison of the suite of mRNAs most sensitive to both mutations with those uniquely sensitive to disruption of the entire complex sheds new light on the specific roles of individual subunits of the eIF3 complex.

Keywords: eIF3, translation initiation, translational regulation, mRNA recruitment, ribosome, ribosome profiling, ribo-seq

INTRODUCTION

Translation initiation is the rate-limiting and most regulated phase of translation (Sonenberg and Hinnebusch, 2009; Jackson et al., 2010). Translation initiation in eukaryotes requires the ribosome—the macromolecular machine responsible for synthesizing the proteins encoded by messenger RNA molecules in all kingdoms of life—to dock at the very 5′ end of a mRNA molecule and then scan to identify the start codon for translation, usually the first AUG. The sequence through which the ribosome must scan, known either as the 5′-untranslated region (5′-UTR) or the transcript leader (TL), can be in excess of a 1,000 nucleotides in length and contain regions of defined secondary structure or upstream open reading frames (uORFS) demarcated by

either cognate (AUG) or near-cognate start codons and whose translation can regulate translation of the downstream open reading frame (ORF) (Hinnebusch et al., 2016).

At least twelve protein initiation factors (eIFs) collaborate with the ribosome to facilitate its navigation of these obstacles (Aitken and Lorsch, 2012; Shivaya Valasek, 2012; Hinnebusch, 2014; Hinnebusch, 2017). The process begins with the formation of a pre-initiation complex (PIC) comprising the small (40S) ribosomal subunit, a ternary complex (TC) of the initiator methionyl tRNA ($tRNA_i$), the GTPase eIF2, and GTP ($tRNA_i$•eIF2•GTP), and the initiation factors eIF1, eIF1A, eIF5, and eIF3. The PIC then docks at the 5′ end of the mRNA in collaboration with the eIF4F complex comprising the cap-binding protein eIF4E, the scaffolding protein eIF4G, and the helicase eIF4A, which may facilitate initial docking of the PIC by relaxing structural complexity near the 5′ end of the mRNA (Yourik et al., 2017). Once docked at the 5′ end, the PIC scans in the 3′ direction to identify the start codon. Scanning is thought to be facilitated by eIF4A and eIF4B, which binds the 40S subunit (Walker et al., 2013). The helicase Ded1 also plays an important role in scanning, perhaps by resolving defined structural elements within the 5' UTR that might otherwise prevent efficient scanning (Gupta et al., 2018).

The largest and most complex of the initiation factors is eIF3, a multi-subunit complex comprising at least 5 essential subunits in the yeast *S. cerevisiae* and at least 12 subunits in mammalian cells (Hinnebusch, 2006; Valášek et al., 2017). eIF3 participates in every component step of translation initiation. It stabilizes and promotes formation of the PIC via interactions with the 40S subunit, eIF1, and eIF2 within the TC (Asano et al., 2000; Valášek et al., 2002; Majumdar et al., 2003; Valášek et al., 2003; Nielsen et al., 2006; Sokabe and Fraser, 2014). eIF3 is also required, both *in vivo* and *in vitro*, for mRNA recruitment by the PIC (Jivotovskaya et al., 2006; Mitchell et al., 2010; Aitken et al., 2016), a process consisting of PIC docking, scanning, and start-codon recognition. Consistent with this role, eIF3 binds the PIC at the solvent face but projects appendages near both the mRNA-entry and mRNA-exit channels of the ribosome (Aylett et al., 2015; Des Georges et al., 2015; Llácer et al., 2018). At the mRNA-exit channel, the eIF3a subunit (and eIF3d in higher eukaryotes) appears to interact functionally or physically with the mRNA (Szamecz et al., 2008; Munzarová et al., 2011) and the very N-terminal region of eIF3a seems to stabilize the binding of mRNA to the PIC (Aitken et al., 2016). Subunits of the human eIF3 complex bind to eIF4G (Villa et al., 2013), and some of these were found interacting directly with components of the eIF4F complex at the mRNA-exit channel in a recent high-resolution structure of the human 48S PIC (Querido et al., 2020).

Near the mRNA-entry channel, the C-terminal domain (CTD) of eIF3a interacts with 40S elements that mediate the transition between the open (docking- and scanning-competent) and closed (scanning-arresting) conformations of the PIC (Chiu et al., 2010; Dong et al., 2017). High-resolution structural models of eIF3 bound to the PIC reveal that the eIF3a CTD, eIF3b, eIF3i, and eIF3g compose this mRNA-entry-channel arm (Des Georges et al., 2015; Simonetti et al., 2016; Llácer et al., 2018). Moreover, structural models of the PIC either lacking or bound to mRNA reveal distinct positions of this arm (Llácer et al., 2015; Llácer et al., 2018). In the absence of mRNA, these subunits are found bound to the solvent face of the PIC; in the presence of mRNA, but prior to start-codon recognition, the mRNA-entry-channel arm is found at the intersubunit face but then appears to relocate to its original position at the solvent face upon start-codon recognition. Together with the observations that mutations to the eIF3a CTD (Valášek et al., 2002; Chiu et al., 2010), eIF3b (Nielsen et al., 2004; Elantak et al., 2010), eIF3i (Herrmannová et al., 2012), and eIF3g (Cuchalova et al., 2010) elicit phenotypes consistent with defects in the component events of mRNA recruitment and affect the kinetics of mRNA recruitment *in vitro* (Aitken et al., 2016), this suggests that the eIF3 mRNA-entry-channel arm, and its potential repositioning in response to mRNA binding and start-codon recognition, may play an important mechanistic role in mRNA recruitment.

To investigate the role of eIF3 and components of the eIF3 mRNA-entry-channel arm in mRNA recruitment and its component events, we employed ribosome profiling (Ingolia et al., 2009) to follow the repercussions of specific eIF3 mutations on the translational efficiency (TE) of mRNAs across the transcriptome. By comparing the features of mRNAs most sensitive to each mutation with those least sensitive to these mutations, we shed new light on the role of eIF3 and its mRNA-entry-channel arm in mRNA recruitment. This approach has previously been employed to illuminate the transcriptome-scale role of several initiation factors, including eIF1 (Zhou et al., 2020), eIF1A (Martin-Marcos et al., 2017), eIF4A (Sen et al., 2015), eIF4B (Sen et al., 2016), and Ded1 (Sen et al., 2019). Here, we focused on two mutations whose effects on translation initiation have been previously explored with both genetic and biochemical tools. The first of these mutants—$tif32^{td}/prt1^{td}$ (*eIF3a/b Degron*)—expresses temperature sensitive degron (td) alleles of the eIF3a (TIF32) and eIF3b (PRT1) subunits (Jivotovskaya et al., 2006). Growth of this strain under restrictive conditions results in the depletion of eIF3a and eIF3b. This in turn disrupts the entire eIF3 complex, mimicking an eIF3 deletion mutant under these conditions. This disruption of the eIF3 complex further interferes with mRNA binding and 48S formation by the PIC, providing evidence for the role of eIF3 in mRNA recruitment (Jivotovskaya et al., 2006). The second mutation we investigated is a mutation to eIF3i that abrogates eIF3i binding to eIF3b: *eIF3i DDKK* (Herrmannová et al., 2012). Because the binding of both eIF3i and eIF3g to the eIF3 complex depends on this interaction, the *eIF3i DDKK* mutation mimics the absence of both subunits; purification of eIF3 from *eIF3i DDKK* cells via tagged eIF3b yields the wild-type a/b/c sub-complex (Aitken et al., 2016). The *eIF3i DDKK* mutation was previously shown to interfere with scanning and start-codon recognition *in vivo* and in cell extracts (Herrmannová et al., 2012). In addition, subsequent *in vitro* investigation demonstrated that, in the absence of eIF3i and eIF3g, the eIF3 a/b/c sub-complex is unable to promote recruitment of a natural, capped mRNA (Aitken et al., 2016).

By investigating the effects of these two mutations—which mimic the loss of either the entire eIF3 complex or two subunits of the eIF3 mRNA-entry-channel arm—we hoped to disentangle the roles of eIF3i and eIF3g from that of the entire eIF3 complex.

In the presence of both mutations, we observed strong decreases in global translation levels and were able to identify mRNAs whose relative translational efficiency is either more or less sensitive—as compared to the total population of mRNAs—to each mutation. By comparing the features of these mRNAs with each other and with mRNAs sensitive to mutations targeting other initiation factors, we shed further light on the roles of eIF3 and its mRNA-entry-channel arm during mRNA recruitment. Contrasting the effects we observed when disrupting the entire eIF3 complex or targeting its mRNA-entry-channel arm disentangles the contributions of the eIF3i and eIF3g subunits from those of the other subunits of the complex. These analyses provide evidence that eIF3 and its mRNA-entry-channel arm collaborate functionally with eIF4A, eIF4B, and Ded1 to drive initiation on mRNAs with long 5′-UTRs and with a lower propensity to form stable closed-loop structures mediated by eIF4G, eIF4E, and PABP. They further reveal that eIF3 stimulates the translation of mRNAs involved in mitochondrial processes and contributes to the resolution of structurally complex regions during initial docking or scanning, and that these roles require subunits beyond eIF3i and eIF3g.

MATERIALS AND METHODS

Cell Growth and Harvest

We created ribosome profiling libraries from eIF3 mutant and corresponding isogenic WT strains for both the *eIF3a/b Degron* (YAJ34: *MAT**a** trp1Δ leu2-3,112 ura3-52 gcn2::hisG* P_{GAL1}*-myc-UBR1::TRP1::ubr1* P_{CUP1}*-UBI-R-HA-tif32*^{td}*::URA3::tif32* P_{CUP1}*-UBI-R-DHFR*^{ts}*-HA-prt1*^{td}*::URA3::prt1* and YAJ3: MAT**a** *trp1Δleu2-3,112 ura3-52 gcn2::hisG* P_{GAL1}*-myc-UBR1::TRP1::ubr1* pRS316 [*URA3*]) (Jivotovskaya et al., 2006) and *eIF3i DDKK* (H450: *MATa leu2-3,-112 ura3-52::GCN2 trp1Δ tif34Δ* hc TIF34 URA3 transformed with YCp-i/TIF34-D207K-D224K-HA or YCp-i/TIF34-HA, respectively) (Herrmannová et al., 2012) as described previously (Ingolia, 2010; Sen et al., 2015; Sen et al., 2016). We grew two biological replicates of each strain and its matching isogenic WT strain under permissive conditions before harvesting and adding to pre-warmed restrictive media for a duration resulting in an ~90% decrease in bulk translation (as judged by polysome:monosome ratios, **Supplementary Figure S1**) and a final cell density at mid-log phase (OD_{600} = ~0.6). We grew *eIF3a/b Degron* cells at 25°C in SC_{Raff} + Cu^{2+} before shifting them to pre-warmed $SC_{Raff/Gal}$ + BCS at 36°C for 90 min. We grew *eIF3i DDKK* at 30°C in SC media before shifting them to pre-warmed SC media at 37°C for 30 min. We added cycloheximide to a final concentration of 100 μg/ml 2 min prior to harvesting by filtration through a Kontes filtration apparatus and flash freezing in liquid nitrogen with 2 ml of ribosome footprinting buffer (20 mM Tris pH 8.0, 140 mM KCl, 1.5 mM MgCl2, 1% Triton, 100 μg/ml cycloheximide).

Ribosome Profiling and RNA-Seq Library Preparation

We generated sequencing libraries of ribosome footprints and total mRNA as previously described (Ingolia, 2010; Sen et al., 2015; Sen et al., 2016). Briefly, we lysed cells using a freezer mill and then prepared lysates by centrifuging 5 min at 3,000 × g, collecting the supernatant and then centrifuging 12 min at >20,000 × g. We then collected the supernatant and flash-froze in 30 OD_{260} aliquots. We purified ribosome footprints by adding 5 μL RNase1 to one aliquot of purified lysate and incubating 60 min at 26°C with mixing at 700 rpm. We then added 5 μL SuperAsin (Thermo Fisher) and loaded on a 10–50% sucrose gradient and centrifuged at 40,000 rpm for 3 h and then collected the monosome peak using a gradient fractionator. We then purified RNA from purified monosomes via hot phenol extraction. We purified total mRNA from one 30 OD_{260} aliquot of purified lysate using the miRNeasy mini kit (Qiagen) per the vendor's instructions and then randomly fragmented at 70°C for 8 min using Fragmentation Reagent (Invitrogen). We then performed subsequent steps (size selection, linker ligation, reverse transcription, circularization, rRNA subtraction, and PCR amplification) as previously described and had libraries sequenced using an Illumina HiSeq system.

Analysis of Sequencing Data

We processed and analyzed sequencing libraries of ribosome footprints and total mRNA as described previously (Ingolia, 2010; Sen et al., 2015; Sen et al., 2016). We then employed DESeq2 (Love et al., 2014) for statistical analysis of differences in ribosome footprint and RNA-seq read counts, and TE_{rel} values between WT and mutant samples, as previously reported (Martin-Marcos et al., 2017; Kulkarni et al., 2019). We excluded genes with fewer than 128 total mRNA reads in the four samples combined (two replicates of both WT and mutant strains) from the calculation of TE_{rel} values. We then performed subsequent analysis of mRNA features and characteristics within R, using custom scripts, together with previously-reported datasets reporting 5′-UTR lengths, PARS values, closed-loop-forming propensity of individual mRNAs, previously identified uORFs, or ΔTE_{rel} values observed in the presence of mutations targeting eIF4A, eIF4B, Ded1, eIF1, or eIF1A. We performed Gene Ontology analysis using the Gene Ontology Resource PANTHER classification system. Statistical tests were performed as described in the main text and figures.

RESULTS

Disruption of the eIF3 Complex Provokes Severe Translational Defects

To investigate the transcriptome-wide roles of eIF3, we performed ribosome profiling in two *S. cerevisiae* strains in which the eIF3 complex is partially or entirely compromised. The *eIF3a/b Degron* strain expresses temperature-sensitive degron variants of the eIF3a and eIF3b subunits. Depletion of these subunits provokes the loss of the entire eIF3 complex (Jivotovskaya et al., 2006). The *eIF3i DDKK* strain expresses a variant of the eIF3i subunit that is unable to bind stably to eIF3b (Herrmannová et al., 2012). Because both eIF3i and eIF3g depend on this interaction to associate with the remainder of the eIF3 complex, this results in the loss of both subunits, which normally

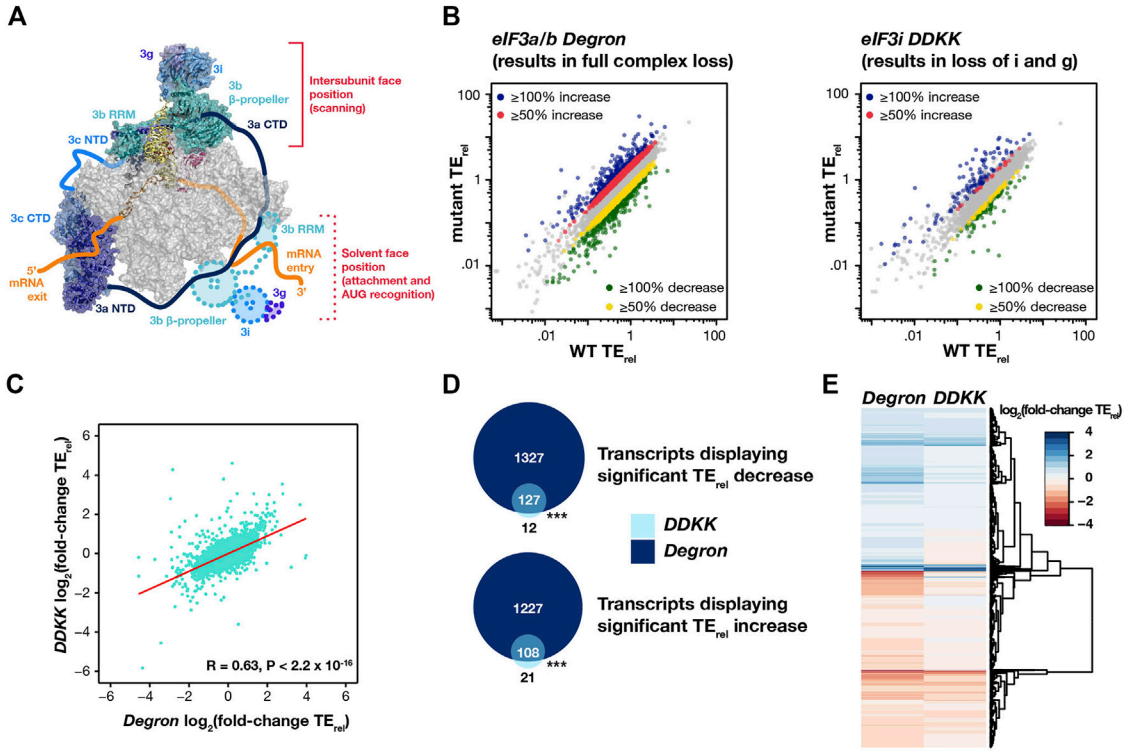

FIGURE 1 | Disruption of the eIF3 complex or its mRNA-entry channel arm provoke strong and overlapping effects on the translation of mRNAs across the transcriptome. **(A)** Structural model of eIF3 bound to the PIC (PDB 6GSM) viewed looking down at top of the small (40S) ribosomal subunit head so as to visualize the path of mRNA as it enters and exits the PIC (Llácer et al., 2021). The small (40S) ribosomal subunit is shown in grey, and the initiator tRNA and mRNA are shown in yellow and orange, respectively (with the path of the mRNA entering and exiting the PIC shown as a cartoon). Subunits of the eIF3 complex are shown in blues and greens, with the mRNA-entry-channel arm shown in two positions: at the intersubunit face of the PIC (identified density seen in this structure) or at the solvent face (cartoons depicting approximate location observed in structures lacking mRNA or after start-codon recognition). **(B)** TE_{rel} correlation plots comparing observed TE_{rel} values in either *eIF3a/b Degron* (left) or *eIF3i DDKK* (right) cells with TE_{rel} values observed in isogenic wild-type cells. Transcripts displaying significant ($P_{adj} < 0.05$) TE_{rel} increases (≥50% red and ≥100% blue) or decreases (≥50% yellow and ≥100% green) as determined by DESeq2 analysis are shown in color. **(C)** Correlation plot comparing observed TE_{rel} changes in *eIF3a/b Degron* and *eIF3i DDKK* cells, with predicted Pearson correlation shown in red. **(D)** Venn diagrams describing the overlap in transcripts displaying significant TE_{rel} decreases (top) or increases (bottom) in *eIF3a/b Degron* (dark blue) or *eIF3i DDKK* (light blue) cells. *** = $P < 10^{-10}$, ** = $P < 10^{-5}$, * = $P < 0.05$, HyperGeometric test. **(E)** Heatmap and dendrogram resulting from hierarchical clustering analysis of significant TE_{rel} changes observed in *eIF3a/b Degron* and *eIF3i DDKK* cells.

contribute to the mRNA-entry-channel arm of eIF3 (**Figure 1A**). This arm has been observed in two distinct locations of the PIC, depending on its functional state (Llácer et al., 2015; Llácer et al., 2018).

Before constructing ribosome profiling libraries, we first investigated the effects of the *eIF3a/b Degron* and *eIF3i DDKK* mutations on global translation levels, as assayed by polysome profiling. For each strain, we grew cells first under permissive conditions and then shifted them to restrictive conditions for 30, 60, 90, and 120 min. Both strains exhibit no growth defect under permissive conditions but manifest severe growth defects at restrictive conditions (Jivotovskaya et al., 2006; Herrmannová et al., 2012). Consistent with this, polysome profiles collected under permissive growth conditions for both strains were similar to those collected for isogenic wild-type strains (**Supplementary Figure S1A**). In contrast, we observed strong decreases in polysome to monosome ratios (P/M) upon shifting to restrictive conditions for both strains, with *eIF3a/b Degron* and *eIF3i DDKK* cells exhibiting an approximately 90% decrease in P/M (as compared to isogenic WT cells grown under the same conditions) after 30 min and 90 min at restrictive conditions, respectively (**Supplementary Figure S1B,C**).

Relative TE Changes Identify mRNAs Most or Least Sensitive to the Disruption of the Entire eIF3 Complex or Its mRNA-Entry-Channel Arm

Given the marked decrease in global translation levels we observed in both strains, we next asked how these global affects translate to individual mRNAs across the transcriptome. To that end, we constructed ribosome profiling and RNA-seq libraries from both the *eIF3i DDKK* and *eIF3a/b Degron* strains (and their corresponding isogenic WT strains) grown under restrictive conditions and calculated relative translational efficiency (TE_{rel}) values for coding sequences (CDS), ignoring reads obtained from the initial 15 codons and

from the final 5 codons to avoid cycloheximide-induced artifacts (Gerashchenko and Gladyshev, 2014). Owing to the absence of an internal read-count standard, read counts from both ribosome profiling and RNA-seq libraries are normalized to the total library size for each condition. The TE_{rel} values we calculate from these normalized read counts thus do not enable direct comparison of absolute TE between samples. Instead, TE_{rel} values provide a measure of the translational status of individual mRNAs as compared to the overall population of mRNAs within each sample. We also calculated TE_{rel} values for a set of previously identified uORFs (Martin-Marcos et al., 2017; Kulkarni et al., 2019) but did not attempt to identify novel translated uORFS owing to the inclusion of cycloheximide in our library preparation. Both ribosome footprint and RNA-seq libraries were highly reproducible across replicates for each condition (**Supplementary Figure S2**).

Using the R DESeq2 package (Love et al., 2014), we then identified transcripts whose TE_{rel} was significantly changed ($P_{adj} < 0.05$) in each strain, as compared to an isogenic WT strain (**Figure 1B**). Owing to the marked decrease in global translational levels we observed in each mutant strain, as well as the normalization to total ribosomal footprint reads performed when calculating TE_{rel}, we interpreted mRNAs exhibiting significant TE_{rel} decreases as having a greater than average dependence on the either the eIF3i and eIF3g subunits lost in *eIF3i DDKK* cells or on the entire eIF3 complex disrupted in *eIF3a/b Degron* cells. We interpreted those mRNAs exhibiting significant TE_{rel} increases as instead having a weaker than average dependance on the regions of the eIF3 complex targeted by each mutation. The significant effects on global translational levels that we observed in both *eIF3i DDKK* and *eIF3a/b Degron* cells in fact suggest that most mRNAs likely experience decreases in their absolute TE. Nonetheless, comparison of these significant changes in TE_{rel} (ΔTE_{rel}) enables identification of those mRNAs whose translation is most or least sensitive to disruption of eIF3 or its mRNA-entry-channel arm in a background where global translational levels are repressed.

In *eIF3a/b Degron* cells—in which the entire eIF3 complex is disrupted—we identified 1,455 transcripts whose TE_{rel} decreased and 1,340 transcripts whose TE_{rel} increased (5,466 total with significant read counts), as compared to TE_{rel} values in an isogenic WT strain (**Figure 1B**). Because eIF3 has been implicated in mediating the translation of specific mRNAs in a number of cell types (Sha et al., 2009; Lee et al., 2015; Rode et al., 2018; Lin et al., 2020; Lamper et al., 2020), we investigated the gene ontology (GO) terms associated with these affected mRNAs. The set of transcripts whose TE_{rel} decreased in *eIF3a/b Degron* cells was enriched for mRNAs with GO terms involved in mitochondrial translation and gene expression, as well as a variety of metabolic processes (**Supplementary Figure S3**). These most sensitive mRNAs were under-enriched in mRNAs involved in RNA processing and ribosome biogenesis. Consistent with this, mRNAs whose TE_{rel} increased in *eIF3a/b Degron* cells were enriched in GO terms associated with RNA processing and under-enriched in terms associated with mitochondrial translation and gene expression (**Supplementary Figure S3**).

In *eIF3i DDKK* cells—in which the eIF3i and eIF3g subunits of the eIF3 mRNA-entry-channel arm are lost from the complex—we identified 139 transcripts whose TE_{rel} decreased and 133 transcripts whose TE_{rel} increased, as compared to TE_{rel} values in an isogenic WT strain (**Figure 1B**). We did not observe any significant over- or under-enrichment of specific GO terms in affected transcripts in these cells, perhaps because the strong global effects on translation in *eIF3i DDKK* cells are more uniformly distributed amongst all mRNAs, resulting in widespread but uniform decreases in absolute TE levels across the transcriptome with more limited effects on the relative TE of individual mRNAs.

In both *eIF3i DDK*K and *eIF3a/b Degron* cells, we observed strong increases in uORF translation (**Supplementary Figure S4A**). Of 4,830 uORFs identified previously, 529 displayed significant ($P_{adj} < 0.05$) increases in TE_{rel} in *eIF3a/b Degron* cells, whereas 21 displayed significant decreases in TE_{rel}. In *eIF3i DDKK* cells, 391 uORFs displayed significant ($P_{adj} < 0.05$) increases in TE_{rel}, whereas 5 displayed significant decreases in TE_{rel}. This global increase in uORF translation in both strains is likely a result of the previously described effects of cycloheximide on read counts near the start codon (Gerashchenko and Gladyshev, 2014), which cannot be discarded as in the calculation of ORF TE_{rel} values owing to the short length of these regions. Thus we focused subsequent analysis of uORF TE_{rel} values on any observed differential behavior between uORFs within the same strain.

Because the eIF3 complex is either partly or entirely disrupted in both cell lines, we investigated the degree to which the TE_{rel} effects we observed were similar in *eIF3i DDKK* and *eIF3a/b Degron* cells. We observed a significant correlation ($R = 0.63$, $P < 2.2 \times 10^{-16}$) between the ΔTE_{rel} values observed in both strains (**Figure 1C**). Additionally, we found a strong overlap between those transcripts exhibiting TE_{rel} decreases in *eIF3i DDKK* and *eIF3a/b Degron* cells (**Figure 1D**), with the changes observed in *eIF3i DDKK* cells appearing to represent a subset of the changes observed in *eIF3a/b Degron* cells. Moreover, the overall portfolio of ΔTE_{rel} values we observe is similar for both strains, as evidenced by heat map comparison of the magnitude and direction of observed changes (**Figure 1E**). Together, these results are consistent with strong translational effects upon disruption of the eIF3 mRNA-entry-channel arm (as in *eIF3i DDKK* cells) or depletion of the entire eIF3 complex (as in *eIF3a/b Degron* cells) and a role for eIF3 in promoting the translation of mRNAs with mitochondrial roles.

mRNAs Most Sensitive to the *eIF3a/b Degron* or *eIF3i DDKK* Mutations Possess Longer 5′-Untranslated Regions

We next investigated the structural features (**Figure 2A**) of mRNAs most or least sensitive to the *eIF3i DDKK* and *eIF3a/b Degron* mutations, as identified by DESeq2 analysis of TE_{rel} changes in each strain. eIF3 is required for the overall process of mRNA recruitment both *in vivo* (Jivotovskaya et al., 2006) and

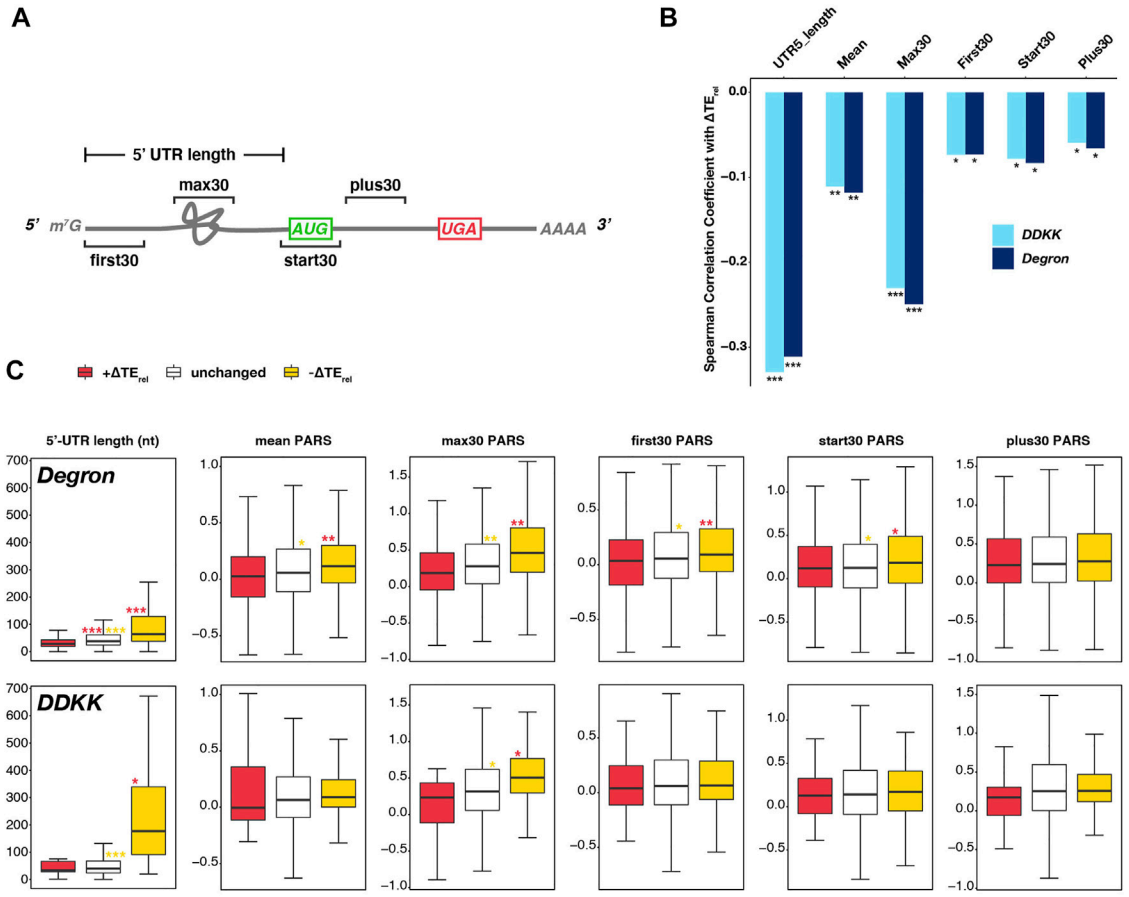

FIGURE 2 | Transcripts most sensitive to disruption of the eIF3 complex or its mRNA-entry-channel arm possess longer 5′-UTRs. **(A)** Cartoon depicting a hypothetical mRNA and detailing the 5′-UTR length and the specific 30-nt windows within which mean PARS values (Kertesz et al., 2010) were calculated as measures of structural complexity. **(B)** Bar plot comparing the Spearman correlation coefficients obtained when comparing observed ΔTE_{rel} values in each mutant eIF3 strain and different measures of 5′-UTR length or complexity. *** = $P < 10^{-10}$, ** = $P < 10^{-5}$, * = $P < 0.05$. **(C)** Box and whisker plots comparing different measures of 5′-UTR length or complexity between mRNAs whose TE_{rel} significantly increases (red), decreases (yellow), or is not significantly changed (white) in *eIF3a/b Degron* (top row) or *eIF3i DDKK* (bottom row) cells. *** = $P_{adj} < 10^{-10}$, ** = $P_{adj} < 10^{-5}$, * = $P_{adj} < 0.05$, color indicates comparison set; Wilcoxon Test for 5′-UTR lengths, ANOVA with post-hoc Tukey test for others.

in vitro (Mitchell et al., 2010; Aitken et al., 2016), and mutations to several eIF3 subunits elicit defects in mRNA recruitment or its component events of initial docking, scanning, and start-codon recognition (Valášek et al., 2002; Nielsen et al., 2004; Chiu et al., 2010; Cuchalova et al., 2010; Elantak et al., 2010; Herrmannová et al., 2012).

To shed light on the contribution of the eIF3 complex and the eIF3i and eIF3g subunits of the mRNA-entry-channel arm to scanning processivity, we first asked if the ΔTE_{rel} values we observed in each strain correlated with 5′-UTR length. Upon restricting our analysis to mRNAs previously shown to have a dominant 5′-UTR isoform (defined as mRNAs for which one isoform accounts for at least 40% of all transcripts and is present at an abundance at least twice that of the next most abundant isoform) (Pelechano et al., 2013; Zinshteyn et al., 2017), we observed significant ($P < 10^{-59}$) negative correlations between 5′-UTR length and ΔTE_{rel} in both the *eIF3i DDKK* and *eIF3a/b Degron* strains (**Figure 2B**). Consistent with this effect, we also observed a negative correlation between ΔTE_{rel} and distance from the 5′ end for a set uORFs identified in previous studies (Martin-Marcos et al., 2017; Kulkarni et al., 2019), though this correlation was significant only in *eIF3i DDKK* cells (**Supplementary Figure S4B**).

To interrogate the roles of eIF3 and the eIF3i and eIF3g subunits in resolving structural impediments during initial mRNA docking or scanning, we next determined the relationship between ΔTE_{rel} and the propensity of specific regions of an mRNA to form secondary structures, as measured by their differential sensitivity *in vitro* to nucleases specific for single- or double-stranded RNA (PARS, **Figure 2A**) (Kertesz et al., 2010). In *eIF3a/b Degron* and *eIF3i DDKK* cells, we observed a significant ($P < 10^{-8}$ and $P < 10^{-7}$, respectively) negative correlation between ΔTE_{rel} and mean 5′-UTR PARS values, as well as with mean PARS scores determined within specific 30 nucleotide (nt) windows located at the first 30 nt of the 5′-UTR (First30; $P < 10^{-3}$ for both), 30 nt centered around the

AUG start codon (Start30; $P < 10^{-4}$ for both), and the first 30 nt downstream of the Start30 window (Plus30; $P < 10^{-3}$ and $P < 10^{-2}$, respectively) (**Figure 2B**) (Sen et al., 2015; Sen et al., 2016). Of the correlations we observed between ΔTE_{rel} and PARS measures, the strongest and most significant was with the maximum PARS score observed within any 30 nt window within the 5′-UTR (Max30; $P < 10^{-32}$ and $P < 10^{-38}$, respectively) (**Figure 2B**).

Having observed these correlations between ΔTE_{rel} and 5′-UTR length or structural complexity in both the *eIF3i DDKK* and *eIF3a/b Degron* strains, we next investigated if we could detect significant differences in the median values of these measures when comparing mRNAs whose TE_{rel} was either significantly decreased or increased in either strain (**Figure 2C**). As before, we restricted our analysis to mRNAs with one dominant 5′ isoform. In *eIF3a/b Degron* cells, mRNAs displaying significant negative ΔTE_{rel} values possess longer 5′-UTRs and those displaying significant positive ΔTE_{rel} values possess shorter 5′-UTRs, as compared to mRNAs whose TE_{rel} was not significantly affected ($P_{adj} < 10^{-28}$ for all pairwise comparisons, Wilcoxon test). Similarly, in *eIF3i DDKK* cells, mRNAs displaying significant negative ΔTE_{rel} values possess longer 5′-UTRs than both unaffected mRNAs ($P_{adj} < 10^{-18}$) and mRNAs displaying significant positive ΔTE_{rel} values ($P_{adj} < 10^{-3}$). However, we did not observe a significant difference in 5′-UTR lengths when comparing mRNAs displaying significant positive ΔTE_{rel} values and unaffected mRNAs in *eIF3i DDKK* cells, perhaps because the set of mRNAs expressed as a dominant transcript isoform and exhibiting significant positive ΔTE_{rel} values in these cells is relatively small (n = 57). In both cell lines, we observed similar results when comparing 5′-UTR values reported in a separate study (Kertesz et al., 2010) (**Supplementary Figure S5A**).

When comparing measures of structural complexity (as measured by PARS values across the 5′-UTR and in distinct windows), we again observed differences between mRNAs whose TE_{rel} either increased or decreased in *eIF3a/b Degron* cells. mRNAs displaying significant TE_{rel} decreases in these cells have higher mean and max30 5′-UTR PARS values, as compared to unaffected mRNAs ($P_{adj} < 10^{-3}$ and $P_{adj} < 10^{-6}$, respectively; ANOVA and post-hoc Tukey test) and mRNAs displaying significant TE_{rel} increases ($P_{adj} < 10^{-9}$ and $P_{adj} < 10^{-6}$, respectively). Similarly, mRNAs whose TE_{rel} decreased in *eIF3a/b Degron* cells have higher PARS values at the 5′ end of their 5′-UTRs (first30) and around their start codons (start30) as compared to mRNAs whose TE_{rel} either increased ($P_{adj} < 10^{-7}$ and $P_{adj} < 10^{-2}$, respectively) or was unaffected ($P_{adj} < 10^{-2}$ for both) in these cells. However, these differences appear more modest than those observed for 5′-UTR length, mean and max30 PARS values. In contrast, there is no significant difference in the PARS values downstream of the start-codon window (plus30) between mRNAs whose TE_{rel} either increased, decreased, or was unaffected in *eIF3a/b Degron* cells.

In *eIF3i DDKK* cells, we did not observe significant differences in most measures of 5′-UTR structural complexity when comparing mRNAs whose TE_{rel} either decreased, increased, or was unaffected. The one exception is the max30 PARS values of

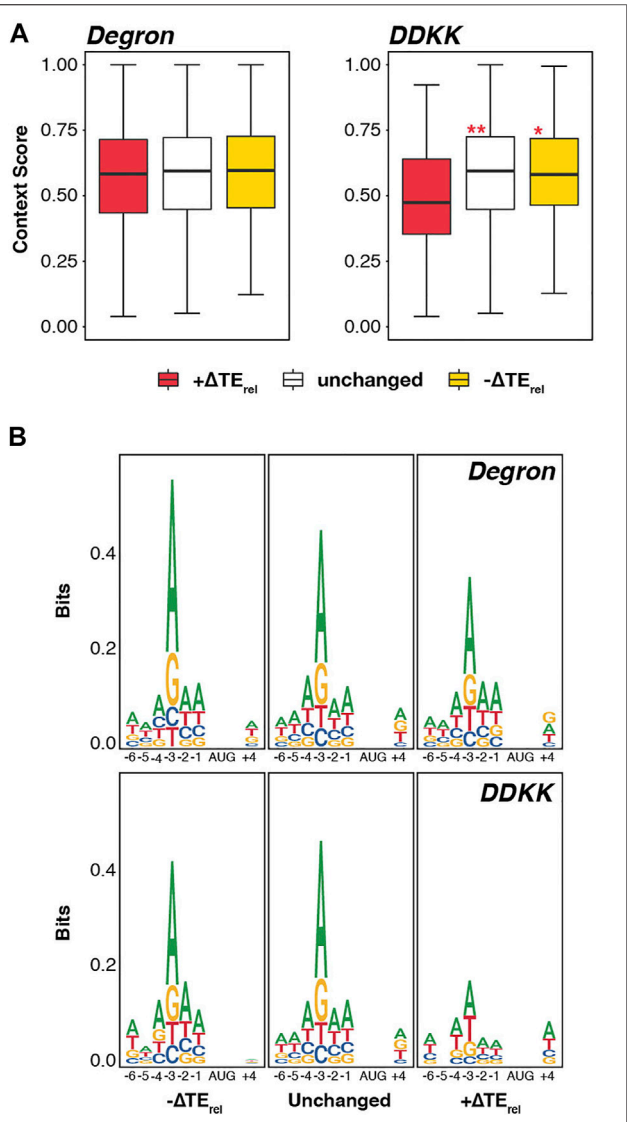

FIGURE 3 | Disruption of the eIF3 mRNA-entry-channel arm interferes with discrimination against start codons appearing in poor Kozak sequence context. **(A)** Box and whisker plots comparing the Kozak sequence context (nt -6 thru +4) of transcripts whose TE_{rel} significantly increases (red), decreases (yellow), or is not significantly changed (white) in each eIF3 mutant strain. *** = $P_{adj} < 10^{-10}$, ** = $P_{adj} < 10^{-5}$, * = $P_{adj} < 0.05$, color indicates comparison set; ANOVA with post-hoc Tukey test. **(B)** Sequence logos of nt -6 to +4 of transcripts whose TE_{rel} significantly increases, decreases, or is not significantly changed in each eIF3 mutant strain.

mRNAs whose TE_{rel} decreased in these cells, which is higher than for mRNAs whose TE_{rel} was not significantly affected ($P_{adj} < 10^{-3}$) and modestly different than for transcripts whose TE_{rel} increased in these cells ($P_{adj} < 0.02$), perhaps because the number of transcripts displaying significant TE_{rel} increases in these cells and with available PARS scores is limited (n = 17). Nonetheless, these observations are consistent with a role for eIF3 and its mRNA-entry-channel arm in processive scanning through longer 5′-UTRs. eIF3 also appears to contribute to resolving structural complexity within the 5′-UTR during initial docking or scanning,

though the mRNA-entry-channel arm may play a more peripheral role in these events.

Disruption of the eIF3 mRNA-Entry-Channel Arm Exerts Modest Effects on Discrimination Against Start Codons in Poor Kozak Sequence Context

Because various subunits of eIF3 appear to play roles in start-codon recognition (Nielsen et al., 2004; Valasek et al., 2004; Chiu et al., 2010; Cuchalova et al., 2010; Herrmannová et al., 2012), we next asked whether there was a correlation between the observed ΔTE_{rel} values in the *eIF3i DDKK* and *eIF3a/b Degron* strains and the strength of the Kozak consensus sequence surrounding the AUG start codon for each mRNA. However, we did not observe a significant correlation between context scores (calculated for nucleotides −6 to +4) and ΔTE_{rel} values in either *eIF3i DDKK* or *eIF3a/b Degron* cells (**Supplementary Figure S6**).

Consistent with this, we observed no significant difference in the median context scores for mRNAs whose TE_{rel} either increased, decreased, or was unaffected in *eIF3a/b Degron* cells (**Figure 3A**). Nonetheless, we did observe modest but significant differences between the median context scores of mRNAs displaying TE_{rel} increases in *eIF3i DDKK* cells, which are weaker than either those of mRNAs displaying TE_{rel} decreases or those whose TE_{rel} was unaffected ($P_{adj} < 10^{-4}$ and $P_{adj} < 10^{-5}$, respectively).

Given these modest effects, we investigated the sequence logos in the vicinity of the start codons of these distinct mRNAs (**Figure 3B**). Here again, we observed no difference when comparing mRNAs whose TE_{rel} either increased, decreased, or was unaffected in *eIF3a/b Degron* cells. However, consistent with the differences we observed in context scores in *eIF3i DDKK* cells, mRNAs displaying TE_{rel} increases in this background show a weaker preference for an adenine at the −3 nt than do mRNAs whose TE_{rel} is either unaffected or decreases; optimal Kozak consensus sequences contain a purine base (most often adenine) at position −3 and a guanosine at position +4 (Hinnebusch, 2014). Together, these results suggest a peripheral role for the eIF3i and eIF3g subunits of the mRNA-entry-channel arm in discriminating against start codons in poor Kozak context.

The Transcriptome-Wide Effects of the *eIF3a/b Degron* and *eIF3i DDKK* Mutations Most Closely Resemble Those Observed for Mutations Targeting Factors Involved in mRNA Recruitment

In light of previous work implicating eIF3 in both mRNA recruitment and start-codon recognition and our results here, we next compared the effects we observed in *eIF3a/b Degron* and *eIF3i DDKK* cells to those previously reported for mutations targeting other initiation factors. The effects of mutations targeting eIFA, eIF4B, and Ded1—which appear to contribute either to initial PIC docking or scanning—have previously been investigated using ribosome profiling (Sen et al., 2015, 2016). Specifically, these studies investigated the effect of temperature-sensitive alleles of eIF4A and Ded1, and a deletion of eIF4B. Importantly, the sequencing libraries from which these datasets were obtained were prepared by addition of cycloheximide to media in which cells exhibited strong translational defects, as were our sequencing libraries.

We found significant overlaps (**Figure 4A**, left panel) in the specific mRNAs experiencing significant TE_{rel} decreases in *eIF3i DDKK* or *eIF3a/b Degron* cells and those mRNAs whose TE_{rel} was significantly decreased in the presence of mutations targeting eIF4A ($P < 10^{-6}$ and $P < 10^{-19}$ for *eIF3i DDKK* and *eIF3a/b Degron*, respectively; HyperGeometric test), eIF4B ($P < 10^{-20}$ for both), and Ded1 ($P < 10^{-20}$ and $P < 10^{-11}$). We similarly found significant overlaps when comparing the sets of mRNAs whose TE_{rel} increased in the presence of these mutations (eIF4A, $P < 10^{-20}$ and $P < 10^{-17}$; eIF4B, $P < 10^{-13}$ and $P < 10^{-20}$; Ded1, $P < 10^{-10}$ and $P < 10^{-11}$). Consistent with these overlapping effects, we also observed significant positive correlations between the ΔTE_{rel} values we observed in both *eIF3i DDKK* and *eIF3a/b Degron* cells and ΔTE_{rel} values observed in the presence of mutations targeting eIF4A, eIF4B, and Ded1 (**Figure 4B** and **Supplementary Figure S7**). Global comparison of the magnitude and direction of observed ΔTE_{rel} values from these distinct experiments further revealed a similar transcriptome-level portfolio of effects (**Figure 4C**, right panel).

Having observed these similarities, we next compared the effects observed in *eIF3i DDKK* and *eIF3a/b Degron* cells to those obtained from cells expressing an eIF1 variant (*L96P*) that increases recognition of both AUG start codons in poor context and near-cognate uORF start codons (Zhou et al., 2020). The sequencing libraries giving rise to this dataset were also prepared under conditions similar to those we employed in our experiments. In contrast to the significant overlaps we observed when comparing to datasets from eIF4A, eIF4B, or Ded1 mutant cells, we only found a significant overlap between mRNAs displaying TE_{rel} decreases in *eIF3i DDKK* and *L96P eIF1* cells ($P < 10^{-5}$) and not in *eIF3a/b Degron* cells or for mRNAs displaying TE_{rel} increases in either eIF3 background (**Figure 4A**). Consistent with this, we observed a significant but negative correlation between ΔTE_{rel} values from *eIF3a/b Degron* and *L96P eIF1* cells and no significant correlation between *eIF3i DDKK* and *L96P eIF1* cells (**Figure 4B** and **Supplementary Figure S7**). Moreover, global comparison of the observed ΔTE_{rel} values from these datasets further revealed a distinct pattern of transcriptome-wide effects in *L96P eIF1* cells when compared to either *eIF3i DDKK* or *eIF3a/b Degron* cells (**Figure 4C**, left panel). We also observed weak but modestly significant correlations in ΔTE_{rel} values when comparing our eIF3 datasets to a ribosome profiling dataset obtained from cells expressing *R13P eIF1A*, in which discrimination against near-cognate codons or AUG codons in poor context was increased (**Supplementary Figure S7**). However, the sequencing libraries for this dataset were prepared from cells harvested in the absence of cycloheximide, which complicates their comparison to our sequencing results.

Together with the more pronounced overlap we observed when comparing our datasets with those obtained from cells expressing mutant versions of eIF4A, eIF4B, and Ded1, these results suggest that eIF3 and its mRNA-entry-channel arm contribute to initial docking and scanning of the mRNA, whereas their contributions to start-codon recognition may be less critical or peripheral to those of eIF1 and eIF1A.

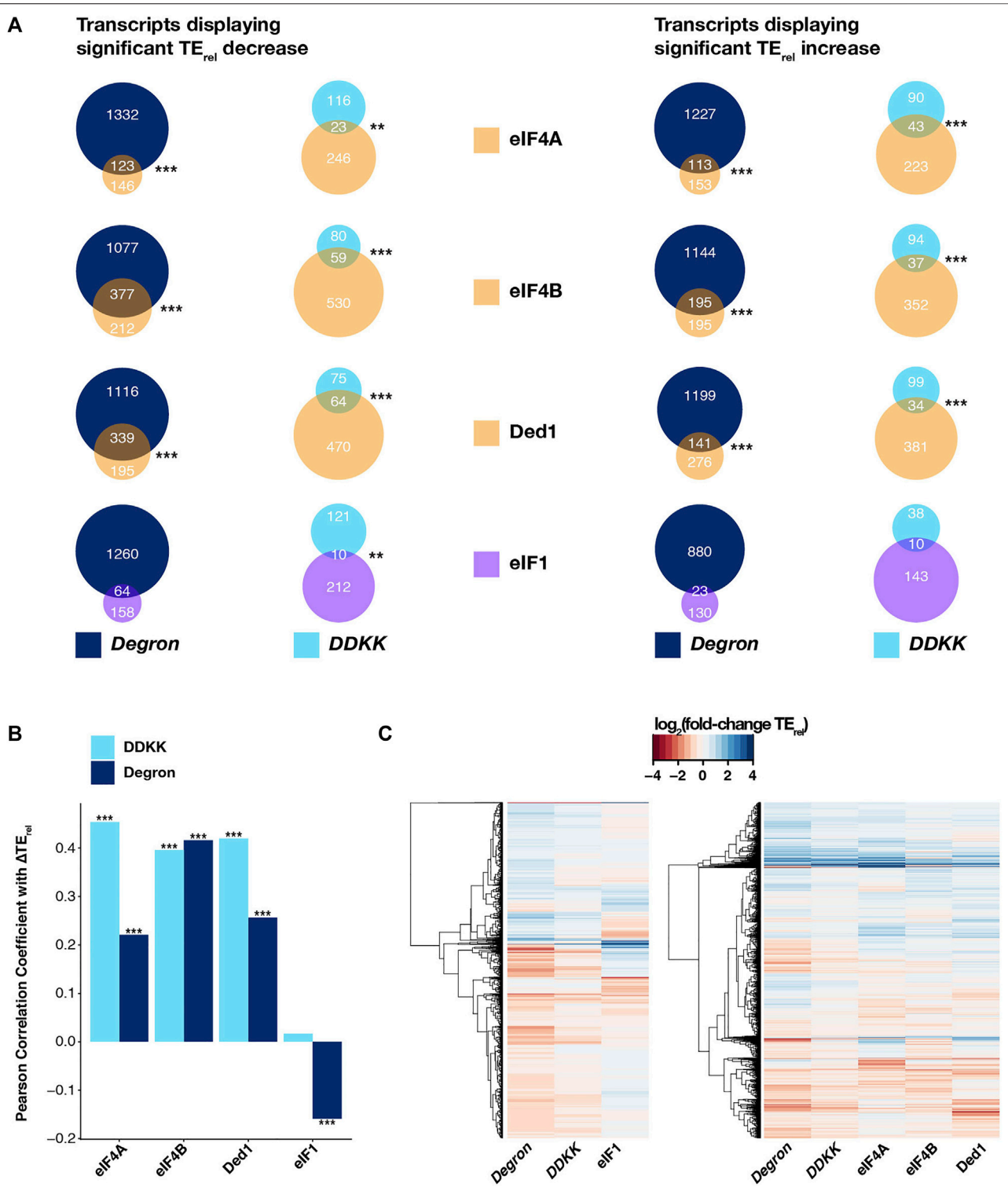

FIGURE 4 | The effects of disruption of the entire eIF3 complex or its mRNA-entry-channel arm are similar to those observed for mutations targeting other initiation factors involved in mRNA recruitment. **(A)** Venn diagrams showing the overlap between mRNAs displaying either TE_{rel} decreases (left) or increases (right) in *eIF3a/b Degron* (dark blue) or *eIF3i DDKK* (light blue) cells and cells expressing mutations targeting other initiation factors that contribute to mRNA recruitment (eIF4A, eIF4B, and Ded1; light orange) or to start-codon recognition (eIF1, purple). *** = $P < 10^{-10}$, ** = $P < 10^{-5}$, * = $P < 0.05$, HyperGeometric test. **(B)** Bar plot showing Pearson correlation coefficients obtained when comparing ΔTE_{rel} values observed in *eIF3a/b Degron* (dark blue) or *eIF3i DDKK* (light blue) cells and those observed in cells expressing mutations targeting eIF4A, eIF4B, Ded1, or eIF1. *** = $P < 10^{-10}$, ** = $P < 10^{-5}$, * = $P < 0.05$. **(C)** Heatmap and dendrograms resulting from hierarchical clustering analysis of significant TE_{rel} changes observed in *eIF3a/b Degron* and *eIF3i DDKK* cells and cells with mutations targeting either eIF1 (left) or eIF4A, eIF4B, and Ded1 (right).

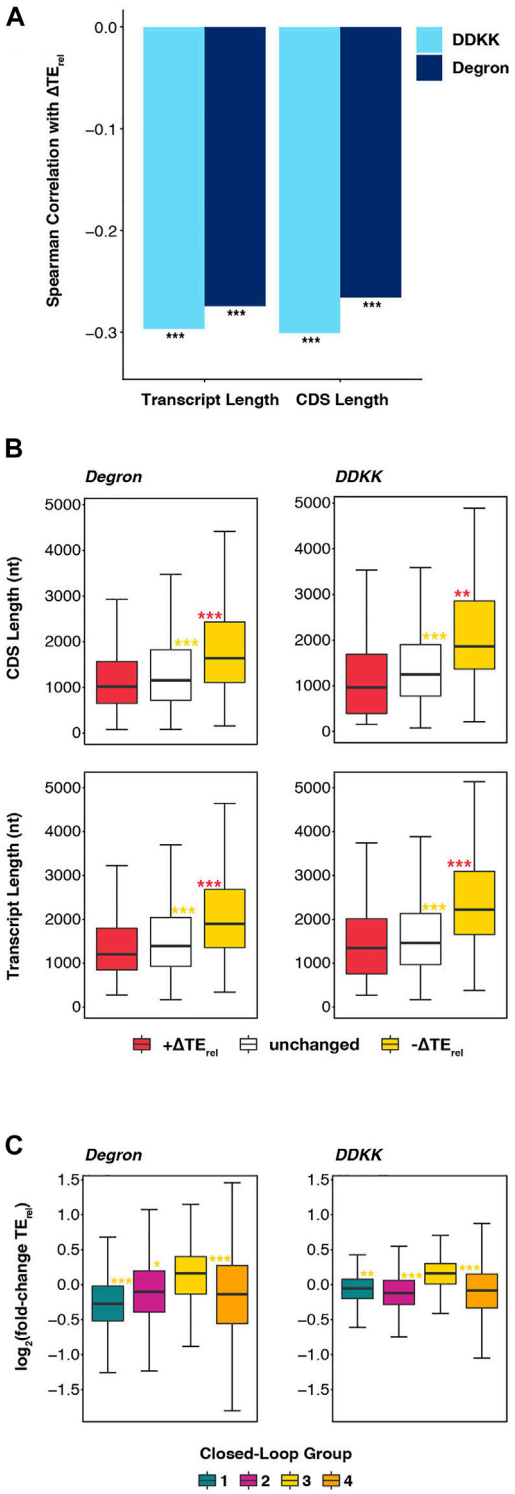

FIGURE 5 | Disruption of the eIF3 complex or its mRNA-entry-channel arm most strongly affect long mRNAs with a weaker dependence on closed loop formation. **(A)** Bar plot showing Spearman correlation coefficients obtained when comparing ΔTE_{rel} values observed in *eIF3a/b Degron* (dark blue) or *eIF3i DDKK* (light blue) cells with overall transcript length and CDS length *** = P < 10^{-10}, ** = P < 10^{-5}, * = P < 0.05, color indicates comparison set; Wilcoxon test. **(B)** Box and whisker plots comparing the TE_{rel} changes observed in either *eIF3a/b Degron* (left) or *eIF3i DDKK* (right) cells for previously identified groups of transcripts (Costello et al., 2015) that differentially associate with closed-loop factors such as eIF4G, eIF4E, and PABP. *** = $P_{adj} < 10^{-10}$, ** = $P_{adj} < 10^{-5}$, * = $P_{adj} < 0.05$, color indicates comparison set; ANOVA and post-hoc Tukey test.

Long Transcripts Less Likely to Form Closed Loop Structures Are More Sensitive to Disruption of the Entire eIF3 Complex or Its mRNA-Entry-Channel Arm

Because of the similarities we observed in the effects of *eIF3i DDKK* and *eIF3a/b Degron* mutations and mutations targeting eIF4A, eIF4B, and Ded1, we investigated whether these similarities extended to the observation that long transcripts and transcripts with lower closed-loop-forming potential are particularly sensitive to deletion of eIF4B or to mutations of eIF4A or Ded1 (Sen et al., 2016). In fact, we observed significant negative correlations between ΔTE_{rel} and both overall transcript length and coding sequence (CDS) length in both *eIF3i DDKK* and *eIF3a/b Degron* cells (**Figure 5A**). Comparing the overall length of mRNAs whose TE_{rel} decreased in each mutant eIF3 background reveals them to be significantly longer than both unaffected mRNAs ($P_{adj} < 10^{-13}$ and $P_{adj} < 10^{-16}$ for *eIF3i DDKK* and *eIF3a/b Degron*, respectively; Wilcoxon test) and mRNAs whose TE_{rel} increased ($P_{adj} < 10^{-14}$ and $P_{adj} < 10^{-16}$) (**Figure 5B**). Similarly, the CDS lengths of mRNAs whose TE_{rel} decreased in the presence of each eIF3 mutation is longer than both unaffected mRNAs ($P_{adj} < 10^{-11}$ and $P_{adj} < 10^{-16}$) and mRNAs whose TE_{rel} increased ($P_{adj} < 10^{-5}$ and $P_{adj} < 10^{-16}$).

We further observed that, as in cells expressing mutations of eIF4A or Ded1 or in which the gene coding for eIF4B was deleted, mRNAs identified in a previous study (Costello et al., 2015) as having strong closed-loop-forming potential owing to their enrichment in eIF4G, eIF4E, and PABP (group 3) are less sensitive than other mRNAs to both the *eIF3i DDKK* ($P_{adj} < 10^{-7}$; $P_{adj} < 10^{-14}$; and $P_{adj} < 10^{-14}$ for comparison to groups 1, 2, and 4 respectively) or *eIF3a/b Degron* ($P_{adj} < 10^{-12}$; $P_{adj} < 10^{-4}$; and $P_{adj} < 10^{-15}$) mutations (**Figure 5C**). Moreover, we observed positive median ΔTE_{rel} values for strong closed-loop mRNAs (group 3) and negative median ΔTE_{rel} values for weak closed-loop mRNAs (groups 1 and 2), suggesting that mRNAs with strong closed-loop-forming potential compete more effectively for the initiation machinery when eIF3 or its mRNA-entry-channel arm are disrupted, whereas mRNAs less likely to form closed-loop structures are disadvantaged under these conditions. Taken together, these results suggest that, like eIF4A, eIF4B, and Ded1, eIF3 and its mRNA-entry-channel arm may contribute to driving initiation on long mRNAs less likely to form eIF4G-, eIF4E-, and PABP-dependent closed loop structures *in vivo*. While the translation of most mRNAs likely depends on contributions from these factors, translation of these long and

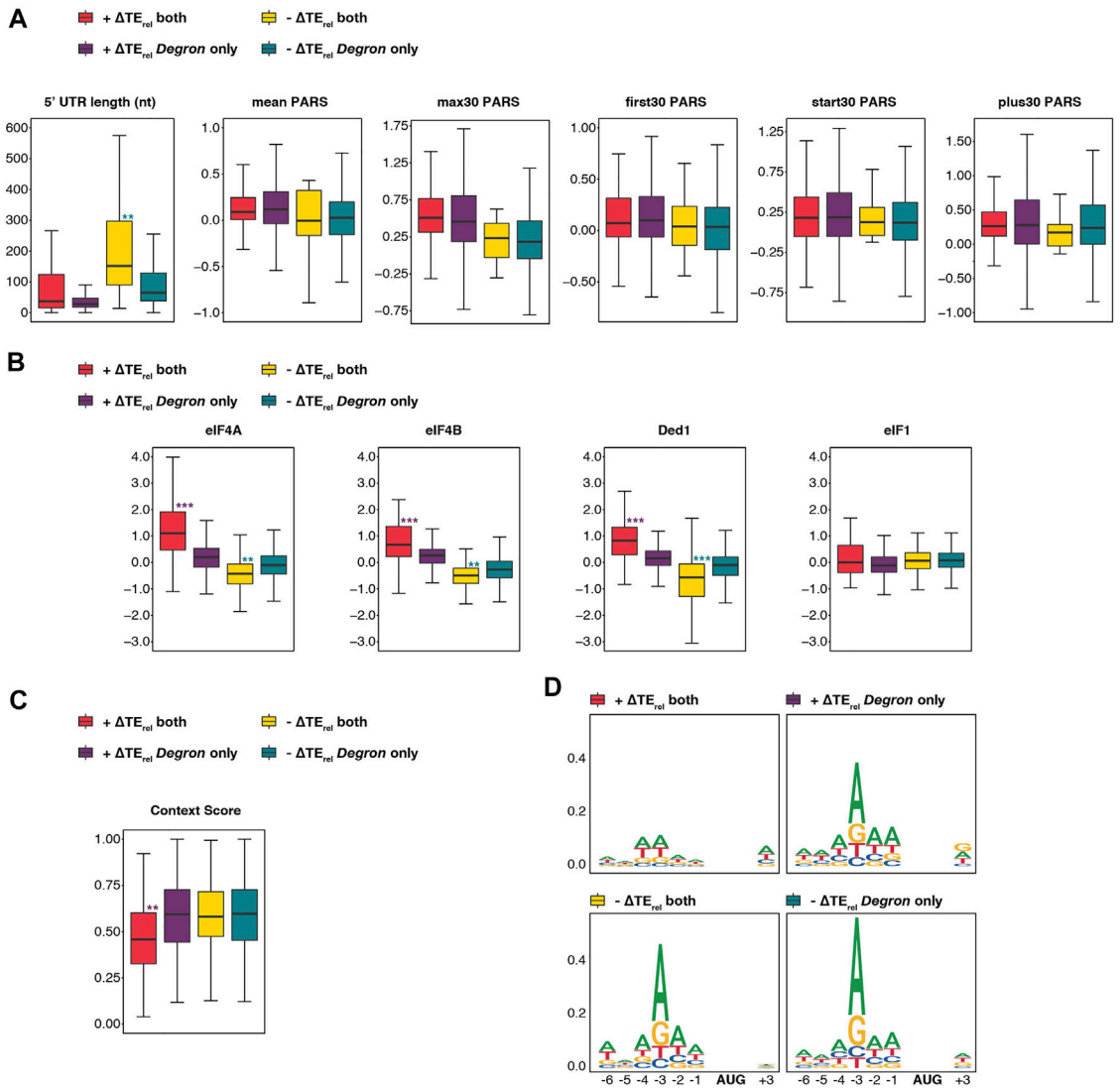

FIGURE 6 | The eIF3 mRNA-entry-channel arm collaborates with eIF4A, eIF4B, and Ded1 to drive initiation on mRNAs with long 5′-UTRs and may also discriminate against poor start-codon context. **(A)** Box and whisker plots comparing different measures of 5′-UTR length or complexity between mRNAs whose TE_{rel} significantly increases or decreases in both *eIF3a/b Degron* and *eIF3i DDKK* cells (red and yellow, respectively) or increases or decreases only in *eIF3a/b Degron* cells (purple and teal, respectively). *** = $P_{adj} < 10^{-10}$, ** = $P_{adj} < 10^{-5}$, * = $P_{adj} < 0.05$, color indicates comparison set; Wilcoxon Test for 5′-UTR lengths, ANOVA with post-hoc Tukey test for others. **(B)** Same as in A, except comparing ΔTE_{rel} values observed in cells expressing mutations targeting eIF4A, eIF4B, Ded1, and eIF1. *** = $P_{adj} < 10^{-10}$, ** = $P_{adj} < 10^{-5}$, * = $P_{adj} < 0.05$, color indicates comparison set; ANOVA with post-hoc Tukey test. **(C)** Same as in A, except comparing the Kozak sequence context (nt -6 thru +4) of affected mRNAs. *** = $P_{adj} < 10^{-10}$, ** = $P_{adj} < 10^{-5}$, * = $P_{adj} < 0.05$. **(D)** Sequence logos of nt -6 to +4 of mRNAs whose TE_{rel} either increases (top panels) or decreases (bottom panels) in both *eIF3a/b Degron* and *eIF3i DDKK* cells (left panels) or only in *eIF3a/b Degron* cells (right panels).

closed-loop-dependent mRNAs is particularly sensitive to their disruption.

Comparing the mRNAs Sensitive to Both eIF3 Mutations With Those Uniquely Sensitive to the *eIF3a/b Degron* Mutation Provides Clues to the Roles of the eIF3i and eIF3g Subunits

Because the *eIF3i DDKK* and *eIF3a/b Degron* mutations mimic the loss of either the eIF3i and eIF3g subunits (*eIF3i DDKK*) or the entire eIF3 complex (*eIF3a/b Degron*), we reasoned that comparing those mRNAs whose TE_{rel} was affected uniquely in *eIF3a/b Degron* cells to those whose TE_{rel} was affected in both *eIF3a/b Degron* and *eIF3i DDKK* cells might disentangle the roles of these distinct regions of the eIF3 complex. mRNAs whose TE_{rel} was affected in both cell lines might depend more heavily on the contributions of the eIF3i and eIF3g subunits of the eIF3 mRNA-entry-channel arm, whereas mRNAs whose TE_{rel} was affected solely in *eIF3a/b Degron* cells might depend more heavily on the contributions of other eIF3 subunits (or the collaboration of subunits within the intact complex) for their translation.

To this end, we compared the features of mRNAs whose TE_{rel} significantly increased or decreased either in both strains or exclusively in *eIF3a/b Degron* cells (**Figure 6A**). mRNAs whose TE_{rel} decreased in both *eIF3i DDKK* and *eIF3a/b Degron* cells possess longer 5′-UTRs than those whose TE_{rel} decreased only in *eIF3a/b Degron* cells, when restricting our analysis to mRNAs previously identified as having a dominant 5′ transcript isoform ($P < 10^{-9}$). In contrast, there is no significant difference in the 5′-UTR lengths of mRNAs whose TE_{rel} increased. We observed similar results when comparing 5′-UTR lengths reported in a separate study (Kertesz et al., 2010) (**Supplementary Figure S5B**). We also observed no difference in the degree of structural complexity, as measured by various PARS metrics (**Figure 2A**), of mRNAs whose TE_{rel} was affected either in both eIF3 mutant backgrounds or solely in *eIF3a/b Degron* cells. These results suggest that the eIF3i and eIF3g subunits of the mRNA-entry-channel arm may be specifically required for the contributions of eIF3 to processive scanning through long 5′-UTRs, whereas the other subunits of the eIF3 complex, either independently or in collaboration with eIF3i and eIF3g, participate in its contribution to the resolution of structural impediments during initial mRNA docking and scanning.

We next compared the differential sensitivity of affected mRNAs within these groups to mutations targeting eIF4A, eIF4B, Ded1, or eIF1 (Sen et al., 2015; Sen et al., 2016; Zhou et al., 2020). mRNAs whose TE_{rel} increased or decreased in both *eIF3i DDKK* and *eIF3a/b Degron* cells were significantly more sensitive to mutations targeting eIF4A, eIF4B, or Ded1 than those uniquely affected in *eIF3a/b Degron* cells: mRNAs whose TE_{rel} decreased in both mutant eIF3 cell lines displayed greater TE_{rel} decreases in response to mutations targeting these factors ($P < 10^{-9}$, $P < 10^{-8}$, and $P < 10^{-12}$ for eIF4A, eIF4B, and Ded1, respectively; ANOVA) and mRNAs whose TE_{rel} increased displayed stronger TE_{rel} increases in these datasets ($P < 10^{-16}$ for all comparisons, **Figure 6B**). In contrast, we observed no significant differences in the relative sensitivity of affected mRNAs to a mutation targeting eIF1. These differential sensitivities are consistent with a role for the mRNA-entry-channel arm in collaborating with eIF4A, eIF4B, and Ded1 during mRNA recruitment.

Finally, mRNAs whose TE_{rel} increased in both *eIF3i DDKK* and *eIF3a/b Degron* cells possess significantly weaker context scores than transcripts whose TE_{rel} increased uniquely in *eIF3a/b Degron* cells ($P < 10^{-8}$, **Figure 6C**). Consistent with this, sequence logos reveal that mRNAs whose TE_{rel} increased in both mutant eIF3 cell lines display a weaker preference for adenine at the -3 position (**Figure 6D**). These observations suggest that eIF3i and eIF3g, and by extension the eIF3 mRNA-entry-channel arm, may play a role in discriminating against AUG codons in poor context.

DISCUSSION

eIF3 is a multisubunit complex that contributes to events throughout the initiation pathway (Hinnebusch, 2006; Valášek et al., 2017). However, disentangling the contributions of eIF3 and its individual subunits to these events has thus far proved challenging.

To shed light on the mechanistic roles of eIF3 and its component subunits, we interrogated the effects of disrupting either the entire eIF3 complex or the eIF3i and eIF3g subunits—both components of the mRNA-entry-channel arm of eIF3—using ribosome profiling. Our results suggest that the eIF3 complex contributes to driving initiation on mRNAs with long and structurally complex 5′-UTRs and a lower propensity for forming closed-loop structures mediated by eIF4G, eIF4E, and PABP. To a lesser degree, eIF3 may also contribute to discriminating against mRNAs whose start codons appear in weak sequence context. Our results further suggest that eIF3i and eIF3g and thus the eIF3 mRNA-entry-channel arm contribute to the role of eIF3 in facilitating scanning through longer 5′-UTRs, perhaps in collaboration with eIF4A, eIF4B, and Ded1. These subunits may also contribute to discriminating against weak sequence context surrounding the start codon. However, they appear less critical for the role eIF3 plays in resolving structurally complex 5′-UTRs. Instead, the eIF3a, eIF3b, and eIF3c subunits—or all five subunits in collaboration—are required for this role.

Consistent with the strong growth defects provoked by both the *eIF3i DDKK* and *eIF3a/b Degron* mutations (Jivotovskaya et al., 2006; Herrmannová et al., 2012), we observed strong global translational defects in the presence of both mutations. Our ribosome profiling results further identified mRNAs in both mutant backgrounds whose TE_{rel} was significantly affected, as compared to the overall distribution of ΔTE_{rel} values we observed. Whereas the strong global translational effects we observe suggest that the absolute TE of most mRNAs likely decreases in the presence of both mutations, these absolute effects are removed by the normalization of read counts to library size within each sample. Instead, we focus on the relative changes in TE (TE_{rel}) we observe in each mRNA, as compared to the overall population of mRNAs across the transcriptome. In the background of global translational suppression that we observe in both cell lines, we interpret these TE_{rel} changes as indicating mRNAs whose translation is more dependent (in the case of negative ΔTE_{rel} values) or less dependent (positive ΔTE_{rel} values) than the overall population of mRNAs.

Despite the strong effects on global translation that we observe in both mutant eIF3 strains, we identify many more mRNAs whose TE_{rel} is significantly affected in *eIF3a/b Degron* cells. Intriguingly, the set of mRNAs most sensitive ($-\Delta TE_{rel}$) to the *eIF3a/b Degron* mutation was enriched in mRNAs involved in processes such as mitochondrial translation or metabolism. eIF3 was recently implicated in driving the translation of mitochondrial mRNAs in both fission yeast (Shah et al., 2016) and mammalian cells (Lin et al., 2020), a role which was attributed to the eIF3e and eIF3d subunits. eIF3d has also been linked to the preferential translation of mRNAs involved in cell proliferation pathways in human cells (Lee et al., 2015; Lee et al., 2016). This latter regulatory role appears to involve a cap-independent initiation mechanism driven by eIF3. This emerging regulatory role for eIF3 may also be linked to the observation that

eIF3 binding to the PIC persists through early rounds of elongation in both yeast and mammalian systems (Bohlen et al., 2020; Lin et al., 2020; Wagner et al., 2020). However, neither eIF3d nor eIF3e is present in the budding yeast complex. Our results suggest that the five subunits of the yeast core complex may nonetheless be capable of driving the selective translation of specific mRNAs. More targeted disruption of these subunits might further illuminate the origin of these effects and whether they involve the participation of eIF3 during initiation or early elongation cycles.

In contrast, we did not observe significant enrichment of specific GO terms in the sets of transcripts whose TE_{rel} was affected in *eIF3i DDKK* cells. We further observed a narrower set of transcripts whose translation is affected either more or less strongly than the overall population of mRNAs in the presence of this specific disruption of the eIF3 mRNA-entry-channel arm. That these cells still display strong defects in global translation—and thus likely decreases in the absolute TE of most mRNAs—suggests that the eIF3i and eIF3g subunits might contribute to aspects of mRNA recruitment required more universally across the transcriptome, as opposed to being required to drive translation of specific classes of mRNAs. This was recently suggested for eIF4A in light of the observation that ribosome profiling of cells expressing a temperature-sensitive eIF4A variant that provokes strong global translational defects did not identify substantial numbers of mRNAs more or less sensitive than the overall population, consistent with *in vitro* measurements suggesting a universal role for eIF4A in alleviating structural complexity within mRNAs (Sen et al., 2015; Yourik et al., 2017).

While our results point to potentially distinct roles for eIF3 and its mRNA-entry-channel arm in either mediating initiation on specific classes of mRNAs or driving the translation of mRNAs across the transcriptome, they also further illuminate the role of eIF3 and its mRNA-entry-channel arm in contributing to mRNA recruitment and its component events of PIC docking, scanning, and start-codon recognition. We show that mRNAs possessing longer 5′-UTRs are more sensitive to disruption of both the entire complex or targeted disruption of the mRNA-entry-channel arm. This is consistent with the identification of mutations throughout the eIF3 complex that affect scanning, with several of these mutations targeting eIF3i (Herrmannová et al., 2012), eIF3g (Cuchalova et al., 2010), and other constituents of the mRNA-entry-channel arm (Nielsen et al., 2006; Chiu et al., 2010; Cuchalova et al., 2010).

We also observed that the effects of both eIF3 mutations are similar to those observed via ribosome profiling of cells expressing mutations targeting eIF4A, eIF4B, and Ded1 (Sen et al., 2015; Sen et al., 2016; Zhou et al., 2020), all of which are thought to contribute either to initial PIC docking to the mRNA or subsequent scanning. These similarities extend to the observation that mRNAs likely to form stable closed-loop structures are least sensitive to mutations targeting these initiation factors and to both eIF3 mutations, whereas mRNAs less likely to form stable closed-loop structures are more sensitive. Together, these observations suggest that eIF3 may collaborate with eIF4A, eIF4B, and Ded1 to drive initiation on mRNAs with longer 5′-UTRs and a weaker dependence on the initiation factors eIF4G, eIF4E, and PABP. eIF3—via the eIF3a CTD component of the eIF3 mEnC arm—interacts with eIF4B (Methot et al., 1996) and with the 40S latch (Chiu et al., 2010). Moreover, eIF3 is present in both the mRNA-entry and -exit channels of the ribosome in both yeast and mammalian structures (Aylett et al., 2015; Simonetti et al., 2016). In a recent structure of the human 48S complex, eIF3g was observed binding to ribosomal RNA and protein elements within the mRNA-entry channel and eIF3k, eIF3l, and eIF3e were found adjacent to eIF4A near the mRNA-exit channel (Querido et al., 2020). And yet, eIF3k, -l, and -e are absent from the yeast eIF3 complex, where eIF3a and eIF3c are alone found near the mRNA-exit channel of the ribosome. However, *in vitro* studies reveal that, in addition to eIF3d and eIF3e, eIF3c (which is present in budding yeast) is also able to bind to components of the eIF4F complex (Villa et al., 2013). Together with our results here, these observations together raise several possibilities for direct or functional collaboration between eIF3 and these other factors.

eIF3 has also been implicated in driving cap-independent initiation mechanisms (Lee et al., 2016; Rode et al., 2018; Bhardwaj et al., 2019) and in directly recruiting the PIC to specific classes of mRNAs (Lee et al., 2015; Lee et al., 2016; Shah et al., 2016; Lin et al., 2020; Lamper et al., 2020), both of which may circumvent the requirement for eIF4G-, eIF4E-, and PABP-mediated closed-loop formation. Our observation that these effects manifest upon targeting either the entire eIF3 complex or simply the mRNA-entry-channel arm point to a role for the mRNA-entry-channel arm in collaborating with these other factors to mediate initiation in the absence of stable closed-loop formation. In fact, eIF3 and eIF4A were recently shown to collaborate in a non-canonical initiation pathway that circumvents eIF4E and eIF4G during neuronal development in *Drosophila* (Rode et al., 2018).

In contrast, we observed stronger effects of mRNA structural complexity when disrupting the entire eIF3 complex than when specifically targeting its mRNA-entry-channel arm. Certainly, this does not exclude the possibility that either or both eIF3i and eIF3g contribute to resolving regions of structural complexity within the 5′-UTR. Mutations targeting these subunits have previously been shown to interfere with initiation on reporter mRNAs containing stable stem loop structures (Cuchalova et al., 2010; Herrmannová et al., 2012). Nonetheless, our results point to the remaining eIF3 subunits—eIF3a, eIF3b, and eIF3c, either alone or in collaboration with eIF3i and eIF3g—playing a role in resolving structural complexity during initial PIC docking or scanning. Both eIF3a (via its CTD) and eIF3b contribute to the mRNA-entry-channel arm (Aylett et al., 2015; Llácer et al., 2015; Simonetti et al., 2016; Llácer et al., 2018) and mutations targeting the eIF3a CTD disrupt initiation on reporter mRNAs containing stem loop structures (Chiu et al., 2010). In addition, eIF3a interacts physically and functionally with mRNA near the mRNA-exit channel of the ribosome (Szamecz et al., 2008; Munzarová et al., 2011; Aitken et al., 2016; Llácer et al., 2018) and eIF3c binds components of the eIF4F complex (Villa et al., 2013) that have recently been visualized near the mRNA-exit channel in the human 48S PIC (Querido et al., 2020).

Whereas we observed relatively strong effects on either initial docking or scanning in the presence of both eIF3 mutations, we observed more nuanced effects on start-codon recognition upon disruption of the eIF3 mRNA-entry-channel arm. In contrast to the similarities between the effects of both eIF3 mutations and those previously observed for mutations targeting eIF4A, eIF4B, and Ded1, we observed relatively little similarity with those observed in previous ribosome profiling experiments targeting eIF1. Nonetheless, our observation that those mRNAs least sensitive to the *eIF3i DDKK* mutation exhibit weaker start-codon context does suggest that the eIF3 mRNA-entry-channel arm plays a role in discriminating against AUG codons in weak context. Consistent with this, mutations targeting several components of the mRNA-entry-channel arm elicit defects in either the accuracy or efficiency of start-codon recognition (Nielsen et al., 2004, 2006; Chiu et al., 2010; Cuchalova et al., 2010; Herrmannová et al., 2012). The fact that we observe these modest effects but do not observe similarities between our dataset and ribosome profiling data from eIF1 mutant cells suggests that these effects do not arise from disruption of the functional collaboration between eIF3 and eIF1(Valasek et al., 2004; Llácer et al., 2015; Llácer et al., 2018). Instead, it is possible that disruption of the eIF3 mRNA-entry-channel arm might disrupt its modulation of the equilibrium between the open and closed states of the PIC via interaction with the 40S latch. Indeed, mutations targeting this nexus produce start-codon recognition defects (Chiu et al., 2010; Dong et al., 2017).

Overall, we observed striking similarities between the effects of the *eIF3i DDKK* and *eIF3a/b Degron* mutations. Consistent with their disruption of either a portion of the eIF3 mRNA-entry-channel arm (*eIF3i DDKK*) or the entire complex (*eIF3a/b Degron*), the affected mRNAs we identified in *eIF3i DDKK* cells comprise subsets of those we identified in *eIF3a/b Degron* cells. Nonetheless, comparison of those transcripts whose TE_{rel} was affected in both eIF3 mutant backgrounds with those affected solely in *eIF3a/b Degron* cells identifies telling differences that suggest roles for the eIF3i and eIF3g subunits of the eIF3 mRNA-entry-channel arm. mRNAs whose TE_{rel} decreases in both backgrounds—suggesting that their translation depends more strongly on the eIF3i and eIF3g subunits affected by both mutations—have 5′-UTRs that are longer but are no more structurally complex than those whose TE_{rel} decreases only when the entire eIF3 complex is disrupted. mRNAs sensitive to both mutations are also more strongly affected by mutations targeting eIF4A, eIF4B, and Ded1. mRNAs whose TE_{rel} decreased in both backgrounds displayed stronger TE_{rel} decreases in the presence of these other mutations than mRNAs whose TE_{rel} decreased solely in *eIF3a/b Degron* cells. mRNAs whose TE_{rel} increased in both mutant eIF3 backgrounds similarly display stronger TE_{rel} increases in cells expressing mutants of eIF4A, eIF4B, or Ded1. mRNAs whose TE_{rel} increased in both eIF3 backgrounds further possess weaker start-codon sequence context than those whose TE_{rel} increased solely in *eIF3a/b Degron* cells.

Together, these observations again point to roles for eIF3i and eIF3g, and by extension the eIF3 mRNA-entry-channel arm, in functional collaboration with eIF4A, eIF4B, and Ded1 to drive processive scanning through longer 5′-UTRs on mRNAs whose translation is less dependent on the formation of a stable closed loop. Surprisingly, effects on scanning processivity were not previously observed using a set of reporter constructs in extracts derived from cells expressing *eIF3i DDKK* cells (Herrmannová et al., 2012), perhaps because other features present in natural mRNAs or mRNPs are required to elicit these effects. Distinct mutations targeting either eIF3i or eIF3g, however, do manifest defects in scanning processivity (Cuchalova et al., 2010). Our results also suggest that eIF3i and eIF3g play a role in discriminating against weak start-codon context during start-codon recognition. Previous experiments following the effects of the *eIF3i DDKK* mutation using a series of reporter mRNAs observed leaky scanning of AUG codons, suggesting these subunits might contribute to efficient start-codon recognition (Herrmannová et al., 2012). However, the effect of codon context was not reported.

While the eIF3i and eIF3g subunits of the eIF3 mRNA-entry-channel arm appear to contribute to scanning processivity, the remaining subunits (or the entire complex) appear to contribute to resolving structural complexity within 5′-UTRs. We observed stronger and more significant effects of various measures of structural complexity throughout the 5′-UTRs of mRNAs in *eIF3a/b Degron* cells than we did in *eIF3i DDKK* cells. That we do not observe these effects in *eIF3i DDKK* cells but still observe strong similarities with those effects observed in mutant eIF4A, eIF4B, or Ded1 cells (and find that mRNAs sensitive only to the *eIF3a/b Degron* mutation are less sensitive to mutations targeting these factors) might suggest that eIF3 can also contribute to the resolution of structural complexity independently of any collaboration with these factors. Another possibility is that eIF3 does indeed collaborate with these factors but via distinct functional mechanisms to resolve stable structural impediments near the 5′ cap or within downstream 5′-UTR regions.

Finally, we also found that mRNAs whose translation is most sensitive to the disruption of the entire eIF3 complex were enriched in mRNAs involved in mitochondrial translation and metabolism. This observation echoes the recently identified role of eIF3 in preferentially mediating translation on these classes of mRNAs in fission yeast and mammalian cells (Shah et al., 2016; Lin et al., 2020). That role appears to involve the eIF3d subunit, which has also been implicated in mediating the translation of mRNAs involved in cell proliferation (Lee et al., 2016), as well as the ability of eIF3 to remain bound during early rounds of elongation (Bohlen et al., 2020; Lin et al., 2020; Wagner et al., 2020). Because eIF3d is absent in budding yeast cells, our observations suggest that at least one subunit of the core complex is capable of reprising aspects of this role. A potential candidate is eIF3a which, like eIF3d, is positioned near the mRNA-exit channel of the ribosome and appears to interact physically and functionally with the mRNA there (Szamecz et al., 2008; Aitken et al., 2016; Llácer et al., 2018). eIF3a has also previously been implicated in mediating sequence-dependent reinitiation events, a function

which requires direct interaction with specific mRNA sequence elements (Szamecz et al., 2008; Munzarová et al., 2011). The mechanistic origin of these effects in budding yeast, and whether they involve the participation of eIF3 during initiation, early rounds of elongation, or both, emerge as intriguing questions.

Our work sheds light on the specific roles of the eIF3 mRNA-entry-channel arm and its other subunits during the component events of mRNA recruitment. It further points to a potential role for eIF3 in mediating the translation of specific classes of mRNAs, as in higher eukaryotic cells. Nonetheless, experiments following the fate of reporter constructs containing the 5′-UTRs of sensitive mRNAs in *eIF3i DDKK* and *eIF3a/b Degron* cells or cell extracts or the requirements of sensitive mRNAs for eIF3 or eIF3i and eIF3g in mRNA recruitment assays *in vitro* might further strengthen the case for these roles. Still further investigation is necessary to determine the mechanism whereby eIF3 mediates translation of these mRNAs, how it functions to facilitate initiation on mRNAs with structurally complex 5′-UTRs, and how its mRNA-entry-channel arm collaborates with other initiation factors to drive initial docking and scanning on mRNAs independent of closed-loop formation.

DATA AVAILABILITY STATEMENT

Sequencing data from this study have been submitted to the NCBI Gene Expression Omnibus (GEO; http://www.ncbi.nlm.nih.gov/geo/) under accession number GSE190601.

AUTHOR CONTRIBUTIONS

CA performed the experiments, wrote the manuscript, prepared final versions of the figures, and performed data analysis. AS performed significant data preparation, analysis, and interpretation. JL performed data analysis and interpretation. LF and SGH performed data analysis. SK performed sample preparation and data preparation.

FUNDING

CEA is supported by R15 GM140372 (NIH/NIGMS). AS is an undergraduate student in the Computer Science Department at Vassar College. JL is an undergraduate student in the Biochemistry Program at Vassar College; LF and SGH are undergraduate students in the Biology Department at Vassar College and are supported by R15 GM140372 (NIH/NIGMS).

ACKNOWLEDGMENTS

CEA would like to acknowledge Jon R. Lorsch and Alan G. Hinnebusch of the National Institutes of Health for their support and guidance during the initial phases of this project. In addition, CEA would like to acknowledge Jennifer Kennell and Zachary Donhauser of the Vassar College Biochemistry Program, Justin Touchon of the Vassar College Biology Department, and Shardul Kulkarni of the Department of Biochemistry & Molecular Biology at Penn State Eberly College of Science for their comments and guidance during the preparation of this manuscript.

SUPPLEMENTARY MATERIAL

The Supplementary Material for this article can be found online at: https://www.frontiersin.org/articles/10.3389/fmolb.2021.787664/full#supplementary-material

Supplementary Figure 1 | Disruption of the eIF3 complex or its mRNA-entry-channel arm provoke strong global translational defects. **(A)** Polysome profiles collected from *eIF3a/b Degron* and *eIF3i DDKK* cells and isogenic wild-type cells grown under permissive conditions. **(B,C)** Polysome profiles collected from biological replicates used to prepare ribosome profiling libraries for *eIF3i DDKK* **(B)** and *eIF3a/b Degron* (**C**) cells and isogenic wild-type cells upon shifting to growth under restrictive conditions for 30 min (*eIF3i DDKK*) or 90 min (*eIF3a/b Degron*).

Supplementary Figure 2 | mRNA fragment and Ribosome footprint libraries obtained from biological replicates of *eIF3i DDKK* and *eIF3a/b Degron* cells are highly reproducible. Correlation plots of read counts obtained from mRNA fragment and ribosome footprint libraries prepared from biological replicates of *eIF3i DDKK* and *eIF3a/b Degron* cells and matching isogenic wild-type cells.

Supplementary Figure 3 | Disruption of the eIF3 complex affects the translation of mRNAs associated with mitochondrial processes. Bar plots showing the percent over- or under-representation of specific biological process GO terms in the list of mRNAs whose TE_{rel} either significantly decreases (left) or increases (right) in *eIF3a/b Degron* cells. Color scale indicates P_{adj} values.

Supplementary Figure 4 | Disruption of eIF3 or its mRNA-entry-channel arm result in global increases in relative uORF translation that are strongest for uORFs closest to the 5' end. **(A)** Correlation of uORF TE_{rel} values observed in either *eIF3a/b Degron* (left) or *eIF3i DDKK* (right) cells and those observed in isogenic wild-type cells. uORFs displaying significant ($P_{adj} < 0.05$) TE_{rel} increases (>50% red, > 100% blue) or decreases (>50% yellow, >100% green) as determined by DESeq2 analysis are shown in colors. **(B)** Correlation of observed ΔTE_{rel} values and distance from the 5' end for individual uORFs in *eIF3a/b Degron* (left) and *eIF3i DDKK* (right) cells. Spearman correlation fits shown in red.

Supplementary Figure 5 | Disruption of eIF3 or its mRNA-entry-channel arm affect the translation of mRNAs with long 5'-UTRs. **(A)** Box and whisker plots comparing 5'-UTR lengths (reported by Kertesz, et al., Nature 2010) between mRNAs whose TE_{rel} significantly increases (red), decreases (yellow), or is unaffected (white) in each eIF3 mutant strain. *** = $P_{adj} < 10^{-10}$, ** = $P_{adj} < 10^{-5}$, * = $P_{adj} < 0.05$, color indicates comparison set; Wilcoxon test. **(B)** Same as in A, except comparing 5'-UTR lengths between mRNAs whose TE_{rel} significantly increases or decreases in both *eIF3a/b Degron* and *eIF3i DDKK* cells (red and yellow, respectively) or increases or decreases only in *eIF3a/b Degron* cells (purple and teal, respectively). *** = $P_{adj} < 10^{-10}$, ** = $P_{adj} < 10^{-5}$, * = $P_{adj} < 0.05$, color indicates comparison set; Wilcoxon test.

Supplementary Figure 6 | Observed ΔTE_{rel} values in *eIF3a/b Degron* and *eIF3i DDKK* cells are not correlated with the AUG sequence context of individual mRNAs. Correlation plots comparing observed ΔTE_{rel} values in *eIF3a/b Degron* (left) or *eIF3i DDKK* (right) cells and the AUG sequence context (nt –6 to +4) of individual mRNAs. Predicted Spearman correlations shown in red.

Supplementary Figure 7 | ΔTE_{rel} values observed in *eIF3a/b Degron* and *eIF3i DDKK* cells strongly correlate with those observed in the presence of mutations targeting eIF4A, eIF4B, and Ded1 but not eIF1 or eIF1A. Correlation plots comparing observed ΔTE_{rel} values in *eIF3a/b Degron* (top) or *eIF3i DDKK* (bottom) cells and those observed for mutations targeting eIF4A, eIF4B, Ded1, eIF1, and eIF1A. Predicted Spearman correlations shown in red.

REFERENCES

Aitken, C. E., Beznosková, P., Vlčkova, V., Chiu, W.-L., Zhou, F., Valášek, L. S., et al. (2016). Eukaryotic Translation Initiation Factor 3 Plays Distinct Roles at the Mrna Entry and Exit Channels of the Ribosomal Preinitiation Complex. *Elife* 5, 1. doi:10.7554/eLife.20934

Aitken, C. E., and Lorsch, J. R. (2012). A Mechanistic Overview of Translation Initiation in Eukaryotes. *Nat. Struct. Mol. Biol.* 19, 568–576. doi:10.1038/nsmb.2303

Asano, K., Clayton, J., Shalev, A., and Hinnebusch, A. G. (2000). A Multifactor Complex of Eukaryotic Initiation Factors, eIF1, eIF2, eIF3, eIF5, and Initiator tRNAMet Is an Important Translation Initiation Intermediate *In Vivo*. *Genes Dev.* 14, 2534–2546. doi:10.1101/gad.831800

Aylett, C. H. S., Boehringer, D., Erzberger, J. P., Schaefer, T., and Ban, N. (2015). Structure of a Yeast 40S-eIF1-eIF1A-eIF3-eIF3j Initiation Complex. *Nat. Struct. Mol. Biol.* 22, 269–271. doi:10.1038/nsmb.2963

Bhardwaj, U., Powell, P., and Goss, D. J. (2019). Eukaryotic Initiation Factor (eIF) 3 Mediates Barley Yellow Dwarf Viral mRNA 3′-5′ UTR Interactions and 40S Ribosomal Subunit Binding to Facilitate Cap-independent Translation. *Nucleic Acids Res.* 47, 6225–6235. doi:10.1093/nar/gkz448

Bohlen, J., Fenzl, K., Kramer, G., Bukau, B., and Teleman, A. A. (2020). Selective 40S Footprinting Reveals Cap-Tethered Ribosome Scanning in Human Cells. *Mol. Cel.* 79, 561–574. doi:10.1016/j.molcel.2020.06.005

Brito Querido, J., Sokabe, M., Kraatz, S., Gordiyenko, Y., Skehel, J. M., Fraser, C. S., et al. (2020). Structure of a Human 48 S Translational Initiation Complex. *Science* 369, 1220–1227. doi:10.1126/SCIENCE.ABA4904

Chiu, W.-L., Wagner, S., Herrmannova´, A., Burela, L., Zhang, F., Saini, A. K., et al. (2010). The C-Terminal Region of Eukaryotic Translation Initiation Factor 3a (eIF3a) Promotes mRNA Recruitment, Scanning, and, Together with eIF3j and the eIF3b RNA Recognition Motif, Selection of AUG Start Codons. *Mol. Cell. Biol.* 30, 4415–4434. doi:10.1128/mcb.00280-10

Costello, J., Castelli, L. M., Rowe, W., Kershaw, C. J., Talavera, D., Mohammad-Qureshi, S. S., et al. (2015). Global mRNA Selection Mechanisms for Translation Initiation. *Genome Biol.* 16, 1. doi:10.1186/s13059-014-0559-z

Cuchalova´, L., Kouba, T., Herrmannova´, A., Da´nyi, I., Chiu, W.-l., Vala´šek, L., et al. (2010). The RNA Recognition Motif of Eukaryotic Translation Initiation Factor 3g (eIF3g) Is Required for Resumption of Scanning of Posttermination Ribosomes for Reinitiation on GCN4 and Together with eIF3i Stimulates Linear Scanning. *Mol. Cell. Biol.* 30, 4671–4686. doi:10.1128/mcb.00430-10

Des Georges, A., Dhote, V., Kuhn, L., Hellen, C. U. T., Pestova, T. V., Frank, J., et al. (2015). Structure of Mammalian eIF3 in the Context of the 43S Preinitiation Complex. *Nature* 525, 491–495. doi:10.1038/nature14891

Dong, J., Aitken, C. E., Thakur, A., Shin, B.-S., Lorsch, J. R., and Hinnebusch, A. G. (2017). Rps3/uS3 Promotes mRNA Binding at the 40S Ribosome Entry Channel and Stabilizes Preinitiation Complexes at Start Codons. *Proc. Natl. Acad. Sci. USA* 114, E2126–E2135. doi:10.1073/pnas.1620569114

Elantak, L., Wagner, S., Herrmannová, A., Karásková, M., Rutkai, E., Lukavsky, P. J., et al. (2010). The Indispensable N-Terminal Half of eIF3j/HCR1 Cooperates with its Structurally Conserved Binding Partner eIF3b/PRT1-RRM and with eIF1A in Stringent AUG Selection. *J. Mol. Biol.* 396, 1097–1116. doi:10.1016/j.jmb.2009.12.047

Gerashchenko, M. V., and Gladyshev, V. N. (2014). Translation Inhibitors Cause Abnormalities in Ribosome Profiling Experiments. *Nucleic Acids Res.* 42, e134. doi:10.1093/NAR/GKU671

Gupta, N., Lorsch, J. R., and Hinnebusch, A. G. (2018). Yeast Ded1 Promotes 48S Translation Pre-initiation Complex Assembly in an mRNA-specific and eIF4F-dependent Manner. *Elife* 7, 1. doi:10.7554/eLife.38892

Herrmannová, A., Daujotytė, D., Yang, J.-C., Cuchalová, L., Gorrec, F., Wagner, S., et al. (2012). Structural Analysis of an eIF3 Subcomplex Reveals Conserved Interactions Required for a Stable and Proper Translation Pre-initiation Complex Assembly. *Nucleic Acids Res.* 40, 2294–2311. doi:10.1093/nar/gkr765

Hinnebusch, A. G. (2006). eIF3: a Versatile Scaffold for Translation Initiation Complexes. *Trends Biochem. Sci.* 31, 553–562. doi:10.1016/j.tibs.2006.08.005

Hinnebusch, A. G., Ivanov, I. P., and Sonenberg, N. (2016). Translational Control by 5′-untranslated Regions of Eukaryotic mRNAs. *Science* 352, 1413–1416. doi:10.1126/science.aad9868

Hinnebusch, A. G. (2017). Structural Insights into the Mechanism of Scanning and Start Codon Recognition in Eukaryotic Translation Initiation. *Trends Biochem. Sci.* 42, 589–611. doi:10.1016/j.tibs.2017.03.004

Hinnebusch, A. G. (2014). The Scanning Mechanism of Eukaryotic Translation Initiation. *Annu. Rev. Biochem.* 83, 779–812. doi:10.1146/annurev-biochem-060713-035802

Ingolia, N. T. (2010). Genome-Wide Translational Profiling by Ribosome Footprinting. *Methods Enzymol.* 470, 119–142. doi:10.1016/S0076-6879(10)70006-9

Ingolia, N. T., Ghaemmaghami, S., Newman, J. R. S., and Weissman, J. S. (2009). Genome-wide Analysis *In Vivo* of Translation with Nucleotide Resolution Using Ribosome Profiling. *Science* 324, 218–223. doi:10.1126/science.1168978

Jackson, R. J., Hellen, C. U. T., and Pestova, T. V. (2010). The Mechanism of Eukaryotic Translation Initiation and Principles of its Regulation. *Nat. Rev. Mol. Cel. Biol.* 11, 113–127. doi:10.1038/nrm2838

Jivotovskaya, A. V., Vala´šek, L., Hinnebusch, A. G., and Nielsen, K. H. (2006). Eukaryotic Translation Initiation Factor 3 (eIF3) and eIF2 Can Promote mRNA Binding to 40S Subunits Independently of eIF4G in Yeast. *Mol. Cell. Biol.* 26, 1355–1372. doi:10.1128/mcb.26.4.1355-1372.2006

Kertesz, M., Wan, Y., Mazor, E., Rinn, J. L., Nutter, R. C., Chang, H. Y., et al. (2010). Genome-wide Measurement of RNA Secondary Structure in Yeast. *Nature* 467, 103–107. doi:10.1038/nature09322

Kulkarni, S. D., Zhou, F., Sen, N. D., Zhang, H., Hinnebusch, A. G., and Lorsch, J. R. (2019). Temperature-dependent Regulation of Upstream Open reading Frame Translation in *S. cerevisiae*. *BMC Biol.* 17, 1. doi:10.1186/s12915-019-0718-5

Lamper, A. M., Fleming, R. H., Ladd, K. M., and Lee, A. S. Y. (2020). A Phosphorylation-Regulated eIF3d Translation Switch Mediates Cellular Adaptation to Metabolic Stress. *Science* 370 (6518), 1853–856. doi:10.1126/science.abb0993

Lee, A. S. Y., Kranzusch, P. J., and Cate, J. H. D. (2015). EIF3 Targets Cell-Proliferation Messenger RNAs for Translational Activation or Repression. *Nature* 522, 111–114. doi:10.1038/nature14267

Lee, A. S. Y., Kranzusch, P. J., Doudna, J. A., and Cate, J. H. D. (2016). EIF3d Is an mRNA Cap-Binding Protein that Is Required for Specialized Translation Initiation. *Nature* 536, 96–99. doi:10.1038/nature18954

Lin, Y., Li, F., Huang, L., Polte, C., Duan, H., Fang, J., et al. (2020). eIF3 Associates with 80S Ribosomes to Promote Translation Elongation, Mitochondrial Homeostasis, and Muscle Health. *Mol. Cel.* 79, 575–587. doi:10.1016/j.molcel.2020.06.003

Llácer, J. L., Hussain, T., Dong, J., Villamayor, L., Gordiyenko, Y., and Hinnebusch, A. G. (2021). Large-Scale Movement of eIF3 Domains During Translation Initiation Modulate Start Codon Selection. *Nucleic Acids Research* 49 (20), 11491–11511. doi:10.1093/nar/gkab908

Llácer, J. L., Hussain, T., Marler, L., Aitken, C. E., Thakur, A., Lorsch, J. R., et al. (2015). Conformational Differences between Open and Closed States of the Eukaryotic Translation Initiation Complex. *Mol. Cel.* 59, 399–412. doi:10.1016/j.molcel.2015.06.033

Llácer, J. L., Hussain, T., Saini, A. K., Nanda, J. S., Kaur, S., Gordiyenko, Y., et al. (2018). Translational Initiation Factor eIF5 Replaces eIF1 on the 40S Ribosomal Subunit to Promote Start-Codon Recognition. *Elife* 7, 1. doi:10.7554/ELIFE.39273

Love, M. I., Huber, W., and Anders, S. (2014). Moderated Estimation of Fold Change and Dispersion for RNA-Seq Data with DESeq2. *Genome Biol.* 15, 550. doi:10.1186/s13059-014-0550-8

Majumdar, R., Bandyopadhyay, A., and Maitra, U. (2003). Mammalian Translation Initiation Factor eIF1 Functions with eIF1A and eIF3 in the Formation of a Stable 40 S Preinitiation Complex. *J. Biol. Chem.* 278, 6580–6587. doi:10.1074/jbc.m210357200

Martin-Marcos, P., Zhou, F., Karunasiri, C., Zhang, F., Dong, J., Nanda, J., et al. (2017). eIF1A Residues Implicated in Cancer Stabilize Translation Preinitiation Complexes and Favor Suboptimal Initiation Sites in Yeast. *Elife* 6, 1. doi:10.7554/eLife.31250

Méthot, N., Song, M. S., and Sonenberg, N. (1996). A Region Rich in Aspartic Acid, Arginine, Tyrosine, and glycine (DRYG) Mediates Eukaryotic Initiation Factor 4B (eIF4B) Self-Association and Interaction with eIF3. *Mol. Cell. Biol.* 16, 5328–5334. doi:10.1128/mcb.16.10.5328

Mitchell, S. F., Walker, S. E., Algire, M. A., Park, E.-H., Hinnebusch, A. G., and Lorsch, J. R. (2010). The 5′-7-Methylguanosine Cap on Eukaryotic mRNAs Serves Both to Stimulate Canonical Translation Initiation and to Block an Alternative Pathway. *Mol. Cel.* 39, 950–962. doi:10.1016/j.molcel.2010.08.021

Munzarová, V., Pánek, J., Gunišová, S., Dányi, I., Szamecz, B., and Valášek, L. S. (2011). Translation Reinitiation Relies on the Interaction between eIF3a/TIF32 and Progressively Folded Cis-Acting mRNA Elements Preceding Short uORFs. *Plos Genet.* 7, e1002137. doi:10.1371/journal.pgen.1002137

Nielsen, K. H., Szamecz, B., Valášek, L., Jivotovskaya, A., Shin, B.-S., and Hinnebusch, A. G. (2004). Functions of eIF3 Downstream of 48S Assembly Impact AUG Recognition and GCN4 Translational Control. *EMBO J.* 23, 1166–1177. doi:10.1038/sj.emboj.7600116

Nielsen, K. H., Vala´šek, L., Sykes, C., Jivotovskaya, A., and Hinnebusch, A. G. (2006). Interaction of the RNP1 Motif in PRT1 with HCR1 Promotes 40S Binding of Eukaryotic Initiation Factor 3 in Yeast. *Mol. Cell. Biol.* 26, 2984–2998. doi:10.1128/mcb.26.8.2984-2998.2006

Pelechano, V., Wei, W., and Steinmetz, L. M. (2013). Extensive Transcriptional Heterogeneity Revealed by Isoform Profiling. *Nature* 497, 127–131. doi:10.1038/nature12121

Rode, S., Ohm, H., Anhäuser, L., Wagner, M., Rosing, M., Deng, X., et al. (2018). Differential Requirement for Translation Initiation Factor Pathways during Ecdysone-dependent Neuronal Remodeling in Drosophila. *Cel. Rep.* 24, 2287–2299. e4. doi:10.1016/J.CELREP.2018.07.074

Sen, N. D., Gupta, N., K. Archer, S., Preiss, T., Lorsch, J. R., and Hinnebusch, A. G. (2019). Functional Interplay between DEAD-Box RNA Helicases Ded1 and Dbp1 in Preinitiation Complex Attachment and Scanning on Structured mRNAs *In Vivo*. *Nucleic Acids Res.* 47, 8785–8806. doi:10.1093/nar/gkz595

Sen, N. D., Zhou, F., Harris, M. S., Ingolia, N. T., and Hinnebusch, A. G. (2016). eIF4B Stimulates Translation of Long mRNAs with Structured 5′ UTRs and Low Closed-Loop Potential but Weak Dependence on eIF4G. *Proc. Natl. Acad. Sci. USA* 113, 10464–10472. doi:10.1073/pnas.1612398113

Sen, N. D., Zhou, F., Ingolia, N. T., and Hinnebusch, A. G. (2015). Genome-wide Analysis of Translational Efficiency Reveals Distinct but Overlapping Functions of Yeast DEAD-Box RNA Helicases Ded1 and eIF4A. *Genome Res.* 25, 1196–1205. doi:10.1101/gr.191601.115

Sha, Z., Brill, L. M., Cabrera, R., Kleifeld, O., Scheliga, J. S., Glickman, M. H., et al. (2009). The eIF3 Interactome Reveals the Translasome, a Supercomplex Linking Protein Synthesis and Degradation Machineries. *Mol. Cel.* 36, 141–152. doi:10.1016/j.molcel.2009.09.026

Shah, M., Su, D., Scheliga, J. S., Pluskal, T., Boronat, S., Motamedchaboki, K., et al. (2016). A Transcript-specific eIF3 Complex Mediates Global Translational Control of Energy Metabolism. *Cel. Rep.* 16, 1891–1902. doi:10.1016/J.CELREP.2016.07.006

Shivaya Valasek, L. (2012). 'Ribozoomin' - Translation Initiation from the Perspective of the Ribosome-Bound Eukaryotic Initiation Factors (eIFs). *Cpps* 13, 305–330. doi:10.2174/138920312801619385

Simonetti, A., Brito Querido, J., Myasnikov, A. G., Mancera-Martinez, E., Renaud, A., Kuhn, L., et al. (2016). eIF3 Peripheral Subunits Rearrangement after mRNA Binding and Start-Codon Recognition. *Mol. Cel.* 63, 206–217. doi:10.1016/j.molcel.2016.05.033

Sokabe, M., and Fraser, C. S. (2014). Human Eukaryotic Initiation Factor 2 (eIF2)-GTP-Met-tRNAi Ternary Complex and eIF3 Stabilize the 43 S Preinitiation Complex. *J. Biol. Chem.* 289, 31827–31836. doi:10.1074/JBC.M114.602870

Sonenberg, N., and Hinnebusch, A. G. (2009). Regulation of Translation Initiation in Eukaryotes: Mechanisms and Biological Targets. *Cell* 136, 731–745. doi:10.1016/j.cell.2009.01.042

Szamecz, B., Rutkai, E., Cuchalová, L., Munzarová, V., Herrmannová, A., Nielsen, K. H., et al. (2008). eIF3a Cooperates with Sequences 5′ of uORF1 to Promote Resumption of Scanning by post-termination Ribosomes for Reinitiation on GCN4 mRNA. *Genes Dev.* 22, 2414–2425. doi:10.1101/gad.480508

Valásek, L., Mathew, A. A., Shin, B. S., Nielsen, K. H., Szamecz, B., and Hinnebusch, A. G. (2003). The Yeast eIF3 Subunits TIF32/a, NIP1/c, and eIF5 Make Critical Connections with the 40S Ribosome *In Vivo*. *Genes Dev.* 17, 786–799. doi:10.1101/gad.1065403

Valásek, L., Nielsen, K. H., Zhang, F., Fekete, C. A., and Hinnebusch, A. G. (2004). Interactions of Eukaryotic Translation Initiation Factor 3 (eIF3) Subunit NIP1/c with eIF1 and eIF5 Promote Preinitiation Complex Assembly and Regulate Start Codon Selection. *Mol. Cell. Biol.* 24, 9437–9455. doi:10.1128/MCB.24.21.9437-9455.2004

Valášek, L., Nielsen, K. H., and Hinnebusch, A. G. (2002). Direct eIF2-eIF3 Contact in the Multifactor Complex Is Important for Translation Initiation *In Vivo*. *EMBO J.* 21, 5886–5898. doi:10.1093/emboj/cdf563

Valášek, L. S., Zeman, J., Wagner, S., Beznosková, P., Pavlíková, Z., Mohammad, M. P., et al. (2017). Embraced by eIF3: Structural and Functional Insights into the Roles of eIF3 across the Translation Cycle. *Nucleic Acids Res.* 45, 10948–10968. doi:10.1093/nar/gkx805

Villa, N., Do, A., Hershey, J. W. B., and Fraser, C. S. (2013). Human Eukaryotic Initiation Factor 4G (eIF4G) Protein Binds to eIF3c, -d, and -e to Promote mRNA Recruitment to the Ribosome. *J. Biol. Chem.* 288, 32932–32940. doi:10.1074/JBC.M113.517011

Wagner, S., Herrmannová, A., Hronová, V., Gunišová, S., Sen, N. D., Hannan, R. D., et al. (2020). Selective Translation Complex Profiling Reveals Staged Initiation and Co-translational Assembly of Initiation Factor Complexes. *Mol. Cel.* 79, 546–560. doi:10.1016/j.molcel.2020.06.004

Walker, S. E., Zhou, F., Mitchell, S. F., Larson, V. S., Valasek, L., Hinnebusch, A. G., et al. (2013). Yeast eIF4B Binds to the Head of the 40S Ribosomal Subunit and Promotes mRNA Recruitment through its N-Terminal and Internal Repeat Domains. *RNA* 19, 191–207. doi:10.1261/rna.035881.112

Yourik, P., Aitken, C. E., Zhou, F., Gupta, N., Hinnebusch, A. G., and Lorsch, J. R. (2017). Yeast eIF4A Enhances Recruitment of mRNAs Regardless of Their Structural Complexity. *Elife* 6, 1. doi:10.7554/eLife.31476

Zhou, F., Zhang, H., Kulkarni, S. D., Lorsch, J. R., and Hinnebusch, A. G. (2020). eIF1 Discriminates against Suboptimal Initiation Sites to Prevent Excessive uORF Translation Genome-wide. *RNA* 26, 419–438. doi:10.1261/rna.073536.119

Zinshteyn, B., Rojas-Duran, M. F., and Gilbert, W. V. (2017). Translation Initiation Factor eIF4G1 Preferentially Binds Yeast Transcript Leaders Containing Conserved Oligo-Uridine Motifs. *RNA* 23, 1365–1375. doi:10.1261/RNA.062059.117

Conflict of Interest: The authors declare that the research was conducted in the absence of any commercial or financial relationships that could be construed as a potential conflict of interest.

Publisher's Note: All claims expressed in this article are solely those of the authors and do not necessarily represent those of their affiliated organizations, or those of the publisher, the editors and the reviewers. Any product that may be evaluated in this article, or claim that may be made by its manufacturer, is not guaranteed or endorsed by the publisher.

Advantages of publishing in Frontiers

OPEN ACCESS
Articles are free to read for greatest visibility and readership

FAST PUBLICATION
Around 90 days from submission to decision

HIGH QUALITY PEER-REVIEW
Rigorous, collaborative, and constructive peer-review

TRANSPARENT PEER-REVIEW
Editors and reviewers acknowledged by name on published articles

Frontiers
Avenue du Tribunal-Fédéral 34
1005 Lausanne | Switzerland

Visit us: www.frontiersin.org
Contact us: frontiersin.org/about/contact

REPRODUCIBILITY OF RESEARCH
Support open data and methods to enhance research reproducibility

DIGITAL PUBLISHING
Articles designed for optimal readership across devices

FOLLOW US
@frontiersin

IMPACT METRICS
Advanced article metrics track visibility across digital media

EXTENSIVE PROMOTION
Marketing and promotion of impactful research

LOOP RESEARCH NETWORK
Our network increases your article's readership